Comments on

Dynamic Energy and Mass budgets in Biological Systems

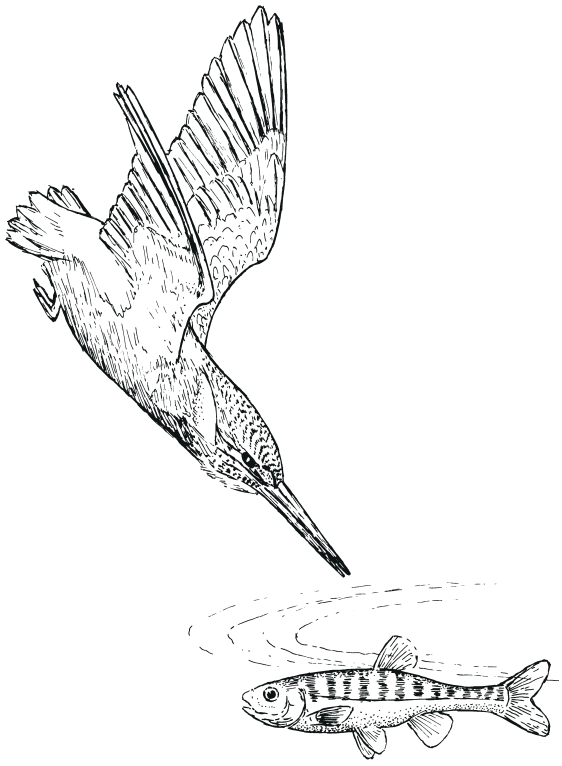

S. A. L. M. Kooijman 2000

Cambridge University Press, 2nd edition

http://www.bio.vu.nl/thb/deb/ 2008/06/10

The comments in this document resulted from discussions with colleagues and students and from further research. The numbers in curled braces in the margin refer to page numbers of the DEB book [289]; the positive numbers behind 'l' refer to line number from the top of the page, the negative numbers from the bottom of the page; the numbers behind 'p' refer to paragraph, and 'Eq' stands for equation. Derivations for particular equations are presented here in detail. The numbers separated by dots refer to section numbers.

Many items in this book are illustrated with sheets that can be found at (and downloaded from) `http://www.bio.vu.nl/thb/deb/sheets/`. Other supporting material, such as errata, quizzes and exercises can be found at `http://www.bio.vu.nl/thb/deb/material.html`. This site also shows question & answer, essay and theses collections that resulted from the international tele-courses on DEB theory that have been organized, see `http://www.bio.vu.nl/thb/deb/course/deb/`. All these files are updated every now and then.

Each figure of the DEB book has an Octave/Matlab file in DEBtool/fig at `http://www.bio.vu.nl/thb/deb/deblab/debtool/`; these files set the data points, define the models, fit the models to the data, present parameter values and their standard deviations, and show the figure in color. Replacing these data by your own data provides a rapid mean the apply DEB theory to your data. DEBtool can also be used for further illustrations and new applications of DEB theory.

DEB papers before the DEB-book [281]: 1979–1993

[323, 326, 270, 269, 268, 272, 271, 273, 313, 274, 275, 276, 140, 174, 277, 317, 603, 184, 315, 139, 138, 278, 279, 324, 182, 280, 471, 580, 596, 185]

DEB papers since the DEB-book [281] till [289]: 1993–2000

[116, 132, 137, 201, 185, 457, 470, 469, 605, 604, 27, 29, 28, 55, 183, 186, 239, 257, 258, 267, 283, 282, 322, 409, 465, 469, 571, 181, 245, 259, 284, 411, 468, 570, 302, 285, 305, 303, 304, 310, 314, 319, 320, 401, 402, 472, 597, 175, 249, 248, 260, 286, 306, 598, 602, 57, 240, 251, 250, 288, 287, 308, 400, 466, 601, 600, 599, 45, 58, 252, 261, 321]

DEB papers since the DEB-book [289]: 2000–2009

[9, 47, 46, 56, 66, 179, 180, 229, 262, 307, 325, 357, 403, 128, 421, 59, 177, 176, 246, 254, 255, 290, 348, 410, 446, 467, 502, 567, 64, 178, 243, 263, 265, 311, 346, 449, 451, 67, 244, 247, 256, 298, 338, 340, 345, 347, 349, 356, 448, 566, 65, 123, 211, 155, 172, 264, 292, 291, 297, 318, 335, 337, 334, 339, 343, 422, 452, 572, 2, 210, 214, 316, 327, 352, 359, 365, 423, 447, 462, 480, 559, 558, 4, 3, 6, 18, 83, 84, 85, 124, 213, 231, 266, 293, 309, 391, 390, 428, 450, 455, 459, 530, 554, 556, 563, 565, 16, 17, 48, 76, 82, 199, 212, 234, 235, 301, 300, 312, 330, 350, 555, 384, 385, 528, 427, 429, 560, 60, 77, 130, 131, 145, 209, 253, 294, 299, 329, 440, 441, 443, 444, 442, 529, 557, 54, 61, 62, 146, 295, 296, 216, 166, 366, 367, 382, 392, 439, 458, 481, 485, 551, 564, 584]

Third edition of the DEB book

I started systematic research on DEB theory in august 1979, some thirty years ago. Research, results and acceptance accelerated since then. The international tele-courses on DEB theory (2001, 2003, 2005, 2007) played an important role in the acceleration. The research group AQUAdeb and international research projects further simulated research with practical applications in aquaculture, ecotoxicity and economics. This necessitated a new edition of the DEB book [289] to remain an effective stimulus for further developments.

- Title: *The Dynamic Energy Budget theory for metabolic organization*
- Links with DEBtool (m-file for each figure)
- Support on the web (derivations); helpdesk
- Inclusion of a selection of these comments
- Reduction of preface
- Elimination of chapter 1 (some material transfer to other chapters)
- Update of chapter 2

  2.3.1 weak, strong, structural homeostasis: mechanisms

  2.4 → Synthesizing Units: extension, transfer from chap5
- Update of chapter 4

  ageing, with acceleration of ageing linked to mitochondria

  entropy estimates, effect of pressure in deep ocean

  dynamics of isotopes
- Update of chapter 8

  new primary parameters

  tables with estimates of species parameters
- Update of chapter 9

  reduction of population dynamics

  parasite dynamics in hosts; effects on hosts

  extension of system dynamics; biomass spectra
- New chapter on evolution & system earth

DEB symposium in Brest, April 2009

To enhance the essential link between eduction and research the fifth international telecourse on DEB theory with be linked to a DEB symposium. This symposium is planned for April 2009 in Brest (see DEB info page on the web); At the symposium we plan to present

- a second special issue of the *Journal of Sea Research* on DEB applications by the group AQUAdeb
- the third edition of the DEB book by Bas Kooijman
- an introductory DEB book for ecologists by Jaap van der Meer
- a book on ecotoxicological applications of DEB theory by Tjalling Jager

Chapter 1

Energetics and models

Pores in egg shells and plant leaves

{3}, l25

The example of the pore frequency in egg shells has a parallel with the stomata frequency in plant leaves. Data from fossil plants from Greenland show a dramatic drop in stomata frequency at the end of the Triassic (208 Ma ago), which has been linked to a steep rise of the atmospheric CO_2 concentration to three times the present values, possibly as a result of the activity of volcanoes that mark the breakup of Pangaea [31, p98]. The plants no longer needed many stomata, and reduced the number to reduce the water loss by evaporation.

A weird world at small scales

{7},1.2.1

The standard approach to the problem of understanding complex systems is to start from the low organization level, to collect all possible information and use it to explain processes at higher organization levels. Although spectacular progress has been booked in the last decades on qualitative aspects of molecular biology, little is known about quantitative ones, which are substantially more difficult to tackle. Chemical kinetics, and enzyme kinetics, are developed for (large) homogeneous reactors with constant volumes that have diluted concentrations of substrates and enzymes that perform simple transformations, not for small inhomogeneous cells that change in volume and are packed with macro molecules that each partake in very few but complex transformations only. Basic to chemical kinetics is the law of mass action: transformation rates are proportional to meeting frequencies, which are taken proportional to the product of concentrations of substrate. This rests on transport by diffusion or convection. A few observations might help to reveal that the application of classic chemical kinetics in cellular metabolism is problematic. This even holds for the concept 'concentration' of a compound inside cells.

An example from [290]: Consider a typical bacterial cell of volume 0.25 μm^3 and an internal pH of 7. The intra-cellular compartments of eukaryotic cells are about the same size. It must have 15 free protons, but random dissociation of water, and random association of protons and hydroxyl ions make this number fluctuate wildly [389]. Figure 1.1 shows that the (asymptotic) frequency distribution of the number of protons, and so of pH, dramatically increases in variance for decreasing cell sizes for volumes smaller that 0.5

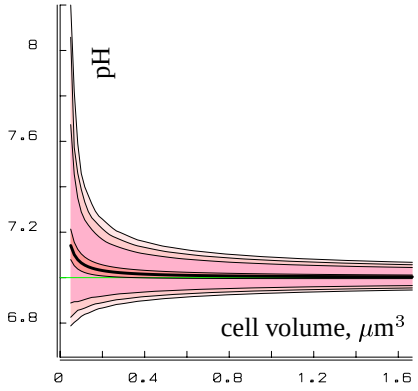

Figure 1.1: The 95%, 90%, 80% and 60% confidence intervals of pH in cells of pure water with pH 7 as a function of the cell size. They increase dramatically for decreasing cell sizes for cells (or cell compartments) less than 0.5 μm^3. The thick curve represents the mean pH, which goes up sharply for very small cell sizes.

μm^3. We have to think in terms of pH *distributions* rather than pH *values*. Many chemical properties of compounds depend on the pH, which makes matters really complex.

A water molecule is created, by association of a proton and a hydroxyl ion, and is annihilated by dissociation about twice a day at 25 °C. Brownian motion transports a water molecule about 3 cm between creation and annihilation, while protons and hydroxyl ions are transported some 3 μm, on average. However, these distances do not fit into a cell (or cell compartment), which must lead to the conclusion that undisturbed diffusion does not occur in cells. These expectations are based on pure water, but a more realistic cytoplasm composition does not eliminate the problem.

Water in very small volumes behaves as a liquid crystal [75, 22], rather than as a liquid, which has substantial consequences for kinetics. Electrical potentials reveal the crystalline properties. They decay exponentially as a function of distance L, so they are proportional to $\exp\{-L/L_D\}$. The parameter L_D, called the Debye distance, is about 0.1 μm for water at 25 °C [579], which means the electrical potential of a proton would be felt through most of the cell, even if it did not move.

Organelles crawl around in cells, divide, merge and may be destroyed. Substrates are delivered to enzymes by transporter proteins, that follow paths along the endoplasmatic reticulum; products are removed from their site of origin in a similar way. Active allocation of substrates to particular transformations is common. The small number of molecules of any type requires stochastic rather than deterministic specification of their dynamics. Many enzymes are only active if bounded to membranes. Many substrates play a role in a metabolic network, which given complex connections. The cell follows a cell cycle, and many sub-cellular structures and activities have complex links to this cycle. All these aspects make that transformations that are based on the law of mass action are problematic for living cells.

Central role for individuals in DEB theory

{10}, Fig 1.2

The reasons why the individual play a central role in DEB theory for metabolic organization are

- input and output of mass and energy is most accessible at this level
- the individual is the primary unit of evolutionary selection, the survival machine life
- behaviour is key to food intake and food selection; food fuels metabolism. Behaviour is also key to mate selection; reproduction controls survival across generation in many species. Behaviour is primarily linked to the level of the individual

The delineation of the individual level is not always sharp; the section on evolution (Chapter 8) discusses this in more detail. Many species are unicellular, so the cellular and individual levels coincide for them. Multicellular species that sport reproduction start their life cycle as a unicellular, which is relevant to DEB theory because it deals with the full life cycle. Some species are multicellular in the embryo stage, but unicellular in the adult stage, which illustrates that the various levels of organisation are more complex than illustrated in this scheme.

Estimation of DEB parameters

{14},1.2.4

The sequence of estimation steps that is discussed in [328] basically concerns a mixture of statistics (e.g. the von Bertalanffy growth rate) and observations. We did this because sometimes this is the only information that is available, but in the first place to reveal the logical relationships between these quantities and DEB parameters. From a statistical point of view, it is better to use data directly [390], rather than via these statistics. This strategy also allows for a wider choise of types of data that can be used to obtain values for parameters. Data on embryo development, for instance, can be used to extract the energy conductance $\dot{v}$ and the somatic maintenance rate coefficient $\dot{k}_M$, see [289, p101]. The basic idea is to use all available information simultaneously.

The regression routines of software package DEBtool can handle an arbitrary number of data set simultaneously using algorithms, that vary from slow with a large domain of attraction (genetic algorithms, Nead-Melder method), to fast with a small domain of attraction (Newton-Raphson method). It is easy to change from fixing parameters at particular values and subjecting them to optimasation. The routines allow for continuation, i.e. the resulting parameters from one call can be used as starting point for a next call. Since the possibility always exist that the resulting estimates correspond with a local minimum of the sum of weighted squared deviations, rather than with a global minimum, it is good idea to try several values for initial estimates, and select the result with the smallest deviation.

A basic problem in estimating parameters from several data sets simultaneously is that it is less easy to figure out if the combined data do determine the parameters that are subjected to optimasation. A useful test is to check for non-singularity using the Newton-Raphson method (a warning appears for singularity); this test is not "waterproof", however. Moreover, a parameter might be determined by the combined data, but very imprecisely only. The standard deviations might indicate this, (DEBtool has a function for the covariance matrix of parameter estimates, from which standard deviations are derived), but one should not conclude from a small standard deviation that the corresponding parameter is

precisely determined by the data; a mistake that is easy to make. The simultaneous confidence interval with highly correlated parameters might be large. Moreover parameters might depend on each other in non-linear ways that are poorly quantified by the correlation matrix. Profile likelyhood functions give a much more reliable idea about the real confidence of parameter values (DEBtool has functions for them), but the computation of these profile likehood functions can easily be demanding.

It is always a good idea to finalize the estimation with the Newton Raphson method (because it is most accurate), and to check the results graphically (DEBtool has facilities for this); no formalized method can compete with the human eye.

Apart from optimizing the goodness of fit we want to have physiological consistency. These different criteria frequently, but not always, coincide; a very unrealistic parameter value might give a slightly better fit than a realistic one. As long as the fit is not too bad, realism is a stronger criterion. Such an endpoint can be obtained using the concept of sloppy constraints, where "pseudo observations" are fitted for particular parameters, simultaneously with real observations. Choosing large weight coefficients in the regression procedure that minimizes the weighted sum of squared deviations for the pseudo observations, the sloppy constraints become real constraints and the parameters are set to the "observed" values. By decreasing the weight coefficients, we can allow deviations from these values; if the weight coefficients equal zero, the "observation" is completely ignored. This procedure has relationships with Baysian methods, but has a better biological foundation. See the first estimation step for the logic of this procedure.

DEB theory can handle varying food conditions and temperatures, which are inherent to seasonal forcing. The implementation of the more advance applications typically requires some data set specific coding.

Implicit Monod

{16},Fig 1.3

Note that the solution for Monod degradation has been given implicitly only. It cannot be given explicitly because $X(t)$ as well as $\ln X(t)$ occur in the equation. It is not difficult, however, to solve $X(t)$ numerically from the equation that has been given.

More intros to DEB theory

{19}

Meanwhile we wrote papers that introduce DEB theory conceptually [421, 290, 390]. The role of the central nervous system in the regulation of food intake in demand systems is discussed by [408].

Chapter 2

Basic concepts

Supply versus demand systems

{19}

Since the DEB theory is supposed to be applicable to all organisms, both supply and demand systems follow the same rules within the DEB theory. An explanation might be that demand systems evolved from supply systems, froze the existing metabolic rules, lost metabolic flexibility (to deal with extreme starvation conditions), but increased in behavioural flexibility. All demand systems are animals, i.e. organisms that feed on other organsims; they are often mobile and move to there were the food is and this food typically consists of other organisms. Hence they encounter less frequently extreme starvation conditions; they typically cannot shrink during starvation, but die. The increased behavioural flexibility gives them the possibility to specialize on one type of food species and translates in a small value for the half saturation coefficient for demand systems. They also have a relatively large difference between the peak and the standard metabolic rate, and have typically closed circulation systems (efficient transport under extreme metabolic performance), some developed endothermy (birds and mammals) and many have higly developed sensors. Supply organisms typically move less and find their food via a kind of (activated) diffusion process. They can better deal with starvation (shrinking). They have less developed sensors and are metabolically more flexible. Especially those that do not live of other organisms typically have a number of reserves equal to the number of complementary resources. By far the majority of species are supply systems, but the few demand systems got relatively more research attention.

Size variation via food intake

{21}, Fig 2.1

We here focus on spatially homogeneous situations, and create ourselves a stochastic model for feeding of a single individual on a single type of food particles. We then extend the model to more individuals and see how social interaction can amplify size differences. This section is meant to present a mechanism behind the phenomenon depicted in Figure 2.1 at {21}.

The stochastic feeding model is constructed such that the expected feeding rate is $\dot{J}_{XA} = f\{\dot{J}_{XAm}\}L^2$ with $f = X/(K+X)$, where $\dot{J}_{XA}$ is quantified as mass of particles per

time and food density X and saturation constant K as mass of food particles per volume. The mass of a food particle is M_X (in C-mole). In number of food particles, we write $\dot{h}_X = f\{\dot{h}_{Xm}\}L^2$ with $\{\dot{J}_{XAm}\} = -\{\dot{h}_{Xm}\}M_X$, and $f = X_\#/(K_\# + X_\#)$, with $X = X_\# M_X$ and $K = K_\# M_X$. (Notice that $\dot{J}_{XA} < 0$ and $\dot{h}_X > 0$.) At high food density $X_\#$, for $f = 1$, searching takes a negligible amount of time, and the mean time it takes to handle a single food item is $t_h = 1/\dot{h}_{Xm} = \{\dot{h}_{Xm}\}^{-1}L^{-2}$. Since $\dot{h}_X = (t_s + t_h)^{-1}$, the time for searching is $t_s = 1/\dot{h}_X - 1/\dot{h}_{Xm} = K_\{\dot{h}_{Xm}\}^{-1}X_\#^{-1}L^{-2}$.

Suppose that the food particles at a given time are randomly distributed in space with mean density $X_\#$. The probability that the nearest food particle is at a distance larger than L from an individual at a random site is

$$\mathrm{Prob}\{\underline{L}_d > L\} = \exp(-X_\# L^3 \pi 4/3)$$

So, the nearest food particle is at mean distance

$$\mathcal{E}\underline{L}_d = \int_0^\infty \mathrm{Prob}\{\underline{L}_d > L\}\, dL = \Gamma(4/3)(X_\# \pi 4/3)^{-1/3} = aX_\#^{-1/3}$$

with $a = \Gamma(4/3)(\pi 4/3)^{-1/3} \simeq 0.554$. Traveling at speed $\dot{S}$, the time to reach this particle is $t_s = \mathcal{E}\underline{L}_d/\dot{S} = aX_\#^{-1/3}/\dot{S}$, so the speed is $\dot{S} = aX_\#^{-1/3}/t_s = aK_\#^{-1}\{\dot{h}_{Xm}\}X_\#^{2/3}L^2 = \dot{b}X_\#^{2/3}L^2$ for $\dot{b} = aK_\#^{-1}\{\dot{h}_{Xm}\}$.

We now construct a feeding process of a single individual in a unit cube of habitat on the basis of the following rules

R1 a new food particle appears at a random site within the cube at the moment one of the resident particles disappears. It stays on this site till it disappears; the total number of food particles remains constant.

R2 a food particle disappears at a constant probability rate μ, or because it is eaten by the individual.

R3 the individual travels in a straight line to the nearest visible food particle at speed $\dot{S} = \dot{b}X_\#^{2/3}L^2$, eats the particle upon arrival and waits at this site for a time $t_h = \{\dot{h}_{Xm}\}^{-1}L^{-2}$. The individual changes direction if the food particle at which it is aiming disappears or a nearer new one appears. It changes speed because of changes in length.

R4 the individual grows following the DEB rules for an isomorph, i.e. the food particle converts to reserve instantaneously; the scaled reserve density e of an individual of structural volume L^3 makes a jump from e to $e + (L_X/L)^3$ upon feeding; scaled reserve density is used for metabolism at rate $\frac{d}{dt}e = -e\{\dot{h}_{Xm}\}L_X^3/L$; reserve converts to structure and the length changes at rate $\frac{d}{dt}L = \frac{\{\dot{h}_{Xm}\}L_X^3 e - L\dot{k}_M g}{3(e+g)}$. At time $t = 0$ the length is $L = L_b$, and the reserve density $e = f$.

R5 all food particles are visible.

We now extend the rules for N individuals that interact not only by competition, but also by social intimidation using the following rule that replaces R5

R5 a food particle becomes invisible for an individual of length L_1, if an individual of length L_1 is within a distance $L_s(L_2/L_1)^2$ from the food particle, irrespective of being aimed at.

Notice that even for the intimidation length $L_s \to 0$ the individuals interact (weakly) by competition because the mean traveling distance will increase, despite the replacement of disappearing food particles. The differences in length will amplify for increasing intimidation length.

The interpretation of the food length L_X is $L_X^3 = M_X y_{EX}/[M_{Em}]$, which makes that $L_m = \frac{-\{\dot{J}_{XAm}\}y_{EX}}{k_M g[M_{Em}]} = \frac{\kappa\{\dot{J}_{EAm}\}}{j_{EM}[M_V]} = -\frac{\kappa\{-\dot{J}_{XAm}\}}{j_{XM}[M_V]}$ (cf {122} Table 3.4). Notice that by increasing mass M_X, while keeping $\{\dot{J}_{XAm}\}$ constant, the maximum length will increase as well. Keeping $\{\dot{J}_{XAm}\}$ constant, however, will result in an increase in variance. The speed can be made independent of food density and proportional to length, rather than squared length, by inserting more detail in the feeding process (especially in the visibility module). We here want to minimize the number of parameters that needs to be specified.

The food density X and the particle disappearance rate μ are environmental parameters. Although our food particles do not move, the replacement scheme has the effect as if the particles move at infinite speed to another random location at random points in time. The mean distance between two random points on a unit edge is 1/3, on a unit square it is 0.521405, and on a unit cube it is 0.65853. So the mean speed of a food particle in a cube with edge L_D is $0.65853 L_D \mu$. If this is in the same order of magnitude as the speed of the organism, it strongly affects the feeding process; if it is much larger, the individuals will starve to death.

We have two different spatial units, that of the individual (in $\{\dot{h}_{Xm}\}$, L_b and L_X) and of the environment (in X, K and L_s), here chosen as cm and m, respectively. Speed is primarily controlled by the saturation constant K. The social interaction increases with decreasing number of food particles per individual. The variance increases with food length L_X, but decreases in time because of the smoothing capacity of the individual increases with size (the catabolic flux is inversely proportional to a length measure.

We have 8 parameters $X_\#$, $K_\#$, L_b, L_X, $\{\dot{h}_{Xm}\}$, $\dot{k}_M$, g, μ for feeding and growth of a single individual with state variables scaled reserve density e and structural length L, and one extra parameter, L_s, for the feeding and growth of N individuals. Notice that $\{\dot{h}_{Xm}\}L_X^3$ plays the role of the energy conductance $\dot{v}$ in the standard DEB formulation, which does not account for stochasticity and the discreteness of food particles. This stochastic extension, therefore, does not come with an increase in the number of parameters, while we need a single parameter to introduce social interaction. We can out-scale one parameter, if our interest is in relative length $l = L/L_m$ with $L_m = \{\dot{h}_{Xm}\}L_X^3/\dot{k}_M g$, and another one by choosing the spatial scale such that $K_\# = 1$, and a final one if we out-scale time, e.g. by choosing the maintenance rate coefficient $\dot{k}_M^{-1}$ as unit of time. The core of the problem of how the variance in length builds up as function of time t, food density X, number of interacting individuals N and the intimidation length L_s has thus 6 parameters.

Figure 2.1 illustrates simulation results; notice that both individuals have exactly the same parameter values, although they seem to follow different growth curves! Stochastic growth is retarded relative to the deterministic expectations because of the border effects (which increase the traveling distances), and the stochastic displacements of food particles. Even in the single individual case, the variance behaves different, compared to the random telegraph process, as described in section 7.1.1 at {221} and Figure 7.1. Notice also how

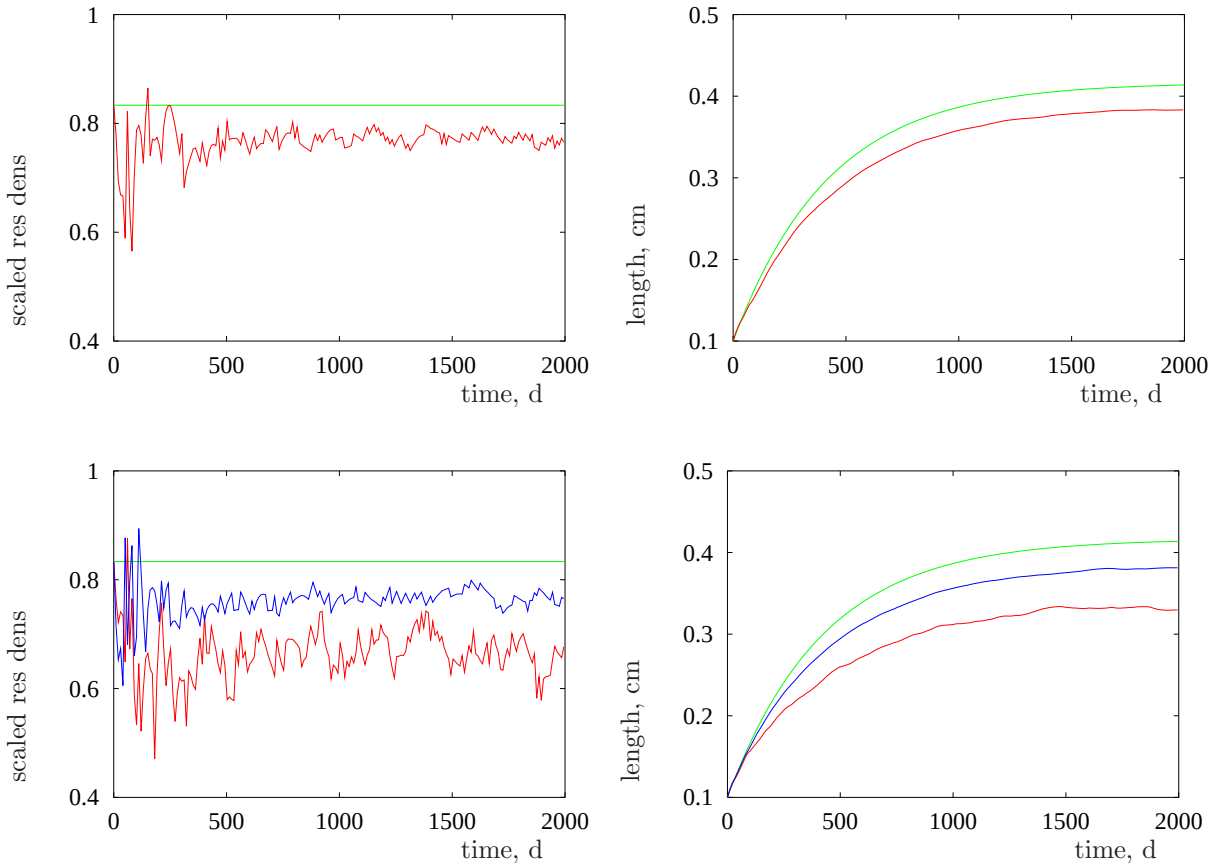

Figure 2.1: The scaled reserve density e and the length L, in the single (top) and the two (bottom) individual situation. The green lines give the deterministic expectation without interaction. Parameters: $\mu = 2$ d^{-1}, $X_\# = 10$ m^{-3}, $K_\# = 2$ m^{-3}, $\{\dot{h}_{Xm}\} = 10$ d^{-1}cm^{-2}, $L_b = 0.1$ cm, $L_X = 0.1$ cm, $\dot{k}_M = 0.01$ d^{-1}, $g = 2$, $L_s = 0.2$ m.

effectively reserve smooths out stochastic fluctuations in food availability.

{25}, 2.2.1

Exoskeletons

Isomorphism itself poses no constraints on shape, but if organisms have a permanent exoskeleton, then stringent constraints on shape exist and as most animals with a permanent exoskeleton actually meet these constraints, it is helpful to work them out. This is done in [281].

A grasshopper remains isomorphic and has an exoskeleton, but it grows by moulting, thus the exoskeleton is not permanent and isomorphism poses no constraints in this case. The same holds for an organism which resembles a sphere, such as a sea urchin; it cannot have a permanent (rigid) exoskeleton, because the curvature of its surface changes during growth. A cylindrical organism that grows in length only, is not isomorphic. A cylindrical organism that grows isometrically has only its caps as a permanent exoskeleton; thus

this includes only the caps, i.e. two growing disks separated by a growing distance. The permanent exoskeleton generally represents a (curved) surface in three dimensional space, which can be described in a simple way using logarithmic spirals. The idea of the logarithmic spiral or *spira mirabilis* (in the plane) goes back to Descartes' studies of *Nautilus* in 1638 and to Bernoulli in 1692. The function has been used by Thompson [552], Rudwick [495, 496] and Raup [473, 474] to describe the shape of brachiopods, ammonites and other molluscs. I will rephrase their work in modern mathematical terms and extend the idea a bit.

A natural starting point for a description of the isomorphic permanent exoskeleton is the mouthcurve. This is a closed curve in three dimensional space that describes the 'opening' of the permanent exoskeleton (shell). This is where the skeleton synthesizing tissue is found. The development of the exoskeleton can, in most cases, be retraced in time to an infinitesimally small beginning, giving the permanent exoskeleton just the one 'opening'. This method avoids the problem of the specification of the shape of an invisibly small object. To follow the mouth curve back in its development, we introduce a dummy variable l, which has the value 0 for the present mouth curve and $-\infty$ at the start of development. By placing the start of development at the origin, the test on isomorphism of the developing exoskeleton is reduced to mapping one exoskeleton to another by multiplication and rotation only (so no translation). We can always orient the exoskeleton such that the rotation is around the x-axis. Let $\boldsymbol{R}(l)$ denote the rotation matrix

$$\boldsymbol{R}(l) \;=\; \begin{pmatrix} 1 & 0 & 0 \\ 0 & \cos l & \sin l \\ 0 & -\sin l & \cos l \end{pmatrix}$$

The closed mouthcurve $\boldsymbol{m}$ at an arbitrary value for the dummy variable l, can be described by

$$\boldsymbol{m}(l) = c^{l/2\pi}\boldsymbol{R}(-l)\boldsymbol{m}(0) \tag{2.1}$$

where c is a constant describing how fast the mouth curve reduces in size when the exoskeleton rotates over an angle 2π. If c is very large, it means that the exoskeleton does not rotate during its reduction in size. Size reduction relates in a special way to the rotation rate to ensure (self) isomorphism. It follows from the requirement that for any two points $\boldsymbol{m}_0$ and $\boldsymbol{m}_1$ on the mouthcurve, the distance $\|\boldsymbol{m}_1(l+h) - \boldsymbol{m}_0(l)\|$ depends on l in a way that does not involve the particular choice of points. The rotation matrix is here evaluated at argument $-l$, because most gastropods form left handed coils. For right handed coiling l, rather than $-l$, should be used. The mouth curve, together with the parameter c determine the shape of the exoskeleton.

An arbitrary point on the mouth curve will describe a logarithmic spiral to the origin. To visualize this, it helps to realize that a simple function such as the standard circle is given by $\boldsymbol{f}(l) = (\sin l, \cos l)$, where the dummy variable l takes values between $-\infty$ and ∞. A graphical representation can be obtained by plotting $\sin l$ against $\cos l$. Similarly, the logarithmic spiral with the vertex at the origin through the point $\boldsymbol{m}(0) \equiv (m_1, 0, m_3)$ is given by

$$\boldsymbol{f}(l) = c^{l/2\pi}(m_1, m_3 \sin -l, m_3 \cos -l) \tag{2.2}$$

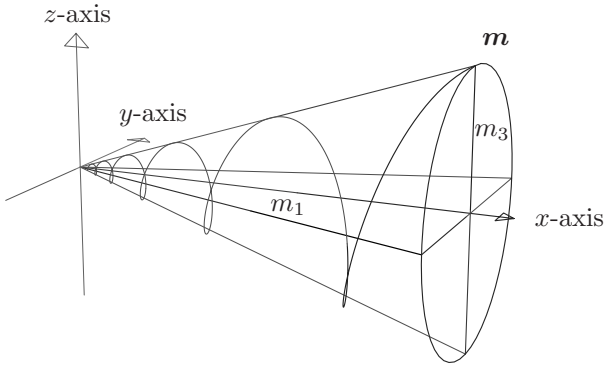

It lies on a cone around the x-axis with vertex at the origin, and tangent m_3/m_1 of the diverging angle with respect to the x-axis. For increasing l, the normalized direction vector of the spiral from the vertex, $(m_1, m_3 \sin -l, m_3 \cos -l)/\|\boldsymbol{m}\|$, with $\|\boldsymbol{m}\| = \sqrt{m_1^2 + m_3^2}$, describes a circle in the y, z-plane at x-value $m_1/\|\boldsymbol{m}\|$.

Until now, no explicit reference to time has been made. If the length measure of the animal follows a von Bertalanffy growth pattern, i.e. $1 - \exp\{-\dot{r}_B t\}$ for $t \in (0, \infty)$, the relationship $c^{l/2\pi} = 1 - \exp\{-\dot{r}_B t\}$ results. So, $l = \frac{2\pi}{\ln c} \ln\{1 - \exp\{-\dot{r}_B t\}\}$. This is realistic when food density and temperature remain constant. In winter, when growth ceases in the temperate regions and calcification partially continues in molluscs, a thickening of the shell occurs, which is visible as a ridge ringing the shell. If the gradual transitions between the seasons can be neglected, these ridges will be found at $l = \frac{2\,pi}{\ln c} \ln\{1 - \exp\{-\dot{r}_B i\}\}$, $i = 1, 2, 3, ..$, when the unit of time is one growth season. In principle, this offers the possibility of determining the von Bertalanffy growth rate $\dot{r}_B$ from a single shell found on the sea shore.

The mouth curve in living animals with a permanent exoskeleton frequently lies more or less in a plane, which reduces the specification of the three dimensional mouth curve to a two dimensional one, plus the specification of the plane of the mouth curve, which involves two extra parameters. The exoskeleton can always be oriented such that the plane of the mouth curve is perpendicular to the x, y-plane and the mouth opening is facing negative y-values.

Let $\boldsymbol{p} \equiv (p_1, p_2, 0)$ denote a point in the plane of the mouth curve, such that this plane is perpendicular to the vector $\boldsymbol{p}$ and $p_2 \leq 0$. (Remember that the axis of the spiral is the x-axis with the vertex at the origin so that the orientation of the exoskeleton is now completely fixed.) The mouth curve $\boldsymbol{n}$ in the plane is now measured using the point $\boldsymbol{p}$ as origin. If the mouth curve is exactly in a plane, a series of two coordinates suffice to describe the exoskeleton together with c, p_1 and p_2.

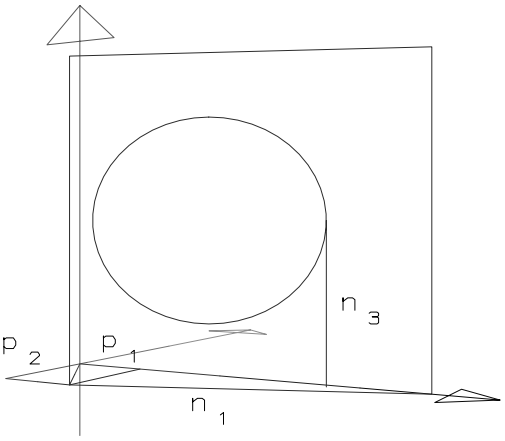

If it is not exactly in a plane, we can interpret the plane as a regression plane and still use three coordinates, where the y-values are taken to be small. The relationship between $\boldsymbol{n}$ measured in the coordinate system with the plane of the mouth curve as x, z-plane and $\boldsymbol{p}$ as origin with the original three dimensional mouth curve $\boldsymbol{m}$ is:

$$\boldsymbol{m} = \boldsymbol{p} + \begin{pmatrix} -p_2/\|\boldsymbol{p}\| & -p_1/\|\boldsymbol{p}\| & 0 \\ p_1/\|\boldsymbol{p}\| & -p_2/\|\boldsymbol{p}\| & 0 \\ 0 & 0 & 1 \end{pmatrix} \boldsymbol{n} \tag{2.3}$$

More specifically, if the mouth curve is a circle with radius r and the centre point at $(q_1, 0, q_3)$, we get $\boldsymbol{n}(\phi) = (q_1 + r\sin\phi, 0, q_3 + r\cos\phi)$, for an arbitrary value of ϕ between 0 and 2π. This dummy variable just scans the circle. The 6 parameters c, p_1, p_2, q_1, q_2 and r completely fix both shape and size of all isomorphic exoskeletons with circular mouth curves. If only the shape is of interest, we can choose r as the unit of distance, which leaves 5 free parameters for a full specification.

This class of morphs is too wide because it includes physically impossible shapes. The orientation of the mouth curve should be such that a mouth opening results and the shape may not 'bite' itself when walking along the spiral. This constraint can be translated into the constraint that the intersections of the exoskeleton with the x, z-plane should not intersect each other. The intersections of the mouth curve with the x, z-plane are easy to construct, given points on the mouth curve. When the point $\boldsymbol{m}_1 \equiv (m_1, m_2, m_3)$ on the mouth curve $\boldsymbol{m}(0)$ spirals its way back to the vertex, it intersects the x, z-plane at $c^{l_i/2\pi}\boldsymbol{R}(l_i)\boldsymbol{m}_1$, with $l_i = i\pi - \arctan m_2/m_3$ for $i = 0, -1, -2, \cdots$.

The distinction Raup [473] made between a generating curve and a biological one is purely arbitrary and has neither biological nor geometric meaning; Raup raises the problem that realistic values for the parameters he uses to characterize shape tend to cluster around certain values. Schindel [506] correctly pointed out that this depends on the particular way of defining parameters, and he used the intersection of (2.1) with the x, z-plane to characterize shape and showed that realistic values for parameters of this curve did not cluster. Any parameterization, however, is arbitrary unless it follows the growth mechanism. This shape of permanent exoskeletons is dealt with here to show that the shape is a result of the isomorphic constraint.

Nautilus has a fixed number of septa per revolution. This is to be expected as it makes a septum as soon as the end chamber in which it lives exceeds a given proportion of its body size. (The fact that the septa in subsequent revolutions frequently make contact implies that *Nautilus* somehow knows the number π.) These septa cause the shell to be no longer isomorphic in the strict sense, but to be what can be called periodically isomorphic, by which I mean that isomorphism no longer holds for any two values of l, but for values that differ by a certain amount. Many gastropods are sculptured at the outer surface of their shell; this sculpture is formed by the mantle curling around the shell edge. The distance from the shell edge and the height of the sculpture relates to the actual body size, the result being a shell that is also periodically isomorphic. Sculpture patterns that do not follow the mouth curve, but follow the logarithmic spirals, do not degrade isomorphism. Some shells of fully grown ammonites and gastropods have a last convolution that deviates in shape from the previous ones, showing a change in physiology related to life stage.

Most shapes are simple and correspond to special cases where the mouth curve lies in a plane. For $p_1 = 0$, the mouth curve lies in a plane parallel to the x, z-plane; shapes such as *Planorbis* and *Nautilus* result if the mouth curve is symmetrical around the x, y-plane. A growing sheet is obtained when $p_1 \to 0$ and $p_2 = 0$ so that the mouth curve lies in the y, z-plane. Age ridges can still show logarithmic spirals (in the plane), depending on the value of c. Figure 2.2 gives a sample of possible shapes. Although the shell of *Spirula* is internal rather than external, this does not spoil the argument.

From an abstract point of view, the closed mouth curve can secrete exoskeletons to

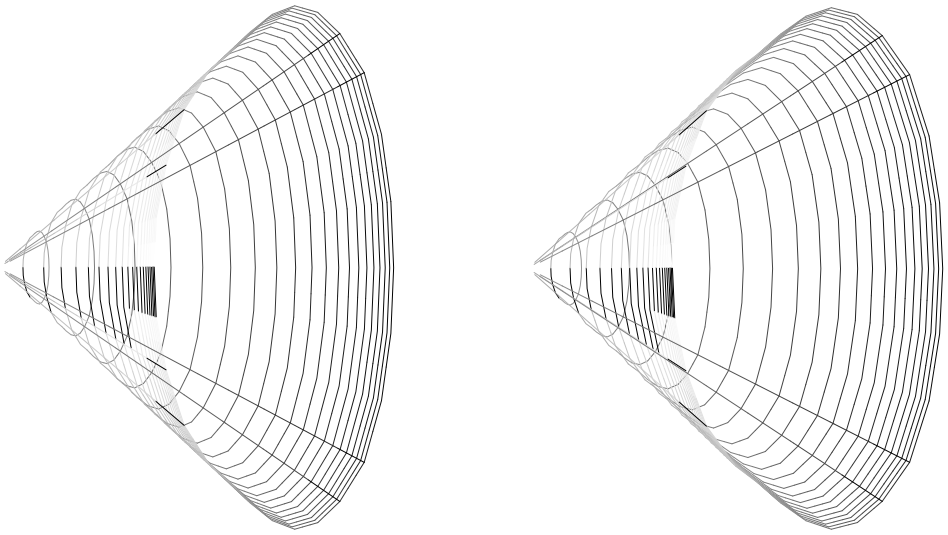

Patella, $c \to \infty$, $p_2 = 0$

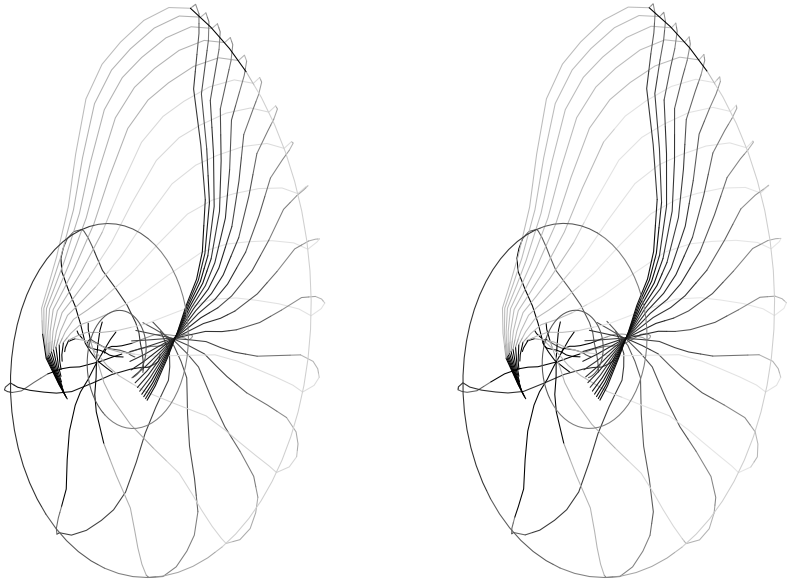

Nautilus, $c = 3$, $p_1 = 0$, $p_2 \to 0$

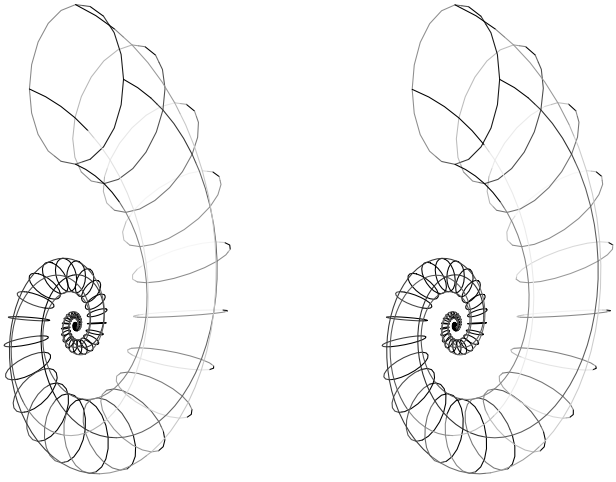

Spirula, $c = 5$, $p_1 = 0$, $p_2 \to 0$

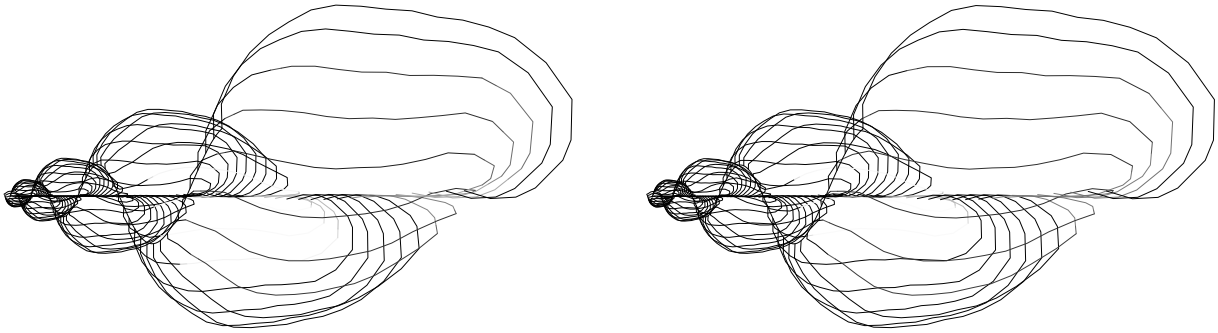

Lymnaea, $c = 2$, $p_1 = 0$, $p_2 \to 0$

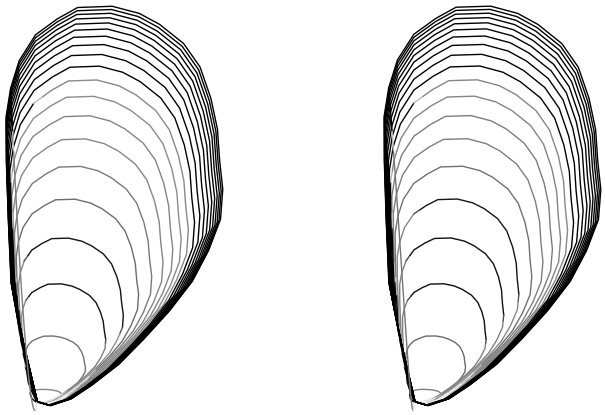

Mytilus, $c = 10^4$, $p_1 \to 0$, $p_2 = 0$

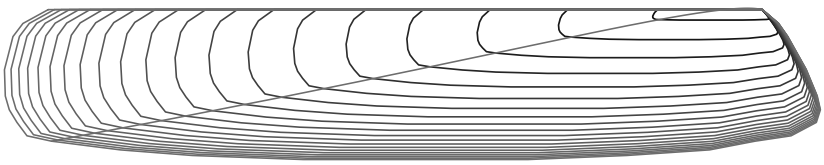

Ensis, $c = 10^5$, $p_1 \to 0$, $p_2 = 0$

Figure 2.2: A sample of possible shapes of isomorphs with permanent exoskeletons. The mouth curves are shown at equal steps for the dummy argument (*Lymnaea*, *Spirula*) or for time. Illuminate well and evenly to obtain the stereo effect. Hold your head about 50 cm from the page with the axis that connects your eyes exactly parelell to that for the figures. Do not focus at first on the page but on an imaginary point far behind the page. Try to merge both middle images of the four you should see this way. Then focus on the merged image. If this fails, try stereo glasses. If the grey is in front, rather than at the background, you are looking with your right eye to the left picture. Prevent this with a sheet of paper placed between your eyes and the page. About 10% of people actually look with one eye only and thus fail to see depth. If necessary, test this by raising one finger in front of your nose and counting the number of raised fingers that you see while focusing at infinity.

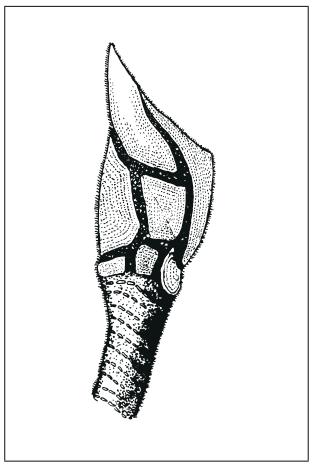

Figure 2.3: The goose barnacle (*Scalpellum scalpellum*) has an exoskeleton with a large number of components, each belonging to the family (2.1); it is an example of a branched mouth curve. Tetrahedrons provide an example of permanent exoskeletons with three branching points in the mouth curve and cubes with eight. If the (branched) mouth curve is a globular network, the exoskeleton can even resemble a sphere.

either side and no formal restrictions exist for the parameters describing their surfaces. (The biological reality is that two mouth curves are lined up and can be moved apart to let the animal interact with the environment.) Animals such as bivalves have two logarithmic spirals sharing the same mouth-curve, one turns clockwise, one anti-clockwise. Many gastropods also have a second exoskeleton, the plane-like operculum, which is so small that it easily escapes notice. Gastropods of the genera *Berthelinia*, *Julia* and *Midorigai* have two valves, much like the bivalva. As illustrated in figure 2.3, more complex shape are possible when the mouth curve is branched.

Surface areas vs volumes

{27}, l2

The fact that the surface area of an isomorph is proportional to volume$^{2/3}$ has been discussed in 2.2.2.
Line 13-14: "The different body sizes can be obtained through multiplying the x-values by some scalar..." , rather than the 'x-axis'. (Comments by Dmitrii Logofet)

Derivation of L_d

{29}, l7

The formula for L_d is derived as follows:
$V_d = (L_d - \delta L_d)\pi\delta^2 L_d^2/4 + \frac{4}{3}\pi\delta^3 L_d^3/8$; the first term is the volume in the cylinder of length $L_d - \delta L_d$ and radius $\delta L_d/2$, excluding the caps, the second term is the volume in the two hemispheres. These two hemispheres together make up a sphere with radius $\delta L_d/2$. Rearrangement of terms gives $V_d = \pi\delta^2 L_d^3(1 - \delta/3)/4$. We now write L_d as function of V_d, rather than vice versa.

Although it is not required for the shape correction function, we will later need length as a function of volume. The cylindric part of the cell is growing, so is the total cell length L, and the cell volume V, while the diameter remains constant. The volume at division V_d is taken as a reference value. We can express the cell length L as a function of cell volume V. The derivation is as follows:
$V = (L - \delta L_d)\pi\delta^2 L_d^2/4 + \frac{4}{3}\pi\delta^3 L_d^3/8$; the first term is again the volume in the cylinder, the second term is the volume in the two hemispheres. Rearrangement of terms gives

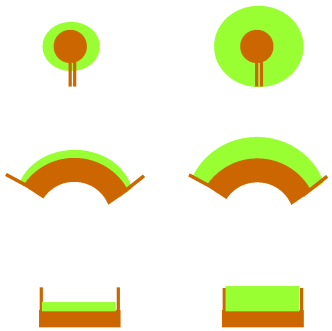

Figure 2.4: Biofilms (green) on the surface of a sphere (brown) can behave between an isomorph (top; radius of sphere $V_1 = 0$) and a V0-morph (bottom; radius of sphere $V_1 = \infty$). The shape correction function is $\mathcal{M}(V) = \left(\frac{V_d}{V} \frac{V_1+V}{V_1+V_d}\right)^{2/3}$.

$V = L\pi\delta^2 L_d^2/4 - \pi\delta^3 L_d^3/12$ or $L = \frac{\delta}{3} L_d + \frac{4V}{\pi\delta^2 L_d^2}$. We now substitute the expression for L_d as function of V_d and obtain directly the expression for L as a function of V; note that length is *linear* in volume, which is characteristic for a mixture between a V0- and a V1-morph. This is the reason why the result is presented in this section.

Biofilms

{29}

Figure 2.4 shows that a biofilm on a curved surface can behave somehwere between a V0 and an isomorph.

Reserve & structure

{30}

DEB theory partitions biomass into one or more reserves and one or more structures. Reserves complicate the dynamics of the individual and the application of the model considerably, so it make sense to think about its necessity and become motivated to deal with this more complex dynamics.

We need reserve because of the following reasons

- to include metabolic memory. The metabolic behaviour of an individual does not depend on the actual food availability, but of that of the (recent) past. At constant food availabilities the argument is less convincing, but since an embryo does not eat, and a juvenile and adult do, reserve is essential to include the embryonic stage, even in constant environments.

- the chemical composition of the individual depends on the growth rate

- fluxes (e.g. dioxygen, carbon dioxide, nitrogen waste, heat) are linear sums of three basic energy fluxes: assimilation, dissipation and growth (as we will see). The method of indirect calorimetry is based on this fact. Without reserve, using a single structure only, two rather than three basic energy fluxes would suffice, while experimental evidence shows that this is not true.

- to explain observed patterns in respiration and in body size scaling relationships. Eggs decrease in mass during development, but increase in respiration, while juveniles increase in mass as well as in respiration. This cannot be understood without reserve.

We will see that reserve plays a key role in body size scaling relationships, and to understand, for instance, why respiration increases approximately with weight to the power 3/4 among species.

- to understand how the cell decides on the use of a particular (organic) substrate, as building block or as source of energy. This problem will be discussed in the section on organelle-cytoplasm interactions (in these comments).

The term reserve does *not* mean 'set apart for later use'; reserve can have active metabolic functions. The primary difference between reserve and structure is in their dynamics: all chemical compounds in the reserve have the same turnover time, in structure they can be different. An implication is that structure requires somatic maintenance, reserve does not. A freshly laid egg consists (almost) fully of reserve and does hardly respire; a simple and direct empirical support for this statement.

{30}, l-16

Muscle tissue: structure or reserve?

'muscle tissue .. must be considered as structural material' is a confusing formulation. Muscles, like all tissues, have structural as well as reserve components. If reserve is used during starvation, and restored after subsequent feeding, the individual is in its original state. If structure is used during (extreme) starvation, the individual can suffer from permanent damage, and never recovers fully. An example is the degradation of muscle tissue during extreme starvation. The example is not meant to imply that muscle tissue does not have reserve.

{34}, l4

C-mole

One mole of glucose equals 6 C-moles of glucose.

{34}

Generalized compounds

We need the link between generalized and "pure" chemical compounds in applications of isotopes, for instance. Like generalized compounds, we quantify organic compounds in terms of C-moles. Suppose that compound i is present in M_{V_i} (C-)moles in structure, for example. So structure has mass $M_V = \sum_i M_{V_i} n_{CV_i}$, where n_{CV_i} is either 0 (anorganic compounds) or 1 (organic compounds). The chemical indices of the generalized compound relate to that of the chemical compounds as

$$n_{*V} = \frac{\sum_i M_{V_i} n_{*V_i}}{\sum_i M_{V_i} n_{CV_i}} = \frac{\sum_i M_{V_i} n_{*V_i}}{M_V} = \sum_i w_i n_{*V_i} \quad \text{with } w_i = M_{V_i}/M_V \text{ and } i \in \{C, H, O, N\}$$

This decomposition can also be done for other generalized compounds, such as reserve and food. Notice that any chemical compound can potentially partake in all generalized compounds and all chemical elements can be included.

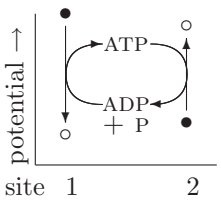

Figure 2.5: The ATP/ADP shuttle transports energy from a site where an energy producing transformation occurs, to a site where an energy requiring transformation occurs. If both transformations occur at the same place and time, and thermodynamics allows, the shuttle is not required. Variations in the free energy of an ATP molecule affect the speed of the shuttle, but not necessarily the transformation rates. Form [290].

Molar mass

{34}, l-14

When a biologist uses the word "weight", he/she actually means mass expressed in grams, not force. The book follows this tradition. The term 'molar mass' gives confusion. It here stands for 'mass expressed in (C-)moles', as opposed to mass expressed in grams, for instance. (The definition of a C-mole is given in the glossary). The main difference between mass expressed in grams or moles is that comparisons of grams allow differences of chemical composition, while that of moles typically do not. An inconsistency in the notation of the dimension crept in. In table 3.4 at {122} m denotes mass (expressed in moles), while in the notation list it denotes mass expressed in weight (grams for instance, see symbol W), while mass expressed in moles is indicated by the number-symbol # (see symbol M). Since a mole is a unit, not a dimension, the dimension identifier for W and M should be the same. Yet their role in checking mass conservation is very different, which makes it handy to link the symbol to the way mass is quantified.

ATP

{35}

Bio-energetics studies the processes of ATP* generation and use, because cells use ATP to drive energy requiring transformations. ATP turnover is considered to organize metabolism. The energy charge, i.e. the ratio

$$[\text{ATP}]/([\text{AMP}]+[\text{ADP}]+[\text{ATP}]),$$

changes, and therefore the free energy* of ATP. This complicates the understanding of slow transformations in terms of generation and use of ATP. Slow transformations are controlled by polymers (proteins, lipids and carbohydrates), however, which do not suffer from fluctuating free energies. They are spatially organized in granules, and attacked from the periphery. Their amount, or exposed surface area, would quantify their metabolic significance much better than their concentration; see Figure 2.5.

Entropy

{35}

Later developments of the theory replaced the assumption that the entropy of biomass is zero by the assumption that the specific entropies of reserve and structure is constant (because of the strong homeostasis assumption), see [530, 328]. These specific entropies can be obtained indirectly for mass and energy balances. It turned out that the specific entropy of structure is lower than that of reserve, as expected. See comment for {154}.

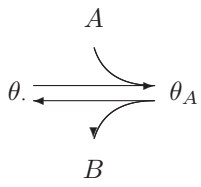

Figure 2.6: Uptake of a single substrate is well quantified on the basis of a fixed handling time of substrate (prey) by the uptake machinery. The time need not be constant, but it must be independent of substrate density [395, 396]. The handling time not only includes mechanical handling but also metabolic processing. This is why eating prey by predators and transformation rate by enzymes depend in a similar way on substrate (food) density. From [290]

{41}

SUs

SUs are generalized enzymes that follow the rules of classic enzyme kinetics with two modifications: transformation is based on fluxes, rather than on concentrations of substrates, and the backward fluxes are assumed to be negligibly small in the transformation

$$S + \mathcal{E} \leftrightarrow S\mathcal{E} \leftrightarrow P\mathcal{E} \leftrightarrow P + \mathcal{E},$$

where S stands for substrate, P for product and $\mathcal{E}$ for enzyme, see Figure 2.6. The backward fluxes might be small, not because of enzyme performance as such, but because of the spatial organization of the supply of substrate and the removal of product by transporters. The differences from classic enzyme kinetics do not affect the simple one-substrate one-product conversion in spatially homogeneous environments, but do affect more complex transformations. The arrival flux can be taken to be proportional to the density in spatially homogeneous environments. So for compound S present in concentration S, with binding probability ρ and affinity $\dot{b}$, the arrival flux $\dot{J}_S$ relates to the concentration as $\rho \dot{J}_S = \dot{b} S$

{43}

More on SUs

The theory on synthesizing units is substantially extended; [410] presents applications in an evolutionary context; [64] gives extensions for multiple substrates, inhibition, and co-metabolism; [327] presents closed handshanking slightly different from the book to ensure that a set of SUs that perform closed hank-shaking can act as if it is just a single SU; [297] apply the theory to quantify the nutritional value of prey for the predator; [335, 336, 334] introduces multiple reserves that can be used supplementary, both for maintenance and growth. These extensions turn out to have remarkable consequences for ecosystem dynamics. A short review on further developments is given in [330].

{44}

Number of SUs

The section on SU ends with brief remarks on the effect of the number of SUs. The section can use some expansion in the form of a simple application that supplements the section on the functional response {73}.

Think of a V1-morph with structural mass M_V (in C-mol) that feeds on a single substrate that is present in concentration X in the environment. The number of SUs S per C-mol of structure V is given by chemical index n_{SV}; the total number of SUs is thus $N = n_{SV} M_V$. The arrival flux per SU is $\dot{J}_X$. The binding probability per molecule of

substrate is ρ. Since the environment is homogeneous, we can work with the concentration of substrate and write $\rho \dot{J}_X = \dot{b}X$, where $\dot{b}$ quantifies the transport of substrate through the medium to an SU, already corrected for the binding efficiency of the SU; $\dim(\dot{b}) =$ time^{-1} length (of environment)^3 amount (of substrate)$^{-1}$. The dissociation rate equals $\dot{k}$; $\dim(\dot{k}) =$ time^{-1}. The change in the fraction of unbound SUs is $\frac{d}{dt}\theta_\cdot = \theta_X \dot{k} - \theta_\cdot \dot{b} X$, with $1 = \theta_X + \theta_\cdot$. At equilibrium we have $\theta_\cdot^* = \frac{\dot{k}}{\dot{k}+\dot{b}X} = \frac{K}{K+X}$, with half saturation constant $K = \dot{k}/\dot{b}$; $\dim(K) =$ amount (of substrate) length (of environment)$^{-3}$. The flux of disappearing substrate per SU is $-\theta_\cdot^* \dot{b} X = \frac{-\dot{k}X}{K+X}$. The total flux is N times as large, which means that the maximum substrate uptake rate is $\dot{J}_{Xm} = N\dot{k}$, and the maximum specific substrate uptake rate is $j_{Xm} = \dot{J}_{Xm}/M_V = n_{SV}\dot{k}$. The rate of reserve production can be linked to the substrate uptake flux like $\dot{J}_E = -y_{EX}\dot{J}_X$. Alternatively, it can be obtained directly from the SUs kinetics $\dot{J}_E = N y_{EX} \theta_X^* \dot{k}$, which should give the same result.

Handshaking protocols

{48}

Consider the transformation $X_{i-1} \to y_{X_i X_{i-1}} X_i$ for $i = 1, \cdots, n$, see [327]. We take $y_{X_i X_{i-1}} = 1$ for simplicity. After an introduction of the behaviour of a single Synthesizing Unit (SU), we discuss closed and open handshaking, followed by mixtures of these two extremes. Finally we discuss synthesis from two substrates, to model cyclic pathways.

Chain of length $n = 1$

For a given flux $\dot{J}_{X_0,F}$ of substrate to the M_{S_1} SUs, we have

$$\text{Change in unbound fraction:} \quad \frac{d}{dt}\theta_1 = (1-\theta_1)\dot{k}_1 - \theta_1 \rho_1 \dot{J}_{X_0,F}/M_{S_1} \tag{2.4}$$

$$\text{Steady state unbound fraction:} \quad \theta_1^* = \left(1 + \rho_1 \dot{J}_{X_0,F}(\dot{k}_1 M_{S_1})^{-1}\right)^{-1} \tag{2.5}$$

$$\text{Production flux:} \quad \dot{J}_{X_1,P} = \dot{k}_1 M_{S_1}(1-\theta_1^*) = \frac{\rho_1 \dot{J}_{X_0,F}}{1 + \rho_1 \dot{J}_{X_0,F}(\dot{k}_1 M_{S_1})^{-1}} \tag{2.6}$$

Closed handshaking at all nodes

Closed handshaking is defined as an interaction between subsequent SUs in a linear pathway such that, given perfect binding, the product of SU i is directly piped to the SU $i+1$ for further processing. To find appropriate expressions for the dynamics of SUs that have this property, we introduce (yet) unknown functions $\dot{b}_i$ of the θ_i's that specify the appearance of unbound fractions. The dynamics of the last SU is simple, because the release of product does not depend on the binding state of any other SU. The release rate of product from the last SU-product complex is proportional to the bound fraction, so $\dot{b}_n = (1-\theta_n)\dot{k}_n$. We now have

$$\frac{d}{dt}\theta_1 = \dot{b}_1 - \theta_1 \rho_1 \dot{J}_{X_0,F}/M_{S_1} \tag{2.7}$$

$$\frac{d}{dt}\theta_i = \dot{b}_i - \dot{b}_{i-1}M_{S_{i-1}}/M_{S_i} \quad \text{for } i = 2, \cdots, n-1 \tag{2.8}$$

$$\frac{d}{dt}\theta_n = (1-\theta_n)\dot{k}_n - \dot{b}_{n-1}M_{S_{n-1}}/M_{S_n} \tag{2.9}$$

$$\dot{J}_{X_n,P} = \dot{k}_n M_{S_n}(1-\theta_n^*) = \frac{\rho_1 \dot{J}_{X_0,F}}{1+\rho_1 \dot{J}_{X_0,F}\sum_j (\dot{k}_j M_{S_j})^{-1}} \tag{2.10}$$

The latter follows from the idea that $(\dot{k}_i M_{S_i})^{-1}$ acts as a resistance, and that the n-chain should operate as if it is a single SU; compare (2.6) with (2.10). At steady state, we have $\dot{b}_i^* M_{S_i} = \dot{b}_{i-1}^* M_{S_{i-1}}$, so $\dot{b}_1^* M_{S_1} = \dot{b}_{n-1}^* M_{S_{n-1}}$. From (2.10) follows

$$\dot{b}_i^* = \frac{\rho_1 \dot{J}_{X_0,F}/M_{S_i}}{1+\rho_1 \dot{J}_{X_0,F}\sum_{j=1}^n (\dot{k}_j M_{S_j})^{-1}} \tag{2.11}$$

$$\theta_1^* = \frac{1}{1+\rho_1 \dot{J}_{X_0,F}\sum_i (\dot{k}_i M_{S_i})^{-1}} \tag{2.12}$$

$$\theta_n^* = \frac{1+\rho_1 \dot{J}_{X_0,F}\sum_{j=1}^{n-1} (\dot{k}_j M_{S_j})^{-1}}{1+\rho_1 \dot{J}_{X_0,F}\sum_{j=1}^n (\dot{k}_j M_{S_j})^{-1}} \tag{2.13}$$

We see that

$$\theta_{i+1}^* - \theta_i^* = \frac{\rho_1 \dot{J}_{X_0,F}(\dot{k}_i M_{S_i})^{-1}}{1+\rho_1 \dot{J}_{X_0,F}\sum_{j=1}^n (\dot{k}_j M_{S_j})^{-1}}$$

which suggests

$$\dot{b}_i = (\theta_{i+1} - \theta_i)\dot{k}_i \tag{2.14}$$

Substitution into (2.7) - (2.9) gives

$$\frac{d}{dt}\theta_1 = (\theta_2 - \theta_1)\dot{k}_1 - \theta_1 \rho_1 \dot{J}_{X_0,F}/M_{S_1} \tag{2.15}$$

$$\frac{d}{dt}\theta_i = (\theta_{i+1} - \theta_i)\dot{k}_i - (\theta_i - \theta_{i-1})\dot{k}_{i-1}M_{S_{i-1}}/M_{S_i} \quad \text{for } i = 2, \cdots, n-1 \tag{2.16}$$

$$\frac{d}{dt}\theta_n = (1-\theta_n)\dot{k}_n - (\theta_n - \theta_{n-1})\dot{k}_{n-1}M_{S_{n-1}}/M_{S_n} \tag{2.17}$$

For the purpose of mixing this dynamics with open handshaking, we substitute the feeding fluxes $\dot{J}_{X_{i-1},F} = \dot{J}_{X_{i-1},P} = (\theta_i - \theta_{i-1})\dot{k}_{i-1}M_{S_{i-1}}$ and allow for non-perfect binding ($0 \leq \rho_i \leq 1$). Moreover, we remove θ_1 in front of the flux of X_0 that arrives to the pathway to avoid leaks of X_0. (This can be done because the open handshaking already has this factor.) The result is

$$\frac{d}{dt}\theta_1 = (\theta_2 - \theta_1)\dot{k}_1 - \rho_1 \dot{J}_{X_0,F}/M_{S_1} \tag{2.18}$$

$$\frac{d}{dt}\theta_i = (\theta_{i+1} - \theta_i)\dot{k}_i - \rho_i \dot{J}_{X_{i-1},F}/M_{S_i} \quad \text{for } i = 2, \cdots, n-1 \tag{2.19}$$

$$\frac{d}{dt}\theta_n = (1-\theta_n)\dot{k}_n - \rho_n \dot{J}_{X_{n-1},F}/M_{S_n} \tag{2.20}$$

The steady state unbound fractions are

$$\theta_i^* = 1 - \dot{J}_{X_0,F} \sum_{j=n+1-i}^{n} (\dot{k}_j M_{S_j})^{-1} \Pi_{k=1}^{j} \rho_k = 1 - j_{X_0,F} \sum_{j=n+1-i}^{n} (\dot{k}_j m_{S_j})^{-1} \Pi_{k=1}^{j} \rho_k$$

with $m_{S_j} = M_{S_j}/M_V$ and $j_{X_0,F} = \dot{J}_{X_0,F}/M_V$. The production fluxes are

$$\dot{J}_{X_i,P} = \dot{k}_i M_{S_i} (\theta_{i+1}^* - \theta_i^*) = \dot{J}_{X_0,F} \Pi_{k=1}^{i} \rho_k$$

Open handshaking at all nodes

Open handshaking is defined as the lack of any interaction between subsequent SUs in a linear pathway. We here simply have (compare with (2.4))

$$\frac{d}{dt}\theta_i = (1-\theta_i)\dot{k}_i - \theta_i \rho_i \dot{J}_{X_{i-1},F}/M_{S_i} \quad \text{for } i = 1, \cdots, n \tag{2.21}$$

$$\theta_i^* = \left(1 + \rho_i \dot{J}_{X_{i-1},F} (\dot{k}_i M_{S_i})^{-1}\right)^{-1} \tag{2.22}$$

$$\dot{J}_{X_i,P} = \dot{k}_i M_{S_i} (1 - \theta_i^*) = \frac{\rho_i \dot{J}_{X_{i-1},F}}{1 + \rho_i \dot{J}_{X_{i-1},F} (\dot{k}_i M_{S_i})^{-1}} \tag{2.23}$$

General handshaking

We now combine the dynamics of (2.18) - (2.20) and (2.21) linearly with n handshaking parameters α_i and arrive for $i = 1, \cdots, n-1$ at

$$\frac{d}{dt}\theta_i = \left(1 - \alpha_i(1-\theta_{i+1}) - \theta_i\right) \dot{k}_i - \left(\theta_i + \alpha_{i-1}(1-\theta_i)\right) \rho_i \dot{J}_{X_{i-1},F}/M_{S_i} \tag{2.24}$$

$$\frac{d}{dt}\theta_n = (1-\theta_n)\dot{k}_n - \left(\theta_n + \alpha_{n-1}(1-\theta_n)\right) \rho_n \dot{J}_{X_{n-1},F}/M_{S_n} \tag{2.25}$$

We can check that the system reduces to closed handshaking for $\alpha_i = 1$ and open handshaking for $\alpha_i = 0$ for $i = 1, \cdots, n-1$. The motivation for the linear combination of the two handshaking protocols is that a fraction α_i of the SUs is following the open handshaking protocol, and a fraction $1 - \alpha_i$ the closed one. Notice that α_0 controls the flux from the cell to the pathway, while the other α_i's only deal with the metabolite traffic between SU i and $i+1$.

Trophic modes

{51}

Trophic strategies are labeled with respect to the energy and the carbon source, as indicated Table 2.1. Animals typically feed on other organisms, which makes them organochemotrophs, and so heterotrophs. If these organisms are only animals, we call then carnivores, if they are only veridiplants (glaucophytes, rhodophytes, or chlorophytes, including plants), we call them herbivores, and in all other cases we call them omnivores. The implication is that daphnids, which also feed on heterokonts, ciliates and dinoflagellates, should be classified as omnivores, although many authors call them herbivores. Many trophic classifications are very imprecise and sensitive to the context.

trophy	hetero-	auto-
energy source	chemo	photo
carbon source	organo	litho

Table 2.1: The classification of trophic modes among organisms.

Central metabolism

{51}

The central metabolic pathway of many prokaryotes and almost all eukaryotes (Figure 2.14) consists of four main modules [316].

The Pentose Phosphate (PP) Cycle comprises a series of extra-mitochondrial transformations by which glucose-6-phosphate is oxidized with the formation of carbon dioxide, reduced NADP and ribulose 5-phosphate. Some of this latter compound is subsequently transformed to sugar phosphates with 3 to 7 or 8 carbon atoms, whereby glucose-6-phosphate is regenerated. Some ribulose 5-phosphate is also used in the synthesis of nucleotides and amino acids. Higher plants can use the same enzymes also in reverse, thus running the reductive pentose phosphate cycle. The PP cycle is primarily used to inter-convert sugars as a source of precursor metabolites and to produce reductive power. Theoretical combinatorial optimization analysis indicated that the number of steps in the PP cycle is evolutionarily minimized [394, 393], which maximizes the flux capacity [194, 575].

The Glycolytic Pathway (aerobically) converts glucose-6-phosphate to pyruvate or (anaerobically) to lactate, ethanol or glycerol, with the formation of 2 ATP. The transformations occur extra-mitochondrially in the free cytoplasm. However, in kinetoplastids they are localized in an organelle, the glycosome, which is probably homologous to the peroxisome of other organisms [20, 89]. The flux through this pathway is under control by phospho fructokinase and by hormones. Heinrich & Schuster [194] studied some design aspects of the glycolytic pathway. Most pyruvate is converted to acetyl and bound to coenzyme A.

The TriCarboxylic Acid (TCA) Cycle also known as the citric acid or the Krebs cycle, oxidizes (without the use of dioxygen) the acetyl group of acetyl coenzyme A to two carbon dioxide molecules, under the reduction of 4 molecules NAD(P) to NAD(P)H. In eukaryotes that contain them, these transformations occur within their mitochondria. Some plants and micro-organisms have a variant of the TCA cycle, the glyoxylate cycle, which converts pyruvate to glyoxylate and to malate (hence a carbohydrate) with another pyruvate. Since pyruvate can also be obtained from fatty acids, this route is used for converting fatty acids originating from lipids into carbohydrates. Some plants possess the enzymes of the glyoxylate cycle in specialized organelles, the glyoxysomes.

The Respiratory Chain oxidizes the reduced coenzyme NAD(P)H, and succinate with dioxygen, which leads to ATP formation through oxidative phosphorylation. Similarly to the TCA cycle it occurs inside mitochondria. Amitochondriate eukaryotes

process pyruvate through pyruvate-ferredoxin oxidoreductase, rather than through the pyruvate dehydrogenase complex. If the species can live anaerobically, the respiratory chain can use fumarate, nitrate, or nitrite as electron acceptors in the absence of dioxygen [553].

In combination with nutrients (phosphates, sulphates, ammonia, iron oxides, etc), the first three pathways of the central metabolic pathway provide almost all the essential cellular building blocks, including proteins, lipids, and RNA. The universality of this central metabolic pathway is partly superficial or, if you like, the result of convergent evolution because the enzymes running it can differ substantially. This diversity in enzymes partly results from the modular make-up of the enzymes themselves. Some variation occurs in the intermediary metabolites as well.

Obviously, glucose plays a pivotal role in the central metabolism. However, its accumulation as a monomer for providing a metabolism with a permanent source of substrate would give all sorts of problems, such as osmotic ones. This also applies to metabolic products. To solve these problems, cells typically store the supplies in polymeric form (polyglucose (i.e. glycogen), starch, polyhydroxyalkanoate, polyphosphate, sulphur, proteins, RNA), which are osmotically neutral. Their storage involves so-called inclusion bodies, the inherent solid/liquid interface of which controlling their utilization dynamics (see reserve dynamics in chap 8).

Autotrophy in eukaryotes

{52}

Several eukaryotes can respire nitrate non-symbiotically. The ciliate *Loxodes* (*Karyorelicta*) reduces nitrate to nitrite; the fungi *Fusarium oxysporum* and *Cylindrocarpon tonkinense* reduce nitrate to nitrous oxide; the foraminifera *Globobulimina* and *Nonionella* live in anoxic marine sediments and are able to denitrify nitrate completely to N_2 [487].

Patterns in Arrhenius temperatures

{54}

The catalizing rate of enzymes in metabolic transformations can be adapted by the individual to the current temperature by changing the tertiary configuration. This takes time, upto days to weeks depending on the detailed nature of the adaptation. Species living in habitats that typically sport large (and rapid) temperature fluctuations (e.g. intertidal zones of sea coasts) have to use enzymes that function well in a broad temperature range, with the result that they have a relatively low Arrhenius temperature (around 6 kK). Species that live in habitats with a rather constant temperature (e.g. the pelagic, or the deep ocean) typically have a large Arrhenius temperature (around 12 kK).

Temperature dependence of assimilation

{55}

In the case of multiple reserves, physiological rates can depend on temperature in more complex ways. Photosynthesis, for instance is known to depend on temperatue at high light levels, but hardly so at low light levels [51, 383]. This can be understood by realizing

that the binding of photons is insensitive to temperature, but that of carbon dioxide and other nutrients is. The consequence is a build up of carbohydrate reserve at low temperature, so a shift in the composition in biomass, which affects its nutritional value for consumers of this biomass. In the case of a single generalized reserve, this flexibility is absent, and the other rates (growth, reproduction, etc) must follow the temperature dependence of the assimilation process to avoid changes in conversion efficiencies. Given an invariant biochemical machinery for the transformations, such changes in efficiency are hard to implement from an evolutionary perspective.

Dodo

{59}, l22

Although examples exist where germination of seeds is stimulated by passage through a gut, this example of the tambulacoque tree and the dodo is perhaps not the best one. It is based on a publication by Temple in *Science*, but is questioned by Quammen [461, p349] (Comment by Cor Zonneveld).

Chapter 3

Energy acquisition and use

Holling type II

{73}, eq (3.1)

The Holling type II functional response (Holling, 1959) represents in fact the Michaelis Menten kinetics (Michaelis & Menten, 1913). Food has the role of substrate, food density that of substrate concentration, ingested material that of product formation. Let $\theta_.$ denote the fraction of animals that are searching for food, and the 'handling' fraction is $\theta_X = 1 - \theta_.$. The 'searching' fraction changes like

$$\frac{d}{dt}\theta_. = \dot{k}\theta_X - \dot{b}X\theta_.$$

where $\dot{k}^{-1}$ represents the mean handling time, and $\dot{b}$ quantifies the searching efficiency, which includes activity levels of both feeder and food (if it is alive). The steady state fraction $\theta_.^*$ obeys $0 = \dot{k}\theta_X^* - \dot{b}X\theta_.^*$, which results in $\theta_.^* = \dot{k}/(\dot{k} + \dot{b}X)$ (cf {42}). The mean feeding rate is $\dot{J}_X = \dot{b}X\theta_.^* = \dot{J}_{Xm}f$ with scaled functional response $f = X/(K + X)$, maximum ingestion rate $\dot{J}_{Xm} = \dot{k}$ and saturation constant $K = \dot{k}/\dot{b}$. This is the hyperbolic functional response indeed. Notice that this very simple model classifies all behavioural components in either 'searching' or 'handling', so 'handling' includes the whole period that the animal is not searching (such as sleeping, courtship, social interaction etc). See the comment for {168}.

Specific food uptake

{75}, l-1

The dimension of parameter $\{\dot{J}_{Xm}\}$ is mol.time^{-1}.length^{-2}. It applies to an isomorph, while the parameter j_{Xm} with dimension mol.mol^{-1}.time^{-1} is later frequently used for a V1-morph. To improve comparability, DEBtool uses $j_{Xm} = \{\dot{J}_{Xm}\}/([M_V]L_d)$ for isomorphs, with characteristic length $L_d = \dot{v}\, m_{Em}/(y_{EX}\, j_{Xm})$ as compound parameter and $\dot{v}$, m_{Em} and y_{EX} as primary parameters. This type of rescaling is always possible, and sometimes convenient, cf {122}.

Dual function

{77}, 3.1.4

Almost all compounds (including proteins) in a cell cq individual can be used to extract energy as well as building blocks. Maintenance requires primarily energy (capacity to do work), but also some building blocks (to compensate for the leaks in protein turnover, for example). Lipids and carbohydrates can be used to generate energy with no harmful by-products (just carbon dioxide and water), but they cannot cover the requirements for building blocks. Proteins can cover both requirements, but their use to cover energy requirements comes with harmful by-products (primarily ammonia, which is toxic even at rather low concentrations). Kuijper [335, 334, 336] discusses two-reserve situations (proteins versus carbohydrates plus lipids) that are partly substitutable in covering maintenance costs.

Effect of storage

{78}, 3.1.5

The effect of storage (inside or outside the individual) on population dynamics depends very much on the turnover rates of the stored material relative to the fluctuations in food (prey) density. Some aspects are discussed in chapter 9 on population dynamics. If a predator stores its food (dead prey) for later use, rather than converts prey into more predator directly, a temporary peak in food availability does not translate into an increase in predator biomass, so the prey-population will suffer less from the predator after the peak for two reasons. First the amount of predators is less (compared with no storage), second because the predator (partly) feeds on the stored material, rather than on living (rare) prey. This only "helps" the prey if the dip in its abundance is short relative to the time the storage lasts. If this dip lasts longer the opposite effect applies. Storages help the predator to maintain a relative high abundance, which translates into a high predation pressure on the prey in the dip. Without storage, the predator population would have declined together with the prey.

Gradient in gut

{83}, Figure 3.10

The transition between digested and undigested daphnids' gut contents is perhaps not easy to see for the non-specialist. The black band of digested material in the gut tappers to the left, the undigested material appears as light gray and tappers to the right. Just above the black compound eye, you can see the two digestive ceaca, and above those, a bit to the right, a wider part of the gut, filled with undigested algal material.

Derivation of formula without number

{83}, l15

The formula for reserve density dynamics that is not numbered can be derived as follows. The general formula for reserve dynamics is $\frac{d}{dt}[E] = [\dot{p}_A] - F([E], V)$, for some function F of the state variables $[E]$ and V. We now use the weak homeostasis assumption, which states that $[E]$ is independent of V if $\frac{d}{dt}[E] = 0$, while $[\dot{p}_A] \propto V^{-1/3}$. The essential point of this assumption is that the individual can grow under constant environmental conditions,

but does this in such a way the the reserve density does not change. This means that the function F has to be inversely proportional to length as well, and, at equilibrium, F can be written as $F([E]^*, V) = V^{-1/3}H([E]^*|\boldsymbol{\theta})$, where function H does not depend on V, but on $[E]$ only. Weak homeostasis only applies at equilibrium. When we generalize this result to non-equilibrium conditions, we must add a general term that disappears in the equilibrium. We do this by choosing some general function G, like F, and multiply it with the factor $([E]^* - [E])$ to make sure that it disappears at equilibrium. This directly results in the not-numbered formula on {83}. To demonstrate that the function $G^\circ([E]^*, [E], V) = ([E]^* - [E])G([E]^*, [E], V)$ must equal zero, we differentiate to $[E]^*$ and require that it is independent of $[E]^*$ by imposing $\frac{d}{d[E]^*}G^\circ = 0$, which leads to $0 = G + ([E]^* - [E])\frac{d}{d[E]^*}G$. Separation of variables leads to the solution $G([E]^*, [E], V) = G^*([E], V)/([E]^* - [E])$, for some general function G^*. This is only independent of $[E]^*$, so of food density, if $G^*([E], V) = 0$, which leaves us at $\frac{d}{dt}[E] = [\dot{p}_A] - V^{-1/3}H([E]|\boldsymbol{\theta})$ at steady state, as well as non-steady state conditions. The key argument around function G is that an arbitrary function of $[E]$ and V that disappears at steady state $[E]^*$ must depend on the value $[E]^*$, while this value depends on food density. We assumed, however, that the use of reserve does not depend on food density, so we can forget about such a function G and $\frac{d}{dt}[E] = [\dot{p}_A] - V^{-1/3}H([E]|\boldsymbol{\theta})$ fully covers the set of all possibilities, given the assumptions.

Derivation of Eq (3.7)

{83}

The derivation of (3.7) is as follows: We have $\frac{d}{dt}E = \dot{p}_A - \dot{p}_C$, while $[E] = EV^{-1}$, so

$$\begin{aligned}
\frac{d}{dt}[E] &= V^{-1}\frac{d}{dt}E - EV^{-2}\frac{d}{dt}V \\
&= V^{-1}\frac{d}{dt}E - [E]V^{-1}\frac{d}{dt}V \\
&= V^{-1}\frac{d}{dt}E - [E]\frac{d}{dt}\ln V \\
&= \dot{p}_A/V - \dot{p}_C/V - [E]\frac{d}{dt}\ln V \\
&= [\dot{p}_A] - [\dot{p}_C] - [E]\frac{d}{dt}\ln V
\end{aligned}$$

Eq (3.8) follows from (3.7) and $\kappa\dot{p}_C = \dot{p}_M + [E_G]\frac{d}{dt}V$, by realizing that $\frac{d}{dt}\ln V = V^{-1}\frac{d}{dt}V$.

Reserve dynamics

{85}

Notice that the reserve density dynamics is independent of any allocation rule; the mobilization of reserves is prior to and independent of allocation. Therefore, the parameters $[\dot{p}_M]$ (specific somatic maintenance costs) and $[E_G]$ (specific costs for structure) do not occur in the parameter list $\boldsymbol{\theta}$ (cf the first formula on {85}). The book introduces $[E_G]$ as 'costs for growth', but this description can be misleading because the allocation to growth, $\dot{p}_G$ can be zero. The parameter vector $\boldsymbol{\theta}$ should better be renamed to $\boldsymbol{\theta}^\circ$, because the earlier introduced parameter vector $\boldsymbol{\theta}$ relates to $\boldsymbol{\theta}^\circ$ as $\boldsymbol{\theta} = [[\dot{p}_M], [E_G], \boldsymbol{\theta}^\circ]$ (we simply take

two parameters apart in the list of parameters; the status of the specific costs for structure $[E_G]$ is indeed a constant parameter because of the strong homeostasis assumption. That of $[\dot{p}_M]$ is more complex, because we did not yet make the assumption that is a constant, it might still be a function of structure V). In summary: the assumption is made that each of the processes assimilation, mobilization and allocation don't "know" each other's activities directly. They do, however, react to the consequences of activities, namely the built up of reserve (as a consequence of assimilation) and the dilution by growth (as a consequence of allocation to growth).

The definition of partitionability in the formula on line 5 should be read as follows: if we multiply $[E]$, $[\dot{p}_M]$ and $[E_G]$ with some number κ_A between 0 and 1 (as is done in the right-hand side), the effect is that $[\dot{p}_C]$ is multiplied with that number (as is done in the left-hand side). The criterion applies to dynamics of the reserve density $[E]$, not to the dynamics of the amount of reserve E. The reason is in the smooth merging of reserves in an evolutionary time frame. Single-reserve systems evolved from multi-reserve systems. Moreover, symbiogenesis frequently occurred in evolution, where two syntrophic species merge into a single one. Since DEB theory is supposed to apply to all organisms, consistency arguments show that both partners prior to merging, as well are the merged new species must follow the DEB rules. To do this in a smooth way, we need a mergebility argument, which is the inverse partitionability argument. The reasoning is spelled out in [298].

The step from the partitionability requirement to the requirement for H and κ follow after substitution of (3.9) in the definition of partitionability, together with the observation that it must apply for all values of V. The latter observation boils that to the argument that the substitution of $[\dot{p}_C]$ in the left- and right-hand side of the partitionability definition results in the equality of two ratios of terms in V, and so to equality of each of the terms.

Mergeability

{85}

The derivation of reserve dynamics can be simplified considerably by replacing the requirement of partitionability by that of mergeability. Mergeability means that reserves can be added without effects on the reserve (density) dynamics if assimilation of the resources to synthesize the reserves is coupled and the total intake is constant.

Definition: Given $\frac{d}{dt}[E_i] = [\dot{p}_{A_i}] - \dot{F}([E_i], V)$ for $i = 1, 2, \cdots$ and $[\dot{p}_{A_i}] = \kappa_{A_i}[\dot{p}_A]$ with $\sum_i \kappa_{A_i} = 1$, two reserves E_1 and E_2 are mergeable if $\frac{d}{dt}\sum_i[E_i] = [\dot{p}_A] - \dot{F}(\sum_i[E_i], V)$.

Weak homeostasis implies that $\dot{F}([E], V) = V^{-1/3}\dot{H}([E])$ (see {83}), so together with the mergeability requirement this translates into the requirement that $\sum_i \dot{H}([E_i]) = \dot{H}(\sum_i[E_i])$ or $\kappa_A\dot{H}([E]) = \dot{H}(\kappa_A[E])$ for an arbitrary positive value of κ_A. In other words: H must be first degree homogeneous in $[E]$. From this follows $\dot{H}([E]) = \dot{v}[E]$.

Since the first organisms (prokaryotes) had (and prokaryotes still have) many reserves, and the number of reserves reduced during evolution [330] (homeostasis), the mergeability of reserves is unavoidable for theories that are not species-specific. The mergeability requirement is also essential to understand symbiogenesis in a DEB theory context: Given that species 1 and 2 each follow DEB rules, and species 1 evolves into an endosymbiont of species 1, the new symbiosis again should follow the DEB rules (else the theory becomes

species-specific). This process is discussed in detail in [298]. All eukaryotes once possessed endosymbionts (mitochondria), some lost them subsequently. Various forms of symbiosis are key processes in life. Evolution might have found several mechanisms to obtain mergeability of reserves, but the fact that they are mergeable is essential for evolution.

Mergeability is almost equivalent to partitionability

Since from partitionability also follows that κ is a zero-th degree homogeneous function in E, while this does not follow from mergeability, the latter requirement is less restrictive. In other words, partitionability imposes constraints on the fate of mobilised reserve, mergeability does not. More specifically, partitionability involves maintenance explicitly, mergeability does not.

To demonstrate the difference we now translate the mergebility constraint on $\dot{F}$ to a constraint on the mobilisation flux $\dot{p}_C$. These two fluxes relate to each other as $\dot{F} = [\dot{p}_C] + [E]\dot{r}$, where the specific growth rate $\dot{r} = [\dot{p}_G]/[E_G] = (\kappa[\dot{p}_C] - [\dot{p}_M])/[E_G]$. So

$$\begin{aligned} \dot{F} &= [\dot{p}_C] + (\kappa[\dot{p}_C] - [\dot{p}_M])[E]/[E_G] \\ &= \left(1 + \frac{\kappa[E]}{[E_G]}\right)[\dot{p}_C] - \frac{[E]}{[E_G]}[\dot{p}_M] \end{aligned}$$

The mergeability constraint $\kappa_A \dot{F}([E], V) = \dot{F}(\kappa_A[E], V)$ can be written as

$$\kappa_A \left(1 + \frac{\kappa[E]}{[E_G]}\right)[\dot{p}_C]([E], V) - \kappa_A \frac{[E]}{[E_G]}[\dot{p}_M] = \left(1 + \frac{\kappa_A\kappa[E]}{[E_G]}\right)[\dot{p}_C](\kappa_A[E], V) - \frac{\kappa_A[E]}{[E_G]}[\dot{p}_M]$$

or

$$\kappa_A \left(1 + \frac{\kappa[E]}{[E_G]}\right)[\dot{p}_C]([E], V) = \left(1 + \frac{\kappa_A\kappa[E]}{[E_G]}\right)[\dot{p}_C](\kappa_A[E], V)$$

or

$$\kappa_A[\dot{p}_C]([E], V) = [\dot{p}_C](\kappa_A[E], V)\frac{[E_G] + \kappa_A\kappa[E]}{[E_G] + \kappa[E]}$$

while the partitionability constraint is

$$\kappa_A[\dot{p}_C]([E], V|[\dot{p}_M], [E_G], \kappa) = [\dot{p}_C](\kappa_A[E], V|\kappa_A[\dot{p}_M], \kappa_A[E_G], \kappa)$$

In combination with weak homeostasis, both partitionability and mergability imply the result

$$\dot{p}_C = \frac{[E_G][E]}{[E_G] + \kappa[E]}G(V) \quad \text{with } G(V) = V^{2/3}\dot{v} + V\frac{[\dot{p}_M]}{[E_G]}$$

Both the partionability and the mergeability derivations allow the extension of the specific maintenance costs with terms that depend on structural volume, such as terms that are linked with surface area. So $[\dot{p}_M]$ might depend on V (but not on $[E]$).

Partitionability follows from weak and strong homeostasis

{85}

[529] demonstrate that partitionability is implied by weak and strong homeostasis. In other words: it does not represent a new assumption. The consequence is that reserve dynamics follows from weak and strong homeostasis, given that the flux of mobilized reserve does not depend on assimilation and fuels all non-assimilatory metabolic activity.

Effects of parasites

{89}

The effects of the parasite *Schistosoma* on the DEB of the pond snail *Lymnaea stagnalis* and its molecular aspects are discussed in [219].

Derivation of Eq (3.18)

{94}

Formula (3.18) can be derived as follows: Eq (3.12) reads $\dot{p}_C = [E](\dot{v}V^{2/3} - \frac{d}{dt}V)$. Substitution in Eq (3.17) gives

$$\kappa[E](\dot{v}V^{2/3} - \frac{d}{dt}V) = [E_G]\frac{d}{dt}V + \dot{p}_M + \dot{p}_T \quad \text{which gives} \tag{3.1}$$

$$\frac{d}{dt}V = \frac{\kappa[E]\dot{v}V^{2/3} - \dot{p}_T - \dot{p}_M}{\kappa[E] + [E_G]} \tag{3.2}$$

The volume-related somatic maintenance costs are given in Eq (3.15) as $\dot{p}_M = [\dot{p}_M]V$, while the surface area-related somatic maintenance costs are specified by Eq (3.16): $\dot{p}_T = \{\dot{p}_T\}V^{2/3}$. Substitution in the expression for growth gives

$$\begin{aligned}
\frac{d}{dt}V &= \frac{V^{2/3}[E]\dot{v}\kappa - V^{2/3}\dot{\{}p_T\} - V[\dot{p}_M]}{\kappa[E] + [E_G]} \quad \text{take out } \dot{v} \\
&= \dot{v}\frac{V^{2/3}[E]\kappa - V^{2/3}\dot{\{}p_T\}/\dot{v} - V[\dot{p}_M]/\dot{v}}{\kappa[E] + [E_G]} \quad \text{divide by } \kappa[E_m] \\
&= \dot{v}\frac{V^{2/3}[E]/[E_m] - V^{2/3}\frac{\dot{\{}p_T\}}{\dot{v}[E_m]\kappa} - V\frac{[\dot{p}_M]}{\dot{v}[E_m]\kappa}}{[E]/[E_m] + \frac{[E_G]}{\kappa[E_m]}} \quad \text{substitute } \dot{v} = \frac{\{\dot{p}_{Am}\}}{[E_m]} \text{ see \{85\} or \{412\}} \\
&= \dot{v}\frac{V^{2/3}[E]/[E_m] - V^{2/3}\frac{\dot{\{}p_T\}}{\kappa\{\dot{p}_{Am}\}} - V\frac{[\dot{p}_M]}{\kappa\{\dot{p}_{Am}\}}}{[E]/[E_m] + g} \quad \text{substitute } V_m^{1/3} = \frac{\kappa\{\dot{p}_{Am}\}}{[\dot{p}_M]} \\
&= \dot{v}\frac{V^{2/3}[E]/[E_m] - V^{2/3}\frac{\dot{\{}p_T\}}{[\dot{p}_M]}V_m^{-1/3} - V/V_m^{1/3}}{[E]/[E_m] + g} \quad \text{substitute } V_h^{1/3} = \frac{\{\dot{p}_T\}}{[\dot{p}_M]} \\
&= \dot{v}\frac{V^{2/3}[E]/[E_m] - V^{2/3}(V_h/V_m)^{1/3} - V/V_m^{1/3}}{[E]/[E_m] + g} = \dot{v}V^{2/3}\frac{e - l_h - (V/V_m)^{1/3}}{e + g}
\end{aligned}$$

for $e = [E]/[E_m]$ and $l_h = (V_h/V_m)^{1/3}$. The last equation is (3.18). In some applications some further scaling is handy:

$$\frac{d}{dt}\frac{V}{V_m} = \frac{\dot{v}}{V_m^{1/3}}\left(\frac{V}{V_m}\right)^{2/3}\frac{e - l_h - (V/V_m)^{1/3}}{e + g} \quad \text{substitute } l^3 = \frac{V}{V_m} \text{ and } \dot{k}_M = \frac{[\dot{p}_M]}{[E_G]}$$

$$\frac{d}{dt}l^3 = g\dot{k}_M l^2 \frac{e - l_h - l}{e + g} \quad \text{while } \frac{d}{dt}l^3 = 3l^2\frac{d}{dt}l$$
$$\frac{d}{dt}l = \frac{g\dot{k}_M}{3}\frac{e - l_h - l}{e + g}$$

Notice that heating only occurs in (juvenile and adult) endotherms, and V_h or l_h quantifies the surface area-related somatic maintenance costs. Apart from heating, it also includes osmotic work, which is especially relevant for fresh-water organisms.

Maximum weight

{95}

On the island Gough, the house mouse *Mus musculus* changed diet and turned to prey on the chicks of the Tristan albatross *Diomedea dabbenena* and the Atlantic petrel *Pterodroma incerta*, despite the fact that these birds weigh 250 times their own weight. From an energy point of view, this had the remarkable effect that the weight of the adult mice are 40 g, rather than the typical 15 g. The reason is probably that the conversion efficiency from birds to mice is higher than their typical conversion efficiency. This supports the idea that ultimate weight represents the ratio of assimilation and maintenance. From a nature conservation point of view the problem is that 99 % of the world population these two bird species live on this island; the birds are now threatened with extinction.

Derivation of Eq (3.20)

{95}

Notice that (3.20) implies that

$$\frac{d}{dt}V = 3\dot{r}_B(V_\infty^{1/3}V^{2/3} - V)$$

which is used at {137} line 2, and only holds for constant food. Just differentiate (3.20) and substitute V, to see that this result is true. The von Bertalanffy growth rate relates to DEB parameters as

$$r_B = (3/k_M + 3L_\infty/v)^{-1} = [p_M](3[E_G] + 3f\kappa[E_m])^{-1}$$

so it does not depend on the specific maximum assimilation flux $\{\dot{p}_{Am}\}$.

Empirical support for maternal effects [294]

{97}

Experimental support for the assumption that the reserve density at birth equals that of the mother at egg formation have been found in e.g. birds [417], reptiles, amphibians [364], fishes [192], insects [388, 493, 492], crustaceans [163], rotifers [593] (see [6]), echinoderms and bivalves [42]. However, some species seem to produce large eggs under poor feeding conditions, e.g. some poeciliid fishes [482], daphnids [164] and *Sancassania* mites [35]. Moreover, egg size can vary within a clutch [133, 578, 416], according to geographical distribution [524], with age [388] and race.

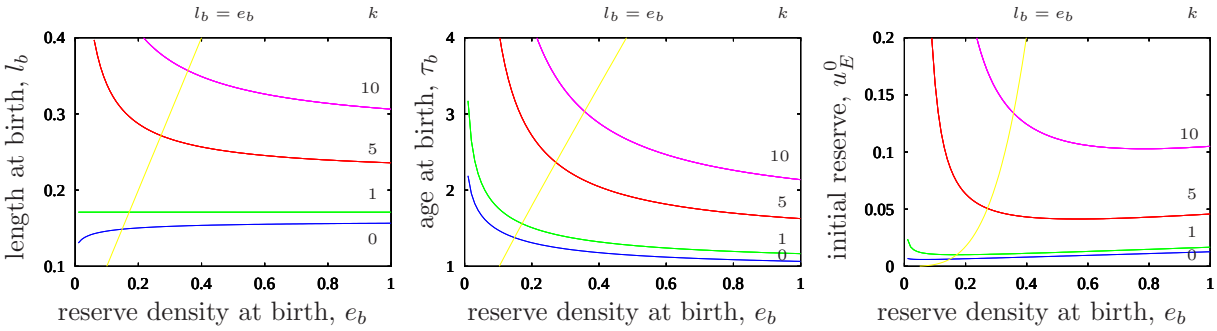

Figure 3.1: The scaled length at birth (left), age at birth (middle), and initial reserve (right) as function of the scaled reserve at birth for various values of k. The length, age and reserve at $l_b = e_b$ is also indicated; the structure is shrinking at birth for smaller values of e_b. Parameters: $\kappa = .8$, $g = 0.5$, $u_H^b = .001$.

Cell separation [294]

{103}

Hart [187] studied the effect of separation of the embryonic cells of the sea urchin *Strongylocentrotus droebachiensis* in the two-cell stage on the energetics of larval development. Both the size and the feeding capacity of the resulting larva were reduced by about one-half, but the time to metamorphosis is about the same (7 d at 8–13 °C). The maximum clearance rate of dwarf and normal larvae was found to be the same function of the ciliated band length. Larvae fed at smaller ration had longer larval periods, but food ration hardly affected size at metamorphosis. Egg size affected juvenile test diameter only slightly.

DEB theory predicts an elongation of the embryonic period if the initial amount of reserve is reduced, while the cumulative energy investment to complete the embryonic stage is the same. The mechanism is that reducing the amount of reserve reduces the use of reserve, so it takes longer to cumulate a particular investment into development. This is found for the crested penguin *Eudyptes*, which sports egg dimorphy (Figure 3.17, {103}). If the separation of the cells would affect the required cumulative investment in development, however, other predictions result. It is then quite well possible that incubation is hardly affected, while size at birth is. Standard DEB theory correctly predicts that a reduction of the feeding level elongates the larval period and hardly affects size at puberty for a particular relationship between the somatic and maturity maintenance costs.

The effects of cell separation are discussed further in the comments for chapter 8.

Removal of some initial reserve [294]

{103}

The removal of an amount of reserve at the start of the development, as is frequently done [144, 215, 524, 406, 217] elongates of the incubation time (as observed in the gypsy moth [493]), and reduces the reserve at hatching, see Figure 3.1. This experiment simulates the natural situation, where the nutritional status of the mother affects to initial amount of reserve. The pattern is rather similar to that of the separation of cells at an early stage,

because reductions of structure and maturity at an early stage have little effect. Although not very obvious in these plots, the initial amount of reserve is a U-shaped function of the reserve at birth. The right branch is explained by the larger amount of reserve at birth, the left branch by the larger age at birth, which comes with larger cumulative somatic maintenance requirements.

The size of neonates of trout and salom, was found to increase with initial egg size [133, 192], suggesting that $k < 1$ for samonids. This also applies to the emu [127], and probably represents a general pattern.

Mother-foetus system

{103}

Vitellogenin in eggs and casein in milk have similar metabolic functions. The three vitellogenin-encoding genes were progressively lost in the mammalia around 30–70 Ma ago, except in the protherians, while casein-encoding genes already appeared in the mammallian ancestor some 200–310 Ma ago [69]. The transition from egg laying to placental development went probably incremental. The protherians still lay yolky eggs, the marsupial oocyte still has some yolk, that of the eutherians has not.

The mother-foetus system can be analysed in a DEB context in more detail, as a result of interaction with Tânia Sousa and Tiago Domingos.

Foetus

The foetus is ectothermic, so $\{\dot{J}_{ET}\} = 0$; in placentalia the mother keeps the foetus warm. The mother provides the foetus with a reserve flux $\dot{J}^F_{EA} = \{\dot{J}^F_{EA}\}L^2$ through the placenta, which is proportional to the squared length of the foetus, while $\{\dot{J}^F_{EA}\}$ is assumed to be constant, but might depend on the general nutritional status of the mother. This supply bypasses the assimilatory system of the foetus, which only becomes functional in the juvenile stage.

All parameters in the following equations for the change in reserve mass M_E and structural mass M_V refer to that of the foetus, and are probably close to that of the mother.

$$\begin{aligned}
\frac{d}{dt}M_E &= \dot{J}^F_{EA} - \dot{J}_{EC} \\
&\quad \dot{J}_{EC} = \{\dot{J}_{EAm}\}L^2\frac{ge}{g+e}\left(1+\frac{L}{gL_m}\right) \quad \text{with } g = \frac{\dot{v}[M_V]}{\kappa\{\dot{J}_{EAm}\}y_{VE}} \\
\frac{d}{dt}M_V &= (\kappa\dot{J}_{EC} - \dot{J}_{EM})y_{VE} \quad \text{with } \dot{J}_{EM} = [\dot{J}_{EM}]L^3
\end{aligned}$$

where the scaled reserve density $e \equiv \frac{m_E}{m_{Em}} = \frac{M_E\dot{v}}{L^3\{\dot{J}_{EAm}\}}$ (dimensionless) and the reserve density $m_E = M_E/M_V = M_E(L^3[M_V])^{-1}$ (in $\mathrm{mol\,mol^{-1}}$) represent ratios of masses of reserve and structure.

Initial structural length L_0 is very small, while $M^0_V = M_V(0) = [M_V]L^3_0$. The reserve density of the foetus e equals that of the mother, so $M^0_E = M_E(0) = eL^3_0\{\dot{J}_{EAm}\}/\dot{v}$,

which implies that if the mother is experiencing a constant food level for a long time $\{\dot{J}^F_{EA}\} = f\{\dot{J}_{EAm}\}$.

The growth curve of the foetus is the von Bertalanffy growth curve. Since length at birth is small relative to the ultimate length, length will increase in time linearly. This can be seen as follows. Since $M_V = [M_V]L^3$, so $L = (M_V/[M_V])^{1/3}$, we have for $y_{EV} = 1/y_{VE}$

$$\begin{aligned}
\frac{d}{dt}L &= \frac{1}{3[M_V]}\left(\frac{M_V}{[M_V]}\right)^{-2/3}\frac{d}{dt}M_V = \frac{\kappa\{\dot{J}_{EAm}\}L^2\frac{ge}{g+e}\left(1+\frac{L}{gL_m}\right) - [\dot{J}_{EM}]L^3}{3y_{EV}[M_V]L^2} \\
&\simeq \frac{\kappa\{\dot{J}_{EAm}\}\frac{ge}{g+e} - [\dot{J}_{EM}]L}{3y_{EV}[M_V]} \simeq \frac{\kappa\{\dot{J}_{EAm}\}ge}{3y_{EV}[M_V](g+e)} \\
L(t) &\simeq \frac{\kappa\{\dot{J}_{EAm}\}get}{3y_{EV}[M_V](g+e)} \quad \text{for } L_0 \downarrow 0
\end{aligned}$$

Mother

The assimilation of the mother is up-regulated during pregnancy, where the surface area of the placenta is added to that of the mother. The idea behind this construct is that for demand systems like most organisms that produce foetuses, food uptake capacity is proportional to the gut surface area, where not only the actual transport of metabolites across the gut surface limits uptake, but also the further processing of the metabolites to reserve. The transport across the placenta accelerates this process. The assimilation process of the mother of length L and a foetus of length L_F then amounts to

$$\dot{J}_{EA} = f\{\dot{J}_{EAm}\}(L^2 + \delta L_F^2)$$

At constant food levels the extra assimilation will match the foetal needs, so

$$f\{\dot{J}_{EAm}\}(L^2 + \delta L_F^2) = f\{\dot{J}_{EAm}\}L^2 + \{\dot{J}^F_{EA}\}L_F^2, \quad \text{so } \{\dot{J}^F_{EA}\} = f\{\dot{J}_{EAm}\}\delta$$

The export of reserve from the mother to the foetus is from the somatic branch of the catabolic flux and has priority over the somatic maintenance of the mother unless starvation conditions are so severe that spontaneous abortus occurs.

The parameters in the following specification of the changes in reserve M_E and structure M_V refer to that of the mother:

$$\begin{aligned}
\frac{d}{dt}M_E &= \dot{J}_{EA} - \dot{J}_{EC} \quad \text{with } \dot{J}_{EC} = \{\dot{J}_{EAm}\}L^2\frac{ge}{g+e}\left(1+\frac{L_h+L}{gL_m}\right) \\
\frac{d}{dt}M_V &= (\kappa\dot{J}_{EC} - \dot{J}_{EM} - \dot{J}_{ET} - \dot{J}^F_{EA})y_{VE} \quad \text{with } \dot{J}_{EM} = [\dot{J}_{EM}]L^3 \text{ and } \dot{J}_{ET} = \{\dot{J}_{ET}\}L^2
\end{aligned}$$

where $L_h = \{\dot{J}_{ET}\}/[\dot{J}_{EM}]$ and $L_m = \kappa\{\dot{J}_{EAm}\}/[\dot{J}_{EM}]$.

Notice that the foetus increases the assimilation of the mother, but not the catabolic rate directly, only indirectly via the increase of the reserve of the mother that is the consequence of the actions of the foetus. This is qualitatively consistent with empirical observations.

Since allocation to the foetal system has priority over somatic maintenance, and so over growth, the foetus might reduce the growth of the mother. If the mother is already fully grown at pregnancy, somatic maintenance might be reduced, e.g. by reducing activity, which typically comprises some 5 till 10 % of the somatic maintenance costs. This too is qualitatively consistent with observations. It is probably no coincidence that species that sport foetal reproduction frequently developed advanced social systems to avoid the translation of a reduction in activity into a reduction in food intake or an increase in hazard rate via an increased risk of being catched by a predator.

Suppose that food density, and so f, as well as M_V, and so L, are constant at the start of pregnancy, so $\kappa \dot{J}_{EC} = \dot{J}_{EM} + \dot{J}_{ET} + \{\dot{J}^F_{EA}\} L_F^2$ and $L = f L_m - L_h$. The catabolic flux reduces to $\dot{J}_{EC} = \{\dot{J}_{EAm}\} L^2 \frac{f+g}{e+g} e$. We now study the reduction of $[\dot{J}_{EM}]$ that is required to cope with foetal development. The value relative to the pre-pregnancy period and the dynamics of scaled reserve density amounts for $y_{TA} = \{\dot{J}_{ET}\}/\{\dot{J}_{EAm}\}$ and $y_{FA} = \{\dot{J}^F_{EA}\}/\{\dot{J}_{EAm}\}$ to

$$\begin{aligned} \frac{[\dot{J}_{EM}](t)}{[\dot{J}_{EM}](0)} &= \frac{\kappa e(t) \frac{f+g}{e(t)+g} - y_{TA} - y_{FA} L_F^2/L^2}{\kappa f - y_{TA}} \\ \frac{d}{dt} e &= \left(f + f\delta L_F^2/L^2 - e\right) \dot{v}/L \end{aligned}$$

This dynamics implies a maximum reduction of somatic maintenance costs, and might match the fraction that activity takes in the somatic maintenance costs. In this way foetal reproduction could evolve without mayor metabolic adaptations.

In many placentalia pregnancy is followed by a period of lactation. This product by the mother is also paid from the somatic branch of the catabolic flux, and also has the effect that the assimilation capacity is up-regulated to match this drain of reserve. It is typically a demand-driven process where the flux of milk taken by the baby is proportional to its squared length. The consequence is that the reserve of the mother remains elevated above the normal level during this period. In the marsupials, the foetal development is really short, meaning that the length at birth is very small, but the lactation period is relatively long.

Incomplete beta function

{107}

The incomplete beta function in Eq (3.31) can be written explicitly as a hypergeometric function, which partly removes the need for approximation (3.32). The result is

$$\begin{aligned} B_x(\tfrac{4}{3}, 0) &= \int_0^x y^{1/3} (1-y)^{-1} \, dy \\ &= \frac{3}{4} x^{4/3} {}_2F_1(1, \tfrac{4}{3}, \tfrac{7}{3}, x) = \frac{3}{4} \frac{\Gamma(7/3)}{\Gamma(4/3)} \sum_{n=0}^{\infty} \frac{\Gamma(n+4/3)}{\Gamma(n+7/3)} x^{n+4/3} \\ &= \sqrt{3} \left(\arctan \frac{1+2x^{1/3}}{\sqrt{3}} - \arctan \frac{1}{\sqrt{3}} \right) + \frac{1}{2} \log(1 + x^{1/3} + x^{2/3}) - \log(1 - x^{1/3}) - 3x^{1/3} \end{aligned}$$

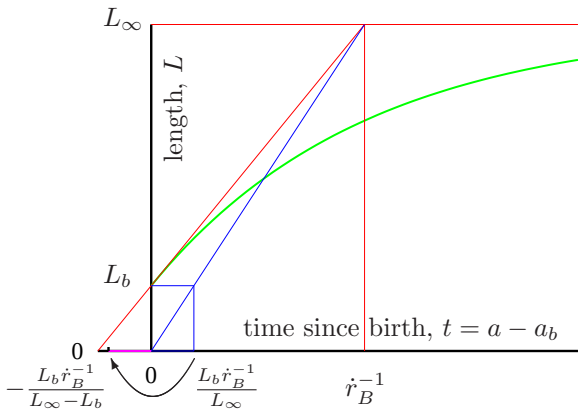

Figure 3.2: The von Bertalanffy growth curve $\frac{d}{dt}L = \dot{r}_B(L_\infty - L)$, with the geometric interpretation of the von Bertalanffy growth rate $\dot{r}_B$, and the maximum possible age at birth $\frac{L_b\dot{r}_B^{-1}}{L_\infty}$ in the context of DEB theory. The tangent line at $t = 0$ intersects the asymptote at time $\dot{r}_B^{-1}$; the line from the origin to this intersection point hits level L_b at time $\frac{L_b}{L_\infty \dot{r}_B}$, which is the maximum possible incubation time.

Range for age at birth

{107}

The age at birth simplifies for small g and large $\dot{k}_M$, while $\dot{r}_B = \frac{\dot{k}_M g}{3(e_b+g)}$ remains fixed [329]:

$$\begin{aligned} a_b &= \frac{3}{\dot{k}_M}\int_0^{x_b} \frac{dx}{(1-x)x^{2/3}(3gx_b^{1/3}l_b^{-1} - B_{x_b}(\tfrac{4}{3},0) + B_x(\tfrac{4}{3},0))} \\ &\overset{g,\dot{k}_M^{-1}\text{small}}{\simeq} \frac{1}{3e_b\dot{r}_B}\int_0^{x_b} \frac{dx}{(1-x)x^{2/3}x_b^{1/3}(l_b^{-1} - (x_b^{4/3} - x^{4/3})/(4e_b))} \\ &\overset{g,\dot{k}_M^{-1}\to 0}{=} \frac{l_b}{e_b\dot{r}_B} \end{aligned}$$

where $x_b \equiv \frac{g}{e_b+g}$. The significance of this result is in the fact that for fixed $\dot{r}_B$, L_b and L_∞, $g \to 0$ while $\dot{k}_M \to \infty$ if a_b is running from 0 to this upper boundary. See Figure 3.2 for a graphical interpretation.

The foetal special case, where $a_b = 3L_b/\dot{v} = \frac{3l_b}{\dot{k}_M g}$ (Eq. (3.36)) represents a lower boundary for the age at birth (of eggs). For $e_b = f$ and $\dot{r}_B = \frac{1}{3}\frac{\dot{k}_M g}{f+g}$ (Eq. (3.22)), the upper boundary can be written as $\frac{3l_b}{\dot{k}_M g}(1 + g/f)$, which makes that

$$\frac{3l_b}{\dot{k}_M g} < a_b < \frac{3l_b}{\dot{k}_M g}(1 + g/f) \quad \text{or} \quad 1 < a_b\frac{\dot{k}_M g}{3l_b} < 1 + g/f$$

Find a_b, L_b, U_E^0 given U_H^b, U_E^b for $\dot{k}_J \neq \dot{k}_M$ [294]

{107}

The standard DEB model for embryonic development amounts to

$$\frac{d}{da}U_E = -S_C \quad \text{with } S_C = L^2\frac{ge}{g+e}\left(1 + \frac{\dot{k}_M L}{\dot{v}}\right) \text{ and } e \equiv \frac{U_E\dot{v}}{L^3} \tag{3.3}$$

$$\frac{d}{da}L = \frac{\dot{v}e - \dot{k}_M g L}{3(e+g)} \tag{3.4}$$

$$\frac{d}{da}U_H = (1-\kappa)S_C - \dot{k}_J U_H \tag{3.5}$$

Table 3.1: The dimensionless scaled variables and parameters that are used to find the initial amount of scaled reserve.

$\tau = a\dot{k}_M$	$\tau_b = a_b\dot{k}_M$	$l = Lg\dot{k}_M/\dot{v}$	$l_b = L_b g\dot{k}_M/\dot{v}$
$u_E = U_E g^2\dot{k}_M^3/\dot{v}^2$	$u_E^0 = U_E^0 g^2\dot{k}_M^3/\dot{v}^2$	$u_H = U_H g^2\dot{k}_M^3/\dot{v}^2$	$u_H^b = U_H^b g^2\dot{k}_M^3/\dot{v}^2$
$e = gu_E/l^3$	$e_b = gu_E^b/l_b^3$	$e_H = gu_H/l^3$	$e_H^b = gu_H^b/l_b^3$
$x = \frac{g}{e+g}$	$x_b = \frac{g}{e_b+g}$	$\alpha = 3gx^{1/3}/l$	$\alpha_b = 3gx_b^{1/3}/l_b$
$y = \frac{xe_H}{1-\kappa}$	$y_b = \frac{x_b e_H^b}{1-\kappa} = gx_b v_H^b l_b^{-3}$	$v_H^b = \frac{u_H^b}{1-\kappa}$	$k = \dot{k}_J/\dot{k}_M$

where the variable (U_E, L, U_H) evolves from value $(U_E^0, 0, 0)$ at $a = 0$ to value (U_E^b, L_b, U_H^b) at $a = a_b$, which is at birth. Apart from the five parameters $\dot{k}_M$, $\dot{k}_J$, $\dot{v}$, g, κ, only the scaled maturity at birth U_H^b and the (dimensionless) scaled reserve density at birth $e_b = \dot{v}U_E^b L_b^{-3}$ are given and the problem is to find U_E^0 and so a_b, U_E^b and L_b. For the special case $k = 1$ (i.e. $\dot{k}_J = \dot{k}_M$), the solution is given in [289], but the present problem is to find expressions for the general case that $k \neq 1$.

In [294] I first remove 2 parameters by scaling to dimensionless quantities; Table 3.1 gives the dimensionless quantities that are involved. The reformulated problem is now: Find τ_b, l_b, u_E^0 given u_H^b, k, g, κ and $u_E^b = e_b l_b^3/g$.

The reformulated problem is now: Find τ_b, l_b, u_E^0 given u_H^b, k, g, κ and $u_E^b = e_b l_b^3/g$. We also have $0 < k < (1-\kappa)e_b^3/u_H^b$ and $u_H^b < 1 - \kappa$.

For the variable (τ, u_E, l, u_H) evolving from the value $(0, u_E^0, 0, 0)$ to the value $(\tau_b, u_E^b, l_b, u_H^b)$, the scaled model amounts to

$$\frac{d}{d\tau}u_E = -u_E l^2 \frac{g+l}{u_E + l^3} \tag{3.6}$$

$$\frac{d}{d\tau}l = \frac{1}{3}\frac{gu_E - l^4}{u_E + l^3} \tag{3.7}$$

$$\frac{d}{d\tau}u_H = (1-\kappa)u_E l^2 \frac{g+l}{u_E + l^3} - ku_H \tag{3.8}$$

or alternatively for variable (τ, e, l, e_H) evolving from the value $(0, \infty, 0, e_H^0)$ to the value $(\tau_b, e_b, l_b, e_H^b)$

$$\frac{d}{d\tau}e = -g\frac{e}{l} \tag{3.9}$$

$$\frac{d}{d\tau}l = \frac{g}{3}\frac{e-l}{e+g} \tag{3.10}$$

$$\frac{d}{d\tau}e_H = (1-\kappa)\frac{ge}{l}\frac{l+g}{e+g} - e_H\left(k + \frac{g}{l}\frac{e-l}{e+g}\right) \tag{3.11}$$

where $e_H^0 = (1-\kappa)g$ is such that $\frac{d}{d\tau}e_H(0) = 0$, else $\frac{d}{d\tau}e_H(0) = \pm\infty$. If $k = 1$ we have $e_H(\tau) = e_H^0$ for all τ and $u_H(\tau) = (1-\kappa)l_b^3$. For $k > 1$, e_H is decreasing in (scaled) age, and for $k < 1$ increasing.

I first observe that

$$\begin{aligned}
\alpha_b - \alpha &= B_{x_b}(\frac{4}{3},0) - B_x(\frac{4}{3},0) && (3.12)\\
\frac{3gx_b^{1/3}}{l_b} - \frac{3gx^{1/3}}{l} &= B_{x_b}(\frac{4}{3},0) - B_x(\frac{4}{3},0) && (3.13)\\
\frac{1}{l} &= \frac{1}{l_b}\left(\frac{x_b}{x}\right)^{1/3} - \frac{B_{x_b}(\frac{4}{3},0) - B_x(\frac{4}{3},0)}{3gx^{1/3}} && (3.14)\\
-l^{-2}\frac{dl}{dx} &= \frac{-1}{3l_b}\frac{x_b^{1/3}}{x^{4/3}} + \frac{x^{1/3}}{(1-x)3gx^{1/3}} + \frac{B_{x_b}(\frac{4}{3},0) - B_x(\frac{4}{3},0)}{9gx^{4/3}} && (3.15)\\
\text{using (3.13):}\quad \frac{dl}{dx} &= \frac{l^2}{3l_b}\frac{x_b^{1/3}}{x^{4/3}} - \frac{l^2}{3g(1-x)} - l^2\frac{3gx_b^{1/3}/l_b - 3gx^{1/3}/l}{9gx^{4/3}} && (3.16)\\
&= \frac{l}{3}\left(\frac{1}{x} - \frac{l}{g(1-x)}\right) && (3.17)\\
&= \left(\frac{g(1-x)-lx}{3}\right)\left(gx\frac{1-x}{l}\right)^{-1} && (3.18)\\
&= \frac{dl}{d\tau}\frac{d\tau}{dx} && (3.19)
\end{aligned}$$

The last step follows from Eq (3.9 - 3.10) and shows that Eq (3.12) follows from the latter two ode's for embryonic development; all earlier steps follow from the definitions in Table 3.1.

Scaled age at birth τ_b

The scaled age at birth τ_b and its derivation is given by

$$\begin{aligned}
\tau_b &= 3\int_0^{x_b} \frac{dx}{(1-x)x^{2/3}(\alpha_b - B_{x_b}(\frac{4}{3},0) + B_x(\frac{4}{3},0))} && (3.20)\\
\text{using (3.12)} &= 3\int_0^{x_b} \frac{dx}{\alpha(1-x)x^{2/3}} && (3.21)\\
&= \int_0^{x_b} \frac{l\,dx}{gx(1-x)} && (3.22)\\
d\tau &= \frac{l\,dx}{gx(1-x)} && (3.23)\\
\frac{dx}{d\tau} &= gx\frac{1-x}{l} && (3.24)
\end{aligned}$$

The latter follows from Eq (3.9) and the definition of x in Table 3.1, which shows that Eq (3.20) follows for Eq (3.9 - 3.10). Notice that τ_b requires l_b in α_b, which is given below.

Scaled initial amount of reserve u_E^0

From $x^{-1} = 1 + u_E l^{-3}$ (using definitions of x and u_E in Table 3.1), we have $l^3 + u_E = l^3/x = (3g/\alpha)^3$. The last step follows again from from Table 3.1).

Now we let $l \to 0$, so that $u_E \to u_E^0$, substitute α using Eq (3.12) and arrive at

$$u_E^0 = \left(\frac{3g}{\alpha_b - B_{x_b}\left(\frac{4}{3}, 0\right)} \right)^3 \tag{3.25}$$

which again requires l_b in α_b.

Scaled length at birth l_b

The *pièce de resistance* for solving our boundary value problem is finding l_b, which turns out to be rather straightforward once the appropriate transformation of variables is found (namely $y(x)$, see Table 3.1). For the variable (τ, x) evolving from the value $(0, 0)$ to the value (τ_b, x_b) and the variable (τ, e_H) evolving from the value $(0, e_H^0)$ to the value (τ_b, e_H^b) we have

$$\frac{d}{d\tau}x = gx\frac{1-x}{l(x)}; \quad \frac{d}{d\tau}e_H = (1-\kappa)g(1-x)\left(\frac{g}{l(x)}+1\right) - e_H\left(k - x + g\frac{1-x}{l(x)}\right)$$

Now consider the variable (x, e_H) evolving from the value $(0, e_H^0)$ to the value (x_b, e_H^b) or the variable (x, y) evolving from the value $(0, 0)$ to the value (x_b, y_b):

$$\begin{aligned} \frac{d}{dx}e_H &= \frac{e_H^0}{x}\left(\frac{l(x)}{g}+1\right) - \frac{e_H}{x}\left(\frac{k-x}{1-x}\frac{l(x)}{g}+1\right) \quad \text{for } e_H^0 = e_H(0) = (1-\kappa)g \\ \frac{d}{dx}y &= r(x) - ys(x) \quad \text{for } r(x) = g + l(x); \quad s(x) = \frac{k-x}{1-x}\frac{l(x)}{gx} \end{aligned} \tag{3.26}$$

where $l(x)$ is given in (3.14). The ode for y can be solved to

$$y(x) = v(x)\int_0^x \frac{r(x_1)}{v(x_1)}dx_1 \quad \text{with } v(x) = \exp(-\int_0^x s(x_1)\,dx_1)$$

The quantity l_b must be solved from $y_b = y(x_b) = gx_b v_H^b l_b^{-3}$, see Table 3.1. So we need to find the root of t as function of l_b with

$$t(l_b) = \frac{x_b g v_H^b}{v(x_b) l_b^3} - \int_0^{x_b} \frac{r(x)}{v(x)}dx = 0 \tag{3.27}$$

From this equation it becomes clear that the parameters κ and u_H^b affect l_b only via $v_H^b = \frac{u_H^b}{1-\kappa}$; a conclusion that is more difficult to obtain using the ode for the scaled maturity density e_H rather than that for abstract variable y. Notice that the solution of l_d (and that of u_E^0 and τ_b) for the boundary value problem for the ode for (u_E, l, e_H) as given in Eq. (3.6–3.8) depends on the four parameters g, k, v_H^b and e_b only. The solution for l_b must be substituted into Eq. (3.25) to obtain u_E^0 and in Eq. (3.20) to obtain τ_b; the scaled reserve at birth is $u_E^b = e_b l_b^3/g$.

Numerical solution for scaled length at birth l_b

The shooting method turns out to be rather stable, where $y(x_b) = y_b$ is evaluated by integrating $\frac{d}{dx}y$ using $l_b = \left(v_H^b\right)^{1/3}$ as starting value. It is exact for $k = 1$ and has been the motivation for the choice of the symbol v_H^b, which appears to have the interpretation as a scaled volume.

Alternatively the Newton Raphson procedure $l_b^{i+1} = l_b^i - t(l_b^i)/t'(l_b^i)$ can be used to solve (3.27) with

$$\begin{aligned}
l(x) &= \left(\frac{1}{l_b}\left(\frac{x_b}{x}\right)^{1/3} - \frac{B_x(\frac{4}{3},0) - B_{x_b}(\frac{4}{3},0)}{3gx^{1/3}}\right)^{-1}; \quad l'(x) = \frac{l^2(x)}{l_b^2}\left(\frac{x_b}{x}\right)^{1/3} \\
v(x) &= \exp\left(-\int_0^x \frac{k-x_1}{1-x_1}\frac{l(x_1)}{g}\frac{dx_1}{x_1}\right); \quad v'(x) = v(x)\exp\left(-\int_0^x \frac{k-x_1}{1-x_1}\frac{l'(x_1)}{g}\frac{dx_1}{x_1}\right) \\
r(x) &= g + l(x); \quad r'(x) = l'(x) \\
t(l_b) &= \frac{x_b g u_H^b}{(1-\kappa)v(x_b)l_b^3} - \int_0^{x_b}\frac{r(x)}{v(x)}dx \\
t'(l_b) &= -\frac{x_b g u_H^b}{(1-\kappa)v(x_b)l_b^3}\left(\frac{3}{l_b} + \frac{v'(x_b)}{v(x_b)}\right) - \int_0^{x_b}\left(\frac{r'(x)}{r(x)} - \frac{v'(x)}{v(x)}\right)\frac{r(x)}{v(x)}dx
\end{aligned}$$

The problem here is in the accurate evaluation of the integrals. Euler integration requires many steps if $k > 1$, but is nonetheless much faster.

Special case $e \to \infty$: foetal development

The special case $e \to \infty$, which is approximative for foetal development, makes that $\frac{d}{d\tau}l = g/3$, or $l(\tau) = g\tau/3$. We further have

$$\begin{aligned}
\frac{d}{d\tau}u_H &= (1-\kappa)l^2(g+l) - ku_H \\
u_H(\tau) &= \frac{g^3(1-\kappa)}{3^3k^4}\left(k^2\tau^2(3k + k\tau - 3) + 6(k-1)(1 - \tau - \exp(-k\tau))\right)
\end{aligned}$$

The equation $u_H(\tau_b) = u_H^b$ has to be solved numerically for τ_b, but for $k = 1$ we have $u_H^b = (1-\kappa)3^{-3}g^3\tau_b^3 = (1-\kappa)l_b^3$. The solution of this equation is stable and fast; the resulting scaled length at birth $l_b = g\tau_b/3$ can be used to start the Newton Raphson procedure. This start is preferable if k is substantially different from 1. From $l_b < 1$, so $\tau_b < 3/g$, we can derive the constraint

$$\frac{k^2u_H^b}{1-\kappa} < k + g(k-1) + g^3\frac{k-1}{k^2}\frac{1 - 3/g - \exp(-3k/g)}{9/2}$$

It can be shown that $1 < \frac{g\tau_b}{3l_b} < 1 + \frac{g}{e_b}$ generally holds, see [329]; the range in the foetus case being restricted to zero.

For $u_E^b = u_E(\tau_b)$, the cost for a foetus amounts to

$$u_E^0 = u_E^b + \kappa l_b^3 + u_H^b + \int_0^{\tau_b}(\kappa l^3(\tau) + ku_H(\tau))\,d\tau = u_E^b + l_b^3 + \frac{3}{4}\frac{l_b^4}{g}$$

where the five terms correspond with the costs of reserve, structure, maturity, somatic and maturity maintenance, respectively. The second equality follows from the structure of DEB theory: the investment in maturity plus maturity maintenance equals $\frac{1-\kappa}{\kappa}$ times the investment in structure plus somatic maintenance and $l(\tau) = g\tau/3$.

Growth of V1-morphs

{108}

The derivation of growth for V1-morphs can be very much simplified, using the reasoning that leads to (5.15), but now applied to a single reserve only. We have for the increase of structure:

$$\begin{aligned} \dot{J}_{VG} &= \frac{d}{dt}M_V = \frac{\dot{J}_{EG}}{y_{EV}} = \frac{\dot{J}_{EC} - \dot{J}_{EM}}{y_{EV}} \\ &= \frac{M_E(\dot{k}_E - \dot{r}) - \dot{J}_{EM}}{y_{EV}} \\ \dot{r} &= \frac{\dot{J}_{VG}}{M_V} = j_{VG} = \frac{m_E(\dot{k}_E - \dot{r}) - j_{EM}}{y_{EV}} \\ &= \frac{m_E\dot{k}_E - j_{EM}}{m_E + y_{EV}} \end{aligned}$$

Part of the notation is introduced later. Notice that the term $\dot{r}$ in the numerator of the right argument at line two relates to 'dilution by growth' and gives rise to the term m_E in the denominator at the last line. So $m_E\dot{k}_E$ is the specific flux that is mobilized from the reserve, j_{EM} is lost for maintenance, while the cost for new biomass has a structural component y_{EV} and a reserve component m_E.

The maximum specific growth rate is

$$\dot{r}_m = \frac{m_{Em}\dot{k}_E - j_{EM}}{m_{Em} + y_{EV}} = \frac{j_{EAm} - j_{EM}}{j_{EAm}/\dot{k}_E + y_{EV}} = \frac{\dot{k}_E - \dot{k}_M g}{1+g} = \dot{k}_E\frac{1-l_d}{1+g}$$

so that $g = \frac{\dot{k}_E - \dot{r}_m}{\dot{k}_M + \dot{r}_m}$ and $j_{EAm} = y_{EV}\frac{\dot{r}_m + \dot{k}_M}{1 - \dot{r}_m/\dot{k}_E} = y_{EV}\dot{k}_E/g$ for $j_{EM} = y_{EV}\dot{k}_M$. Notice that the maximum throughput rate of a chemostat is less than the maximum specific growth rate, but the difference decreases for increasing concentration of substrate in the feed.

As stated in the comment for {315}, V1-morphs have the reserve density dynamics

$$\frac{d}{dt}m_E = j_{EA} - \dot{k}_E m_E$$

so that the steady state reserve density is $m_E^* = j_{EA}/\dot{k}_E$ and the maximum reserve density is $m_{Em} = j_{EAm}/\dot{k}_E$.

Maturity

{111}

It would behave been conceptually more clear to introduce a state variable E_H that quantifies the level of maturity (expressed as cumulative energy investment), while the maturity

maintenance costs $\dot{p}_J$ are taken to be proportional to E_H, so the maturity maintenance rate coefficient $\dot{k}_J = \dot{p}_J/E_H$ is constant. The transition from embryo to juvenile occurs if $E_H > E_H^b$, and from juvenile to adult if $E_H = E_H^p$. (The notation E_b and E_p is already in use for the reserve E at structural volume V_b and V_p, respectively; these are not constant.) Since allocation to the increase of the state of maturity ceases, we never have $E_H > E_H^p$. Eq (3.45) should have been preceded by

$$\begin{aligned}(1-\kappa)\dot{p}_C &= \dot{p}_J + \frac{d}{dt}E_H = \dot{k}_J E_H + \frac{d}{dt}E_H \quad \text{for } E_H < E_H^p \\ &= \dot{k}_J E_H^p + \dot{p}_R \quad \text{for } E_H = E_H^p\end{aligned}$$

where $\dot{p}_R$ is the allocation to reproduction. We now consider the special case that $\dot{k}_J E_H^p = V_p[\dot{p}_M]\frac{1-\kappa}{\kappa}$, where we have the situation that E_H reaches E_H^p at exactly the same moment when V reaches V_p. In this special case stage transitions occur if the structure exceeds a threshold; in all other cases the structural volume at which stage transitions occur depend on food history. This reasoning can be reversed: by observing how structural volume at stage transitions depend on food levels, we have indirect access to the value of rate $\dot{k}_J$. Notice that $\dot{k}_J = [\dot{p}_J]V_p/E_H^p = [\dot{p}_J]V_b/E_H^b$.

A similar situation applies to the transition from embryo to juvenile. So, if $(1-\kappa)[\dot{p}_M] \neq \kappa[\dot{p}_J]$, we can find the age at birth a_b, the reserve at birth E_b and the structural volume at birth V_b from

$$\begin{aligned}E_H^b &= \frac{1-\kappa}{\kappa}[E_G]V_b + \left(\frac{1-\kappa}{\kappa}[\dot{p}_M] - [\dot{p}_J]\right)\int_0^{a_b} V(a)\,da \\ \frac{d}{da}V &= \dot{r}V \quad \text{with } \dot{r} = \dot{v}\frac{E/L - [E_m]V/L_m}{E + [E_G]V/\kappa} \text{ and } V(0) \simeq 0 \\ \frac{d}{da}E &= E\left(\dot{r} - \frac{\{\dot{p}_{Am}\}}{L[E_m]}\right) \quad \text{with } E(0) = E_0\end{aligned}$$

for $L = V^{1/3}$ and $L_m = V_m^{1/3} = \kappa\{\dot{p}_{Am}\}/[\dot{p}_M]$ and given the initial amount of reserve E_0 of the egg. Notice that eggs are ectotherm, also those from endotherm adults (although there is still a need to think about the temperature during incubation). We still can impose the constraint $E_b = f[E_m]V_b$, where f is the scaled functional response as experienced by the mother, and we can solve E_0. These computations are done in routine "egg" in DEBtool/animal.

Low reproduction close to L_p

{112}, l15

The formulation is somewhat confusing. Individuals with an asymptotic length just lower than L_p don't reproduce, with or without maturity maintenance. The key is in the reproduction rate of individuals with an asymptotic length just larger than L_p; they hardly reproduce in practice, but without maturity maintenance they would reproduce at a substantial rate.

Effect of starvation on maturity

{113}, l-8

Little is known about variations in the state of maturity and how starvation can affect it. Thomas & Ikeda [550] concluded from studies on laboratory populations of *Euphausia superba* that female krill can regress from the adult to the juvenile state during starvation.

Derivation of Eq (3.48)

{114}

Eq (3.48) can be derived as follows. $\dot{R}$ denotes the reproductive rate in terms of numbers of eggs per time, and relates to the energy investment into reproduction $\dot{p}_R$ as $\dot{R} = \kappa_R \dot{p}_R / E_0$, where the fraction $1 - \kappa_R$ of $\dot{p}_R$ goes lost into the environment as overhead costs of reproduction, and $E_0 = e_0 E_m = e_0 [E_m] V_m$ is the energy costs of an egg, which is further quantified at {117}. Using (3.46) and (3.47) we have for $e = [E]/[E_m]$

$$\begin{aligned}
\dot{p}_R &= (1-\kappa)\dot{p}_C - \dot{p}_J \\
&= \frac{(1-\kappa)g[E]}{g + [E]/[E_m]} \left(\dot{v} V^{2/3} + \dot{k}_M V_h^{1/3} V^{2/3} + \dot{k}_M V \right) - \frac{1-\kappa}{\kappa} [\dot{p}_M] V_p \\
\dot{R} &= \frac{\kappa_R}{e_0 V_m} (1-\kappa) \left(\frac{ge}{g+e} \left(\dot{v} V^{2/3} + \dot{k}_M V_h^{1/3} V^{2/3} + \dot{k}_M V \right) - \frac{V_p}{\kappa} \frac{[\dot{p}_M]}{[E_m]} \frac{[E_G]}{[E_G]} \right) \\
&= \frac{\kappa_R}{e_0 V_m} (1-\kappa) \left(\frac{ge}{g+e} \left(\dot{v} V^{2/3} + \dot{k}_M V_h^{1/3} V^{2/3} + \dot{k}_M V \right) - g \dot{k}_M V_p \right)
\end{aligned}$$

for $\dot{k}_M = \frac{[\dot{p}_M]}{[E_G]}$ and $g = \frac{[E_G]}{\kappa [E_m]}$.

Buffer handling rules

{116}

Collaborative work with Laure Pecquerie on anchovy, which is a multiple spawner: Batch preparation is initiated if temperature in spring exceeds $T_R = 14°\mathrm{C}$ in individuals with $U_H > U_H^p$. Individual that mature after this time point have to wait with batch preparation till the next spring. The batch size is $E_B^* = \min(E_R, [E_B] L^3)$ for constant $[E_B]$. Batch preparation is ceased for that spawning season if $E_R = 0$.

The rate of batch preparation equals the allocation to reproduction in an individual if e would equal 1 (which implies a maximum rate of allocation) so

$$\dot{p}_B = (1-\kappa)\dot{p}_{Cm} - \dot{p}_J \quad \text{with } \dot{p}_{Cm} = [E_m] \frac{\dot{v}^* L^2 + \dot{k}_M L^3}{1 + 1/g}$$

and a batch is completed if the batch size equals E_B^*. The rate still depends on length of the individual and is motivated by the avoidance of an unbounded accumulation of the reproduction buffer at abundant food (during the whole year). The spawning season, however, lasts less than a year, so the rate of batch preparation is divided by the fraction of the year that has good spawning conditions, which is about 7/12. Notice that only in the last batch of the spawning season the batch size will be smaller than the target size $E_B = [E_B] L^3$. If food would be abundant, this rule for spawning implies that spawning, once initiated, continues till death.

The number of eggs per batch $N_B = \kappa_R E_B^*/E_0 = \kappa_R U_B^*/U_E^0$, where $1-\kappa_R$ is the overhead costs of reproduction, which is paid at the moment of conversion of (part of) the reproduction buffer to eggs. Furthermore $U_B^* = E_B^*/\{\dot{p}_{Am}\} = \min(U_R^*, L^3/\dot{v}_B)$, with $\dot{v}_B = \{\dot{p}_{Am}\}/[E_B]$, and $U_E^0 = E_0/\{\dot{p}_{Am}\}$. The initial reserve of an egg,E_0, depends on the reserve density of the mother at spawning, since the reserve density at birth (= at the moment of mouth-opening) equals that of the mother at spawning. This means that if the scaled functional response decreases during the spawning season, the numbers of eggs increases (if length would remain constant).

At spawning the reproduction buffer makes a step down of E_B^* if enough is available, else it is emptied fully. So if t_B denotes the time point at a spawning event, we have

$$\begin{aligned} E_R(t_B+dt) &= E_R(t_B) - \min(E_R(t_B), E_B^*) \quad \text{and } E_B(t_B+dt) = 0 \\ U_R(t_B+dt) &= \frac{E_R(t_B+dt)}{\{\dot{p}_{Am}\}} = U_R(t_B) - \min(U_R(t_B), U_B^*) \end{aligned}$$

To find the spawning events t_i, we have to solve t_i, $i = 1, 2, \cdots$, from $b(t_i) = 1$ for

$$b(t) = \frac{\int_{t_{i-1}}^t \dot{p}_B\, dt}{E_B} \quad \text{so} \quad \frac{d}{dt}b = \frac{\dot{p}_B}{E_B} - \frac{3b}{L}\frac{d}{dt}L = \frac{\dot{v}_B S_B}{L^3} - \frac{3b}{L}\frac{d}{dt}L$$

where t_0 is implicitly given by $T(t_0) = T_R$ and

$$S_B = \frac{\dot{p}_B}{\{\dot{p}_{Am}\}} = (1-\kappa)S_{Cm} - S_J \quad \text{with } S_{Cm} = \frac{L^2}{g+1}(\mathcal{M}(U_H)g + L/L_m)$$

To this end we evaluate $t_1 = \int_{b=0}^1 \frac{dt}{db}\, db$, reset $b = 0$ at t_1 and repeat to find t_2, etc.

Frames of reference

{120}

The changes in reserve and structure are given in several frames of reference. Eq (3.55) and (3.56) are the mass-form of volume-form Eq (3.10) and (3.18). Eq (3.11) gives the scaled form for reserve density, but that for length is not given. Table 3.5 gives the power-form, while Eq (4.7) and (4.8) give the relationship between the power and the scaled form. The overview is for isomorphs given in Table 3.2.

Parameter estimation

{120}

The (compound) DEB parameters that only have time and length in their dimension can be obtained from growth and reproduction data [329] with functions in DEBtool. These parameters don't depend on food level, while the growth and reproduction data do. To emphasize this, the quantities that depend on food level are printed bold in the following table:

Growth at a single food level: debtool/animal/get_pars_g

$$(L_b, \boldsymbol{L}_\infty, \boldsymbol{a}_b, \dot{\boldsymbol{r}}_B \text{ at } \boldsymbol{f}_1) \longrightarrow (g, \dot{k}_M = \dot{k}_J, \dot{v}; \boldsymbol{U}_E^0, \boldsymbol{U}_E^b \text{ at } \boldsymbol{f}_1)$$

Table 3.2: Changes in reserve density $[E]$ (energy per structural volume), structural volume V, reserve density m_E (moles per structural mole), structural mass M_V (moles), scaled reserve density e (dimensionless), and scaled length l (dimensionless) for the standard DEB model for isomorphs (top) and V1-morphs (bottom). The specific assimilation rate is $j_{EAm} = \{j_{EAm}\} M_V^{-1/3} [M_V]^{-2/3}$ for isomorphs and $j_{EAm} = [\dot{J}_{EAm}][M_V]^{-1}$ for V1-morphs.

form	reserve	structure
volume	$\frac{d}{dt}[E] = \frac{\{\dot{p}_{Am}\}}{V^{1/3}} \left(f - \frac{[E]}{[E_m]}\right)$	$\frac{d}{dt}V = \dot{v} \frac{V^{2/3}[E]/[E_m] - V^{2/3}(V_h/V_m)^{1/3} - V/V_m^{1/3}}{[E]/[E_m] + g}$
mass	$\frac{d}{dt} m_E = j_{EAm} \left(f - \frac{m_E}{m_{Em}}\right)$	$\frac{d}{dt} M_V = M_V \frac{j_{EAm}(m_E/m_{Em} - l_h) - j_{EM}/\kappa}{m_E + y_{EV}/\kappa}$
scaled	$\frac{d}{dt} e = \frac{\dot{k}_M g}{l}(f - e)$	$\frac{d}{dt} l = \frac{\dot{k}_M g}{3(e+g)}(e - l_h - l)$
volume	$\frac{d}{dt}[E] = [p_{Am}] \left(f - \frac{[E]}{[E_m]}\right)$	$\frac{d}{dt}V = \dot{k}_E V \frac{[E]/[E_m] - (V_d/V_m)^{1/3}}{[E]/[E_m] + g}$
mass	$\frac{d}{dt} m_E = j_{EAm} \left(f - \frac{m_E}{m_{Em}}\right)$	$\frac{d}{dt} M_V = M_V \frac{j_{EAm} m_E/m_{Em} - j_{EM}/\kappa}{m_E + y_{EV}/\kappa}$
scaled	$\frac{d}{dt} e = \dot{k}_E (f - e)$	$\frac{d}{dt} l = \frac{\dot{k}_M g}{3(e+g)}(e - l_d)$

Growth at several food levels: debtool/animal/get_pars_h

$$\left(\begin{array}{l} \boldsymbol{L}_b, \boldsymbol{L}_\infty, \dot{\boldsymbol{r}}_B \text{ at } \boldsymbol{f}_1 \\ \boldsymbol{L}_b, \boldsymbol{L}_\infty, \dot{\boldsymbol{r}}_B \text{ at } \boldsymbol{f}_2 \end{array} \right) \longrightarrow \left(\begin{array}{l} \dot{k}_M, \dot{k}_J, \dot{v}, \ \boldsymbol{U}_E^0, \boldsymbol{U}_E^b \text{ at } \boldsymbol{f}_1 \\ \qquad\qquad\quad \boldsymbol{U}_E^0, \boldsymbol{U}_E^b \text{ at } \boldsymbol{f}_2 \end{array} \right)$$

Growth at several food levels: debtool/animal/get_pars_i

$$\left(\begin{array}{l} L_b, \ \boldsymbol{L}_\infty, \dot{\boldsymbol{r}}_B \text{ at } \boldsymbol{f}_1 \\ \qquad\quad \boldsymbol{L}_\infty, \dot{\boldsymbol{r}}_B \text{ at } \boldsymbol{f}_2 \end{array} \right) \longrightarrow \left(\begin{array}{l} \dot{k}_M = \dot{k}_J, \dot{v}, \ \boldsymbol{U}_E^0, \boldsymbol{U}_E^b \text{ at } \boldsymbol{f}_1 \\ \qquad\qquad\quad\ \ \boldsymbol{U}_E^0, \boldsymbol{U}_E^b \text{ at } \boldsymbol{f}_2 \end{array} \right)$$

Growth & reproduction at a single food level: debtool/animal/get_pars_r

$$(L_b, L_p, \boldsymbol{L}_\infty, \boldsymbol{a}_b, \dot{\boldsymbol{r}}_B, \dot{\boldsymbol{R}}_\infty \text{ at } \boldsymbol{f}_1) \overset{\text{given } \kappa_R}{\longrightarrow} (\kappa, g, \dot{k}_J = \dot{k}_M, \dot{v}, U_H^b, U_H^p; \boldsymbol{U}_E^0, \boldsymbol{U}_E^b, \boldsymbol{U}_E^p \text{ at } \boldsymbol{f}_1)$$

Growth & reproduction at several food levels: debtool/animal/get_pars_s

$$\left(\begin{array}{l} \boldsymbol{L}_b, \boldsymbol{L}_p, \boldsymbol{L}_\infty, \dot{\boldsymbol{r}}_B, \dot{\boldsymbol{R}}_\infty \text{ at } \boldsymbol{f}_1 \\ \boldsymbol{L}_b, \boldsymbol{L}_p, \boldsymbol{L}_\infty, \dot{\boldsymbol{r}}_B, \dot{\boldsymbol{R}}_\infty \text{ at } \boldsymbol{f}_2 \end{array} \right) \overset{\text{given } \kappa_R}{\longrightarrow} \left(\begin{array}{l} \kappa, g, \dot{k}_J, \dot{k}_M, \dot{v}, U_H^b, U_H^p, \ \boldsymbol{U}_E^0, \boldsymbol{U}_E^b, \boldsymbol{U}_E^p \text{ at } \boldsymbol{f}_1 \\ \qquad\qquad\qquad\qquad\quad\ \ \boldsymbol{U}_E^0, \boldsymbol{U}_E^b, \boldsymbol{U}_E^p \text{ at } \boldsymbol{f}_2 \end{array} \right)$$

Growth & reproduction at several food levels: debtool/animal/get_pars_t

$$\left(\begin{array}{l} L_b, L_p, \ \boldsymbol{L}_\infty, \dot{\boldsymbol{r}}_B, \dot{\boldsymbol{R}}_\infty \text{ at } \boldsymbol{f}_1 \\ \qquad\quad\ \ \boldsymbol{L}_\infty, \dot{\boldsymbol{r}}_B, \dot{\boldsymbol{R}}_\infty \text{ at } \boldsymbol{f}_2 \end{array} \right) \overset{\text{given } \kappa_R}{\longrightarrow} \left(\begin{array}{l} \kappa, g, \dot{k}_J = \dot{k}_M, \dot{v}, U_H^b, U_H^p, \ \boldsymbol{U}_E^0, \boldsymbol{U}_E^b, \boldsymbol{U}_E^p \text{ at } \boldsymbol{f}_1 \\ \qquad\qquad\qquad\qquad\quad\ \ \boldsymbol{U}_E^0, \boldsymbol{U}_E^b, \boldsymbol{U}_E^p \text{ at } \boldsymbol{f}_2 \end{array} \right)$$

The parameter κ_R must be obtained from mass balances. Notice that the assumption $\dot{k}_J = \dot{k}_M$ can only be avoided if info at several food levels is available. Notice also that scaled reserve $U_E = M_E/\{\dot{J}_{EAm}\}$ and scaled maturity $U_H = M_H/\{\dot{J}_{EAm}\}$ play a role here, while the unscaled reserve M_E and maturity M_H require moles, and so knowledge

of $\{\dot{J}_{EAm}\}$. This can be obtained from observations on the feeding process and the mass at zero and birth. These extra observations also results in the yield coefficients y_{EX} and y_{VE}, see Chapter 4. DEBtool also has functions iget_pars that do the inverse mapping from (compound) DEB parameters to easy-to-measure quantities. This can be used for checking the mapping and testing against empirical data.

Assumptions

{121}

Table with assumptions for the standard model: assumptions 3, 5 and 7 should be modified slightly, see [529]

3 Embryos start their development with neglectable level of maturity and amount of structure. Daughters of dividing cells have equal amounts of structure and reserve, and reset their maturity level.

5 Somatic maintenance is a weighted sum of structural volume and surface area, maturity maintenance is proportional to the level of maturity.

7 The use of reserve does not depend on food availability and is weakly homeostatic. So reserve density converges to a constant value in constant environments, despite growth.

It is shown in [529] that the partitionability of reserve kinetics follows from weak and strong homeostasis assumptions 1 and 7. This makes that the original assumption 7 can be simplified.

Conversions

{122}

Table with conversions: We need conversions, because we need volumes, masses and energies at different moments in working with the DEB theory. An individual has structural volume V, structural mass M_V and reserve mass M_E. These quantities change in a coherent way in time, as specified by the DEB theory. Because of strong homeostasis $[M_V] = M_V/V$ is a constant. For a given structural mass M_V, the reserve mass can vary between some small positive number, and a maximum amount M_{Em}. The lower boundary cannot be zero, because the use of reserves would be zero as well, and the individual can no longer pay maintenance. (See 7.1 for more discussion on starvation.) At high food levels, the individual can grow to a maximum structural mass M_{Vm}, which is a simple function of DEB parameters. Also for this structural mass we have a maximum reserve mass M_{Em}, but this value has not got a special symbol in the book. So, while M_{Vm} is a number, M_{Em} changes during growth, but $[M_{Em}] = M_{Em}/V$ and $m_{Em} = M_{Em}/M_V$ are constants because of the weak homeostasis assumption. Notice that we also have that $m_{Em} = M_{Em}/M_{Vm}$, because the amounts of reserve and structure are taken from to the same individual, and this time we apply it to an individual with structural mass M_{Vm}.

Maximum length equals $L_m = V_m^{1/3} = \frac{\dot{v}}{\dot{k}_M g}$, and at maximum length we have

$$\kappa \dot{J}_{EAm} = \dot{J}_{EM}$$

$$\begin{aligned}
\kappa\{\dot{J}_{XAm}\}L_m^2 y_{EX} &= j_{EM}[M_V]L_m^3 \\
\kappa\{\dot{J}_{XAm}\}y_{EX} &= \dot{k}_M y_{EV}[M_V]L_m \\
\kappa\{\dot{J}_{XAm}\}y_{EX} &= y_{EV}[M_V]\dot{v}/g \\
y_{EX} &= \frac{y_{EV}[M_V]\dot{v}}{g\kappa\{\dot{J}_{XAm}\}} \\
g\kappa\{\dot{J}_{EAm}\} &= y_{EV}[M_V]\dot{v}
\end{aligned}$$

Since $\dot{v} = y_{EX}\frac{\{\dot{J}_{XAm}\}}{[M_{Em}]}$, it follows that

$$g\kappa[M_{Em}] = y_{EV}[M_V] \quad \text{and} \quad y_{EX} = \frac{[M_{Em}]\dot{v}}{\{\dot{J}_{XAm}\}}$$

By definition we have $M_E = E/\mu_E$, and since $[\dot{E}_m] = \{\dot{p}_{Am}\}/\dot{v} = \mu_E\{\dot{J}_{EAm}\}/\dot{v}$, we have $[M_{Em}] = [E_m]/\mu_E = \{\dot{J}_{EAm}\}/\dot{v}$. Notice that $\{\dot{J}_{XAm}\} = \{\dot{J}_{EAm}\}y_{XE}$.

Other useful conversions and relationships are given in Table 3.3, where M_H is the maturity, quantified as the cumulative investment into maturation, expressed as C-mol of reserve, using the choice of primary parameters as given in Table 3.4. Since this choice no longer supports $[\dot{p}_J] = [\dot{p}_M](1-\kappa)/\kappa$, the maturity maintenance costs are no longer proportional to the amount of structure, but to the maturity, so $\dot{p}_J = \dot{k}_J E_H$.

In the initial stages of estimation of DEB parameters [329], it is useful to avoid the use of moles and energies, which motivates the use of scaled reserve U_E and scaled maturity U_H. The initial scaled reserve U_E^0 can be known from g, $\dot{k}_M$, $\dot{k}_J$, $\dot{v}$, and f, or from L_b, L_∞, a_b, $\dot{r}_B$ and f, using the assumption $\dot{k}_M = \dot{k}_J$.

Suppose that the amount of carbon in a freshly laid egg M_E^0 and in a neonate $M_W^b = M_E^b + M_V^b$ are known, in combination with U_E^0. We first use the information in M_E^0 and obtain $\{\dot{J}_{EAm}\} = M_E^0/U_E^0$, and then $y_{EX} = \{\dot{J}_{EAm}\}/\{\dot{J}_{XAm}\}$, $M_H^b = \{\dot{J}_{EAm}\}/U_H^b$, $M_H^p = \{\dot{J}_{EAm}\}/U_H^p$, $M_E^b = U_E^b\{\dot{J}_{XAm}\}$. We then use the information in M_W^b, and obtain $M_V^b = M_W^b - M_E^b$ and $[M_V] = M_V^b L_b^{-3}$ (in actual length, if L_b is in actual length), $y_{VE} = \dot{v}[M_V](\kappa\{\dot{J}_{EAm}\}g)^{-1}$, $[\dot{J}_{EM}] = \dot{k}_M[M_V]/y_{VE}$.

If the weight of a freshly laid egg W_0 and of a neonate W_b is known, as well as the moles of carbon in a freshly laid egg M_E^0, we can obtain the molecular weights of reserve and structure: $w_E = W_0/M_E^0$, $W_V^b = W_b - w_E M_E^b$ and $w_V = W_V^b/M_V^b$. The shape coefficient is $\delta_{\mathcal{M}} = (M_V^b/[M_V])^{1/3}/L_b = (d_V^{-1}W_V^b)^{1/3}/L_b$.

The systematic use of the choice of primary parameters as in Table 3.4 comes with the need to treat maturity as an explicit state variable. The changes in reserve mass and length and the reproduction rate are for $m_E = M_E/M_V = M_E(L^3[M_V])^{-1}$, so $e \equiv \frac{m_E}{m_{Em}} = \frac{M_E\dot{v}}{L^3\{\dot{J}_{EAm}\}}$

$$\frac{d}{dt}M_E = f\{\dot{J}_{EAm}\}L^2 - \dot{J}_{EC} \quad \text{with } f = 0 \quad \text{if } M_H < M_H^b \tag{3.28}$$

$$\frac{d}{dt}L = \frac{\dot{v}}{3}\frac{e - (L+L_h)/L_m}{e+g} \quad \text{with } L_h = 0 \quad \text{if } M_H < M_H^b \tag{3.29}$$

$$\frac{d}{dt}M_H = (1-\kappa)\dot{J}_{EC} - \dot{k}_J M_H \quad \text{for } M_H < M_H^p \tag{3.30}$$

Table 3.3: Conversions and compound parameters

relationship	unit	description
$K = \frac{\{\dot{J}_{EAm}\}}{y_{EX}\{\dot{b}\}}$	$\mathrm{mol\,m^{-3}}$	half-saturation constant
$\{\dot{J}_{XAm}\} = \{\dot{J}_{EAm}\}/y_{EX}$	$\mathrm{mol\,m^{-2}d^{-1}}$	maximum specific ingestion rate
$M_{Vm} = L_m^3[M_V]$	mol	maximum structural mass
$[M_V] = d_V/w_V$	$\mathrm{mol\,m^{-3}}$	specific structural mass
$[M_{Em}] = \{\dot{J}_{EAm}\}/\dot{v}$	$\mathrm{mol\,m^{-3}}$	maximum reserve density
$m_{Em} = [M_{Em}]/[M_V]$	$\mathrm{mol\,mol^{-1}}$	maximum reserve density
$m_E = M_E/M_V$	$\mathrm{mol\,mol^{-1}}$	reserve density
$[E_m] = \{\dot{p}_{Am}\}/\dot{v}$	$\mathrm{J\,m^{-3}}$	maximum reserve density
$L_m = \kappa\frac{\{\dot{J}_{EAm}\}}{[\dot{J}_{EM}]} = \kappa\frac{\{\dot{p}_{Am}\}}{[\dot{p}_M]} = \frac{\dot{v}}{\dot{k}_M g}$	m	maximum structural length
$L_h = \{\dot{p}_T\}/[\dot{p}_M]$	m	heating length
$U_E = M_E/\{\dot{J}_{EAm}\} = E/\{\dot{p}_{Am}\}$	$\mathrm{d\,m^2}$	scaled reserve
$U_H = M_H/\{\dot{J}_{EAm}\} = E_H/\{\dot{p}_{Am}\}$	$\mathrm{d\,m^2}$	scaled maturity
$\{\dot{p}_{Am}\} = \mu_E\{\dot{J}_{EAm}\}$	$\mathrm{J\,d^{-1}\,m^{-2}}$	maximum specific assimilation energy flux
$\{\dot{p}_T\} = \{\dot{J}_{ET}\}\mu_E$	$\mathrm{J\,d^{-1}\,m^{-3}}$	surface area-specific maintenance energy flux
$[\dot{p}_M] = [\dot{J}_{EM}]\mu_E = \dot{k}_M\mu_{GV}[M_V]$	$\mathrm{J\,d^{-1}\,m^{-3}}$	specific somatic maintenance energy flux
$[\dot{p}_J] = \mu_E\dot{J}_{EJ}L^{-3} = \dot{k}_J E_H L^{-3}$	$\mathrm{J\,d^{-1}\,m^{-3}}$	specific maturity maintenance energy flux
$\dot{k}_M = [\dot{p}_M]/[E_G] = j_{EM}y_{VE}$	$\mathrm{d^{-1}}$	somatic maintenance rate coefficient
$\dot{J}_{EJ} = \dot{k}_J M_H$	$\mathrm{mol\,d^{-1}}$	maturity maintenance mass flux
$j_{EM} = [\dot{J}_{EM}]/[M_V]$	$\mathrm{mol\,mol\,d^{-1}}$	specific somatic maintenance flux
$E_H = \mu_E M_H$	J	maturity
$[E_G] = \mu_E[M_V]/y_{VE}$	$\mathrm{J\,m^{-3}}$	energy costs per structural volume
$\mu_E = \{\dot{p}_{Am}\}/\{\dot{J}_{EAm}\}$	$\mathrm{J\,mol^{-1}}$	chemical potential of reserve
$\mu_{GV} = [E_G]/[M_V] = \mu_E/y_{VE}$	$\mathrm{J\,mol^{-1}}$	energy-mass coupler for growth
$g = \frac{[E_G]}{\kappa[E_m]} = \frac{\dot{v}[M_V]}{\kappa\{\dot{J}_{EAm}\}y_{VE}}$	–	energy investment ratio
$f = X/(K+X)$	–	scaled functional response
$e = \frac{m_E}{m_{Em}} = \frac{M_E\dot{v}}{L^3\{\dot{J}_{EAm}\}}$	–	scaled reserve density
$M_V = L^3[M_V]$	mol	structural mass

$$\dot{R} = \kappa_R((1-\kappa)\dot{J}_{EC} - \dot{k}_J M_H^p)/M_E^0 \quad \text{for } M_H > M_H^p \tag{3.31}$$

$$\dot{J}_{EC} = \{J_{EAm}\}L^2\frac{ge}{g+e}\left(1 + \frac{L_h + L}{gL_m}\right) \quad \text{with } L_h = 0 \quad \text{if } M_H < M_H^b \tag{3.32}$$

where $\dot{J}_{EC}$ has the interpretation of the flux of mobilized reserve, which can be seen in Eq (3.28).

The initial amount of structure, $L(0) \simeq 0$ is negligibly small and the reserve density at birth m_E^b equals that of the mother at the moment of egg formation. That means, if the mother is living at function response f, the reserve density of the embryo at birth equals $m_E^b = f m_{Em}$. These initial conditions imply von Bertalanffy growth at constant food availability right after birth, but the initial amount of reserve M_{E0} and the length L_b

Table 3.4: The 12 primary parameters of the standard DEB model in a length-mass frame. The maturity maintenance costs can have arbitrary values (in principle, but the feasible range in very much restricted).

symbol	unit	description	process
$\{\dot{J}_{EAm}\}$	$\mathrm{mol\,d^{-1}m^{-2}}$	surface area-specific max assimilation rate	assimilation
$\{\dot{b}\}$	$\mathrm{m^3m^{-2}d^{-1}}$	surface area-specific searching rate	feeding
y_{EX}	$\mathrm{mol\,mol^{-1}}$	yield of reserve on food	digestion
y_{VE}	$\mathrm{mol\,mol^{-1}}$	yield of structure on reserve	growth
$\dot{v}$	$\mathrm{m\,d^{-1}}$	energy conductance	mobilization
$\{\dot{J}_{ET}\}$	$\mathrm{mol\,d^{-1}m^{-2}}$	surface area-specific maint. costs	heating/osmosis
$[\dot{J}_{EM}]$	$\mathrm{mol\,d^{-1}m^{-3}}$	volume-specific somatic maintenance	turnover/activity
$\dot{k}_J$	$\mathrm{d^{-1}}$	specific maturity maintenance	regulation/defense
κ	-	allocation fraction	allocation
κ_R	-	reproduction efficiency	egg formation
M_H^b	mol	maturation at birth	life history
M_H^p	mol	maturation at puberty	life history

and at age a_b at birth must be obtained numerically. So

$$(M_H, M_E, L) : (0, M_E^0, 0)\Big|_{a=0} \rightarrow (M_H^b, fL_b^3\{\dot{J}_{EAm}\}/\dot{v}, L_b)\Big|_{a=a_b}$$

The development of a foetus is rarely limited by the availability of reserve, because it gets reserve from the mother *via* the placenta. This can be used as a first approximation to obtain the cost of an egg. Since $L(0) \simeq 0$ and e is very large, the catabolic flux initially equals $\dot{J}_{EC} = \{J_{EAm}\}gL^2\left(1 + L\dot{k}_M/\dot{v}\right)$ and the change in length $\frac{d}{dt}L = \dot{v}/3$. So length as a function of age becomes $L(a) = a\dot{v}/3$. The maturity as function of age can now be solved and amounts to

$$M_H(a) = \frac{1-\kappa}{\kappa}\frac{\delta_1 + \delta_2 + \delta_3}{(a\dot{k}_J)^3}M_V \quad \left\{\begin{array}{rcl} \delta_1 &=& 3(a\dot{k}_J(a\dot{k}_J - 2) + 2) \\ \delta_2 &=& (a\dot{k}_J(a\dot{k}_J(a\dot{k}_J - 3) + 6) - 6)\dot{k}_M/\dot{k}_J \\ \delta_3 &=& 6(\dot{k}_M/\dot{k}_J - 1)\exp(-a\dot{k}_J) \end{array}\right. \tag{3.33}$$

The gestation (incubation) time a_b can be found numerically from $M_H(a_b) = M_H^b$, and the initial amount of reserve of an embryo equals

$$\begin{aligned} M_E^0 &= M_E^b + \int_0^{a_b} \dot{J}_{EC}(a)\,da \\ &= \{\dot{J}_{EAm}\}\left(f + (1-\kappa)g(1 + a_b\dot{k}_M/4)\right)L_b^3/\dot{v} \end{aligned}$$

This underestimates the cost of an egg, because its development eventually slows down due to depletion of reserve, which increases the maintenance costs.

Because endothermic species are ectothermic during the embryo stage, the change in the mass of structure can be written as

$$\frac{d}{dt}M_V = (\kappa\dot{J}_{EC} - j_{EM}M_V)y_{VE}$$

From this equation it can be seen that if $\dot{k}_M(1-\kappa) = \dot{k}_J\kappa$, the structure-specific maturity remains constant, and stage transitions occur at fixed amounts of structure. That is $m_H \equiv M_H/M_V = y_{VE}^{-1}\frac{1-\kappa}{\kappa}$, or $M_H = \frac{[M_V]}{y_{VE}}\frac{1-\kappa}{\kappa}L^3$. For a foetus we have $M_H^b = \frac{[M_V]}{y_{VE}}\frac{1-\kappa}{\kappa}(a_b\dot{v}/3)^3$, so $a_b = 3L_b/\dot{v}$ with $L_b = (M_H^b\frac{y_{VE}}{[M_V]}\frac{\kappa}{1-\kappa})^{1/3}$. This expression for the age at birth, a_b, can be used to initiate the numerical procedure that solves $M_H^b(a) = M_H^b$ using Eq (3.33) if $\dot{k}_M(1-\kappa) \neq \dot{k}_J\kappa$; the solution for a_b can be used to find M_E^0 for a foetus, which can be used to initiate the numerical procedure to find M_E^0 for an egg. The latter is necessary to find M_E^b and L_b for an egg.

In absence of growth the catabolic flux reduces to $\dot{J}_{EC} = M_E\dot{v}/L$. In absence of surface-related maintenance costs, $\{\dot{J}_{ET}\} = 0$, the catabolic flux just covers the somatic maintenance costs if $\kappa\dot{J}_{EC} = [\dot{J}_{EM}]L^3$. For $e = M_E/M_{Em}$, this amounts to the threshold $e = \frac{[\dot{J}_{EM}]L}{\kappa\{\dot{J}_{EAm}\}}$. If food density is constant, we have $e = f$, so this threshold then applies to f. The maturity can only exceed the threshold at birth if $(1-\kappa)\dot{J}_{EC} > \dot{k}_J M_H^b$, so if $M_H^b < (1-\kappa)\frac{M_E^b\dot{v}}{L_b\dot{k}_J}$. Substitution of the previous threshold gives the constraints for viable eggs

$$f > \frac{[\dot{J}_{EM}]L_b}{\kappa\{\dot{J}_{EAm}\}} = l_b \quad \text{and} \quad M_H^b < \frac{1-\kappa}{\kappa}\frac{[\dot{J}_{EM}]}{\dot{k}_J}L_b^3 = \frac{1-\kappa}{\kappa}\frac{j_{EM}}{\dot{k}_J}M_V^b$$

where length at birth L_b is an implicit function of primary parameters that is determined by the relationships just discussed.

Volume, mass & energy

{120}

Equivalent ways to quantify reserve, structure and maturity are given in Table 3.5. Mass is typically expressed in C-moles if the chemical composition does not change, and in grams when it can change (such as total body weight). Specific density d converts volume (cm^3) to mass (g); molecular weight w converts mass (mol) to mass (g); specific mass $[M_V] = d_V/w_V$ converts structural volume (cm^3) to structural mass (mol). The chemical potential converts mol (mol) to energy (J).

Since maturity results from an energy and/or mass conservation principle, it makes little sense to quantify it as volume because there is no conservation law for volume. Maturity is quantified in *invested* reserve (in mass or energy). It does not represent a mass or energy pool, but information; in this way we avoid the explicit conversion from reserve to information.

To avoid explicit use of moles or energy, we work with scaled reserve $U_E = M_E/\{\dot{J}_{EAm}\} = E/\{\dot{p}_{Am}\}$ and scaled maturity $U_H = M_H/\{\dot{J}_{EAm}\} = E_H/\{\dot{p}_{Am}\}$, with $\dim(U_E) = \dim(U_H) = t\,L^2$.

Table with powers

{123}

The entries in the tables have to be multiplied by $\mu_E M_{Em}\dot{k}_M g = \{\dot{p}_{Am}\}L_m^2$ to arrive at the powers (energy fluxes). Please realize that $\dot{p}_C = \dot{p}_M + \dot{p}_J + \dot{p}_T + \dot{p}_G + \dot{p}_R$, and $\kappa\dot{p}_C = \dot{p}_M + \dot{p}_T + \dot{p}_G$. These relationships are used to calculate $\dot{p}_R$.

Table 3.5: The state variables of the standard DEB model, expressed in three different ways. The notation for energy in reserve $E_E \equiv E$ and volume of structure $V_V \equiv V$ is simplified. Energy is assessed via mass (in C-mole) by multiplication with the chemical potential ($\overline{\mu}_E$ and $\overline{\mu}_V$).

	reserve E	structure V	maturity H
volume V	V_E	$V \equiv L^3$	
mass M	M_E	$M_V = [M_V]V$	M_H
energy E	$E = \overline{\mu}_E M_E$	$E_V = \overline{\mu}_V M_V$	$E_H = \overline{\mu}_E M_H$

Chapter 4

Uptake and use of essential compounds

From compound to primary parameters

{129}

The mixture of primary and compound parameters of the previous chapter suffices for many applications already (e.g. to predict growth and reproduction in different situations), but other applications require more primary parameters explicitly. We need to supplement the measured quantities with other type of measurements (involving weight, mass or energy) to make the step to the primary parameters, if necessary.

The last missing information to obtain the full set of primary parameters for isomorphic ectotherms ($\{\dot{J}_{ET}\} = 0$; see Table 3.4) can be extracted from the amount of carbon in a freshly laid egg M_E^0 and in a neonate $M_W^b = M_E^b + M_V^b$. We first use the information in M_E^0 and obtain $\{\dot{J}_{EAm}\} = M_E^0/U_E^0$, and then $y_{EX} = \{\dot{J}_{EAm}\}/\{\dot{J}_{XAm}\}$, $M_H^b = \{\dot{J}_{EAm}\}/U_H^b$, $M_H^p = \{\dot{J}_{EAm}\}/U_H^p$, $M_E^b = U_E^b\{\dot{J}_{XAm}\}$. We then use the information in M_W^b, and obtain $M_V^b = M_W^b - M_E^b$ and $[M_V] = M_V^b L_b^{-3}$ (in actual length, if L_b is in actual length), $y_{VE} = \dot{v}[M_V](\kappa\{\dot{J}_{EAm}\}g)^{-1}$, $[\dot{J}_{EM}] = \dot{k}_M[M_V]/y_{VE}$.

If the weight of a freshly laid egg W_0 and of a neonate W_b is known, we can obtain the molecular weights of reserve and structure: $w_E = W_0/M_E^0$, $W_V^b = W_b - w_E M_E^b$ and $w_V = W_V^b/M_V^b$. On the assumption that the specific density of structure is $d_V = 1$ $\mathrm{g\,cm^{-3}}$ (i.e. that of water), the shape coefficient is $\delta_{\mathcal{M}} = (d_V^{-1} W_V^b)^{1/3}/L_b$. We can now convert actual lengths into volumetric lengths and correct the primary parameters that have length in their dimension: $\delta_{\mathcal{M}}\dot{v}$, $\delta_{\mathcal{M}}^{-2}\{\dot{J}_{EAm}\}$, $\delta_{\mathcal{M}}^{-2}\{\dot{b}\}$, $\delta_{\mathcal{M}}^{-3}[\dot{J}_{EM}]$. The parameter $[M_V]$ is not a primary one because it only converts one size-measure into another, but it is best to convert it to $\delta_{\mathcal{M}}^{-3}[M_V]$ for comparative purposes.

The map

$$\Big(\{\dot{J}_{XAm}\}, K, M_E^0, M_W^b; \kappa, \kappa_R, g, \dot{k}_J, \dot{k}_M, \dot{v}, U_H^b, U_H^p\Big) \longrightarrow \Big(\{\dot{J}_{EAm}\}, \{\dot{b}\}, y_{EX}, y_{EV}, \dot{v}, [\dot{J}_{EM}], \dot{k}_J, \kappa, \kappa_R, M_H^b, M_H^p, [M_V]\Big)$$

is made by function get_pars_u of software package DEBtool. This completes the full set of

primary parameters of the standard DEB model in absence of somatic maintenance costs that are linked to surface areas (ectotherms).

At constant food density the weight of juveniles increases proportional to cubed length (in the standard model), and the proportionality constant relates to the (constant) reserve density. The weights in adults are typically above this weight-length curve, due to contributions of the buffer of reserve that is allocated to reproduction. The deviation can be used to quantify the size of this buffer, and to study the buffer handling rules for the transformation of the allocated reserve to offspring.

Composition parameters

{129}

The elemental composition of reserve and structure is required if predictions about fluxes of specific compounds (such as ammonia, carbon dioxide and dioxygen) are to be made. If the elemental composition of a freshly laid egg (so of reserve) and that of a neonate is known, the chemical index of structure, i.e. the frequency of element $*$ in structure, relative to carbon, is given by

$$n_{*V} = n_{*W} m_W^b - n_{*E} m_E^b \quad \text{for } * = H, O, N, \cdots$$

where $m_W^b = M_W^b / M_V^b$.

This is just one of a series of related techniques to unravel the composition of reserve and structure using measurements of biomass. Suppose that we have the elemental frequencies of two individuals of the same length (so the same amount of structure) at two scaled functional responses. We have $M_W = M_V + M_E$, and $M_E = f m_{Em} M_V$, where $m_{Em} = (m_W - 1)/f$ is the maximum reserve density. The structural mass M_V of an individual of total mass M_W equals $M_V = M_W/(1 + m_E)$. Moreover, if an organism has physical length L and structural mass M_V, the shape coefficient is $\delta_{\mathcal{M}} = (M_V/[M_V])^{1/3}/L$.

We also have

$$M_W \, n_{*W} = M_V \, n_{*V} + M_E \, n_{*E}$$

so the chemical indices of reserve and structure are

$$n_{*E} = \frac{f_1}{m_{W1} - 1} \frac{m_{W1} - m_{W2}}{f_1 - f_2} \quad n_{*V} = m_{W1} n_{*W} - f_1 \frac{m_{W1} - m_{W2}}{f_1 - f_2}$$

This technique to compute the concentrations in reserve and structure can also be applied to compounds rather than chemical elements. The contribution of the reproduction buffer in the weight (and composition) of adults should be taken into account, but for juveniles we don't have these complications.

Knowledge about the chemical indices can be used to determine the molecular weights of reserve and structure, so to link masses and weights. A pertinent question is to include or exclude water in mass, volume and weight measurements. If water replaces reserve in starving organisms (likely in aquatic arthropods and other taxa with exoskeletons), strong homeostasis can only apply when we exclude water. In many other cases the inclusion of water is more handy.

Derivation of $\dot{J}_E + \dot{J}_{E_R}$

{129}, p-1

The derivation of why the sum of $\dot{J}_E$ and $\dot{J}_{E_R}$ is a weighted sum of the three basic powers, but $\dot{J}_E$ and $\dot{J}_{E_R}$ are not, is given on {131}, third paragraph.

Derivation of Eq (4.2)

{130}

The notation can be confusing because some symbols can have different meanings, depending on the context. This specially applies to elements and compounds. The symbol N is, for instance used to denote the chemical element nitrogen as well as the compound 'nitrogen waste'. The first index in chemical index n_{NN} refers to the element, the second one to the compound. Compounds can be transformed into other compounds, but elements are conserved. So we make a mass balances for elements, can study fluxes of compounds; the N in $\dot{J}_N$ denotes the compound 'nitrogen waste'. A similar confusion can arise with the symbol E, for instance, which can stand for the (generalized) compound reserve, as well as for the amount of energy in the reserve.

The motivation behind these notational choices is that writing out the name of the compound systematically is not an option, because many formulas will become very long. Finding new symbols is also problematic, because many are used already, and this strategy can easily make it hard to remember what symbols denotes what, so I tried the use 'natural' symbols for the compounds, which made it necessary to use the context of the symbols to tell the meaning apart. See further the notation section.

Derivation of Eq (4.5)

{130}

Eq (4.5) is general for the product formation for the standard DEB system (one type of food, one reserve, one structure). In the case of faeces, we have $\eta_{PD} = \eta_{PG} = 0$ (see first line at {131}), but one can also think of other products, such as hair, skin flakes, sweat (see section 4.8) etc. Goldfish produces e.g. ethanol at low dioxygen levels; organisms other than animals have an even wider set of possible products.

Conversions

{130}, l-7

μ_X stands for the chemical potential of X, so of food. $\mu_{AX} = \mu_E y_{EX}$ stands for the energy per C-mole of food that is fixed in reserve, after the transformation, so $\dot{p}_A = -\mu_{AX}\dot{J}_X = \mu_E \dot{J}_{EA} = -\mu_E y_{EX}\dot{J}_X$. The difference $\mu_X - \mu_{AX}$ went lost for the organism. Part of this difference is still conserved in the faeces, some of it sits in e.g. the carbon dioxide production and in heat production that are associated with assimilation. The partitioning of the mineral fluxes to the three basic powers is discussed in 4.3.1. The energy balances are discussed in more detail in 4.9. The notation in μ_{AX} is somewhat uneasy, because first the process (assimilation A) is identified, and then the compound (food X). The reason is in the relationship $\mu_{AX} = \eta_{XA}^{-1}$, which has nice notational properties.

For the assimilation process we can work out the balance as follows. We first define the

matrix of mineral mass-energy couplers

$$\boldsymbol{\eta}_{\mathcal{M}} = \begin{pmatrix} \eta_{CA} & \eta_{CD} & \eta_{CG} \\ \eta_{HA} & \eta_{HD} & \eta_{HG} \\ \eta_{OA} & \eta_{OD} & \eta_{OG} \\ \eta_{NA} & \eta_{ND} & \eta_{NG} \end{pmatrix} \equiv \begin{pmatrix} \boldsymbol{\eta}_{\mathcal{M}A} & \boldsymbol{\eta}_{\mathcal{M}D} & \boldsymbol{\eta}_{\mathcal{M}G} \end{pmatrix}$$

As explained on {131}, these are not new parameters; they are given by $\boldsymbol{\eta}_{\mathcal{M}} = -\boldsymbol{n}_{\mathcal{M}}^{-1}\boldsymbol{n}_{\mathcal{O}}\boldsymbol{\eta}_{\mathcal{O}}$, where the organic mass-energy couplers $\boldsymbol{\eta}_{\mathcal{O}}$ are given in eq (4.5), and the chemical indices $\boldsymbol{n}_{\mathcal{M}}$ and $\boldsymbol{n}_{\mathcal{O}}$ in eq (4.2). So the mineral fluxes that are released in the environment in association with assimilation are $\dot{\boldsymbol{J}}_{\mathcal{M}A} = \dot{p}_A\boldsymbol{\eta}_{\mathcal{M}A}$. This represents an energy drain $\dot{p}_{\mathcal{M}A} = \boldsymbol{\mu}_{\mathcal{M}}^T\dot{p}_A\boldsymbol{\eta}_{\mathcal{M}A}$. The energy drain in product that is associated with assimilation (think e.g. of faeces for animals) amounts to $\dot{p}_{PA} = \dot{p}_A\mu_P\eta_{PA}$, as explained on {130}. The energy balance for assimilation process thus amounts to

$$\begin{aligned} -\mu_X\dot{J}_X &= \dot{p}_A + \dot{p}_{PA} + \dot{p}_{\mathcal{M}A} + \dot{p}_{TA} \\ &= \dot{p}_A(1 + \mu_P\eta_{PA} + \boldsymbol{\mu}_{\mathcal{M}}^T\boldsymbol{\eta}_{\mathcal{M}A}) + \dot{p}_{TA} \\ \mu_X &= \mu_{AX}(1 + \mu_P\eta_{PA} + \boldsymbol{\mu}_{\mathcal{M}}^T\boldsymbol{\eta}_{\mathcal{M}A}) - \dot{p}_{TA}/\dot{J}_X \end{aligned}$$

where $\dot{p}_{TA}$ is the heat that dissipates into the environment in association with the assimilation process; its amount follows from this energy balance. So the terms in the right argument stands for the energy flux fixed in reserve, product en minerals, followed by the dissipating heat. Only the reserve stays in the individual, the rest dissipates into the environment. Food disappears so the flux $\dot{J}_X$ is taken to be negative.

It is possible to express the basic powers as weighted sums of organic fluxes as

$$\begin{pmatrix} \dot{p}_A \\ \dot{p}_D \\ \dot{p}_G \end{pmatrix} = \begin{pmatrix} -\mu_{AX} & 0 & 0 & 0 \\ -\mu_{AX} & -\mu_{GV} & -\mu_E & 0 \\ 0 & \mu_{GV} & 0 & 0 \\ 0 & 0 & 0 & 0 \end{pmatrix} \begin{pmatrix} \dot{J}_X \\ \dot{J}_V \\ \dot{J}_E + \dot{J}_{E_R} \\ \dot{J}_P \end{pmatrix} \quad \text{or} \quad \dot{\boldsymbol{p}} = \boldsymbol{\eta}_{\mathcal{O}}^{-1}\dot{\boldsymbol{J}}_{\mathcal{O}}$$

for $\mu_{AX} = \eta_{XA}^{-1}$ and $\mu_{GV} = \eta_{VG}^{-1}$. If $\boldsymbol{n}_{\mathcal{O}}^{-1}$ exists, the basic powers can also be written as weighted sums of mineral fluxes: $\dot{\boldsymbol{p}} = -\boldsymbol{\eta}_{\mathcal{O}}^{-1}\boldsymbol{n}_{\mathcal{O}}^{-1}\boldsymbol{n}_{\mathcal{M}}\dot{\boldsymbol{J}}_{\mathcal{M}}$. This quantification is likely to be sensitive to inaccuracies.

Since $Y_{VX} = -\frac{\dot{J}_V}{\dot{J}_X} = \frac{\eta_{VG}\dot{p}_G}{\eta_{XA}\dot{p}_A} = \frac{\eta_{VG}j_{EG}\mu_E}{\eta_{XA}j_{EA}\mu_E} = \frac{\eta_{VG}y_{EV}\dot{r}}{\eta_{XA}y_{EX}j_{XA}} = \frac{\eta_{VG}\dot{r}}{\eta_{XA}j_{XA}}y_{VX}^{-1}$, we clearly see that $Y_{VX} \neq y_{VX}$. The first quantity is variable, the second one is fixed.

From macro- to micro-chemical reaction equations

{131}

A chemical transformation of chemical compounds A and B is typically denoted by, for instance, A + 2 B → 4 C, or more generally A + Y_{BA} B → Y_{CA} C. Alternatively we can write $0 = Y_{AA}\mathrm{A} + Y_{BA}\mathrm{B} + Y_{CA}\mathrm{C}$, if we include the fact that A and B disappear in the (negative) sign of the yield coefficients $Y_{AA} = -1$ and Y_{BA}. The choice of relating the disappearance rate of B and the appearance rate of C to the disappearance rate of A is arbitrary. We might also have written $0 = Y_{AC}\mathrm{A} + Y_{BC}\mathrm{B} + Y_{CC}\mathrm{C}$, for instance, with

$Y_{CC} = 1$. The notation does not specify the rate at which the transformation occurs, and this rate is sensitive to the choice of the reference compound. The absence of information on rates is probably the reason for the popularity of the notation in microbiology. The yield coefficients can (by definition) be written as ratios of rates: $Y_{ij} = \dot{J}_i/\dot{J}_j$. If one or more of the compounds stand for some generalized compound, rather than pure compounds, we speak of a macrochemical reaction equation, which can typically be split up into two or more microchemical reactions equations. Mass en energy conservation constraints apply to the values of the yield coefficients, and the dissipating heat could be included explicitly. If appropriate, these constraints could be extended with e.g. constraints on electrical charge and isotopes.

Applied to metabolic systems, a macrochemical reaction equation is a chemical reaction equation of the type

$$0 = \sum_{i \in \mathcal{M},\mathcal{O}} Y_{iX}\, i$$

where $\mathcal{M}$ and $\mathcal{O}$ represent all mineral and organic compounds that are involved in the transformation, and substrate (= food) X and biomass W (or structure and reserve) are among them. Notice that the macrochemical reaction equation is not a mathematical equation; i in this equation stands for a label (i.e. a type), not for a concentration or other quantity. The chemical indices of biomass, n_{HW}, n_{OW} and n_{NW}, depend on the specific growth rate, so on nutrient availability, which is why Y rather than y is used.

The yield coefficients can be collected in a matrix $\boldsymbol{Y}^k$, where element Y_{ij}^k represents the yield of compound i on compound j in transformation k. Likewise the chemical indices can be collected in matix $\boldsymbol{n}$, where element n_{ij} represents the chemical index of chemical element i in compound j. Conservation of chemical elements implies $\boldsymbol{n}\boldsymbol{Y}^k = \boldsymbol{0}$. Multiplication with the flux of the compound that is used to normalize the yield coefficients results in $\boldsymbol{n}\dot{\boldsymbol{J}}_{*k} = \boldsymbol{0}$, where $\dot{\boldsymbol{J}}_{*k}$ is the column matrix of fluxes of all compounds that partake in transformation k. For all transformations simultaneously we can write $\boldsymbol{n}\dot{\boldsymbol{J}} = \boldsymbol{0}$

Suppose that there are not one but several chemical transformations simultaneously. Let $\boldsymbol{M}$ be the column matrix of the masses of all compounds. Then $\frac{d}{dt}\boldsymbol{M} = \dot{\boldsymbol{J}}\boldsymbol{1}$, where the summation is over all transformations.

Anabolism & catabolism

Substrate and reserve serve a dual function; they are a sources of energy as well as building blocks. For this reason, assimilation, dissipation as well as growth can be partitioned into a catabolic and an anabolic flux, see Table 4.1 for aerobic metabolism. The table does not present the anabolic aspect of dissipation because the stuctural compounds are degraded and synthesized at the same rate with additional use of reserve, making that the overall stoichiometry is identical to the catabolic aspects. This turnover of structure complicates the behaviour of isotopes, however. In anaerobic metabolism dioxygen O is replaced by another electron acceptor, but otherwise the derivations are similar. If other than the mineral products are formed, such feaces for animals, we need extra information of how this product formation is linked to the catabolic and anabolic aspects to be able to partition the flux. In the catabolic aspect, substrates are transformed to extract energy

Table 4.1: The yield coefficients (upper panel) and the chemical indices (lower panel) for the 8 compounds that are involved in the 5 transformations with one reserve and one structure; the energy and carbon substrates, X and S respectively, are frequently identical. Assimilation, dissipation and growth have a catabolic and an anabolic aspect; that of dissipation is discussed in the section on isotopes. The yield coefficients stand for

$Y^a_{CS} = 0$ $Y^a_{HS} = n_{HS}/2 - n_{HE}/2 - Y^a_{NS}3/2$ $Y^a_{OS} = n_{OS}/2 - n_{OE}/2 - Y^a_{HS}/2$ $Y^a_{NS} = n_{NS} - n_{NE}$
$Y^c_{C*} = n_{C*}$ $Y^c_{H*} = -n_{N*}3/2 + n_{H*}/2$ $Y^c_{O*} = -1 + n_{O*}/2 - Y^a_{H*}/2$ $Y^c_{N*} = n_{N*}$
$Y^a_{CE} = 0$ $Y^a_{HE} = n_{HE}/2 - n_{HV}/2 - Y^a_{NE}3/2$ $Y^a_{OE} = n_{OE}/2 - n_{OV}/2 - Y^a_{HE}/2$ $Y^a_{NE} = n_{NE} - n_{NV}$

Following microbiological tradition, substrate is chosen as reference in the yield coefficients for assimilation and reserve for dissipation and growth. The specific rates $j_{EA} = \dot{p}_A/\mu_E$, $j_{ED} = \dot{p}_D/\mu_E$ and $j_{EG} = \dot{p}_G/\mu_E$ are specified by the DEB theory (see Tables 3.5 and 3.6). The specific dissipation flux $j_{ED} = j_{EM}/\kappa$ for V1-morphs (or $j_{ED} = j_{EM}$ if $\kappa = 1$).

symbol	processes	C: carbon dioxide	H: water	O: dioxygen	N: ammonia	X: E-substrate	S: C-substrate	E: reserve	V: structure	specific rates
A_c	assim. (cat)	Y^c_{CX}	Y^c_{HX}	Y^c_{OX}	Y^c_{NX}	-1	0	0	0	$(y_{XE} - 1)j_{EA}$
A_a	assim. (ana)	0	Y^a_{HS}	Y^a_{OS}	Y^a_{NS}	0	-1	1	0	j_{EA}
D	dissipation	Y^c_{CE}	Y^c_{HE}	Y^c_{OE}	Y^c_{NE}	0	0	-1	0	j_{ED}
G_c	growth (cat)	Y^c_{CE}	Y^c_{HE}	Y^c_{OE}	Y^c_{NE}	0	0	-1	0	$(1 - y_{VE})j_{EG}$
G_a	growth (ana)	0	Y^a_{HE}	Y^a_{OE}	Y^a_{NE}	0	0	-1	1	$y_{VE}j_{EG}$
C	carbon	1	0	0	0	n_{CX}	1	1	1	
H	hydrogen	0	2	0	3	n_{HX}	n_{HS}	n_{HE}	n_{HV}	
O	oxygen	2	1	2	0	n_{OX}	n_{OS}	n_{OE}	n_{OV}	
N	nitrogen	0	0	0	1	n_{NX}	n_{NS}	n_{NE}	n_{NV}	

and all the products are excreted. Since the catabolic aspect of growth concerns the use of reserve, just like maintenance, the stoichiometries of the two processes are identical, and different from the anabolic aspect of growth. In the anabolic aspect, some of the substrates are incorporated in biomass, others are excreted; anabolic processes typically require energy derived from catabolic processes. Since the anabolic aspect is a fixed fraction of the total flux (both for assimilation and for growth), this partitioning does not imply an extension of the number of independent fluxes in the total metabolism, which remains 3 (assimilation, dissipation and growth). Phosphates and other micro-nutrients are not included for simplicity's sake.

If we assemble a matrix of chemical indices $\boldsymbol{n}$, with 4 elements in the rows and 8 compounds in the columns, and a matrix of yield coefficients $\boldsymbol{Y}$, with 8 compounds in the rows and 5 transformations in the columns (Table 4.1 presents the transposed $\boldsymbol{Y}$ rather than $\boldsymbol{Y}$, for typographic reasons), then the conservation law for elements implies that $\boldsymbol{nY} = \boldsymbol{0}$; it takes only simple book keeping and some patience to solve these yield

coefficients.

The assimilation flux of reserves depends on the concentrations of the complementary compounds substrates, dioxygen and ammonia. The SU rule for the assimilation rate of reserves j_{EA} for $x = X/K_X$, $s = S/K_S$, $o = O/K_O$, $n = N/K_N$ work out as follows:

$$\begin{aligned} j_{EA} &= \frac{j_{EAm}}{1 + \sum_i A_i^{-1} - \sum_i B_i^{-1} + \sum_i C_i^{-1} - D^{-1}} \quad \text{with} \\ & A_i = x,\, s,\, o,\, n; \quad B_i = x+s,\, x+o,\, x+n,\, s+o,\, s+n,\, o+n \\ & C_i = x+s+o,\, x+s+n,\, x+o+n,\, s+o+n; \quad D = x+s+o+n \end{aligned}$$

where X, S, O and N are the concentrations of energy substrate, carbon substrate, dioxygen and ammonia, K_X, K_S, K_O and K_N are the half saturation constants; j_{EAm} is the maximum specific assimilation rate of reserves. The consumption of substrates, dioxygen and ammonia follow from the production of reserve via fixed coupling coefficients. A rather small range of concentrations of substrates, dioxygen and ammonia limit assimilation simultaneously. In many practical applications we have at abundant dioxygen and $x \ll n$ or $x \gg n$

$$j_{EA} \simeq \frac{j_{EAm}}{1 + x^{-1}} = \frac{j_{EAm} X}{K_X + X} \quad \text{or} \quad j_{EA} \simeq \frac{j_{EAm}}{1 + n^{-1}} = \frac{j_{EAm} N}{K_N + N}$$

This is the familiar standard formulation for single-substrate limitation. If energy and carbon substrate is identical, we should $s \to \infty$ to remove the extra limitation by carbon. This might seem to be counter intuitive, because we in fact have $x = s$. The explanation is that a single molecule is used for both energy and carbon, so we remove waiting time compared to the situation for two different molecules.

The specific rate of appearance of ammonia in association with maintenance, for instance, is $j_{NM} = n_{NE} j_{EM}$; that of dioxygen is $Y^c_{OE}\, j_{EM}$. If we assemble the rates in Table 4.1 in a 5-vector $\dot{\boldsymbol{k}}$, the 8-vector of specific rates of appearances or disappearances of compounds is given by $\boldsymbol{Y}\dot{\boldsymbol{k}}$, where each rate can be positive as well as negative.

Reserve density dynamics of V1-morphs is $\frac{d}{dt} m_E = j_{EA} - \dot{k}_E m_E$, where $\dot{k}_E$ is the reserve turnover rate. The specific maintenance flux of reserve is constant at rate $j_{EM} = y_{EV}\, \dot{k}_M$. The specific growth rate is $\dot{r} = \frac{m_E \dot{k}_E - j_{EM}}{m_E + y_{EV}}$, where $m_E \dot{k}_E - j_{EM}$ is the reserve flux that is released from the reserves minus the losses through maintenance; $m_E + y_{EV}$ are the specific costs for new reserve plus structure. So the growth rate depends on the reserve density m_E, not on the nutrient concentrations directly; growth ceases at reserve density $m_E = j_{EM}/\dot{k}_E$, where all mobilized reserves are used for maintenance. The flux of reserve associated with growth is $j_{EG} = y_{EV}\dot{r}$.

The assumption by [530] that the specific entropy of a compound is constant directly translates in the entropy balance equation for compound $*$

$$\overline{s}_* = Y^c_{C*}\overline{s}_C + Y^c_{H*}\overline{s}_H + Y^c_{O*}\overline{s}_O + Y^c_{N*}\overline{s}_N$$

which gives the specific entropy of compound $*$, $\overline{s}_*$, given the specific entropies of C, H, O and N, as presented in Table 4.4.

It is important to realize that the microchemical reaction equations are still far away from a detailed chemical description of metabolism. Compounds can be produced in one

part of the pathway, and used in another part, and do not occur in the micro- or macro-chemical reaction equation.

[297] gives such a decomposition for methanotrophy and [64] for the anaerobic oxidation of ammonia (anammox). In the example of methanotrophy, the energy and carbon source are identical, in the anammox the are different. The example for anammox shows how additional biochemical information can be used in these decompositions and how the number of conserved quantities can be extended. Here with eletrical charge, but extensions with other chemical elements work out similarly.

Type I methanotrophy

The macro-chemical reaction equation for methanotrophs is

$$\mathrm{CH_4} + Y_{CX}\,\mathrm{CO_2} + Y_{OX}\,\mathrm{O_2} + Y_{NX}\,\mathrm{NH_3} + Y_{HX}\,\mathrm{H_2O} \rightarrow Y_{WX}\,\mathrm{CH}_{n_{HW}}\mathrm{O}_{n_{OW}}\mathrm{N}_{n_{NW}}$$

Methanotrophs use methane (CH_4) as energy source; methane is the only carbon source in Type I methanotrophs, such as *Methylomonas*, *Methylomicrobium*, *Methylobacter* and *Methyloccus*, which use the monophosphate pathway to process formaldehyde (CH_2O), a metabolite of methane. Methane and carbon dioxide (CO_2) are carbon sources for Type II methanotrophs, such as *Methylosinus* and *Methylocystis*, which use the serine pathway to process formaldehyde. These organisms can also fix dinitrogen. We here selected type I methanotrophs to illustrate the stoichiometric principles because very simple compounds are involved only, see [297]. So we have $n_{CX} = n_{CS} = 1$, $n_{HX} = n_{HS} = 4$, $n_{OX} = n_{OS} = 0$ and $n_{NX} = n_{NS} = 0$.

Figure 4.1 gives the specific fluxes of compounds as functions of the specific growth rate. It also gives the ratio of the carbon dioxide and dioxygen fluxes, and that of ammonia and dioxygen. Many text books deal with these ratios as being proportional to the specific growth rate. This obviously does not apply here.

The result we obtained is that we can relate the yield coefficients and chemical indices of biomass to (varying) concentrations of nutrients in the environment, and to a (varying) reserve density, which involves a number of constant energy budget parameters. These constant parameters are the specific maintenance rate $\dot{k}_M$, the reserve turnover $\dot{k}_E$, the yield of structure on reserve y_{VE}, the chemical indices of reserve and structure, and the parameters of the assimilation process. Some text books mention that methanotrophs consume two methane molecules for each produced carbon dioxide molecule. Our analysis shows, however, that such a fixed relationship does not exist; it is very sensitive to environmental conditions.

Methane burning in assimilations' catabolic transformation should generate enough energy to drive assimilations' anabolic component. For the chemical potential μ_X of methane and μ_E of reserve, we have $\mu_X\, j^C_{XA} > (\mu_E - \mu_X) j^A_{XA}$ or $\mu_X(1 - y_{EX}) > (\mu_E - \mu_X) y_{EX}$ or $y_{EX} > \mu_E/\mu_X$.

Notice that ammonia is taken up as well as excreted; a phenomenon that only recently attracted attention in algal physiology. We know a priori that ammonium uptake always exceeds excretion at steady state.

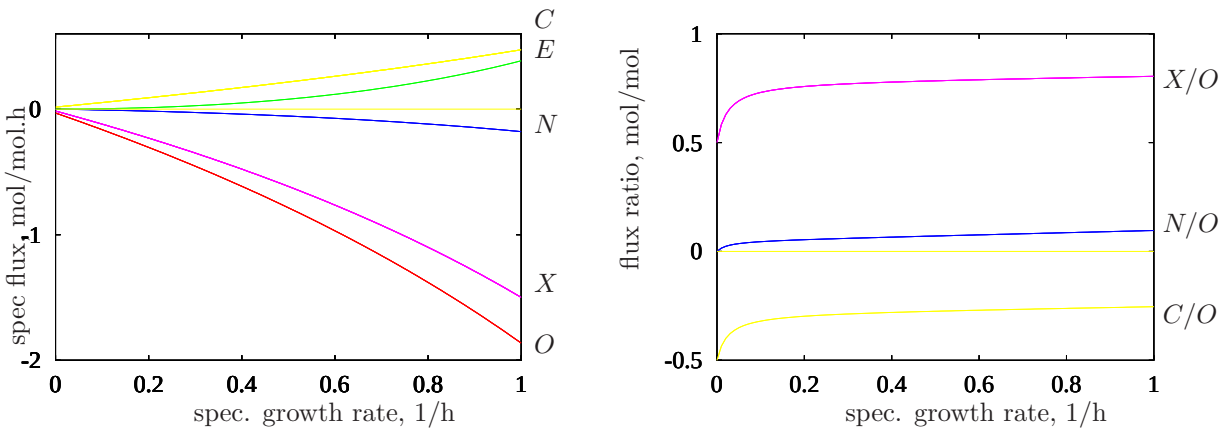

Figure 4.1: The specific fluxes (left graph) of (from top to bottom) carbon dioxide C, reserves E, ammonia N, methane X and dioxygen O as a function of the specific growth rate of a methanotroph. That of water and structure are not shown. The ratio of the fluxes (right graph) of methane (top curve), carbon dioxide (bottom curve) and ammonia (middle curve), with that of dioxygen. Parameters: max spec assimilation rate (of E) $j_{EAm} = 1.2$ mol/(h.mol), yield coefficients $y_{EX} = 0.8$ mol/mol and $y_{VE} = 0.8$ mol/mol, maintenance rate constant $\dot{k}_M = 0.01$ 1/h, reserve turnover rate $\dot{k}_E = 2.00$ 1/h. Chemical indices of reserve and structure: $n_{HE} = 1.8$; $n_{OE} = 0.3$; $n_{NE} = 0.3$; $n_{HV} = 1.8$; $n_{OV} = 0.5$; $n_{NV} = 0.1$.

Anammox

The anammox (anaerobic ammonia oxidation) process is only known from the chemolithotrophic planctomycete *Brocadia anammoxidans*. It generates energy from $NH_4^+ + NO_2^- \rightarrow N_2 + 2\,H_2O$, and fixes carbon from $CO_2 + 2\,NO_2^- + H_2O \rightarrow CH_2O + 2\,NO_3^-$. The measured macrochemical reaction equation at specific growth rate $\dot{r} = 0.0014$ h^{-1} is [540]

$$1\,NH_4^+ + 1.32\,NO_2^- + 0.066\,HCO_3^- + 0.13\,H^+ \rightarrow \\ 1.02\,N_2 + 0.26\,NO_3^- + 0.066\,CH_2O_{0.5}N_{0.15} + 2.03\,H_2O$$

Also is known that N_2 comes from NH_4^+ and NO_2^- and that N in biomass comes from NH_4^+. The coefficients depend on the growth rate in a way that has been evaluated by Bernd Brandt [64] who also corrected and detailed the equation. We here extend the elemental balance equations with that for the electric charge. Table 4.2 presents the summary of the decomposition of the macrochanical reaction equation.

Figure 4.2 shows how the fluxes of the compounds that are involved in the anammox transformation depend on the growth rate. The chemical indices for biomass depend on the specific growth rate as $n_{iw} = \frac{n_{iV} + m_E n_{iE}}{1 + m_E}$ where the reserve density is given by $m_E = j_{EA}/\dot{k}_E = y_{EV}\frac{\dot{k}_M + \dot{r}}{\dot{k}_E - \dot{r}}$. The specific growth flux equals $j_{EG} = \dot{r} y_{EV}$ and the specific maintenance flux $\dot{k}_M y_{EV}$. For further discussion see [64].

Isotopes

{133}

Isotope dynamics can be followed in the context of DEB theory, due to the fact that DEB theory specifies *all* mass fluxes. We here derive the dynamics, excluding physiological

Table 4.2: The yield coefficients (upper panel) and the chemical indices (lower panel) for the nine compounds that are involved in the five transformations by anammox bacteria. The yield coefficients are

$$Y^A_{CS} = -n^{-1}_{NE} \qquad Y^A_{H_1S} = Y^A_{CS}$$
$$Y^A_{HS} = (3 + Y^A_{CS}(n_{HE} - 2))/2 \qquad Y^A_{N_3S} = (3 - n_{OE})Y^A_{CS} + Y^A_{HS}$$
$$Y^M_{N_3E} = (-4 - n_{HE} + 2n_{OE} + 3n_{NE})/6 \qquad Y^M_{SE} = n_{NE} - Y^M_{N_3E}$$
$$Y^M_{H_1E} = 1 + Y^M_{N_3E} \qquad Y^M_{HE} = n_{OE} - 2Y^M_{N_3E} - 3$$
$$Y^G_{N_3E} = Y^M_{N_3E} - (-4 - n_{HV} + 2n_{OV} + 3n_{NV})/6 \qquad Y^G_{H_1E} = Y^G_{N_3E}$$
$$Y^G_{HE} = -2Y^G_{N_3E} + n_{OE} - n_{OV} \qquad Y^G_{SE} = -Y^G_{N_3E} + n_{NE} - n_{NV}$$

Following microbiological tradition, substrate is chosen as reference in the yield coefficients: ammonium for assimilation, and reserve for maintenance and growth. The yield coefficients follow from the conservation law for elements and electrical charge. The DEB theory provides the specific rates j_{EA}, j_{EM}, and j_{EG} (see text). Note that the yield coefficients for the catabolic aspect of growth equal those for maintenance.

symbol	processes	C: HCO_3^-	H_1: H^+	H: H_2O	S: NH_3	N: N_2	N_3: NO_2^-	N_5: NO_3^-	E: reserve	V: structure	specific rates
A_C	assim. (cat.)	0	–1	2	–1	1	–1	0	0	0	$(y_{SE} - n_{NE})j_{EA}$
A_A	assim. (ana.)	Y^A_{CS}	$Y^A_{H_1S}$	Y^A_{HS}	–1	0	$Y^A_{N_3S}$	$-Y^A_{N_3S}$	$-Y^A_{CS}$	0	$n_{NE}j_{EA}$
M	maintenance	1	$Y^M_{H_1E}$	Y^M_{HE}	Y^M_{SE}	0	$Y^M_{N_3E}$	0	–1	0	j_{EM}
G_C	growth (cat.)	1	$Y^M_{H_1E}$	Y^M_{HE}	Y^M_{SE}	0	$Y^M_{N_3E}$	0	–1	0	$(1 - y_{VE})j_{EG}$
G_A	growth (ana.)	0	$Y^G_{H_1E}$	Y^G_{HE}	Y^G_{SE}	0	$Y^G_{N_3E}$	0	–1	1	$y_{VE}\, j_{EG}$
C	carbon	1	0	0	0	0	0	0	1	1	
H	hydrogen	1	1	2	3	0	0	0	n_{HE}	n_{HV}	
O	oxygen	3	0	1	0	0	2	3	n_{OE}	n_{OV}	
N	nitrogen	0	0	0	1	2	1	1	n_{NE}	n_{NV}	
$+$	charge	–1	1	0	0	0	–1	–1	0	0	

effects of isotopes. Applications of isotope dynamics could include history reconstructions and monitoring particular fluxes.

We neglect the decay of isotopes, so if this decay can't be neglected (e.g. for unstable isotopes), the present treatment should be adjusted. We assume that transformations convert substrates into products, that the isotope ratios of the substrates are known. The isotope ratios of the products are assumed to be known at time zero only, and the task is to specify the trajectory of the ratio given a specification of the transformation rate as function of time. We first discuss the process of reshuffling of atoms in transformations, which leads to a re-distribution of isotopes, then we study fractionation, and finally we apply the theory to the standard DEB model and discuss some applications.

We take the fluxes of substrate in a transformation to be negative by definition and that of products positive. Since the roles of substrates and products are asymmetrical with respect to isotope transduction, the next section assumes that all substrates and products are specified, even if they happen to be chemically identical. Some transformations might use e.g. water both as substrate and as product; water should then appear twice in the equation for the transformation. Table 4.3 introduces the notation. Notice that n_{ij}^{0k} only gives the frequency of isotope 0 of element i relative to carbon if compound j actually has

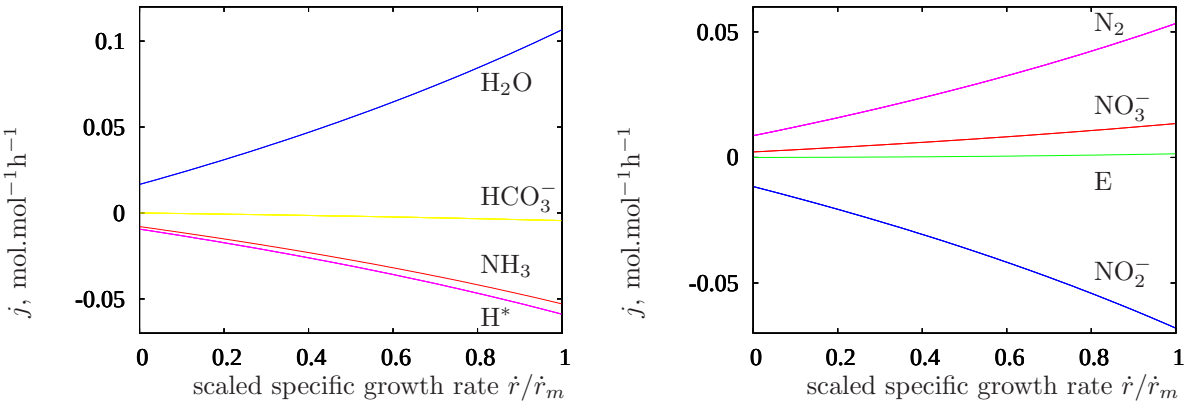

Figure 4.2: The specific fluxes of the compounds as a function of the specific growth rate as fraction of the maximum of $\dot{r}_m = 0.003$ h^{-1} of the anammox bacteria. DEB Parameters: $\dot{k}_E = 0.0127$ h^{-1}, $\dot{k}_M = 0.000811$ h^{-1}, $y_{SE} = 8.80$, $y_{VE} = 0.8$ C-mol/C-mol reserve. Composition parameters: $n_{HE} = 2$, $n_{OE} = 0.46$, $n_{NE} = 0.25$, $n_{HV} = 2$, $n_{OV} = 0.51$, $n_{NV} = 0.125$.

carbon; otherwise the same strategy should be followed as for n_{ij}, which leaves open the possibility to work in e.g. H-moles for compounds that have no carbon, or in N-moles.

The literature on isotope distributions, see e.g. [97], uses the isotope ratio R, which stands for the ratio of the frequencies of one isotope of a certain element (typically the rare type) and that of another (typically the most common type). Sometimes R is the ratio of masses, rather than frequences. This ratio relates to δ^0_{ij} as $R = \frac{\delta^0_{ij}}{1-\delta^0_{ij}}$. Data typically refer to isotope frequencies relative to a standard "ref" and are denoted by

$$\delta_i = 1000\frac{R_i - R_{\text{ref}}}{R_{\text{ref}}} = 1000\left(\frac{\delta^0_{ij}}{1-\delta^0_{ij}}\frac{1-\delta^{0\text{ref}}_{ij}}{\delta^{0\text{ref}}_{ij}} - 1\right)$$

This notation does not make explicit the compound(s) in which the element i occurs. If the compound occurs in phases A and B, two other frequently used definitions are

$$\Delta_{A-B} = \delta_A - \delta_B; \quad \alpha_{A-B} = \frac{1000+\delta_A}{1000+\delta_B} = \frac{\delta^{0A}_{ij}}{1-\delta^{0A}_{ij}}\frac{1-\delta^{0B}_{ij}}{\delta^{0B}_{ij}}$$

n_{ij}	frequency of element i in compound j
n^0_{ij}	frequency of isotope 0 in element i of compound j in the pool M_j
n^{0k}_{ij}	frequency of isotope 0 in element i of compound j in transformation k
δ^0_{ij}	frequency of isotope 0 of element i in compound j rel. to element i of compound j
Y^k_{ps}	yield of compound p on compound s in transformation k
M_j	mass of compound j in (C-)mole
$\dot{J}_{jk}$	flux of compound j in transformation k in (C-)mole/time
α^{ik}_{ps}	reshuffle parameter of substrate s for product p for element i in transformation k
β^{0k}_{ij}	odds ratio for isotope 0 in transformation k of element i in compound j

Table 4.3: List of symbols for isotope dynamics.

We use this notation only in auxiliary theory (to link predictions to measurements) because in the core theory we need more notational detail in compounds and transformations and a closer link to the underlying processes.

Reshuffling in a single transformation

Let $\mathcal{S}$ be the set of substrates and $\mathcal{P}$ be the set of products. The transformation is completely defined by the set of fluxes $\{\dot{\boldsymbol{J}}_{\mathcal{S}k}, \dot{\boldsymbol{J}}_{\mathcal{P}k}\}$, where the column vectors have elements $\dot{J}_{sk}$ with $s \in \mathcal{S}$ and $\dot{J}_{pk}$ with $p \in \mathcal{P}$, respectively. These fluxes are subjected by the constraints

$$\mathbf{0} = \boldsymbol{n}_{\mathcal{P}}\dot{\boldsymbol{J}}_{\mathcal{S}k} + \boldsymbol{n}_{\mathcal{S}}\dot{\boldsymbol{J}}_{\mathcal{P}k}$$

where matrix $\boldsymbol{n}_{\mathcal{P}}$ has elements n_{ip} for $p \in \mathcal{P}$, and similarly for $\boldsymbol{n}_{\mathcal{S}}$. The number of constraints equals the number of chemical elements that are followed; the constraints can be used to specify some of the fluxes.

The dimensionless reshuffling parameter α_{ps}^{ik}, with $0 \leq \alpha_{ps}^{ik} \leq 1$ specifies what fraction of the atoms of chemical element i in substrate s ends up in product p in transformation k. Given the coefficients n_{is}^{0k} for $s \in \mathcal{S}$, the coefficients n_{ip}^{0k} are given for $p \in \mathcal{P}$ by

$$0 = n_{ip}^{0k}\dot{J}_{pk} + \sum_{s\in\mathcal{S}} \alpha_{ps}^{ik} n_{is}^{0k}\dot{J}_{sk} \quad \text{or} \quad n_{ip}^{0k} = -\sum_{s\in\mathcal{S}} \alpha_{ps}^{ik} n_{is}^{0k}/Y_{ps}^{k}$$

with $1 = \sum_{p\in\mathcal{P}} \alpha_{ps}^{ik}$. If n_s substrates and n_p products exist, the number reshuffle parameters α is $(n_p - 1)n_s$.

In matrix notation we can write

$$\mathbf{0} = \dot{\boldsymbol{J}}_{\mathcal{P}k}^{0i} + \boldsymbol{\alpha}^{ik}\dot{\boldsymbol{J}}_{\mathcal{S}k}^{0i} \quad \text{with} \quad \mathbf{1}^T\boldsymbol{\alpha}^{ik} = \mathbf{1}^T$$

where (column) vector $\dot{\boldsymbol{J}}_{\mathcal{S}k}^{0i}$ has elements $n_{is}^{0k}\dot{J}_{sk}$ and vector $\dot{\boldsymbol{J}}_{\mathcal{P}k}^{0i}$ has elements $n_{ip}^{0k}\dot{J}_{pk}$ and matrix $\boldsymbol{\alpha}^{ik}$ has elements α_{ps}^{ik} with $p \in \mathcal{P}$ and $s \in \mathcal{S}$. Notice that the use of the reshuffling parameters is via the product with the chemical indices, $\alpha_{ps}^{ik}n_{ns}^{0k}$, so the requirement that the sum of the rows of each column of $\boldsymbol{\alpha}^{ik}$ equals 1 is only essential for elements that actually occur in that substrate. If element i does not occur in substrate s, the entries of $\boldsymbol{\alpha}^{ik}$ in column s don't matter. From the conservation of elements and isotopes, we must have

$$0 = \mathbf{1}^T\dot{\boldsymbol{J}}_{\mathcal{P}k}^{i} + \mathbf{1}^T\dot{\boldsymbol{J}}_{\mathcal{S}k}^{i} \quad \text{and} \quad 0 = \mathbf{1}^T\dot{\boldsymbol{J}}_{\mathcal{P}k}^{0i} + \mathbf{1}^T\dot{\boldsymbol{J}}_{\mathcal{S}k}^{0i}$$

where vector $\dot{\boldsymbol{J}}_{\mathcal{S}k}^{i}$ and $\dot{\boldsymbol{J}}_{\mathcal{P}k}^{i}$ have elements $n_{is}\dot{J}_{sk}$ and $n_{ip}\dot{J}_{pk}$, respectively.

To illustrate the application of the reshuffling matrix, consider the oxygenic photosynthesis L:

$$\mathrm{CO_2} + 2\,\mathrm{H_2O} + \text{light} \rightarrow \mathrm{CH_2O} + \mathrm{H_2O} + \mathrm{O_2} \quad \text{or} \quad C + 2\,H \rightarrow X + H' + O$$

where the oxygen atoms of dioxygen are known (from biochemistry) to come from water, not from carbon dioxide; this is why water is both substrate and product in this transformation. Water as product is labelled H' because its isotope composition can deviate for water as substrate H. For this transformation L and isotopes ^{13}C, ^{2}H and ^{18}O we have

$$\begin{array}{cccc} \alpha_{XC}^{CL} = 1 & \alpha_{XH}^{HL} = \frac{1}{2} & \alpha_{XC}^{OL} = \frac{1}{2} & \alpha_{XH}^{OL} = 0 \\ \alpha_{H'C}^{CL} = 0 & \alpha_{H'H}^{HL} = \frac{1}{2} & \alpha_{H'C}^{OL} = \frac{1}{2} & \alpha_{H'H}^{OL} = 0 \\ \alpha_{OC}^{CL} = 0 & \alpha_{OH}^{HL} = 0 & \alpha_{OC}^{OL} = 0 & \alpha_{OH}^{OL} = 1 \end{array} \quad : \quad n_{CX}^{13L} = n_{CC}^{13L} \quad : \quad \begin{array}{c} n_{HX}^{2L} = n_{HH}^{2L} \\ n_{HH'}^{2L} = n_{HH}^{2L} \end{array} \quad : \quad \begin{array}{c} n_{OX}^{18L} = \frac{1}{2}n_{OC}^{18L} \\ n_{OH'}^{18L} = \frac{1}{2}n_{OC}^{18L} \\ n_{OO}^{18L} = 2n_{OH}^{18L} \end{array}$$

$\alpha^{OL}_{XC} = \frac{1}{2}$ tells that half of the oxygen of carbon dioxide ends up in carbohydrate; $\alpha^{OL}_{OH} = 1$ tells that all of the oxygen of water ends up in dioxygen. So the oxygen-isotope distribution in carbon dioxide has no relevance for that in dioxygen (in this transformation).

Suppose we have the absurd reaction mechanism that all substrate atoms of element i are allocated to product molecules after complete randomisation. The isotope ratios of that element are equal in all products, so for product $p \in \mathcal{P}$ we have

$$\frac{n^{0k}_{ip}}{n_{ip}} = \frac{\mathbf{1}^T \dot{\boldsymbol{J}}^{0i}_{\mathcal{S}k}}{\mathbf{1}^T \dot{\boldsymbol{J}}^{i}_{\mathcal{S}k}} \quad \text{or} \quad \dot{\boldsymbol{J}}^{0i}_{\mathcal{P}k} = \dot{\boldsymbol{J}}^{i}_{\mathcal{P}k} \frac{\mathbf{1}^T \dot{\boldsymbol{J}}^{0i}_{\mathcal{S}k}}{\mathbf{1}^T \dot{\boldsymbol{J}}^{i}_{\mathcal{S}k}} \quad \text{and} \quad \alpha^{ik}_{ps} = \frac{\dot{J}^{i}_{pk}}{\mathbf{1}^T \dot{\boldsymbol{J}}^{i}_{\mathcal{P}k}} \quad \text{or} \quad \boldsymbol{\alpha}^{ik} = \frac{\dot{\boldsymbol{J}}^{i}_{\mathcal{P}k} \mathbf{1}^T}{\mathbf{1}^T \dot{\boldsymbol{J}}^{i}_{\mathcal{P}k}}$$

Division of the numerator and denumerator by one of the fluxes, typically a flux of substrate, converts fluxes to yield coefficients which are not time-dependent. Although the mechanism is unrealistic, this choice of reshuffle coefficients can serve as baseline to reduce the number of parameters in specific applications where no information about the mechanism is available. If the transformation is really complex, like in living systems, complete reshuffling might be not too far from reality.

Addition of transformations

Macrochemical reaction equations are typically additions of several (or even many) equations. Transfer of isotopes comes with an asymmetry of the roles of substrates and products, which makes that a particular compound in a macrochemical reaction equation can play both roles, even if no net synthesis or decay of that compound occurs.

Before adding transformations k and l, we extend the set of substrates $\mathcal{S}$ and products $\mathcal{P}$, such that these sets include *all* substrates and compounds, and allow that some of the fluxes are zero, and some compounds occur in both sets. Let $\{\dot{\boldsymbol{J}}_{\mathcal{S}m}, \dot{\boldsymbol{J}}_{\mathcal{P}m}\} = \{\dot{\boldsymbol{J}}_{\mathcal{S}k} + \dot{\boldsymbol{J}}_{\mathcal{S}l}, \dot{\boldsymbol{J}}_{\mathcal{P}k} + \dot{\boldsymbol{J}}_{\mathcal{P}l}\}$ be the sets of fluxes of the total transformation. To define transformation m properly, we must have $n^{0k}_{is} = n^{0l}_{is} = n^{0m}_{is}$ for $s \in \mathcal{S}$, so $\dot{\boldsymbol{J}}^{0i}_{\mathcal{S}m} = \dot{\boldsymbol{J}}^{0i}_{\mathcal{S}k} + \dot{\boldsymbol{J}}^{0i}_{\mathcal{S}l}$. Although generally we will have $n^{0k}_{ip} \neq n^{0l}_{ip}$, we still have $\dot{\boldsymbol{J}}^{0i}_{\mathcal{P}m} = \dot{\boldsymbol{J}}^{0i}_{\mathcal{P}k} + \dot{\boldsymbol{J}}^{0i}_{\mathcal{P}l}$. Further $\alpha^{im}_{ps} \dot{J}^{i}_{sm} = \alpha^{ik}_{ps} \dot{J}^{i}_{sk} + \alpha^{il}_{ps} \dot{J}^{i}_{sl}$. We then have

$$\mathbf{0} = \dot{\boldsymbol{J}}^{0i}_{\mathcal{P}m} + \boldsymbol{\alpha}^{im} \dot{\boldsymbol{J}}^{0i}_{\mathcal{S}m} \quad \text{with} \quad \mathbf{1}^T \boldsymbol{\alpha}^{im} = \mathbf{1}^T$$

and

$$\boldsymbol{\alpha}^{im} \mathrm{diag}(\dot{\boldsymbol{J}}_{\mathcal{S}m}) = \boldsymbol{\alpha}^{ik} \mathrm{diag}(\dot{\boldsymbol{J}}_{\mathcal{S}k}) + \boldsymbol{\alpha}^{il} \mathrm{diag}(\dot{\boldsymbol{J}}_{\mathcal{S}l})$$

Notice that the reshuffle parameters become time-dependent if the ratio of the rates of transformation k and l changes in time. The practice we will only add fully coupled transformations.

Fractionation

Preamble: Fisher's noncentral hypergeometric distribution. Suppose we have m_0 white balls with weight β_0 each and $m_1 = m - m_0$ black balls with weight β_1. The number of white balls in a sample of size n follows Fisher's noncentral hypergeometric distribution if selection is non-interactive, only depends on weight and selection probability is proportional

to weight. For odds ratio $\beta = \beta_0/\beta_1$ and $n \in (0, m)$, the expected number of white balls in the sample is

$$n_0 = P_1/P_0 \quad \text{with } P_k = \sum_{y=\max(0,n-m_1)}^{\min(n,m_0)} \left(\begin{array}{c} m_0 \\ y \end{array} \right) \left(\begin{array}{c} m_1 \\ n-y \end{array} \right) \beta^y y^k$$

or

$$n_0 \approx \frac{-2c}{b - \sqrt{b^2 - 4ac}} = \frac{rm_0\beta}{r\beta + 1} \quad \text{with } r > 0 \text{ such that } n = \frac{rm_0\beta}{r\beta+1} + \frac{rm_1}{r+1}$$

where $a = \beta - 1$, $b = n - m_1 - (m_0 + n)\beta$, $c = m_0 n\beta$. Multivariate extensions are known. For isotope applications we focus on fractions m_0/m in the total flux and n_0/n in the sub-flux (the anabolic flux). The fluxes are converted to pools by integration over a time increment, which makes that n is not necessarily small relative to m_0 and m_1.

For large m_0 and m_1 relative to n, this non-central hypergeometric distribution converges to the binomial distribution with mean $n_0 = \frac{nm_0\beta}{m_0\beta+m_1}$. This applies if isotope selection occurs from the pool, such as that of dioxygen or carbon dioxide. Notice that this mean only depends on $\frac{m_0}{m_1} = \frac{\delta^0_{ij}}{1-\delta^0_{ij}}$, and not on m_0 and m_1 separately.

Fractionation from pools

Fractionation can occur in the selective uptake of dioxygen and carbon dioxide (mostly by phototrophs) and in the selective release of carbon dioxyde, N-waste and water. The latter might be of some importance for terrestrial organisms, where this release is associated with a phase transition for liquid (= organism) to gas.

The selective uptake of dioxygen, where the isotope frequency in assimilation, dissipation and growth follows a binomial distribution with

$$n^{0k}_{ij} = \frac{n_{ij}\beta^{0k}_{ij}}{\beta^{0k}_{ij} - 1 + 1/\delta^0_{ij}}, \quad \text{so } n^{0k}_{OO} = \frac{2\beta^{0k}_{OO}}{\beta^{0k}_{OO} - 1 + 1/\delta^0_{OO}}$$

For odds ratio $\beta^{0k}_{ij} = 1$, this gives $n^{0k}_{ij} = n_{ij}\delta^0_{ij}$. In the case of dioxygen, there is little reason to expect that this relationship depends on the transformation k.

Suppose that the odds ratio equals the ratio of molecular velocities and that ^{10}O and ^{16}O combine randomly in dioxygen. So a fraction $(1-\delta^{18}_{OO})^2$ of the dioxygen molecules has velocity $\dot{v}_{32}$, a fraction $(\delta^{18}_{OO})^2$ has velocity $\dot{v}_{36}$, and a fraction $2\delta^{18}_{OO}(1-\delta^{18}_{OO})$ has velocity $\dot{v}_{34}$ at some given temperature. All dioxygen molecules have the same kinetic energy so $32\dot{v}^2_{32} = 34\dot{v}^2_{34} = 36\dot{v}^2_{36}$. So

$$\beta^{18k}_{OO} = \frac{(1-\delta^{18}_{OO})\dot{v}_{34} + \delta^{18}_{OO}\dot{v}_{36}}{(1-\delta^{18}_{OO})\dot{v}_{32} + \delta^{18}_{OO}\dot{v}_{34}} = \frac{1 - \delta^{18}_{OO} + \delta^{18}_{OO}\sqrt{34/36}}{(1-\delta^{18}_{OO})\sqrt{34/32} + \delta^{18}_{OO}} \simeq \sqrt{\frac{32}{34}} = 0.97$$

The latter approximation applies for small δ^{18}_{OO}. However, it is very doubtfull that this simple reasoning applies; the link between molecular and macroscopic phenomena is typically less direct.

The observations for ^{13}C in the oxydative photosynthesis L are: $^{13}\delta\, C = -8$ for CO_2 in the atmosphere, and -28 from carbohydrate in C_3-plants [152, p44]. The $R_{\text{ref}} = 0.01191$ for carbon in the PDB standard [152, p34]. So $R = 0.011091$ for $^{13}CO_2$ and 0.010750 for $^{13}CH_2O$. This gives $\delta^{13}_{CC} = R/(1+R) = 0.010969$ for $^{13}CO_2$ and $\delta^{13}_{CX} = 0.010750$ for $^{13}CH_2O$. The odds ratio for $^{13}CO_2$ is $\beta^{13\,L}_{CC} = \frac{1/\delta^{13}_{CC}-1}{1/\delta^{13}_{CX}-1} = 0.97982$; a small deviation from 1 gives a strong fractionation.

Selection from food, reserve and structure as pools is less likely. Food is processed as whole items; at the interface of reserve and structure mobilization SUs are at work locally with no "knowlegde" of the neighbouring reserve molecules. Selection is more likely in mobilized fluxes that have several fates; isotopes can affect binding strength in a molecule and so the energy required to transform the compound; compounds with light isotopes are more easily degraded, so more likely to be used for catabolic, rather than anabolic purposes.

Fractionation from fluxes

Definition: Suppose that a molecule of a compound has more than one possible fate in a transformation. Selection occurs if the probability on the fate of a molecule depends on the presence of one or more isotopes. Notice that a change in isotope ratio can well be the result of reshuffling, rather than selection. Reshuffling always occurs, selection will be rare. We here assume that each molecule in a well-mixed pool has the same probability to be selected to partake in a transformation, independent of its isotope composition; selection only interferes with the fate of the mobilized molecule. It is conceivable, however, that selection occurs in the mobilization process, not in the destination.

Suppose that the fluxes of substrates $\dot{\boldsymbol{J}}_{\mathcal{S}k}$ are partitioned into two fluxes (e.g. a catabolic and an anabolic one) as $\dot{\boldsymbol{J}}_{\mathcal{S}k_a} = \kappa^a_k \dot{\boldsymbol{J}}_{\mathcal{S}k}$ and $\dot{\boldsymbol{J}}_{\mathcal{S}k_c} = \kappa^c_k \dot{\boldsymbol{J}}_{\mathcal{S}k}$, with $1 = \kappa^c_k + \kappa^a_k$. The partitioning is, however, selective for the isotope of element i in compound j.

We must have $n^{0k}_{ij}\dot{J}_{jk} = n^{0k_a}_{ij}\dot{J}_{jk_a} + n^{0k_c}_{ij}\dot{J}_{jk_c}$ or $n^{0k}_{ij} = n^{0k_a}_{ij}\kappa^a_k + n^{0k_c}_{ij}\kappa^c_k$. Again we write $n^{0k}_{ij} = \delta^0_{ij} n_{ij}$ and introduce an odds ratio $\beta^{0k_a}_{ij}$ on an isotope of type 0 of element i in compound j in transformation k_a. The number of isotopes in the anabolic flux integrated times a time increment follows Fisher's noncentral hypergeometric distribution. This results in the approximation

$$\begin{aligned} n^{0k_a}_{ij} &\simeq \frac{2n^{0k}_{ij}\beta^{0k_a}_{ij}}{\sqrt{B^2 + 4(1-\beta^{0k_a}_{ij})\beta^{0k_a}_{ij} n^{0k}_{ij}\kappa^a_k} - B} \quad \text{with } B = n^{0k}_{ij} - \kappa^c_k - (n^{0k}_{ij} + \kappa^a_k)\beta^{0k_a}_{ij} \\ n^{0k_c}_{ij} &= \frac{n^{0k}_{ij} - n^{0k_a}_{ij}\kappa^a_k}{\kappa^c_k} \end{aligned}$$

If $\beta^{0k_a}_{ij} = 1$, we have $n^{0k_a}_{ij} = n^{0k}_{ij}$ and the process is unselective. We must have

$$n^{0k}_{ij} \geq n^{0k_a}_{ij}\kappa^a_k \quad \text{and} \quad B^2 + 4(1-\beta^{0k_a}_{ij})\beta^{0k_a}_{ij} n^{0k}_{ij}\kappa^a_k \geq 0$$

Notice that only molecules can be selected on the basis of having a particular isotope of a particular element; the selection is not on elements independently. Once the selective

element i is determined for a compound j, $\beta_{hj}^{0k_a} = 1$ for all $h \neq j$. The selection on a single isotope of a particular atom in a particular compound is the simplest possibility; many more complex forms of selection can exist.

Suppose that substrate S is subjected to selection with respect to element I and that $\boldsymbol{\alpha}^{ik_a}$ and $\boldsymbol{\alpha}^{ik_c}$ are the reshuffling parameters of the anabolic and the catabolic sub-fluxes. So the fractions κ_k^a and κ_k^c apply to flux $\dot{J}_S$. Let $n_{IS}^{0k} = n_{IS}\delta_{IS}^0$. In adding these two fluxes, we should take into account that the anabolic flux experiences a different isotope frequency for element I than the catabolic flux: $\dot{J}_{Sk}^{0I} = \dot{J}_{Sk_a}^{0I} + \dot{J}_{Sk_c}^{0I} = (n_{IS}^{0k_a}\kappa_k^a + n_{IS}^{0k_c}\kappa_k^c)\dot{J}_{Sk}$. Let $\dot{\boldsymbol{J}}_{\mathcal{S}k}^{0I*}$ be $\dot{\boldsymbol{J}}_{\mathcal{S}k}^{0I}$, but with element S replaced by this modified flux $\dot{J}_{Sk}^{0I}$. The reshuffle parameters $\boldsymbol{\alpha}^{Ik}$ are not affected by selection. The coefficients n_{Ip}^{0I} in $\dot{\boldsymbol{J}}_{\mathcal{P}k}^{0I}$ are now given by

$$\mathbf{0} = \dot{\boldsymbol{J}}_{\mathcal{P}k}^{0I} + \boldsymbol{\alpha}^{Ik}\dot{\boldsymbol{J}}_{\mathcal{S}k}^{0I*} \quad \text{with} \quad \boldsymbol{\alpha}^{Ik}\text{diag}(\dot{\boldsymbol{J}}_{\mathcal{S}k}) = \boldsymbol{\alpha}^{Ik_a}\text{diag}(\dot{\boldsymbol{J}}_{\mathcal{S}k_a}) + \boldsymbol{\alpha}^{Ik_c}\text{diag}(\dot{\boldsymbol{J}}_{\mathcal{S}k_c})$$

Application to the standard DEB model

The focus is on the isotope dynamics of reserve E and structure V with food X as substrate in the standard DEB model. This model assumes that dioxygen is a non-limiting substrate, which excludes applications in micro-aerobic environments (e.g. parasites inside hosts), where we have to deal with transitions from aerobic metabolism to fermentation. Drinking is an extension of the standard model (and includes modules for evaporation), see section 4.8.1 for remarks on isotope dynamics linked to double labelled water.

The three basic fluxes assimilation, dissipation and growth each have a catabolic and an anabolic aspect. The rato of the use of dioxygen in the anabolic and catabolic fluxes is not equal to that of the organic substrate, so the situation is more complex than described in the previous section. For simplicity's sake, we now assume that the atoms of the mineral products all originate from the organic substrate or from dioxygen. Since it is known that e.g. carbon dioxyde is both product and substrate, at least in some transformations, this assumption need not be correct and applications might urge to change this assumption.

Under extreme starvation conditions shrinking might occur; the anatomy of this transformation is basically identical to that of dissipation.

The chemical indices for the minerals $\mathcal{M} = (C, H, O, N)$ and the organic compounds $\mathcal{O} = (X, V, E, P)$

$$\boldsymbol{n}_{\mathcal{M}} = \begin{pmatrix} 1 & 0 & 0 & n_{CN} \\ 0 & 2 & 0 & n_{HN} \\ 2 & 1 & 2 & n_{ON} \\ 0 & 0 & 0 & n_{NN} \end{pmatrix}; \quad \boldsymbol{n}_{\mathcal{O}} = \begin{pmatrix} n_{CX} & n_{CV} & n_{CE} & n_{CP} \\ n_{HX} & n_{HV} & n_{HE} & n_{HP} \\ n_{OX} & n_{OV} & n_{OE} & n_{OP} \\ n_{NX} & n_{NV} & n_{NE} & n_{NP} \end{pmatrix}$$

are assumed to be known and $\mathbf{0} = \boldsymbol{n}_{\mathcal{M}}\boldsymbol{Y}_{\mathcal{M}s}^k + \boldsymbol{n}_{\mathcal{O}}\boldsymbol{Y}_{\mathcal{O}s}^k$ so $\boldsymbol{Y}_{\mathcal{M}s}^k = -\boldsymbol{n}_{\mathcal{M}}^{-1}\boldsymbol{n}_{\mathcal{O}}\boldsymbol{Y}_{\mathcal{O}s}^k$ for any choice of organic substrate s. Many aquatic organisms use ammonia as N-waste, so $n_{CN} = 0$, $n_{HN} = 3$, $n_{ON} = 0$, $n_{NN} = 1$. Since $\boldsymbol{n}_{\mathcal{M}}^{-1}$ is well-defined, $\boldsymbol{Y}_{\mathcal{M}s}^k$ is known, once $\boldsymbol{Y}_{\mathcal{O}s}^k$ is given.

Assimilation

Assimilation A is defined as the transformation

$$Y_{XE}^A X + Y_{OE}^A O \rightarrow Y_{EE}^A E + Y_{PE}^A P + Y_{HE}^A H + Y_{NE}^A N + Y_{CE}^A C$$

for food X, dioxygen O, reserve E, feaces P, water H, N-waste N, carbon dioxide C. The organic yield coefficients are

$$\boldsymbol{Y}^A_{\mathcal{O}E} = (\ Y^A_{XE} \quad Y^A_{VE} \quad Y^A_{EE} \quad Y^A_{PE}\ )^T = (\ -\tfrac{1}{y_{EX}} \quad 0 \quad 1 \quad \tfrac{y_{PX}}{y_{EX}}\ )^T$$

from which follow the mineral yield coefficients $\boldsymbol{Y}^A_{\mathcal{M}E} = (\ Y^A_{CE} \quad Y^A_{HE} \quad Y^A_{OE} \quad Y^A_{NE}\ )^T = -\boldsymbol{n}^{-1}_{\mathcal{M}}\boldsymbol{n}_{\mathcal{O}}\boldsymbol{Y}^A_{\mathcal{O}E}$; the assimilation flux $\dot{J}_{EA}$ is determined by DEB theory.

The anabolic fraction is $\kappa^a_A = y_{EX} = 1/y_{XE}$, so $\kappa^c_A = 1 - y_{EX}$. If $y_{EX} + y_{PX} = 1$, we have $Y^A_{CX} = 0$.

If selection occurs for isotope 0 of element I of food X in assimilation A, we need to use the apparent coefficient $n^{0A_a}_{IX}$ for reserve, rather than the actual coefficient n^{0A}_{IX}, using $\beta^{0A_a}_{IX}$. Likewise we need to use $n^{0A_c}_{IX}$ for feaces with $\beta^{0A_c}_{IX}$. We have isotope flux $\dot{J}^{0I}_{XA} = (n^{0A_a}_{IX}\kappa^a_A + n^{0A_c}_{IX}\kappa^c_A)\dot{J}_{XA}$.

Dissipation

The catabolic aspect of dissipation just oxidises reserve into minerals. Somatic maintenance, which is one of the components of the dissipation flux, is partly used for the turnover of structure, which means that structure is both a substrate and a product. No net synthesis of structure occurs in association with dissipation.

Dissipation D is defined as the transformation

$$Y^D_{EE}E + Y^D_{VE}V + Y^D_{OE}O \rightarrow -Y^D_{VE}V + Y^D_{HE}H + Y^D_{NE}N + Y^D_{CE}C$$

for reserve E, structure V, dioxygen O, water H, N-waste N, carbon dioxide C.

$$\boldsymbol{Y}^D_{\mathcal{O}E} = (\ Y^D_{XE} \quad Y^D_{VE} \quad Y^D_{EE} \quad Y^D_{PE}\ )^T = (\ 0 \quad 0 \quad 1 \quad 0\ )^T$$

from which follow the mineral yield coefficients $\boldsymbol{Y}^D_{\mathcal{M}E} = (\ Y^D_{CE} \quad Y^D_{HE} \quad Y^D_{OE} \quad Y^D_{NE}\ )^T - \boldsymbol{n}^{-1}_{\mathcal{M}}\boldsymbol{n}_{\mathcal{O}}\boldsymbol{Y}^D_{\mathcal{O}E}$; the dissipation flux $\dot{J}_{ED}$ is given by DEB theory. The parameter $Y^D_{VE} = y^D_{VE}$ is new, and only plays a role in isotope dynamics, because in the bookkeeping of elements the substrate term cancels against the product term. The definition of this parameter is $\dot{J}_{VD_a} = y^D_{VE}\dot{J}_{ED}$, so it links the decomposition of structure to the full dissipation flux of reserve.

The anabolic fraction is κ^a_D, is also a new model parameter and $\kappa^c_D = 1 - \kappa^a_D$. Part of the atoms from the newly synthesized structure might originate from structure, so there is some modeling flexability here for the isotope dynamics. The simplest assumption is that all structure originates from reserve. So for selection of isotope 0 of element i in reserve E in the dissipation process D, we might use the appearent coefficient $n^{0D_a}_{iE}$ for structure with $\beta^{0D_a}_{iX}$. We have isotope flux $\dot{J}^{0i}_{ED} = (n^{0D_a}_{iE}\kappa^a_D + n^{0D_c}_{iE}\kappa^c_D)\dot{J}_{ED}$.

During shrinking, the product-yield of structure is less than the substrate-yield, but otherwise also some synthesis of structure still occurs and the equations remain the same.

Growth

Growth G is defined as the transformation

$$Y_{EV}^G E + Y_{OV}^G O \to Y_{VV}^G V + Y_{HV}^G H + Y_{NV}^G N + Y_{CV}^G C$$

for reserve E, dioxygen O, structure V, water H, N-waste N, carbon dioxide C.

$$\boldsymbol{Y}_{\mathcal{O}E}^G = (\ Y_{XE}^G \quad Y_{VE}^G \quad Y_{EE}^G \quad Y_{PE}^G\ )^T = (\ 0 \quad -y_{VE} \quad 1 \quad 0\ )^T$$

from which follow the mineral yield coefficients $\boldsymbol{Y}_{\mathcal{M}E}^G = (\ Y_{CE}^G \quad Y_{HE}^G \quad Y_{OE}^G \quad Y_{NE}^G\ )^T = -\boldsymbol{n}_{\mathcal{M}}^{-1}\boldsymbol{n}_{\mathcal{O}}\boldsymbol{Y}_{\mathcal{O}E}^G$; the growth flux $\dot{J}_{EG}$ is determined by DEB theory.

The anabolic fraction is $\kappa_G^a = y_{VE} = 1/y_{EV}$, so $\kappa_G^c = 1 - y_{VE}$. We must have $y_{EV} > 1$. Since all structure originates from reserve in the anabolic route. If selection occurs on reserve with isotope 0 in element I in reserve E in growth G, we need to use the appearent coefficient $n_{IE}^{0G_a}$ for structure, rather than the actual coefficient n_{IE}^{0G}, using $\beta_{IE}^{0G_a}$. We have isotope flux $\dot{J}_{EG}^{0I} = (n_{IE}^{0G_a}\kappa_G^a + n_{IE}^{0G_c}\kappa_G^c)\dot{J}_{EG}$.

Changes in isotope fractions

The previous sections quantified the coefficients n_{ij}^{0k}, i.e. the isotope frequency in element i of compound j, relative to the carbon frequency in that compound in the various fluxes. Now we focus on the dynamics of the fraction of isotopes in the pools.

Let fraction δ_{ij}^0 denote the amount isotopes of element i in the pool of compound j as a fraction of the amount of element i in that pool, i.e. $n_{ij}M_j$ and let $n_{ij}^0 M_j$ denote the amount of isotopes of type 0 of element i in the pool of compound j. So

$$\begin{aligned}\frac{d}{dt}\delta_{ij}^0 &= \frac{d}{dt}\frac{n_{ij}^0 M_j}{n_{ij}M_j} = \frac{\frac{d}{dt}n_{ij}^0 M_j}{n_{ij}M_j} - \delta_{ij}^0\frac{\frac{d}{dt}M_j}{M_j} = \frac{\sum_k n_{ij}^{0k}\dot{J}_{jk}}{n_{ij}M_j} - \delta_{ij}^0\frac{\sum_k \dot{J}_{jk}}{M_j}\\ &= \sum_k\left(\frac{n_{ij}^{0k}}{n_{ij}} - \delta_{ij}^0\right)\frac{\dot{J}_{jk}}{M_j} = \sum_k\left(\frac{n_{ij}^{0k}}{n_{ij}} - \delta_{ij}^0\right)\frac{\max(0,\dot{J}_{jk})}{M_j}\end{aligned}$$

The last equality holds because for the processes with $\dot{J}_{jk} < 0$, so for which compound j serves as substrate rather than as product, we have $n_{is}^{0k} = \delta_{is}^0 n_{is} = n_{is}^0$.

We now apply this for $j = E, V$ and $k = A, D_a, G$ to the standard DEB model. The changes in isotope fractions δ_{iE}^0 and δ_{iV}^0, given those in the substrates $\delta_{iX}(t)$ and $\delta_{OO}(t)$ are

$$\begin{aligned}\frac{d}{dt}\delta_{iE}^0 &= \left(\frac{n_{iE}^{0A}}{n_{iE}} - \delta_{iE}^0\right)\frac{\dot{J}_{EA}}{M_E};\quad \frac{d}{dt}M_E = \dot{J}_{EA} + \dot{J}_{EC}\\ \frac{d}{dt}\delta_{iV}^0 &= \left(\frac{n_{iV}^{0G}}{n_{iV}} - \delta_{iV}^0\right)\frac{\dot{J}_{VG}}{M_V} - \left(\frac{n_{iV}^{0D_a}}{n_{iV}} - \delta_{iV}^0\right)\frac{\dot{J}_{VD_a}}{M_V};\quad \frac{d}{dt}M_V = \dot{J}_{VG} + \dot{J}_{VD_s}\end{aligned}$$

where $\dot{J}_{VD_a}$ represents the (negative) flux of structure turnover as part of the somatic maintenance process and the (negative) flux $\dot{J}_{VD_s}$ the shrinking, which only occurs during extreme starvation.

Effects of temperature

Temperature affects rates, and selection depends on odds ratios, which are dimensionless. So effects of temperature on fractionation is only indirect, via effects on physiological rates (assimilation, dissipation, growth). A promising candidate for selection is dissipation. An increase in temperature causes an increase in dissipation, so an increase in the rate at which the isotope-fraction in structure increases. Isotope-enrichment in the food chain has several components: 1) the isotope-fraction of food increases, which cause an increase in the isotope fraction of reserve and structure of the predator 2) body size typically increases with the trophic level, so the life span and mean age, which makes that dissipation-linked enrichment has more time to proceed (independent of food characteristics). So the observation that isotope-fractions increase with the trophic level does not imply an enrichment in the assimilation process.

If the trajectory of isotope-enrichment is well-captured with enrichment in dissipation only (including responses to changes in food availebility and temperature), this would give support for the position of maintenance in the metabolic organisation within the context of DEB theory. Notice that the Marr-Pirt model (for prokaryotes) specifies that structure is used for maintenance, rather than reserve, so it would be impossible to obtain enrichment linked to dissipation with this model.

Products

Apart from faeces, other products can be formed, and products that accumulated in solid form (hair, nails, shells, bones, earplugs, otoliths, wood) are of special interest, because these products 'write' a record of the food-temperature history, which can be reconstructed using chemical identifiers, including the isotope signal. DEB theory specifies that these products are formed in the catabolic fluxes of assimilation, dissipation and/or growth. Given that fractionation occurs at the separation of the anabolic and catabolic sub-fluxes of assimilation, dissipation and growth, the isotope frequency of an element in the products of any of these three fluxes might equal that before separation, that of the catabolic or that of the anabolic flux.

Derivation of Eq (4.7) & (4.8)

{133}

The derivation is as follows, using Table 3.4 at {122} for conversions

$$\begin{aligned}
\frac{d}{dt}l &= \frac{d}{dt}(M_V/M_{Vm})^{1/3} = \frac{\frac{d}{dt}M_V}{3M_V^{2/3}M_{Vm}^{1/3}} \\
&= \frac{\dot{p}_G\eta_{VG}}{3M_V^{2/3}M_{Vm}^{1/3}} = \frac{\dot{p}_G\eta_{VG}}{3l^2M_{Vm}} = \frac{\dot{p}_G}{3l^2\mu_{GV}M_{Vm}} \\
&= \frac{\dot{p}_G}{3l^2[E_G]M_{Vm}/[M_V]} = \frac{\dot{p}_G}{3l^2[E_G]V_m} = \frac{\dot{p}_G}{3l^2[E_G]E_m/[E_m]} \\
&= \frac{\dot{p}_G}{3l^2\kappa g E_m}
\end{aligned}$$

$$\begin{aligned}
\frac{d}{dt}e &= \frac{d}{dt}\frac{M_E M_{Vm}}{M_V M_{Em}} = \frac{M_{Vm}}{M_{Em}}\frac{d}{dt}\frac{M_E}{M_V} = \frac{M_{Vm}}{M_{Em}}\left(M_V^{-1}\frac{d}{dt}M_E - \frac{M_E}{M_V^2}\frac{d}{dt}M_V\right)\\
&= \frac{M_{Vm}}{M_V M_{Em}}\left(\frac{d}{dt}M_E - \frac{M_E}{M_V}\frac{d}{dt}M_V\right) = \frac{M_{Vm}}{M_V M_{Em}}\left(\frac{\dot p_A - \dot p_C}{\mu_E} - \frac{M_E}{M_V}\dot p_G \eta_{VG}\right)\\
&= \frac{1}{l^3 M_{Em}}\left(\frac{\dot p_A - \dot p_C}{\mu_E} - \frac{M_E}{M_V}\dot p_G \eta_{VG}\right) = \frac{1}{l^3 \mu_E M_{Em}}\left(\dot p_A - \dot p_C - \dot p_G \frac{M_E}{M_V}\frac{\mu_E}{\mu_{GV}}\right)\\
&= \frac{1}{l^3 \mu_E M_{Em}}\left(\dot p_A - \dot p_C - \dot p_G\, e\, m_{Em}\frac{\mu_E}{\mu_{GV}}\right) = \frac{1}{l^3 \mu_E M_{Em}}\left(\dot p_A - \dot p_C - \dot p_G\, e\, \frac{y_{EV}}{\kappa g}\frac{\mu_E}{\mu_{GV}}\right)\\
&= \frac{1}{l^3 \mu_E M_{Em}}\left(\dot p_A - \dot p_C - \dot p_G \frac{e}{\kappa g}\right) = \frac{1}{l^3 E_m}\left(\dot p_A - \dot p_C - \dot p_G \frac{e}{\kappa g}\right)
\end{aligned}$$

The maintenance process is here assumed to produce ammonia as single nitrogen waste. It is theoretically also possible that some dinitrogen is formed in this process. The results of [64] show that this hardly affect to macrochemical reaction equation.

Derivation of Eq (4.9)

{133}

Notice that

$$\begin{pmatrix} w_E & w_V \end{pmatrix}\begin{pmatrix} e_0 & e_b l_b^3 \\ 0 & l_b^3 \end{pmatrix} = \begin{pmatrix} w_E e_0 & w_E e_b l_b^3 + w_V l_b^3 \end{pmatrix}.$$

If the write out the product with the factor $[M_{Em}]V_m$, we arrive at the initial wet weight $W_w(0) = [M_{Em}]V_m w_E e_0$, where $[M_{Em}]V_m e_0$ is the initial amount of C-moles of reserve. The wet weight at birth is $W_w(a_b) = [M_{Em}]V_m\,(w_E e_b l_b^3 + w_V l_b^3)$, where $[M_{Em}]V_m e_b l_b^3$ is the C-moles of reserve at birth and $[M_{Em}]V_m l_b^3$ is the C-moles of structure at birth. If we replace the molecular weights w_E and w_V, by those corresponding to dry-weights, we get the result in dry-weights, rather than wet weights.

Derivation of Eq (4.10)

{133}, l-1

Notice that $[M_V]V_b$ stands for the C-moles of the structure of a neonate, so having volume V_b. Further, $E_0 - E_b$ is the energy that is used from the reserve during the incubation period, so $\mu_E^{-1}(E_0 - E_b)$ is the number of C-moles that is used from the reserve during this period.

Multiple-reserve systems can behave as one-reserve systems

{134}, 4.3.4

The section on the composition of reserve and structure is illustrated with a bacterium that lives on glycerol, which must have many, rather than a single reserve (see comments on evolution). This is still consistent with DEB theory for multiple reserves discussed at 5.2, if the concentrations of the nutrients don't limit growth and all rejected reserve fluxes are excreted, $\kappa_{E_i} = 0$. In that case we have $m_{E_i} = j_{E_i A}/\dot k_E$ in steady state (see Eq (5.18) for $\frac{d}{dt}m_{E_i} = 0$), which means that m_{E_i} is constant if $j_{E_i A}$ is constant, so if the concentration of the i-th nutrient in the medium is constant. Figure 4.2 presents the

situation in a chemostat, which means that the concentration of nutrients depend on the growth rate. If the concentration of the non-limiting nutrients is large relative to the half saturation constant, we have $j_{E_iA} \simeq j_{E_iAm}$, which is independent of the growth rate and the non-limiting reserves count as parts of the structure in the analysis of the chemical composition.

Powers as polynomials

{135}, l12

Table 3.5 shows that all powers are cubic polynomials in the (scaled) length, which means that the basic powers assimilation, dissipation (see (3.58) at {134} for the definition) and growth can be written as

$$\begin{pmatrix} \dot{p}_A \\ \dot{p}_D \\ \dot{p}_G \end{pmatrix} = \begin{pmatrix} c_{A0} & c_{A1} & c_{A2} & c_{A3} \\ c_{D0} & c_{D1} & c_{D2} & c_{D3} \\ c_{G0} & c_{G1} & c_{G2} & c_{G3} \end{pmatrix} \begin{pmatrix} l^0 \\ l^1 \\ l^2 \\ l^3 \end{pmatrix} \equiv \boldsymbol{cl}$$

for appropriate choices for the coefficients c. The flux of dioxygen (one way to quantify respiration) can by written as

$$\begin{aligned} \dot{J}_O &= \begin{pmatrix} \eta_{OA} & \eta_{OD} & \eta_{OG} \end{pmatrix} \begin{pmatrix} \dot{p}_A \\ \dot{p}_D \\ \dot{p}_G \end{pmatrix} = \begin{pmatrix} \eta_{OA} & \eta_{OD} & \eta_{OG} \end{pmatrix} \boldsymbol{cl} \\ &= \begin{pmatrix} c_{O0} & c_{O1} & c_{O2} & c_{O3} \end{pmatrix} \boldsymbol{l} \end{aligned}$$

In other words, this flux, like all other mass fluxes, are cubic polynomials in length as well (for isomorphs). Notice that some of the coefficients c depend on the reserve, so on the nutritional status of the organism, and some coefficients are zero. Figure 4.3 illustrates that this is very similar to allometric functions, using the same number of parameters and having an equally good fit. The big difference is that there is a very good explanation for the polynomials, and no explanation for the allometric function. This matters when we want to predict effects of nutrition for instance.

Derivation of Eq (4.12)

{135}

The derivation of Eq (4.12) is as follows. We use (4.3) and (4.5) to find $\dot{\boldsymbol{J}}_{\mathcal{M}} = -\boldsymbol{n}_{\mathcal{M}}^{-1}\boldsymbol{n}_{\mathcal{O}}\boldsymbol{\eta}_{\mathcal{O}}\dot{\boldsymbol{p}}$. The first element of this vector is the one that we need if we exclude assimilation by $\dot{p}_A = 0$ and product formation by $\eta_{PD} = \eta_{PG} = 0$. From Eq (4.5) we find

$$\boldsymbol{\eta}\dot{\boldsymbol{p}} = \begin{pmatrix} 0 & \eta_{VG}\dot{p}_G & -(\dot{p}_D + \dot{p}_G)/\mu_E & 0 \end{pmatrix}^T$$

The first row of $\boldsymbol{n}_{\mathcal{M}}^{-1}\boldsymbol{n}_{\mathcal{O}}$ is for $n_{C*} = 1$, because we work in C-moles:

$$\begin{pmatrix} 1 - n_{NX}\frac{n_{CN}}{n_{NN}} & 1 - n_{NV}\frac{n_{CN}}{n_{NN}} & 1 - n_{NE}\frac{n_{CN}}{n_{NN}} & 1 - n_{NP}\frac{n_{CN}}{n_{NN}} \end{pmatrix}$$

Minus the product of this first row and $\boldsymbol{\eta}\dot{\boldsymbol{p}}$ directly gives Eq (4.5)

Respiration vs catabolism

{136}, last para

Respiration (use of dioxygen or production of carbon dioxide) in absence of assimilation is only approximately proportional to the catabolic rate if the overhead costs of growth are relatively large. If not, respiration can deviate from this and the more general expression (4.12) should be used, with has a less direct link with $\dot{k}_M$. If constraint (4.4) applies, however, and the respiration quotient is constant (independent of the length of the organism), respiration in absence of assimilation is proportional to the catabolic rate.

Aging

{139}

Meanwhile we have developed a theory for aging in which damage-amplification occurs during aging, to account for the survival patterns that are found in endotherms [346]. Effects of caloric restrictions on life span are well predicted. The model has many similarities with the one discussed at {139}, but also some differences and is also more complex. A curiosity is that Gompertz model is a special case of the new model, while the Weibull model is a special case of the model that is discussed in the DEB book.

Derivation of Eq (4.23)

{144}

Eq (4.23) can be derived as follows. We know that volume $V \propto l^3$, and from Table 3.6 at {123} we learn that the catabolic power $\dot{p}_C \propto el^3/(g+e)$. Notice that several constants disappear in the proportionality sign, only the scaled reserve density e and the scaled length l vary. The hazard rate is proportional to $\dot{p}_C/V$, so to $e/(g+e)$. Therefore, it can be written as $\dot{h}(e,l) = \dot{h}_a e \frac{1+g}{e+g}$. The term $1+g$ might seem to fall out of the blue sky. It is just a constant, which is introduced to give the proportionality constant $\dot{h}_a$ a simple interpretation: the maximum hazard rate. This interpretation follows from the fact that e can vary only between 0 and 1. We were allowed to introduce this new constant $1+g$, because it is a constant and it does not introduce a new parameter, since g was already present.

Derivation of Eq (4.24)

{144}

Eq (4.24) can be derived as follows. We know that volume $V \propto l^3$, and from (3.44) we learn that the catabolic power $\dot{p}_C \propto e(l^2\dot{v}/L_m + \dot{k}_M l^3)/(g+e) \propto el^3(g/l+1)/(g+e)$. Notice that $V_h = 0$ for unicellular isomorphs, because they do not heat their body to maintain a constant temperature. Following the same argumentation as is used for (4.23), we now introduce two new constants, $1+g$ and $1+g/l_d$ for the purpose of giving $\dot{h}_a$ the interpretation of a maximum aging rate.

Otoliths as composite products

{147}

Like wood of plants and shells of molluscs, otoliths in fish can be considered as products which helps to convert observations from otoliths to expectations for growth and food

intake in the past (collaborative work with Laure Pecquerie). We assume that otoliths remain isomorphic, except at metamorphosis, where they make an instantaneous change from a disc-like shape to a more complex one. The shape correction function of otoliths can be quantified as $\mathcal{M}_\emptyset(U_H) = \mathcal{M}_\emptyset^b + (U_H > U_H^j)(\mathcal{M}_\emptyset^p - \mathcal{M}_\emptyset^b)$. So $\frac{d}{dt}\mathcal{M} = 0$, except at $U_H = U_H^j$. The physical otolith length $\mathcal{L}_\emptyset$ relates to the volumetric otolith length $L_\emptyset$ as $\mathcal{L}_\emptyset = L_\emptyset/\delta_{\mathcal{L}\emptyset}$, where $\delta_{\mathcal{L}\emptyset} = \delta_{\mathcal{L}\emptyset}^b$ or $\delta_{\mathcal{L}\emptyset}^p$, depending on U_H. The physical otolith surface area (which we need for the degradation process of otoliths) is proportional to the squared volumetric otolith length, but the proportionality factor makes a jump at metamorphosis.

Suppose that otoliths are products with volume $V_\emptyset$ and volumetric length $L_\emptyset = V_\emptyset^{1/3}$. Like all product formation, change in otolith volume is a weighted sum of contributions from assimilation, dissipation and growth. The otolith is in the otosac and suppose that the otosac is isomorphic with volume $\delta_S V$, that the use of otolith material in the fluid in the otosac is proportional to the concentration of otolith material in this fluid and that the precipitation of utilized material is proportional to the volume of fluid in the otosac, relative to the volume of the otosac. The rest of mobilized otolith material is excreted into the environment. The change in otolith volume then becomes

$$\frac{d}{dt}V_\emptyset = \left(\frac{\dot{p}_A}{[E_{\emptyset A}]} + \frac{\dot{p}_D}{[E_{\emptyset D}]} + \frac{\dot{p}_G}{[E_{\emptyset G}]}\right)\left(1 - \frac{V_\emptyset}{\delta_S V}\right)$$

The change in otolith volumetric length is $\frac{d}{dt}L_\emptyset = \frac{1}{3}L_\emptyset^{-2}\frac{d}{dt}V_\emptyset$ and change in (body) volumetric length $\frac{d}{dt}L = \frac{1}{3}L^{-2}\frac{d}{dt}V = \frac{1}{3}L^{-2}\dot{p}_G/[E_G]$. So the change in volumetric length as function of the change in otolith volumetric length is

$$\begin{aligned}\frac{d\mathcal{L}}{d\mathcal{L}_\emptyset} &= \frac{\delta_{\mathcal{L}\emptyset}}{\delta_{\mathcal{L}}}\frac{\frac{1}{3}L^{-2}\dot{p}_G/[E_G]}{\frac{1}{3}L_\emptyset^{-2}(\dot{p}_A/[E_{\emptyset A}] + \dot{p}_D/[E_{\emptyset D}] + \dot{p}_G/[E_{\emptyset G}])(1 - L_\emptyset^3/\delta_S L^3)}\\ &= \frac{\delta_{\mathcal{L}\emptyset}}{\delta_{\mathcal{L}}}\frac{\dot{p}_G/[E_G]}{(\dot{p}_A/[E_{\emptyset A}] + \dot{p}_D/[E_{\emptyset D}] + \dot{p}_G/[E_{\emptyset G}])(L^2/L_\emptyset^2 - L_\emptyset/\delta_S L)}\end{aligned}$$

where

$$\begin{aligned}\dot{p}_A &= \{\dot{p}_{Am}^*\}fL^2; \quad \dot{p}_D = \dot{p}_M + \dot{p}_J + (1-\kappa_R)\dot{p}_R; \quad \dot{p}_M = [\dot{p}_M]L^3\\ \dot{p}_J &= \dot{k}_J E_H; \quad \dot{p}_R = (1-\kappa)\dot{p}_C - \dot{p}_J; \quad \dot{p}_G = \kappa\dot{p}_C - \dot{p}_M; \quad \dot{p}_C = [E]\frac{\dot{v}^* L^2 + \dot{k}_M L^3}{1 + \kappa[E]/[E_G]}\end{aligned}$$

with $f = 0$ for $U_H < U_H^b$, $\kappa_R = 0$ for $U_H < U_H^p$. Furthermore $\{\dot{p}_{Am}^*\} = \{\dot{p}_{Am}\}\mathcal{M}(L)$.

We can remove energies via division by $\{\dot{p}_{Am}\}$ at a reference temperature and maturity, i.e. $S_i = \dot{p}_i/\{\dot{p}_{Am}\}$, with $i = A, D, G, C, R, B, M, J$ with $\dim(S_i) = L^2$:

$$S_C = \frac{\dot{p}_C}{\{\dot{p}_{Am}\}} = \frac{L^2 e}{g+e}(\mathcal{M}(L)g + L/L_m); \quad S_M = \frac{\dot{p}_M}{\{\dot{p}_{Am}\}} = \frac{\kappa L^3}{L_m}; \quad S_J = \frac{\dot{p}_J}{\{\dot{p}_{Am}\}} = \dot{k}_J U_H$$

to obtain

$$\begin{aligned}\frac{d\mathcal{L}}{d\mathcal{L}_\emptyset} &= \frac{\delta_{\mathcal{L}\emptyset}}{\kappa g \delta_{\mathcal{L}}}\frac{\dot{v}S_G}{(\dot{v}_{\emptyset A}S_A + \dot{v}_{\emptyset D}S_D + \dot{v}_{\emptyset G}S_G)(L^2/L_\emptyset^2 - L_\emptyset/\delta_S L)}\\ \frac{d}{dt}\mathcal{L}_\emptyset &= \frac{(\dot{v}_{\emptyset A}S_A + \dot{v}_{\emptyset D}S_D + \dot{v}_{\emptyset G}S_G)(1 - L_\emptyset^3/\delta_S L^3)}{3\delta_{\mathcal{L}\emptyset}L_\emptyset^2}\end{aligned}$$

with

$$S_A = \mathcal{M}(L) f L^2; \quad S_D = S_M + S_J + (1-\kappa_R) S_R; \quad S_G = \kappa S_C - S_M; \quad S_R = (1-\kappa) S_C - S_J$$

and

$$\dot{v}_{\emptyset A} = \{\dot{p}_{Am}\}/[E_{\emptyset A}]; \quad \dot{v}_{\emptyset D} = \{\dot{p}_{Am}\}/[E_{\emptyset D}]; \quad \dot{v}_{\emptyset G} = \{\dot{p}_{Am}\}/[E_{\emptyset G}]$$

Notice that $\dim(\dot{v}_i) = L/t$, with $i = \emptyset A, \emptyset D, \emptyset G, \emptyset$. The removal of energies from the equations comes with a reduction of one parameter, namely

$$U_H^b, U_H^j, U_H^p, \dot{k}_M, \dot{k}_J, g, \kappa, \dot{v}, \dot{v}_\emptyset$$

combined with

$$[E_G], [E_{\emptyset A}], [E_{\emptyset D}], [E_{\emptyset G}] \quad \textit{versus} \quad \dot{v}_{\emptyset A}, \dot{v}_{\emptyset D}, \dot{v}_{\emptyset G},$$

given $f(t)$. If food density $X(t)$ is given, rather than scaled functional response $f(t)$, we need one extra parameter, the half saturation coefficient K. The conversion from the energy allocated to reproduction $\dot{p}_R$ to eggs involves the overhead factor $1 - \kappa_R$. The module for the buffer handling rule has additional parameters. The velocities $\dot{v}_i$ might be negative, provided that $L_\emptyset > 0$ for all possible environmental scenario's for which the individual can survive. They do not depend on temperature, because we obtained them by via $\{\dot{p}_{Am}\}$ at a standardized temperature. Notice also that if $\dot{v}_{\emptyset A} = \dot{v}_{\emptyset D} = 0$ and δ_S large, we have $\frac{d\mathcal{L}}{d\mathcal{L}_\emptyset} = \frac{\delta_{\mathcal{L}\emptyset}}{\delta_\mathcal{L}} \frac{L_\emptyset^2}{\kappa g L^2} \frac{\dot{v}}{\dot{v}_{\emptyset G}}$ and $\mathcal{L}^3 = \frac{\delta_{\mathcal{L}\emptyset}}{\delta_\mathcal{L}} \frac{\dot{v}}{\kappa g \dot{v}_{\emptyset G}} \mathcal{L}_\emptyset^3$ if $L_\emptyset = 0$ when $L = 0$.

Otolith color

Otoliths typically have layers of transparent keratine-like protein, and opaque aragonite plus protein. This observed sequence of layers can be explained if the deposition on the otolith that is associated with growth and (possibly) assimilation has aragonite, and that linked to dissipation has not. Otoliths of embryos are opaque, and embryos don't have assimilation, so contribution from growth and/or maintenance must have aragonite. In winter, when food intake is so low that somatic maintenance costs is partly paid from the reproduction buffer and growth is ceased, otolith depositions have no aragonite, so the contribution from dissipation must be positive and must have no aragonite, while that of growth must also be positive and must have aragonite. If fully grown the deposition has no aragonite, so if the contribution of assimilation is positive, it can have no aragonite. On the assumption that degradation does not affect the opacity, opacity is given by

$$O(t) = \frac{\dot{v}_{\emptyset A} S_A + \dot{v}_{\emptyset G} S_G}{\dot{v}_{\emptyset A} S_A + \dot{v}_{\emptyset D} S_D + \dot{v}_{\emptyset G} S_G}$$

which assumes value 1 if aragonite content is maximum, and 0 in complete absence of aragonite. The relative contributions of assimilation and growth linked depositions to opacity can be weighted unequally.

The color bands are used to assess growth. The human eye recognizes the band boundaries as maximum changes in color. Color change (in length of otolith) is given by

$$\frac{dO}{d\mathcal{L}_\emptyset} = \frac{dO}{dt} \frac{dt}{d\mathcal{L}_\emptyset} = \frac{\sum_k \dot{v}_{\emptyset k} \frac{d}{dt} S_k - O \sum_i \dot{v}_{\emptyset i} \frac{d}{dt} S_i}{(\sum_i \dot{v}_{\emptyset i} S_i) \delta_{\mathcal{L}\emptyset}^{-1} \frac{d}{dt} L_\emptyset} \quad \text{for } i = A, D, G; \quad k = A, G$$

where we need

$$\begin{aligned}
\frac{d}{dt}S_A &= fL^2\frac{d}{dt}\mathcal{M} + \mathcal{M}L^2\frac{d}{dt}f + \mathcal{M}f2L\frac{d}{dt}L \\
\frac{d}{dt}\mathcal{M} &= (U_H > U_H^b)(U_H < U_H^j)(\frac{d}{dt}U_H/U_H^b)/(3\mathcal{M}^2) \\
\frac{d}{dt}f &= f^2\frac{K}{X^2}\frac{d}{dt}X \\
\frac{d}{dt}S_D &= \frac{d}{dt}S_M + \frac{d}{dt}S_J + (1-\kappa_R)\frac{d}{dt}S_R \\
\frac{d}{dt}S_G &= \kappa\frac{d}{dt}S_C - \frac{d}{dt}S_M \\
\frac{d}{dt}S_R &= (1-\kappa)\frac{d}{dt}S_C - \frac{d}{dt}S_J \\
\frac{d}{dt}S_C &= \frac{L}{g+e}(\mathcal{M}g + \frac{L}{L_m})(\frac{gL}{g+e}\frac{d}{dt}e + 2e\frac{d}{dt}L) + \frac{L^2e}{g+e}(g\frac{d}{dt}\mathcal{M} + \frac{d}{dt}\frac{L}{L_m}) \\
\frac{d}{dt}S_M &= \frac{3\kappa L^2}{L_m}\frac{d}{dt}L \\
\frac{d}{dt}S_J &= \dot{k}_J\frac{d}{dt}U_H
\end{aligned}$$

If $X(t)$ is described by a cubic spline or a Fourier series, the evaluation of $\frac{d}{dt}X$ is straightforward.

Isotopes in otoliths

To follow isotopes in otoliths, it is most convenient to work with masses, rather than energies or lengths. We also need more chemical detail. The chemical composition of the contributions from assimilation, dissipation and growth to the otolith can differ; the chemical indices are denotes by n_{ij}^k for $k = A, D, G$. Each C-mole contributes differently to volume, which makes that the otolith volume relates to the otolith mass as

$$V_\emptyset = M_\emptyset^A/[M_\emptyset^A] + M_\emptyset^D/[M_\emptyset^D] + M_\emptyset^G/[M_\emptyset^G]$$

where the parameters $[M_\emptyset^A]$, $[M_\emptyset^D]$ and $[M_\emptyset^G]$ are treated as constants. If $[M_\emptyset^A] = [M_\emptyset^D] = [M_\emptyset^G] = [M_\emptyset]$, the volume of the otolith simplifies to $V_\emptyset = (M_\emptyset^A + M_\emptyset^D + M_\emptyset^G)/[M_\emptyset]$, which might be used as a first approximation to reduce the number of parameters.

Working with masses invites for working with yields, so we apply the relationships

$$[M_\emptyset^A]\dot{v}_{\emptyset A} = \{\dot{J}_{EAm}\}y_{\emptyset E}^A; \quad [M_\emptyset^D]\dot{v}_{\emptyset D} = \{\dot{J}_{EAm}\}y_{\emptyset E}^D; \quad [M_\emptyset^G]\dot{v}_{\emptyset G} = \{\dot{J}_{EAm}\}y_{\emptyset E}^G.$$

Product formation, including otoliths, affects mineral fluxes. This can be avaluated by extending the sets of organic yields for assimilation, dissipation and growth with that on product formation, and the organic chemical indices with those of for otoliths, and obtain the mineral fluxes from the elemental balance equaltion. Since otoliths are very small, the correction is likely to be minute.

The changes in mass of otolith, the color, the chemical indices, the isotope indices and the isotope fractions of the otolith amount to

$$\begin{aligned}
\frac{d}{dt}M_{\emptyset}^{A} &= y_{\emptyset E}^{A}\dot{J}_{EA}\left(1-\frac{V_{\emptyset}}{\delta_S V}\right)\\
\frac{d}{dt}M_{\emptyset}^{D} &= -y_{\emptyset E}^{D}\dot{J}_{ED}\left(1-\frac{V_{\emptyset}}{\delta_S V}\right)\\
\frac{d}{dt}M_{\emptyset}^{G} &= -y_{\emptyset E}^{G}\dot{J}_{EG}\left(1-\frac{V_{\emptyset}}{\delta_S V}\right)\\
O(t) &= \frac{y_{\emptyset E}^{A}\dot{J}_{EA}-y_{\emptyset E}^{G}\dot{J}_{EG}}{y_{\emptyset E}^{A}\dot{J}_{EA}-y_{\emptyset E}^{D}\dot{J}_{ED}-y_{\emptyset E}^{G}\dot{J}_{EG}}\\
n_{i\emptyset}(t) &= \frac{n_{i\emptyset}^{A}y_{\emptyset E}^{A}\dot{J}_{EA}-n_{i\emptyset}^{D}y_{\emptyset E}^{D}\dot{J}_{ED}-n_{i\emptyset}^{G}y_{\emptyset E}^{G}\dot{J}_{EG}}{y_{\emptyset E}^{A}\dot{J}_{EA}-y_{\emptyset E}^{D}\dot{J}_{ED}-y_{\emptyset E}^{G}\dot{J}_{EG}}\\
n_{i\emptyset}^{0}(t) &= \frac{n_{i\emptyset}^{0A}y_{\emptyset E}^{A}\dot{J}_{EA}-n_{i\emptyset}^{0D}y_{\emptyset E}^{D}\dot{J}_{ED}-n_{i\emptyset}^{0G}y_{\emptyset E}^{G}\dot{J}_{EG}}{y_{\emptyset E}^{A}\dot{J}_{EA}-y_{\emptyset E}^{D}\dot{J}_{ED}-y_{\emptyset E}^{G}\dot{J}_{EG}}\\
\delta_{i\emptyset}^{0}(t) &= \frac{n_{i\emptyset}^{0}(t)}{n_{i\emptyset}(t)}
\end{aligned}$$

with $\dot{J}_{EA}, \dot{J}_{EG} \leq 0$. Notice that the chemical indices n_{ij} and the isotope indices n_{ij}^{0} are relative to carbon and that $n_{C\emptyset}^{A} = n_{C\emptyset}^{D} = n_{C\emptyset}^{G} = n_{C\emptyset} = 1$. Notice also that the otolith is not mixed, so we don't have dilution by growth of the otolith.

Several possibilities can be delineated for $n_{i\emptyset}^{0k}$. The simplest set of possiblities is that no fractionation occurs at otolith formation, which we will examine in more detail. The isotope indices $n_{i\emptyset}^{0k}$ are obtained from $n_{i\emptyset}^{0k} = -\sum_s \alpha_{\emptyset s}^{ik} n_{is}^{0k}/Y_{\emptyset s}^{k}$, where for elements $i = C, H, N$ we have substrate $s = X$ for transformation $k = A$ and $s = E$ for $k = D, G$. For the element oxygen, $i = O$, we have two substrates, the second one being dioxygen, $s = O$. Since otoliths are very small, the effect of their production on the reshuffling parameters α will be minute, and we can link the isotope indices directly to that of reserve or structure. The contribution of dioxygen for oxygen in otoliths should be reconsidered. Since fractionation occurs at the anabolic/catabolic forks of the three fluxes, the allocation to otoliths can occur before or after the forks, so we have three possibilities per flux

$$\begin{aligned}
n_{i\emptyset}^{0A} &= n_{i\emptyset}^{A}\frac{n_{iX}^{0A}}{n_{iX}} \quad \text{or } n_{i\emptyset}^{A}\frac{n_{iX}^{0A_a}}{n_{iX}} \quad \text{or } n_{i\emptyset}^{A}\frac{n_{iX}^{0A_c}}{n_{iX}}\\
n_{i\emptyset}^{0D} &= n_{i\emptyset}^{D}\frac{n_{iE}^{0D}}{n_{iE}} \quad \text{or } n_{i\emptyset}^{D}\frac{n_{iE}^{0D_a}}{n_{iE}} \quad \text{or } n_{i\emptyset}^{D}\frac{n_{iE}^{0D_c}}{n_{iE}}\\
n_{i\emptyset}^{0G} &= n_{i\emptyset}^{G}\frac{n_{iE}^{0G}}{n_{iE}} \quad \text{or } n_{i\emptyset}^{G}\frac{n_{iE}^{0G_a}}{n_{iE}} \quad \text{or } n_{i\emptyset}^{G}\frac{n_{iE}^{0G_c}}{n_{iE}}
\end{aligned}$$

This does not exhaust all possibilities; part of the atoms in otoliths can originate from structure in the anabolic sub-flux of somatic maintenance. If we include the contribution from growth into the anabolic flux (the second option), we have $\kappa_G^a = y_{VE} + y_{\emptyset E}^{G}$ and $\kappa_G^c = 1 - \kappa_G^a$ and for assimilation $\kappa_A^a = y_{EX} + y_{\emptyset E}^{A}$ and $\kappa_A^c = 1 - \kappa_A^a$. For dissipation the situation is simpler because κ_D^a is a free parameter, independent of other parameters.

Formula	State	Enthalpy kcal/mol	Entropy cal/mol.K
CO_2	g	-94.05	51.07
H_2O	l	-68.32	16.71
O_2	g	0	49.00
NH_3	aq.	-19.20	26.63

Table 4.4: Formation enthalpies and absolute entropies of CO_2, H_2O and O_2 at 25 $^\circ$C were taken from [102]. The formation enthalpy and absolute entropy for NH_3 at 25 $^\circ$C were taken from [14].

With the presently available information, we can neglect the contribution from assimilation to otoliths, $y^A_{\emptyset E} = 0$, but future work with biomarkers might change that.

Simulation results show that, even in absence of effects of temperature on the odds ratios, seasonal cycles in temperature result in a covariance of temperature and the isotope fractions in otoliths.

Thermodynamic parameters

{154}

The entropies and chemical potentials for microbial populations in a chemostat are discussed in [530], for individual isomorphs in [328]. The value of the entropy of living biomass did differ from Battley's empirical rule [26] and destructive methods. We expect that changes in entropy are especially important in transients from anaerobic and aerobic conditions and in large transients in pressure (deep ocean to surface). This comment presents the results in [328] for an isomorph.

Strong homeostasis implies that the specific enthalpies, chemical potentials and entropies of reserve and structure are constant. Our methods can be applied under anaerobic as well as aerobic conditions if we replace dioxygen by the products that are formed.

Enthalpy and dissipating heat

Given the molar enthalpies for the minerals, $\overline{\boldsymbol{h}}^T_{\mathcal{M}} = \begin{pmatrix} \overline{h}_C & \overline{h}_H & \overline{h}_O & \overline{h}_N \end{pmatrix}$ from the literature (see Table 4.4), the molar enthalpies of the organic compounds, $\overline{\boldsymbol{h}}^T_{\mathcal{O}} = \begin{pmatrix} \overline{h}_X & \overline{h}_V & \overline{h}_E & \overline{h}_P \end{pmatrix}$ can be obtained from the energy balance equation

$$0 = \overline{\boldsymbol{h}}^T_{\mathcal{M}} \dot{\boldsymbol{J}}_{\mathcal{M}} + \overline{\boldsymbol{h}}^T_{\mathcal{O}} \dot{\boldsymbol{J}}_{\mathcal{O}} + \dot{p}_{T+} = \left(\overline{\boldsymbol{h}}_{\mathcal{O}} - \overline{\boldsymbol{h}}_{\mathcal{M}} \boldsymbol{n}^{-1}_{\mathcal{M}} \boldsymbol{n}_{\mathcal{O}}\right)^T \dot{\boldsymbol{J}}_{\mathcal{O}} + \dot{p}_{T+},$$

by measuring the net heat dissipated heat by the organism, i.e. $\dot{p}_{T+}$. This heat can be negative if heat from the environment is required to keep the temperature of the individual constant. Generally measurements of dissipating heat at four different food levels are required to obtain the four enthalpies for the organic compounds; if the enthalpies of food X and faeces P are known then only measurements of dissipated heat at two different food densities are required.

The dissipated heat can be estimated for other food densities, knowing the enthalpies of organic compounds, using the method of indirect calorimetry that establishes a linear dependence between the mineral fluxes and the dissipated heat (see also [289, p155]).

The specific enthalpy of biomass equals $\overline{h}_W = \frac{m_E \overline{h}_E + \overline{h}_V}{m_E + 1}$.

Chemical potentials and entropy

The specific chemical potential $\overline{\mu}$ of a compound converts a flux of this compound (in moles per time) into a flux of Gibbs energy, for instance the assimilation energy flux is $\dot{p}_A = \overline{\mu}_E \dot{J}_{EA}$. The chemical potentials $\overline{\mu}$ have to be computed simultaneously with the molar entropies $\overline{s}$. Work that is involved in changes in volumes are typically negligibly small at the surface of the earth, but in the deep ocean, this work has profound effects on energetics and biochemistry [160, 513]. Neglecting this effect, the chemical potential and entropies of food $\overline{\mu}_X$ and $\overline{s}_X$, structure $\overline{\mu}_V$ and $\overline{s}_V$, reserve $\overline{\mu}_E$ and $\overline{s}_E$, and faeces $\overline{\mu}_P$ and $\overline{s}_P$ can be obtained with

$$\begin{aligned} 0 &= (\overline{\boldsymbol{\mu}}_{\mathcal{M}} + T\overline{\boldsymbol{s}}_{\mathcal{M}})^T \dot{\boldsymbol{J}}_{\mathcal{M}} + (\overline{\boldsymbol{\mu}}_{\mathcal{O}} + T\overline{\boldsymbol{s}}_{\mathcal{O}})^T \dot{\boldsymbol{J}}_{\mathcal{O}} + \dot{p}_{T+} \\ &= \left(\left(\overline{\boldsymbol{h}}_{\mathcal{M}} - \overline{\boldsymbol{\mu}}_{\mathcal{M}} - T\overline{\boldsymbol{s}}_{\mathcal{M}}\right) \boldsymbol{n}_{\mathcal{M}}^{-1} \boldsymbol{n}_{\mathcal{O}} - \overline{\boldsymbol{h}}_{\mathcal{O}} + \overline{\boldsymbol{\mu}}_{\mathcal{O}} - T\overline{\boldsymbol{s}}_{\mathcal{O}}\right)^T \dot{\boldsymbol{J}}_{\mathcal{O}}, \end{aligned}$$

by measuring the temperature T of the organisms and computing the organic and mineral flows at 8 different food densities (or 4 different food densities if molar entropies and chemical potentials of food X and faeces P are known), where $\overline{\boldsymbol{\mu}}_{\mathcal{M}}$ and $\overline{\boldsymbol{s}}_{\mathcal{M}}$ collect the values of the molar chemical potentials and molar entropies for the four minerals, while $\overline{\boldsymbol{\mu}}_{\mathcal{O}}$ and $\overline{\boldsymbol{s}}_{\mathcal{O}}$ do that for the organic compounds, as before.

The rate of entropy production by the organism $\dot{\sigma}$ is a measure of the amount of dissipation that is occurring. It can be quantified for each food density if the temperature of the organism and the entropies of the organic compounds are known:

$$0 = \dot{\sigma} + \frac{\dot{p}_{T+}}{T} + \overline{\boldsymbol{s}}_{\mathcal{M}}^T \dot{\boldsymbol{J}}_{\mathcal{M}} + \overline{\boldsymbol{s}}_{\mathcal{O}}^T \dot{\boldsymbol{J}}_{\mathcal{O}}.$$

The chemical potentials of organic compounds are essential to obtain the energy parameters $\{\dot{p}_{Am}\}$, $[E_G]$, $\{\dot{p}_T\}$, $[\dot{p}_M]$ and $[\dot{p}_J]$, see Table 3.3.

The specific entropy of biomass equals $\overline{s}_W = \frac{m_E \overline{s}_E + \overline{s}_V}{m_E + 1}$

Aerobic conditions

Formula are simpler for aerobic conditions because for most important reactions in aerobic biological systems $T\,\Delta\overline{s}$ is very small compared to $\Delta\overline{h}$ and therefore the enthalpy of the reaction $\Delta\overline{h}_+$ is approximated using its Gibbs energy $\Delta\overline{\mu}_+$, since at constant temperature we have $\Delta\overline{\mu} = \Delta\overline{h} - T\,\Delta\overline{s} \simeq \Delta\overline{h}$ [156].

The entropies of the organic compounds $\overline{\boldsymbol{s}}_{\mathcal{O}}$ can be obtained with

$$\mathbf{0} = \overline{\boldsymbol{s}}_{\mathcal{M}}^T \dot{\boldsymbol{J}}_{\mathcal{M}} + \overline{\boldsymbol{s}}_{\mathcal{O}}^T \dot{\boldsymbol{J}}_{\mathcal{O}},$$

by computing the organic and mineral flows at 4 different food densities (or 2 different food densities if molar entropies of food X and faeces P are known) and constant temperature.

The specific chemical potentials of the organic compounds $\overline{\boldsymbol{\mu}}_{\mathcal{O}}$ can be computed with

$$\mathbf{0} = \dot{p}_{T+}^{\circ} + \overline{\boldsymbol{\mu}}_{\mathcal{O}}^T \dot{\boldsymbol{J}}_{\mathcal{O}} + \overline{\boldsymbol{\mu}}_{\mathcal{M}}^T \dot{\boldsymbol{J}}_{\mathcal{M}},$$

where $\dot{p}^\circ_{T+}$ is the net heat release by all chemical reactions. If the temperature of the organism is constant, the net heat release $\dot{p}^\circ_{T+}$ is equal to the net heat dissipated by the organism $\dot{p}_{T+}$. The computation can be done by measuring directly the dissipated heat $\dot{p}_{T+} \simeq \dot{p}^\circ_{T+}$, at 4 different food densities (or 2 different food densities if chemical potentials of food X and faeces P are known), that is approximately equal to the total heat release by all chemical reactions $\dot{p}^\circ_{T+}$. Alternatively the dissipated heat can be obtained with the method of indirect calorimetry.

The rate of entropy production by the organism $\dot{\sigma}$ can be quantified if the temperature of the organism is known: $\dot{\sigma} = -\frac{\dot{p}_{T+}}{T}$.

Heat $\propto$ dioxygen flux

{154}

In microbiology, heat is frequently taken to be proportional to the dioxygen flux. We can now try to understand how this translates to constraints on biomass composition, and we can specify the proportionality factor in terms of DEB parameters.

Let

$$\boldsymbol{n}_{\mathcal{M}}^{-1} = \boldsymbol{u}_{\mathcal{M}} = \begin{pmatrix} \boldsymbol{u}_C \\ \boldsymbol{u}_H \\ \boldsymbol{u}_O \\ \boldsymbol{u}_N \end{pmatrix} = \begin{pmatrix} 1 & 0 & 0 & -\frac{n_{CN}}{n_{NN}} \\ 0 & 2^{-1} & 0 & -\frac{n_{HN}}{2n_{NN}} \\ -1 & -4^{-1} & 2^{-1} & \frac{n}{4n_{NN}} \\ 0 & 0 & 0 & n_{NN}^{-1} \end{pmatrix}; \quad n \equiv 4n_{CN} + n_{HN} - 2n_{ON}$$

and

$$\boldsymbol{n}_{\mathcal{O}} = \begin{pmatrix} n_{CX} & n_{CV} & n_{CE} & n_{CP} \\ n_{HX} & n_{HV} & n_{HE} & n_{HP} \\ n_{OX} & n_{OV} & n_{OE} & n_{OP} \\ n_{NX} & n_{NV} & n_{NE} & n_{NP} \end{pmatrix} = \begin{pmatrix} \boldsymbol{n}_X & \boldsymbol{n}_V & \boldsymbol{n}_E & \boldsymbol{n}_P \end{pmatrix}$$

and

$$\boldsymbol{\eta}_{\mathcal{O}} = \begin{pmatrix} -\eta_{XA} & 0 & 0 \\ 0 & 0 & \eta_{VG} \\ \mu_E^{-1} & -\mu_E^{-1} & -\mu_E^{-1} \\ \eta_{PA} & \eta_{PD} & \eta_{PG} \end{pmatrix} = \begin{pmatrix} \boldsymbol{\eta}_A & \boldsymbol{\eta}_D & \boldsymbol{\eta}_G \end{pmatrix}$$

The dioxygen flux can thus be written as $\dot{J}_O = -\boldsymbol{u}_O \boldsymbol{n}_{\mathcal{O}} \dot{\boldsymbol{J}}_{\mathcal{O}}$, see Eq (4.3). Dissipating heat is given by

$$\begin{aligned} \dot{p}_{T+} &= -\boldsymbol{\mu}_{\mathcal{M}}^T \dot{\boldsymbol{J}}_{\mathcal{M}} - \boldsymbol{\mu}_{\mathcal{O}}^T \dot{\boldsymbol{J}}_{\mathcal{O}} \\ &= (\boldsymbol{\mu}_{\mathcal{M}}^T \boldsymbol{n}_{\mathcal{M}}^{-1} \boldsymbol{n}_{\mathcal{O}} - \boldsymbol{\mu}_{\mathcal{O}}^T) \dot{\boldsymbol{J}}_{\mathcal{O}} \end{aligned}$$

see Eq (4.36) and (4.3). The question now translates as: under what constraints do we have $\dot{p}_{T+} = -\mu_{OT} \dot{J}_O$, and how does the constant μ_{OT} relate to parameter values? So we have that

$$\mu_{OT} = -\frac{\dot{p}_{T+}}{\dot{J}_O} = \frac{(\boldsymbol{\mu}_{\mathcal{M}}^T \boldsymbol{n}_{\mathcal{M}}^{-1} \boldsymbol{n}_{\mathcal{O}} - \boldsymbol{\mu}_{\mathcal{O}}^T) \dot{\boldsymbol{J}}_{\mathcal{O}}}{\boldsymbol{u}_O \boldsymbol{n}_{\mathcal{O}} \dot{\boldsymbol{J}}_{\mathcal{O}}} = \frac{(\boldsymbol{\mu}_{\mathcal{M}}^T \boldsymbol{u}_{\mathcal{M}} \boldsymbol{n}_{\mathcal{O}} - \boldsymbol{\mu}_{\mathcal{O}}^T) \boldsymbol{\eta}_O \dot{\boldsymbol{p}}}{\boldsymbol{u}_O \boldsymbol{n}_{\mathcal{O}} \dot{\boldsymbol{\eta}}_{\mathcal{O}} \dot{\boldsymbol{p}}}$$

must be constant, while the three elements of $\dot{\boldsymbol{p}}$ can vary. This can only happen if this relationship applies to each of the three powers $\dot{\boldsymbol{p}}$:

$$\mu_{OT} = \frac{(\boldsymbol{\mu}_{\mathcal{M}}^T \boldsymbol{u}_{\mathcal{M}} \boldsymbol{n}_{\mathcal{O}} - \boldsymbol{\mu}_{\mathcal{O}}^T)\boldsymbol{\eta}_A}{\boldsymbol{u}_O \boldsymbol{n}_{\mathcal{O}} \boldsymbol{\eta}_A} = \frac{(\boldsymbol{\mu}_{\mathcal{M}}^T \boldsymbol{u}_{\mathcal{M}} \boldsymbol{n}_{\mathcal{O}} - \boldsymbol{\mu}_{\mathcal{O}}^T)\boldsymbol{\eta}_D}{\boldsymbol{u}_O \boldsymbol{n}_{\mathcal{O}} \boldsymbol{\eta}_D} = \frac{(\boldsymbol{\mu}_{\mathcal{M}}^T \boldsymbol{u}_{\mathcal{M}} \boldsymbol{n}_{\mathcal{O}} - \boldsymbol{\mu}_{\mathcal{O}}^T)\boldsymbol{\eta}_G}{\boldsymbol{u}_O \boldsymbol{n}_{\mathcal{O}} \boldsymbol{\eta}_G}$$

so

$$\boldsymbol{\mu}_{\mathcal{M}}^{T*} \boldsymbol{u}_{\mathcal{M}} \boldsymbol{n}_{\mathcal{O}} \boldsymbol{\eta}_{\mathcal{O}} = \boldsymbol{\mu}_{\mathcal{O}}^T \boldsymbol{\eta}_{\mathcal{O}} \quad \text{with } \boldsymbol{\mu}_{\mathcal{M}}^{T*} = \begin{pmatrix} \mu_C & \mu_H & \mu_O - \mu_{OT} & \mu_N \end{pmatrix}$$

If $\boldsymbol{\eta}_{\mathcal{O}}^{-1}$ exists, this further reduces to the constraint $\boldsymbol{\mu}_{\mathcal{M}}^{T*} \boldsymbol{u}_{\mathcal{M}} \boldsymbol{n}_{\mathcal{O}} = \boldsymbol{\mu}_{\mathcal{O}}^T$. It still depends on some coefficients η via μ_{OT}, which is in $\boldsymbol{\mu}_{\mathcal{M}}^{T*}$.

Faeces as only product

Suppose $\eta_{PD} = \eta_{PG} = 0$, while $\eta_{PA} \neq 0$. This situation occurs when faeces is the only product, as in animals; $\boldsymbol{\eta}_{\mathcal{O}}^{-1}$ does not exist. Substitution for dissipation gives

$$\mu_{OT} = \frac{\boldsymbol{\mu}_{\mathcal{M}}^T \boldsymbol{u}_{\mathcal{M}} \boldsymbol{n}_E - \mu_E}{\boldsymbol{u}_O \boldsymbol{n}_E}$$

which does not depend on any coefficient η. Let

$$\boldsymbol{\mu}^T = \boldsymbol{\mu}_{\mathcal{M}}^{T*} \boldsymbol{u}_{\mathcal{M}} \boldsymbol{\eta}_{\mathcal{O}} = \begin{pmatrix} \mu_1 & \mu_2 & \mu_3 & \mu_4 \end{pmatrix}$$

We then must have that $\mu_2 = \mu_V$, $\mu_3 = \mu_E$, and $\eta_{PA}\mu_4 - \eta_{XA}\mu_1 = \eta_{PA}\mu_P - \eta_{XA}\mu_X$.

No product

Suppose $\eta_{PA} = \eta_{PD} = \eta_{PG} = 0$ (no product; this situation can occur with bacteria). We now have $\mu_1 = \mu_X$, so the constraints no longer depend on coefficients η. Substitution of the η's gives

$$\begin{aligned} \mu_{OT} &= \frac{\boldsymbol{\mu}_{\mathcal{M}}^T \boldsymbol{u}_{\mathcal{M}} (\boldsymbol{n}_E - \mu_E \eta_{XA} \boldsymbol{n}_X) - \mu_E (1 - \mu_X \eta_{XA})}{\boldsymbol{u}_O (\boldsymbol{n}_E - \mu_E \eta_{XA} \boldsymbol{n}_X)} \\ &= \frac{\boldsymbol{\mu}_{\mathcal{M}}^T \boldsymbol{u}_{\mathcal{M}} \boldsymbol{n}_E - \mu_E}{\boldsymbol{u}_O \boldsymbol{n}_E} \\ &= \frac{\boldsymbol{\mu}_{\mathcal{M}}^T \boldsymbol{u}_{\mathcal{M}} (\boldsymbol{n}_E - \mu_E \eta_{VG} \boldsymbol{n}_V) - \mu_E (1 - \mu_V \eta_{VG})}{\boldsymbol{u}_O (\boldsymbol{n}_E - \mu_E \eta_{VG} \boldsymbol{n}_V)} \end{aligned}$$

or, for $\boldsymbol{n}_{\mathcal{O}} = \begin{pmatrix} \boldsymbol{n}_X & \boldsymbol{n}_V & \boldsymbol{n}_E \end{pmatrix}$ and $\boldsymbol{\mu}_{\mathcal{O}}^T = \begin{pmatrix} \mu_X & \mu_V & \mu_E \end{pmatrix}$

$$\begin{aligned} \boldsymbol{\mu}_{\mathcal{O}}^T &= \boldsymbol{\mu}_{\mathcal{M}}^{T*} \boldsymbol{u}_{\mathcal{M}} \boldsymbol{n}_{\mathcal{O}} = (\boldsymbol{\mu}_{\mathcal{M}}^T \boldsymbol{u}_{\mathcal{M}} - \mu_{OT} \boldsymbol{u}_O) \boldsymbol{n}_{\mathcal{O}} \\ \boldsymbol{u}_O \boldsymbol{n}_E \boldsymbol{\mu}_{\mathcal{O}}^T &= (\boldsymbol{\mu}_{\mathcal{M}}^T \boldsymbol{u}_{\mathcal{M}} \boldsymbol{u}_O \boldsymbol{n}_E - \boldsymbol{\mu}_{\mathcal{M}}^T \boldsymbol{u}_{\mathcal{M}} \boldsymbol{n}_E \boldsymbol{u}_O + \mu_E \boldsymbol{u}_O) \boldsymbol{n}_{\mathcal{O}} \\ &= \left(\boldsymbol{\mu}_{\mathcal{M}}^T \boldsymbol{u}_{\mathcal{M}} (\boldsymbol{u}_O \boldsymbol{n}_E - \boldsymbol{n}_E \boldsymbol{u}_O) + \mu_E \boldsymbol{u}_O\right) \boldsymbol{n}_{\mathcal{O}} \end{aligned}$$

Notice that $\boldsymbol{u}_O \boldsymbol{n}_E$ is a scalar and $\boldsymbol{n}_E \boldsymbol{u}_O$ a (4×4)-matrix. Although the result does not depend on the detailed dynamics of the DEB model, it does depend on an important property of the standard DEB model: all mass fluxes are weighted sums of assimilation, dissipation and growth.

Ammonia as N-waste

$n_{CN} = 0$, $n_{HN} = 3$, $n_{ON} = 0$ and $n_{NN} = 1$, so $n = 3$ and

$$\boldsymbol{u}_{\mathcal{M}} = \frac{1}{4}\begin{pmatrix} 4 & 0 & 0 & 0 \\ 0 & 2 & 0 & -6 \\ -4 & -1 & 2 & 3 \\ 0 & 0 & 0 & 4 \end{pmatrix}$$

This can be used to work out a numerical example.

Frame of reference

{155}, l-8

The idea is that we start in an aerobic situation, using a combustion frame of reference, and then correct for product formation under anaerobic conditions. So we replace the chemical potential of dioxygen (set to zero in the combustion frame of reference) by that of ethanol.

Chapter 5

Multivariate DEB models

Classification of substrates

{160}

The substrates are classified as substitutable or complementary and binding schemes as sequential or parallel. These four classes comprise the standard kinetics see Figure 5.1. Let us characterize the states of the SUs in bounded fractions with vector $\boldsymbol{\theta}$, while $\mathbf{1}^T\boldsymbol{\theta} = 1$ and $0 \leq \theta_i < 1$ for all states i. The change in bounded fractions of SUs can be written as $\frac{d}{dt}\boldsymbol{\theta} = \dot{\boldsymbol{k}}\boldsymbol{\theta}$, for a matrix of rates $\dot{\boldsymbol{k}}$ with diagonal elements $\dot{k}_{ii} = -\sum_{j\neq i}\dot{k}_{ij}$, while $\dot{k}_{ij} \geq 0$, so $\mathbf{1}^T\dot{\boldsymbol{k}} = \mathbf{0}$. Using a time scale separation argument, a flux of metabolite X can be written as $\dot{J}_X = \dot{\boldsymbol{J}}^T\boldsymbol{\theta}^*$, with weight coefficients $\dot{\boldsymbol{J}}$ and fractions $\boldsymbol{\theta}^*$ such that $\mathbf{0} = \dot{\boldsymbol{k}}\boldsymbol{\theta}^*$. Mixtures of the four classes of standard kinetics have the property that $\dot{\boldsymbol{k}} = \sum_i \dot{\boldsymbol{k}}_i$, where $\dot{\boldsymbol{k}}$ is the matrix of rates of the mixture, and $\dot{\boldsymbol{k}}_i$ that of a standard type. Such mixtures are discussed in [298] in connection with the gradual transition from substitutable to complementary compounds.

SUs can be organized in a metabolic chain or network, sometimes they are spatially organized in a metabolon and pass intermediate metabolites to each other by channeling. They might use the open-handshaking protocol for dissociation, meaning that the dissociation process is independent of the binding state of the neighbouring SUs, the closed-handshaking protocol, meaning that dissociation only occurs if the neighbouring SUs are in the free unbounded state, or a mixture of both protocols. Closed handshaking involves communication, and typically physical contact (so spatial structure). If handshaking is fully closed, the whole metabolon acts as if it is a single SU. For an application of this to the TCA cycle see [327].

Sequential processing

{160}

The derivation of the uptake flux for two substrates under sequential processing is as follows for N_1 being the number of carriers bound to substrate 1, and N_2 that to substrate 2, with the total number of carriers $N = N_0 + N_1 + N_2$ being constant:

$$\begin{aligned} \frac{d}{dt}N_0 &= N_1\dot{k}_1 + N_2\dot{k}_2 - N_0(\rho_1\dot{J}_1 + \rho_2\dot{J}_2) \\ \frac{d}{dt}N_1 &= N_0\rho_1\dot{J}_1 - N_1\dot{k}_1 \end{aligned}$$

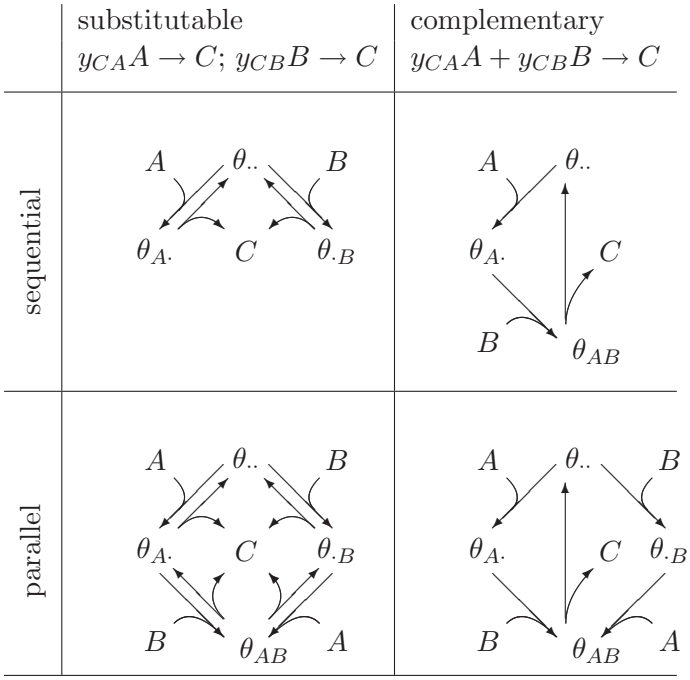

Figure 5.1: Interaction of substrates A and B in transformations into product C can be understood on the basis of a classification of substrates into substitutable and complementary, and of binding into sequential or parallel. The symbol $\theta_{*_1*_2}$ represents a SU that is bound to the substrates $*_1$ and $*_2$, the dot representing no substrate, so $\theta_{..}$ represents a free SU. The symbol $y_{*_1*_2}$ denotes a stoichiometric coupling coefficient. The schemes can be generalized to more complex transformations to include co-metabolism and intermediate cases between substitutability and complementarity, without involving new theoretical problems. From [290].

$$\frac{d}{dt}N_2 = N_0\rho_2\dot{J}_2 - N_2\dot{k}_2$$

The steady state frequencies are

$$N_0^* = \frac{N}{1+\rho_1\dot{J}_1/\dot{k}_1+\rho_2\dot{J}_2/\dot{k}_2} \quad N_1^* = \frac{N\rho_1\dot{J}_1/\dot{k}_1}{1+\rho_1\dot{J}_1/\dot{k}_1+\rho_2\dot{J}_2/\dot{k}_2} \quad N_2^* = \frac{N\rho_2\dot{J}_2/\dot{k}_2}{1+\rho_1\dot{J}_1/\dot{k}_1+\rho_2\dot{J}_2/\dot{k}_2}$$

In Eq (5.1) the term $(N-N_0)\dot{k}_X$ corresponds with $N_1\dot{k}_1 + N_2\dot{k}_2$, so

$$\begin{aligned}\dot{k}_X &= \frac{N_1^*\dot{k}_1 + N_2^*\dot{k}_2}{N-N_0^*} = \frac{\rho_1\dot{J}_1+\rho_2\dot{J}_2}{\rho_1\dot{J}_1/\dot{k}_1+\rho_2\dot{J}_2/\dot{k}_2}\\ \dot{k}_X^{-1} &= \frac{\rho_1\dot{J}_1}{\rho_1\dot{J}_1+\rho_2\dot{J}_2}\dot{k}_1^{-1} + \frac{\rho_2\dot{J}_2}{\rho_1\dot{J}_1+\rho_2\dot{J}_2}\dot{k}_2^{-1} = \theta_1\dot{k}_1^{-1} + (1-\theta_1)\dot{k}_2^{-1}\end{aligned}$$

We have found formulations of Synthesizing Units that embrace sequential and parallel processing, as well as substitutable and complementary compounds [64, 67, 297]. Such theory is essential to understand e.g. why cows can do with much less grass if you give them some proteins in addition, and co-metabolism. We also developed formulations for the dynamics of the carriers for the uptake of various substrates by micro-organisms [64, 65]. Such theory is necessary to understand diauxic growth, where one substrate is used first, before another one is consumed. This theory also comes with an extension of the SU theory to include uni- and bi-lateral inhibition.

Figure 5.2: Left: Interaction between the conversions $S_1 \rightarrow P$ and $S_2 \rightarrow P$, with preference for the first transformation. θ_* indicates the fraction of synthesizing units that are bound to substrates. Right: The standard inhibition scheme, where S_2 inhibits the transformation $S_1 \rightarrow P$.

Derivation of Eq (5.2)

{161}

The derivation of Eq (5.2) from (5.1) is as follows. The equilibrium number of carriers in the binding phase N_0^* is found from $\frac{d}{dt}N_0 = 0$, which leads to $(N - N_0^*)\dot{k}_X = N_0^*(\rho_1\dot{J}_1 + \rho_2\dot{J}_2)$, and gives $N_0^* = \frac{N\dot{k}_X}{\dot{k}_X+\rho_1\dot{J}_1+\rho_2\dot{J}_2}$. The fraction of carriers in the binding phase is $\theta = N_0^*/N = \frac{\dot{k}_X}{\dot{k}_X+\rho_1\dot{J}_1+\rho_2\dot{J}_2}$ and the number of carriers is here taken to be proportional to the amount of structure, with proportionality constant n. The assimilation equals the bounded substrate. Substrate i binds with rate $n\rho_i\dot{J}_i\theta$ per unit of structure, so the total specific assimilation equals $j_X = n\rho_1\dot{J}_1\theta + n\rho_2\dot{J}_2\theta = n\frac{\dot{k}_X(\rho_1\dot{J}_1+\rho_2\dot{J}_2)}{\dot{k}_X+\rho_1\dot{J}_1+\rho_2\dot{J}_2}$. This directly simplifies to Eq (5.2).

Inhibition and preference

{164}

We here deal with interacting substitutable substrates that are bound in a parallel fashion. Standard inhibition makes part of the SUs unavailable for catalyzing transformations (Figure 5.2). Stronger forms of interaction can occur if one substrate is able to replace another that is already bound to an SU (Figure 5.2).

Let j_{S_1} and j_{S_2} be the fluxes of substrate S_1 and S_2 that arrive at an SU, and ρ_{S_1} and ρ_{S_2} be the binding probabilities. The binding kinetics, *i.e.* the changes in the bounded fractions of SUs, for scaled fluxes $j'_{S_1} = \rho_{S_1}j_{S_1}$, $j'_{S_2} = \rho_{S_2}j_{S_2}$ and $1 = \theta. + \theta_{S_1} + \theta_{S_2}$ are

$$\begin{aligned}\frac{d}{dt}\theta_{S_2} &= j'_{S_2}\theta. - (j'_{S_1} + \dot{k}_{S_2})\theta_{S_2},\\ \frac{d}{dt}\theta_{S_1} &= j'_{S_1}(\theta. + \theta_{S_2}) - \dot{k}_{S_1}\theta_{S_1},\end{aligned}$$

where $\dot{k}_{S_1}$ and $\dot{k}_{S_2}$ are the dissociation constants of the SU-substrate complexes.

Supply kinetics

For the binding fraction at steady state, the production flux of P equals $j_P = y_{PS_1}j^+_{S_1} + y_{PS_2}j^+_{S_2}$, while the fluxes of S_1 and S_2 that are used are

$$j^+_{S_1} = \dot{k}_{S_1}\theta^*_{S_1} = \frac{\dot{k}_{S_1}j'_{S_1}}{\dot{k}_{S_1} + j'_{S_1}},$$

$$j_{S_2}^+ = \dot{k}_{S_2}\theta_{S_2}^* = \frac{\dot{k}_{S_1}\dot{k}_{S_2}j'_{S_2}}{\dot{k}_{S_2} + j'_{S_1} + j'_{S_2}}.$$

Although their derivation has been set up slightly differently, this formulation is used in [65] to model substrate preference and diauxic growth in microorganisms. The use of genes coding for substrate-specific carriers is here linked to the use of carriers; the expression of one gene inhibits the expression of the other. When embedded in a batch culture, the uptake rate of substrates S_1 and S_2 by biomass X (of V1-morphs) with reserve density m_E in a batch culture is given by

$$\begin{aligned}
\frac{d}{dt}S_1 &= -j_{S_1}X; \quad j_{S_1} = \kappa_{S_1}j_{S_1m}f_{S_1}; \quad f_{S_1} = \frac{S_1}{S_1 + K_{S_1}},\\
\frac{d}{dt}S_2 &= -j_{S_2}X; \quad j_{S_2} = \kappa_{S_2}j_{S_2m}f_{S_2}; \quad f_{S_2} = \frac{S_2}{S_2 + K_{S_2}}; \quad \kappa_{S_2} = 1 - \kappa_{S_1},\\
\frac{d}{dt}X &= \dot{r}X; \quad \dot{r} = \frac{\dot{k}_E m_E - \dot{k}_M}{m_E + y_{EV}},\\
\frac{d}{dt}m_E &= y_{ES_1}j_{S_1} + y_{ES_2}j_{S_2} - m_E\dot{k}_E,\\
\frac{d}{dt}\kappa_{S_1} &= (\dot{r} + \dot{h})\left(\frac{w'_{S_1}\kappa_{S_1}f_{S_1}}{w'_{S_1}\kappa_{S_1}f_{S_1} + w'_{S_2}\kappa_{S_2}f_{S_2}} - \kappa_{S_1}\right),
\end{aligned}$$

where j_{*m} is the maximum specific uptake flux of substrate $*$, f_* is the scaled functional response and K_* the half-saturation coefficient for substrate $*$. The coefficient y_{E*} is the yield of reserve E on substrate $*$, $\dot{k}_E$ the reserve turnover rate, $\dot{k}_M$ the maintenance rate coefficient and $\dot{r}$ the specific growth rate. The fraction κ_{S_1} between 0 and 1 quantifies the relative gene expression for the carrier of substrate S_1 and w'_{S_1} the inhibition of the expression of the gene for the carrier of substrate S_1 by the expression of the gene for the carrier of substrate S_2; without loss of generality we can assume that $1 = w'_{S_1} + w'_{S_2}$. Notice that a single substrate induces full gene expression ($\kappa_{S_1} \to 1$ if $f_{S_2} = 0$). The typically very low background expression rate $\dot{h}$ serves an antenna function for substrates that have been absent for a long time. This readily extends to an arbitrary number of substrates. See Figure 7.19 and [65] for an illustration of the application of this theory.

Demand kinetics

If the flux of P is given (and constant), we require that

$$j_P = y_{PS_1}\dot{k}_{S_1}\theta_{S_1} + y_{PS_2}\dot{k}_{S_2}\theta_{S_2}$$

is constant at value $\dot{k}_P$, say, by allowing $\dot{k}_{S_1}$ and $\dot{k}_{S_2}$ to depend on θ_*. The following rates fulfill the constraint:

$$\dot{k}_{S_1} = \dot{k}_P/\theta \text{ and } \dot{k}_{S_2} = w\dot{k}_P/\theta \quad \text{with } \theta = y_{PS_1}\theta_{S_1} + y_{PS_2}w\theta_{S_2},$$

where the preference parameter $w = \dot{k}_{S_2}/\dot{k}_{S_1}$ has the interpretation of the ratio of dissociation rates. For the fractions in steady state, the fluxes of S_1 and S_2 that are used to

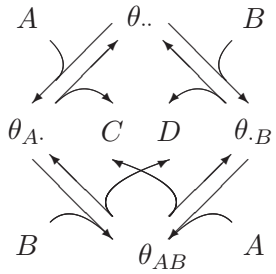

Figure 5.3: The scheme for general co-metabolism of the transformations $A \to C$ with $B \to D$.

produce P are

$$j_{S_1}^+ = (\dot{k}_P - y_{PS_2} j_{S_2}^+) y_{S_1 P} \quad \text{and} \quad j_{S_2}^+ = w \dot{k}_P \frac{\theta_{S_2}^*}{\theta^*} = \frac{2a\dot{k}_P / y_{PS_2}}{2a + y_{PS_1}(\sqrt{b^2 - 4ac} - b)},$$

with $a = w j'_{S_2} \dot{k}_P y_{PS_2}$, $b = y_{PS_1} c + ((1-w) j'_{S_1} + j'_{S_2}) \dot{k}_P$, $c = -j'_{S_1}(j'_{S_1} + j'_{S_2})$. Tolla [554] proposed this model to quantify the preference to pay maintenance (flux j_P) from reserve (flux j_{S_1}) rather than from structure (flux j_{S_2}). Only under extreme starvation conditions, when reserve is insufficient, is maintenance met from structure. This is less efficient, because structure is synthesized from reserve. Since the structure-specific maintenance cost is constant, this formulation is demand driven, rather than the more typical supply driven. The DEB model specifies the reserve flux j_{S_1}. Since the turnover of structure is constant, j_{S_2} is constant. We want to minimize payment of maintenance costs from structure; the worst case is that $j_{S_1} = 0$ and all must be paid from structure, which gives $j'_{S_2} = \dot{k}_P y_{S_2 P}$. The preference parameter w allows for an absolute preference for reserve for $w \to 0$, and a preference for structure for $w \to \infty$. Figure 5.2 presents a numerical study that shows that this model can mimic a switch model, without having a switch.

Another variation on the demand version of (partly) substitutable compounds was studied by [336], where carbohydrate reserve is preferred above protein reserve for paying the energy-maintenance in zooplankton, but protein reserve is required to pay the building-block maintenance. This increase in metabolic flexibility has the consequence that a nutrient-light-phytoplankton-zooplankton system evolves to a situation in which it becomes both energy and nutrient limited, rather than a single limitation only.

Co-metabolism

{164}

Suppose that substrates A and B are substitutable and are bounded parallelly and that the binding probability of each substrate depends on binding with the other substrate as described and applied in [67]. We study the process $1\,A \to y_{CA}\,C$ and $1\,B \to y_{CB}\,C$. So we have three binding probabilities of each substrate; for substrate A we have the binding probabilities

0 if A is already bounded

ρ_A if A and B are not bounded

ρ_{AB} if B is bounded, but A is not

No interaction occurs if $\rho_A = \rho_{AB}$; full co-metabolism occurs if $\rho_A = 0$. See Figure 5.3. Sequential processing occurs if $\rho_{AB} = \rho_{BA} = 0$. The dissociation rates $\dot{k}_A$ and $\dot{k}_B$ of product C, and the stoichiometric coefficients y_{AC} and y_{BC}, might differ for both substrates. The binding period is measured as the period between arrival of substrate and dissociation of product, so it includes the production period.

For $j'_A = j_A\rho_A$, $j''_A = j_A\rho_{AB}$, $j'_B = j_B\rho_B$, $j''_B = j_B\rho_{BA}$, the fractions of bounded SUs follow the dynamics

$$\begin{aligned}
1 &= \theta_{..} + \theta_{A.} + \theta_{.B} + \theta_{AB} \\
\frac{d}{dt}\theta_{..} &= -(j'_A + j'_B)\theta_{..} + \dot{k}_A\theta_{A.} + \dot{k}_B\theta_{.B} \\
\frac{d}{dt}\theta_{A.} &= j'_A\theta_{..} - (\dot{k}_A + j''_B)\theta_{A.} + \dot{k}_B\theta_{AB} \\
\frac{d}{dt}\theta_{.B} &= j'_B\theta_{..} - (\dot{k}_B + j''_A)\theta_{.B} + \dot{k}_A\theta_{AB} \\
\frac{d}{dt}\theta_{AB} &= j''_B\theta_{A.} + j''_A\theta_{.B} - (\dot{k}_A + \dot{k}_B)\theta_{AB}
\end{aligned}$$

Assuming pseudo steady state (i.e. $\frac{d}{dt}\theta_{**} = 0$ for $\theta_{**} = \theta^*_{**}$), the production flux amounts to

$$\begin{aligned}
j_C &= j_{C,A} + j_{C,B} = y_{CA}\dot{k}_A(\theta^*_{A.} + \theta^*_{AB}) + y_{CB}\dot{k}_B(\theta^*_{.B} + \theta^*_{AB}) \\
&= \frac{y_{CA}\dot{k}_A\left(j'_A\dot{k}_B + j''_A\frac{j'_B(\dot{k}_A+\dot{k}_B)+j''_B(j'_A+j'_B)}{j''_A+j''_B+\dot{k}_A+\dot{k}_B}\right) + y_{CB}\dot{k}_B\left(j'_B\dot{k}_A + j''_B\frac{j'_A(\dot{k}_A+\dot{k}_B)+j''_A(j'_A+j'_B)}{j''_A+j''_B+\dot{k}_A+\dot{k}_B}\right)}{j'_A\dot{k}_B + j'_B\dot{k}_A + \dot{k}_A\dot{k}_B + \frac{j''_Aj'_B\dot{k}_B+j''_Bj'_A\dot{k}_A+j''_Aj''_B(j'_A+j'_B)}{j''_A+j''_B+\dot{k}_A+\dot{k}_B}}
\end{aligned}$$

If B represents a xenobiotic substrate, and A a natural one, the case $\rho_A = \rho_{AB}$ and $\rho_B = 0$ is of special interest. The use of A is not effected by B, but B can only be processed if A is present. The expression for the product flux simplifies for $j'_A = j''_A$ and $j'_B = 0$ to

$$j_C = \frac{y_{CA}\dot{k}_A}{1 + \dot{k}_Aj'^{-1}_A} + \frac{y_{CB}\dot{k}_B}{1 + \dot{k}_Aj'^{-1}_A}\,\frac{j''_B(j'_A + \dot{k}_A + \dot{k}_B)}{j''_B(j'_A + \dot{k}_B) + \dot{k}_B(j'_A + \dot{k}_A + \dot{k}_B)}$$

The accepted flux of substrate B, so the specific biodegradation rate of B, is $j^+_B = y_{BC}j_{C,B}$ with $y_{BC} = y^{-1}_{CB}$, and $j_{C,B}$ is given by the second term in the expression for j_C. We need this scheme for co-metabolism to describe e.g. that the conversion of grass to cow and of sheep brain to cow is much less efficient than of the combination.

Derivation of Eq (5.7)

{165}

Eq (5.7) first gives the simple product flux for an SU that is processing single substrate (namely a photon-flux). It then gives an approximation $j_{L_2,A} \simeq -z_{L_2}j_{L,F}$ that is motivated by the reasoning that the maximum photosynthesis is dominated by the maximum of the next step, namely the photon-flux $j_{L_1,Am}$. The numerical effect of $j_{L_2,Am}$ can only be felt if its value is small relative to $j_{L_1,Am}$; so the approximation is motivated to reduce the number of parameters.

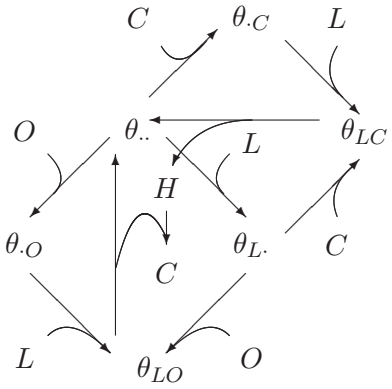

Figure 5.4: The couple photo-synthesis – photo-respiration in the transformations from carbon dioxide C plus photons (light) L (plus water) to hydrocarbon H (plus dioxygen), $C + L \rightarrow H$, and from dioxygen O plus photons plus hydrocarbon to carbon dioxide (plus water), $O + L + H \rightarrow C$.

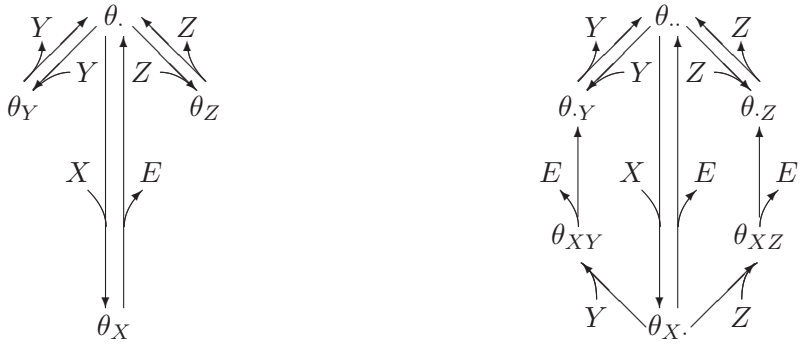

Figure 5.5: The various associations of an individual of species Y with substrate X, which leads to a conversion $X \rightarrow E$, or with other individuals of species Y or Z. The left scheme treats food processing as a process sequential to socialization, the right one as parallel.

Derivation of Eq (5.10)

{166}

Eq (5.10), and the eq just above this one, has a term $(1+z_C^{-1})$ to give the parameter $j_{C_h,Am}$ the interpretation of the maximum specific assimilation flux of carbohydrates. This can be seen by letting the substrate fluxes $j_{C,A}$ (CO_2-flux) and $j_{L,F}$ (photon-flux) go to infinity. (For $X_C \rightarrow \infty$ we have $f_C \rightarrow 1$.) Since $j_{C_H,Am}$ as well as $(1 + z_C^{-1})$ are just numbers, their product is also just a number. The advantage of this notation is that we can now write for the carbohydrate assimilation $j_{C_H,A} = f_{C_H} j_{C_H,Am}$, where $0 \leq f_{C_H} < 1$ is a scaled functional response.

Photosynthesis & photorespiration

{167}

Figure 5.4 illustrates the scheme of photo-synthesis and photo respiration.

Behaviour

{168}

SU dynamics is build on the conservation of time, where an SU can be either in the binding or in the handling phase. Applications in feeding, especially of animals, frequently require more than two states of the SU.

Social interaction [330]

Especially among animals at the demand end of the supply-demand spectrum can be seen as an association between two individuals that dissociates without transformation; the effect on the feeding rate is *via* loss of time that depends in a particular way on the population density; the process is formally equivalent to an inhibition process of a special type. Figure 5.5 shows schemes for the cases that socialization can be initiated during food processing (parallel case) or can not (sequential case), while searching for food cannot be initiated during socialization. Socialization can be intra- and/or inter-specific.

For species Y that interacts intra-specifically only and feeds on food X, the possible "binding" fractions are $1 = \theta_{..} + \theta_{X.} + \theta_{.Y} + \theta_{XY}$. The changes in the "binding" fractions for the parallel case are

$$\begin{aligned} \frac{d}{dt}\theta_{..} &= \dot{k}_X\theta_{X.} + \dot{k}_Y\theta_{.Y} - (\dot{b}_X X + \dot{b}_Y Y)\theta_{..}, \\ \frac{d}{dt}\theta_{X.} &= \dot{b}_X X\theta_{..} + \dot{k}_Y\theta_{XY} - \dot{b}_Y Y\theta_{X.}, \\ \frac{d}{dt}\theta_{.Y} &= \dot{b}_Y Y\theta_{..} + \dot{k}_X\theta_{XY} - \dot{b}_X X\theta_{.Y}, \end{aligned}$$

where $\dot{b}_*$ are the affinities and $\dot{k}_*$ dissociation rates. For the sequential case, we exclude all double binding.

The scaled functional response equals $f = \theta^*_{.}x$ with

$$\begin{aligned} \theta^*_{.} &= (1+x+y)^{-1} \quad \text{sequential case} \\ &= \left(1 + x + y + \frac{xy}{1+w'+w'y}\right)^{-1} \quad \text{parallel case} \end{aligned}$$

where scaled food density $x = X/K_X$ and scaled population density $y = Y/K_Y$ are scaled with saturation constants $K_X = \dot{k}_X/\dot{b}_X$ and $K_Y = \dot{k}_Y/\dot{b}_Y$, *i.e.* ratios of the dissociation rates and the affinities. The socialization parameter $w' = \dot{k}_X/\dot{k}_Y$ is the ratio of the dissociation rates for food and social interaction and plays the role of an inhibition parameter.

If food X is supplied to a population of socially interacting consumers Y in a chemostat run at throughput rate $\dot{h}$, the changes in food and population densities are given by

$$\frac{d}{dt}X = \dot{h}(X_r - X) - f j_{Xm} Y, \tag{5.1}$$

$$\frac{d}{dt}Y = (\dot{r} - \dot{h})Y, \tag{5.2}$$

with specific growth rate $\dot{r} = \frac{\dot{k}_E f - \dot{k}_M g}{f+g}$, where $\dot{k}_M$ is the maintenance rate coefficient, $\dot{k}_E$ the reserve turnover rate and g the energy investment ratio. At steady state we have $\dot{h} = \dot{r}$.

Figure 5.6 illustrates the effects of socialization in a single-species situation. After finishing a food-processing session, a sequentially interacting individual starts food searching, but one interacting in parallel first has to complete any social interaction that started during food processing. If social interaction is parallel, it can always be initiated; if sequential,

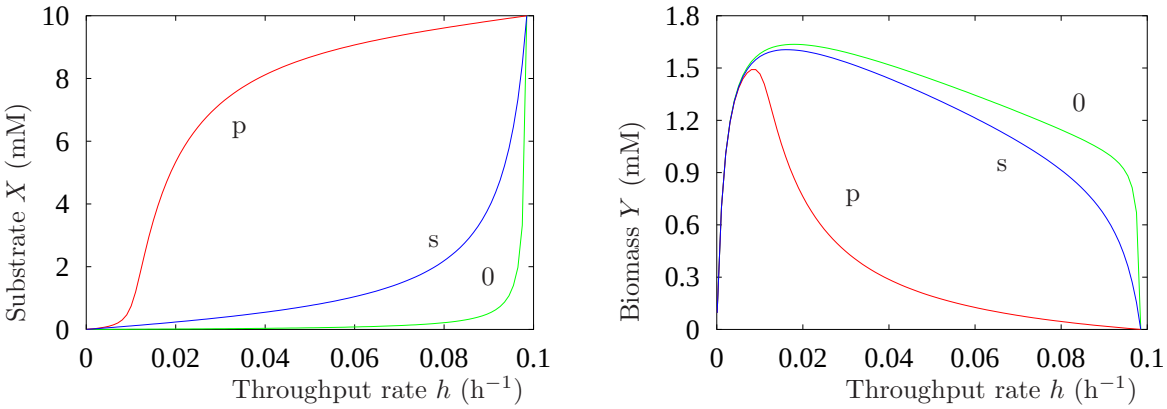

Figure 5.6: No socialization (0), and sequential (s) and parallel (p) socialization in a single-species population in a chemostat. Parameter values: substrate concentration in the feed $X_r = 10$ mM, maximum specific substrate uptake rate $j_{Xm} = 1$ h^{-1}, energy investment ratio $g = 1$, maintenance rate coefficient $\dot{k}_M = 0.002$, reserve turnover rate $\dot{k}_E = 0.2$ h^{-1}, half-saturation coefficients $K_x = 0.1$ mM and $K_y = 0.1$ mM, socialization $w' = 0.01$. The latter parameter only occurs in the parallel case.

it can only be initiated during searching. This explains the substantial difference between both models; sequential socialization has relatively little impact because low growth rates accompany low densities (because of maintenance), and so rare social encounters, whereas high growth rates accompany high food levels, so most time is spend on food processing and not on social interaction. The models are more similar for higher values of K and/or w'. While the sequential model is well known [30, 103], the parallel model is here formulated for the first time.

Sleeping [330]

The neuronal system is, sensitive to ROS, and requires sleep for repair [519, 520]. Since the required sleeping time tends to be proportional to the specific respiration rate, large-bodied individuals have more time to search for food, which partly compensates the disadvantage that the require minimum higher food levels, with consequences for intra- and inter-specific competition. The size-dependent time allocation to sleeping gives, in principle, deviations from the standard DEB model, but it a way that will be difficult to detect empirically.

The link between ageing, sleeping and energetics is *via* the respiration rate (which is fully specified by DEB theory) and the time-budget.

κ in V1-morphs

{168}

Section 5.2 on several reserves is primarily intended for V1-morphs with bacteria and "algae" in mind. For this reason, little attention is given to the κ-rule for allocation to reproduction, and its implications. Its explicit inclusion would involve a set of rules for the buffers of reserves that are allocated to reproduction, a specification of the reserves at hatching and a more elaborate set of rules for excretion and feed back of unused reserves.

Maintenance and excretion

{170}

For a k-reserve system, we have $2k$ maintenance parameters: j_{E_iM} and j_{VM_i} for $i = 1, ., k$, where $j_{VM_i} \geq y_{VE_i} j_{E_iM}$. The actual fluxes of reserve and structure allocated to maintenance are $j_{E_i}^M$ and $j_V^{M_i}$, respectively, and might vary in time, where $j_{E_i}^M \leq j_{E_iM}$ and $j_{VM_i} \leq j_{VM_i}$. See the section on "Maintenance from reserve and structure" of chapter 7.

If no structure is used to pay (somatic) maintenance costs the specific gross growth rate $j_V G$ equals the specific net growth rate $\dot{r}$, but if (some) maintenance is paid from structure at rate $j_V^M < \sum_i j_{VM_i}$, then the growth rates relate to each other as $\dot{r} = j_{VG} - j_V^M$ and the specific rejected flux Eq (5.16) becomes

$$j_{E_iR} = (\dot{k}_{E_i} - \dot{r}) m_{E_i} - j_{E_i}^M - y_{E_iV}(\dot{r} + j_V^M)$$

where $j_{E_i}^M < j_{E_iM}$ is the specific flux of reserve i spend on somatic maintenance. The decision to allocate structure to maintenance is made for each reserve separately, so $j_V^M = \sum_i j_V^{M_i}$.

The dilution by growth is controlled by the specific net growth rate, so $j_{E_iC} = (\dot{k}_E - \dot{r}) m_{E_i}$, and the balance equation for the reserve density Eq (5.17) becomes

$$\frac{d}{dt} m_{E_i} = j_{E_iA} - j_{E_iC} + \kappa_{E_i} j_{E_iR}$$

Organs, tumours & flocs

{177}

We have extended the theory for organs and tumours [349, 345]. Later work revealed that the model for tumour growth is the workload model for allocation that is discussed below. The growth of microbial flocs and tumours have similarities and is further discussed in [66, 349]. The host-tumour interactions allow us to understand why particular tumors continue to grow, while others don't, and why tumours in young individuals grow faster than in older ones. The growth-trajectory of tumours depends very much on parameter values. Caloric restriction reduces tumour growth, but the effect of it fades eventually.

Static generalization of the κ-rule: heart

{179}

Suppose that we decompose structural volume V in that of some organ (e.g. the heart) V_H and of the rest V_R, so $V = V_R + V_H$, and generalize the κ rule as

$$\begin{aligned} \kappa \kappa_H \dot{p}_C &= [E_{GH}] \frac{d}{dt} V_H + [\dot{p}_{MH}] V_H \\ \kappa(1-\kappa_H) \dot{p}_C &= [E_G] \frac{d}{dt} V_R + [\dot{p}_M] V_R (1 + L_h V_R^{-1/3}) \\ \dot{p}_C &= \frac{g[E]}{g + [E]/[E_m]} \left(\dot{v} V_R^{2/3} + \dot{k}_M V_R (1 + L_h V_R^{-1/3}) \right) \end{aligned}$$

Suppose that $[E] = f[E_m]$ is constant. Substituting

$$\frac{\kappa[\dot{p}_C]}{[E_G]} = \dot{k}_C(V) = \frac{f}{f+g} \left(\frac{\dot{v}}{V^{1/3}} + \dot{k}_M \left(1 + \frac{L_h}{V^{1/3}} \right) \right)$$

gives for $e_H = [E_G]/[E_{GH}]$ and $\dot{k}_{MH} = [\dot{p}_{MH}]/[E_{GH}]$

$$\begin{aligned} \frac{d}{dt}V_H &= e_H\kappa_H\dot{k}_C V_R - \dot{k}_{MH}V_H \\ \frac{d}{dt}V_R &= (1-\kappa_H)\dot{k}_C V_R - \dot{k}_M V_R(1 + L_h V_R^{-1/3}) \end{aligned}$$

This dynamics still has full isomorphy as special case, and can show near-allometric relationships between organ and whole body weight. See Figure 5.7.

Dynamic generalization of the κ-rule: Velum vs Gut

{179}

The differential growth of velum and gut in bivalve larvae turns out to be described well by a work-load model [453], see Figure 5.8; in retrospection the tumour growth model is a workload model as well (see below).

We assume that the filtering rate is fully controlled by the size of filtering organ (velum) of volume V_F, and the digestion by the food-processing organ (gut) of volume V_X. The total structural volume thus amounts to $V = V_F + V_X + V_G$, where V_G is the general, i.e. non-assimilatory part of the body.

Isomorphs are organisms that do not change in shape during growth. Isomorphy implies that $V_F = \theta_F V$, for constant fraction θ_F, while $\dot{F} = \{\dot{F}\}(V_F/\theta_F)^{2/3}$, where $\{\dot{F}\}$ does not depend on the size of structure. The same applies for V_X, and $\dot{J}_X = \{\dot{J}_X\}(V_X/\theta_X)^{2/3}$. This couples organ size and function.

The arrival rate of food particles in density X at the individual that filters at rate $\dot{F}$ equals $\dot{F}X$. We assume a parsimonious design, so the filtering rate is such that $\dot{F}X = \dot{J}_X$ and the amount of rejected particles is negligibly small. This makes that the filtering rate equals $\dot{F} = (\dot{F}_m^{-1} + X\dot{J}_{Xm}^{-1})^{-1}$, and half-saturation constant equals

$$K = \frac{\dot{J}_{Xm}}{\dot{F}_m} = \frac{\{\dot{J}_{Xm}\}}{\{\dot{F}_m\}}\left(\frac{V_X/\theta_X}{V_F/\theta_F}\right)^{2/3} = \frac{\{\dot{J}'_{Xm}\}}{\{\dot{F}'_m\}}\left(\frac{V_X}{V_F}\right)^{2/3} = K'\left(\frac{V_X}{V_F}\right)^{2/3}$$

with $\{\dot{J}'_{Xm}\} = \{\dot{J}_{Xm}\}\theta_X^{-2/3}$ and $\{\dot{F}'_m\} = \{\dot{F}_m\}\theta_F^{-2/3}$ and $K' = \{\dot{J}'_{Xm}\}/\{\dot{F}'_m\}$. The feeding rate amounts to $\dot{J}_X = f\{\dot{J}'_{Xm}\}V_X^{2/3}$ with scaled functional response $f = \frac{X}{K+X}$.

Notice that this expression for the half-saturation constant is identical with that for nutrient uptake by plant roots [289, p153], where this uptake depends on the transport of water in the soil, and so on the evaporation by the shoot, thus on the surface area of the shoot. This resemblance of saturation constants is more than superficial if we look beyond morphology to functions of organs, where shoot and velum or root and gut have functional properties in common.

According to the DEB theory, the assimilation and catabolic powers are, for reserve density $[E] = E/V$, given by

$$\begin{aligned} \dot{p}_A &= \mu_{EA}\dot{J}_X = f\{\dot{p}'_{Am}\}V_X^{2/3} \\ \dot{p}_C &= [E](\dot{v}V^{2/3} - \frac{d}{dt}V) \end{aligned}$$

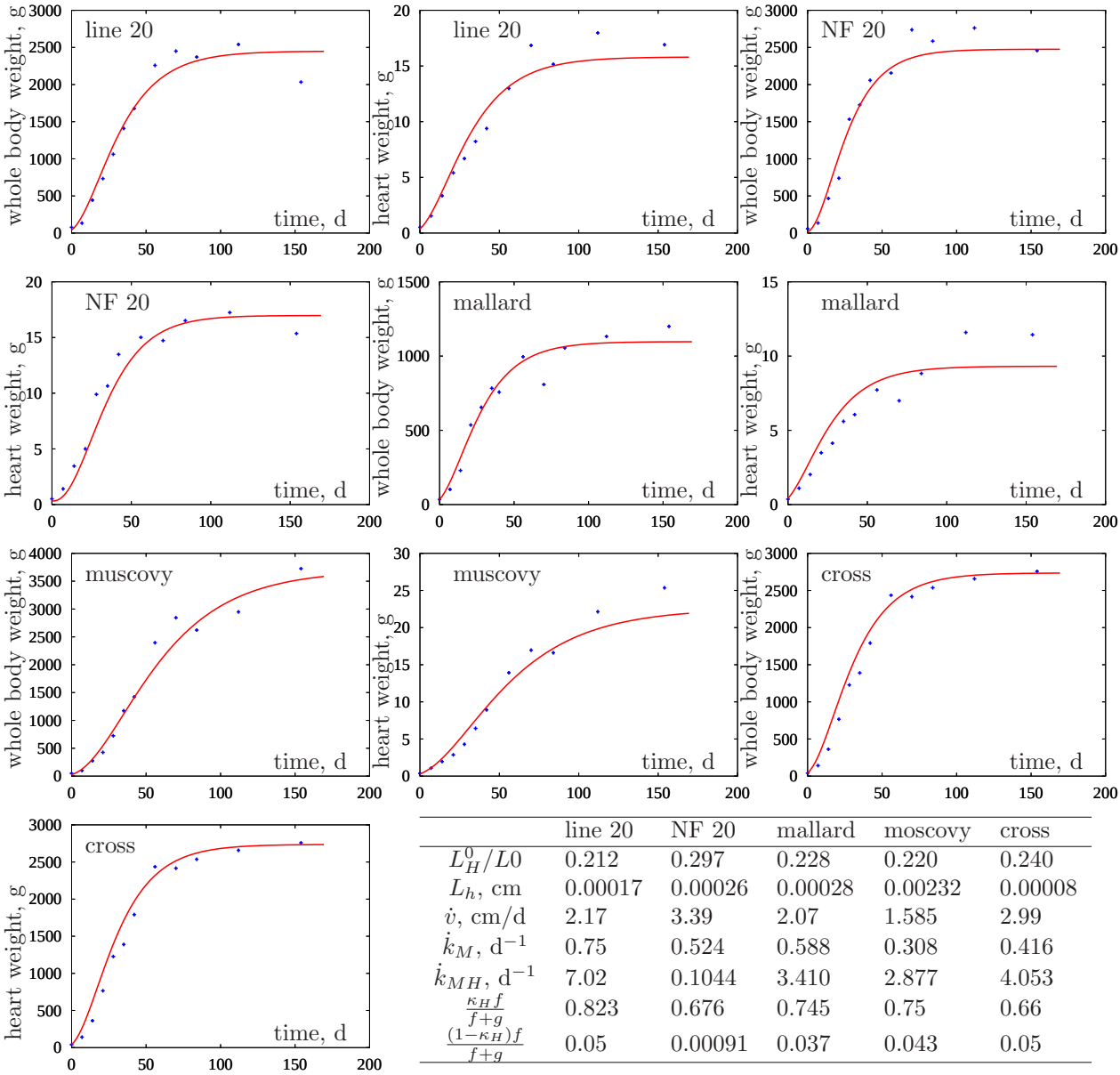

	line 20	NF 20	mallard	moscovy	cross
$L_H^0/L0$	0.212	0.297	0.228	0.220	0.240
L_h, cm	0.00017	0.00026	0.00028	0.00232	0.00008
$\dot{v}$, cm/d	2.17	3.39	2.07	1.585	2.99
$\dot{k}_M$, d^{-1}	0.75	0.524	0.588	0.308	0.416
$\dot{k}_{MH}$, d^{-1}	7.02	0.1044	3.410	2.877	4.053
$\frac{\kappa_H f}{f+g}$	0.823	0.676	0.745	0.75	0.66
$\frac{(1-\kappa_H)f}{f+g}$	0.05	0.00091	0.037	0.043	0.05

Figure 5.7: Whole body weight and heart weigth as function of time since birth in duck species. Data from [161]. The static generalisation of the κ-rule can capture the recreasing relative size of the heart.

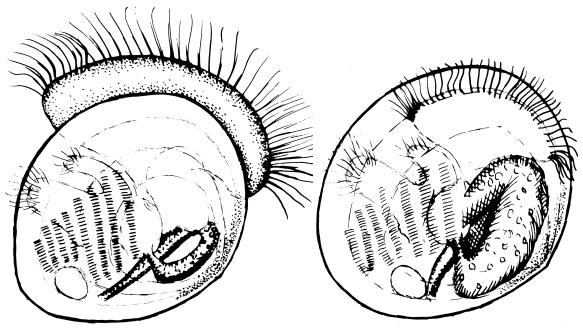

Figure 5.8: *Macoma* larvae develop a large velum and a small gut at low food levels (left), and the other way around at high food levels (right).

with $\{\dot{p}'_{Am}\} = \mu_{EA}\{\dot{J}'_{Xm}\}$ and energy conductance $\dot{v} = \{\dot{p}_{Am}\}/[E_m]$, where $\{\dot{p}_{Am}\} = \mu_{EA}\{\dot{J}_{Xm}\}$ and $[E_m]$ is the reserve density capacity. Reserve dynamics is given by $\frac{d}{dt}E = \dot{p}_A - \dot{p}_C$, or for scaled reserve density $e = [E]/[E_m]$

$$\frac{d}{dt}e = f\dot{v}'V_X^{2/3}/V - e\dot{v}V^{-1/3}$$

with energy conductance $\dot{v}' = \{\dot{p}'_{Am}\}/[E_m]$

The workload of the filtering and digestion organs can be defined as

$$f_F = \dot{F}/\dot{F}_m = 1 - f_X \quad \text{and} \quad f_X = \dot{J}_X/\dot{J}_{Xm} = f$$

We further make the observations that

$$\frac{d}{dV_F}\dot{J}_X = \frac{2}{3}\,\dot{J}_X\,\frac{1-f}{V_F} \quad \text{and} \quad \frac{d}{dV_X}\dot{J}_X = \frac{2}{3}\,\dot{J}_X\,\frac{f}{V_X}$$

Allocation

So far, this is all standard DEB theory; we just introduced some notation that prepares for differentiated growth of organs. This can be done naturally within the framework of the DEB theory by a generalization of the κ-rule, see [289]. Assuming that the costs of structure and its somatic maintenance are independent of the type of structure, the κ-rule can be generalized for $\kappa_F = 1 - \kappa_X$ as

$$\begin{aligned}
\kappa\kappa_A\kappa_F\dot{p}_C &= [E_G]\frac{d}{dt}V_F + [\dot{p}_M]V_F \\
\kappa\kappa_A\kappa_X\dot{p}_C &= [E_G]\frac{d}{dt}V_X + [\dot{p}_M]V_X \\
\kappa(1-\kappa_A)\dot{p}_C &= [E_G]\frac{d}{dt}V_G + [\dot{p}_M]V_G
\end{aligned}$$

where κ_A is the fraction of the catabolic power that is allocated to the assimilation machinery, i.e. to $V_A = V_F + V_X$ and $1 - \kappa$ to maturity maintenance plus maturation (or reproduction in adults). Summing these three equations gives

$$\begin{aligned}
\kappa\dot{p}_C &= [E_G]\frac{d}{dt}V + [\dot{p}_M]V = \kappa[E](\dot{v}V^{2/3} - \frac{d}{dt}V) \quad \text{(see former section), so} \\
\frac{d}{dt}V &= \frac{\dot{v}eV^{2/3} - \dot{k}_M gV}{e+g} \quad \text{and} \quad \frac{\kappa\dot{p}_C}{[E_G]} = \frac{e}{e+g}(\dot{v}V^{2/3} + \dot{k}_M V)
\end{aligned}$$

with maintenance rate coefficient $\dot{k}_M = [\dot{p}_M]/[E_G]$ and investment ratio $g = [E_G]/\kappa[E_m]$.

Using the catabolic power we just obtained and dividing by $[E_G]$ we arrive at

$$\begin{aligned}
\frac{d}{dt}V_F &= \kappa_A\kappa_F\frac{e}{e+g}(\dot{v}V^{2/3} + \dot{k}_M V) - \dot{k}_M V_F \\
\frac{d}{dt}V_X &= \kappa_A\kappa_X\frac{e}{e+g}(\dot{v}V^{2/3} + \dot{k}_M V) - \dot{k}_M V_X \\
\frac{d}{dt}V_G &= (1-\kappa_A)\frac{e}{e+g}(\dot{v}V^{2/3} + \dot{k}_M V) - \dot{k}_M V_G
\end{aligned}$$

Together with given volumes at birth, V_{Fb}, V_{Xb} and V_{Gb}, and the expression for $\frac{d}{dt}e$ we already obtained, these equations fully determine growth of body parts. As long as the fractions κ are constant, this is still the standard DEB model if $V_{Fb} = \kappa_A\kappa_F V_b$ and $V_{Xb} = \kappa_A\kappa_X V_b$, which makes that $V_F = \kappa_A\kappa_F V$ and $V_X = \kappa_A\kappa_X V$ at any time, so $\theta_F = \kappa_A\kappa_F$ and $\theta_X = \kappa_A\kappa_X$.

We now deviate from this standard by allowing that κ_F (and so $\kappa_X = 1 - \kappa_F$) is not longer constant, but can vary in time, depending on the feeding conditions (where food density X varies in time); fractions κ_A and κ are kept constant and the parameters with primes as well. Moreover we assume that the coupling between organ size and function does not change with the relative size of the organ.

We will study two models for allocation of reserve to organs:

$$\begin{aligned}
&\text{workload model:} && \kappa_F = f_F \\
&\text{efficiency model:} && \kappa_F = \frac{d}{dV_F}\dot{J}_X\left(\frac{d}{dV_F}\dot{J}_X + \frac{d}{dV_X}\dot{J}_X\right)^{-1} = \left(1 + \frac{V_F}{V_X}\frac{X}{K}\right)^{-1}
\end{aligned}$$

and compare their numerical behaviour with the standard DEB model.

Model properties

Numerical studies of the body parts as functions of age require the specification of food density $X(t)$, modified saturation constant K', energy conductance $\dot{v}$, modified energy conductance $\dot{v}'$, allocation fraction κ_A, investment ratio g and maintenance rate coefficient $\dot{k}_M$. Moreover we need to specify the situation at birth for the structures V_F, V_X and V_G, and the scaled reserve density e. In this section we analyze some properties of the models at constant food density.

If $V_{Gb} = (1-\kappa_A)V_b$, the relative general structure will not change in time. Further if $e_b = f_b\frac{\dot{v}'}{\dot{v}}\left(\frac{V_{Xb}}{V_b}\right)^{2/3}$, with $f_b = \frac{X}{K_b+X}$ and $K_b = K'\left(\frac{V_{Xb}}{V_{Fb}}\right)^{2/3}$, the scaled reserve density $e(t)$ will not change in time for the standard DEB model. The choice $\dot{v}' = \dot{v}\kappa_A^{-2/3}$ seems natural because it scales the scaled reserve density between 0 and 1.

Weak homeostasis still applies if the relative sizes of the organs become constant, which is well before growth ceases; although relative growth is not a first order process, the time constant $\dot{k}_M^{-1}$ quantifies the rate at which relative growth ceases. The scaled reserve density is no longer confined to the interval (0,1) for arbitrary choices of $\dot{v}'$, also not for the standard

DEB model, because we now link uptake to the size of an organ, rather to that of the whole body. The steady state value is $e^* = f^* \left(\kappa_A \kappa_X^*\right)^{2/3} \dot{v}'/\dot{v}$ and the asymptotic total structural volume is $V^* = V_\infty = \left(\frac{e^* \dot{v}}{g \dot{k}_M}\right)^3$.

The assimilatory machinery is a fixed fraction of the total structure for all models. The steady state relative volumes of V_F and V_X and their ratio equals

$$\frac{V_F^*}{V^*} = \kappa_A \kappa_F^*; \quad \frac{V_X^*}{V^*} = \kappa_A \kappa_X^*; \quad \frac{V_F^*}{V_X^*} = \frac{\kappa_F^*}{\kappa_X^*}$$

We obtain the following results at steady state for $e_A = \kappa_A^{2/3} \dot{v}'/\dot{v}$

quantity	workload	efficiency
half-saturation constant K^*	$K'^{3/5} X^{2/5}$	$K'^{1/2} X^{1/2}$
functional response f^*	$(1 + (K'/X)^{3/5})^{-1}$	$(1 + (K'/X)^{1/2})^{-1}$
partition fraction κ_X^*	f^*	$\left(1 + (K'/X)^{3/4}\right)^{-1}$
scaled reserve density e^*	$f^{*5/3} e_A$	$f^* \kappa_X^{*2/3} e_A$

These functional responses are special cases of what is known as Hill's functional response $f(X) = (1 + (K/X)^n)^{-1}$; this model has an origin in biochemistry [198], and its application in ecology was empirical only.

Both the workload and efficiency models usually show enhanced growth, compared to the standard DEB model, both at low and high food densities. This is revealed by the steady state value of the scaled reserve density; the ultimate (total) volumetric length is proportional to this quantity, see Figure 5.9. The steady state relative size of the filtering organ decreases with the food density more steeply in the efficiency model, compared to the workload model. There are parameter combinations for which the standard DEB model shows more growth than the efficiency model, but the workload model always showed most growth, apart from a short initial period for some parameter combinations. Allocation proportional to relative maintenance workload was also found to be realistic for tumour growth [349], in relation to the state of the host and effects of caloric restriction. Moreover the workload model links up better with the adaptation model [65] that was found to be adequate to capture diauxic growth of micro-organisms. This model for the regulation of the relative abundance of carriers for the uptake of various substrates also uses the workload of the carriers as key for the production of the various substrate-specific carriers.

The conclusion is that the workload model allows for an adequate adaptive behaviour of the morphology to the current food situation. This extension of the standard DEB model 'costs' two extra parameters, V_{Fb} and V_{Xb}, given the restrictions that are mentioned in this section. (The standard DEB model requires the specification of V_b; together with V_{Fb} and V_{Xb} this specifies V_{Gb}, and we choose $\kappa_A = 1 - V_{Gb}/V_b$. There is little need to quantify V_F and V_X explicitly in the standard DEB model, but if we want to do this, we will need V_{Fb} and V_{Xb} as well, so that our extension to variable organ size is then without new parameters.) This extension seems to be most effective in terms of the number of extra parameters that are required. Moreover it gives a mechanistic explanation of Hill's functional response with the important restriction that our Hill's functional response only applies to steady state uptake, after morphological adaptations are completed. The organ

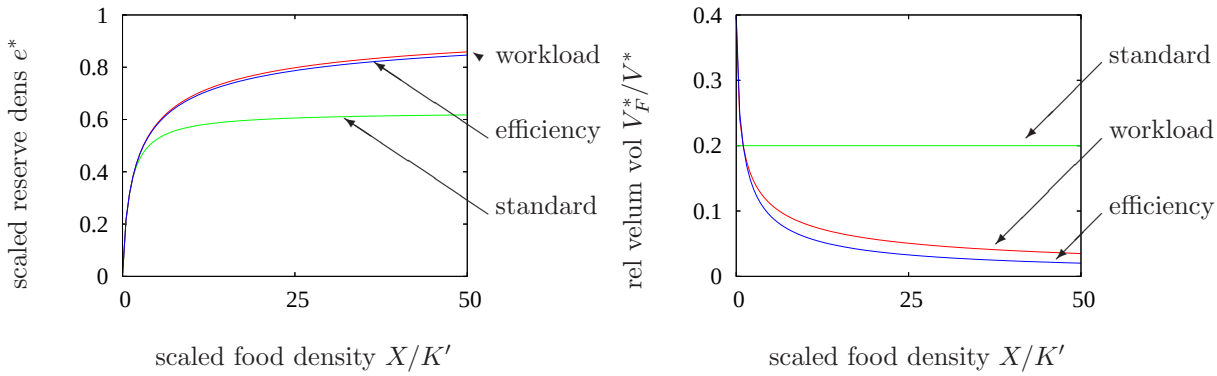

Figure 5.9: The scaled reserve density e^* (left), and the relative size of the velum V_F^*/V^* (right) as a function of the scaled food density X/K' at steady state. Three models are shown: the standard DEB, the workload and the efficiency model. The ultimate volumetric length is proportional to the scaled reserve density. Parameter values: ratio of energy conductances $\dot{v}'/\dot{v} = \kappa_A^{-2/3}$, and allocation to assimilation machinery $\kappa_A = 0.4$.

sizes will generally deviate substantially from the allometry relationship with total body size during growth.

State of plants

{180}, l2 below table

The sentence "structure, and three reserves for root and shoot" is meant to mean that both root and shoot have a structure and three reserves, which makes 8 state variables in total.

Comparison of interactions

{182}

Figure 5.10 compares the various form of interaction between autotrophic and heterotrophic (sub)systems to illustrate the gradual transition between symbiontic and non-symbiontic systems.

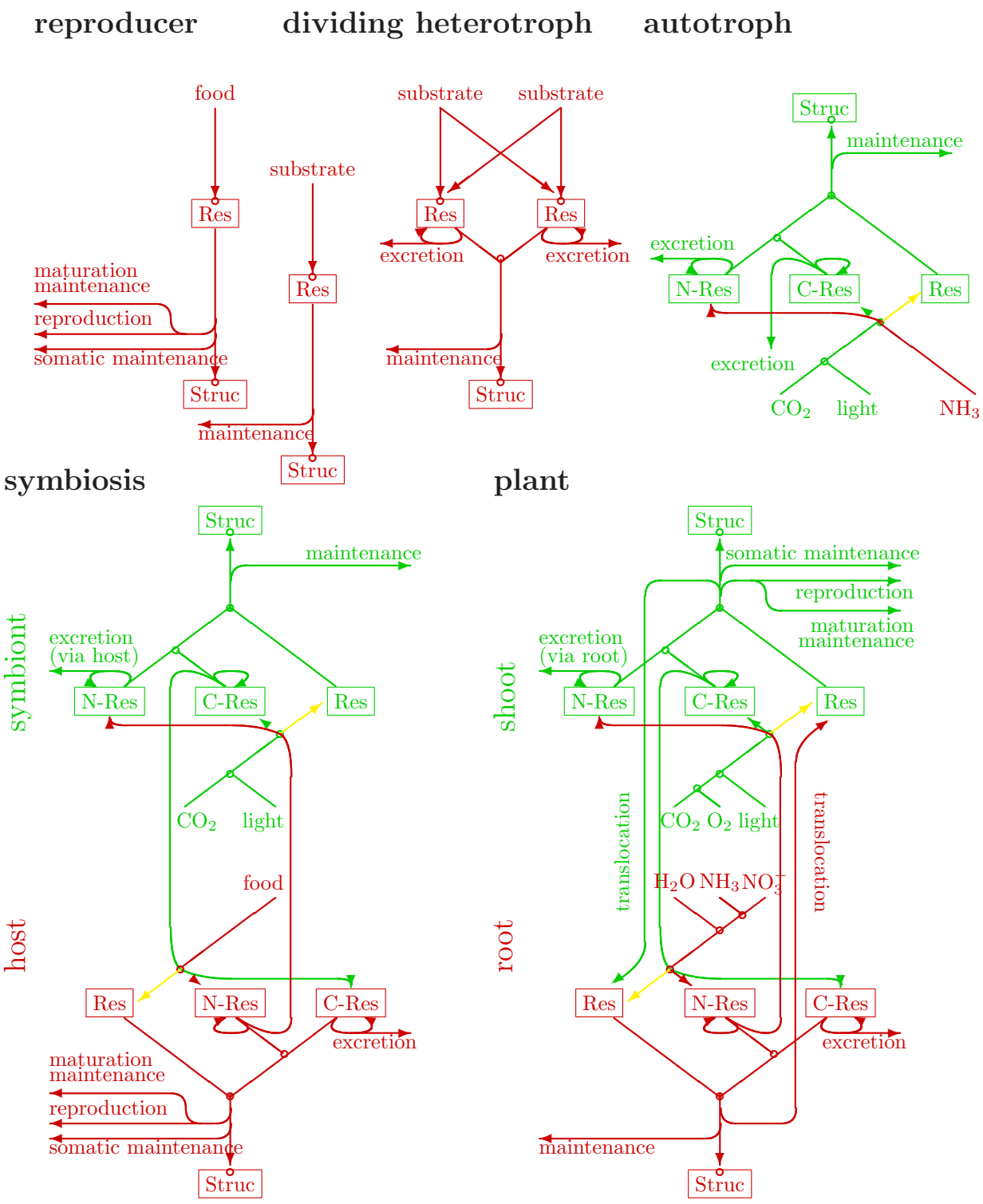

Figure 5.10: The upper-left diagram shows fluxes as appropriate for a reproducing heterotroph*, such as many animals. A simplification is possible for dividing heterotrophs, which remain in the juvenile phase, by combining allocations to somatic and maturity maintenance, and to somatic and maturity growth (second diagram). An extension is required to cope with simultaneous limitation of substrate, which involves excretion (third diagram). Autotrophs require three reserves (a generalized, carbon and nitrogen one; fourth diagram). Symbiontic partners (e.g. in coral, lower left diagram) link excretion fluxes, while plants have extra translocation processes between root and shoot. From [290].

Chapter 6

Uptake and effects of non-essential compounds

1,1-compartment model [318]

{191}

We here derive why and how uptake and elimination parameters covary for the different chemicals, with direct consequences for how toxicity parameters (NEC and killing rate) covary. We also show how variations on the one-compartment model translate in variations in these scaling relationships. The type of reasoning has similarities with the body size scaling relationships; like the partition coefficient, the ultimate length of isomorphs is a ratio of two rates.

We think of a cylinder filled with two homogeneous media that do not mix, and a compound that can move freely from one medium to another across the interface with surface area S. The total number of molecules of the compound is taken to be constant, contrary to a 1-compartment model where the concentration on the environment of the compartment is taken to be constant or a specified forcing function of time. N_i molecules are in medium i of constant volume $\mathcal{V}_i$, with $i = 0, 1$, so the concentration is $c_i = N_i/\mathcal{V}_i$. We introduce a one-dimensional spatial axis, perpendicular on the plane of the interface between the two media, and do not correct for a possible curvature of this interface; the depth of medium i is $\mathcal{L}_i = \mathcal{V}_i/S$. The standard 1,1-compartment model amounts for $j = 1 - i$ to

$$\frac{d}{dt}c_i = \mathcal{L}_i^{-1}(v_{ji}c_j - v_{ij}c_i) \quad \text{or} \quad \frac{d}{dt}N_i = k_{ji}N_j - k_{ij}N_i \tag{6.1}$$

where v_{ij} is the exchange velocity (i.e. a mass transfer coefficient) and $k_{ij} = v_{ij}/\mathcal{L}_i$ the exchange rate of the compound. At equilibrium we have that $\frac{c_i}{c_j} = \frac{v_{ji}}{v_{ij}} = \frac{\mathcal{L}_j}{\mathcal{L}_i}\frac{k_{ji}}{k_{ij}} = P_{ij}$, where P_{ij} is called the partition coefficient.

To simplify the notation, we write x for the partition coefficient P_{01}, choose $\mathcal{L}_0 = \mathcal{L}_1$ and try to find how the elimination rate depends on x. Let us say that the elimination rate k_{01} is some function f of x, i.e. $k_{01} \propto f(x)$, which we want to know. We solve the problem in two steps.

We first demonstrate that the partition coefficient can be written as a quotient of two similar terms, one depending only on i, and the other only on j. For this purpose we

suppose that an extremely thin slice separates two media; the compound can cross the slice freely. The assumption of well-mixed compartments, which is basic to one-compartment models, excludes any concentration gradients. If M denotes the number of molecules in the slice, we get

$$\frac{d}{dt}N_i = h_i M - k_i N_i \tag{6.2}$$

$$\frac{d}{dt}M = k_i N_i + k_j N_j - h_+ M \tag{6.3}$$

where the hazard rate h_i quantifies the specific escape rate from the slice to medium i, while $h_+ = h_i + h_j$. On each side of the slice, the compound cannot 'feel' the presence of the other medium; only in the slice can the compound 'sense' both media, k_i does not depend on any property of medium j. We have that M is very small with respect to the total amount of molecules, implying that $h_i \gg k_i$ and that the dynamics of M is fast with respect to that of N_i.

Suppose that M is in pseudo-equilibrium, so $M^* = k_i N_i/h_+ + k_j N_j/h_+$. Substitution of this result in (6.2) gives

$$\frac{d}{dt}N_i = N_j k_j h_i/h_+ - N_i k_i h_j/h_+ \tag{6.4}$$

From (6.1) it follows that $k_{ij} = k_i h_j/h_+$. The exchange rate, therefor, depends on the properties of medium i *and* j. The partition coefficient is $P_{ij} = \frac{\mathcal{L}_j}{\mathcal{L}_i}\frac{k_j}{k_i}\frac{h_i}{h_j} = \frac{g_i}{g_j}$, with $g_i = h_i k_i^{-1}\mathcal{L}_i^{-1}$. The partition coefficient can thus indeed be written as a ratio of two similar terms, each depending on a single medium only. The term g_i is the value of some function of properties of the compound and medium i that we could quantify with a variable y_i, for instance, while g_j is the value of that same function, but now applied to medium j rather than i. If the elimination rate can be written as $k_{ij} \propto f'(y_i)/f'(y_j)$, we have the condition $f(x) = 1/f(1/x)$. This means that the unknown function f belongs to the class of the power functions: $f(x) = x^\alpha$, for some arbitrary value of the coefficient α (at this moment in our reasoning).

The second step in our derivation is the use of the skew-symmetry argument, which boils down to interchanging media. We know that the uptake rate $k_{10} = f(1/x)$, so we have that $\frac{f(1/x)}{f(x)} = x$. This condition allows for a large class of functions, but in combination with our previous condition $f(1/x) = 1/f(x)$, it leads to a unique solution, namely $f(x)^{-2} = x$ or $f(x) = x^{-1/2}$.

The final result is that

$$k_{ij} \propto v_{ij} \propto 1/\sqrt{P_{ij}} \quad \text{and} \quad k_{ji} \propto v_{ji} \propto \sqrt{P_{ij}}$$

which relates rate parameters to a steady state. The argument for these relationships are all basic to the one-compartment model, apart from the assumption that the rates *can* be written as a function of the partition coefficient, which is by no means self evident. Notice that the temperature, mixing rates, molecular size of the compound, surface area

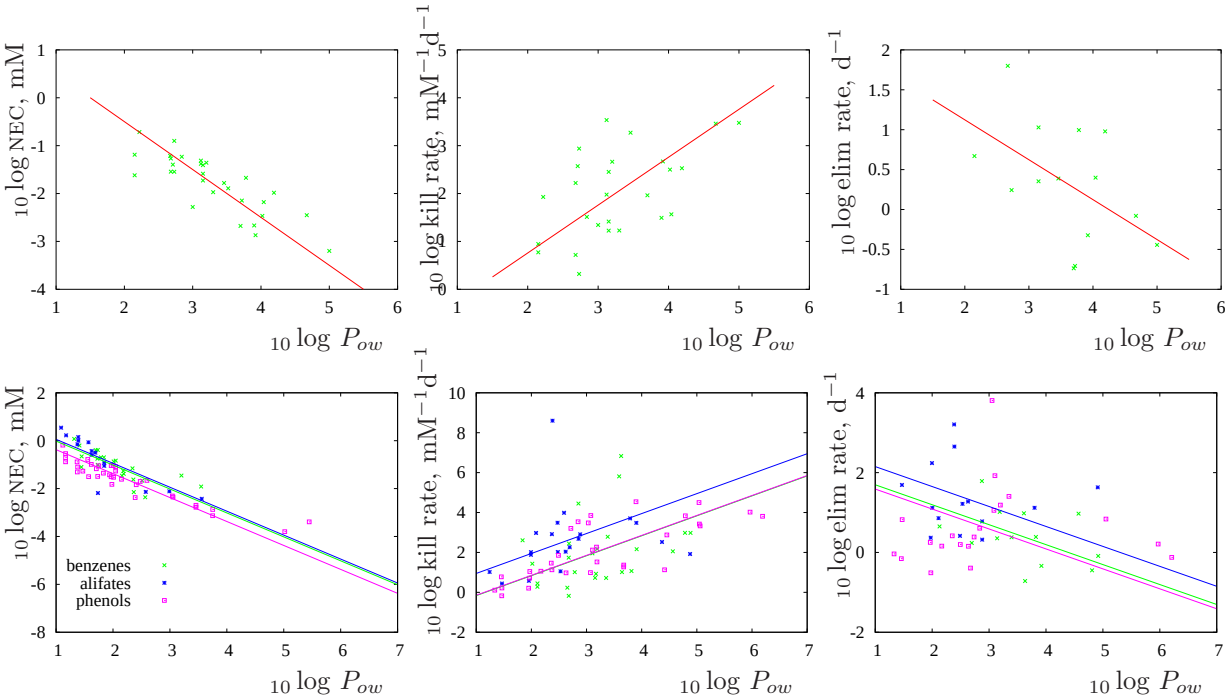

Figure 6.1: The $_{10}$log NEC (left), killing rate (middle) and elimination rate (right) of alkyl benzenes (top) and benzenes, alifatic compounds and phenols (bottom) as a function of the $_{10}$log octanol/water partition coefficient. The slopes of the lines, i.e. -1, 1 and -0.5, respectively, follow from simple theoretical considerations. The data in the top panels are from the 4d bio-assays on survival of the fathead minnow, as presented in [158]. The partition coefficients were obtained from [483] or calculated according to [479]. The data in the bottom panels are from [368] (NECs, killing rates), [190] (elimination rates). The toxicity data originate from [73, 157, 74, 71, 72], as reported in [159].

of exchange, and other modifying factors affects the proportionality constants of the rates, not how they depend on the partition coefficient.

If medium 0 represents some organism, and medium 1 the aquatic environment in which the concentration is constant at level c_1, the model reduces to 1,0-compartment model, better known as the 1-compartment model

$$\begin{aligned} c_0(t) &= c_0(0)\exp\{-k_{01}t\} + c_1P_{01}\left(1-\exp\{-k_{01}t\}\right) \\ &= c_0(0)\exp\{-k_{01}t\} \quad \text{for } c_1 = 0 \\ &= c_1P_{01}\left(1-\exp\{-k_{01}t\}\right) \quad \text{for } c_0(0) = 0 \end{aligned}$$

The rate k_{01} now has the interpretation of the elimination rate. The time we have to wait to saturate the tissue of a blanc organism to a fraction x of the ultimate level is $t_x = -k_{01}^{-1}\ln(1-x)$. It is independent of the concentration in the environment and of the uptake rate, and equals the time required to reach a fraction $1-x$ of the original concentration in the tissue if an exposed organism experiences a blanc environment. We mention these trivialities in preparation of further discussions.

Figure 6.1 presents tests against the empirical evidence of the relationship between

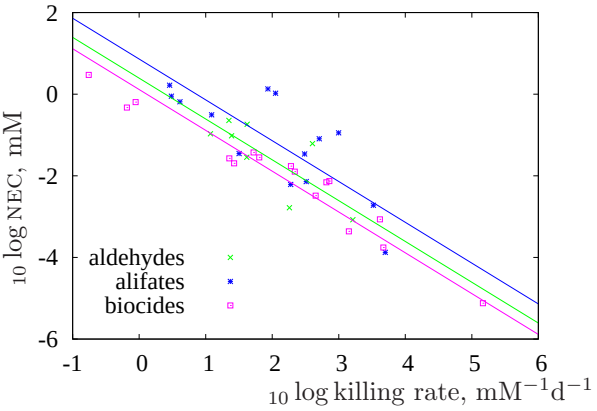

Figure 6.2: The log NEC as a function of the log killing rate for aldehydes, alifates and biocides. Data from [159]. The slope is -1, as resulting from theoretical predictions.

killing rate, elimination rate and NEC with the partition coefficient, and Figure 6.2 does so for the relationship between the killing rate and the NEC. The latter test avoids the uncertainties involved in the relationships with the partition coefficient and is, therefore, more direct. LC50 values at a fixed exposure time are functions of the toxicity parameter, and so covary in predictable ways among chemicals with a related physiological mode of action, see Figure 6.3.

The one compartment model is obviously a very simple one, in which both media are well mixed. We will now study an extension of the model, in which the media are no longer well-mixed.

Film models

{195}

Film models are widely used in environmental chemistry. They are popular because they account for spatial structure of transport in a very simple, yet appealing way, but they suffer from the problem that the films, i.e. the non-mixed layers, can typically not be identified in a direct way. This complicates the link between model predictions and data, as discussed in [318].

Suppose that the media are now separated by rather thin layers of thickness L_i, see Figure 6.4. We will use the notation that the depth of the layer $L = 0$ at the mixed bulk for both media, and $L = L_i$ at the interface. The volume between lengths L_a and L_b is given $V(L_a, L_b) = (L_b - L_a)S$, in both media. The density n of the compound in layer i relates to the number of molecules as $N_i(L_a, L_b, t) = \int_{L_a}^{L_b} n_i(L, t)\, dL$; we have concentration $c_i(L_a, L_b, t) = N_i(L_a, L_b, t)/V(L_a, L_b)$. If the bulk has depth $\mathcal{L}_i$, there are $N_i = n_i(0)\mathcal{L}_i$ molecules in the bulk, which makes that the total amount of molecules in medium i is $N_i^+ = n_i(0)\mathcal{L}_i + N_i(0, L_i)$. The volume of the well-mixed medium is $\mathcal{V}_i = \mathcal{L}_i S$, and of the total medium is $V_i^+ = (\mathcal{L}_i + L_i)S$, so the (mean) concentration is $c_i^+ = N_i^+/V_i^+$. The concentration in the bulk is $c_i = c_i(0) = n_i(0)/S$. We need this notation to compare the different models that we will discuss.

Assuming that the initial densities $n_i(L, 0)$ are given such that the boundary conditions in (6.7), the dynamics for the densities is given for $i = 1-j$ by partial differential equations

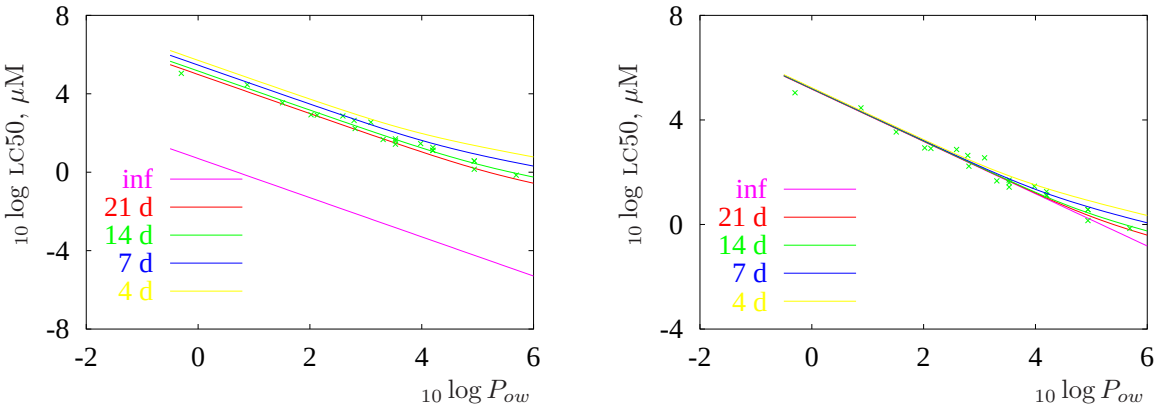

Figure 6.3: LC50.14 d of chlorinated aromatics for guppies as a function of P_{ow}. Data from [242]. Curves for other exposure times are for comparison and follow from the three parameters: NEC (c_0), killing rate (b) and elimination rate (k_e).

par	c_0	b	k_e
units	μM	$\mathrm{d}^{-1}\mu\mathrm{M}^{-1}$	d^{-1}
Left	$5/P_{ow}$	$3.413\,10^{-7}P_{ow}$	$45.03/\sqrt{P_{ow}}$
Right	$1.5\,10^{5}/P_{ow}$	$8.21\,10^{-6}P_{ow}$	$30.17/\sqrt{P_{ow}}$

The LC50 data give little information about the NEC's (c_0). The relationships demonstrate that the extrapolation to other exposure times is very sensitive to this.

(pde's)

$$0 = \frac{\partial}{\partial t}n_i(L,t) - d_i\frac{\partial^2}{\partial L^2}n_i(L,t) \quad \text{for } L \in (0, L_i) \tag{6.5}$$

with boundary conditions at $L = 0$ for $v_i = d_i/L_i$

$$0 = \frac{\partial}{\partial t}n_i(0,t) - v_i\frac{\partial}{\partial L}n_i(0,t) \tag{6.6}$$

and boundary conditions at $L = L_i$

$$0 = v_{ji}n_j(L_j,t) - v_{ij}n_i(L_i,t) + d_i\frac{\partial}{\partial L}n_i(L_i,t) \tag{6.7}$$

The latter boundary conditions are believed to be new, despite the popularity of the film-models.

For increasing diffusivity's d_i, and/or decreasing thickness of the non-mixed layers L_i, this two-film model reduces to the 1,1-compartment model of the last section (to be discussed in the following sections). So it is an extension of the same idea that accounts for lack of mixing in the boundary area.

This model has rather complex properties, so we will study simplifications of it.

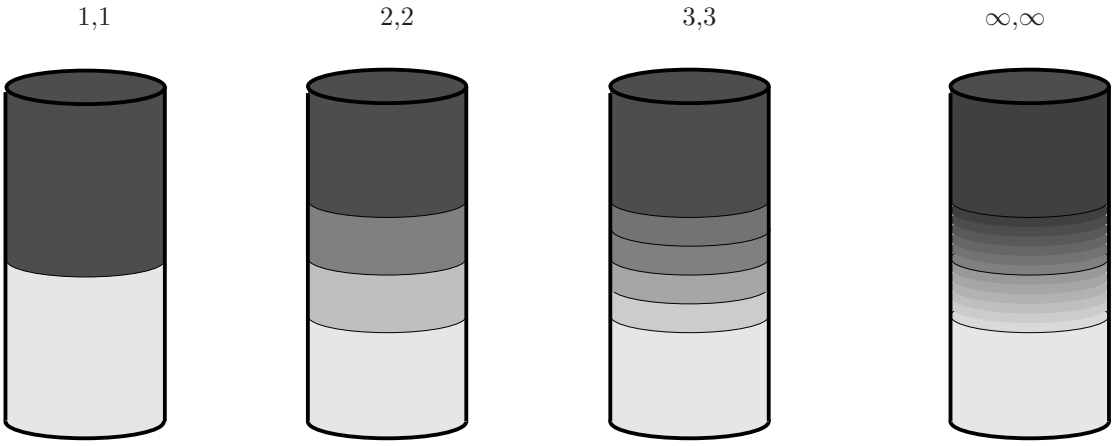

Figure 6.4: The sequence of physical systems that we study in this paper, called n,n-compartments. The medium 0 is confined to the upper compartment in the cylinder, medium 1 to the lower one; they cannot cross the thin line that separates them, while the compound can but with possibly different concentration-specific rates. The compound can also cross the very thin lines within the media, but with the same specific rates. Starting from the simplest situation at the left, $n = 1$, the system converges for $n = 2, 3, \cdots$ to the two-film system at the right in which we have continuous concentration gradients in the layers on each side of the interface between the media.

Steady-flux approximation

Suppose now that transport in the films is steady, i.e. the density profiles do not change in time, so $\frac{\partial}{\partial t} n_i(L,t) = 0$. Suppressing argument t, we then have according to (6.5) that

$$0 = \frac{d^2}{dL^2} n_i(L) \text{ for } L \in (0, L_i)$$

The density profiles in the films are thus linear:

$$\frac{d}{dL} n_i(L) = \left(n_i(L_i) - n_i(0)\right)/L_i$$

The mass balance across the bi-film gives $L_i \frac{d}{dt} n_i(0) = -L_j \frac{d}{dt} n_j(0)$, which leads via (6.6) to $(n_j(L_j) - n_j(0))v_j = -(n_i(L_i) - n_i(0))v_i$. Substitution of this result in (6.7) gives $n_i(L_i)$ as a weighted sum of $n_i(0)$ and $n_j(0)$. Back-substitution in (6.6) finally leads to the first order kinetics for the bulk densities $\frac{d}{dt} n_i(0) = k_e(P_{ij} n_j(0) - n_i(0))$ with elimination rate

$$k_e = k_i(1 + P_{ij} v_i/v_j - v_i/v_{ij})^{-1}$$

for $v_i v_j < v_{ij} v_j + v_{ji} v_i$. The restriction of this approximation is that the change in bulk densities n_i is sufficiently small to allow the transport flux in the bi-film to be steady and that transport within the film is strictly limiting; this is not necessarily true. If the transport within the bi-film is very slow, relative to the exchange velocities across the interface, $v_i v_j \ll v_{ij} v_j + v_{ji} v_i$, the elimination rate simplifies to $k_e \simeq k_i(1 + P_{ij} v_i/v_j)^{-1}$,

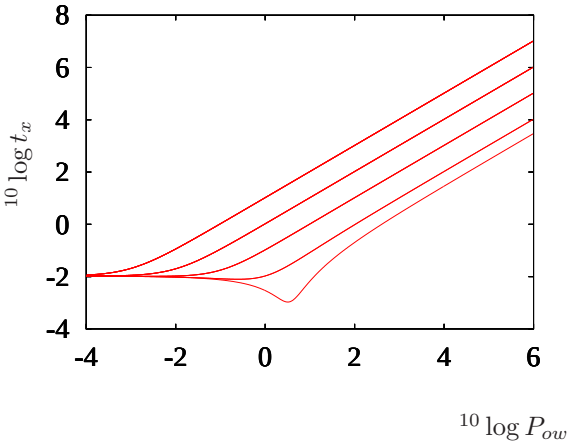

Figure 6.5: A log-log plot of the time to reach an x-level saturation in the tissues of an organism exposed in an environment with a constant concentration of a compound in a two-film model, using the steady-flux approximation. The curves correspond with different values of the velocity v_1; the upper curve has the lowest velocity. Parameters: $v_0 = 1$, $v_1 = .001$, $.01$, $.1$, 1, 3.6 mm h^{-1}. $v_{01} = P_{ow}^{-1/2}$, $v_{10} = P_{ow}^{1/2}$, $k_0 = 10$ h^{-1}, $x = 0.1$. Notice that the $v_1 = 3.6$ mm h^{-1} is close its maximum value in this parameter combination to ensure positive elimination rates; the steady-flux approximation is probably very poor in this situation.

while $n_i(L_i) \simeq P_{ij} n_j(L_j)$. Boundary condition (6.7) shows that this can only be a crude approximation indeed, because a gradient is required to drive diffusive transport, and the concentration jump across the interface only equals the partition coefficient in absence of a gradient in the films.

The time we have to wait to saturate the tissue of a blanc organism to a fraction x of the ultimate level is $t_x = -k_e^{-1} \ln(1 - x)$. Figure 6.5 illustrates how this time relates to the P_{ow}. We see that the elimination rate k_e is now a hyperbolic function of the partition coefficient. This result is reported by Schwarzenbach et al [512] for air-water exchange, by Flynn and Yalkowsky [147] for artificial membranes, and by Gobas and Opperhuizen [165] for fish. For low P_{ow} values, the elimination rate hardly depends on the P_{ow} and for large values it is inversely proportional to P_{ow}. As a consequence, the opposite holds for the uptake rate. The result of Thomann [549] is largely consistent with this relationship, if applied to the proper range of P_{ow} values. Notice that this reasoning does not make use of the considerations for how the exchange rates k_{ij} depend on P_{ij} as presented in the earlier section; this is because they do not occur independently in this steady-state flux model, but only in combination as a ratio in the form of P_{ij}.

The steady-flux approximation of two-film model has a one-film model as special case, where e.g. $L_j \to 0$ or $v_j \to \infty$. The elimination rates then reduces to $k_e = k_i(1 - v_i/v_{ij})^{-1}$, and we must have that $v_i < v_{ij}$. Since $v_{ij} \propto 1/\sqrt{P_{ij}}$, this approximation is only valid in a limited range of P_{ij} values, depending on the value of v_i.

This illustrates a serious problem with this steady-flux approximation: contrary to the full pde formulation, we cannot reduce this approximation in a smooth way to the well-mixed special case of a one-compartment model. If we would increase the diffusivities d_i and/or reduce the thickness of the non-mixed layers L_i, we are forced to increase the exchange rates k_{ij} as well to ensure that the transport in the layers is still in pseudo steady-state. In other words: the dynamics of the system disappear, and the whole system equilibrates instantaneously. We will see k_{01} and k_{10} will occur independently in other approximations of the two-film pde model that do not suffer from this problem. This

approximation is popular in situations where the bulk volumes are infinitely large and represent the ocean and the atmosphere, for instance. It than becomes a reasonable assumption to take a constant flux from one medium into the other, without changes in the bulk concentrations. This application is quite different from that in toxico-kinetics, where one medium represents a initially blanc fish, and the other an aquarium with a compound, and we study the toxico-kinetics and effects in transient states.

2,2- and 2-compartment approximations

In this approximation we assume that the layers adjacent to the interface are well-mixed and write N_{i1} for the amount in the boundary layer of medium i, and N_i for the amount in the bulk of medium i (see Figure 6.4). The volume of the layer is V_{i1} and of the bulk $\mathcal{V}_i$, which makes that the concentration in the layer is $c_{i1} = N_{i1}/V_{i1}$ and in the bulk $c_i = N_i/\mathcal{V}_i$. The total amount in medium i is $N_i^+ = N_i + N_{i1}$, the total volume is $V_i^+ = \mathcal{V}_i + V_{i1}$, and the total (mean) concentration $c_i^+ = N_i^+/V_i^+$. The set of pde's is now approximated by the linear ordinary differential equations (ode's) for $k_i = v_i/L_i$ and $l_i = L_i\mathcal{L}_i^{-1}$

$$\frac{d}{dt}\boldsymbol{c} = \boldsymbol{k}\boldsymbol{c} \quad \text{with} \quad \boldsymbol{c} = \begin{pmatrix} c_0 \\ c_{01} \\ c_{10} \\ c_1 \end{pmatrix} \quad \text{and} \quad \boldsymbol{k} = \begin{pmatrix} -k_0 l_0 & k_0 l_0 & 0 & 0 \\ k_0 & -k_0 - k_{01} & k_{10} & 0 \\ 0 & k_{01} & -k_1 - k_{10} & k_1 \\ 0 & 0 & k_1 l_1 & -k_1 l_1 \end{pmatrix}$$

This linear system can be integrated explicitly, with solution $\boldsymbol{c}(t) = \exp\{\boldsymbol{k}t\}\boldsymbol{c}(0)$.

For large k_0, the model for N_0^+ reduces to the one-compartment model, just as the pde model, for which this model is an approximation. The link between this 2,2-compartment model and the two-film pde model is discussed in the next subsection.

In order to compare this model with the one compartment one, we again study the time t_x we have to wait saturate the tissue of a blanc organism to a fraction x of the ultimate level. This study has to be done numerically, and Figure 6.6 summarizes the results. The small rate dominates the waiting time; for large P_{ow}, this is the elimination rate; the diffusivity does not depend systematically on P_{ow}. The figure shows that the second film acts as an extra resistance, which becomes stronger for increasing P_{ow}. While the one-film model has slope 0.5 in the linear sections, the slope is 1 for the two-film model at low diffusivities, and 0.5 for large ones. For low diffusivities, the relationship is similar to the one we found for the steady-flux approximation (i.e. hyperbolic). The results for the two-film model clearly show that we can smoothly go from a hyperbolic relationship (transport dominated by diffusion in the film) to a square-root relationship (transport dominated by exchange across the interface), by changing the parameters of the system.

n,n-compartment approximations

We can partition the single mixed-layers of the 2,2-compartment model into $2, 3, \cdots, n$ layers. We write $V_{ij} = L_{ij}S$ for the volume, and L_{ij} for the depth of sublayer j in medium i, with $j = 1, 2, \ldots, n$. For the sake of notational simplicity, we here take the numbers of sub-layers equal in both media and choose all sub-layers in each medium of equal depth,

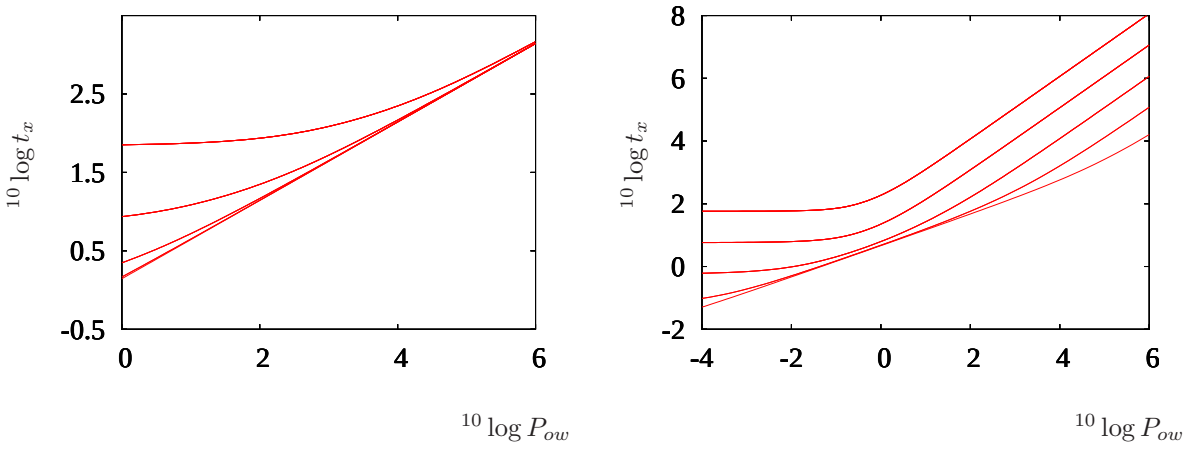

Figure 6.6: A log-log plot of the time to reach an x-level saturation in the tissues of an organism exposed in an environment with a constant concentration of a compound with a single film (left) and a double film (right). The curves correspond with different values of the diffusivity in a two-compartment model; the upper curve has the lowest diffusivity. Parameters: $l_0 = 1$, $k_{01} = P_{ow}^{-1/2}$, $k_{10} = P_{ow}^{1/2}$, $k_0 = 0.01, 0.1, 1, 10, 100$ h^{-1} (left), $k_0 = k_1 = 0.04, 0.4, 4, 40, 400$ h^{-1} (right), $x = 0.1$. Notice that the one-film model has slope 0.5, while the two-film model has slope 1 in the linear sections for low diffusivities and high partition coefficients (i.e. low elimination rates), and 0.5 for large diffusivities.

which gives $L_{ij} = L_i/n$. Both V_{ij} and L_{ij} decrease inversely proportional to n if the depth of the (total) boundary layer $L_i = \sum_{j=1}^{n} L_{ij}$ is taken to be constant. The vector of concentrations and the matrix of coefficients become for $k_i = v_i/L_i$ and $l_i = L_i\mathcal{L}_i^{-1}$

$$\boldsymbol{c} = \begin{pmatrix} c_0 & c_{01} & \cdots & c_{0n} & c_{1n} & \cdots & c_{11} & c_1 \end{pmatrix}^T$$

and

$$\boldsymbol{k} = \begin{pmatrix} -k_0'l_0' & k_0'l_0' & & & & & & \mathbf{0} \\ k_0' & -2k_0' & k_0' & & & & & \\ & \ddots & \ddots & \ddots & & & & \\ & & k_0' & -2k_0' & k_0' & & & \\ & & & k_0' & -k_0' - k_{01}' & k_{10}' & & \\ & & & & k_{01}' & -k_1' - k_{10}' & k_1' & \\ & & & & & k_1' & -2k_1' & k_1' \\ & & & & & & \ddots & \ddots \\ & & & & & & k_1' & -2k_1' \\ \mathbf{0} & & & & & & & k_1'l_1' \end{pmatrix} \begin{matrix} \\ \\ \\ \\ \\ \\ \\ k_1' \\ \\ -k_1'l_1' \end{matrix}$$

The first item to discuss is how the values for rates k_i' and k_{ij}' and the scale length l_i' relate to each other for different choices of the number of sub-layers n. The mean residence time of a molecule in the (total) boundary layer should not depend on the number of sub-layers.

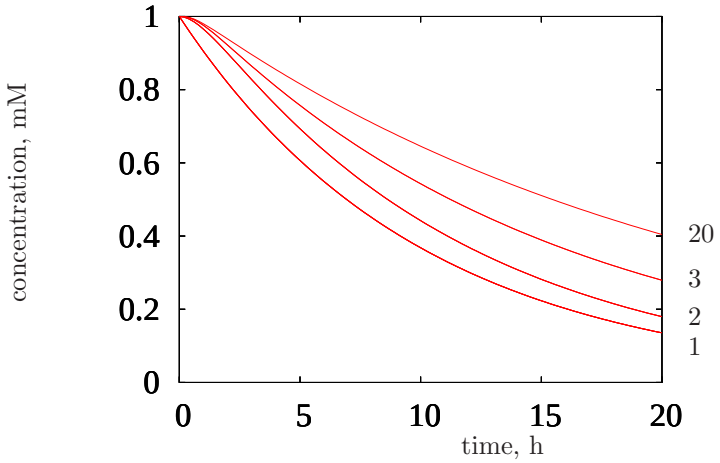

Figure 6.7: The time trajectory of the concentration in the bulk $c_0(t)$, for $n = 1, 2, 3, 20$ compartments in medium 0 and no compartments in medium 1, while the concentration in the medium 1 is zero, $c_1 = 0$. The diffusivities are $k_0 = 0.1n^2$ h^{-1}, while the scaled length $l_0 = 1/(n-1)$. Notice that for $n = 1$ we do not have a diffusion layer and the value for the diffusivity and scaled length are irrelevant; the bulk then eliminates exponentially.

By requiring $k_i' = n^2 k_i$ and $k_{ij}' = (1+n)k_{ij}$ and $l_i' = l_i/(n-1)$, we achieve that an increase of n increases the level of detail of the model, without affecting the overall properties.

By increasing the number of sub-layers $n \to \infty$, while decreasing the depth of each sublayer dL such that the depth of the non-mixed layer $L_i = n\,dL$ is constant, this set of ode's converges to the pde model, with the concentration in sublayer j becomes the surface area-specific density: $c_{ij}(t) \to n_i(L_i j/n, t)/S$, and $k_i \to d_i L_i^{-2}$ and $k_{ij} \to v_{ij} L_i^{-1}$.

Numerical analysis shows that the increase of the number of layers does not have a large quantitative effect, see Figure 6.7.

Derivation of Eq (6.14)

{195}

Section 6.3 formula (6.14) is derived as follows. We start from (6.1) at {190} on the basis of mass, rather than concentration. Remember that the elimination flux is proportional to the internal *concentration* ($[M_Q]$), rather that to the *amount*, and both exchange fluxes are proportional to surface area. So we multiply the accumulation rate ($\dot{k}_a V_m$) and the elimination rate ($\dot{k}_e$) with a squared scaled length. Then we divide by volume and account for the dilution by growth. Finally we divide by the BCF:

$$\begin{aligned}
\frac{d}{dt}M_Q &= (\dot{k}_a c_d - \dot{k}_e [M_Q]) V_m l^2 \\
&= (\dot{k}_a c_d - \dot{k}_e [M_Q]) V_m l^2 \\
&= (P_{Vd} c_d - [M_Q]) V_m \dot{k}_e l^2 \\
\frac{d}{dt}[M_Q] &= (P_{Vd} c_d - [M_Q]) \dot{k}_e / l - [M_Q] \frac{d}{dt} \ln V \\
\frac{d}{dt}c_V &= (c_d - c_V) \dot{k}_e / l - c_V \frac{d}{dt} \ln l^3
\end{aligned}$$

where $V = V_m l^3$, $[M_Q] = M_Q/V$, $P_{Vd} = \dot{k}_a/\dot{k}_e$, $c_V = [M_Q]/P_{Vd}$, $\frac{d}{dt}\ln V = V^{-1}\frac{d}{dt}V = l^{-3}\frac{d}{dt}l^3$.

Derivation of Eq (6.15)

{197}

Eq (6.15) can be understood as follows. The mass of compound Q in the body is partitioned into three pools: that in structure V, in reserve E and in the reproduction buffer E_R, so $M_Q = M_{QV} + M_{QE} + M_{QR}$. We assume that the partitioning is in equilibrium. This means that $M_{QE} = M_{QV}P_{EV}M_E/M_V$, where P_{EV} is the reserve-structure partitioning coefficient defined as $P_{EV} = \frac{M_{QE}/M_E}{M_{QV}/M_V}$ at equilibrium with respect to the transport of compound Q between the (three) pools. The reserve and the reproduction buffer have the same chemical composition, so $M_{QR} = M_{QV}P_{EV}M_{ER}/M_V$. Substitution gives $M_Q = M_{QV}(1+P_{EV}(M_E + M_{ER})/M_V)$. Table 3.4 at {122} gives $M_E = eM_{Em}$, and likewise we write $M_{ER} = e_R M_{Em}$. This leads to $M_Q = M_{QV}(1 + \frac{M_{Em}}{M_V}P_{EV}(e+e_R)) = M_{QV}(1 + \frac{[M_{Em}]}{[M_V]}P_{EV}(e+e_R))$. The significance of the last equality is that $[M_V]$ and $[M_{Em}]$ are constants, because of the strong homeostasis assumption. The final step is to substitute the biomass-structure partition coefficient $P_{WV} = 1+\frac{[M_{Em}]}{[M_V]}P_{EV}(e+e_R)$. For individuals that do not build up a reproduction buffer ($e_R = 0$), and live in a constant environment (which means that e settles at a constant value), P_{WV} becomes constant as well.

Internal concentrations

{202}

We present further evidence that toxic effects should be linked to internal concentrations in [196, 211]. Effects disappear as soon as internal concentrations are below a threshold value and re-appear if they are above this value [449]. Theory for effects during variations of external concentrations is given in [446].

NEC

{206}

We demonstrated that the NEC estimates has nice statistical properties, and that confidence intervals obtained via profile likelihood functions are valid, even for a very small number of test organisms [9]. Even if the NEC varies in value among individuals, its mean is recovered accurately from a low number of test organisms; the accurate recovery of the scatter requires more individuals [17].

Half saturation constant

{211}

The half saturation constant for *Daphnia* can be interpreted as the ratio of the maximum feeding rate and the maximum filtering rate, see {74}: $K = J_{Xm}/F_m$ and the scaled functional response is $f = \frac{X}{K+X}$. So if a compound affects the maximum feeding rate only, the half saturation constant is affected as well. The same applies for the maximum filtering rate. If both rates are reduced by the same factor, the half saturation constant is independent of the chemical stress. If experiments are done at abundant food, the half saturation constant is irrelevant.

The reserve dynamics (in the blank) is given by Eq (3.10):

$$\begin{aligned} \frac{d}{dt}[E] &= (f\{\dot{p}_{Am}\} - \dot{v}[E])V^{-1/3} \\ \frac{d}{dt}e &= (f\{\dot{p}_{Am}\}/[E_m] - \dot{v}e)V^{-1/3} \end{aligned}$$

In the evaluation of effects of toxicants it matters which two of the three parameters $\{\{\dot{p}_{Am}\}, [E_m], \dot{v}\}$ are considered as the primary parameters, and which one as a compound parameter. The most natural choice is to consider $[E_m] = \{\dot{p}_{Am}\}/\dot{v}$ as a compound parameter and the energy investment ratio is $g = \frac{[E_G]\dot{v}}{\kappa\{\dot{p}_{Am}\}}$. Under stress on the parameter $\{\dot{p}_{Am}\}$, the reserve dynamics then becomes

$$\frac{d}{dt}e_s = (f - e_s)\dot{v}V^{-1/3}$$

with the implication that the effects on assimilation reduces the reserve density $[E]$, but not the scaled reserve density e, because the effect is scaled out, i.e. $0 < e_s \leq 1$. In other words: the reserve density is not scaled with the maximum one in the blank, but with the maximum one in the stressed situation. This dynamics only applies if the compound affects the digestion efficiency, so the food uptake rate in not affected, but the assimilation rate is. It also applies if the maximum feeding rate is affected, but then only at abundant food, so $e = 1$ (which makes that the half saturation constant is irrelevant).

The reproduction rate (in the blank) is given by Eq (3.48). Using Eq (3.52) for the maximum reproduction rate

$$\dot{R}_m = \kappa_R[\dot{p}_M]\frac{1-\kappa}{\kappa E_0}(V_m - V_p)$$

In the stressed situation for effects on the max spec assimilation rate, the costs for structure, for an egg or on the specific maintenance costs we have

$$\dot{R}_{ms} = \kappa_{Rs}[\dot{p}_M]_s\frac{1-\kappa}{\kappa E_0}(V_{ms} - V_p)$$

or

$$\frac{\dot{R}_{ms}}{\dot{R}_{m0}} = \frac{\kappa_{Rs}}{\kappa_{R0}}\frac{[\dot{p}_M]_s}{[\dot{p}_M]_0}\frac{(l_{ms}/l_{m0})^3 - l_p^3}{1 - l_p^3}$$

The reason for linking affects to κ_R rather than E_0 is pragmatic only, because the rule that the reserve density of the embryo at birth equals that of the mother at egg formation leads to a complex expression for the costs of an egg that involves maintenance and costs for structure parameters. By replacing that rule by a numerically simpler one, namely that the reserve density at birth is independent of the nutritional status of the mother avoids all these problems, but introduces an extra parameter, namely the costs of an egg. An additional implication is that growth at constant food cannot longer be exactly von Bertalanffy, except for a single special food density.

Stage transitions occur if the cumulative investment into maturation exceeds a threshold. This only occurs when the amount of structure exceeds a threshold if $[\dot{p}_J] = [\dot{p}_M](1 -$

$\kappa)/\kappa$. If the compound affects $[\dot{p}_M]$, but not $[\dot{p}_J]$, stage transitions no longer occur at a fixed amount of structure (and becomes dependent on food history). For simplicity's sake, we assume that $[\dot{p}_M]$ and $[\dot{p}_J]$ are affected in the same way, with the implication that V_p is not affected.

For the reproduction rate we arrive at

$$\dot{R} = \frac{\dot{R}_m}{V_m - V_p}\left(\frac{e}{g+e}\left(\frac{\dot{v}}{\dot{k}_M}V^{2/3} + V\right) - V_p\right)_+$$

We can check that $\dot{R} = \dot{R}_m$ if $e = 1$ and $V = V_m = (\frac{\dot{v}}{g\dot{k}_M})^3$. In the case of stress we have for $l = (V/V_{m0})^{1/3}$

$$\begin{aligned}
\dot{R}_s &= \frac{\dot{R}_{ms}}{V_{ms} - V_p}\left(\frac{e}{g_s+e}\left(\frac{\dot{v}}{\dot{k}_{Ms}}V^{2/3} + V\right) - V_p\right)_+ \\
&= \frac{\dot{R}_{ms}}{(l_{ms}/l_{m0})^3 - l_p^3}\left(\frac{el^2}{g_s+e}\left(\frac{\dot{v}}{\dot{k}_{Ms}V_{m0}^{1/3}} + l\right) - l_p^3\right)_+ \\
&= \frac{\dot{R}_{ms}}{(l_{ms}/l_{m0})^3 - l_p^3}\left(\frac{el^2}{g_s+e}\left(\frac{l_{ms}}{l_{m0}}g_s + l\right) - l_p^3\right)_+ \\
&= \frac{\dot{R}_{m0}}{1-l_p^3}\frac{\kappa_{Rs}}{\kappa_{R0}}\frac{[\dot{p}_M]_s}{[\dot{p}_M]_0}\left(\frac{el^2}{g_s+e}\left(\frac{l_{ms}}{l_{m0}}g_s + l\right) - l_p^3\right)_+
\end{aligned}$$

If we consider $\dot{v}$ as a primary parameter, effects on $\{\dot{p}_{Am}\}$ do not have consequences for $\dot{v}$, so $\dot{v}_s/\dot{v}_0 = 1$ in the table at {213}.

If the toxicant increases the cost of an egg proportional to the internal concentration, we have to multiply e_0 by $(1+s)$, which amounts to the same as dividing the fraction of energy that is fixed in embryos, κ_R, by $(1+s)$.

The various modes of action affect the scaled parameter as follows

model	target	$\frac{\kappa_{Rs}}{\kappa_{R0}}$	$\frac{g_s}{g_0}$	$\frac{\dot{k}_{Ms}}{\dot{k}_{M0}}$	$\frac{[\dot{p}_M]_s}{[\dot{p}_M]_0}$	$\frac{l_{ms}}{l_{m0}}$
hazard	$\dot{h}_{\text{ovum}}$	$\exp\{-s\}$	1	1	1	1
costs	κ_R	$(1+s)^{-1}$	1	1	1	1
maint.	$[\dot{p}_M]$	1	1	$1+s$	$1+s$	$(1+s)^{-1}$
struct.	$[E_G]$	1	$1+s$	$(1+s)^{-1}$	1	1
assim.	$\{\dot{p}_{Am}\}$	1	$(1-s)^{-1}$	1	1	$1-s$

The list of possible modes of action is not complete. Compounds might well effect e.g. the energy conductance $\dot{v}$, and endocrine disruptors are likely to affect the partitioning fraction κ.

Receptor-mediated effects

{213}

By considering several endpoints simultaneously, we have found empirical support for receptor-mediated effects [214].

Table 6.1: The following notation is used for discssing the effects of mixtures of chemical compounds.

c_A, c_B	mM	external conc for compound A, B
k_A, k_B	d^{-1}	elimination rate for A, B
P_{Ad}, P_{Bd}	$\mathrm{l\,C\text{-}mol}^{-1}$	BCF for A, B
Q_A^0, Q_B^0	$\mathrm{mmol\,C\text{-}mol}^{-1}$	internal NECs for A and B
C_A^0, C_B^0	mM	external NECs for A and B
B_A, B_B	$\mathrm{C\text{-}mol\,mmol}^{-1}\mathrm{d}^{-1}$	killing rate for internal compound A, B
b_A, b_B	$\mathrm{mM}^{-1}\mathrm{d}^{-1}$	killing rate for external compound A, B
D_{AB}	$\mathrm{C\text{-}mol}^2\,\mathrm{mmol}^{-2}\mathrm{d}^{-2}$	internal interaction rate between A, B
d_{AB}	$\mathrm{mM}^{-2}\mathrm{d}^{-2}$	external interaction rate between A, B
h_0	d^{-1}	hazard rate in the blank

Population consequences

{217}

The population consequences of effects on individuals is discussed in [307].

Effects of mixtures of chemical compounds

{217}

Several possibilities exists for how combinations of chemical compounds interact in the NEC [16], which are discussed below. See Table 6.1 for the notation.

Hazard rate

Suppose that compounds A and B compete for capacity to cancel effects and that Q_A^0 and Q_B^0 are the internal NECs. No effects occur if

$$1 > Q_A/Q_A^0 + Q_B/Q_B^0$$

If this condition is not fullfilled, compounds A an B take fractions

$$w_A = \frac{Q_A}{Q_A^0}\left(\frac{Q_A}{Q_A^0} + \frac{Q_B}{Q_B^0}\right)^{-1}; \quad w_B = \frac{Q_B}{Q_B^0}\left(\frac{Q_A}{Q_A^0} + \frac{Q_B}{Q_B^0}\right)^{-1}$$

of the effect cancel capacity. The internal concentrations of A and B that cause effect are

$$Q_A^e = \max(0, Q_A - w_A Q_A^0); \quad Q_B^e = \max(0, Q_B - w_B Q_B^0)$$

The internal concentrations and the hazard rate is given by

$$\begin{aligned} Q_A(t) &= c_A P_{Ad}(1 - \exp(-tk_A)); \quad Q_B(t) = c_B P_{Bd}(1 - \exp(-tk_B)) \\ h_c(t) &= B_A Q_A^e(t) + B_B Q_B^e(t) + D_{AB} Q_A^e(t) Q_B^e(t) \end{aligned}$$

Compounds A and B do not interact if $D_{AB} = 0$. This situation seems to be called "concentration addition" or "independent action", which are two words for the same concept in this context.

From internal to external concentrations

Substitute $C_A = Q_A/P_{Ad}$; $C_B = Q_B/P_{Bd}$; $b_A = B_A P_{Ad}$; $b_B = B_B P_{Bd}$; $d_{AB} = D_{AB} P_{Ad} P_{Bd}$.

$$\begin{aligned}
C_A(t) &= c_A(1-\exp(-tk_A)); \quad C_B(t) = c_B(1-\exp(-tk_B)) \\
w_A(t) &= \frac{C_A(t)}{C_A^0}\left(\frac{C_A(t)}{C_A^0}+\frac{C_B(t)}{C_B^0}\right)^{-1}; \quad w_B(t) = \frac{C_B(t)}{C_B^0}\left(\frac{C_A(t)}{C_A^0}+\frac{C_B(t)}{C_B^0}\right)^{-1} \\
C_A^e(t) &= \max(0, C_A(t) - w_A(t)C_A^0); \quad C_B^e(t) = \max(0, C_B(t) - w_B(t)C_B^0) \\
h_c(t) &= b_A C_A^e(t) + b_B C_B^e(t) + d_{AB} C_A^e(t) C_B^e(t)
\end{aligned}$$

The complete hazard rate is given by $h(t) = h_0 + h_c(t)$, where h_0 is the hazard rate in the blank.

Effects occur at finite time t_0 if

$$1 < c_A/C_A^0 + c_B/C_B^0$$

A consequence of this competition model for cancel capacity is that $C_A^e > 0$ if $C_B^e > 0$, and *vice versa*. This occurs at time t_0, where

$$\begin{aligned}
1 &= C_A(t_0)/C_A^0 + C_B(t_0)/C_B^0 \\
&= (1-\exp(-t_0k_A))c_A/C_A^0 + (1-\exp(-t_0k_B))c_B/C_B^0
\end{aligned}$$

This time point t_0 must be obtained numerically, but with octave's fsolve convergence is fast from the initial choice $t_0 = 0$.

From hazard rate to survival probability

The survivor probability is given by

$$S(t) = \exp(-\int_0^t h(s)\,ds) = \exp(-h_0 t) \quad \text{for } t < t_0$$

For $t > t_0$ the integration of the hazard rate should be done numerically.

For relative large negative vlues of the interaction rate, the hazard rate can become negative, which means that we have take the maximum of zero and the specified value. For positive values, the hazard rate is not necessarily monotonous in time. This is not a formal problem, but somewhat counter-intuitive.

Fixed cancel capacity

The formulation above allows changes in the use of the cancel capacity after the moment effects show up. This corresponds perhaps better to a receptor-based situations. Alternatively the use of this capacity can be frozen at the moment effects show up. We then have constant values for

$$\begin{aligned}
C_A^{0B} &= (1-\exp(-t_0k_A))c_A; \quad C_B^{0A} = (1-\exp(-t_0k_B))c_B \\
w_A &= (1-\exp(-t_0k_A))c_A/C_A^0; \quad w_B = (1-\exp(-t_0k_B))c_B/C_B^0
\end{aligned}$$

The survivor probability can now be evaluated analytically (given the numerically obtained value for t_0) fot $t > t_0$

$$\begin{aligned}
S(t) &= \exp(-h_0 t - b_A g_A(t) - b_B g_B(t) - d_{AB} g_{AB}(t)) \\
g_A(t) &= -c_A t_A + (c_A - C_A^{0B})(t - t_0); \quad g_B(t) = -c_B t_B + (c_B - C_B^{0A})(t - t_0) \\
g_{AB}(t) &= c_A c_B t_{AB} - c_A (c_B - C_B^{0A}) t_A - (c_A - C_A^{0B}) c_B t_B + (c_A - C_A^{0B})(c_B - C_B^{0A})(t - t_0) \\
t_A &= k_A^{-1}(\exp(-k_A t_0) - \exp(-k_A t)); \quad t_B = k_B^{-1}(\exp(-k_B t_0) - \exp(-k_B t)) \\
t_{AB} &= (k_A + k_B)^{-1}(\exp(-(k_A + k_B) t_0) - \exp(-(k_A + k_B) t))
\end{aligned}$$

Implementation

The formulation with the fixed weight coefficients is coded in debtool/tox/fomort2, with the dynamic weight coefficients in debtool/tox/fomort2r; the "r" relates to "receptor". The script file mydata_fomort2 illustrates how to use it, including the generation of Monte Carlo data (using debtool/lib/prob/surv_count), and the formal statistical test $d_{AB} = 0$. The routines /debtool/lib/regr/scsurv3, nmsurv3, psurv3, dev3 have been written to estimate par values.

Note: the numerical derivatives in scsurv3 are found to be not accurate enough for the numerical integrations in fomort2r.

Chapter 7

Case studies

Varying half saturation constants due to pseudo-faeces

{221}

Filter feeders like bivalves filter material that does not make it to the gut, but nonetheless affect their feeding. We partition feeding into acquisition A with N_A functional units and digestion D with N_D functional units. The numbers N_* are proportional to the surface area of the individual; an acquisition unit might be a filtering hair, and a digestion unit a site in the gut wall at which absorption occurs. Food X is present in density X and non-digestible particles Y (here called silt particles) in density Y. Food is passed from the acquisition units to the digestion units by channeling using a closed handshaking protocol (so no acquired food is spoiled) and silt is excreted as pseudo-faeces and is not passed to the digestion units.

We now find expressions for the feeding and filtering rates, where food and silt compete for access to the acquisition units, in a way that is consistent with the standard DEB model, which specifies that in absence of silt, food intake can be written as $J_X = \{J_{Xm}\} f V^{2/3}$ with $f = X/(X+K)$.

Closed handshaking between A and D

We follow [327] for closed handshaking, and include pseudo-faeces production. For $1 = \theta_\cdot^A + \theta_X^A + \theta_Y^A$ and $1 = \theta_\cdot^D + \theta_X^D$, the changes in the fractions of A and D are

$$\begin{aligned}
\frac{d}{dt}\theta_\cdot^A &= (\theta_X^D - \theta_X^A)k_X + \theta_Y^A k_Y - \theta_\cdot^A(b_X X + b_Y Y) \\
\frac{d}{dt}\theta_Y^A &= \theta_\cdot^A b_Y Y - \theta_Y^A k_Y \\
\frac{d}{dt}\theta_\cdot^D &= \theta_X^D k_D - (\theta_X^D - \theta_X^A)k_X N_A/N_D
\end{aligned}$$

where b_X and b_Y are the affinities of X and Y; k_X^{-1} and k_Y^{-1} are the mean handling times of X and Y by the acquisition machinery, and k_D^{-1} is the mean handling time of X by the digestion machinery. The steady state fractions are

$$\theta_\cdot^{A*} = k_X k_Y k_D N_D/\Theta$$

$$\begin{aligned}
\theta_X^{A*} &= k_Y b_X X(k_X N_A - k_D N_D)/\Theta \\
\theta_Y^{A*} &= k_X k_D N_D b_Y Y/\Theta \\
\theta_X^{D*} &= k_X k_Y N_A b_X X/\Theta \\
\Theta &= k_X k_Y N_A b_X X + k_D N_D (k_X k_Y - k_Y b_X X + k_X b_Y Y)
\end{aligned}$$

Feeding & pseudo-faeces production

The feeding and pseudo-faeces production rates are

$$\begin{aligned}
J_X &= N_A \theta_\cdot^{A*} b_X X = N_D \theta_X^{D*} k_D = \frac{k_X k_Y k_D N_A N_D b_X X}{k_X k_Y k_D N_D + (k_X N_A - k_D N_D) k_Y b_X X + k_D N_D k_X b_Y Y} \\
J_Y &= N_A \theta_\cdot^{A*} b_Y Y = N_A \theta_Y^{A*} k_Y = \frac{k_X k_Y k_D N_A N_D b_Y Y}{k_X k_Y k_D N_D + (k_X N_A - k_D N_D) k_Y b_X X + k_D N_D k_X b_Y Y}
\end{aligned}$$

Consistency test with standard DEB model: $Y = 0$

$$J_X = \frac{k_X k_D N_A N_D b_X X}{k_X k_D N_D + (k_X N_A - k_D N_D) b_X X} = \frac{\{J_{Xm}\} V^{2/3} X}{K + X}$$

for $\{J_{Xm}\} V^{2/3} = \frac{k_X k_D N_A N_D}{k_X N_A - k_D N_D}$ and $K = \frac{k_X k_D N_D}{(k_X N_A - k_D N_D) b_X}$. Result: the model is DEB-consistent for $N_A, N_D \propto V^{2/3}$; the half saturation coefficient K is then independent of structural volume V and the maximum food uptake $J_{Xm} \propto V^{2/3}$.

Re-parametrization

To remove parameters that are difficult to measure from the behaviour of individuals, we introduce the silt saturation coefficient $K_Y = k_Y/b_Y$ and relative affinity $\delta_{YX} = b_Y/b_X$. Substitution gives the ingestion rates for food and silt particles

$$\begin{aligned}
J_X &= \frac{\{J_{Xm}\} V^{2/3} X}{K'(Y) + X} \quad \text{with } K'(Y) = K(1 + Y/K_Y) \\
J_Y &= \delta_{YX}\, J_X\, Y/X
\end{aligned}$$

If no selection in acquisition occurs, we have $\delta_{YX} = 1$, which means that this model for how silt affects food uptake has one extra (compound) parameter K_Y which is inverse to the product of the mean handling time of a silt particle, k_Y^{-1}, and its affinity, b_Y; its dimension is silt density. Faeces production is proportional to food consumption; the conversion depends on food quality parameters. Pseudo-faeces production equals silt consumption J_Y; mucus production might also have a contribution, depending on the choice of quantifiers.

The filtering rate of an individual that completely clears the filtered water equals $F(X,Y) = J_X/X = J_Y/Y$ for $\delta_{YX} = 1$. The maximum filtering rate is at $X = 0$, $Y = 0$, so

$$F_m = F(0,0) = \frac{J_{Xm}}{K} = \frac{k_X k_D N_A N_D}{k_X N_A - k_D N_D} \frac{(k_X N_A - k_D N_D) b_X}{k_X k_D N_D} = N_A b_X$$

Apparent saturation coefficient

Notice that if food density X would vary at constant silt density Y, we have that the apparent half saturation coefficient $K'(Y) = K(1 + Y/K_Y)$ is constant, and the standard DEB formulation applies, but its value depends on the constant silt density Y. Suppose that Y is site-specific, then K' is linear in the silt density Y. We can invert the argument and obtain $Y = K_Y(K'/K - 1)$, where K is the minimum among K''s if there is a "clean" site in the set of measurements. If measurements of (mean) silt densities Y are available, we can test the relationship between K' and Y, and arrive at an estimate for silt saturation coefficient $K_Y = Y/(K'/K - 1)$.

Starvation

{221}

As long as growth is non-negative, standard dynamics applies. If (full or partial) starvation continues, the response can be at the following levels

1 continue the standard reserve dynamics till death follows; don't change the κ-rule for allocation; use the buffer for reproduction (little data are available to tell us how exactly, but see [129] for studies on polychaetes and [440] for studies on anchovy); if necessary shrink (i.e. pay somatic maintenance from structure). Variant: migrate to better locations.

2 continue the standard reserve dynamics till death follows; change the κ-rule for allocation; reduce on maturation maintenance and reproduction; use buffer for reproduction if necessary; shrink if necessary.

3 change the reserve dynamics to pay somatic maintenance only; no allocation to maturity maintenance and reproduction use buffer for reproduction if necessary; shrink if necessary. Variant: switch to dormant state, partially reducing somatic maintenance costs.

4 change the reserve dynamics by converting reserve to eggs (seeds); convert structure to eggs (as far as possible). This is the case of emergency reproduction, typically followed by death. Popular strategy among plants.

Sometimes systems start to respond at level 1, but then continue to level 2, 3 and 4.

Maintenance from reserve and structure

Caroline Tolla [555, 554] proposed that somatic maintenance is payed from reserve as well as from structure with a (strong) preference for payment from reserve. If reserves are not sufficient, the payment from structure gradually becomes more important, without any switch. The motivation comes from the turnover of structure as part of the somatic maintenance costs. The formal significance is to relate the Droop to the Marr-Pirt model. If reserve turnover increases, the maximum reserve capacity decreases, but in the limit, maintenance costs are paid from assimilation in the DEB model and from structure in the Marr-Pirt model, where maintenance is not distinguishable from death as far as the change in state variables is concerned, but an obvious difference exists in term of products. The difference between payment from assimilation rather than from structure is felt when growth switches sign.

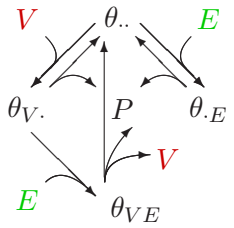

Figure 7.1: The interaction between the conversions $E \to P$ and $V \to P$, with preference to the first transformation. See the comment for {164} for a simplified version.

$$\begin{aligned}
\frac{d}{dt}\theta_{..} &= \dot{k}_V\theta_{.V} + \dot{k}_{EV}\theta_{EV} + \dot{k}_E\theta_{E.} - \rho_V j_V\theta_{..} - \rho_E j_E\theta_{..} \\
\frac{d}{dt}\theta_{.V} &= \rho_V j_V\theta_{..} - \rho_{EV} j_E\theta_{.V} - \dot{k}_V\theta_{.V} \\
\frac{d}{dt}\theta_{EV} &= \rho_{EV} j_E\theta_{.V} - \dot{k}_{EV}\theta_{EV} \\
\frac{d}{dt}\theta_{E.} &= \rho_E j_E\theta_{..} - \dot{k}_E\theta_{E.}
\end{aligned}$$

For a given size, the flux of maintenance products P is constant, so we require that

$$j_P = y_{PE}\dot{k}_E\theta_{E.} + y_{PE}\dot{k}_{EV}\theta_{EV} + y_{PV}\dot{k}_V\theta_{.V}$$

is constant by allowing $\dot{k}_E$, $\dot{k}_{EV}$ and $\dot{k}_V$ to depend on θ_{**}.

Equal dissociation rates

Proposal for rates that fulfill the constraint:

$$\dot{k}_E = \dot{k}_{EV} = \dot{k}_V = \dot{k}_P/\theta \quad \text{with } \theta = y_{PE}\theta_{E+} + y_{PV}\theta_{.V} \text{ and } \theta_{E+} = \theta_{E.} + \theta_{EV}$$

for constant $\dot{k}_P$. We must have that $j_P = \dot{k}_P$.

Constant flux of structure to SU for maintenance

Within the context of the DEB theory, the flux j_V is constant, because the turnover of structure represents an substantial part of the maintenance costs. Substitution of $\dot{k}_*$ and j_V in

$$\begin{aligned}
\frac{d}{dt}\theta_{..} &= \dot{k}_P(1-\theta_{..})/\theta - (\rho_V j_V + \rho_E j_E)\theta_{..} \\
\frac{d}{dt}\theta_{.V} &= \rho_V j_V\theta_{..} - \rho_{EV} j_E\theta_{.V} - \dot{k}_P\theta_{.V}/\theta \\
\frac{d}{dt}\theta_{E+} &= j_E(\rho_{EV}\theta_{.V} + \rho_E\theta_{..}) - \dot{k}_P\theta_{E+}/\theta
\end{aligned}$$

The steady state solutions are explicit, but complicated. For $\rho_E = \rho_{EV}$ and $\rho_E j_E = j'_E$ and $\rho_V j_V = j'_V$, the steady state solutions simplify considerably.

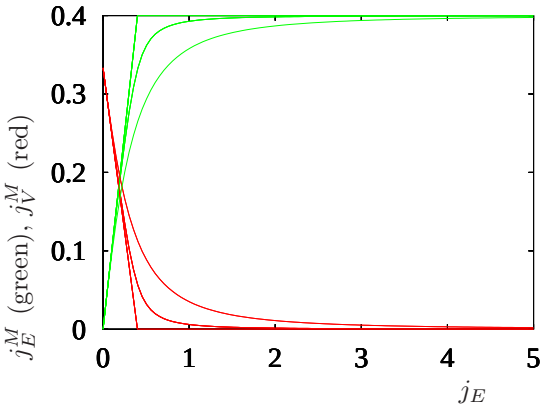

Figure 7.2: The flux of reserve and of structure for somatic maintenance. Numerical study for $\alpha = 0$ (switch model), 0.1 and 1 (equal dissociation rates), $\dot{k}_P = 0.04$, $y_{PV} = .12$, $y_{PE} = .1$, $\rho_E = 1$, $\rho_{EV} = 1$. Reserve has absolute priority over structure to pay somatic maintenance costs in the switch model.

The fluxes of reserve and structure that are allocated to maintenance are

$$\begin{aligned} j_V^M &= \theta^*_{.V}\dot{k}_P/\theta^* \\ j_E^M &= (\dot{k}_P - y_{PV}j_V^M)y_{EP} \end{aligned}$$

while j_E is released from the reserve. For V1-morphs: $j_E = (\dot{k}_E - \dot{r})M_E$, with $\dot{r}$ being the specific growth rate.

Unequal dissociation rates

Suppose now that $\dot{k}_V = \alpha\dot{k}_P/\theta$; substitution in the constraint that j_P is constant learns for $j_P = \dot{k}_P$ that $\theta = y_{PE}\theta_{E+} + \alpha\theta_{.V}y_{PV}$. If j_V is constant again, we must have $\rho_V j_V = \dot{k}_P y_{VP}$. Substitution of $\dot{k}_*$ and j_V in

$$\begin{aligned} \frac{d}{dt}\theta_{..} &= \dot{k}_P(\alpha\theta_{.V} + \theta_{E+})/\theta - (\dot{k}_P y_{VP} + \rho_E j_E)\theta_{..} \\ \frac{d}{dt}\theta_{.V} &= \dot{k}_P y_{VP}\theta_{..} - \rho_{EV} j_E \theta_{.V} - \alpha\dot{k}_P\theta_{.V}/\theta \\ \frac{d}{dt}\theta_{E+} &= j_E(\rho_{EV}\theta_{.V} + \rho_E\theta_{..}) - \dot{k}_P\theta_{E+}/\theta \end{aligned}$$

The fluxes of reserve and structure that are allocated to maintenance are

$$\begin{aligned} j_V^M &= \alpha\theta^*_{.V}\dot{k}_P/\theta^* \\ j_E^M &= (\dot{k}_P - y_{PV}j_V^M)y_{EP} \end{aligned}$$

For $\rho_{EV} = \rho_E$, $j'_E = \rho_E j_E$, $j'_V = \rho_V j_V$, the flux of structure that is allocated to maintenance is

$$j_V^M = \frac{2A\dot{k}_P/y_{PV}}{2A + y_{PE}(\sqrt{B^2 - 4AC} - B)}$$

with $A = \alpha j'_V \dot{k}_P y_{PV}$, $B = y_{PE}C + ((1-\alpha)j'_E + j'_V)\dot{k}_P$, $C = -j'_E(j'_E + j'_V)$.

Figure 7.2 illustrates the effect of unequal dissociation rates; they span the whole range from equal dissociation rates to the switch model.

From the microscopic to the macroscopic level

We now consider the individual-level implications of the preference model. The maintenance product P is a generalized compound consisting of CO_2, H_2O, O_2 (negative flux), NH_3, and possibly other compounds. To translate the microscopic level to the macroscopic level without lost of generality, we can assume $y_{PE} = 1$, $\dot{k}_P = j_{EM}$, $y_{PV} = j_{EM}/j_{VM}$, where j_{EM} is the specific reserve flux for maintenance if all would have been paid from researve, and j_{VM} is the specific structure flux for maintenance is all would be paid from structure. Notice that j_{EM} and j_{VM} are parameters; the actual maintenance fluxes are j_E^M and j_V^M, with $j_E^M \leq j_{EM}$ and $j_V^M \leq j_{VM}$. The fluxes j'_E and j'_V have formal dimension number-per-time and can, therefor, be added at the molecular level. At the macroscopic level, however, fluxes of different generalized compounds cannot be added in a meaningful way. To solve this problem we have to convert the flux of structure to a flux of reserve and take $j'_V = y_{EV} j_{VM}$, $j'_E = j_{EC}$. An implicit constraint is $j_{VM} \geq j_{EM}/y_{EV}$.

Substitution of these values gives

$$j_E^M = j_{EM}(1 - j_V^M/j_{VM}); \quad j_V^M = j_{VM}\frac{2A}{2A + \sqrt{B^2 - 4AC} - B}$$

with $A = \alpha j_{EM}^2$, $B = C + ((1-\alpha)j_{EC} + y_{EV}j_{VM})j_{EM}$, $C = -j_{EC}(j_{EC} + y_{EV}j_{VM})$.

Switch model

For $\alpha \to 0$ the preference model approaches the switch model, which amounts to

$$j_E^M = \min\{j_{EM}, j_{EC}\} \quad \text{and} \quad j_V^M = j_{VM}(1 - j_E^M/j_{EM})$$

Marr-Pirt model

Maintenance in the Marr-Pirt model always paid from structure, so the loss-fluxes to maintenance are

$$j_E^M = 0 \quad \text{and} \quad j_V^M = j_{VM}$$

Notice that this model cannot be obtain from the simplified preference model, because reserve can replace structure in the SU-structure complex. We need to remove this simplification to arrive that the Marr-Pirt limit.

Growth of V1-morphs with one reserve

For V1-morphs, the mobilized reserve flux amounts to $j_{EC} = m_E(\dot{k}_E - \dot{r})$. The specific growth rate is

$$\begin{aligned} \dot{r} &= y_{VE}(j_{EC} - j_E^M) - j_V^M \\ &= y_{VE}((\dot{k}_E - \dot{r})m_E - j_E^M) - j_V^M \\ &= \frac{m_E\dot{k}_E - j_E^M - y_{EV}j_V^M}{m_E + y_{EV}} \end{aligned}$$

Preference model

j_V^M is a function of $j_E = (\dot{k}_E - \dot{r})m_E$, and so of $\dot{r}$; we indicate this with $j_V^M(\dot{r})$. The sequence

$$\dot{r}_{i+1} = \frac{m_E\dot{k}_E - j_{EM} - (y_{EV} - j_{EM}/j_{VM})j_V^M(\dot{r}_i)}{m_E + y_{EV}}$$

rapidly converges, $\dot{r}_i \to \dot{r}$, in a few steps, starting from $\dot{r}_0 = 0$. If $j_{VM} = j_{EM}/y_{EV}$, the growth rate reduces to $\dot{r} = \frac{m_E\dot{k}_E - j_{EM}}{m_E + y_{EV}}$.

Switch model

Payment from structure starts when

$$j_{EC} = j_E^M; \quad j_V^M = 0; \quad \dot{r} = 0; \quad m_E = j_{EM}/\dot{k}_E \equiv m_E^s$$

The growth rate after this moment switches from $\dot{r} = \frac{m_E\dot{k}_E - j_{EM}}{m_E + y_{EV}}$ to

$$\begin{aligned}
\dot{r} &= \frac{m_E\dot{k}_E - j_E^M - y_{EV}j_V^M}{m_E + y_{EV}} \\
&= \frac{m_E\dot{k}_E - j_E^M - y_{EV}(1 - j_E^M/j_{EM})j_{VM}}{m_E + y_{EV}} \\
&= \frac{m_E\dot{k}_E - y_{EV}j_{VM} - (1 - y_{EV}j_{VM}/j_{EM})j_E^M}{m_E + y_{EV}} \\
&= \frac{m_E y_{EV}\dot{k}_E j_{VM}/j_{EM} - y_{EV}j_{VM}}{y_{EV} + m_E y_{EV}j_{VM}/j_{EM}} \\
&= \frac{m_E\dot{k}_E - j_{EM}}{m_E + j_{EM}/j_{VM}}
\end{aligned}$$

Since $\lim_{m_E \uparrow m_E^s} \dot{r} = \lim_{m_E \downarrow m_E^s} \dot{r} = 0$, the growth rate is continuous around the switch, but not differentiable for $j_{VM} \neq j_{EM}/y_{EV}$. This also applies to $\frac{d}{dt}m_E$. For $j_{VM} = j_{EM}/y_{EV}$ the preference and the switch model are identical for growth.

Droop-Marr-Pirt model

We have

$$\dot{r} = \frac{m_E\dot{k}_E}{m_E + y_{EV}} - j_{VM}$$

Growth of V1-morphs with multiple reserves

Since for each reserve we have a contribution to maintenance, it is theoretically most elegant to mobilise structure for each reserve separately, and at each maintenance SU it is decided how much reserve and how much structure is used. So the total specific flux of

structure that is used amounts to $j_V^M = \sum_i j_V^{M_i}$, where the summation is over all reserves. Writing $\dot{r} = j_V^G - j_V^M$, the specific growth rate for two reserves ($i = 1, 2$) follows from

$$j_V^G = \dot{r} + j_V^M = \left(\sum_i \left(\frac{m_{Ei}(\dot{k}_{Ei} - \dot{r}) - j_{Ei}^M}{y_{Ei,V}} \right)^{-1} - \left(\sum_i \frac{m_{Ei}(\dot{k}_{Ei} - \dot{r}) - j_{Ei}^M}{y_{Ei,V}} \right)^{-1} \right)^{-1}$$

Food intake after starvation

{222}

A phenomenon shared by many taxa is that food (substrate) intake after a period of starvation is substantially higher during a short period. Morel [404] modeled a fast short-term uptake (at maximum specific rate j_{XAm}^h) in combination with a much lower longer-term uptake (at maximum specific rate j_{XAm}^l) in algae by assuming empirically that nutrient uptake decreases linearly with the reserve density like

$$\begin{aligned} j_X(X, m_E) &= f\left(j_{XAm}^h - (j_{XAm}^h/j_{XAm}^l - 1)m_E\dot{k}_E/y_{EX}\right) \quad \text{with} \quad f = \frac{X}{K+X} \\ \frac{d}{dt}m_E &= y_{EX} f j_{XAm}^h - (1 - f + f j_{XAm}^h/j_{XAm}^l)m_E\dot{k}_E \\ m_E^* &= \frac{y_{EX} f j_{XAm}^h/\dot{k}_E}{1 - f(1 - j_{XAm}^h/j_{XAm}^l)} = \frac{X y_{EX} j_{XAm}^l/\dot{k}_E}{X + K j_{XAm}^l/j_{XAm}^h} \end{aligned}$$

The maximum reserve density is $m_{Em} = y_{EX} j_{XAm}^l/\dot{k}_E$. If nutrients are just internalized, rather than transformed, we typically have $y_{EX} = 1$. For $j_{XAm}^h \to j_{XAm}^l$, the standard food intake is recovered. A change in assimilation does not affect the way how growth depends on reserve (density), so $\dot{r} = \frac{m_E\dot{k}_E - j_{EM}/\kappa}{m_E + y_{EV}/\kappa}$.

A problem with this empirical extension to include fast short-term uptake is that it modifies the well-tested long-term uptake. A variant of this idea that leaves the long-term uptake unaltered is

$$\begin{aligned} j_X(X, m_E) &= f j_{XAm}^h - (j_{XAm}^h/j_{XAm}^l - 1)m_E\dot{k}_E/y_{EX} \quad \text{with} \quad f = \frac{X}{K+X} \\ \frac{d}{dt}m_E &= y_{EX} f j_{XAm}^h - m_E\dot{k}_E j_{XAm}^h/j_{XAm}^l \quad \text{with} \quad m_E^* = y_{EX} f j_{XAm}^l/\dot{k}_E \end{aligned}$$

To avoid negative uptake rates, we must have

$$\frac{\dot{k}_E}{j_{XAm}^l} - \frac{\dot{k}_E}{j_{XAm}^h} > \frac{f y_{EX}}{m_E}$$

In animals very short-term food uptake after starvation is typically even higher due to filling of the digestive system (stomach plus gut). This can be modeled similarly and linked to a more detailed module for digestion, as discussed in 7.3 at {239}.

Food intake reconstruction from weight data

{227}

The reconstruction of food intake is as follows: From $W_w = (d_V + d_E e)V$, we know that $V = W_w/(d_V + d_E e)$ and $\frac{d}{dt}W = (d_V + d_E e)\frac{d}{dt}V + d_E V \frac{d}{dt}e$, which gives $\frac{d}{dt}e = (d_V + d_E e)(\frac{d}{dt}\ln W_w - \frac{d}{dt}\ln V)/d_E$. From Eq (3.18) at {94} we know that $\frac{d}{dt}\ln V = \dot{v}(V^{-1/3}(e - l_h) - L_m^{-1})/(e + g)$. Given observed values for $W_w(t)$, and so of $\frac{d}{dt}W_w(t)$, this allows us to obtain $e(t)$ by numerical integration, starting from $e(0)$. Now we use Eq (3.11) at {85} to get $f(t) = e(t) + V^{1/3}(t)\frac{d}{dt}e/\dot{v}$ or $V^{2/3}(t)f(t) = e(t)V^{2/3}(t) + V(t)\frac{d}{dt}e/\dot{v}$.

Composition of reserve & structure

{227}

The linear decrease of compounds during starvation can be used to gain info on the composition of reserve and structure, using the following reasoning.

We first try to understand the decrease of a compound C in an organism during starvation, having measurements of how the amount M_C (in C-mol) changes in time t. At the start of the experiment, the organism has amounts of structure M_V and reserve M_E. Suppose that reserve mobilization during starvation is just enough to cover the somatic maintenance costs. The amount of structure M_V remains constant, so if we focus on some compound C, e.g. protein, and follow it backward in time, with the time origin at the moment on which the reserve is fully depleted, we have

$$M_C(t^*) = M_{CV} + (M_{CE}/M_E)t^* \dot{J}_{EM}$$

where $M_C(t^*)$ is the amount of compound at revered time t^*, M_{CV} the (constant) amount of compound in structure, M_{CE}/M_E the constant density of the compound in reserve and $\dot{J}_{EM}$ the (constant) rate of use of reserve for somatic maintenance purposes.

Reverting time back into the standard direction, we substitute $t = t_0 - t^*$ and obtain

$$\begin{aligned} M_C(t) &= M_{CV} + (M_{CE}/M_E)(t_0 - t)\dot{J}_{EM} \\ &= M_{C0} - t\dot{J}_{CM} \quad \text{with } \dot{J}_{CM} = (M_{CE}/M_E)\dot{J}_{EM} \text{ and } M_{C0} = M_{CV} + \dot{J}_{CM}t_0 \end{aligned}$$

This shows that each compound can decrease linearly at its own rate, even under the strong homeostasis assumption, which prescribes that the densities of the compound in reserve M_{CE}/M_E and in structure M_{CV}/M_V remain constant.

It also shows that, if we only know how the compound changes in time, we have access to M_{C0} and $\dot{J}_{CM}$, but not to the more informative M_{CV} and M_{CE} (i.e. info on the composition of structure and reserve).

We do have some relative information on the composition of reserve, if we know the time trajectories of several compounds: $\dot{J}_{C_1M}/\dot{J}_{C_2M} = M_{C_1E}/M_{C_2E}$. If we would know when the reserve is depleted (namely at time t_0), we have access to the composition of structure M_{CV}/M_V, since $M_C(t_0) = M_{CV}$, but the individual will probably start to use structure to pay maintenance costs during prolonged starvation (causing deviations from linear decrease). Moreover it is likely that the reserve buffer that is allocated to reproduction is used under extreme starvation. This makes it difficult to have access to t_0.

Suppose now that we have info for *all* compounds, that is $\sum_i M_{C_iV} = M_V$ and $\sum_i M_{C_iE} = M_E$. Although the actual number of chemical compounds is formidable, they can be

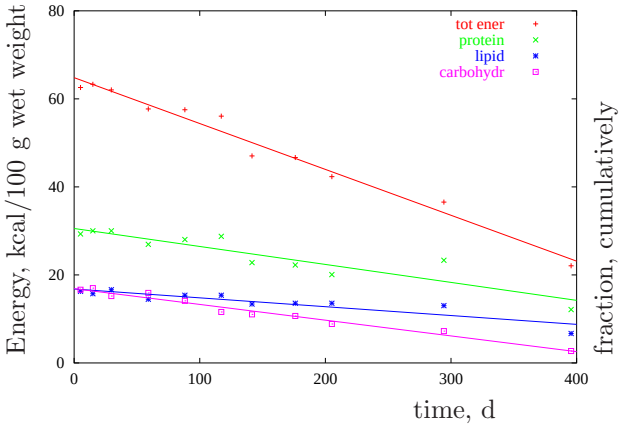

Figure 7.3: The amounts of energy in starving oyster. Data from [583]. Parameters are presented in Table 7.1.

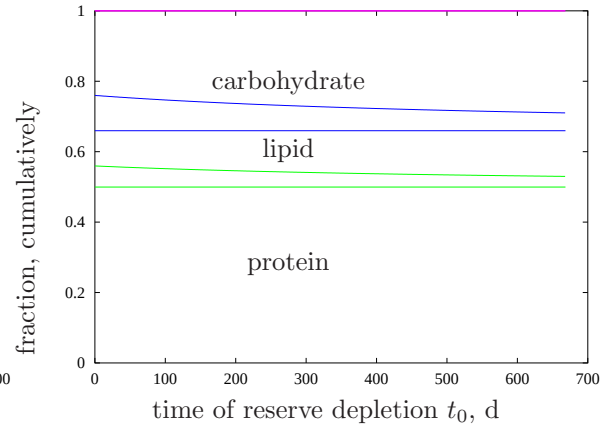

Figure 7.4: Composition of reserve (horizontal lines) and structure (curves) of the oyster as derived from Table 7.1. The maximum time at which the reserve could have been depleted is 668 d. The fractions are plotted cumulatively, assuming that proteins, lipids and carbohydrates together comprise 100 % of all biomass. Structure has less carbohydrates than reserve and more protein and lipid.

grouped into a limited number of chemical categories (e.g. proteins, lipids etc). We have $\sum_i \dot{J}_{C_iM} = \dot{J}_{EM}$, so $\dot{J}_{C_iM}/\sum_j \dot{J}_{C_jM} = M_{C_iE}/M_E$. We also have $\sum_i M_{C_i0} = M_V + \dot{J}_{EM}t_0$, so $M_V = \sum_i M_{C_i0} - t_0 \sum_i \dot{J}_{C_iM}$, which we know if we would have and estimate for t_0. We obviously must have that $t_0 < \sum_i M_{C_i0}/\sum_i \dot{J}_{C_iM}$. The composition of structure is then found from $M_{C_iV}/M_V = (M_{C_i0} - t_0 J_{C_iM})/M_V$.

Figures 7.3 and 7.4 give an example of application. Remark that RNA might also contribute to biomass, but is neglected here. A puzzling thing in this example is that the data seem to concern energies per 100 g wet weight. Is the rest of the weight water only? I treated the data as if they refer to 100 g wet weight *at time zero*.

Food intake reconstruction from reproduction data

{227}

Collaborative work with Stella Berger: Food intake can also be reconstructed from reproduction data of e.g. *Daphnia hyalina*. Data include body length, egg length, width & number of eggs in the brood pouch in weekly hauls from enclosures. The general idea is to reconstruct food density and then try to link measured quantities in the enclosures, such as chlorophyll concentration, POM, and DOC to this reconstructed food density to learn more about the nutritional value of these quantities for daphnids. These links are less than direct (daphnids cannot digest chlorophyll or cellulose)and involves the (unknown) half saturation constant.

These data also allow the study of maternal effects: is the reserve density at birth indeed equal to the reserve density of the mother at egg formation as the DEB theory assumes? Eggs initially fully consist of reserve. If reserve density at birth is small, initial

Table 7.1: The parameter estimates from Figure 7.3, conversions, and their translation into composition info for 3 choices for the time at which the reserve is depleted; 1 cal = 4.184 J; the caloric values are from Kooijman (2000) {137}.

100 g wet weight	total	protein	lipid	carbohydrate
$\mu_C M_{C0}$, kcal	64.81	30.54	16.80	16.87
$\mu_C \dot{J}_{CM}$, kcal/d	0.1042	0.0408	0.0200	0.0358
μ_C, kJ/C-mol		401	616	516
M_{C0}, C-mol	0.570	0.319	0.114	0.137
$\dot{J}_{CM}$, mmol/d		0.426	0.136	0.290
M_{CE}/M_E, mol/mol		0.500	0.159	0.341
M_{CV}/M_V, mol/mol, $t_0 = 200$ d		0.546	0.191	0.263
M_{CV}/M_V, mol/mol, $t_0 = 400$ d		0.537	0.185	0.278
M_{CV}/M_V, mol/mol, $t_0 = 600$ d		0.531	0.181	0.288

egg size will be small as well, but less than linear: a low amount of initial reserve leads to low maturation, so long incubation and high cumulated maintenance costs. Hatching (which coincides with start of feeding in *Daphnia*) occurs if maturity exceeds a threshold value. The differences in egg size are small only since only half of the initial reserve is used during the embryo stage in daphnids [328].

Two different ideas on the main sources of scatter are evaluated

1 each individual experienced a different food history and I use the observed number of eggs N to estimate the scaled functional response f for each individual. To find f, $N = t_R \dot{R}$ with reproduction rate $\dot{R}$ given in Eq 3.31 was solved numerically for each individual, starting from the analytical solution using the scaled reserve U_E^0 for $f = 1$. Using these values of f, the sum of squared deviations between observed egg volumes and expected egg volume $\dot{v}_0 U_E^0$ was minimized to find an estimate for the conversion factor $\dot{v}_0$. In this scenario all scatter is in the local food density of individual daphnids. The environment is supposed to be spatially and temporary heterogeneous. These individuals have identical parameter values. Since eggs grow in volume during incubation (see below), we need to correct the measured egg volumes for growth during development. The "observed" initial egg volume V_{Oi} of individual i is estimated by $\sum_j w_j V_{0j} / \sum_j w_j$, where $w_{ij} = \exp\{-c_f(f_i - f_j)^2 - c_V(V_{Oj} - V_{Om})^2\}$ and V_{0m} is the minimum observed egg volume. So the closer the reconstructed functional response is to the individual at hand and the smaller the egg volume is, the larger is the weight coefficient for the estimated initial egg volume.

2 individuals in a single haul experienced the same food history and I use the different individuals in one haul to estimate a common scaled functional response. To find f, the sum of squared deviations was minimized between the observed number of eggs N and the expected number of eggs $t_R \dot{R}$ with $\dot{R}$ given in Eq 3.31 for individuals of different lengths, simultaneously with that between observed and expected egg

volumes. In this scenario part of the scatter is in the translation of food to eggs, and part in difference of parameter values amount individuals. Since eggs grow in volume during incubation (see below), the smallest egg volume each haul represents the best estimate for the initial volume for that scaled functional response if individuals do not synchronize moulting cycles.

Reproduction rate is given by

$$\begin{aligned} \dot{R} &= ((1-\kappa)S_C - \dot{k}_J U_H^p)\kappa_R / U_E^0 \\ &\text{with } S_C = \frac{\dot{J}_{EC}}{\{\dot{J}_{EAm}\}} = L^2 \frac{ge}{g+e}\left(1 + \frac{L}{gL_m}\right) \end{aligned}$$

where the scaled reserve density e is replaced by the scaled functional response f. The initial scaled reserve U_E^0 is computed in debtool/animal/initial_scaled_reserve and depends on κ, g, $\dot{k}_J$, $\dot{k}_M$, $\dot{v}$, U_H^b.

The volume of an ellipse of radii a, b, c equals $4\pi abc/3$. Expressed in egg length $L_l = 2a$ and egg width $L_w = 2b = 2c$, egg volume equals $V_e = L_l L_w^2 \pi/6$.

We have no reproduction, $\dot{R} = 0$, if $(1-\kappa)S_C = \dot{k}_J U_H^p$, which happens for

$$f_R^0 = \left((1-\kappa)(L^2 + L^3 \dot{k}_M/\dot{v})/(\dot{k}_J U_H^p) - g^{-1}\right)^{-1}$$

Using only individuals with eggs, we know that the reconstructed f must be in the interval $(f_R^0, 1)$. Notice that the larger the individual, the lower the reserve density can be to continue reproduction. We have no growth, $\frac{d}{dt}L^3 = 0$, if $\kappa S_C = \kappa L^3/L_m$, which happens for

$$f_G^0 = L/L_m$$

Notice that the larger the individual, the higher the reserve density must be to fulfill the somatic maintenance costs.

Reproduction is at maximum for an individual at length L for $f = 1$ at level

$$\dot{R}_m = \left(\frac{1-\kappa}{g+1}\left(g + \frac{L}{L_m}\right)L^2 - S_H^p\right)\frac{\kappa_R}{U_E^0}$$

The maximum number of eggs accumulated over a time interval t_R is $N_m = t_R \dot{R}_m$, so if N_m represents the maximum observed number we have $t_R \geq N_m/\dot{R}_m$. If t_R does not meet this constraint we can obtain estimates of f that exceed the value 1.

The range of lengths of individuals with eggs is (1.12, 2.36) mm, which translates in estimates $L_p = 1$ mm and $L_m = 2.75$ mm. The latter value is well above the maximum observed length because maximum length can only be reached after prolonged exposure to abundant food, which is not likely in natural situations. The range of egg lengths is (0.137, 0.488) mm, which translates in an estimate $L_b = 0.48$ mm. The range of egg volumes is (0.0006, 0.1) mm^3, this covers a range of a factor 16. In view of the finding that around half of the initial reserve is still present at birth in *D. magna* [328], this factor is much too large to be explained by differences in initial reserve. I conclude that during the incubation period, the volume of the egg must grow due to the uptake of water.

The values $\kappa = 0.8$, $\dot{v} = 3.24$ mm d^{-1}, $\dot{k}_J = \dot{k}_M = 1.7$ d^{-1} are chosen from *D. magna* [328] for a reference temperature of 20°C, while $g = 0.44\,4.48/2.75 = 0.69$ was corrected for differences in max body length. This leads to $U_H^b = 0.0046$ d mm^2 and $U_H^p = 0.042$ d mm^2 to arrive at the mentioned values for L_b and L_p. The implications are age at birth $a_b = 0.51$ d and von Bertalanffy growth rate $\dot{r}_B = 0.23$ d^{-1} at $f = 1$. About half of the initial reserve is used during the embryonic stage at $f = 1$ with these parameter settings.

The maximum number of eggs in the brood pouch is 41 in an individual of length 2.24 mm. To accommodate all these eggs with the above-mentioned parameter values, we need an inter-moult period of $t_R\kappa_R = 4.8$ d, which seems somewhat long for $\kappa_R = 0.95$. If data on the real period would be available, this could be used to adjust κ or g, which both have a large effect on the minimum period that is required. Two large observed number of eggs, depress the reconstructed scaled considerably.

The conversion from $\dot{v}_0$ initial scaled reserve U_E^0 to initial volume was obtained by regression, like the scale functional responses. Notice that all parameters with length in their units refer to physical length, not volumetric length. The shape coefficient for *D. hyalina* is probably close to $\delta_{\mathcal{M}} = 0.54$.

The estimates can be improved by including ecophysiological info on DEB parameters of *D. hyalina*.

Both scenario's produced similar $f(t)$ reconstructions, see Figure 7.5. The 4 experiments showed a very similar profile, but the peak in experiment 1 and 2 is before that of 3 and 4. A major difference is that in the scenario 1, some individuals have such a large number of eggs, that the DEB parameters are forced to values such the mean scaled functional response in rather low. If only scenario 2 would have been tried, a wider choice of DEB parameters would have been possible, such that the reconstructed mean scaled functional response fluctuates on wider range of values. The large number of eggs in few individuals is then explained by deviating parameter values for those individuals. Scenario 2 involves relationships between number of eggs in the brood pouch and body length. Given the scatter, these relationships generally applied well.

The maternal effect is supported weakly only, see Figure 7.5, but reports in the literature on the contrary, i.e. that large eggs are produced at low food density (e.g. [164]), are not confirmed; I did not check the empirical basis of their claims. Apart from the problem of an increase in egg volume during development, another source of scatter in egg volume is that some individuals are likely to be in the stage of converting the reproduction buffer to eggs in the brood pouch. The number of eggs in the brood pouch might be small at the moment of sampling, but much larger a few moments later. Notice that the expected initial egg size is an U-shaped function of the functional response. The left branch has no ecological relevance because at the minimum of the function we have $f = L_b/L_m = f_G^0$, so no growth at birth. For $\dot{k}_J = \dot{k}_M$ this also means no maturation, so no birth. This calls for a revision of the parameter values, so for more info on the energetics of *D. hyalina*.

By decomposing observed egg volume into contributions from reserve and structure, they can also be used to study to what extend synchronization of moulting cycles occur among individuals. The dry weights can be used to further test ideas on reserve, in combination with reproduction. Weights have contributions from structure, reserve, reproduction buffer, and eggs. By adding assumptions about the relationship between number

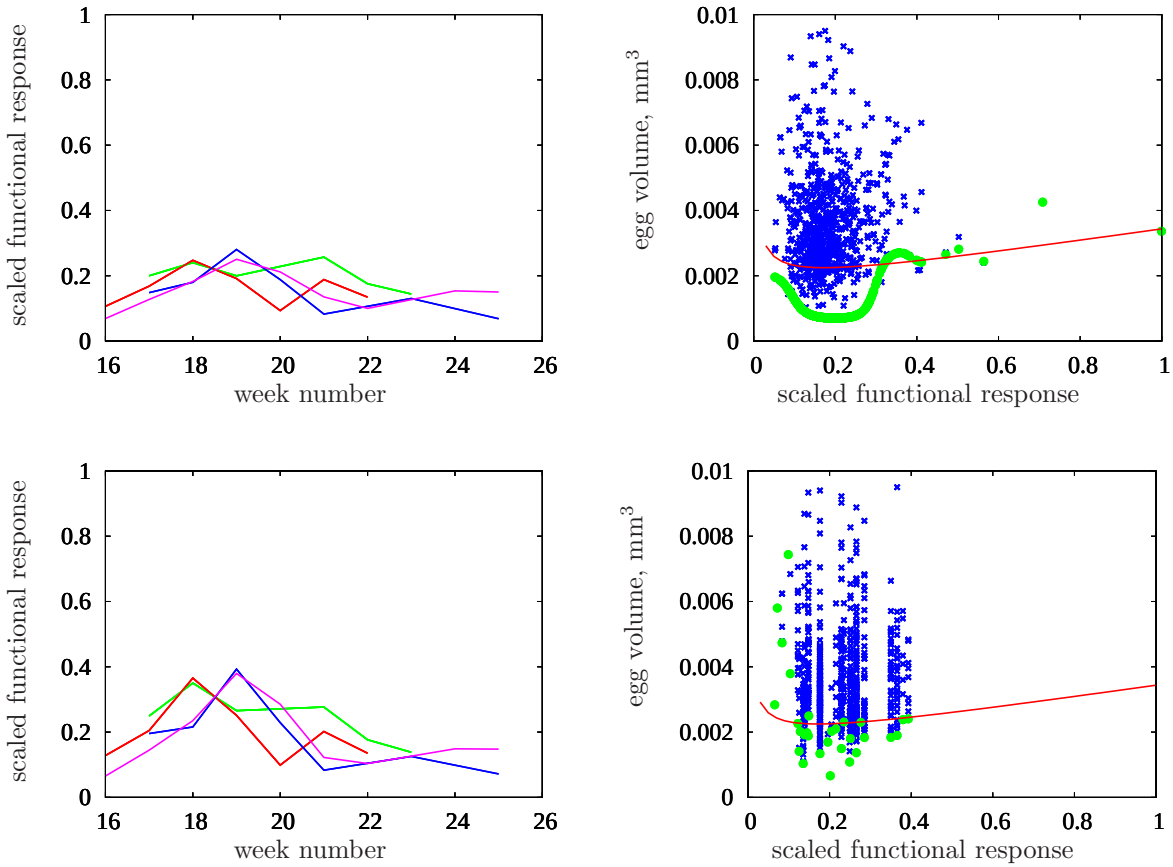

Figure 7.5: The reconstructed scaled functional response as function of the week number (left), and the egg volume as function of the scaled functional response (right), for scenario 1 (top) and 2 (bottom). Colour coding for the functional responses: Experiment 1 green, 2 red, 3 blue, 4 magenta. The blue crosses represent measured egg volumes, the green points the estimated initial egg volumes and the red curve the expected initial egg volume.

of individuals in a haul and that in the enclosure, these data can also be used to study population dynamics and the effect of sampling on population dynamics.

Food intake reconstruction from otolith data [442]

{227}

Collaborative work with Laure Pecquerie: Suppose that the opacity O as function otolith length L_O is known from data for a particular individual fish as well as all required parameter values. How can we find the scaled functional response $f(t)$ for $t \in (t_b, t_\dagger)$, where t_b is the time at mouth opening. First feeding is often detected on the otolith by a specific check.

We here make a number of simplifications, but none of them is essential, however, and all of them can be avoided. We assume that the maturity and somatic maintenance rate coefficients are equal, $\dot{k}_J = \dot{k}_M$ and so we have the scaled maturity $U_H = V(1-\kappa)g/\dot{v}$

and $\frac{d}{dt}U_H = 3(1-\kappa)\frac{L^2}{\dot{k}_M L_m}\frac{d}{dt}L$ and $S_J = \frac{1-\kappa}{\kappa}S_M$, $S_R = \frac{1-\kappa}{\kappa}S_G$. Temperature affects $\dot{k}_M$ and $\dot{v}$ given at reference temperature T_{ref} via a temperature correction factor $c_T = \exp\left(\frac{T_A}{T_{\text{ref}}} - \frac{T_A}{T}\right)$. Since the temperature effects on these two rates cancel in $L_m = \frac{\dot{v}}{\dot{k}_M g}$, we only have to take those on $\dot{v}$ into account. The estimation of T translates into the estimation of $T = T_A(T_A/T_{\text{ref}} - \ln c_T)$. We can also use more elaborate methods to relate physiological rates to temperatures that take deviations from the Arrhenius relationship into account at the high and low boundaries of the environmental temperature range. We further assume that shrinking does not occur. This typically can happen at extreme starvation when the individual is relatively large, and we assume that the reproduction buffer of such individuals is large enough to cover maintenance costs.

The final simplification is for the food density, where we will not reconstruct the food density itself, but the scaled functional response f, defined as the ingestion rate as a fraction of the maximum ingestion rate for an individual of that size. The scaled functional response is a dimensionless scalar between zero and one. The motivation is that this method does not involve the identification of the food source. On the contrary, reconstructed scaled functional responses then can be used to identify the food source.

The available info is now

$$\frac{dO}{dL_O} = \left(\dot{v}_{OG}\frac{d}{dt}S_G - O\sum_i \dot{v}_{Oi}\frac{d}{dt}S_i\right)\frac{3O^2L_O^2}{\dot{v}_{OG}^2 S_G^2(1 - L_O^3/\delta_S L^3)} \quad \text{for } i = D, G$$

with

$$\begin{aligned}
S_D &= (S_M + (1 - (L > L_p)\kappa_R)(1-\kappa)S_G)/\kappa \\
S_G &= \kappa S_C - S_M \\
S_C &= L^2 e\frac{g + L/L_m}{g+e} \\
S_M &= \frac{\kappa L^3}{L_m} \\
\frac{d}{dt}S_D &= (\frac{d}{dt}S_M + (1 - (L > L_p)\kappa_R)(1-\kappa)\frac{d}{dt}S_G)/\kappa \\
\frac{d}{dt}S_G &= \kappa\frac{d}{dt}S_C - \frac{d}{dt}S_M \\
\frac{d}{dt}S_C &= \frac{L}{g+e}(g + \frac{L}{L_m})(\frac{gL}{g+e}\frac{d}{dt}e + 2e\frac{d}{dt}L) + \frac{L^2 e}{g+e}\frac{d}{dt}\frac{L}{L_m} \\
\frac{d}{dt}S_M &= 3\kappa\frac{L^2}{L_m}\frac{d}{dt}L \\
\frac{d}{dt}e &= ((L > L_b)f - e)\dot{v}/L \\
\frac{d}{dt}L &= \frac{\dot{v}}{3}\frac{e - L/L_m}{e+g}
\end{aligned}$$

We assume that T_{ref} and the 11 parameters T_A, L_b, L_p, κ, κ_R, g, $\dot{k}_M$, $\dot{v}$, $\dot{v}_{OD}$, $\dot{v}_{OG}$, δ_S are known. Given $O(t_0)$, $L_O(t_0)$, $L(t_0)$ and $e(t_0)$ we might try to find $f(t_0)$, $c_T(t_0)$ and work our

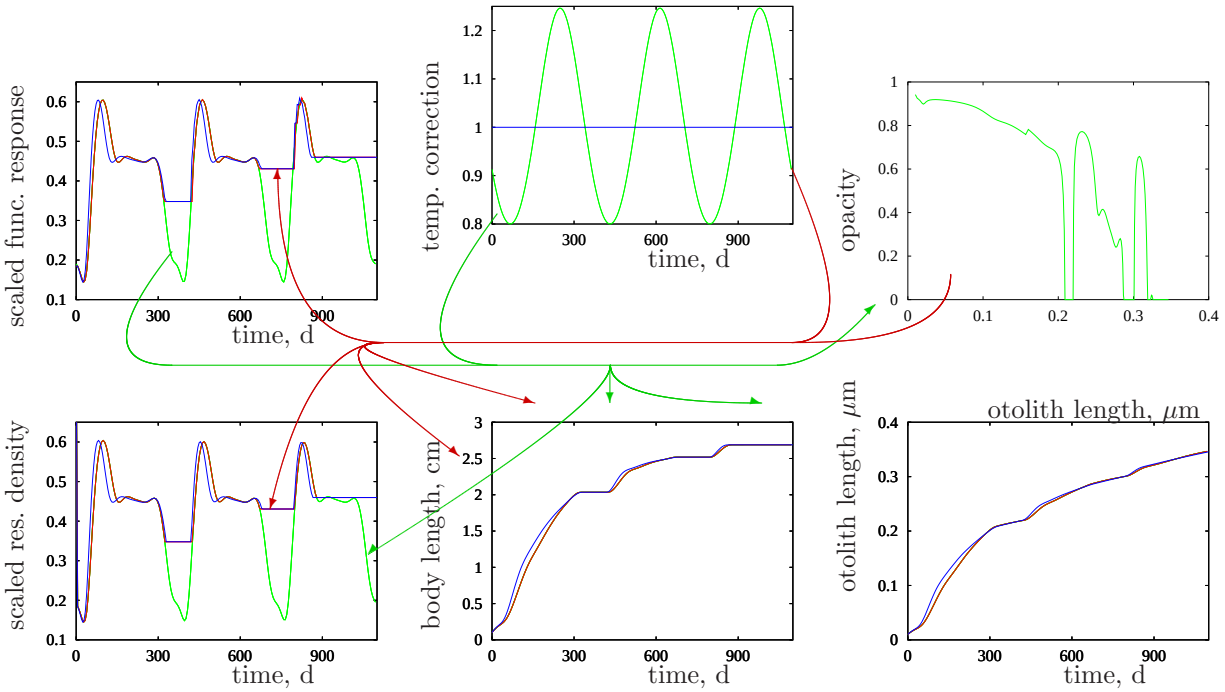

Figure 7.6: The construction (green) of the opacity profile from the functional response trajectory and reconstruction of the functional response trajectory from the opacity profile. The first reconstruction (red) uses the 'true' trajectory of the correction factor for temperature, the second reconstruction (blue) assumes a constant temperature correction factor. The match of the first reconstruction with the construction is almost perfect, so the green curves hide behind the red ones. Parameters: $L_b = 1$ cm, $L_p = 1.5$ cm, $\dot{v} = 0.526$ cm d^{-1}, $\dot{v}_{OD} = 1.186 \times 10^{-5}$ cm d^{-1}, $\dot{v}_{OG} = 1.1 \times 10^{-4}$ cm d^{-1}, $\dot{k}_M = 0.015$ d^{-1}, $g = 6$, $\kappa = 0.65$, $\kappa_R = 0.95$, $\delta_S = 1/20$.

way backwards in time. This scheme, however, turns out to be hopelessly unstable, to the extend that it is useless. A stable scheme is to start from birth and integrate over otolith length, not time. This is possible because otolith length increases strictly monotoneously in time (contrary to body length). Feeding starts at birth, so opacity at birth has no information about the food level. So we have to assumme that between the first and the second data point food density is constant, and changes linearly in time since then at rates that we reconstruct from opacity data.

A continuation method for this change from one data point to the next one turns out to be satisfactory, except when growth is resumed after starvation. For these points we need a more robust method.

Figure 7.6 illustrates the reconstruction using parameters that are appropriate for anchovy. The first reconstruction uses the 'true' trajectory of the correction factor for temperature and reconstructs the otolith and body length trajectories perfectly. The scaled functional response and the reserve density trajectories are also perfectly reconstructed, except if the reserve density no longer supports growth. The second reconstruction assumes a constant temperature correction factor of 1, still leading to a very good reconstruction.

The reconstruction of $f(t)$ from $O(L_O)$ data is coded in routine `o2f}`in toolbox "animal" of software package "debtool". The inverse routine, to construct $O(L_O)$ from $f(t)$ data,

as done in routine `f2o}`can be useful for checking the method. The comparison of the reconstructed body length at otolith collection with the measured one is other very useful check for consistency of the reconstruction method.

A weak component of our reconstruction method is the required knowlegde about the temperature trajectory during the lifetime of the fish. It turns out, however, that the (irrealistic) assumption that the temperature was constant, depite that fact that it changed in reality, hardly affected the reconstructed food history in our simulations. The second reconstruction in Figure 7.6 illustrates this.

Modifications of this reconstruction can make use of other types of data and/or information, for instance that temperature extremes should match known points on the yearly cycle. Such calibrations transform an "exact" reconstruction problem into a minimization of deviations between predictions and measurements, but doubtlessly will improve the quality of the reconstruction.

Shrinking

{231}

The process of shrinking ideally involves an extra parameter j_{VM} that quantifies the specific flux of structure that is required to cover the maintenance costs if no reserve is available to contribute to these costs. The specific growth rate for V1-morphs amounts to

$$\dot{r} = \dot{k}_E \frac{(e - l_d)_+}{e + g} - j_{VM} \frac{(l_d - e)_+}{l_d}$$

where index + indicates: take the maximum of zero and the value between the brackets, as usual. Either the first or the second term on the right-hand side is zero. In this formulation reserve kinetics does not change during shrinking, so it remains $\frac{d}{dt} e = (f - e)\dot{k}_E$, see {86}, and reserve has absolute priority above structure to pay the maintenance costs. We also do not account for adjustments of κ in this formulation, because its role remains hidden for V1-morphs.

Diffusion limitation

{235}

The theory on diffusion limitation has been extended and applied to describe how flocs of micro-organisms grow, where the big flocs develop a dead kernel, destabilize and disintegrate [66]. Almost all microbial growth in sewage plants is in this mode.

Excretion of digestive enzymes

{238}

Prokaryotes have no phagocytosis and, therefore, they have to excrete enzymes to digest substrate molecules that cannot pass the membrane. These enzymes transform substrate into product (metabolites); the resulting metabolites can be taken up and used for metabolism. We here compare this digestion mode with endocellular digestion, assuming that the concentration of (solid) substrate is very large relative to the biomass (so the decrease of solid substrate is negligibly small) and the enzyme molecules have a limited active life span.

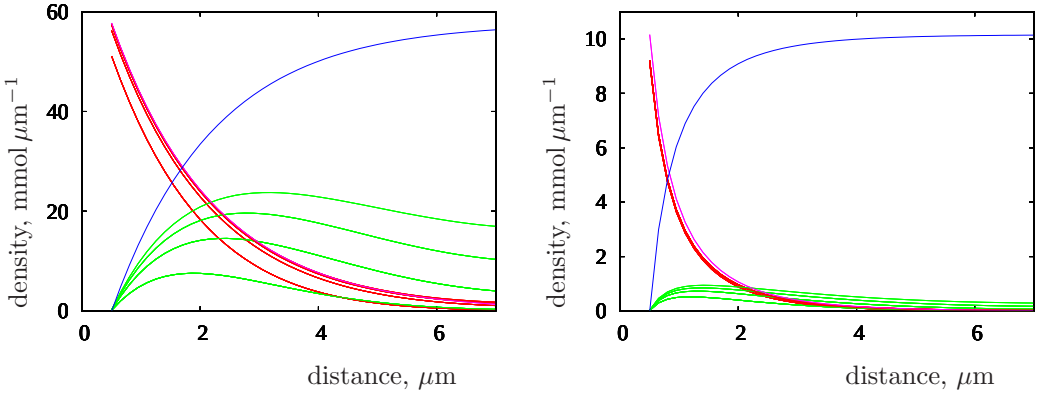

Figure 7.7: The enzyme (red) and metabolite (green) profiles for social (top left) and solitary (top right) digestion for times 100, 200,., 500 h. The magenta and blue curves are the steady state profiles for enzyme and metabolite. Parameters: $\dot{J}_E = 1$ mmol h^{-1}, $\dot{D}_E = 0.03$ μm^2 h^{-1}, $\dot{D}_P = 0.03$ μm^2 h^{-1}, $\dot{k}_E = 0.01$ h^{-1}, $\dot{k}_P = 0.01$ h^{-1}, $\dot{k} = 20$ h^{-1}, $L_R = 0.5$ μm. See Figure 7.8 for the yield of metabolite on enzyme as function of time.

At lower substrate concentrations, extracellular feeding becomes rapidly even less efficient, because enzymes loose time in their unbound state.

Intracellular digestion

Suppose the digestive enzyme becomes inactive at constant specific rate $\dot{k}_E$, and the mean production time per product molecule is $\dot{k}_P^{-1}$. The maximum yield of product per enzyme molecule thus amounts to $y^m_{PE} = \dot{k}_P/\dot{k}_E$ and serve as a reference for extracellular digestion. Although no metabolites become lost, this mode of digestion comes with costs of phagocytosis, and processing of inactive enzymes. The latter might represent a cost or a further benefit.

Social digestion

Suppose now that bacteria are tightly packed in a one-cell thick layer a solid substrate, and they excrete enzyme molecules at specific rate $\{\dot{J}_E\}$ (moles per surface area of cell per time). If the cells are spherical with radius L_R, they excrete enzymes at rate $\{\dot{J}_E\}4\pi L_R^2$. One cell occupies surface πL_R^2 in the layer, so a unit surface area has $(\pi L_R^2)^{-1}$ cells. In surface area S of medium enzymes are excreted at rate $\dot{J}_E = 4\{\dot{J}_E\}S$ (mol/t). Assuming that the cells are half embedded in the medium and the maximum specific uptake rate $\{J_{Pm}\}$ is large enough to ensure that the concentration $n_E(L_R)/S$ at the cell membrane is small, the uptake rate of a cell is $\{J_{Pm}\}\pi L_R^2 \frac{n_E(L_R)}{n_{EK}}$, where n_{EK} is the half saturation density. In surface area S of medium the uptake rate is $J_P = \{J_{Pm}\}S\frac{n_E(L_R)}{n_{EK}}$ (mol/t). The yield of metabolite on enzyme equals $y_{PE} = \frac{\{J_{Pm}\}}{\{J_E\}}\frac{n_E(L_R)}{4n_{EK}} = \frac{\{J_{Pm}\}}{J_E}\frac{n_E(L_R)}{n_{EK}}$.

Choosing the origin of length L in the center of a cell on the solid medium (for reasons

that are obvious in the case of solitary feeding), the change in densities of enzyme and product concentrations is for diffusivities $\dot{D}_E$ and $\dot{D}_P$

$$\begin{aligned} 0 &= \dot{J}_E + D_E \frac{\partial}{\partial L} n_E(L_R, t) \\ 0 &= \frac{\partial}{\partial t} n_E(L,t) + \dot{k}_E n_E(L,t) - \dot{D}_E \frac{\partial^2}{\partial L^2} n_E(L,t) \\ 0 &= \dot{J}_P - D_P \frac{\partial}{\partial L} n_P(L_R, t) \\ 0 &= \frac{\partial}{\partial t} n_P(L,t) - \dot{k}_P n_E(L,t) - \dot{D}_P \frac{\partial^2}{\partial L^2} n_P(L,t) \end{aligned}$$

The steady state profiles follow from the balance for enzyme molecules $\int_{L_R}^{\infty} n_E(L)\, dL = \dot{J}_E/\dot{k}_E$, which have solution

$$\begin{aligned} n_E(L) &= \frac{\dot{J}_E L_E}{\dot{D}_E} \exp\left(\frac{L_R - L}{L_E}\right) \quad \text{for } L_E = \sqrt{\dot{D}_E/\dot{k}_E} \\ n_P(L) &= \frac{\dot{k}_P}{\dot{k}_E} \frac{\dot{D}_E}{\dot{D}_P} \left(\frac{\dot{J}_E L_E}{\dot{D}_E} - n_E(L)\right) \end{aligned}$$

We have $\frac{d}{dL} n_P(L_R) = \frac{\dot{J}_E \dot{k}_P}{\dot{D}_P \dot{k}_E}$. The uptake equals $\dot{J}_P(t) = \dot{D}_P \frac{d}{dL} n_P(L_R, t)$, while $\dot{J}_E \dot{k}_P/\dot{k}_E$ metabolites is produced when the extracellular enzyme buffer is full. The difference is lost in the environment. The yield coefficient at infinite time is $y_{PE} = \dot{J}_P/\dot{J}_E$. We define the relative efficiency to be $\theta = \frac{y_{PE}}{y^m_{PE}} = \frac{\dot{J}_P \dot{k}_E}{\dot{J}_E \dot{k}_P}$. Initially, when $n_E(L,0) = n_P(L,0) = 0$, we have $\theta = 0$; it takes a long time to build up to $\theta = 1$, when all of the medium (apart from the direct neighborhood of the bacteria) has metabolite density $n_P(\infty)$.

Solitary digestion

Suppose now that a single spherical cell of radius L_R lives half embedded on a homogeneous medium and excretes enzyme molecules at specific rate $\{\dot{J}_E\}$ (moles per cell's surface area per time) or at rate $\dot{J}_E = \{\dot{J}_E\} 4\pi L_R^2$ in total. Cell's uptake rate of metabolites is $\{J_{Pm}\} 2\pi L_R^2 \frac{n_E(L_R)}{n_{EK}}$, so the yield of metabolites on enzyme is $y_{EP} = \frac{\{J_{Pm}\}}{\{\dot{J}_E\}} \frac{n_E(L_R)}{2 n_{EK}}$.

The change in densities of enzyme and product concentrations is for diffusivities $\dot{D}_E$ and $\dot{D}_P$

$$\begin{aligned} 0 &= \dot{J}_E + D_E \frac{\partial}{\partial L} n_E(L_R, t) \\ 0 &= \frac{\partial}{\partial t} n_E(L,t) + \dot{k}_E n_E(L,t) - \dot{D}_E \frac{\partial^2}{\partial L^2} n_E(L,t) - 2\frac{\dot{D}_E}{L} \frac{\partial}{\partial L} n_E(L,t) \\ 0 &= \dot{J}_P - D_P \frac{\partial}{\partial L} n_P(L_R, t) \\ 0 &= \frac{\partial}{\partial t} n_P(L,t) - \dot{k}_P n_E(L,t) - \dot{D}_P \frac{\partial^2}{\partial L^2} n_P(L,t) - 2\frac{\dot{D}_P}{L} \frac{\partial}{\partial L} n_P(L,t) \end{aligned}$$

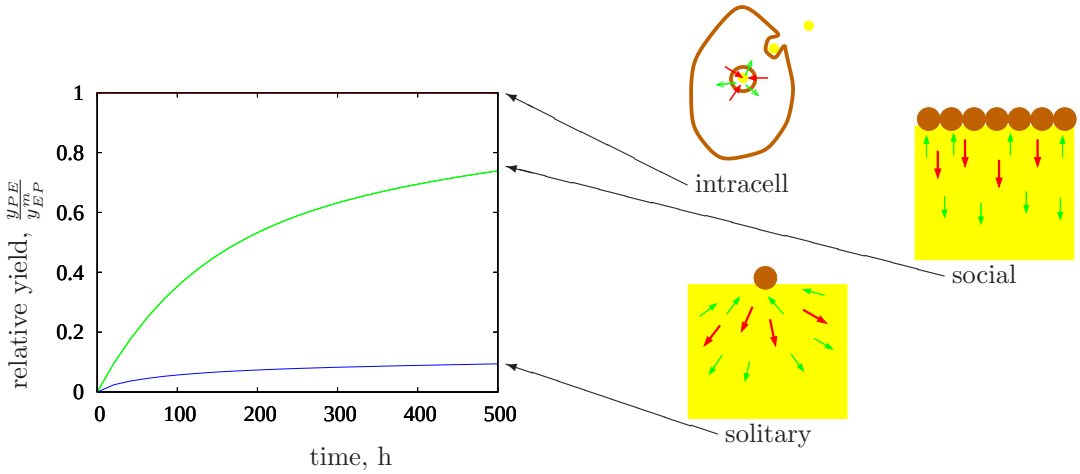

Figure 7.8: The relative to the yield of metabolite on enzyme for intracellular digestion, the yield for social extracellular digestion builds up slowly in time, while that for solitary digestion really takes a long time and builds up to a lower level. The red arrows stand for enzyme flux, the green ones for metabolite flux.

The steady state profile of the enzyme and metabolite is

$$\begin{aligned} n_E(L) &= \frac{\dot{J}_E}{\dot{D}_E} \frac{L_E L_R^2/L}{L_E + L_R} \exp\left(\frac{L_R - L}{L_E}\right) \\ n_P(L) &= \frac{\dot{k}_P}{\dot{k}_E} \frac{\dot{D}_E}{\dot{D}_P} \left(\frac{\dot{J}_E}{\dot{D}_E} \frac{L_E L_R}{L_E + L_R} - n_E(L)\right) \end{aligned}$$

Figure 7.7 compares enzyme and metabolite profiles for the social and solitary digestion modes. Although the results depend on parameter values, quite a bit of metabolites are unavailable for the cell, and the problem is much worse for solitary cells. It also takes a long time to build up some yield, compared with intracellular digestion. The enzyme profile reaches its steady state much earlier than the metabolite profiles; the metabolites first must flush the whole medium before a steady state profile can build up.

Notation

{241}, Fig 7.15

The notation in the caption of figure 7.15 is not fully consistent, since $\{\dot{J}_{Xm}\}$ is here quantified in mg POM/h, while the symbol assumes that it is quantified in C-mol per time. The book has no symbol for "weight per time", so we have to use w_X to convert C-mol to weight of food. So a better notation for the assimilation power is $\dot{p}_A = \dot{J}_X\{\dot{p}_{Am}\}/\{\dot{J}_{Xm}\} = w_X \dot{J}_X \{\dot{p}_{Am}\}(w_X\{\dot{J}_{Xm}\})^{-1}$, where $\{\dot{p}_{Am}\}(w_X\{\dot{J}_{Xm}\})^{-1} = 11.5$ J mg POM^{-1}.

Yield of biomass on substrate

{243}

The table below (9.12) gives the yield $Y = Y_g \frac{g}{f} \frac{f - l_d}{f}$, while the specific growth rate is $r = \dot{k}_e \frac{f - l_d}{f + g}$ for V1-morphs (see {108}). Simple substitution of f and $l_d = g\dot{k}_M/\dot{k}_E$ gives

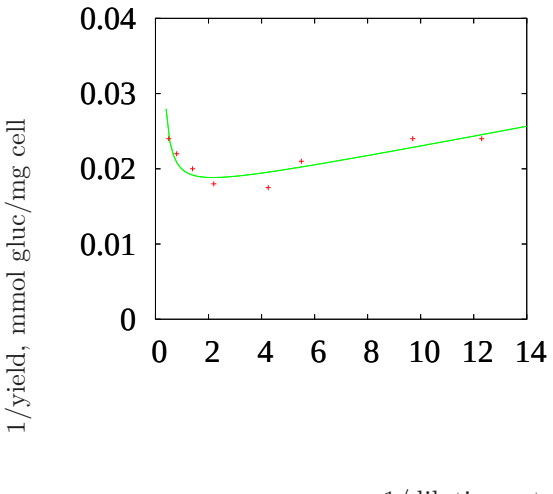

Figure 7.9: When the inverse yield is plotted against the inverse growth rate, an U-shaped curve results. The parameters are $Y_g = 62.84$ mg cell/mmol glucose, $\dot{k}_E = 5.93$ h^{-1} and $\dot{k}_M = 0.042$ h^{-1}. This data set is used by [497] to demonstrate that bacteria down-regulate their maintenance in association with substrate availability. The fit shows, however, that this is not the only possible explanation for these data, since the DEB theory assumes that the specific maintenance costs do not depend on food density and still fits the data.

$Y^{-1} = \frac{\dot{k}_E}{Y_g} \frac{1+\dot{k}_E l_d/(gr)}{\dot{k}_E - r} = Y_g^{-1} \frac{1+\dot{k}_M/r}{1-r/\dot{k}_E}$. This specifies a three-parameter relationship between $1/Y$ and $1/r$, which fits the data of Russell & Baldwin (1979) on *Streptococcus bovis* in glucose-limited medium as reported in [497] very well. See Figure 7.9.

The yield of biomass on substrate Y_{WX} is not a DEB parameter, and depends on the growth rate. Since the specific growth rate of 0.2 h^{-1} is rather large, the contribution of maintenance is small. If we include bacteria with low reserve capacities Y_{WX} is about equal to $y_{VX} = y_{VE}\, y_{EX}$, where only y_{EX} is likely to depend on the chemical potential of the substrate, i.e. $y_{VX} \simeq \eta_{VA} \mu_X$ with $\eta_{VA} = 0.001$ C-mol/ kJ. Since animals are biotrophs, so their food mainly consists of polysaccharides, lipids and proteins, we expect that $y_{VX} = 0.4$ till 0.6 C-mol/C-mol for animals (see the table at {137}).

Mechanism for reserve dynamics

{246}

The simplest catabolic flux that partially obeys the weak homeostasis and partitionability requirements is first-order kinetics, $[p_C] = k_E[E]$, which is implied if all reserve molecules have a constant probability rate for being used by metabolism for maintenance and growth. This results in the specific growth rate $\dot{r} = \frac{d}{dt} \ln V = (\dot{k}_E[E] - [\dot{p}_M])/[E_G]$ and reserve density kinetics $\frac{d}{dt}[E] = [\dot{p}_A] - (\dot{k}_E + \dot{r})[E]$. As long as surface area is proportional to volume (these morphs are called V1-morphs, this kinetics is weakly homeostatic because reserve density $[E]$ settles for constant $[\dot{p}_A] = \dot{p}_A/V$ at a value that does not depend on the size of the organism. It is not weakly homeostatic for other morphs, such as isomorphs, i.e. organisms that do not change in shape during growth, surface area is proportional to volume$^{2/3}$. This specific catabolic flux is first-degree homogeneous in the reserve density and zero-

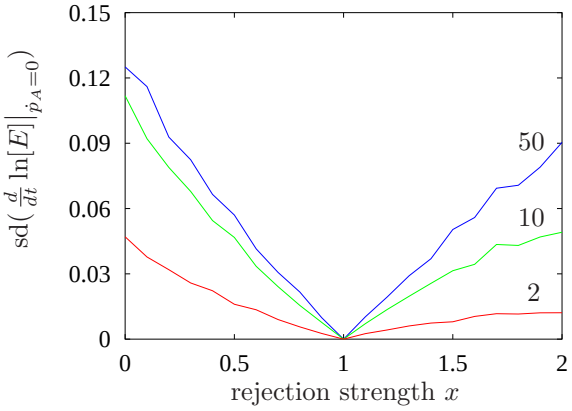

Figure 7.10: The standard deviation of the specific change of reserve density as function of the rejection strength, if the assimilation rate k_A jumps randomly between 0 and $1\,\mathrm{h}^{-1}$. The hazard rate at level 0 is 2, 10 and $50\,\mathrm{h}^{-1}$ and at level 1 is $10\,\mathrm{h}^{-1}$. The standard deviations are estimated from Monte Carlo simulations over 200 h, using turnover rate $\dot{k}_E = 1.5\,\mathrm{h}^{-1}$ and maintenance rate coefficient $\dot{k}_M = 0.01\,\mathrm{h}^{-1}$.

degree homogeneous in structure, but also in the specific maintenance and growth costs (because that latter three quantities do not occur in the specific catabolic rate). First-order dynamics is, therefore, not partitionable.

Since reserve primarily consists of polymers (RNA, proteins, carbohydrates, lipids), an interface exists between reserve and structure. For isomorphs structural homeostasis means that the surface area of the reserve-structure interface is proportional to the ratio of the amount of reserve and a length measure for the structure; for V1-morphs this means that it is proportional to the amount of reserve. The mobilization rate of reserve is now taken to be proportional to the surface area of the reserve-structure interface and allocated to the SUs for maintenance and growth, called the catabolic SUs. The mobilized reserve flux that cannot be bounded to these units is returned to the reserve, while the bounded flux is further processed for maintenance and growth. Maintenance is demand-driven and the flux is proportional to the amount of structure, while growth is supply-driven. The amount of SUs is such that weak homeostasis results, which turns out to be proportional to the amount of structure. Originally this proportionality constant would not have been the value that results in weak homeostasis, as illustrated in Figure 7.10, so the proper setting in an evolutionary achievement.

Polymers as such do not take part in metabolism as substrates, their use as substrate involves monomerization. The decomposition of many types of source polymers and other compounds into a limited number of types of central metabolites before polymerization into biomass (growth) is known as the 'funnel' concept [236]. The next step in the evolutionary development of reserve dynamics is to avoid the rejection of mobilized reserve by the creation of local pools of monomers from which the SUs take their substrate, and linking the pool size of the monomers of reserves to that of the polymers (this is implied by the strong homeostasis assumption). The avoidance of rejection of mobilized reserve is especially important for large body sizes (in eukaryotes) and reproduction via eggs or seeds (so much later in the evolution). The result for V1-morphs is that $[\dot{p}_C] = (\dot{k}_E - \dot{r})[E]$, with the consequence that the specific growth rate amounts to $\dot{r} = \frac{\dot{k}_E[E]-[\dot{p}_M]}{[E]+[E_G]}$ and the reserve density kinetics to $\frac{d}{dt}[E] = [\dot{p}_A] - \dot{k}_E[E]$.

Now more technically recapitulated, the derivation of the reserve dynamics has the following steps

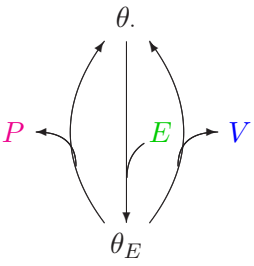

Figure 7.11: The interaction between the conversions from reserve E to maintenance products P and structure V.

- reserve and structure are spatially segregated
- the mobilization of reserve is at a rate proportional to the surface area of the reserve-structure interface and allocated to catabolic SUs
- rejection of mobilized reserve occurs because the catabolic SUs being busy; the rejected flux returns to the reserve
- the bounded (somatic) catabolic SUs dissociate to the demand-driven maintenance SUs and via growth, see Figure 7.11
- the number of catabolic SUs is such that weak homeostasis is achieved, which depends on the specific rate of reserve mobilization relative to the dissociation rate, see Figure 7.10

The surface area of the interface of reserve and structure is proportional to M_E for V1-morphs and to M_E/L for isomorphs (for which length $L \propto M_V^{1/3}$) if structural homeostasis applies. The reserve is mobilized at rate $\dot{J}_{EC} = M_E \dot{k}_E$ for V1-morphs and at rate $\dot{J}_{EC} = M_E \dot{v}/L$ for isomorphs.

The dynamics of the fraction of unbounded SUs for V1-morphs is

$$\frac{d}{dt}\theta_{\cdot} = (1-\theta_{\cdot})\dot{k} + j_{EM}/n - \theta_{\cdot}\dot{k}_E m_E/n$$

where $n = N/M_V$ denotes the specific number for SUs, $\dot{k}$ the dissociation rate of the SUs and $j_{EM} = \dot{J}_{EM}/M_V$ the specific somatic maintenance costs. The steady state fraction of unbounded SUs then amounts to

$$\theta_{\cdot}^* = \frac{\dot{k} + j_{EM}/n}{\dot{k} + \dot{k}_E m_E/n}$$

while the specific growth rate equals $\dot{r} = (1-\theta_{\cdot}^*) n\, y_{VE}\, \dot{k} = \frac{m_E \dot{k}_E - j_{EM}}{m_E x + y_{EV}}$ for $x = \frac{y_{EV}\dot{k}_E}{n\dot{k}}$. The mobilized reserve flux of size $M_E \dot{k}_E$ is partitioned into the flux $M_E(\dot{k}_E - \dot{r})$ that is accepted and used for somatic maintenance at rate $j_{EM} M_V$ and growth (i.e. structure is synthesized at rate $\dot{r} M_V$), and the flux $M_E x \dot{r}$ that is rejected and returned to the reserve. The latter flux can be seen (formally) as a synthesis of reserve, which helps to see that for $x = 1$

Table 7.2: Three steps in the evolution of reserve dynamics, and the implications for the specific catabolic flux, the specific growth rate and the dynamics of the reserve density. Symbols: $[E] = E/V$ reserve density, V structural volume, $L = V^{1/3}$ structural length, $[\dot{p}_C] = \dot{p}_C/V$ specific catabolic flux, $[\dot{p}_M] = \dot{p}_M/V$ specific maintenance flux, $[\dot{p}_A] = \dot{p}_A/V$ (volume-)specific assimilation flux, $\{\dot{p}_A\} = \dot{p}_A/L^2$, surface area-specific maintenance flux, $[E_G]$ specific costs for structure, $\dot{k}_E$ reserve turnover rate, v energy conductance.

module	spec catab $[\dot{p}_C]$	spec growth $\dot{r} = \frac{d}{dt}\ln V$	reserve density $\frac{d}{dt}[E]$
first order	$[E]\dot{k}_E$	$\frac{[E]\dot{k}_E - [\dot{p}_M]}{[E_G]}$	$[\dot{p}_A] - [E](\dot{k}_E + \dot{r})$
V1-morphs	$[E](\dot{k}_E - \dot{r})$	$\frac{[E]\dot{k}_E - [\dot{p}_M]}{[E]+[E_G]}$	$[\dot{p}_A] - [E]\dot{k}_E$
isomorphs	$[E](\dot{v}/L - \dot{r})$	$\frac{[E]\dot{v}/L - [\dot{p}_M]}{[E]+[E_G]}$	$(\{\dot{p}_A\} - [E]\dot{v})/L$

(so $n = y_{EV}\dot{k}_E/\dot{k}$), homeostasis is most effective because reserve is then synthesized at the same specific rate as structure, so the reserve density is not affected.

The dynamics of the reserve density becomes

$$\frac{d}{dt}m_E = j_{EA} - m_E(\dot{k}_E + \dot{r}(1-x))$$

where j_{EA} is the specific assimilation rate, which depends on substrate density and so typically fluctuates in time. The catalyzing SUs at the reserve-structure interface experience a local chemical environment that changes with $-\frac{d}{dt}\ln m_E|_{j_{EA}=0}$. Figure 7.10 gives the standard deviation of this quantity as function of x, when the assimilation rate jumps randomly between 0 and some fixed value; so the assimilation process follows an alternating Poisson process. This standard deviation equals zero for $x = 1$, but increases almost proportional to the deviation from this value. The tuning of the number of SUs can be seen as one of the mechanisms organisms use to improve homeostasis.

The specific catabolic flux $[p_C] = [E_G]\dot{r} + [\dot{p}_M] = [E](\dot{k}_E - x\dot{r})$ is partitionable for all positive values of x. This is because $[\dot{p}_C] = [E]\frac{[E_G]\dot{k}_E + x[\dot{p}_M]}{x[E]+[E_G]} = [E]\frac{[E_G]'\dot{k}_E + [\dot{p}_M]}{[E]+[E_G]'}$. So, x only affects the apparent growth costs, $[E_G]' = [E_G]/x$. In the specific growth rate r, and also affects the apparent turnover rate and the maintenance rate. The abundance of SUs, therefore, affects parameter values, not model structure.

Monomers being part of the reserve, the strong homeostasis assumption implies that the amount of monomers M_F is a fixed fraction of the reserve, $M_F \propto M_E$. It might be by rapid inter-conversion of the first order type. The problem is then how the cost is paid, because the energy drain that is involved should be evident in the respiration rate, while eggs hardly respire initially. A more likely possibility is that monomerization is product inhibited and ceases if the monomers per polymer reach a threshold. The monomerization cost is then covered by maintenance and growth. For an individual with an amount of

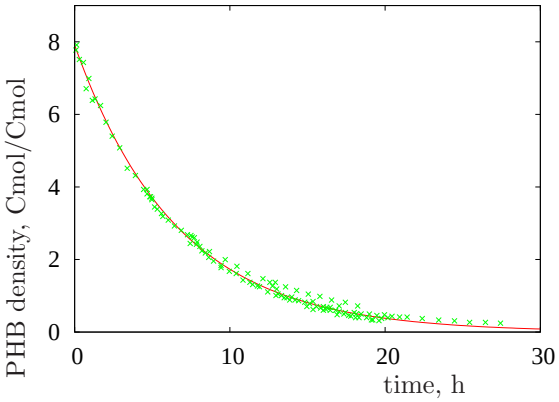

Figure 7.12: The poly-β-hydroxybutyrate (PHB) density (on the basis of C-mol/C-mol) in aerobic activated sludge at 20°C. The fitted curve is an exponential one with parameter 0.15 h. Data from [43]. She pointed in her thesis to [11] who found that the number of PHB granules per cell is fixed at the earliest stage of polymer accumulation. This supports the structural homeostasis hypothesis.

structure M_V and reserve M_E, the kinetics of the amount of monomers M_F could be

$$\frac{d}{dt}M_E = -M_E(\dot{k}_{EF} - \frac{m_F}{m_E}\dot{k}_{FE}); \quad \frac{d}{dt}M_F = y_{FE}M_E(\dot{k}_{EF} - \frac{m_F}{m_E}\dot{k}_{FE})$$

with $m_E = M_E/M_V$ and $m_F = M_F/M_V$. This kinetics makes that in steady state $\frac{m_F^*}{m_E^*} = \frac{\dot{k}_{EF}}{\dot{k}_{FE}}$. The monomerization occurs at the E-V interface, which has a surface area proportional to E/L in isomorphs, where structural length $L \propto M_V^{1/3}$. This makes that k_{EF} and k_{EF} are proportional to L^{-1} as well.

Empirical support for reserve dynamics

{247}

Janneke Beun obtained empirical support for the first order dynamics of reserves on the basis of densities. See Figure 7.12.

Structural homeostasis, derivation of Eq (7.12) - (7.22)

{247}

Eq (7.12)-(7.22) can be derived as follows.

The κ-rule states: $\kappa\dot{p}_C = \dot{p}_G + \dot{p}_M$. Since $\dot{p}_G = \mu_{GV}\frac{d}{dt}M_V$, we have $\kappa\dot{p}_C = \mu_{GV}\frac{d}{dt}M_V + \dot{p}_M$, or

$$\begin{aligned}
\frac{d}{dt}M_V &= \mu_{GV}^{-1}(\kappa\dot{p}_C - \dot{p}_M) \\
&= \eta_{VG}\kappa\dot{p}_C - \mu_{GV}^{-1}[\dot{p}_M]V \quad \text{for } \eta_{VG} = \mu_{GV}^{-1} \text{ and } [\dot{p}_M] = \dot{p}_M/V \\
&= \dot{p}_C\eta_{VC} - \mu_{GV}^{-1}[\dot{p}_M]M_V/[M_V] \quad \text{for } \eta_{VC} = \eta_{VG}\kappa \text{ and } [M_V] = M_V/V \\
&= \dot{p}_C\eta_{VC} - M_V\dot{k}_M \quad \text{which is (7.14)}
\end{aligned}$$

with $\dot{k}_M = \frac{[\dot{p}_M]}{\mu_{GV}[M_V]} = \frac{[\dot{p}_M]}{[E_G]}$. Eq (7.13) follows by analogy because allocation to membranes is treated similarly as allocation to structure.

From (7.14) we have that

$$\frac{d}{dt}\ln V = \frac{d}{dt}\ln M_V = M_V^{-1}\frac{d}{dt}M_V = [\dot{p}_C]\eta_{VC}/[M_V] - \dot{k}_M.$$

Starting from (7.12) and applying the chain rule for differentiation:

$$\begin{aligned}
\frac{d}{dt}[E] &= [\dot{p}_A] - [\dot{p}_C] - [E]\frac{d}{dt}\ln V \\
&\quad \text{substituting } \tfrac{d}{dt}\ln V \\
\frac{d}{dt}[E] &= [\dot{p}_A] - [\dot{p}_C] - [E]([\dot{p}_C]\eta_{VC}/[M_V] - \dot{k}_M) \\
[\dot{p}_C] &= \frac{[\dot{p}_A] - \frac{d}{dt}[E] + \dot{k}_M[E]}{1 + [E]\eta_{VC}/[M_V]} \quad \text{which is (7.16)}
\end{aligned}$$

From (7.13) we get by division through V

$$\begin{aligned}
[\dot{p}_C] &= \mu_{CC}V^{-1}\left(\frac{d}{dt}M_C + M_C\dot{k}_C\right) \\
&\quad \text{substitute (7.17) and (7.18)} \\
&= \mu_{CC}\frac{\{M_{Cn}\}}{[E_n]}V^{-1/3}\left(\frac{d}{dt}[E] + \frac{2}{3}[E]\frac{d}{dt}\ln V + [E]\dot{k}_C\right) \\
&\quad \text{substitute } \tfrac{d}{dt}\ln V \\
&= \mu_{CC}\frac{\{M_{Cn}\}}{[E_n]}V^{-1/3}\left(\frac{d}{dt}[E] + \frac{2}{3}[E]([\dot{p}_C]\eta_{VC}/[M_V] - \dot{k}_M) + [E]\dot{k}_C\right) \\
&\quad \text{now solve } [\dot{p}_C] \\
&= \frac{\{M_{Cn}\}V^{-1/3}}{[E_n]\eta_{CC}}\,\frac{\frac{d}{dt}[E] + [E](\dot{k}_C - \frac{2}{3}\dot{k}_M)}{1 - \frac{\{M_{Cn}\}V^{-1/3}}{[E_n]\eta_{CC}}\frac{2}{3}\frac{\eta_{VC}}{[M_V]}[E]} \quad \text{with } \eta_{CC} = \mu_{CC}^{-1} \\
&= \frac{\frac{d}{dt}[E] + [E](\dot{k}_C - \frac{2}{3}\dot{k}_M)}{\frac{[E_n]\eta_{CC}}{\{M_{Cn}\}V^{-1/3}} - \frac{2}{3}\frac{\eta_{VC}}{[M_V]}[E]} \\
&= \frac{\frac{d}{dt}[E] + [E](\dot{k}_C - \frac{2}{3}\dot{k}_M)}{\frac{\dot{k}_C}{\dot{v}}V^{1/3} - \frac{2}{3}\frac{\eta_{VC}}{[M_V]}[E]} \quad \text{for } \dot{v} = \frac{\{M_{Cn}\}\dot{k}_C}{[E_n]\eta_{CC}} \\
&\quad \text{equating this to (7.16) and solving for } \tfrac{d}{dt}E \\
\frac{d}{dt}[E] &= \frac{\frac{\dot{k}_C}{\dot{v}}V^{1/3}[\dot{p}_A] - [E]\left(\frac{2}{3}\frac{\eta_{VC}}{[M_V]}[\dot{p}_A] - \frac{\dot{k}_C}{\dot{v}}V^{1/3}\dot{k}_M + \dot{k}_C - \frac{2}{3}\dot{k}_M\right) - [E]^2\dot{k}_C\frac{\eta_{VC}}{[M_V]}}{1 + \frac{\dot{k}_C}{\dot{v}}V^{1/3} + \frac{1}{3}\frac{\eta_{VC}}{[M_V]}[E]} \\
&\quad \text{for } \eta_{CC} \to \infty \text{ and } \dot{k}_C \to \infty \text{ such that } \eta_{CC}/\dot{k}_C, \text{ and so } \dot{v}, \text{ remains constant} \\
&= \frac{\frac{1}{\dot{v}}V^{1/3}[\dot{p}_A] - [E]\left(1 - \frac{1}{\dot{v}}V^{1/3}\dot{k}_M\right) - [E]^2\frac{\eta_{VC}}{[M_V]}}{\frac{1}{\dot{v}}V^{1/3}} \\
&= [\dot{p}_A] - [E]\left(\dot{v}V^{-1/3} - \dot{k}_M\right) - [E]^2\frac{\eta_{VC}}{[M_V]}\dot{v}V^{-1/3} \quad \text{which is (7.22)}
\end{aligned}$$

Number of vesicles

{248}

Paragraph 3 " Suppose that the number of vesicles .. see Figure 7.2" tries to explain the supposed kinetics of vesicles. Suppose that the amount of structure increases, but not the amount of reserves; this cannot happen in the natural dynamics of the system, but we, as experimenters, can simply change the value of the state variables. The amount of membranes is proportional to $EV^{-1/3}$, so the amount of membranes has to shrink, which means that the vesicles have to reorganize themselves into a smaller number of bigger vesicles, with the same total volume (because we did not change the amount of reserve). This reorganization is assumed to be fast relative to the change of the state variables (here the amount of structure). Please realize that when two spherical vesicles of equal size meet and merge into a single vesicle with a double volume, it cannot have a spherical shape. This is because the amount membrane that wraps the merged vesicle is too large for a spherical shape.

Dilution by growth

{249}

Paragraph 4 discusses the problem when effects of dilution by growth on reserve dynamics are small. If reserve dynamics, rather than reserve density dynamics, would be a first order process, we would have $\frac{d}{dt}E = \dot{p}_A - \dot{v}EV^{-1/3}$, so that $\frac{d}{dt}[E] = [\dot{p}_A] - \dot{v}[E]V^{-1/3} - [E]\frac{d}{dt}\ln V$. The effects of dilution by growth are small if $\frac{d}{dt}\ln V \ll \dot{v}V^{-1/3}$, i.e. $V^{-2/3}\frac{d}{dt}V \ll \dot{v}$. Specific growth in volume equals that in C-moles, $V^{-1}\frac{d}{dt}V = [M_V]^{-1}\frac{d}{dt}M_V$, while growth in C-moles relates to growth power as $\frac{d}{dt}M_V = \mu_E^{-1}y_{VE}\dot{p}_G$, which leads to $\frac{d}{dt}\ln V = \frac{\dot{p}_G y_{VE}}{[M_V]\mu_E}$. Using Table 3.5 for $\dot{p}_G$ and Table 3.4 for g, M_{Em} and m_{Em}, and $V_m^{1/3} = \frac{\dot{v}}{\dot{k}_M g}$ we arrive at $V^{-2/3}\frac{d}{dt}V = \frac{\dot{v}}{g}\frac{e-l-l_h}{1+e/g}$. This quantity is much smaller than $\dot{v}$ if $e - l - l_h \ll g + e$, or $g \gg -l - l_h$. Obviously, we always have that $g > 0$. This result simply means that the effects of dilution by growth are small for large g, and the dilution by growth can never dominate reserve dynamics. This latter is obvious, since growth is fueled by the use of reserves, so we can never have the combination of a large dilution by growth and a small use of reserve.

7.1 Organelle-cytosol interactions

{250}

Here we consider the problem of how to deal quantitatively with the dual function of many cellular compounds: their use as source for energy as well as building blocks [327]. Because of this duality, the fate of metabolites should generally depend on the cellular growth rate. To focus ideas, let us briefly discuss a specific example.

The nine transformations of the linear metabolic pathway of the tricarboxylic acid (TCA) cycle amount to the oxidation of the acetyl group of acetyl-CoA to CO_2:

$$C_2H_3O\text{-SCoA} + 3\,NAD^+ + FAD + GDP^{3-} + P_i^{2-} + 2\,H_2O \rightarrow$$
$$2\,CO_2 + 3\,NADH + FADH_2 + GTP^{4-} + 2\,H^+ + H\text{-SCoA}$$

The H-SCoA re-binds to pyruvate or fatty acid for the next cycle; the reduced co-enzymes NADH and $FADH_2$ are re-oxidized by dioxygen in a multi-step transformation. The free

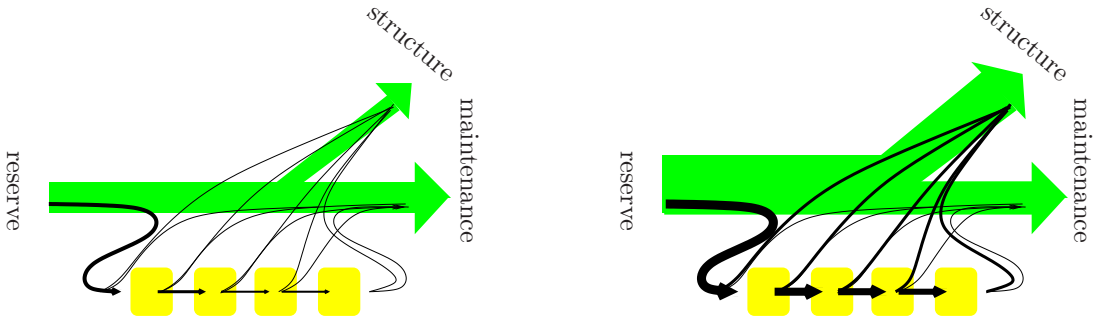

Figure 7.13: The resources that are mobilized from the reserve by the catabolic flux are allocated to maintenance and growth, i.e. increase in structure. When the reserve density increases, the catabolic flux and the allocation to growth increase, but not the allocation to maintenance (right panel; widths of arrows indicate the sizes of fluxes). The flux of substrate to the enzymatic pathway is proportional to the catabolic flux. The mixture of products and intermediary metabolites that are released from a linear pathway and allocated to maintenance (or growth) is constant. This paper solves the problem of how the non-linear dynamics of the pathway should be organized to fulfill this complex task.

energy is used to convert ADP and P_i to ATP via a proton gradient across the mitochondrial inner membrane, as is well known. What is usually less emphasized in text books is that the intermediary metabolites (e.g. citrate, succinate, fumarate, malate) are also used as building blocks. So not all the pyruvate that is passed to mitochondria should be combusted completely. Cells' need for building blocks, relative to that for ATP, depends on the growth rate, and hence on the rate of pyruvate allocation to mitochondria. The six non-membrane-bound enzymes of the TCA cycle are released from the gel-like mitochondrial matrix by gentle ultrasonic vibration as a very large multi-protein complex [363]. This spatial organization suggests interactions between the enzymes that might be responsible for the regulation of the proper ATP/building blocks ratio.

We first reformulating the dual function problem more precisely in quantitative terms and place it in the context of the Dynamic Energy Budget theory. We then show how Synthesizing Units can be used to model cell's regulatory functions for linear and cyclic pathways, and finally we set up a Metabolic Control Analysis for the situation where metabolites are used to synthesize enzymes that transform these metabolites.

7.1.1 Formal problem

Consider an n-step linear metabolic pathway, as illustrated in Figure 7.13, which is mediated by enzymes $S_1, \cdots, S_n$ with the following i-th step:

$$X_{i-1} \rightarrow y_{X_i X_{i-1}} X_i + y_{P_i X_{i-1}} P_i \quad \text{with } i = 1, \cdots, n. \tag{7.1}$$

A molecule of intermediary metabolite X_{i-1} is transformed into $y_{X_i X_{i-1}}$ molecules of another intermediary metabolite X_i and $y_{P_i X_{i-1}}$ molecules of product. (Alternatively, the

yield coefficients y are probabilities that a metabolite transforms respectively to the next metabolite in the pathway or to the product.) Other substrate molecules might be involved as well, but their availability is assumed to be such that they do not limit the rate of transformation. The product P_i might actually be composed of a set of (possibly different) molecules, rather than a single molecule. Products are, therefore, taken to be *generalized compounds*, which are mixtures of chemical compounds such that the chemical composition of the mixture does not change. Without loss of generality we can identify the last intermediary metabolite X_n with the last product P_n. The substrate flux J_{X_0} to the pathway is given by a model for the whole cell and might vary (slowly) in time. If all intermediary metabolites would follow the full pathway (which they generally do not), we have the overall transformation

$$X_0 \rightarrow \sum_{i=1}^{n} y_{P_i X_0} P_i \quad \text{with } y_{P_i X_0} = y_{P_i X_{i-1}} \Pi_{j=1}^{i-1} y_{X_j X_{j-1}} \quad \text{for } i = 2, \cdots, n \tag{7.2}$$

We now consider the situation where some intermediary metabolites follow only part of the pathway and step out of the transformation process at the various nodes of the pathway and become available for two cellular functions: maintenance and growth of structure, see Figure 7.13. Cellular maintenance and growth require the intermediary metabolites X_i and products P_i in possibly different relative amounts:

$$\sum_i y_{X_i X_M} X_i + \sum_i y_{P_{i+1} X_M} P_{i+1} \quad \rightarrow \quad X_M \tag{7.3}$$

$$\sum_i y_{X_i X_G} X_i + \sum_i y_{P_{i+1} X_G} P_{i+1} \quad \rightarrow \quad X_G \tag{7.4}$$

where X_M and X_G are taken to be generalized compounds that are involved in the maintenance and growth process, respectively, and the yield coefficients y are taken to be stoichiometric constants (i.e. fixed constant whose values follow are constraint by mass conservation). *This latter requirement yields the important conclusion that all products and intermediary metabolites that are released from the pathway depend linearly on the growth rate.* To see this, note that the released material at growth rate zero is allocated to maintenance. If more material is released than is needed for maintenance, the extra material is allocated to growth. If, for example, the growth rate is doubled, then twice as much material per unit of time is needed for growth, provided that structure does not change in composition. Maintenance has priority over growth. Accordingly, the flux ratio J_{X_G}/J_{X_M} depends on the flux J_{X_0} in a very special way, as will be discussed below.

The problem now is that the mass balance at the whole-cell level forces us to assume that the chemical composition of the mixture of metabolites and products that is allocated to maintenance is constant. The same applies to the mixture that is allocated to growth, while the composition of both mixtures will differ. This mass balance does not and cannot account for leaks from a pathway, where leaks are defined to be fluxes that are not associated to maintenance or growth (or any other process that the whole-cell model specifies). What does this imply for the dynamics of the pathway? How is pathway kinetics linked to cellular requirements for particular compounds? The cell has many pathways and if each pathway produced compounds that are not allocated to maintenance or growth, any

model at the cellular level would be problematic, unless the cellular model incorporated the details of the then (very large) set of models for all different pathways. Such a complex model would hardly contribute to further insight concerning cellular metabolic functions and would be highly impractical in most applications. Consequently, we here discuss a consistency issue between a whole-cell model and model for the dynamics of a pathway.

The cellular requirements can be expressed in the overall transformation

$$X_0 \rightarrow Y_{X_M X_0} X_M + Y_{X_G X_0} X_G \tag{7.5}$$

where the variable stoichiometric coefficients Y depend on the flux of substrate J_{X_0} to the pathway. Both these coefficients and the flux must be specified by a model for the whole cell, which we will now specify.

7.1.2 Problem in DEB context

To make a clear notational distinction between the two levels of organization (pathway and cell), we will mark all yield coefficients (i.e. mass-mass couplers) that link the levels with $\circ$.

Substrate X_0 is released from the reserve as part of the catabolic flux, so

$$J_{X_0} = y^\circ_{X_0 E} J_{E,C} \quad \text{or for } j_{X_0} = J_{X_0}/M_V \quad j_{X_0} = y^\circ_{X_M E} j_{E,C} \tag{7.6}$$

Generalized compound X_M participates in the maintenance flux, so

$$J_{X_M} = y^\circ_{X_M E} J_{E,M} \quad \text{or for } j_{X_M} = J_{X_M}/M_V \quad j_{X_M} = y^\circ_{X_M E} j_{E,M} \tag{7.7}$$

while generalized compound X_G is used for building structure, so

$$J_{X_G} = y^\circ_{X_G V} J_{V,G} \quad \text{or for } j_{X_G} = J_{X_G}/M_V \quad j_{X_G} = y^\circ_{X_G V} r \tag{7.8}$$

Compound X_G differs from the structure X_V by the inclusion of compounds that are used in the overhead of growth and by that fact that more than one pathway will deliver compounds that are used in growth. For $y_{X_M X_0} = y^\circ_{X_M E}/y^\circ_{X_0 E}$ and $y_{X_G X_0} = y^\circ_{X_G V}/(y^\circ_{X_0 E} y_{EV})$, the variable yield coefficients required in (7.5) can now be expressed in terms of DEB fluxes as

$$Y_{X_M X_0} = \frac{J_{X_M}}{J_{X_0}} = \frac{y_{X_M X_0}}{1 + y_{EV} r/j_{EM}} \quad \text{and} \quad Y_{X_G X_0} = \frac{J_{X_G}}{J_{X_0}} = \frac{y_{X_G X_0}}{1 + j_{EM}/(y_{EV} r)} \tag{7.9}$$

The enzymes that are involved in the metabolic pathway are, by definition, part of the reserve and/or structure since these two components constitute the whole cell. So the amount of the i-th enzyme, M_{S_i}, can be written as weighted sums of reserve and structure:

$$M_{S_i} = n_{S_i E} M_E + n_{S_i V} M_V = (n_{S_i E} m_E + n_{S_i V})\, M_V \quad \text{with} \quad m_E = \frac{j_{EM} + r y_{EV}}{k_E - r}, \tag{7.10}$$

where chemical index n_{ij} specifies how much of i is present in compound j. The first index,i, typically refers to an chemical element present in compound j, but in the situation

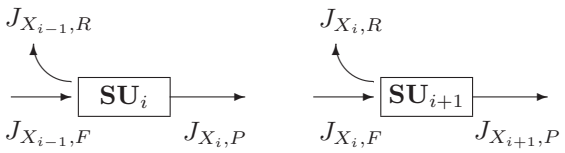

Figure 7.14: The arrival (F, for "feeding"), rejection (R) and production (P) fluxes for two Synthesizing Units that are involved in a metabolic pathway. In a linear pathway for $i = 1, \cdots, n$ we have that $J_{X_i,P} = J_{X_i,F}$.

of a generalized compound j, it can also relate to a compound. The yield coefficient y_{ij} specifies how much of i is formed per (C-)mol of j in a transformation. Both n's and y's are mol mol^{-1}; n's refer to chemical compositions, y's to transformation efficiencies. This notation is standard in microbiology.

The costs for synthesis of the enzymes appear in the yield coefficients for assimilation and growth:

$$y_{XE} = 1/y_{EX} = y^{\circ}_{XE} + \sum_i n_{S_iE}\, y_{XS_i} \tag{7.11}$$

$$y_{EV} = y^{\circ}_{EV} + \sum_i n_{S_iV}\, y_{ES_i} \tag{7.12}$$

Turnover costs of enzymes that are part of the structure should be included in the specific maintenance costs as

$$j_{E,M} = j^{\circ}_{E,M} + k_{S_i}\, n_{S_iV}\, y^{*}_{ES_i} \tag{7.13}$$

where $y^{*}_{ES_i} = y_{ES_i}$ if no reserve components are saved from the decomposition of enzyme S_i; generally we have $y^{*}_{ES_i} \leq y_{ES_i}$. The turnover of enzymes that are part of the reserve is implied by the reserve turnover. If both $n_{S_iE} > 0$ and $n_{S_iV} > 0$, we must have that $k_{S_i} = k_E$ to avoid a distinction between enzyme molecules that are part of the reserve and of the structure.

Notice that the intermediary metabolites of the metabolic pathway, X_i, don't appear in the reserve or structure; strict consistency requires that their amounts are negligibly small, and no need exists to evaluate their concentrations in the highly spatially structured internal environment of the cell. The maintenance compound X_M will be excreted in one form or another, just like part of the growth compound X_G, while another part of X_G will be included in the structure X_V. This completes the placement of our dual function problem in the context of the DEB theory for we now have defined and related the various fluxes at the cellular level that specify the fluxes and the variable yield coefficients in (7.5).

7.1.3 Fluxes through linear pathways

We now specify the fluxes through the linear metabolic pathway as a function of the arrival flux of substrate to the pathway, including the branches of rejected fluxes of intermediary metabolites and products. We need interaction between SUs in the pathway, because without interaction, some intermediate metabolites always escape further transformation, while the cell might not need them for maintenance or growth. For this purpose we introduce $n-1$ *handshaking parameters* α_i, $0 \leq \alpha_i \leq 1$, that affect the release of product and the binding of substrate between SU i and $i+1$. The unbound fraction of the i-th

SU changes such that if the handshaking parameter $\alpha_i = 0$, the handshaking is *open* and the SUs operate independently. If $\alpha_i = 1$, however, the handshaking is *closed* and no intermediary metabolites X_i are released if the binding probability $\rho_i = 1$; an SU only releases its product if the receiving neighbour SU is in the binding state. This coordinates the activities of all the SUs in the pathway and quantifies the distributed release of products and intermediary metabolites. If the handshaking parameter α_i is set to zero, all control is "bottom up" because the SUs do not interact and the behaviour of the whole follows (in complex ways) from the behaviour of the units. If the handshanking parameters are increased, the control becomes increasingly "top down", cf [514] since the behaviour of the whole feeds back to the behaviour of the units. If the handshaking is closed for all SUs in the pathway, $\alpha_i = 1$ for $i = 1, \cdots, n-1$, and binding is sure, $\rho_i = 1$ for $i = 1, \cdots, n$, then the full pathway acts as if it is just a single SU (see appendix) and all metabolites X_0 that are processed are transformed into products. The behaviour of the units is then fully controlled by the behaviour of the whole.

We use a time scale argument to derive the arrival (F), rejection (R) and production (P) fluxes of intermediary metabolites in terms of the steady state binding fractions of the SUs. (We use F for "feeding" to indicate arrival rates to avoid confusion with assimilation, which we also need; when a metabolite flux is "fed" to an SU, it does not mean that all will be "eaten"). All intermediary metabolites X_i that are produced by the i-th SUs, arrive at the $i+1$-th SUs, so $J_{X_i,F} = J_{X_i,P}$. The appendix gives the derivation of the pathway kinetics, which amounts for $i = 1, \cdots, n-1$ to the following changes of unbound fractions, θ_i, of SUs:

$$\frac{d}{dt}\theta_i = (1 - \alpha_i(1-\theta_{i+1}) - \theta_i)\, k_i - (\theta_i + \alpha_{i-1}(1-\theta_i))\, \rho_i J_{X_{i-1},F}/M_{S_i} \tag{7.14}$$

$$\frac{d}{dt}\theta_n = (1-\theta_n)k_n - (\theta_n + \alpha_{n-1}(1-\theta_n))\, \rho_n J_{X_{n-1},F}/M_{S_n} \tag{7.15}$$

Setting the change in the fractions, (7.14, 7.15) equal to zero, we obtain for the unbound fractions of the i-th SUs at steady state (denoted by *) as

$$\theta_i^* = \frac{(1 - \alpha_i + \alpha_i\theta_{i+1}^*)k_i - \alpha_{i-1}\rho_i J_{X_{i-1},F}/M_{S_i}}{k_i + (1-\alpha_{i-1})\rho_i J_{X_{i-1},F}/M_{S_i}} \quad \text{for } i = 1, \cdots, n-1 \tag{7.16}$$

$$\theta_n^* = \frac{k_n - \alpha_{n-1}\rho_n J_{X_{n-1},F}/M_{S_n}}{k_n + (1-\alpha_{n-1})\rho_n J_{X_{n-1},F}/M_{S_n}} \tag{7.17}$$

where the arrival flux $J_{X_0,F}$ of substrate to the pathway is given. Since SU i exists in M_{S_i} copies, and produces $y_{X_iX_{i-1}}$ intermediary metabolites X_i from each molecule X_{i-1}, the production fluxes are

$$J_{X_i,P} = (1 - \alpha_i(1-\theta_{i+1}) - \theta_i)\, k_i\, y_{X_i,X_{i-1}} M_{S_i} \quad \text{for } i = 1, \cdots, n-1 \tag{7.18}$$

$$J_{X_n,P} = (1-\theta_n)k_n\, y_{X_n,X_{n-1}} M_{S_n} \tag{7.19}$$

The set of equations (7.16–7.19) determine the unbound fractions θ_i and arrival rates $J_{X_i,F}$ for all SUs. Since mass conservation implies that the rejection fluxes equal the difference

between the arrived and the processed fluxes, the rejection fluxes are

$$\begin{aligned} J_{X_i,R} &= J_{X_i,P}\left(1-\left(\theta_{i+1}+\alpha_i(1-\theta_{i+1})\right)\rho_{i+1}\right) && (7.20)\\ &= J_{X_i,P}-J_{X_{i+1},P}/y_{X_{i+1},X_i} \quad \text{for } i=0,\cdots,n-1 && (7.21)\\ J_{X_n,R} &= J_{X_n,P} && (7.22) \end{aligned}$$

Note that, if $\alpha_i=\rho_i=1$, no rejection of X_i, $i=0,\cdots,n-1$, occurs, so $J_{X_i,R}=0$. This is how closed handshaking is constructed. A nice property of this construction is that more than once a particular enzyme turns out to be a consortium of several smaller ones. As long as the members of the consortium pass metabolites by direct channeling (i.e. the enzyme-product complex does not release the product molecule into the liquid environment, but the molecule is directly bound to a neighbouring enzyme molecule in a enzyme-substrate complex), such a discovery has no consequence for the pathway model. Constraints apply to parameter values; the handshaking parameters restrict the maximum flux that can be processed. With an open handshaking protocol all excess flux is simply rejected, but that possibility becomes increasingly restricted by gradually closing the handshaking. The physical impossibility to allocate more than can be processed leads to unbound fractions outside the interval (0,1). Any choice of parameter values should be tested for its validity.

This completes the model specification of cells' regulatory functions in terms of the handshaking and the binding parameters. The fluxes and bound fractions can be obtained analytically for $n=2$, but you don't want to see the result. The result is of little relevance for our purpose, fortunately, because the DEB model already specifies the fluxes. Our interest is in the implied constraints; the next section shows that these can be obtained without explicitly solving for the fluxes.

7.1.4 Matching the pathway and the DEB model

We specified the flux of substrate to the pathway (7.6), and the (variable) yield coefficients (7.9), the maintenance flux

$$J_{E,M}\equiv j_{E,M}M_V \tag{7.23}$$

and the growth flux

$$J_{E,G}=J_{E,C}-J_{E,M}=y_{EV}J_{V,G} \quad \text{and} \quad J_{V,G}=rM_V \text{ with } r=\frac{k_E m_E-j_{E,M}}{m_E+y_{EV}}, \tag{7.24}$$

which together quantify the transformation at the cellular level (7.5). We also specified how the fluxes of substrates for maintenance and growth (7.18 – 7.22) as released by the pathway depend on the flux of substrate to the pathway. Now we are ready for the core of this paper: How does the pathway model for metabolites link with the DEB model for the cell under the various growth conditions? The cell will experience a varying concentration of substrate in the environment, which results in a varying reserve density, and hence a varying allocation to growth. Can we avoid leaks under all conditions? We here use the link between two levels of organization to extract information about cells regulatory activities. This exercise will reveal useful constraints on parameter values.

The specific flux of substrate X_0 to the pathway equals by equations $J_{E,C} \equiv j_{E,C} M_V = (k_E - r) M_E$, (7.24) and (7.6)

$$j_{X_0,F} = n_{X_0E}\, j_{E,C} = n_{X_0E}(j_{E,M} + r y_{EV}) = n_{X_0E}(k_E - r) m_E = n_{X_0E} \frac{j_{E,M} + k_E y_{EV}}{1 + y_{EV}/m_E} \quad (7.25)$$

where the specific growth rate r and the reserve density m_E can vary in time. We now equate the release of intermediary metabolites and products from the pathway to their use by the cell. Given (7.3, 7.4), (7.7) and (7.8), the specific required fluxes of intermediary metabolites and products are,

$$\begin{aligned} j_{X_i,P} &= j_{P_i}/y_{P_iX_i} = y^P_{X_iE}\, j_{EM} + y^P_{X_iV}\, r \quad \text{for } i = 1, \cdots, n \qquad (7.26)\\ &\quad \text{with } y^P_{X_iE} = y_{P_iX_M}\, y^\circ_{X_ME}/y_{P_iX_i} \quad \text{and} \quad y^P_{X_iV} = y_{P_iX_G}\, y^\circ_{X_GV}/y_{P_iX_i} \\ j_{X_i,R} &= j_{X_i} = y_{X_iE}\, j_{EM} + y_{X_iV}\, r \quad \text{for } i = 0, \cdots, n-1 \qquad (7.27)\\ &\quad \text{with } y_{X_iE} = y_{X_iX_M}\, y^\circ_{X_ME} = y^P_{X_i,E} - y^P_{X_{i+1},E}/y_{X_{i+1},X_i} \\ &\quad \text{and } y_{X_iV} = y_{X_iX_G}\, y^\circ_{X_GV} = y^P_{X_i,V} - y^P_{X_{i+1},V}/y_{X_{i+1},X_i} \end{aligned}$$

The first equality sign in (7.26), and in (7.27), is a consequence of the following considerations for the links between the fluxes that are required by the cell and those released by the pathway. The released intermediary metabolites X_i, $i = 0, \cdots, n-1$, are the rejected fluxes $J_{X_i,R}$; the released products P_i, $i = 1, \cdots, n$, are linked to the production fluxes of the metabolites one step earlier. Since both intermediate metabolite X_i and product P_i are stoichiometrically linked to X_{i-1}, product P_i is linked to X_i with yield coefficient $y_{P_iX_i} = y_{P_iX_{i-1}}/y_{X_iX_{i-1}}$.

We must have that $j_{X_i,P} > j_{X_i,R}$ for all growth rates r, which implies from (7.26) and (7.27) that $y_{P_iX_M} > y_{P_iX_i}\, y_{X_iX_M}$ and $y_{P_iX_G} > y_{P_iX_i}\, y_{X_iX_G}$.

Are fluxes of substrates for growth proportional the growth rate?

If primes denote differentiation with respect to the specific growth rate r, the linearity of all production and rejection rates in r translates into $j''_{X_i,R} = 0$ and $j''_{X_i,P} = 0$. Double differentiation of (7.16) - (7.22) with respect to r results in the following relationships for $j_{X_iP} = J_{X_iP}/M_V$, and $m_{S_i} = M_{S_i}/M_V = n_{S_iE} m_E + n_{S_iV}$ and scaled reserve density $m_E = \frac{j_{E,M} + r y_{EV}}{k_E - r}$.

$$\begin{aligned} 0 &= \theta''_i\, j_{X_{i-1}P} + 2\theta'_i\, j'_{X_{i-1}P} \quad \text{for } i = 1, \cdots, n \qquad (7.28)\\ 0 &= (\alpha_i \theta''_{i+1} - \theta''_i) m_{S_i} + 2(\alpha_i \theta'_{i+1} - \theta'_i) m'_{S_i} + (1 - \alpha_i(1 - \theta_{i+1}) - \theta_i) m''_{S_i} \qquad (7.29)\\ &\quad \text{for } i = 1, \cdots, n-1 \end{aligned}$$

Consequently, $m'_E = \frac{y_{EV} + m_E}{k_E - r}$ and $m''_E = 2\frac{m'_E}{k_E - r}$. It follows from condition (7.28) that θ_i must be a linear fractional function of r, i.e. $\theta_i = (c_{1i} - c_{2i} r)/j_{X_i,P}$ for appropriate values of c_{1i} and c_{2i}. After substitution of (7.25, 7.27, 7.26), the n relationships (7.18, 7.19) can be rewritten as n equations of the type $0 = \sum_{j=0}^{4} c_{ij} m_E^j$, which only holds for all possible values of m_E if $c_{ij} = 0$ for all $5n$ coefficients c_{ij}. Further analysis shows that this cannot

be true if the relative needs for metabolites and products differ between maintenance and growth. Thus our requirement of exact linearity in r cannot be achieved. However, as will now be shown, this requirement can "almost" be attained.

Numerical studies of (7.16–7.19) reveal that given values for k_i and n_{S_iE}, and n_{S_iV}, the values for α_i and ρ_i can be chosen such that $j_{X_i,P}$ and $j_{X_i,R}$ are almost perfectly linear in the specific growth rate r for $i = 1, \cdots, n$. The best goodness of fit depends on the abundance parameters; for $n_{S_iE} = 0$, i.e. when the concentrations of enzyme are constant and do not depend on the growth rate, the best fit is poor, indeed. The yield coefficients y are in fact parameters at the whole-cell level and have been chosen in Figure 7.15, and the abundances of all enzymes have been chosen equal, so $n_{S_iE} = n_{SE}$ and $n_{S_iV} = n_{SV}$ for all i. The reason is that the channeling mechanism of substrate from one enzyme molecule to another is then most simple. Another reason is to remove some of the parameters from the system. The parameter for the maximum specific assimilation rate only served to fix the maximum specific growth rate; the plots show the full range.

Figure 7.15 (left panel) shows that the production flux of substrate X_0, which is released from the reserve and fed to the pathway, is analytically linear in the growth rate. This is because the fate of all mobilized reserve, including this substrate, is either maintenance or growth. At growth rate zero, all compounds are used for maintenance. The DEB model fully specifies the flux of substrate X_0 to the pathway and the pathway model does not affect it. Intermediary metabolite 4 is produced by the last type of SU in a linear pathway of four types of SUs, and is passed to the cell (and used for maintenance or growth); it, therefore, does not show up in the second panel for rejected fluxes. The difference between the produced and the rejected fluxes for all compounds is used for further processing in the pathway. The last panel shows that the SUs of the first type are very busy (in processing substrate 0), but the other types are much less busy with this parameter choice. Numerical studies indicate that linearity of product and rejected intermediary metabolite fluxes is more difficult to achieve for increasing degrees of business of the SUs.

We checked by simulating (7.14, 7.15) that the pathway is stable for the parameter values that are shown for the full range of growth rates; the speed of convergence to the steady state increases with the specific growth rate. It also holds that, given values for k_i, α_i and ρ_i the values for n_{S_iE}, and n_{S_iV}, can be chosen such that $j_{X_i,P}$ and $j_{X_i,R}$ are close to linear in the specific growth rate r for $i = 1, \cdots, n$. So either the abundance or the control parameters (binding and handshaking parameters) can be fixed, and the other can be chosen such that linearity results approximately. The fit to linearity can be further increased by tuning these four parameters simultaneously for all nodes independently. The significance of this result is that if the reserve is omitted from the cell model, and/or no enzyme is associated with reserve, $n_{S_iE} = 0$, production and rejection fluxes deviate from linearity in the specific growth rate and the pathway model does not match the cell model. The Marr-Pirt model, for instance, which is a limiting case of the DEB model for vanishing reserve, has a consistency problem with this pathway model. We believe that this result is rather general, and applies to a large class of acceptable pathway models.

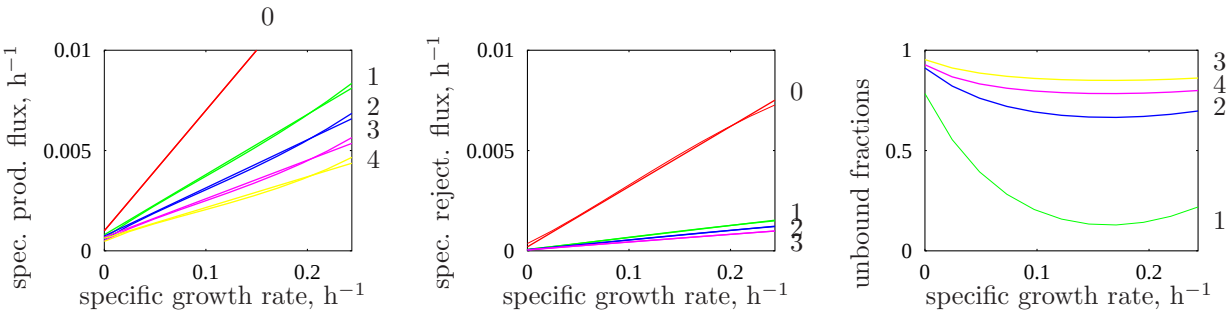

Figure 7.15: The production and rejection fluxes, $J_{X_i,P}$ and $J_{X_i,R}$, and the fraction of unbound SUs, θ_i, as functions of the specific growth rate r in a linear pathway of length $n = 4$. The numbers near the curves indicate the position in the pathway, $i = 1, ., 4$. The handshaking and binding parameters are chosen such that the fluxes are "almost" linear in r (the amount of material required for growth is proportional to the growth rate), which makes the fractions linear fractional functions in r. The linearity is tested by best-fitting linear functions which are plotted as well. The goodness of fit is within the resolution of the figure. The DEB parameters are $y_{EV} = 1.2$, $k_E = 0.4$ h^{-1}, $j_{EM} = 0.02$ h^{-1}, $j_{EAm} = 0.8$ h^{-1} and the substrate concentration for the pathway in the reserve is $n_{X_0E} = 0.05$.

Fixed pathway parameters

i	1	2	3	4
$y_{X_iX_{i-1}}$	1	1	1	1
n_{S_iE}	0.032	0.032	0.032	0.032
n_{S_iV}	0.045	0.045	0.045	0.045
k_i (h^{-1})	0.118	0.186	0.543	0.190

Pathway regulation and yield parameters

i	0	1	2	3	4
α_i	0.7349	0.6652	0.0001	0.2663	
ρ_i		0.6741	0.9134	0.9556	0.9681
$y^P_{X_iE}$	0.0500	0.0400	0.0368	0.0339	0.0311
$y^P_{X_iV}$	0.0600	0.0300	0.0240	0.0192	0.0153
y_{X_iE}	0.0100	0.0032	0.0029	0.0027	0.0311
y_{X_iV}	0.0300	0.0060	0.0048	0.0038	0.0154

7.1.5 Fluxes through cyclic pathways

We can test the robustness of the matching of the pathway model with the DEB model for the whole cell behaviour by studying a metabolic cycle, rather than a linear pathway, where the compound X_n is identical to X_0 and the last SUs follow a handshaking protocol with the first SUs. See Figure 7.16. When α_n denotes the handshaking parameter between SUs number n and 1 we have the following dynamics of the unbound fractions of the first and last SU

$$\begin{aligned}\frac{d}{dt}\theta_1 &= (1-\alpha_1(1-\theta_2)-\theta_1)\,k_1 - (\theta_1+\alpha_0(1-\theta_1))\,\rho_1 J_{X_0,F}/M_{S_1} + \\ &\quad -(\theta_1+\alpha_n(1-\theta_1))\,\rho_1 J_{X_n,F}/M_{S_1} \qquad (7.30)\\ \frac{d}{dt}\theta_n &= (1-\alpha_n(1-\theta_1)-\theta_n)\,k_n - (\theta_n+\alpha_{n-1}(1-\theta_n))\,\rho_n J_{X_{n-1},F}/M_{S_n} \qquad (7.31)\end{aligned}$$

The production flux of metabolite X_n and rejection flux for X_0 are

$$\begin{aligned}J_{X_n,P} &= (1-\alpha_n(1-\theta_1)-\theta_n)\,k_n\,M_{S_n}\,y_{X_n,X_{n-1}} \qquad (7.32)\\ J_{X_0,R} &= J_{X_0,F} + J_{X_n,P} - y_{X_0X_1}J_{X_1,P} \qquad (7.33)\end{aligned}$$

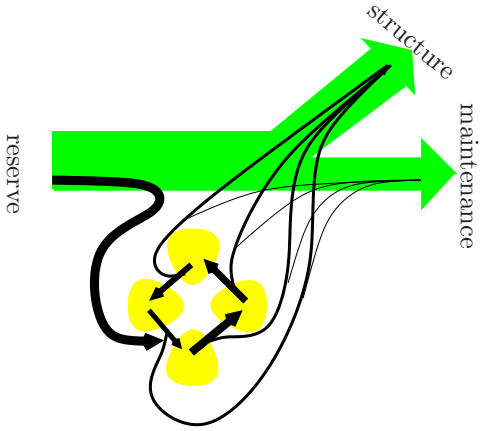

Figure 7.16: The problem we try to solve here is the same as illustrated in Figure 7.13, but now for a cyclic pathway. This is to study the robustness of the solution we found for the allocation problem for maintenance and growth.

The rejection flux of X_0 must again be linear in the specific growth rate r, so that

$$y_{X_0E} = n_{X_0E} + y^P_{X_nE} - y_{X_0X_1}y^P_{X_1E} \quad (7.34)$$

$$y_{X_0V} = n_{X_0E}\, y_{EV} + y^P_{X_nV} - y_{X_0X_1}y^P_{X_1V} \quad (7.35)$$

Figure 7.17 shows the numerical results for the cyclic pathway; the setup of the figure is similar to that for the linear pathway, Figure 7.15. Numerical studies indicate that, compared to linear pathways, the handshaking and binding parameters in cyclic pathways are easier to tune such that the production and rejecting fluxes are (almost) linear in the specific growth rate.

Linearity only seems possible, however, as long as most enzyme is in the unbound state. Although the rejection fluxes are used to minimize the deviations from linearity in the specific growth rate, the computation of both the pathway and the linear fluxes is based on the pathway and linear production fluxes, respectively, using mass conservation. Notice that the yield parameters y_{X_4E} and y_{X_4V} are lacking, because X_4 is assumed to be identical to X_0 and the rejection flux of X_4 is included in that of X_0.

The conclusion must be that the tuning between the pathway model and the whole-cell model is not very sensitive to metabolic "details" of the pathway. This suggests that, probably, branching pathways could also be tuned to consistency with the DEB model for the whole cell; we did not investigate such pathways in much detail.

7.1.6 Cells' design

In what might be called "the principle of parsimony" one expects that the unbound fractions of SUs are low, otherwise the cell is producing non-functional enzymes. These fractions are linear fractional functions of the specific growth rate, which means that for some value of the growth rate, the fractions are minimal, but this value for the growth rate can differ among SUs. Parsimony is a much weaker criterion than optimality, and boils down to the constraint that for each SU a value for the specific growth rate must exist for which the fraction of unbound SU is small. Again we have to rely on numerical analyzes to study how the bound fractions of SUs vary as a function of the growth rate. The numerical

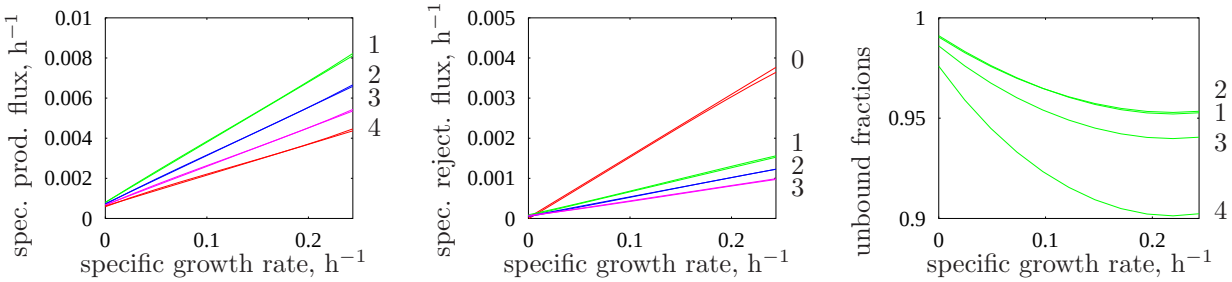

Figure 7.17: The production and rejection fluxes, $J_{X_i,P}$ and $J_{X_i,R}$, and the fraction of unbound SUs, θ_i, as functions of the specific growth rate r in a cyclic pathway of length $n = 4$. The numbers near the curves indicate the position in the pathway, $i = 0, 1, ., 4$. The handshaking, α_i, binding, ρ_i, dissociation, k_i and abundance, n_{S_iE} and n_{S_iV}, parameters are chosen such that the fluxes best fitted the preset linear relationships in r, but all enzymes are assumed to be equally abundant. So all yield parameters y were preset, but those for rejection follow from those for production. The linear relationships are also shown, to check the goodness of fit, which is almost within the graphical resolution. The DEB parameters are $y_{EV} = 1.2$, $k_E = 0.4$ h^{-1}, $j_{EM} = 0.02$ h^{-1}, $j_{EAm} = 0.8$ h^{-1} and the substrate concentration for the pathway in the reserve is $n_{X_0E} = 0.05$.

Pathway parameters

i	1	2	3	4
$y_{X_iX_{i-1}}$	0.5	1	1	1
n_{S_iE}	0.065	0.065	0.065	0.065
n_{S_iV}	0.032	0.032	0.032	0.032
k_i (h^{-1})	2.70	1.11	0.71	0.41

Pathway regulation and yield parameters

i	0	1	2	3	4
α_i	0.5600	0.0018	0.0006	0.0015	0.2350
ρ_i		0.8100	0.8400	0.8500	0.9100
$y^P_{X_iE}$	0.0500	0.0400	0.0368	0.0339	0.0311
$y^P_{X_iV}$	0.0600	0.0300	0.0240	0.0192	0.0154
y_{X_iE}	0.0011	0.0032	0.0029	0.0027	
y_{X_iV}	0.0154	0.0060	0.0048	0.0038	

study is complicated by the fact that it is easy to arrive at combinations of parameter values that result in biologically non-valid values for certain quantities: α_i and ρ_i must be in the interval (0,1) for all i, all other parameters must be positive. Even if these conditions are fulfilled, there can be specific growth rates for which some θ_i become negative, which is obviously invalid. As a consequence, the constraints on parameter values must be such that this situation is avoided too. Since the values of the θ's follow implicitly from (7.16) and (7.17), these constraints can only be tested retrospectively, after having selected a set of parameter values.

Metabolic control theory is a powerful tool to analyze the relative control of design quantities for fluxes of metabolites in steady state [194]. In Figure 7.18 we present the dimensionless (normalized) flux elasticity coefficients $\varepsilon^P_{0i} = \frac{n_{X_0E}}{J_{X_i,P}} \frac{\partial J_{X_i,P}}{\partial n_{X_0E}}$ and $\varepsilon^R_{0i} = \frac{n_{X_0E}}{J_{X_i,R}} \frac{\partial J_{X_i,R}}{\partial n_{X_0E}}$ for all four nodes in a linear pathway as functions of the specific growth rate, using the parameter values given in the legends of Figure 7.15. The relative abundance of substrate

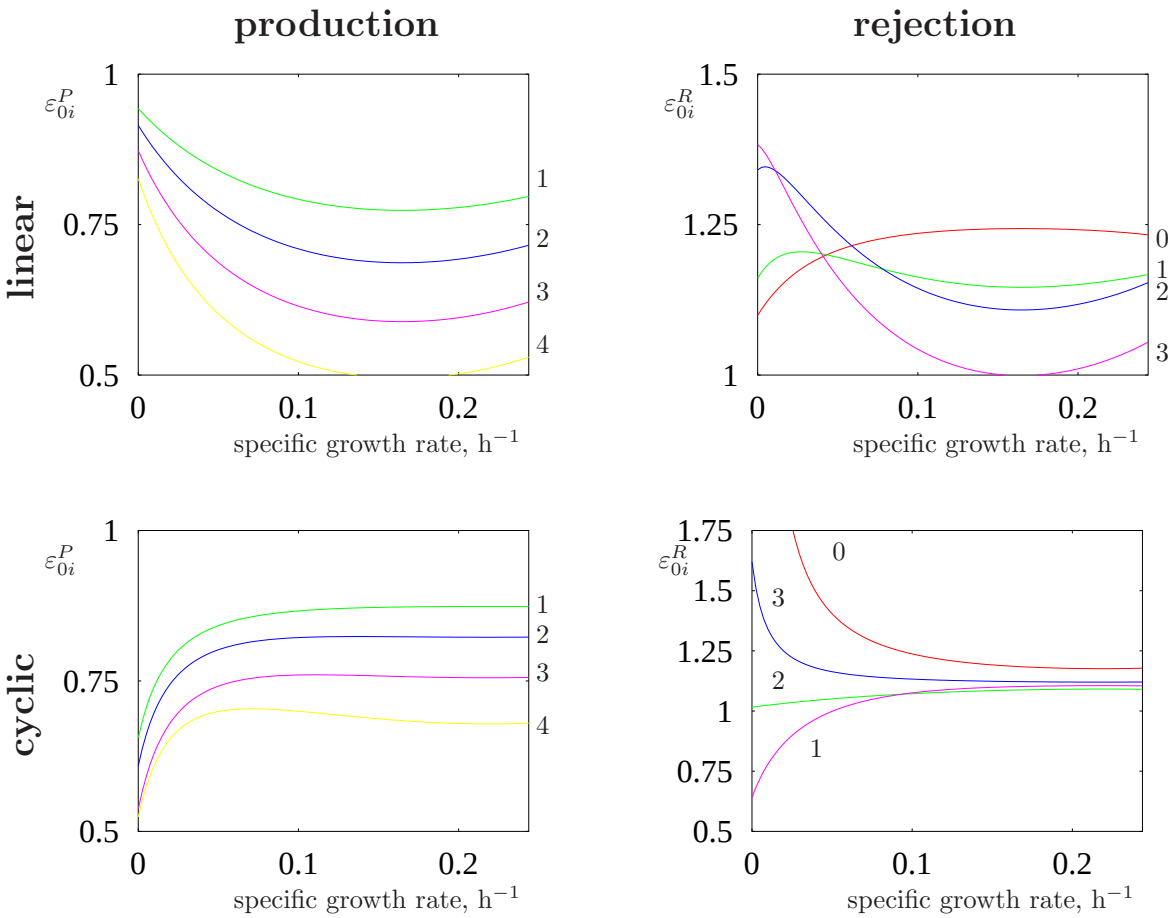

Figure 7.18: The elasticity coefficients for production (left) and rejection (right) fluxes, $J_{X_i,P}$, and $J_{X_i,R}$, with respect to the abundance of substrate to the pathway n_{X_0E}. The upper panels show a linear pathway, with parameters as given in Figure 7.15; the lower panels show a cyclic pathway, with parameters as given in Figure 7.17. We take $\varepsilon^P_{00} = 1$.

X_0 in reserve X_E, i.e. n_{X_0E}, is proportional to the flux of substrate X_0 to the pathway for any value of the specific growth rate. The elasticity coefficients for the production fluxes of the linear pathway are in the range of (0.5-1.0), and for the rejection fluxes in the range of (1.0-1.5). The elasticity coefficient for the rejection of substrate 0 is very high for low growth rates.

We can conclude that no simple relationship exists here between the values of the elasticity coefficients and the transformation rates k_i as was observed in linear pathways where all metabolites follow the full pathway [194]. Moreover the specific growth rate modifies the relationships substantially. Major differences between our pathways and the ones studied in the literature [194, 221, 193, 504, 202, 434] are that in our case only a fraction of the metabolites follow the full pathway and concentrations of intermediate metabolites do not accumulate. It thus appears that the method is very sensitive for such "details".

A major field of application of metabolic control theory is in the evaluation of the effect

of a possible increase or decrease of a particular enzyme on the performance of the whole pathway. Starting from a combination of parameter values for which we have a match between pathway performance and the cell's needs, a change in a concentration of enzyme directly results in a mismatch. This illustrates that the application of control theory in the present context is problematic.

Empirical support for lichen growth

{251}

Strong empirical support for the linear growth of the diameter of the crustose saxicolous lichen *Caloplaca trachyphylla* is given by [96].

Shape changes in plants

{253}

The suggestion for a shape correction function for plants that grow in a closed vegetation is descriptive only. It has just two parameters, V_d and β, and the property that for $V = 0$ we have $\mathcal{M}(V) = (V/V_d)^{1/3}$, which is the shape correction function for V1-morphs, for $V = V_m 3^{-1/\beta}$ we have $\mathcal{M}(V) = 1$, which is the shape correction function for isomorphs, and for $V = V_m$ we have $\mathcal{M}(V) = (V/V_d)^{-2/3}$, which is the shape correction function for V0-morphs, cf {29}. This simple choice can only be an approximation at best; the actual change in shape will depend on the (sizes of the) neighbouring plants, which differs between any two individuals. Notice that a closed vegetation consisting of V0-morphic plants have a lot in common with crusts, that are discussed in 7.7.1 at {250}.

Metamorphosis in juvenile fish

{257}

In collaborative work with Laure Pecquerie, we extend the standard DEB model for anchovy with a juvenile I and II stage, separated by metamorphosis, to accommodate the empirical observation that length increases approximately exponentially with age after birth. Pigmentation occurs at metamorphosis, which marks the metamorphosis event. In the embryo, juvenile II and adult stages, anchovy is isomorphic, but in the juvenile I state V1-morphic. Stage transitions occur for values U_H^b, U_H^j and U_H^p of the scaled maturity $U_H = M_H/\{\dot{J}_{EAm}\} = E_H/\{\dot{p}_{Am}\}$. Notice that $\dim(U_H) = t\,L^2$.

Suppose that between birth b and metamorphosis j the early juvenile changes shape as a V1-morph, while before birth and after metamorphosis is does not change shape and is isomorphic; the shape correction function is $\mathcal{M}(V) = (\min(V, V_j)/V_b)^{1/3}$ for $V > V_b$.

We here assume that physical length $\mathcal{L}$ relates to volumetric length L as $\mathcal{L} = L/\delta_{\mathcal{L}}$, for constant $\delta_{\mathcal{L}}$. In principle the value for $\delta_{\mathcal{L}}$ in the embryo and juvenile II + adult stage could be different, and many possibility for the relationship exists for the juvenile I, since V1-morphy only concerns the relationship between surface area and structural volume.

So the change in scaled reserve, length and scaled maturity is given by for $U_H < U_H^p$:

$$\frac{d}{dt}e = (f - e)\dot{v}^*/L; \quad \frac{d}{dt}L = \frac{\dot{v}^*}{3}\frac{e - L/L_m^*}{e + g}; \quad \frac{d}{dt}U_H = (1 - \kappa)eL^2\frac{g\mathcal{M}(V) + L/L_m}{g + e} - \dot{k}_J U_H$$

with $\dot{v}^* = \dot{v}$ and $f = 0$ for the embryo and $\dot{v}^* = \dot{v}\mathcal{M}(V)$. Furthermore $L_m^* = \frac{\dot{v}^*}{\dot{k}_M g}$ and $L_m = \frac{\dot{v}}{\dot{k}_M g}$. Notice that $\dot{v}^*$ changes in a continuous (but not differentiable) way across stage transitions, as does the reserve turnover rate $\dot{v}^*/L$. For $U_H > U_H^p$ we have $\frac{d}{dt}U_H = 0$, and allocation to reproduction occurs. Notice that for $U_H^j = U_H^b$ we have no juvenile I stage; the individual then remains isomorphic during all stages, with $\dot{v}^* = \dot{v}$ and $\mathcal{M}(V) = 1$. The threshold U_H^j is the only parameter that we introduced for the change in shape.

We also have $L(0) = 0$, $U_H(0) = 0$ and $e(a_b) = f$, where age at birth a_b is given implicitly by $U_H(a_b) = U_H^b$. All rate parameters depend on temperature, including the parameter $\{\dot{J}_{EAm}\}$ or $\{\dot{p}_{Am}\}$ with which we scaled the cumulates investment into maturity; for the scaling, however, we use the constant value that applies to some reference temperature and avoid complex forms of dynamic scaling.

Names of parameters

{260}, l-10

There is a slight inconsistency in names of parameters here. The term 'maximum (volumetric) length' and the symbol L_m should better be reserved for $L_m = \kappa\{\dot{p}_{Am}\}/[\dot{p}_M]$ to be consistent with 'maximum volume' as introduced at {94}. We then also need a new term, such as 'maximum ultimate (volumetric) length' for $L_{\infty m} = L_m - L_h = V_m^{1/3} - V_h^{1/3}$ to be consistent with the label 'ultimate (volumetric) length' for $L_\infty = fL_m - L_h$. In all cases we go from volumetric length to actual length by multiplying with the shape coefficient $\delta_{\mathcal{M}}$; this should come with a specification of how we take the length, given the shape. On top of that we have the complication that reserve can contribute to length, and that it becomes necessary to differentiate between physical length and structural length, see (2.5) at {31}. The symbols L_m and L_∞ only quantify structure, not reserve. Notice that organisms that have maintenance costs that are linked to surface area (heating, osmotic work) cannot reach L_m, they can reach only $L_{\infty m}$ at abundant food.

Diauxic growth: Inhibition and preference.

{263}

Diauxic growth is the property of populations of microorganisms to first grow more or less logistically to a certain level in a batch culture, using one substrate only, and then resume growth to a second higher level, using another substrate. So the use of the second substrate is delayed until the first substrate is exhausted. This behaviour is species as well as substrate-combination specific.

Carriers in the outer membrane typically only transport particular substrates from the environment into the cell. This comes with the requirement to regulate gene expression for carriers of substitutable substrates to match the substrate availability in the environment. Data strongly suggest that allocation to the assimilation machinery is a fixed fraction of the utilized reserve flux, and that the expression of one gene for a carrier inhibits in some cases the expression of another gene. Inhibition strength is linked to the workload of the carriers. This regulation mechanism has similarities to that of differentiation.

Figure 7.19 illustrates this for two data sets on the uptake by *E. coli* K21 of fumarate and pyruvate and of fumarate and glucose (from [330]). Unlike pyruvate, glucose sup-

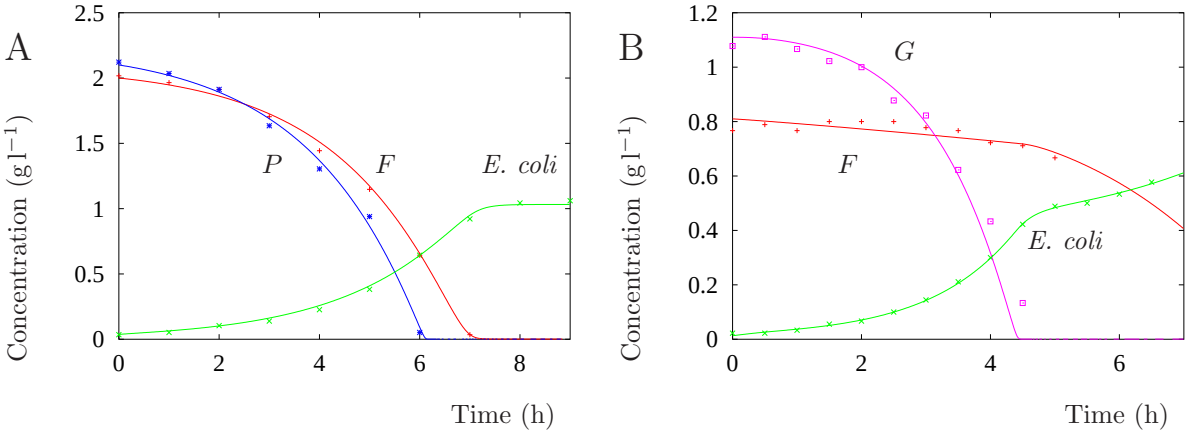

Figure 7.19: The uptake of fumarate (F) and pyruvate (P) (see Figure A), and of fumarate (F) and glucose (G) (see Figure B) by *E. coli* K12 in a batch culture. Data from Narang et al. [418]. Parameters: saturation coefficients (g l^{-1}) $K_F = 0.089$, $K_P = 0.012$, $K_G = 0.013$; yield coefficients (g g^{-1} dry weight) $y_{EF} = 0.577$, $y_{EP} = 0.015$, $y_{EG} = 0.446$, $y_{EV} = 1.2$ (fixed); max. specific uptake rates (g(h g dry weight)$^{-1}$), $j_{Fm} = 1.138$, $j_{Pm} = 40.15$, $j_{Gm} = 2.59$; reserve turnover rate (h^{-1}) $\dot{k}_E = 4.256$; maintenance rate coefficient (h^{-1}) $\dot{k}_M = 0$ (fixed); preference parameter (-) $w_P = 0.941 w_F$ for pyruvate *versus* fumarate; $w_G = 12.15 w_F$ for glucose *versus* fumarate; background expression (h^{-1}) $\dot{h} = 0$ (fixed). Initial conditions: (A) $F(0) = 2.0$ g l^{-1}, $P(0) = 2.1$ g l^{-1}, *E. coli*$(0) = 0.037$ g l^{-1}, $\kappa_F(0) = 0.96$, $m_E(0) = 0.288$ g g^{-1} dry weight; (B) $F(0) = 0.81$ g l^{-1}, $G(0) = 1.11$ g l^{-1}, *E. coli*$(0) = 0.013$ g l^{-1}, $\kappa_F(0) = 0.99$, $m_E(0) = 1.3$ g g^{-1} dry weight

presses the uptake of fumarate. The background expression of carrier synthesis and the maintenance requirements were set to zero, because the data provide little information on this. The yield of structure on reserve was fixed (because the data give no information on biomass composition). The data were fitted simultaneously to ensure that the uptake parameters for fumarate and the reserve turnover rates are identical in the two data sets (so removing degrees of freedom). Apart from the initial conditions, 12 parameters were estimated for six trajectories. The fit is quite good, despite the constraint for the parameter values for fumarate to be identical. The data in Figure 9A clearly show continued growth after depletion of substrates, which requires reserves to capture; this cannot be done with *e.g.* a Monod model.

Although their derivation has been set up slightly differently, the supply formulation for inhibition is used in [65] to model substrate preference and diauxic growth in microorganisms, while [555] used a demand formulation (see comment for {221}). See Figure 5.2. The use of genes coding for substrate-specific carriers is here linked to the use of carriers; the expression of one gene inhibits the expression of the other. When embedded in a batch culture, the uptake rate of substrates S_1 and S_2 by biomass X (of V1-morphs) with reserve density m_E in a batch culture is given by

$$\frac{d}{dt}S_1 \;=\; -j_{S_1}X; \quad j_{S_1} = \kappa_{S_1} j_{S_1 m} f_{S_1}; \quad f_{S_1} = \frac{S_1}{S_1 + K_{S_1}},$$

$$\begin{aligned}
\frac{d}{dt}S_2 &= -j_{S_2}X; \quad j_{S_2} = \kappa_{S_2} j_{S_2 m} f_{S_2}; \quad f_{S_2} = \frac{S_2}{S_2 + K_{S_2}}; \quad \kappa_{S_2} = 1 - \kappa_{S_1}, \\
\frac{d}{dt}X &= \dot{r}X; \quad \dot{r} = \frac{\dot{k}_E m_E - \dot{k}_M}{m_E + y_{EV}}, \\
\frac{d}{dt}m_E &= y_{ES_1} j_{S_1} + y_{ES_2} j_{S_2} - m_E \dot{k}_E, \\
\frac{d}{dt}\kappa_{S_1} &= (\dot{r} + \dot{h}) \left(\frac{w'_{S_1} \kappa_{S_1} f_{S_1}}{w'_{S_1} \kappa_{S_1} f_{S_1} + w'_{S_2} \kappa_{S_2} f_{S_2}} - \kappa_{S_1} \right),
\end{aligned}$$

where j_{*m} is the maximum specific uptake flux of substrate $*$, f_* is the scaled functional response and K_* the half-saturation coefficient for substrate $*$. The coefficient y_{E*} is the yield of reserve E on substrate $*$, $\dot{k}_E$ the reserve turnover rate, $\dot{k}_M$ the maintenance rate coefficient and $\dot{r}$ the specific growth rate. The fraction κ_{S_1} between 0 and 1 quantifies the relative gene expression for the carrier of substrate S_1 and w'_{S_1} the inhibition of the expression of the gene for the carrier of substrate S_1 by the expression of the gene for the carrier of substrate S_2; without loss of generality we can assume that $1 = w'_{S_1} + w'_{S_2}$. Notice that a single substrate induces full gene expression ($\kappa_{S_1} \to 1$ if $f_{S_2} = 0$). The typically very low background expression rate $\dot{h}$ serves an antenna function for substrates that have been absent for a long time. This readily extends to an arbitrary number of substrates. See Figure 7.19 and [65] for an illustration of the application of this theory.

Invariance property

{266}, 8.1

Inge van Leeuwen observed that growth, as specified by (3.18), is not sufficient to derive the invariance property. Reproduction, as specified by (3.48), is also required for this derivation. From (3.48) also follows that $\kappa_{R2} = \kappa_{R1}$; this is mentioned in Table 8.1, but not in the text. The aging process (4.22) is required to derive that $\ddot{h}_{a2} = \ddot{h}_{a1}$.

Chapter 8

Comparison of species

Prokaryotic size range

{267}

Prokaryotes span a huge cellular size range; the largest is the colourless sulphur bacterium *Thiomargarita namibiensis* with a cell volume of $2 \times 10^{-10}\,\mathrm{m}^3$ [510], the smallest is *Pelagibacter ubique* at $10^{-20}\,\mathrm{m}^3$. This small size has the remarkable implication that it has less than a single free proton in its cell if its internal pH is 7 as is typical for bacteria. This has peculiar consequences for the molecular dynamics of metabolism [290].

Fish & molluscs

{267}

The application of body size scaling relationships to marine fish and molluscs is discussed in [567, 566, 83].

Primary parameters

{268}

The shortcut that $[\dot{p}_J] = [\dot{p}_M]\frac{1-\kappa}{\kappa}$, or $[\dot{J}_{EJ}] = [\dot{J}_{EM}]\frac{1-\kappa}{\kappa}$, on {112} should not be implemented in the basic theory for simplicity's sake because this gives problems in some applications. In several cases size at first maturation seems to depend on food history in practice, and if toxicants affect $[\dot{p}_J]$, $[\dot{p}_M]$ or κ, we have to deal with the original rules for stage transitions anyway. So the parameters L_b and L_p should be replaced by $[E_H^b] \equiv E_H^b L_m^{-3}$ and $[E_H^p] \equiv E_H^p L_m^{-3}$, and $[\dot{k}_J]$ should be included explicitly while $[\dot{p}_J]$ should be avoided as a parameter because it is not constant. The state of maturity is treated as information, which requires an energy investment to build up, but this information itself does not represent a mass or energy pool. To avoid a formal conversion from energy to information, the thresholds are quantified in terms of cumulative energy investment. The normalization of the thresholds with respect to maximum volume is to achieve that the parameters become independent of maximum length between species, but the involvement of other parameters is necessary for this. This might not be handy in e.g. toxicity studies.

Moreover, the half-saturation constant should be treated as a compound parameter $K = \{\dot{J}_{XAm}\}/\{\dot{b}\}$, where $\{\dot{b}\}$ is the surface area-specific searching rate with dimension volume of environment per time per surface area of organism. The half-saturation constant

is a phenomenological parameter, and the behavioural parameter $\{\dot{b}\}$ is much closer to the underlying processes.

The parameters $\{\dot{J}_{XAm}\}$ and $\{\dot{J}_{EAm}\}$ can't be subjected independently to evolutionary adaptation since the conversion efficiency $y_{EX} = \{\dot{J}_{EAm}\}/\{\dot{J}_{XAm}\}$ depends on basic biochemical machinery that is conserved among eukaryotes (it is not possible to synthesize more ATP from a glucose molecule). Adaptation of $\{\dot{J}_{XAm}\}$ by changes in the design of the motory and the digestive system seems more easy than in $\{\dot{J}_{EAm}\}$, which involves more of the metabolic machinery (design of liver, kidneys etc). For this reason $\{\dot{J}_{XAm}\} = y_{XE}\{\dot{J}_{EAm}\}$ is probably the best choice for being the compound parameter, and so $\{\dot{J}_{EAm}\}$ the basic design parameter.

In the light of the newly derived mechanism for the reserve dynamics, the maximum reserve density should be a compound parameter $[E_m] = \{\dot{p}_{Am}\}/\dot{v}$, which give a nice parallel with the maximum length $L_m = \kappa\{\dot{J}_{EAm}\}/[\dot{J}_{EM}]$ since both maxima are now the result of underlying input/output processes, like the partition coefficient.

To avoid mass-energy conversions in the set of primary parameters, it seems best to choose mass and volume only for assimilation and maintenance. The resulting set of primary parameters becomes

symbol	**dim**	**description**	**process**
$\{\dot{J}_{EAm}\}$	$\# \mathrm{t}^{-1}\mathrm{L}^{-2}$	surface area-specific max assimilation rate	assimilation
$\{\dot{b}\}$	$\mathrm{l}^3\mathrm{L}^{-2}\mathrm{t}^{-1}$	surface area-specific searching rate	feeding
y_{EX}	$\# \#^{-1}$	yield of reserve on food	digestion
y_{VE}	$\# \#^{-1}$	yield of structure on reserve	growth
$\dot{v}$	$\mathrm{L}\,\mathrm{t}^{-1}$	energy conductance	mobilization
$\{\dot{J}_{ET}\}$	$\# \mathrm{t}^{-1}\mathrm{L}^{-2}$	surface area-specific maint. costs	heating/osmosis
$[\dot{J}_{EM}]$	$\# \mathrm{t}^{-1}\mathrm{L}^{-3}$	volume-specific somatic maintenance	turnover/activity
$[\dot{J}_{EJ}]$	$\# \mathrm{t}^{-1}\mathrm{L}^{-3}$	volume-specific maturity maintenance	regulation/defense
κ	-	allocation fraction	allocation
κ_R	-	reproduction efficiency	egg formation
$[M_H^b]$	$\# \mathrm{L}^{-3}$	spec maturation at birth	life cycle
$[M_H^p]$	$\# \mathrm{L}^{-3}$	spec maturation at puberty	life cycle
$\ddot{h}_a$	t^{-2}	aging acceleration	aging

With this choice of primary parameters only the first parameter depends on maximum length. This simplifies the derivation of the scaling relationships. The replacement of the ageing module, and so of $\ddot{h}_a$ should be considered. The volume-specific maturation parameters are only constant if the maturation is divided by the maximum structural volume, rather than the actual structural volume.

Scaling of length at birth

{270}

If $\dot{k}_J \neq \dot{k}_M$ the length at birth and puberty can no longer be primary parameters and shuold be replaced by the maturity at birth and puberty, which both scale with the cubed zoom factor, z^3; the scaled maturity at birth U_H^b covaries with z^2. This is because the (unscaled)

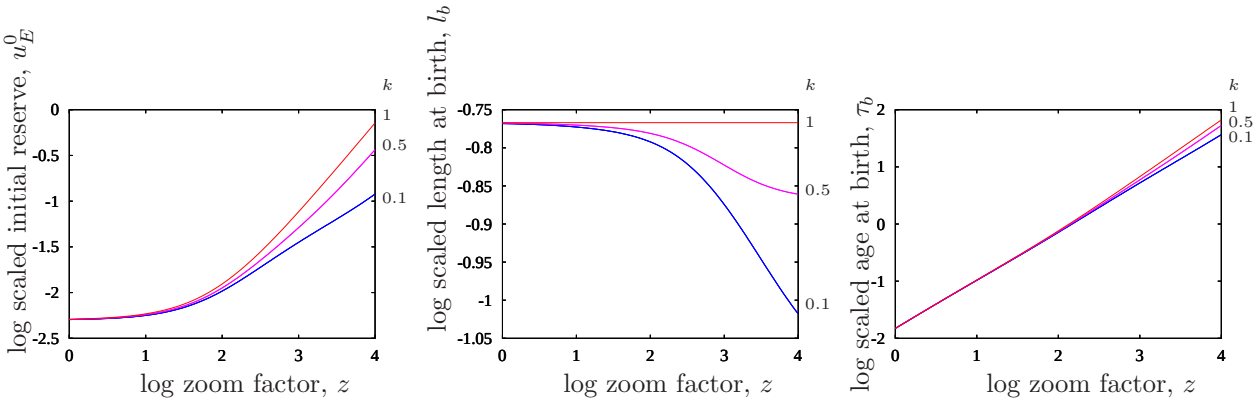

Figure 8.1: The scaled initial reserve (left), length at birth (middle), and age at birth (right) as function of the zoom factor, log-log plotted (base 10). Each plot has three curves, corresponding to maintenance ratio $k = 0.1$ (lower), 0.5 (middle), 1 (upper). Parameters: $g = 80/z$, $u_H^b = 0.005$, $e_b = 1$. The curves are approximately allometric with slopes for large zoom factors

maintenance ratio k	0.1	0.5	1.0
scaled initial reserve u_E^0	0.55	0.83	1.00
scaled length at birth l_b	-0.14	-0.04	0.00
scaled age at birth τ_b	0.85	0.89	0.93

maturity at birth $M_H^b = U_H^b\{\dot{J}_{EAm}\}$ covaries with z^3, and the surface area specific reserve assimilation rate $\{\dot{J}_{EAm}\}$ covaries with z.

If $\dot{k}_J = \dot{k}_M$, the structural volume at birth is proportional to the maturity at birth, so length at birth scales with maximum length. If $\alpha_b >> B_{x_b}(\frac{4}{3}, 0)$, the initial reserve scales approximately with maximum length to the power 4 and age at birth with maximum length. These scalings are confirmed in the analysis presented in Figure 8.1. If scaled initial reserve u_E^0 scales with z, $U_E^)$ scales with z^2 and initial reserve M_E^0 with z^4, as reported Figure 8.6 of [289]. If scaled length at birth l_b scales with z^0, length at birth $L_b = l_b L_m$ scales with z.

Figure 8.1 shows that if $\dot{k}_J \neq \dot{k}_M$, the scaling is more complex, especially for the length at birth and the initial reserve; I presented the approximate scaling exponents to comply with the traditional way to present these types of relationships. It is remarkable that taxa show a wide scatter in scaling relationships for specially these quantities, while age at birth shows much less scatter. This suggests that taxa might differ in the maintenance ratio. The increase in the maintenance ratio $k = \dot{k}_J/\dot{k}_M$ goes with an increase in the relative size at birth for any given value of the zoom factor z, but the effect is bigger for the large bodied species. Since protein turnover is an important component of somatic maintenance costs, and activity typically a minor component, it is not likely that species differ a lot in the somatic maintenance costs. I expect that costs for defense (e.g. the immune system) varies more among species. It is tempting to speculate about the relatively small egg size of dinosaurs (indicating small maturity maintenance costs) versus the relatively large size at birth of mammals (indicating hight maturity maintenance costs).

Table 8.1: Respiration has contributions from growth and maintenance (and assimilation, which is excluded here). Body weight has contributions from reserve and structure; the parameters d_E and d_V stand for the specific density ($\mathrm{g\,cm^{-3}}$) of reserve (E) and structure (V). The amount of structure in this table is proportional to L^3, the cubed volumetric length. The heating length L_h is a positive constant for endotherms, and zero for ectotherms. The length-parameters L_g and L_s are constant (under certain conditions). The inter-species comparison is based on fully grown (adult) individuals. From [301].

	intra-species	inter-species
maintenance	$\propto L_h L^2 + L^3$	$\propto L_h L^2 + L^3$
growth	$\propto L_g L^2 - L^3$	0
$\frac{\text{reserve}}{\text{structure}}$	$\propto L^0$	$\propto L$
$\frac{\text{respiration}}{\text{weight}}$	$\propto \frac{L_s L^2 + L^3}{d_V L^3 + d_E L^3}$	$\propto \frac{L_h L^2 + L^3}{d_V L^3 + d_E L^4}$

Max wet weight

{270}, last line

The maximum wet weight can be derived as follows: For $[E] = [E_m]$ we have from (2.6) that $W_w = (d_V + [E_m](1 + e_R) w_E/\mu_E)V$. Assuming that reserves allocated to reproduction plays a minor role, this reduces to $W_w = (d_V + [E_m] w_E/\mu_E)V = (d_V + w_E[M_{Em}])V$, where $[M_{Em}] = [E_m]/\mu_E$, see Table 3.4 at {122}. The maximum volumetric length is from (3.23) for $f = 1$: $V_\infty^{1/3} = V_m^{1/3} - V_h^{1/3} = V_m^{1/3}(1 - l_h)$, with $l_h = (V_h/V_m)^{1/3}$, see {94}. This makes that the maximum volume is $V = V_m(1 - l_h)^3$. The maximum wet weight thus amounts to $W_w = (d_V + w_E[M_{Em}])V_m^{1/3}(1 - l_h)$.

Scaling of respiration

{273}

The explanation of West and Brown for the inter-specific scaling of respiration, and the application to growth is compared with the DEB theory by [391].

Table 8.1 presents the differences between intra- ad inter-specific scaling of respiration with body size, while numerically they work out rather similar.

Minimum size for separation of embryonic cells [294]

{273}

Suppose that the cells in the two-cell stage of an embryo are identical in terms of amounts of maturity, reserve and structure. If the cells are separated, the three amounts are halved. Figure 8.2 show the expected results of such an event, which sometimes occurs spontaneously. The plots for maturity and structural volume are almost identical in this case because $\dot{k}_J/\dot{k}_M$ is very close to 1; the maturity density then remains constant.

The parameter values for *Daphnia magna* at 20°C are $U_H^b = 012\ \mathrm{d\,mm^2}$, $g = 0.422$, $\dot{k}_J = 1.70\ \mathrm{d^{-1}}$, $\dot{k}_M = 1.71\ \mathrm{d^{-1}}$, $\dot{v} = 3.24\ \mathrm{mm\,d^{-1}}$, which gives a scaled maturity maintenance rate of $k \simeq 1$ and a scaled maturity at birth of $u_H^b = 0.001$ [328]. If one would try to separate cells in this species, the theory predicts that the initial reserve is not enough the cover embryonic development. This result is remarkable because these parameters imply

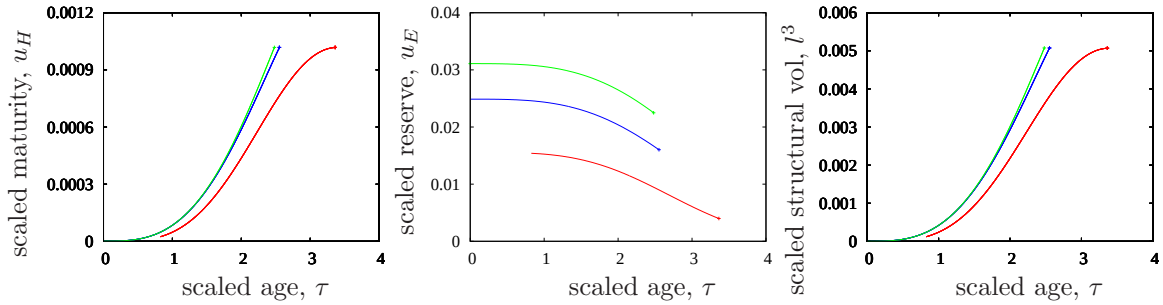

Figure 8.2: The scaled maturity (left), reserve (middle), and structural volume (right) during embryonic development. Each plot has three curves. The left (left and right plots) and upper (middle plot) curves represent the "blank" situation. Then follows the case in which the initial amount of reserve has been reduced by a factor 0.8, and then the case in which the maturity, reserve and structure has been halved. Parameters: $\kappa = .8$, $g = 0.422/1.87$, $k = .99415$; $u_H^b = .001$, $f = 1$ and the age of cell separation is here at $\tau_b/3$.

that a fraction of 0.63 of the initial amount of reserve is still left at birth at abundant food, see [328]. The explanation is that the mobilization of reserve decreases with the reserve density. It might be, of course, that maturity at birth is affected by cell separation, which can still allow this to occur successfully in small bodied species. However, I am unaware of any empirical evidence for this.

The reserve density capacity $[E_m] = \{\dot{J}_{EAm}\}/\dot{v}$ scales with structural length. So species with a larger ultimate body size tend to have a relatively larger reserve capacity. It turned out that for the combination of parameter values as found for *D. magna* we have to apply a zoom factor of at least $z = 1.87$ to arrive at a minimum maximum body size for which cell separation might be successful. The resulting parameter values are used in the figure; the scaling relations only affect the energy investment ratio gz^{-1}, while κ, k and u_H^b are independent of the zoom factor z.

For $k > 1$, the structural volume at birth increases after halving, and decreases for $k < 1$. Since reserve contributes to weight, the weight at birth is close to half of the original weight at birth, irrespective of the value of k. The age of the two-cell stage is probably smaller than $\tau_b/3$, but the results are very similar.

Interactions between QSARs and body size scaling relationships [301]

{292}

Body size affects chemical kinetics in rather complex ways, so do changes in body size. Since DEB theory is about the dynamics of body size, this directly points to the importance of the link between DEB theory and toxico-kinetics. We here briefly review some pertinent items; each of these items can be discussed in much more detail [300], but this would involve more details of the DEB theory, which is beyond the scope of this paper. It is useful to start

with an inventory of the possible uptake and elimination routes of the compounds under consideration, and then consider other chemical and metabolic aspects.

Uptake can be directly from the environment, which is proportional to the surface area of individuals. The implication is that elimination rates are inversely proportional to length. So the time it takes to saturate an organism with a chemical compound is proportional to its (volumetric) length. Uptake can also be via food, and food uptake scales with surface area intra-specifically, but with volume inter-specifically.

Dilution by growth matters, even at low growth rates. The growth rate depends on the size of the individual, relative to the maximum size, so intra- as well as inter-specific scaling relationships contribute.

Elimination can be directly to the environment (involving the surface area), and/or to the gut contents (involving the feeding rate), and/or via reproduction or some other species-specific routes. The possible significance of the latter route is obvious from the observation that a female adult daphnid can produce offspring at the rate of 25% of her own weight *per day*. If chemical compounds are in eggs at formation, this can represent an important elimination route. The reproduction rate (in number of offspring per time) is proportional to a weighted sum of surface area and volume intra-specifically, and inversely proportional to a length inter-specifically. Since the mass per offspring is proportional to volume, allocation to reproduction is proportional to surface area inter-specifically. We hasten to add that the relative size of offspring is a lot more species-specific (so subjected to evolutionary adaptation) than the allocation to reproduction [289, 566, 83].

The *chemical composition* of biomass also depends on size, since the reserve density (so the ratio of the amounts of reserve and structure) is constant intra-specifically, but proportional to a length inter-specifically. Reserve might be more rich in lipids than structure (depending on the taxa that are studied). This observation obviously matters for the comparison of compounds that differ in P_{ow}.

Chemical transformation in an organism is linked to the metabolic activity of the organism. Lipophilic compounds are frequently transformed into less lipophilic ones, which enhances excretion (elimination). These metabolites are, frequently, more toxic. Moreover, uptake and elimination frequently involve metabolic activity. The standard DEB model specifies all metabolic activities, and the rate at which reserves are mobilized seems to be the best candidate to link with (the potential for) metabolic transformation and excretion. It has close links with the respiration rate, a frequently used term, which can stand for a variety of things that are not proportional to each other in the context of the DEB theory as well as in the context of indirect calorimetry: the use of dioxygen, the production of carbon dioxide and of heat. Table 8.1 presents the intra- and inter-specific scaling tendencies of respiration. The numerical behaviour is remarkably close to the well-known observation by Kleiber [232] that respiration scales with body weight$^{3/4}$.

A further modification of the role of metabolic transformation in the toxicity of compounds is when the effects are receptor-mediated [214]. The turnover rate of receptors is possibly linked to the somatic maintenance process, in which case the specific turnover rate is independent of body size, but it might also be linked to the metabolic activity. We still need more experience with the application of receptor-mediated models. The observation that effects are linked to the product of concentration and exposure time motivated many

toxicologists to think about the involvement of receptors, although their biochemical identification remained uncertain. This motivation is incorrect, however, if the hazard rate is linear in the (internal) concentration. This is because even without receptors the effect on the survival probability is already via the product of concentration and exposure time. The significance of receptors is in the contribution of the exposure *history* in the effect, rather than of the actual exposure. This requires an in-depth analysis of how effects build up in time and imposes strong constraints on the quality of data. It is only by analyzing multiple endpoints simultaneously that we found indications that the effects of organophosphorus esters on fish involve receptors.

These considerations invite for a second thought about effects of chemicals. As long as lipophilic compounds are accumulated in metabolically rather inactive lipids, they are less likely to have metabolic effects. Many animals, and especially mammals, have tissues (the adipose tissue) that are specialized in the storage of such lipids. As soon as these lipids are used, however, effects might show up. This calls for a much more dynamic view on the effects of chemicals, and links up with traditions in pharmaco-kinetics and medical research on the effects of chemicals.

Determinate vs indeterminate growth

{293}

The comparison between determinate and indeterminate growth is further extended in [356]. This study helps to understand why both allocation schedules still exist. The two-way classification is too simple in the DEB framework. A copepod (which as a fixed number of moults) follows the expected von-Bertalanffy growth pattern at constant food levels. The asymptotic size (i.e. the size after the final moult) depends on food levels in the expected way. It can only reproduce after the final moult, where it cannot longer grow. This situation is really frequent, and should be classified as indeterminate growth, but the ability to resume growth is finally lost. This also occurs in mammals and birds, for instance (but not in fish). Typical determinate growth is rare, and possibly confined to holo-metabolic insects

Derivation of Eq (8.7)

{296}

Eq (8.7) can be derived as follows: Reproduction is increasing with age, so we focus at a high age, where $V(a) = V_\infty$. If we substitute this and $\{\dot{p}_{Am}\} = \frac{[\dot{p}_M]}{\kappa f} V_\infty^{1/3}$ in the reproduction rate given in (8.3), we get for the constant fraction strategy

$$\dot{R}_c(\infty) = \frac{\kappa}{E_0} \left(V_\infty [\dot{p}_M](1-\kappa)/\kappa - [\dot{p}_J] V_p\right)$$

If we similarly substitute $\{\dot{p}_{Am}\}$ for the bang-bang strategy, we get

$$\dot{R}_b(\infty) = \frac{\kappa}{E_0} \left(V_\infty^{1/3} V_p^{2/3} [\dot{p}_M]/\kappa - [\dot{p}_M] V_p - [\dot{p}_J] V_p\right)$$

So $\dot{R}_c(\infty) > \dot{R}_b(\infty)$ if

$$(1-\kappa) V_\infty - V_\infty^{1/3} V_p^{2/3} + \kappa V_p > 0$$

Evolution

{298}

A proper understanding of metabolic organization cannot be achieved without exploring its historic roots. The metabolism of individuals has adapted over time to overcome the consequences of changing living conditions. The question here is how this might have happened in interaction with the environment. One possibility is through changing the system itself by mutation and selection. This is a very slow process, but essential for building up a basic diversity in metabolic performance between different species. This explains the slow start of evolution. Much faster is the exchange of plasmids that evolved among prokaryotes [117], which is further accelerated by the process of symbiogenesis, typical for eukaryotes. The latter also duplicate DNA and reshuffle parts of their genome, giving adaptive change even more acceleration. Mutation still continues, of course, but the reshuffling of metabolic modules occurs at rates several orders of magnitude higher. The response to changes in the environment is further accelerated by the development of food webs, and therefore of predation, which enhances selection. Owing to their advanced locomotory and sensory systems, animals play an important role in food webs, and so in the acceleration of evolutionary change.

The evolutionary route that is discussed below starts from the speculative abiotic origins of life, then deals with the metabolic diversification that evolved in the prokaryotes, and finally leads the to metabolic simplification, coupled to the organizational diversification of the eukaryotes. We will see how life became increasingly dependent on itself and how life and climate became increasingly coupled. Syntrophy is the basis of biodiversity and supplements Darwin's notion of survival of the fittest, which is based on competitive exclusion [501].

Before the first cells

A possible exergonic process generating energy in the initial stages of life involves the formation of makinawite crusts at the interface of mildly oxidizing, iron-rich acidulous ocean water above basaltic floors from which alkaline seepages arose, e.g. [500]. These crusts consist of FeS layers allowing free electron flow from the reducing environment beneath, generated by the activation of hydrothermal hydrogen. Thus, energy was constantly supplied, which, moreover, could easily be tapped at the steep gradient formed by the crust. FeS can spontaneously form cell-like structures on a solid surface [498, 499, 63, 80], and has a high affinity for the ATP ingredients organophosphates and formaldehyde [484], which can form ribulose [34, p81]. The released energy could stimulate the formation of larger molecules at each inner surface, such as phosphorus or nitrogen compounds. The chemically labile energy-rich inorganic pyrophosphate compounds could have served as energy-transferring molecules [23, 24], whereas the nitrogen-containing molecules on the inner surface of the crust could have developed into nucleic acids or, later, into larger peptides. Of these, the peptides, in turn, could have combined with iron and sulphur complexes in the crust, thus initiating the formation of ferredoxins, or they could have nested themselves within the crust, thus forming the second step in the formation of membranes [499].

ATP generation *via* a proton pump across the outer membrane is probably one of the

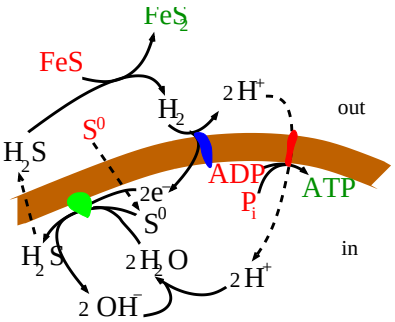

Figure 8.3:
A possible early ATP-generating transformation, based on pyrite formation $FeS + S \rightarrow FeS_2$ [547, 573], that requires a membrane and only three types of enzyme: proto-hydrogenase, proto-ATP-ase and S^0-reductase; modified from [369]. Sulphur is imported in exchange for H_2S.

first steps in the evolution of metabolism. The energy for this ATP generation probably came from some extracellular chemoautotrophic process [573, 498, 499].

A possible scenario for the earliest metabolism is presented in Figure 8.3, which may be found in the archaean *Pyrodictium occulatum* [573]. A few enzymes are required and the substrates are readily available in the deep ocean [120]. Keefe et al. [227], however, argue that the oxidation of FeS gives insufficient energy to fix carbon dioxide through the inverse TCA cycle. Yet, this fixation may have occurred along other pathways using accumulated ATP. Schoonen et al. [508] demonstrated that the energy of this reaction diminishes sharply at higher temperatures. Contrary to pyrite, greigite ($Fe_5Ni_6S_8$) has structural moieties that are similar to the active centers of certain metallo-enzymes, as well as to electron transfer agents (see, for example, [499], and catalyzes the transformation $2\,CO_2 + CH_3SH + 8\,[H] \rightarrow CH_3COSCH_3 + 3\,H_2O$.

Irrespective of the biochemical "details", which are still controversial [431], it rightly places membrane activity central to metabolism, which means that cell size matters. The membranes of membrane-bound vesicles are at the basis of transformations typical for life [515]. Membranes need membranes (plus genes) for propagation; genes only are not enough [88]. Strong arguments in favour of the hypothesis "cells before metabolism" include the abiotic abundance of amphiphilic compounds (even on arriving meteorites), the self-organization of these compounds into membranes and vesicles, and their catalytic properties [101]. This argument only works if amphiphilic compounds tend to accumulate in very specific micro-environments; otherwise they will be too dilute. The modifications of substrates that are taken up from the environment to compounds that function in metabolism were initially probably small, and gradually became substantial. Compartmentalization is essential for the accumulation of metabolites and for any significant metabolism. Norris and Raine [424] suggest that the RNA world succeeded the lipid world, which is unlikely because the archaean lipids consist of isoprenoid ethers, while eubacterial lipids consist of fatty acids (acyl esters) with completely different enzymes involved in their turnover [225, 222, 573]. Lipids were probably synthesized first from pyruvate, the end product of the acetyl-CoA pathway and the reverse TCA cycle, before the extensive use of carbohydrates.

Koga et al. [238] hypothesized that the eubacterial taxa made the transition from non-cellular ancestors to cellular forms independently from the archaea (see also [379]. This seems unlikely, however, because they are similar in the organization of their genes (e.g. in operons) and genomes, and in their transcription and translation machinery [426, 87].

Eubacteria do have a unique DNA replicase and replication initiator proteins, however. These properties apply especially to cells, rather than to pre-cellularly existing forms, and are complex enough to make it very unlikely that they evolved twice. Woese [587] hypothesized that lateral gene transfer could have been intense in proto-cells with a simple organization; diversification through Darwinian mutation and selection could only occur after a given stage in complexity had been reached, that is when lateral gene transfer could have been much less intense. The eubacteria, archaea and eukaryotes would have crossed this stage independently. Since all eukaryotes once seem to have possessed mitochondria, this origin is unlikely for them. Cavalier-Smith [90] argued that archaea and eukaryotes evolved in parallel from eubacteria since about 850 Ma ago, and that eukaryotes have many properties in common with actinomycetes. However, the differences in, for example, lipid metabolism and many other properties between eubacteria and archaea are difficult to explain in this way. Moreover, carbon isotope differences between carbonates and organic matter of 2.8-2.2 Ga ago are attributed to archaean methanotrophs [237]. Although so far the topic remains speculative, a separate existence of eubacteria and archaea before the initiation of the lipid metabolism and before the origin of eukaryotes through symbiogenesis with mitochondria seems to be the least-problematic sequence explaining metabolic properties among these three taxa.

The ionic strength of cytoplasm of all modern organisms equals that of seawater, which suggests that life arose in the sea.

Early substrates and taxa

Since genome size might quantify metabolic complexity, it helps to note that some chemoautotrophs have the smallest genome size of all organisms [316]; The togobacterium *Aquifex* is even more interesting since its metabolism might still resemble that of an early cell. Although it is also aerobic, it tolerates only very low dioxygen concentrations, which may have been present when life emerged [203, 224, 8]. Growing optimally at 85 °C in marine thermal vents, it utilizes H_2, S0 or $S_2 2O_3^-$ as electron donors and O_2 or NO_3^- as electron acceptors. With a genome size of only 1.55 Mbp, its genome amounts to only one third of that of *E. coli*, which is really small for a non-parasitic prokaryote. One of the smallest known genomes for a non-parasitic bacterium is that of *Nanoarchaeum equitans* with 0.5 Mbp [206], but it lives symbiotically with the H_2-producing and sulphur-reducing archaean *Ignicoccus*, which complicates the comparison. The free-living α-proteobacterium *Pelagibacter ubique*, with a genome size of 1.3 Mbp is probably phototrophic (using proteorhopsin) and uses organic compounds as carbon and electron source [162, 464]. Its metabolic needs are uncertain, since it is difficult to culture. The phototrophic cyanobacterium *Prochlorococcus* has 1.7 Mbp [154]. These small genome sizes illustrate that autotrophy is metabolically not more complex than heterotrophy.

The early atmosphere was probably rich in carbon dioxide and poor in methane [224], which changed when methanogens started to convert carbon dioxide into methane so 3.7 Ga ago, using dihydrogen as energy substrate. This problably saved to early earth from becoming deep frozen. Apart from being a product, methane is likely to have been an important substrate (and/or product) during life's origin [191]. Methanogenesis and (anaero-

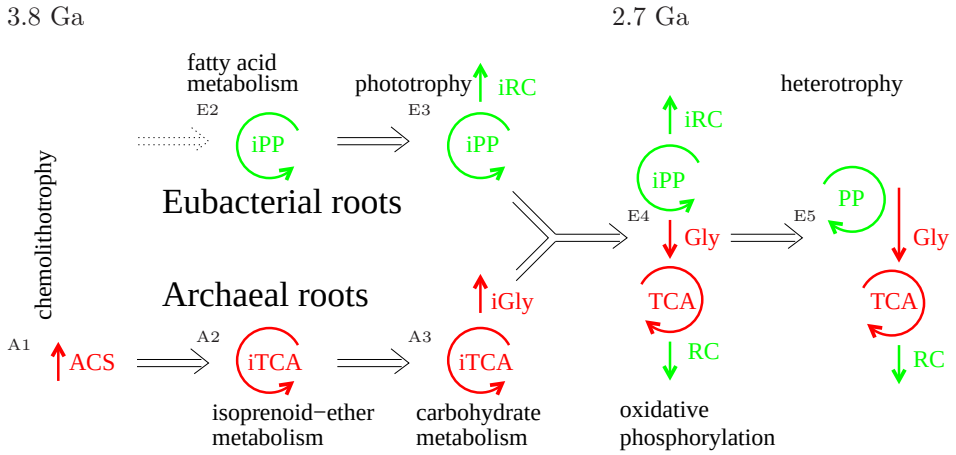

Figure 8.4: Evolution of central metabolism among prokaryotes that formed the basis of eukaryotic organization of central metabolism. ACS = acetyl-coenzyme A synthase pathway, iPP = inverse pentose phosphate cycle (= Calvin cycle), PP = pentose phosphate cycle, iTCA = inverse tricarboxylic acid cycle, TCA = tricarboxylic acid cycle (= Krebs cycle), iGly = inverse glycolysis, Gly = glycolysis, iRC = inverse respiratory chain, RC = respiratory chain. The arrows indicate the directions of synthesis to show where they reversed; all four main components of eukaryote's heterotrophic central metabolism originally ran in the reverse direction to store energy and to synthesize metabolites. The approximate time scale is indicated above the scheme (*i.e.* the origin of life, and that of cyanobacteria and eukaryotes). Contemporary models: A1 *Methanococcus*; A2 *Thermoproteus*; A3 *Sulfolobus*; E2 *Nitrosomonas*; E3 *Chloroflexus*; E4 *Prochlorococcus*; E5 *Escherichia*. Modified from [316]

bic) methylotrophy are perhaps reversible in some archaea [173]; their metabolic pathways share 16 genes, and are present in some archaeal and eubacterial taxa. The most probable scenario for its evolutionary origin is that it first evolved in the planctomycetes, which transferred it to the proteobacteria and the archaea [95]. This remarkable eubacterial taxon is unique in sporting anaerobic ammonium oxidation (anammox). The anammox clade has ether lipids in their membranes and a proteinaceous cell wall like the archaea [541]. They have advanced compartmentation and a nuclear membrane like the eukaryotes [361, 153], and are abundant in (living) stromatolites [436]. Fossil stromatolites resemble the living ones closely [109] and date back some 3.5 Ga ago [576]. Although, this points to a key role in early evolution, planctomycetes seem too complex as a contemporary model for an early cell. Moreover, anaerobic methane oxidation (amo) involves sulphate reduction. Isotope data indicate that sulphate reduction originated 3.47 Ga ago [518]. Sulphate was rare by then [81] and might have been formed photochemically by oxidation of volcanic SO_2 in the upper atmosphere, or phototrophically by green and purple sulphur bacteria (*Chlorobiaceae*, *Chromatiacea*), [454].

Evolution of central metabolism

A closer look at the modern central metabolism in an evolutionary perspective might help to get the broad picture, see Figure 8.4. The four main modules of the central metabolism evolved one by one within the prokaryotes already, and were recombined, reverted and reapplied. It implies considerable conjugational exchange between the archaea and eubacteria, but given the long evolutionary history, such exchanges might have been very rare. The exchange must have been predated by a symbiontic coexistence of archaea and eubacteria to tune their very different metabolic systems.

Dioxygen was rare, if not absent, during the time life emerged on earth which classifies the respiratory chain as an advanced feature. Glucose hardly could have been that central during the remote evolutionary origins of life, since its synthesis and degradation typically involves dioxygen. Like all phototrophic eukaryotes, most chemolitho-autotrophic bacteria fix inorganic carbon in the form of carbon dioxide through the Calvin cycle. At present, this cycle is part of the phototropic machinery, a rather advanced feature in metabolic evolution and which is not found in any archaea [507]. It has glucose as its main product, which suggests that the central position of glucose and, therefore, of carbohydrates, evolved only after oxygenic phototrophy evolved. Like the Calvin cycle, eukaryotic and eubacterial glycolysis (the Embden-Meyerhof pathway) is not found in archaea either; hyperthermophilic archaea possess the Embden-Meyerhof pathway in modified form [507, 516] and generally do not use the same enzymes [379]. This places the pyruvate processing TCA cycle at the origin of the central metabolism. However, if we leave out the glycolysis as a pyruvate-generating device, what process was generating pyruvate?

Interestingly, the eubacteria *Hydrogenobacter thermophilus* and *Aquifex* use the TCA cycle in reverse, binding and transforming CO_2 into building blocks (lipids, cf [353]), including pyruvate. Both species are Knallgas bacteria, extracting energy from the oxidation of dihydrogen. The green sulphur bacterium *Chlorobium*, as well as the archaea *Sulfolobus* and *Thermoproteus* [369] also run the TCA cycle in reverse for generating building blocks. Hartman [188], Wächtershäuser [574] and Morowitz et al. [407] hypothesized the reverse TCA cycle to be one of the first biochemical pathways. The interest in hydrogen bacteria relates to the most likely energy source for the first cells on earth. *Hydrogenobacter* optimally thrives at 70-75 °C in Japanese hot springs. It is an aerobic bacterium, using ammonia and nitrate, but not nitrite and possesses organelles (mesosomes). Several enzymes of the PP cycle and the glycolytic pathway are present although their activities are low [532].

The TCA cycle seems to be remarkably efficient, which explains its evolutionary stability. Moreover, it is reversible, which directly relates to its efficiency and the inherent small steps in chemical potential between subsequent metabolites. Yet, with its nine transformations, the TCA cycle is already rather complex, and must have been preceded by simpler CO_2-binding pathways [430], such as the (linear) acetyl-CoA pathway of homoacetogens: $2\,CO_2 + 4\,H_2 + CoASH \rightarrow CH_3COSCoA + 3\,H_2O$ [207, 362]. Apart from H_2, electron donors for acetogenesis include a variety of organic and C_1-compounds. Coenzyme A, which plays an important role in the TCA cycle, is a ribonucleotide and the main substrate for the synthesis of lipids, a remembrance of the early RNA world [542]. Several eubacteria

and archaea employ the acetyl-CoA pathway; they include autotrophic homoacetogenic and sulphate-reducing bacteria, methanogens, *Closterium*, *Acetobacterium*, and others. The RNA-world is generally thought to predate the protein/DNA-world. RNA originally catalyzed all cellular transformations; protein evolved later to support RNA in this role. Many protein enzymes still have RNA-based cofactors (e.g. ribosomes and spliceozomes), while RNA still has catalytic functions. DNA evolved as a chemically more stable archive for RNA, probably in direct connection with the evolution of proteins, and possibly with the intervention of virusses [148, 149]. The step from the RNA to the protein/DNA world came with a need for the regulation of transcription.

The hyperthermophilic methanogens, such as *Methanococcus*, *Methanobacterium* or *Methanopyrus*, have also been proposed as contemporary models for early cells [360]; they have the acetyl-CoA pathway, which they run in both the oxidative and the reductive direction [523]. Like *Aquifex*, they are thermophilic and taxonomically close to archaea/eubacteria fork (eukaryotes have some properties of both roots), have a small genome (*Methanococcus jannaschii* has 1.66 Mbp, coding for only 1700 genes), and they utilize H_2 as electron donor.

A natural implication of the reversal of the TCA cycle is that the direction of glycolysis was initially reversed as well, and served to synthesize building blocks for e.g. carbohydrates. Comparing the carbohydrate metabolism among various bacterial taxa, Romano and Conway [491] concluded that originally glycolysis must indeed have been reversed. Thus, the reversed glycolytic pathway probably developed as an extension of the reversed TCA cycle, and they both reversed to their present standard direction upon linking to the Calvin cycle, which produces glucose in a phototrophic process. So, what could have been the evolutionary history of phototrophy?

Phototrophy

Phototrophy probably was invented more than 3.2 Ga ago [590]. Recent evidence suggests that phototrophy is also possible near hydrothermal vents at the ocean floor [120], where the problem encountered by surface dwellers, namely that of damage by ultraviolet (UV) radiation, is absent. In an anoxic atmosphere, and therefore without ozone, UV damage must have been an important problem for the early phototrophs though and protection and repair mechanisms against UV damage must have evolved in parallel with phototrophy [110].

The green non-sulphur bacterium *Chloroflexus* probably resembles the earliest phototrophs and is unique in lacking the Calvin cycle, as well as the reverse TCA cycle. In the hydroxypropionate pathway, it reduces two CO_2 to glyoxylate, using many enzymes also found in the thermophilic non-phototrophic archaean *Acidianus*. Its photoreaction centre is similar to that of purple bacteria. The reductive dicarboxylic acid cycle of *Chloroflexus* is thought to have evolved into the reductive TCA cycle as found in *Chlorobium*, and further into the reductive pentose phosphate cycle, which is, in fact, the Calvin cycle [189]. Like sulphur and iron-oxidizing chemolithotrophs, aerobic nitrifying bacteria use the Calvin cycle for fixing CO_2. The substrate of the first transformation of the monophosphate pathway for oxidizing C1-compounds, such as methane, is very similar to the C_1-acceptor of

the Calvin cycle, which suggests a common evolutionary root of these pathways [369]. The first enzyme in the Calvin cycle, RubisCO is present in most chemolithotrophs and phototrophs and even in some hyperthermophilic archaea. It is the only enzyme of the Calvin cycle of which (some of) the code is found on the genome of chloroplasts. The enzymes that are involved in the Calvin cycle show a substantial diversity among organisms and each has its own rather complex evolutionary history [380]. This complicates the finding of its evolutionary roots; see Figure 8.4.

The thermophilic green sulphur bacterium *Chlorobium tepidum* runs the TCA cycle (and glycolysis) in the opposite direction compared to typical (modern aerobic) organisms [369], indicating an early type of organization [188, 574, 407]. In combination with the observations mentioned above, this suggests that the present central glucose-based metabolism evolved when the Calvin cycle became functional in CO_2 binding, and the glycolysis and the TCA cycle reversed to their present standard direction, operating as a glucose and pyruvate processing devices, respectively (see Figure 8.4). Most phototrophs use the Calvin cycle for fixing CO_2 in their cytosol in combination with a pigment system in their membrane for capturing photons. Archaea use a low-efficient retinal-protein and are unable to sustain true autotrophic growth; 5 of the 11 eubacterial phyla have phototrophy. Bacterio-chlorophyll in green sulphur bacteria is located in chlorosomes, organelles bound by a non-unit membrane, attached to the cytoplasmic membrane. Green non-sulphur and purple bacteria utilize photosystem (PS) II; green sulphur and Gram-positive bacteria utilize PS I, whereas cyanobacteria (including the prochlorophytes) utilize both PS I and II [606]. The cyanobacterium *Oscillatoria limnetica* can utilize their PS I and II in conjunction, thus being able to split water and to produce dioxygen. In the presence of H_2S as an electron donor, it uses only PS I, an ability pointing to the anoxic origin of photosynthesis. Oxygenic photosynthesis is a complex process that requires the coordinated translocation of 4 electrons. It evolved more than 2.7 Ga ago [50]. Based on the observation that bicarbonate serves as an efficient alternative for water as electron donor, Dismukes et al. [111] suggested the following evolutionary sequence for oxygenic photosynthesis, starting from green non-sulphur bacterial phytosynthesis that uses organic substrates as electron donor.

The phototrophic system eventually allowed the evolution of the respiratory chain (the oxidative phosphorylation chain), which uses dioxygen that is formed as a waste product of photosynthesis, as well as the same enzymes in reversed order. If the respiratory chain initially used sulphate, for example, rather than dioxygen as electron acceptor, it could well have evolved simultaneously with the phototrophic system.

The production of dioxygen during phototrophy, which predates the oxidative phosphorylation, changed the earth, e.g. [111, 341]. It started to accumulate in the atmosphere around 2.3 Ga ago, which shortened the life time of atmospheric methane molecules from 10000 to 10 years with the consequence that the earth became a "snowball" [224]. The availability of a large amount of energy and reducing power effectively removed energy limitations; primary production in terrestrial environments is mainly water-limited, that in aquatic environments nutrient-limited. This does not imply, however, that the energetic aspects of metabolism could not be quantified usefully; energy conservation also applies in situations where the energy supply is not rate-limiting. Nutrients may have run short of supplies because of oxidation by dioxygen; this would have slowed down the rate of

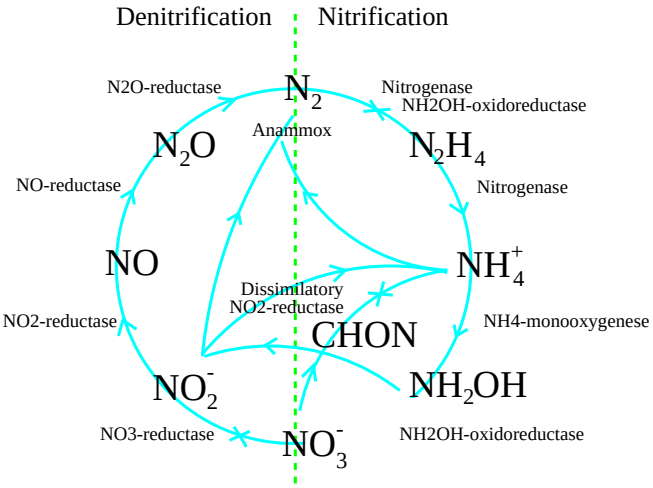

Figure 8.5: Conversions of inorganic nitrogen species by prokaryotes. The compound CHON stands for biomass. Modified from [505].

evolution [8]. First, sulphur precipitated out, followed by iron and toward the end of the Precambrian by phosphate and, since the Cambrium revolution, by calcium as well. Also, under aerobic conditions, nitrogen fixation became difficult, which makes biologically required nitrogen unavailable, despite its continued great abundance of dinitrogen in the environment; see [34, p41]. Since the Calvin cycle produces fructose 6-phosphate, those autotrophic prokaryotes possessing this cycle are likely to have a glucose-based metabolism. Indeed, the presence of glucose usually suppresses all autotrophic activity. Several obligate chemolithotrophic prokaryotes, such as sulphur-oxidizers, nitrifiers, cyanobacteria and prochlorophytes contain this cycle in specialized organelles, the carboxysomes, which are tightly packed with RubisCO. Facultative autotrophs, like purple anoxyphototrophs, use the Calvin cycle for fixing CO_2, although they lack the carboxysomes.

Diversification and interactions

The prokaryotes as a group evolved a wide variety of abilities for the processing of substrates, whilst remaining rather specialized as species (e.g. [7]. The nitrogen cycle in Figure 8.5 illustrates this variety, as well as the fact that the products of one group are the substrate of another.

Some of the conversions of inorganic nitrogen species can only be done by a few taxa. The recently discovered anaerobic oxidation of ammonia is only known from the planctobacterium *Brocadia anammoxidans* [505]. None-the-less, it might be responsible for the removal of one-half to one-third of the global nitrogen in the deep oceans [100]. The aerobic oxidation of ammonia to nitrite is only known from *Nitrosomonas*, the oxidation of nitrite into nitrate is only known from *Nitrobacter*; and the fixation of dinitrogen can only be done by a few taxa, such as some cyanobacteria, *Azotobacter*, *Azospirillum*, *Azorhizobium*, *Klebsiella*, *Rhizobium*, and some other ones [531].

The excretion of polysaccharides (carbohydrates) and other organic products by nutrient-limited photosynthesizers (such as cyanobacteria), stimulated heterotrophs to decompose these compounds through the anaerobically operating glycolytic pathway. Thus, other or-

ganisms came to use these excreted species-specific compounds as resources, and a huge biodiversity resulted. Apart from the use of each others products, prokaryotes, such as the proteobacteria *Bdellovibrio* and *Daptobacter*, invented predation on other prokaryotes. When the eukaryotes emerged, many more prokaryote species turned to predation, with transitions to parasitism causing diseases in their eukaryotic hosts. Predators typically have a fully functional metabolism, while parasites use building blocks from the host, reducing their genome with the codes for synthesizing these building blocks. The smallest genomes occur in viruses, which probably evolved from their hosts and are not reduced organisms [195, 543]. Prokaryotic mats on intertidal mud flats and at methane seeps illustrate that the exchange of metabolites between species in a community can be intense [397, 419]. The occurrence of multi-species microbial flocks, such as in sewage treatment plants [66, 64] further illustrates an exchange of metabolites among species. The partners in such syntrophic relationships sometimes live epibiotically, possibly to facilitate exchange. Internalization further enhances such exchange [297]. The gradual transition of substitutable substrate to become complementary is basic to the formation of obligate syntrophic relationships.

Evolution of individual as dynamic system

The evolution of the organism as a dynamic metabolic system can be described in several steps [330], some of them are illustrated in Figure 8.6.

Variable biomass composition

We start with a living (prokaryotic) cell, surrounded by a membrane. Although it remains hard to define what life is exactly, it represents an activity and, therefore, requires energy. The acquisition of energy and (probably several types of) building blocks to synthesize new structure were separated and the first cells suffered from multiple limitations; they could only flourish if all necessary compounds were present at the same time. Initially there were no reserves and hardly any maintenance costs. A cell's chemical composition varied with the availability of the various substrates. As soon as the membranes were rich in lipids (eubacteria) or isoprenoid ethers (archaea), the accumulation of lipophilic compounds could have been rather passive. The occurrence of lipids and isoprenoid ethers among prokaryotes is only easy to understand if the archaea and eubacteria were already separated before these compounds had a role in metabolism. The excretion of waste products was not well organized.

Strong homeostasis

In a stepwise process, the cells gained control over their chemical composition, which became less dependent on chemical variations in the environment. One mechanism is coupling of the uptake and use of different substrates. How uncoupled uptake of supplementary compounds can gradually change into coupled uptake of complementary compounds is discussed in [298]. With increasing homeostasis, stoichiometric restrictions on growth become more stringent; the cells could only grow if all essential compounds were present at the

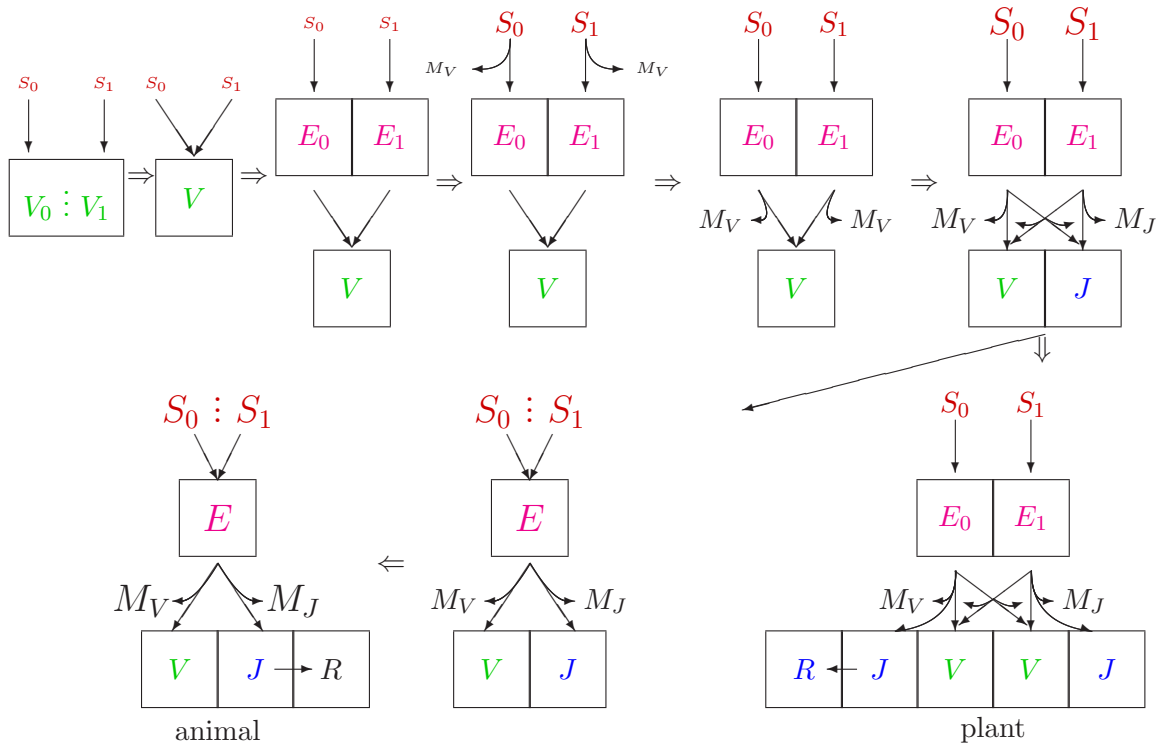

Figure 8.6: Steps in the evolution of the organization of metabolism of organisms. Symbols: S substrate, E reserve, V structure, J maturity, R reproduction, M_V somatic maintenance, M_J maturity maintenance. Only two of several possible types are shown. Font size reflects relative importance. Stacked dots mean sloppy coupling. The top row shows the development of a prokaryotic system, which bifurcated in a plant and an animal line of development. Modified from [330].

same time in the direct environment of the cell. The activity of the cells varied with the environment at a micro-scale, which will typically fluctuate wildly. The reduction in variability of the chemical composition of the cell came with an increased ability to remove waste products, *i.e.* with a process of production of compounds that are released into the environment.

Although the mechanisms of acquiring homeostasis are understood only partially [298], it gradually became more perfect and biomass can be considered as being composed of a single generalized compound called structure. A generalized compound is a mixture of a set of chemical compounds of fixed composition. This (idealized) condition is called strong homeostasis.

Reserves

The increased stoichiometric constraints on growth result in a reduction of possible habitats in which the cell can exist. By internalizing and storing the essential compounds before use, the cells became less dependent on the requirement for all essential compounds to be

present at the same time. In this way, they could smooth out fluctuations in availability at the micro-scale (Figure 8.12). Most substrates are first transported from the environment into the cell across the membrane by carriers before further processing. By reducing the rate of this further processing, storage develops automatically. We will return to this in more detail below. Initially the storage capacity must have been small to avoid osmotic problems, which means that the capacity to process internalized resources is large relative to the capacity to acquire them from the environment. By transforming stored compounds to polymers, these problems could be avoided, and storage capacity could be increased further to smooth out fluctuations more effectively. This can be achieved by increasing the acquisition rate or decreasing the processing rate.

The reason for evolutionary selection toward partitionability might well be in the incremental change in the number of different types of reserves, so in the organizational aspects of metabolism. Partitionability and mergebility are mathematically the same and to some extend probably reversible in evolution. These changes not only occur within individuals, but also during the internalization of symbionts.

Excretion

The DEB reserve dynamics implies that the amount of the most limiting reserve co-varies with growth, and the amounts of non-limiting reserves can or cannot accumulate under conditions of retarded growth, depending on the excretion of mobilized reserve that is not used; excretion is an essential feature of multiple reserve systems to avoid accumulation without boundary. This is because assimilation does not depend on the amount of reserve, so also not on the use of reserve; it only depends on the amount of structure and substrate availability. The excretion process can be seen as an enhanced production process of chemical compounds, but its organization (in terms of the amounts that are excreted under the various conditions) differs from waste production. Waste production is proportional to the source process (assimilation, maintenance, growth). Excretion, on the contrary, reflects an unbalanced availability of resources. The flux is proportional to a fixed fraction of what is rejected by the SU for growth. The theory of SUs quantifies the rejection flux. When the diatom *Pseudonitzschia* becomes silica depleted in an environment that is rich in nitrate, it starts to excrete domoic acids, which drains its nitrogen reserve. Some bacteria produce acetate in environments that are rich in organic compounds, but poor in nutrients, which lowers the pH, which, in turn, has a negative effect on competing species. When only acetates are left, they use these as a substrate.

Empirical evidence has so far [289, Figure 5.5] revealed that the various reserves have the same turnover rate. The reason might be that mobilization of different reserves involves the same biochemical machinery. This possibly explains why the use of *e.g.* stored nitrate follows the same dynamics as that of polymers such as carbohydrates and lipids, although the use of nitrate obviously does not involve monomerization.

Together with waste, excretion products serve an important ecological role as substrate for other organisms [526]. Most notably polysaccharides that are excreted by phototrophs in response to nutrient limitation provide energy and/or carbon substrate for heterotrophs, so they fuel a production process that is known as the microbial loop. Adaptive dynamics

analysis has indicated the importance of syntrophy in evolutionary speciation [114].

Other excretion products are toxic for potential competitors, such as domoic acid produced by the diatom *Pseudonitzschia* spp. in response to nitrogen surplus, which can be highly toxic to a broad spectrum of organisms, including fish. Nitrogen enrichment of the environment by human activity enhances the formation of nitrogen reserves, and so the production of toxicants that contain nitrogen by some algae.

Maintenance

The storing of ions, such as nitrate, creates concentration gradients of compounds across the membrane that have to be maintained. These maintenance costs might originally have been covered by extra-cellular chemoautotrophic transformations, but this requires the presence of particular compounds (*e.g.* to deliver energy). Maintenance can only be met in this way if the organism can survive periods without having to meet such costs, *i.e.* facultative rather than obligatory maintenance. Most maintenance costs are obligatory, however. The next step is to pay the maintenance costs from reserves that are used for energy generation to fuel anabolic work and thus to become less dependent on the local presence of chemoautotrophic substrates. Although extreme starvation, causing exhaustion of reserves, can still affect the ability to meet maintenance costs (see Appendix A.3), such problems will occur much less frequently.

Maintenance requirements were increased further and became less facultative in a number of steps, which we will discuss briefly.

Carriers and regulation

Originally carriers (which transport substrate from the environment into the cell across the membrane) were less substrate-specific and less efficient, meaning that the cell required relatively high concentrations of substrate. The cell increased the range of habitats in which it could exist by using carriers that are not fully structurally stable, meaning that a high-efficiency machinery changes to low efficiency autonomously. The maintenance of a high efficiency involves a turnover of carriers.

High-performance carriers are also more substrate-specific, which introduces a requirement for regulation of their synthesis and for adaptation to substrate availability in the local environment. The expression of genes coding for the carriers of various substitutable substrates becomes linked to the workload of the carriers. The principle that allocation occurs according to relative workload seems to be general and conserved; we will discuss it again in allocation to organs in relation to multicellular eukaryotes.

Turnover of structure

Not only carriers, but many chemical compounds (especially proteins with enzymatic functions) suffer from spontaneous changes that hamper cellular functions. The turnover of these compounds, *i.e.* breakdown and re-synthesis from simple metabolites, restores their functionality [354], but increases maintenance requirements. This mixture of conversion machineries with high and low efficiencies is present in structure and so, due to turnover, to

maintenance, it is converted into structure with high-efficiency machinery. The biochemical aspects of the process are reviewed in [233].

These increased requirements made it even more important to use reserves, rather than unpredictable external resources to cover them. When such reserves do not suffice, maintenance costs are met from structure, and cells shrink. Paying maintenance from structure is less efficient than from reserve directly, because it involves an extra transformation (namely from reserve to structure). The preference for reserve as the substrate rather than structure, would have been weak originally, later becoming stronger. Since the turnover rate of compounds in structure depends on the type of compound (some rates are possibly very low), the metabolites derived from these compounds do not necessarily cover all metabolic needs.

The waste (linked to maintenance and the overhead of growth) and the excreted reserves (linked to stoichiometric restrictions on growth due to homeostasis) serve as substrates for other organisms, so life becomes increasingly dependent on other forms of life even at an early stage. Some of these products were transformed into toxins that suppress competition for nutrients by other species.

Defense systems

The invasion of (micro)habitats where toxic compounds are present, and the production of toxic waste and excretion products by other organisms, required the installation of defense systems, which increase maintenance costs. Prokaryotes developed a diverse family of defense proteins, called bacteriocins [486]. Phototrophy requires protection against UV radiation and these two systems must have been evolved simultaneously [110]. Phototrophy possibly evolved from UV protection systems [454], although it is unlikely that it appeared at the start of evolution, as some authors suggest [585, 86, 189, 52, 53]. The pathways for anaerobic methane oxidation and methanogenesis possibly evolved from a detoxicifation system for formaldehyde; this is another illustration of a change in function of a protection system. A general-purpose protection system against toxic compounds consists of proteins that encapsulate toxic molecules. Another general system is to transform lipophilic compounds into more hydrophilic (and so more toxic) ones to enhance excretion. The development of a complex double cell membrane in the didermata (Gram-negative eubacteria) was possibly a response to the excretion of toxic products by other bacteria [171], although the outer membrane is not a typical diffusion barrier [353]. When dioxygen first occurred in the environment as a waste product of oxygenic photosynthesis, it must have been toxic to most organisms [111, 341]; the present core position of carbohydrates in the central metabolism of eukaryotes and its use in energy storage is directly linked to this waste product. The reactive oxygen species (ROS) play an important role in ageing [346], and induced the development of defense systems using peroxidase dismutases to fight their effects. While eukaryotes learned not only to protect themselves against dioxygen, but even make good use of it, they became vulnerable for hydrogen sulphide that is excreted by anearobically photosynthesysing green and purple sulphur bacteria. Biomarkers (isorenieratene) from these bacteria suggest that the great mass extinctions of the Permian, Devonian and Triassic are linked to the toxic effects of hydrogen sulphide and the lack of

dioxygen [577, 168]. Viruses probably arose early in the evolution of life, and necessitated specialized defense systems that dealt with them. These defense systems further increased maintenance costs.

Increase of reserve capacity

Substrate concentration in the environment is not constant, which poses a problem if there is a continuous need to cover maintenance costs. An increase in maintenance costs therefore requires increased storage capacity in order to avoid situations in which maintenance costs cannot be met. The solution is to further delay the conversion of substrate metabolites to structure, creating a pool of intermediary metabolites. The optimal capacity depends on the variability of substrate availability in the environment and (somatic) maintenance needs. Transformation to polymers (proteins, carbohydrates) and lipids will reduce concentration gradients and osmotic problems, and thus maintenance costs, but involves machinery to perform polymerization and monomerization. The development of vacuoles allows spatial separation of ions and cytoplasm to counter osmotic problems. One example is the storage of nitrate in vacuoles of the colourless sulphur bacteria *Thioploca* spp. [220], which use it to oxidize sulphides first to sulphur, for intracellular storage, and then to sulphate for excretion together with ammonium [433]. Cyanobacteria only develop vacuoles at low pH [595]. Organelles like acidocalcisomes also play a role in the storage of cations [113].

A further step to guarantee that obligatory maintenance costs can be met is to catabolize structure. This is inefficient and involves further waste production (so requiring advanced excretion mechanisms), but at least it allows the organism to survive lean periods.

Reserves can contribute considerably to the variability of biomass composition; phytoplankton composition greatly affects the rate at which phytoplankton bind atmospheric carbon dioxide and transport carbon to deep waters [428], known as the biological carbon pump. The activity of the biological carbon pump strongly influences climate.

Morphological control on metabolism

Morphology will influence metabolism for several reasons: assimilation rate is proportional to surface area, maintenance rate to volume and catabolic rate to the ratio of surface area and volume. This means that surface-area-volume relationships are central to metabolic rates. The shape of the growth curve (and so the timing of developmental events) is directly related to the changes in morphology of the cell.

κ-rule and the emergence of cell cycles

Control on morphology and cell size will increase stepwise. Initially the size at division would be highly variable among cells. This variance will be decreased by the installation of a maturation process, where division is initiated as soon as the investment in maturation exceeds a threshold level. This state of maturity creates maturity maintenance costs. Allocation to this maturation program is a fixed fraction $1 - \kappa$ of the catabolic flux, gradually increasing from zero. Such an allocation is only simple to achieve if the catabolic

flux does not depend on the details of allocation. If the SUs for maturation operate similar to those for somatic maintenance and growth, the fraction κ is constant and depends on the relative abundance and affinity of the maturation SUs.

The metabolic relevance of cell size is in membrane-cytoplasm interactions; many catalyzing enzymes are only active when bound to membranes [24], and cellular compartmentalization affects morphology and metabolism. The turnover of reserve decreases with a length measure for an isomorphic cell, which comes with the need to reset cell size. Apart from the increase of residence time of compounds in the reserve with a length measure, the cell's surface area to volume ratio decreases with increasing cell size, as does the growth potential. The increase in metabolic performance requires an increase in the amount of DNA and in the time spent on DNA duplication. The trigger for DNA duplication is given when investment into maturation exceeds a given threshold, meaning that a large amount of DNA leads to large cell sizes at division. Prokaryotes partly solved this problem by telescoping generations (DNA duplication is initiated before the previous duplication cycle is completed) and by deleting unused DNA [538].

The existence of a maturity investment threshold can be deduced phenomenologically. If the specific maturity maintenance costs $[\dot{p}_J]$ relates to the somatic maintenance costs $[\dot{p}_M]$ as $[\dot{p}_J] = [\dot{p}_M]\frac{1-\kappa}{\kappa}$, the threshold is exceeded if the amount of structure exceeds a threshold; κ represents the fraction of the utilized reserve that is allocated to somatic maintenance plus growth. For all other values of $[\dot{p}_J]$, the amount of structure at the transition depends on the nutritional history. This argument can be used in reverse to estimate the specific maturity maintenance costs from size-at-transition data. If the cells are separated at the two-cell stage of the embryo sea urchin *Strongylocentrotus droebachiensis*, the embryonic period is hardly affected, but the size at the transition to the larval stage is halved [187]. Thus it is possible to manipulate the threshold value experimentally, meaning that its biochemical identification is within reach.

Reduction of number of reserves

Many eukaryotes started feeding on dead or living biomass with a chemical composition similar to themselves. This co-variation in time of all required metabolites for growth removed the necessity to deal with each of those reserves independently. By linking the uptake of various metabolites, the various reserves co-vary fully in time because their turnover times are equal, as was discussed above. This improved homeostasis, and allowed further optimization of enzyme performance.

From an organization point of view, reserves play a key role in product formation. If biomass would have a constant composition (so no reserve), one of the three basic (energy) fluxes of assimilation, maintenance and growth would follow from two of them plus the mass balance. Reserve provides the degree of freedom that is essential to uncouple the three energy fluxes, meaning that all products in single reserve - single structure systems can be written as a weighted sum of these three energy fluxes. These products include water, carbon dioxide, nitrogen waste, faeces, but also products that remain useful to the individual like chitin (in fungi), cellulose and wood (in plants) and carbonates (in corals). These products differ from biomass by not requiring maintenance, which is why

for example fungi, like trees, have low maintenance costs when expressed on the basis of total dry weight. Non-limiting resources, such as dioxygen in aerobic environments, and heat also follow these kinetics. This explains why indirect calorimetry is successful, where dissipating heat is taken to be a weighted sum of the dioxygen, carbon dioxide and nitrogen waste fluxes. The κ-rule means that new allocation destinies (maturity maintenance and maturation or reproduction) do not affect the simple rule that all mass and heat fluxes are weighted sums of the three basic fluxes if we extend the maintenance flux to include the collection of transformations that do not relate to synthesis of biomass.

Syntrophy and compartmentalization.

The evolution of central metabolism testifies from its syntrophic origins [316, 330]. Its possible prokaryotic start is summarized in Figure 8.4. The examples of contemporary models [360, 491] illustrate that the metabolic systems themselves are not hypothetical, but the evolutionary links between these systems obviously are. This is not meant to imply, however, that the taxa also would have these evolutionary links. Some species of *Methanococcus* have most genes of the glycolysis; *Thermoproteus* possesses a variant of the reversible Embden-Meyerhof-Parnas and the Entner-Douderoff pathways; *Sulfolobus* has oxidative phosphorylation. These contemporary models are not just evolutionary relicts; the picture is rather complex.

Some important features are that heterotrophy evolved from phototrophy, which itself evolved from lithotrophy, and that all cycles in the central metabolism of typical modern heterotrophs ran in the opposite direction in the evolutionary past.

This reconstruction suggests that lateral gene exchange between eubacteria and archaea occurred during the evolution of central metabolism. Initially cells could exchange RNA and early strands of DNA relatively easily [587]; restrictions on exchange became more stringent with increasing metabolic complexity. Many authors suggest that considerable lateral gene exchange occurs in extant prokaryotes [386, 171, 331, 377] by conjugation, plasmids and viruses [543].

While prokaryotes passed metabolic properties from one taxon to another by lateral exchange of genes, eukaryotes specialized in symbiotic relationships and even internalization of whole organisms to acquire new metabolic properties.

Mitochondria

The problem of the origins of mitochondria is not fully resolved. Part of the problem is that mitochondria and hosts exchanged quite a few genes, and the genome of mitochondria reduced considerably, down to 1% of its original bacterial genome [141]. The mitochondrial DNA in kinetoplasts, however, is amplified and can form a network of catenated circular molecules [344]. Mitochondria probably evolved from an α-group purple bacterium [13] in an archaean [376, 379, 21]. However, arguments exist for the existence of mitobionts in the remote past [398], from which mitochondria and prokaryotes developed; the mitobionts differentiated before they associated with various groups of eukaryotes. The amitochondriate pelobiont *Pelomyxa palustris* has intracellular methanogenic bacteria that may have com-

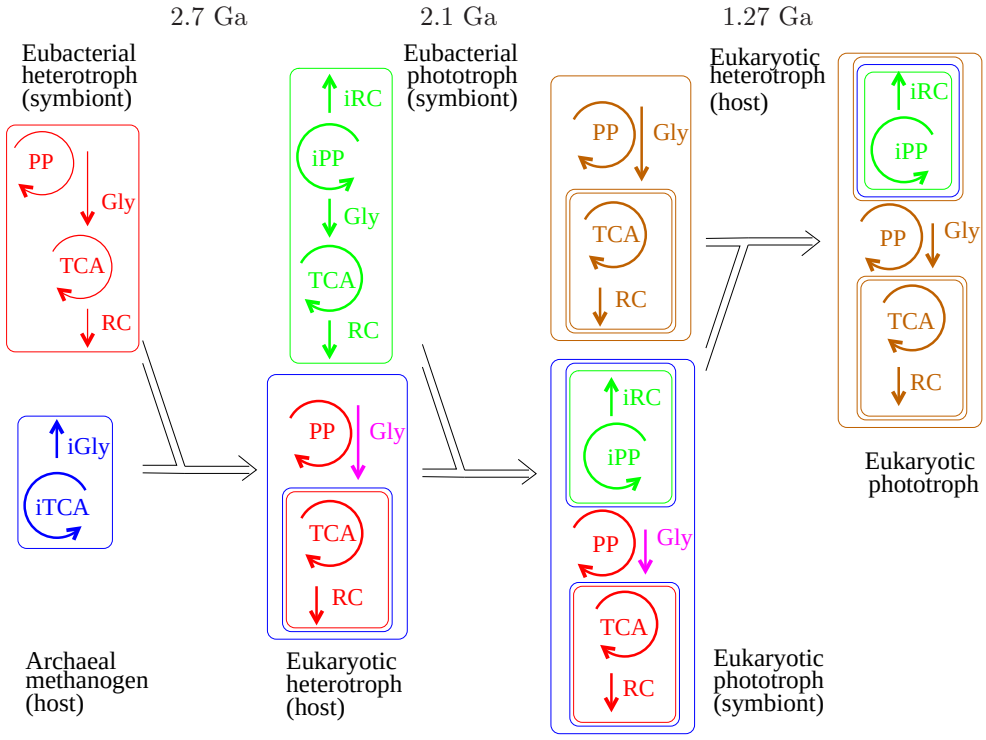

Figure 8.7: Scheme of symbiogenesis events; the first two primary inclusions of prokaryotes (to become mitochondria and chloroplasts respectively), were followed by secondary and tertiary inclusions of eukaryotes. Each inclusion comes with a transfer of metabolic functions to the host. The loss of endosymbionts is not illustrated. See Figure 8.4 for definitions of the modules of central metabolism and for the ancestors of mitochondria and chloroplasts. The outer membrane of the mitochondria is derived from the endosymbiont, and that of the chloroplasts from the host; mitochondria were internalized *via* membrane rupture, chloroplasts *via* phagocytosis. Modified from [316]. The scheme explains why all eukaryotes have heterotrophic capabilities.

parable functions. Other members of the α-group of purple bacteria, such as *Agrobacterium* and *Rhizobium* can also live inside cells and function sport dinitrogen fixation. *Rickettias* became parasites, using their host building blocks and reducing their own genome to viral proportions.

It is now widely accepted that all eukaryotes have or once had mitochondria [490, 171, 228, 134, 521, 533]. Their internalization marks the origin of the eukaryotes, which is possibly some 1.5 Ga [237] or 2.0 Ga [476] or 2.7 Ga [70] ago. In fact the eukaryotes may have emerged from the internalization of a fermenting, facultative anaerobic H_2- and CO_2-producing eubacterium into an autotrophic, obligatory anaerobic H_2- and CO_2-consuming methanogenic archaean [376], the host possibly returning organic metabolites. Once the H_2-production and consumption had been cut out of the metabolism, aerobic environments became available, where the respiratory chain of the symbiont kept the dioxygen concentration in the hosts cytoplasm at very low levels. The internalization of (pro)mitochondria might be a response to counter the toxic effects of dioxygen. This hypothesis for the origin

of eukaryotes explains why the DNA replication and repair proteins of eukaryotes resemble that of archaea, and not that of eubacteria. Notice that the eukaryotization, as schematized in Figure 8.7, just represents a recombination and compartmentation of existing modules of the central metabolism (cf Figure 8.4). Syntrophic associations between methanogens and hydrogenosomes are still abundant; ciliates can have methanogens as endosymbionts and interact in the exchange [142].

The penetration of mitochondria into its host required membrane rupture and healing, without causing cell death. The predatory bacterium *Daptobacter* can penetrate the cytoplasm of its bacterial prey *Chromatium*. This may be analogous to early events in the symbiotic acquisition of cell organelles [170]. The outer membrane of the double membrane around mitochondria might be of negibacterial origin [86], which supports the rupture interpretation. At least one example exists of prokaryotic endosymbiosis (β-proteobacteria that harbour γ-proteobacteria [115]) in absence of phagocytosis. More examples exist of penetration through the membrane without killing the victim instantaneously (e.g. [170]. His present view, shared by others, is that it happened only once and the logical implication is just in a single individual. If phagocytosis would have been well established prior to the entry of a mitochondrion, it is hard to understand why it did not occur more frequently.

The non-lethal penetration that has lead to mitochondria possibly occurred once only, which explains the metabolic similarity among all eukaryotes, compared to the diversity among prokaryotes. Since opisthokonts were the first to branch, and animals probably first appeared in the sea, this internalization event presumably occurred in a marine environment. The fungi, notably the chytrids, diverged from the animals (unicellular relatives of the choanoflagellates) some 0.9 - 1.6 Ga ago [546]. In view of the biology of modern nucleariids and chytrids, this might have occurred in a freshwater environment. This evolutionary origin mitochondria illustrates the narrow borderline between parasitic and symbiotic relationships.

The shape of the cristae of mitochondria is nowadays an important criterion in tracing the evolutionary relationships among protists [438], which points to a slow intracellular evolution. Hydrogenosomes are generally thought to have evolved from mitochondria in anaerobic or micro-aerobic environments. As testified by the presence of mitochondrion-derived genes, some parasitic or commensal groups (entamoebidae, microsporidia, diplomonads, parabasalia, some rumen chytrids, several groups of ciliates) lost their mitochondria [490]. Such genes have not been found (yet) in the amitochondriate oxymonads, retortamonads, *Postgaardi* and *Psalteriomonas*. The absence of mitochondria is perhaps primitive in the pelobionts and the free-living *Trimastrix* [438]. Other organelles, such as peroxysomes and glyoxisomes, probably also have endosymbiotic origins [86, 226]; they follow a growth and fission pattern that is only loosely coupled to the cell cycle. Organelles such as centrioles, undulipodia, and the nuclear membrane, possibly have an endosymbiotic origin [373], but others oppose this point of view.

Membrane plasticity

No prokaryote seems to be able to form vesicles, while membrane transport (including phagocytosis and pinocytosis, vesicle mediated transport) is basic in eukaryotes [125, 169],

and essential for endosymbiotic relationships. Eukaryotes also have ATP-fueled cytoplasmatic mobility driven by myosin and dynein.

The absence of phagocytosis or pinocytosis in prokaryotes has been used as argument in favour of an independent origin of prokaryotes and eukaryotes [86, 586]. The protein clathrin plays a key role in membrane invagination, and is not known in prokaryotes. Similarities in the DNA and RNA code and in the whole biochemical and metabolic organization of prokaryotes and eukaryotes suggest an evolutionary link. Cavalier-Smith [86, 90] argued that eukaryotes descend from some actinobacterium that engulfed a phototrophic posibacterium (an (-proteobacterium) as mitochondrion, which later lost phototrophy, and used it as a slave to produce ATP. The ability to phagotize is central to his reasoning. Actomyosin mediates phagocytosis and actinobacteria have proteins somewhat related to myosin, although they do not phagotize. If he is right that the outer membrane of mitochondria is derived from the original posibacterium, and not from the host, there is little need for the existence of phagocytosis prior to the entry of a posibacterium to become a mitochondrion. Bell [32, 33] proposed that a lysogenic pox-like DNA virus introduced clatrine-like proteins in an archaean that promoted membrane plasticity. This option also helps to understand the origins of the nuclear membrane, of linear chromosomes with short telometic repeats, of capped mRNA and to extrude it across the viral membrane into the cytoplasm. Virusses might have evolved early [149, 150].

The subsequent development of membrane plasticity has been a major evolutionary step, that allowed phagocytosis; cells no longer needed to excrete enzymes to split large molecules of substrate into smaller metabolites for uptake with low efficiency, but digestion could be carried out intracellularly, avoiding waste and the necessity for cooperative feeding. Fungi possibly never developed this ability and animals evolved from fungi [377] suggesting that the animal lineage developed phagocytosis independently. Recent phylogenetic studies [535] place the phagocytotic nucleariids at the base of the fungi, however, suggesting that the fungi lost phagocytosis, and that it only developed once. Most animals also excrete enzymes (like their fungal sisters), but since this is in the gut environment, most metabolites arrive at the gut epithelium for uptake. Plantae (glaucophytes, rhodophytes and chlorophytes) gave up phagocytosis, but chromophytes, which received their plastids in the form of rhodophytes, still sport active phagocytosis [10] despite their acquired phototrophic abilities. Phagocytosis allowed the more efficient use of living and dead organisms as a resource. Scavenging, predation and new forms of endosymbioses became widespread.

We are beginning to understand the evolutionary roots of cell motility [44], including changes in shape in response to environmental stimuli, and extension of protrusions like lamellipodia and filopodia to allow particles to be enclosed in a phagocytotic cup, which is based on the spatially controlled polymerization of actin. The eubacterial pathogens *Listeria monocytogenes* and *Shigella flexneri* exhibit actin-based movement in the host cytoplasm [435]. Actin and tubulin have also been isolated from the togobacterium *Thermatoga maritimum* [136]; apart from their role in motility, these proteins also play a key role in the cytoskeleton of eukaryotes, which is used by transporters for the allocation of metabolites to particular destinations. All eukaryotic cytoskeleton elements are presently known from prokaryotes [167].

The evolution of membrane plasticity must have taken place in a time window of some

700 Ma, since biomarker data suggest that the first eukaryotic cells appeared around 2.7 Ga [70] ago (around the time cyanobacteria evolved).

Before the arrival of plastids, eukaryotes were heterotrophic. Cyanobacteria are mixotrophic, which makes it likely that their plastids before internalization were mixotrophs as well. Very few, if any, eukaryotes with plastids became fully specialized on phototrophy, remaining mixotrophic to some extent. Theoretical studies show that the spontaneous evolutionary specialization of mixotrophs into organo- and phototrophs is difficult in spatially homogeneous environments [559]. In spatially heterogeneous environments, however, such as in the water column where light extinction favours phototrophy at the surface and heterotrophy at the bottom, such specialization is relatively easy [558].

Membrane plasticity had a huge impact on cellular organization. The presence of vacuoles increased the capacity to store nutrients [351], and vesicle-mediated intracellular transport reorganized metabolism [125]. By further improving intracellular transport using the endoplasmatic reticulum and further increasing storage capacity, cells could grow bigger and be more motile. Bigger size favours increased metabolic memory, and increased motility allows the organism to search for favourable sites. The eukaryotic endoplasmatic reticulum, build of actin and tubulin networks has a precursor in prokaryotes in the form of MreB proteins [136], so also here, we see gradual improvement.

Plastids

Long after the origin of mitochondria some cyanobacteria evolved into plastids[372, 545], which made phototrophy available for eukaryotes. Like that of mitochondria, this internalization event possibly occurred only once in eukaryotic history [105, 387, 90, 591, 106, 489], see Figure 8.7, but this is controversial [536].

Sequence data suggest that glaucophytes received the first plastids, and that rhodophytes evolved from them some 2.0 Ga [503, 544] ago (or 1.2 Ga according to [237]), while chlorophytes (including plants) diverged from rhodophytes 1.5 Ga ago. The glaucophytes have a poor fossil record, and now consist of a few freshwater species. Where the plastids of glaucophytes retained most of their genome and properties, whereas that of rhodophytes and chlorophytes became progressively reduced by transfer of thousands of genes to the nucleus [378] and by gene loss.

The present occurrence of glaucophytes weakly suggests that the internalization of a plastid occurred in a freshwater environment. The rhodophytes have their greatest diversity in the sea, and most of their hosts (that possess rhodophyte-derived chloroplasts) are most diverse in the sea, while chlorophytes and their hosts are most diverse in fresh waters. So the habitat in which the internalization occurred is uncertain.

The secondary endosymbiosis event that seeded the chromophytes was some 1.3 Ga ago [592] (see Figure 8.7). Rhodophytes became integrated into heterokonts, haptophytes and cryptophytes, while chlorophytes became integrated into euglenophytes and chlorarachniophytes; heterokonts and haptophytes became integrated into dinoflagellates, which themselves (especially *Gymnodinium adriaticum*) engaged into endosymbiotic relationships with animals (corals, other cnidarians and molluscs). Alveolates, to which dinoflagellates, ciliates and sporozoans belong, generally specialized in kleptoplastides (i.e. functional plastids

that are acquired by feeding). The presence of plastids in the parasitic kinetoplastids and of cyanobacterial genes in the heterotrophic percolozoans (= *Heterolobosea*) suggests that secondary endosymbiosis did not take place in the euglenoids, but much earlier in the common ancestor of all excavates, where chloroplasts became lost in the percolozoans [12]. Apart from dinoflagellates, cryptophytes (especially *Chrysidiella*) and diatoms engaged in endosymbiotic relationships with radiolarians and foraminiferans, and chlorophytes did so with animals (sponges, *Hydra*, rotifers and *Platyhelminthes*). Intracellular chloroplast populations seem to behave more dynamically in kleptomanic and endosymbiotic relationships [537], compared to fully integrated systems. The coupling of the dynamics of the subsystems can be tight as well as less tight.

Vacuoles and cell structures

Apart from membrane plasticity and organelles, a property unknown in prokaryotes is the vacuole [351], which is used for storing nutrients in ionic form and carbohydrates; sucrose, a precursor of many other soluble carbohydrates, typically occurs in vacuoles. This organelle probably evolved to solve osmotic problems that came with storing substrates. The storage of water in vacuoles allowed plants to invade the terrestrial environment; almost all other organisms depend on plants in this environment. The DEB theory predicts that the storage capacity of energy and building-blocks scales with volumetric length to the power of four; since eukaryotic cells are generally larger than prokaryotic ones, storage becomes more important to them. Diatoms typically have extremely large vacuoles, which occupy more than 95% of the cell volume, allowing for a very large surface area (the outer membrane, where the carriers for nutrient uptake are located), relative to their structural mass that requires maintenance. In some species, the large chloroplast wraps around the vacuole like a blanket. Since, according to the DEB theory, reserve does not require maintenance, the large ratio of surface area to structural volume explains why diatoms are ecologically so successful, and also why they are the first group of phytoplankton to appear each spring. Archaea and posibacteria do have gas vacuoles, but their function is totally different from that of eukaryotic vacuoles.

The Golgi apparatus, a special set of flat, staked vesicles, called dictyosomes, develops after cell division from the endoplasmatic reticulum. They appear and disappear repeatedly in the amitochondriate metamonad *Giardia*. The nuclear envelope can disappear in part of the cell cycle in some eukaryotic taxa and it is also formed by the endoplasmatic reticulum. The amitochondriate parabasalid *Trichomonas* does not have a nuclear envelope, while the planctobacterium *Gemmata oscuriglobus* has one. The possession of a nucleus itself is therefore not a basic requisite distinguishing between prokaryotes and eukaryotes. The situation is quite a bit more complex than molecular biology textbooks suggest.; e.g. the macronuclei (sometimes more than one) in ciliates are involved in metabolism, while the micronuclei deal with sexual recombination. Although some prokaryotic cells, such as the planctobacteria, are packed with membranes, eukaryotic cells are generally more compartmentalized, both morphologically and functionally. Compounds can be essential in one compartment, and toxic in another [380]. Eukaryotic cilia differ in structure from the prokaryotic flagella, and are therefore called undulipodia to underline the difference [372].

The microtubular cytoskeleton of eukaryotes is possibly derived from protein constricting the prokaryotic cell membrane during fission, as both use the protein tubulin [136].

Genome organization

The organization of the genome in chromosomes, with a spindle machinery for genome allocation to daughter cells, enhanced the efficiency of cell propagation by reducing the time needed to duplicate DNA [94], and harnessed plastids, whose duplication is only loosely coupled to the cell cycle in prokaryotes. Since animals such as the ant *Myrmecia croslandi* and the nematode *Parascaris univalens* have only a single chromosome [241], acceleration of DNA duplication is not always vital. It allows more efficient methods of silencing viruses, by changing their genome and incorporating it into that of the host (half of eukaryotic "junk DNA" consists of these silenced viral genomes). Eukaryotes had to solve the problem of how to couple the duplication cycles of their nuclear genome and that of their mitochondria and chloroplasts. Dynamin-related guanosine triphosphatases (GTPases) seem to play a role in this synchronization [432]. The nuclear membrane of eukaryotes and planctomycetes possibly allows a better separation of the regulation tasks of gene activity and cellular metabolism by compartmentalization, which might have been essential to the development of advanced gene regulation mechanisms.

Chromosomes are linked to the evolution of reproduction, which includes cell-to-cell recognition, sexuality and mating systems. Moreover, many eukaryotes have haploid as well as diploid life stages, and two or more (fungi, rhodophytes) sexes [230]. Although reproduction may seem to have little relevance to metabolism at the level of the individual, metabolic rates at the population level depend on the amount of biomass and, hence, on rates of propagation. Eukaryotes also have a unique DNA topoisomerase I, which is not related to type II topoisomerase of the archaea [151], which further questions their origins.

Despite all their properties, the eukaryotic genome size can be small; the genome size of the acidophilic rhodophyte *Cyanidoschyzon* is 8 Mbp, only double the genome size of *E. coli* [94]; the chlorophyte *Ostreococcus tauri* has a genome of only 10 Mbp, and the yeast *Saccaromyces cerivisiae* of 12 Mbp [108]. Typical eukaryotic genome sizes are much larger than that of prokaryotes however. Apart from silencing of viruses, most of this extension relates to gene regulation functions that are inherent to cell differentiation and the evolution of life stages.

Merging of individuals in steps

Collaboration in the form of symbioses based on reciprocal syntrophy is basic to biodiversity, and probably to the existence of life [1, 105, 118, 119, 478, 525]. The merging of two independent populations of heterotrophs and autotrophs into a single population of mixotrophs occurred frequently in evolutionary history [477, 548]. This process is known as symbiogenesis [373] and is here discussed following [298].

Endosymbiotic relationships are not always stable on an evolutionary time scale. All of the algal groups have colourless representatives, which imply that they are heterotrophic. Many species with chloroplasts are known to have heterotrophic abilities as well, which

classify them as mixotrophs. Half of the species of dinoflagellates, for instance, do not have chloroplasts, probably due to evolutionary loss [87]. The integration is a step-wise process, where plastids' genome size is reduced by gene loss, substitution and transfer to the hosts' genome, possibly to economize metabolism [86]. Chloroplasts of chlorophytes have a typical genome size of 100 genes, but the genome sizes of chloroplasts of rhodophytes and glaucocystophytes are substantially larger. The chloroplasts of cryptophytes and chlorarachniophytes still contain a nucleomorph with some chromosomes [371], believed to be derived from their earlier rhodophyte and chlorophyte hosts. The endosymbionts of radiolarians, foraminiferans and animals maintained their full genome. The tightness of the integration is, therefore, reflected at the genome level.

Generally little is known about the population dynamics of intracellular organelles [432]. Mitochondria constitute some 20% of the volume of mammalian cells, but this varies per tissue and individuals' condition. Their number per cell varies between 1000 and 1600 in human liver cells, 500 and 750 in rat myoblasts, some 80 in rabbit peritoneal macrophages, and 1 in mammalian sperm cells [36]. In the case of a single mitochondrion, the growth and division of the mitochondrion must be tightly linked to that of the cell, but generally the dynamics of mitochondria is complex and best described by stochastic models [49]. Mitochondria crawl around in eukaryotic cells [36] and can fuse, resulting in a smaller number of larger mitochondria, and can even form a network, as observed in gametes of the green alga *Chlamydomonas*, for instance. In yeast and many unicellular chlorophytes, a single giant mitochondrion alternates cyclically with numerous small mitochondria. Moreover, the host cell can kill mitochondria and lysosomes can decompose the remains. Likewise, chloroplasts can move through the cell, sometimes in a coordinated way. Chloroplasts can transform reversibly into non-green plastids (proplastids, etioplastids and storage plastids) with other cellular functions.

Apart from changes in numbers, plastids can change in function as well. They can reversibly lose their chlorophyll and fulfill non-photosynthetic tasks, which are permanent in the kinetoplasts (e.g. the endoparasite *Tripanosoma*) and in heterotrophic plants (*Petrosaviacea*, *Triurdaceae*, some *Orchidaceae*, *Burmanniaceae*, the prothallium-stage of lycopods and ophioglossids, the thalloid liverwort *Cryptothallus mirabilis* [456, p377]), in parasitic plants (*Lennoaceae*, *Mitrastemonaceae*, *Cytinaceae*, *Hydnoraceae*, *Apodanthaceae*, *Cynomoriaceae*, *Orobanchaceae*, *Rafflesiaceae*, *Balanophoraceae*, some *Convolvulaceae*), and in predatory plants (some *Lentibulariaceae*), for instance. This list of exclusively heterotrophic plants suggests that heterotrophy might be more important among plants than is generally recognized.

The evolution of organelles strongly suggests an increasingly strong coupling between species that were once more independent. This places eukaryotic cellular physiology firmly in an ecological perspective, and motivates the application of ecological methods to subcellular regulation problems. This mutually dependent dynamics is the focus of the present review, and includes that of intracellular parasites.

The physiological basis of endosymbiosis is probably always reciprocal syntrophy, where each species uses the products of the other species. The classic example is a heterotroph-alga/chloroplast symbiosis. The heterotroph feeds on nitrogen-containing organic sources (such as animal prey by corals) and produces ammonia as a waste product; the alga or

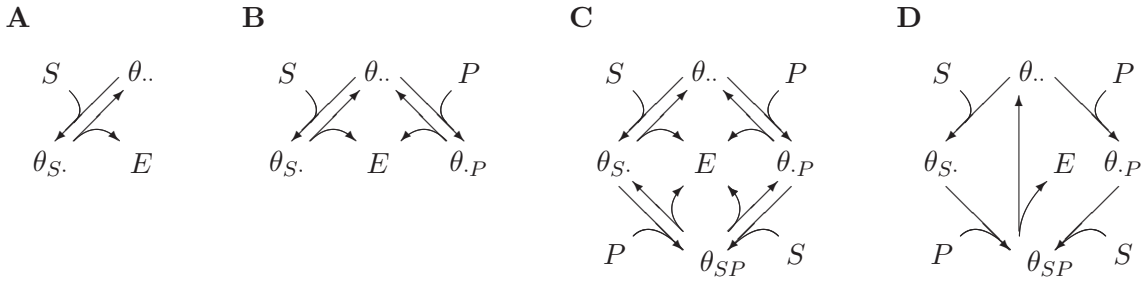

Figure 8.8: The evolution of the transformation from substrate S, and later also from product P, into reserve E. The interaction of substrate and product in the transformation to reserve evolved from sequential-substitutable (B), *via* parallel-substitutable (C), to parallel-supplementary (D). The symbol θ represents a synthesizing unit (SU) that is free $\theta_{..}$, bound to the substrate $\theta_{S.}$, to the product $\theta_{.P}$, or to both θ_{SP}.

chloroplast requires light and carbon dioxide and produces carbohydrates as a waste product (especially if its growth is nutrient limited) [412, 413, 414]; ammonia-carbohydrate exchange forms the basis of the symbiosis. Mitochondria receive pyruvate, FAD, GDP, P, and NAD from the cytoplasm, and return FADH, GTP, NADH and intermediary metabolites from the Krebs cycle. One-way syntrophy, where one species uses the product of the other, but not *vice versa*, is here treated as a special case of reciprocal syntrophy.

This focus on metabolic aspects of symbioses is not meant to imply that other aspects are unimportant. An intriguing example is the α proteobacterial symbiont *Wolbachia* of *Ecdysozoa* (including arthropods and nematodes), which affects sex determination [92, 218, 405, 581]. Other well-known examples are animal symbionts of plants, which promote pollination and seed dispersal. Symbioses on the basis of a mixture of syntrophic and non-metabolic relationships also exist: the Latin-American tree *Cecropia* stores glycogen in specialized plastids in tissue, which is eaten by ants that furiously attack anything that touches the tree.

Starting from two free-living populations in the same environment that follow the DEB rules, eight steps of reductions of degrees of freedom can be delineated to arrive at a fully integrated endosymbiotic system that can be treated as a single population for all practical purposes and again follow the DEB rules. All those steps in the asymptotic behaviour of the populations can be made on an incremental basis, i.e. by a continuous and incremental change in (some) parameter values. The general idea is that the parameter values are under evolutionary control. Figure 8.13 illustrates some of the steps.

1 Reciprocal syntrophy

Originally two species coexist by living on a different substrate each, so they initially might have little interaction and just happen to live in the same environment. Each species excretes products in a well-mixed environment. A weak form of interaction starts when the products are used by the other species as a substitutable compound for their own substrate, a situation which we can call reciprocal syntrophy. Gradually the nutritional nature of the product changes with respect to the substrate from substitutable to supplementary,

and the two species become involved in an obligatory symbiotic relationship; they can no longer live independently of each other; see Figure 8.8. The mechanism can be that the partners' product is a metabolite of an organism's own substrate; eventually the metabolic pathway for that metabolite becomes suppressed and later deleted [538]. A well-known example is the human inability to synthesize vitamin C, which is generally interpreted as an adaptation to fruit eating; the genes for coding vitamin C synthesis are still present in the human genome, but they are not expressed. The theory behind the uptake of compounds that make a gradual transition from being substitutable to supplementary is discussed in [64], together with tests against experimental data on co-metabolism.

Figure 8.9 gives the steady-state amounts of structures of hosts and symbionts as functions of the throughput rate of the chemostat for the various steps in symbiogenesis. The throughput rate equals the specific growth rate at steady-state. The maximum throughput rate is less than the potential maximum growth rate; equality only holds for infinitely high concentrations of substrate in the inflowing medium. The amounts of structures are zero at a throughput rate of zero because of maintenance; the curves for the Monod and Droop models would decrease monotonously. At step 0, where substrates are substitutable to products, the introduction of the partner enhances growth. This is clearly visible in the curve for the host around the maximum throughput rate for the symbiont. Growth stimulation also occurs for the symbiont, of course, but this is less visible in the figure since the host is always present when the symbiont is present with this parameter setting; without the host, the biomass and the maximum throughput rate of the symbiont would be less. The maximum throughput rates for hosts and symbionts can differ as long as substrate and products are substitutable, but not if they are supplementary (steps 1 to 6). The amounts of structures then can't decrease gradually to zero for increasingly high growth rates (steps 1 to 5), because product formation, and thus product concentration, will then also decrease gradually to zero, while the equally rapid growing partner needs a lot of product. Figure 8.9 also shows that the transition from substitutable to supplementary products (from step 1 to 2) comes with a substantial reduction in the maximum growth rate if no other mechanism ensures an easy access to the products; the concentration of products in a well-mixed environment is very low. It is therefore likely that this transition is simultaneous with rather than prior to subsequent steps in symbiogenesis (i.e. spatial clustering, so spatial structure). We will return to this point later.

Examples of product exchange with little spatial clustering can be found among microorganisms in animal guts. The species originally describes as *Methanobacillus omelianskii* turned out to consist of a chemotrophic 'S-organism', which consumes ethanol, and produces di-hydrogen, and a methanogen, which consumes di-hydrogen and dioxide. *Ruminococcus albus* ferments glucose to acetate, ethanol and di-hydrogen, but in the presence of fumarate-fermenting *Vibrio succinogenes*, *R. albus* produces acetate, and not the energetically expensive ethanol; this is only possible when *V. succinogenes* removes di-hydrogen [142]. This exchange pattern is typical for methanogen-partner interactions.

Transitions from syntrophy to competition and parasitism occur. The dung beetle (family *Scarabaeidae*), which feeds on mammalian faeces, is an example of the use of a product that is associated with hosts' assimilation. A transition to competition is found in sharksuckers *Echeneis*, which feed on fish fragments derived from the shark's meals.

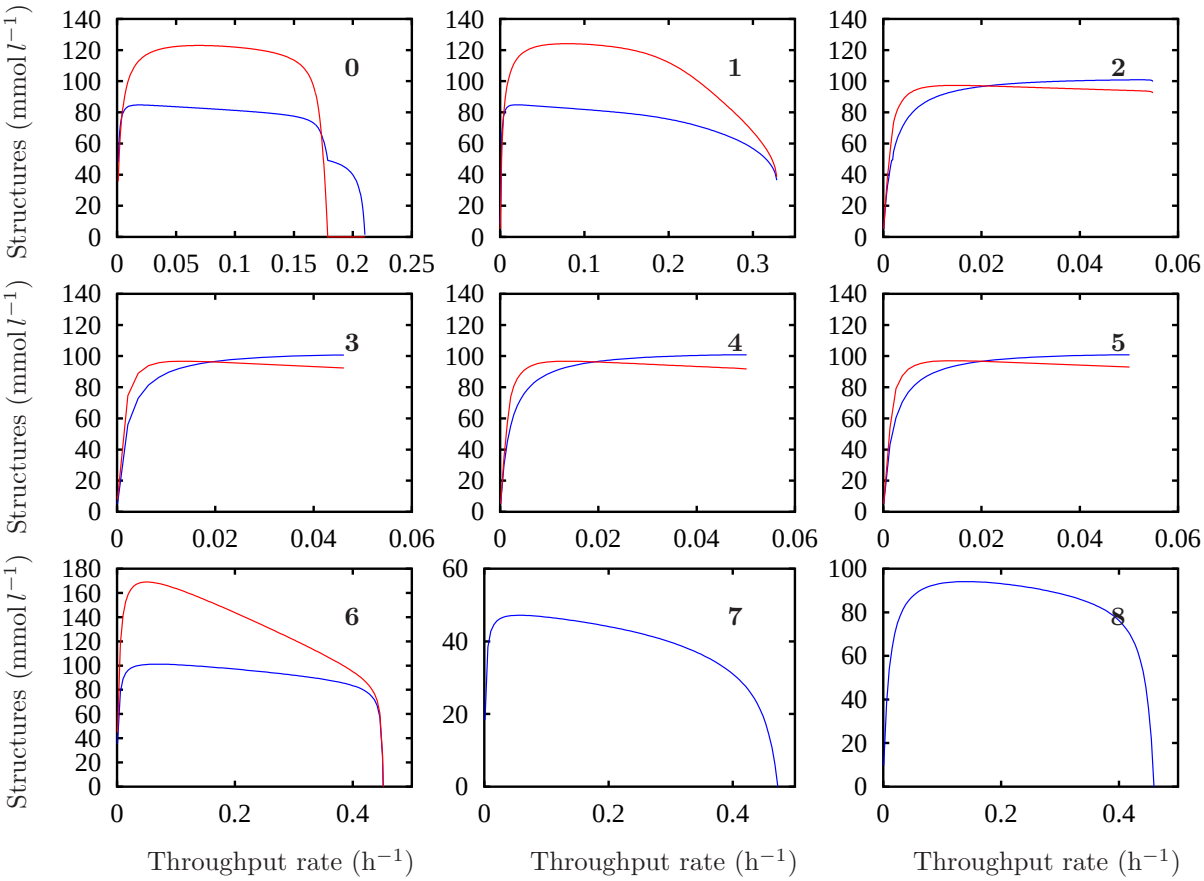

Figure 8.9: Steady-state values of the amounts of structure of hosts (dashed curves) and symbionts (drawn curves) as functions of the throughput rate of the chemostat for the different steps in symbiogenesis. If substrates and products are substitutable (0) symbiosis is facultative and the host can live independently of the symbiont. With this parameter setting the hosts' maximum growth rate is higher. If substrates and products make their transition to become supplementary (1), and especially if they are supplementary (2), symbiosis is obligatory. The environment is homogeneous in steps 0-2 and 5-8, but in step 3 symbionts can live in the free space, in the hosts' mantle space, as well as within the host. The parameter settings are such that the internal population of symbionts out-competes the mantle and free-living populations; the curve for the symbionts in step 3 corresponds to the internal population; other values for the transport parameters allow the coexistence of all three populations, or any selection from these three. Step 4 has internal symbionts only, but the mantle space can differ from the free space in concentrations of substrates and products. These differences disappear in step 5 (by increasing the transport rates between both spaces). Product transfer is on flux basis in step 6, rather than on concentration basis (steps 0-5); the symbioses can grow much faster and the amounts of structure are again zero at the maximum throughput rate. The transition from step 5 to 6 can be smooth if the host can reduce the leaking of product. The merging of both structures (7) and reserves (8) don't have substantial effects at steady-state. The single structure in steps 7 and 8 can handle two substrates; each structure in steps 0-6 handles only one.

Antbirds of the family *Formicariidae* feed on well-camouflaged locusts that jump to escape from an advancing front of army ants (subfamily *Dorylinae*); syntrophy here completes the transition to direct food competition.

We have discussed the use of products in ways that do not affect the production process directly. The use of products can be associated, however, with a change of product flux in complex ways which we will not analyze in depth. The honey guider *Indicator* guides mammals (e.g. badgers and humans) to bees' nests, itself feeding on the wax that is left over after the nest has been opened by the guided animal. The birds' activity might increase its average feeding rate as well as that of the guided animal. The house dust mite *Glycyphagus domesticus* enhances human skin flake production by inducing allergic reactions in humans, and so increases its food supply. The moth *Hypochrosis* increases tear production of big mammals, such as Asian elephants, by poking its tongue into mammals' eye. Both mites and moths 'milk' their hosts, so increasing the hosts' product formation, which is here associated with the hosts' maintenance process. Syntrophy involves a transition to biotrophy in the sucking of mammalian blood by mosquitos or in the extraction of plant saps by mistletoes or aphids. A transition to predation or parasitism is found in young pearl fish *Carapus*, which feed on the gonad tissue of sea cucumbers.

The concentration of products in the environment and the biomass ratios of the species can vary substantially in time. In the unlikely case that substrates, products or biota all remain in a given local homogeneous environment, it initially takes an amount of substrate to build up product concentrations, but once these concentrations and the populations settle to a constant value, the environment no longer acts as a sink and the situation is very similar to a direct transfer of product from one species to the other during steady-state. The inefficiency of product transfer in well-mixed environments becomes clear during transient states and if the product decays away (chemically, by physical transport or biologically mediated). A lot of product will not reach the partner, and population levels will be low.

2 Spatial clustering

Exchange of compounds between the species is enhanced by spatial clustering; most individuals of the small-bodied species live in a narrow mantle around an individual of the large-bodied species, see Figure 8.10. Although the real mantle will not have a sharp boundary with the outer environment, we treat it as a distinct and homogeneous environment that can exchange substrate and products with the outer environment and with the volume inside the host. The individuals of the large-bodied species secrete all product into their mantle; both products and substrates can leave or enter the mantle with certain specific rates according to a generalized diffusion process. We take the mantle's volume (at the population level) just proportional to the structural mass of the large-bodied species (which seems reasonable at the population level). Diffusion and related transport processes mean that the mantle is actually not homogeneous; concentration gradients will build up, as discussed in [289, p235]. This level of detail is not required, however, for our present aim.

The emigration rate of the small-bodied species to and from the mantle space will be relatively small. Since the growth rate will be much higher in the mantle, the small-

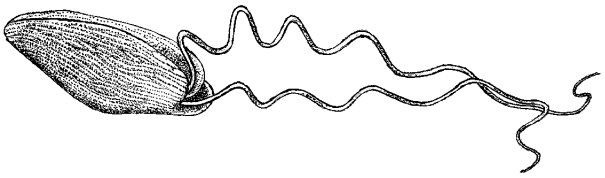

Figure 8.10: The cell surface of the colourless amitochondriate euglenoid *Postgaardi mariagerensis* is fully covered with elongated rod-shaped heterotrophic bacteria. Based on an electronmicrograph in [522]; the length of the cell is 60 μm.

bodied species accumulates in the mantle space of the large-bodied one, depending on the transport rates for substrates and products to the other environment, and on intra-specific competition. Under rather general conditions for the maximum specific assimilation rate, the specific maintenance and growth costs, and the hazard rate (i.e. the instantaneous death rate), the population inside the mantle space even out-competes that outside. This spatial clustering does not involve optimization arguments.

Many species create a special environment to grow their symbionts. Examples are animals intestines, which harbour the gut flora, or pits in the leaves of the floating fern *Azolla* and *Gunnera*, which harbour blue-green bacteria (*Anabaena*) that fix dinitrogen; some flowering plants, such as *Alnus*, leguminosae, *Hippophaë*, have special structures in the roots for harvesting the bacteria *Rhizobium* for the same purpose. Cockroaches lose their gut flora at moulting, and inoculate from mother's faecal supplies. The water flea *Daphnia magna* is a popular species used for ecotoxicity testing [302]. This led to the discovery that repeated media refreshment reduces daphnids' condition, which is probably caused by a wash-out of the gut flora; daphnids natural schooling behaviour thus may be related to re-inoculation of the gut flora.

3 Physical contact: epibionts

The exchanging products now hardly accumulate in the environment, and compound exchange is direct on the basis of fluxes. The exchange is further optimized if the partners live in direct physical contact with each other, since losses will be even smaller. Such situations frequently occur in nature. The surface of the euglenoid *Postgaardi* is completely covered with bacteria (Figure 8.10). Product exchange is probably the reason that many micro-organisms live in flocks, rather than in free suspension [66]. Ascomycetes make physical contact with green algae in lichens. Basidiomycetes do so with vascular plants in ectomycorrhizas. Cyanobacteria, *Prochloron*, live on the outer surface of didemnids.

If the products decay away, the two species can still improve product exchange by internalization, where the small-bodied species (endosymbionts) lives inside the large-bodied one (host). This requires phagocytosis, which is absent in prokaryotes, but widely spread among eukaryotes. During this internalization process, the host acquires the product of its symbiont both from the mantle space, as well as from inside its own body. The natural description of the uptake process of product in the mantle space is on the basis of the concentration of product, in combination with a generalized diffusion process that transports the product to the hosts' product-carriers in the outer membrane. While the symbionts' access to the hosts' product is enhanced by internalization, its access to the substrate can be reduced because that substrate now has to pass through the hosts' outer membrane.

From outside the host the endosymbiont is no longer visible and it appears as if the host is now feeding on two substrates, rather than one. The argument becomes subtle if the host transforms the symbionts' substrate before it reaches the symbiont.

The internal population eventually out-competes the population in the mantle space, and the endosymbiont can lose its capacity to live freely due to adaption to its cytoplasmic environment, which is under the hosts' homeostatic control. It is curious to note that the chloroplasts of chromista (which include diatoms, brown algae and many other "algal" groups), live inside the hosts' endoplasmatic reticulum, while they live outside it in other groups [87]. The passage of the extra membrane during the internalization process is obviously conserved during evolution, which suggests that the internalization process is rare and reveals the evolutionary relationships between these protist taxa.

Our numerical studies did not account for transport mechanisms that enhance the intracellular accumulation of products. A much higher maximum growth rate can be obtained by decreasing the parameters that control the leaking of products and substrates from the cell, for example. The low maximum growth rate shown in Figure 8.9 steps 2-5 suggests that the control of transport may be a rather essential feature of symbiogenesis. These transport parameters also determine the fate of the three populations of symbionts (free-living, epibiotic, and internal). They can all co-exist or each of them can out-compete the others, depending on these parameter values. The competitive exclusion principle, which states that the number of species of competitors cannot exceed the number of types of resources at steady-state, only holds for homogeneous environments. The values that are used in Figure 8.9 step 3 lead to extinction of the epibiotic and free-living populations. The mantle space still can differ in concentrations of substrates and products in step 4, while in step 5 the transport rates of these compounds from the mantle to the free space and *vice versa* are so large that the environment is homogeneous again. It is clear that these differences hardly effect the dynamics with this choice of parameter values, the curves in steps 3, 4 and 5 are very similar; the differences clear for smaller transport rates.

The uptake of product evolves from concentration-based to flux-based (see Figure 8.11); this comes with an increase of the maximum throughput rate and a qualitative change in behaviour of the steady-state amounts of structure around this growth rate: the symbiosis becomes independent of the extracellular product concentration. The role of the products partly degrades from an ecological to a physiological one. Figure 8.9 illustrates this in step 6, where the steady-state amounts of structure at the maximum throughput rate is (again) zero, while the maximum throughput rate is substantially increased compared with that for step 5.

Many examples are known for endosymbioses. The nitrogen-fixing cyanobacterial symbionts of the diatoms *Rhizosolenia* and *Hemiaulus* live between the cell wall and the cell membrane [568, 569]. Pogonophorans (annelids) and *Xyloplax* (echinoderms [19]) do not possess a guts, but harbour chemoautotrophic bacteria inside their tissues. The parabasalian flagellate *Caduceia theobromae* bears two species of ectosymbiotic and one species of endosymbiotic bacteria, which assist wood digestion in termite guts. Cyanobacteria live inside the fungus *Geosiphon* and the diatoms *Richelia*, *Hemiaulus* and *Rhopalodia*. Several species of heterotrophic bacteria live endosymbiotically in *Amoeba proteus*.

The location of mitochondria inside cells further testifies to the optimization of trans-

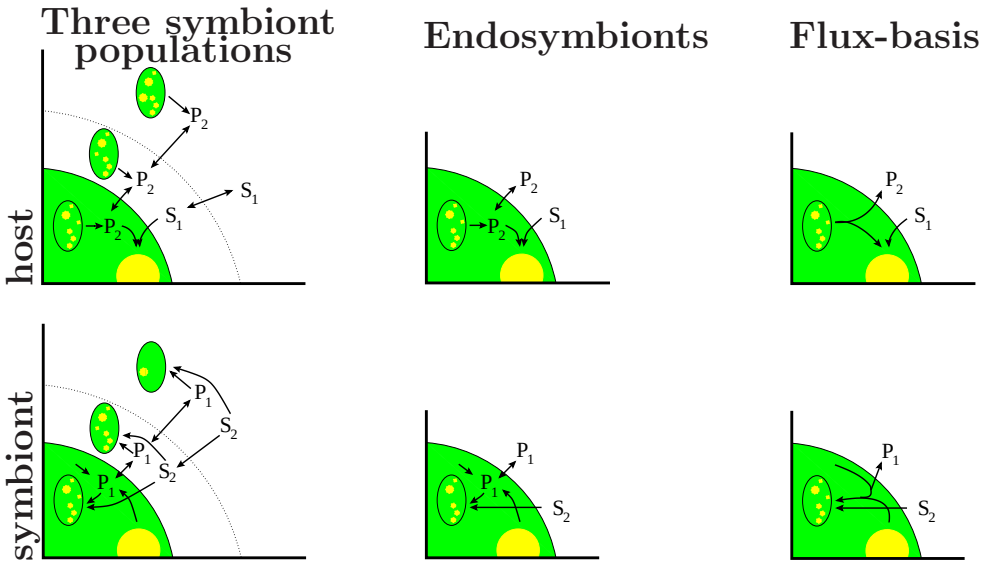

Figure 8.11: The feeding process of host (top) and symbiont (bottom) on substrate (S_1 and S_2) from the environment and product (P_1 and P_2) that is produced by the partner. The first column delineates three populations of symbionts: free, epi- and endosymbionts. The second column only delineates endosymbionts, but still uses intracellular concentrations of products to quantify feeding. With the degradation of intracellular product from an ecological to a physiological variable, feeding is specified in terms of fluxes (third column).

port by spatial clustering. Mitochondria cluster close to blood capillaries in mammalian muscle cells and form interdigitating rows with myofibrils to enable peak performance during contraction [36]. The association of mitochondria with the nuclear envelope is thought to relate to the demand of ATP for synthesis in the nucleus, and to the reduction of damage to DNA by reactive oxygen species. The association of mitochondria with the rough endoplasmatic reticulum is less well understood but might be related to the movement of mitochondria within cells.

4 Weak homeostasis for structure

The ratio of the amounts of structure of the partners varies within a range that becomes increasingly narrow. At constant substrate levels the population sizes grow exponentially, but their ratio becomes constant, a condition that we term 'weak homeostasis' for structure. The ratio might still depend on the substrate levels at steady-state. The importance of products taken up from the environment becomes small; almost all products are exchanged within the body of the host. If the products are fully supplementary to the substrates, some excess product might still leak from host's body, due to stoichiometric restrictions in its use. If part of the product is still substitutable for the substrate, such a leak is unlikely.

Many photosymbionts seem to have a rather constant density in hosts' tissues, although knowledge about digestion of symbionts by hosts as part of a density regulation system is frequently lacking. Our analysis shows that product exchange is such a strong regulation mechanism, that other regulation mechanisms are not necessary to explain a relatively

constant population density of endosymbionts. This does not exclude the existence of regulation mechanisms, of course. Regulation mechanisms might affect the coupling of parameters that control product formation.

5 Strong homeostasis for structure

The ratio of the amounts of structure of the partners becomes fixed and independent of the substrate concentrations at steady-state. We suggest that the mechanism is by tuning the weight coefficients for how product formation depends on assimilation, maintenance and growth.

If the endosymbiont is limited in its growth by hosts' product(s), simple constraints apply to ensure that the endosymbiont and the host have equal specific growth rates, and that the ratio of their structures is independent of the hosts' substrate concentration at steady-state. The constraints are that (1) their reserve turnover times are equal, (2) endosymbionts' assimilation capacity is large with respect to the realized assimilation, (3) no products are produced in association with growth, (4) some products are produced in association with assimilation, (5) the ratio of the weight coefficients for product formation in association with maintenance and growth is the following function of maintenance rate coefficients

$$\frac{y^i_{PM}}{y^i_{PE}} = y^i_{EV}\frac{\dot{k}^j_M/\dot{k}^i_M - 1}{\dot{k}^j_M/\dot{k}_E + 1},$$

where y^i_{PM} is hosts' yield of product on reserve in the maintenance flux, y^i_{PE} is hosts' yield of product on reserve in the assimilation flux, y^i_{EV} is the hosts' yield of structure structure on reserve, $\dot{k}_E$ the reserve turnover rate, $\dot{k}_M$ the maintenance rate coefficient of the host, $\dot{k}^i_M$, and of the endosymbiont, $\dot{k}^j_M$. All yield coefficients are expressed in terms of C-mol per C-mol; a C-mol is a mol of C-atoms, so 1 mol glucose equals 6 C-mol glucose. Hosts' specific product formation is given by $j^i_P = y^i_{PE}j^i_E + y^i_{PM}\dot{k}^i_M$, where j^i_E is the specific assimilation flux, i.e. the synthesis rate of hosts' reserve from substrate and product in terms of C-mol of reserve per C-mol of structure per unit time.

The large assimilation capacity of the endosymbiont (condition 2) is necessary to avoid wastage of hosts' products. If the conditions are not exactly fulfilled, strong homeostasis is not strict and (small) changes in biomass composition remain possible. Strict homeostasis probably only exists in the human mind, but this does not affect the usefulness of the concept. It has an intimate relationship with stoichiometric restrictions on growth; the time-varying resources have to be incorporated into fixed ratios.

The conditions for strong homeostasis are independent of the details of hosts' assimilation process. The host might be product as well as substrate limited. The product and the substrate might also be substitutable compounds, such as in the case of algal symbionts of heterotrophs, where the algal carbohydrates serve as an alternative energy source for the host. The significance of these carbohydrates in the hosts' diet might be complex, while the strong homeostasis condition still holds true. If prey is abundant, and the host's maximum assimilation capacity is reached, the extra carbohydrates contribute little to the hosts' assimilation. This dynamics is consistent with the rules for sequential processing of substitutable substrates by synthesizing units [289] and explains why symbiotic and

aposymbiotic hosts grow equally fast at high substrate levels, as has been observed in ciliates and hydras [223, 415]. At low prey abundance (the typical situation in the oligotrophic waters around coral reefs), the extra carbohydrates do contribute to the hosts' diet and propagation.

The fact that the conditions for strong homeostasis are independent of the hosts' assimilation process also implies the independence of details of the endosymbionts' product formation. This simplifies matters considerably, because the excretion of carbohydrates by algal symbionts is not a process covered by fixed associations with assimilation, maintenance and/or growth. It is an active excretion due to stoichiometric constraints of carbohydrates and ammonia (from the host) to form new algal biomass. This excretion process is discussed in the next step of integration: the single structure-two reserves case, where the algae have a carbon and a nitrogen reserve.

If the host is limited in its growth by endosymbionts' products, similar constraints apply to ensure a constant ratio of structures that is independent of endosymbionts' substrate; the role of host and endosymbionts are just interchanged in this situation. In the case of limitation by substrate of both partners, more stringent constraints apply on energy parameters.

The constraint of small actual assimilation rates might help to explain why symbioses are most frequently found in oligotrophic environments; regulation of relative abundances is more difficult under non-limiting environmental conditions.

Eventually the ratio of amounts of host and symbiont structures also remains constant during transient states, a condition that we term strong homeostasis for structure. We can now replace endosymbionts' and hosts' structure by a single combined structure, with two reserves. The reduction is possible without loss of generality on the basis of the concept of a generalized compound that we introduced earlier. This step is in reality usually accompanied by a transfer of (part of) the endosymbionts' DNA to that of host [381]; endosymbionts are now called organelles.

The numerical effect of the merging of the structures is small with our parameter choice (Figure 8.9 from step 6 to step 7). The technical details of the merging are discussed in Appendix B.

Examples of endosymbioses that approach strong homeostasis are mitochondria, hydrogenosomes, chloroplasts and other plastids and peroxysomes. The number of these organelles per host cell depends very much on the species. Diatoms frequently have just a single chloroplast, which implies that the growth and division cycle of the chloroplast must be tightly linked to that of the cell.

6 Coupling of assimilation pathways

The assimilation routes for the organic substrate(s) become coupled, especially in situations where substrate levels covary in time. The reason for the covariation can be purely physical when the substrates originate from a common source (for example another organism with a rather constant chemical composition, or some erosion process of rocks which extracts minerals in fixed ratios). An alternative possibility is that specialization on a single substrate occurs. Details of product exchange are no longer visible in the dynamics

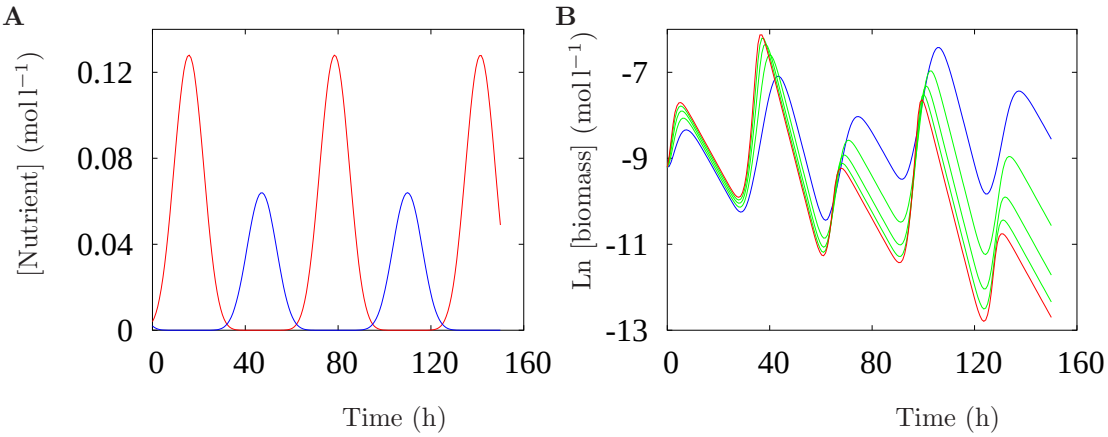

Figure 8.12: (A) A cyclic pattern of two nutrient concentrations, as experienced for example by algae. (B) The expected biomass concentrations in the case of a single structure, and two reserves. The curves correspond to increasing reserve turnover times from top to bottom. The two curves with extreme turnover values are shown with solid lines; the larger this turnover time, the lower the intracellular storage capacity for nutrients. The graphs show that the mean growth rate increases with the storage capacity under these conditions, but that the nutrients must be stored independently.

of the integrated system; products now have a strict physiological role, where they still determine the relative importance of the different sub-structures, and so the substrate uptake capacity. We no longer need to know of their existence to predict how the population responds to environmental factors. If substrates co-vary in fixed ratios in the environment, the range of the ratio of amounts of reserves becomes increasingly narrow.

In situations where substrate abundances do not co-vary in time, coupling of the assimilation processes will not occur, and the host will maintain two reserves (see below). Another pattern of development is then likely: part of the unused reserve that is allocated to growth is returned to that reserve, with the result that each reserve can accumulate and reach very high levels when the other reserve limits growth. The logic is, when the substrate ratio in the environment changes, the reserve density will (eventually) change, so will the ratio of fluxes of used reserves. After paying the maintenance costs, the reduced flux arrives at the synthesizing units for the growth of structure. The chemical composition of structure is constant, however, so there are stoichiometric restrictions on the reserve fluxes that can be used, and part of one of the fluxes will remain unused and will be partly excreted into the environment. This is how algae excrete carbohydrates under nitrogen limitation, or nitrogen-containing toxicants under e.g. silica limitation. Quantitative details are discussed in [289, 297]. An important implication is that the density of the growth-limiting reserve always increases with the growth rate, but the density of the non-limiting reserve can increase as well as decrease with the growth rate; spectacular accumulation of reserves can only occur for the non-limiting reserves at low growth rates.

The functionality of this storing mechanism can be illustrated with algal growth in the sea, where carbohydrate reserves are boosted at the nutrient-poor surface layers where light is plentiful, and the nutrient reserves are filled in the dark bottom layers of the photic zone, which are usually rich in nutrients [311]. Thanks to the uncoupled reserves the alga is

able to grow in an environment that would otherwise hardly allows growth. It is the wind, rather than light or nutrients, that is in proximate control of algal growth (Figure 8.12).

7 Coupling of reserve dynamics

At constant substrate levels, the reserve ratio of the growing populations settles at a constant value, but the value of this ratio can still depend on the substrate levels. This condition has been called weak homeostasis for reserves. The chemical composition of biomass can still depend on the growth conditions in complex ways. If the assimilatory pathways are coupled, reserve dynamics are coupled almost automatically, because the coupling of structures already require that the reserve turnover rates are equal. Data on reserve dynamics in algae so have shown that the reserve turnover rates are equal even when the assimilatory pathways are not coupled [289]. This can be understood from the machinery that is used to mobilize reserves and use them for growth. Ribosomal RNA (rRNA) is an important component of this machinery, and most of the cellular pool of rRNA is directly related to the amount of reserve [289]. This explains why the rRNA content of cells and organisms depends on the growth rate; the coupling is so strict that the rRNA content is sometimes used to measure growth [78, 205].

The numerical effect of the merging of the reserves is small using the present parameter values (Figure 8.9 from step 7 to step 8). The merging only requires that the reserve turnover rates are equal, and the ratio of concentrations of substrate remains constant.

Examples of fully coupled single reserve systems can be found in carnivores, where the rather constant chemical composition of the prey provides the mechanism for the coupling of assimilation of the various nutrients that are required by the carnivore. Parasites also experience a rather constant chemical environment inside their host. Other examples can be found in heterotrophs in eutrophic environments, where a single resource is often limiting, all other resources being available in excess.

8 Strong homeostasis for reserves

The ratio of intra-host reserves becomes fixed and independent of the substrate levels at steady-state. Eventually, the ratio remains fixed during transient states and we arrive at a strong homeostasis for reserves. We can now replace the two reserves by a single combined one. Notice that the reserve ratios no longer depend on growth conditions, but the reserve levels still do. So the chemical composition of biomass also still depends on growth conditions, but in a less complex way.

The increasingly tight coupling of the dynamics of several types of reserves relates to the situation where maintenance and growth drain reserves in fixed and equal ratios. It is the reason why the metabolic performance of cats can be understood using a single reserve, while that of algae cannot. When a carnivore changes its diet over an evolutionary time scale to become a herbivore, using food with a less constant chemical composition, it frequently continues to be less flexible in its metabolism. This is why the metabolic performance of cows can still be understood using a single reserve. The conversion of grass into cow biomass (reserves) is poor from an energy point of view; the conversion

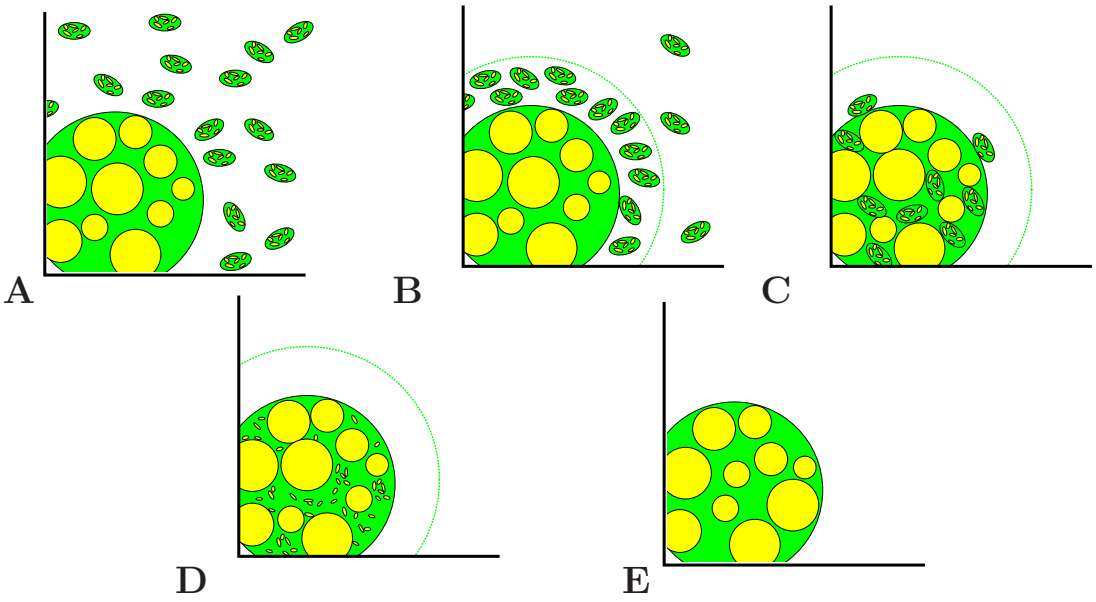

Figure 8.13: Future host (a single individual is indicated) and future symbionts originally live independently (A). When they start exchanging products, an accumulation of symbionts in the hosts' mantle space occurs (B), followed by an internalization (B). A merging of structures then can occur (D), followed by a merging of reserves (E). A new entity then exists. The light areas in the hosts and symbionts indicate reserves, the dark regions indicate structure; reserves integrate after structures. The mantle space around the hosts' body is indicated where hosts' product accumulates that stimulates symbionts' growth. The text describes these and other steps quantitatively.

efficiency can be greatly improved using protein-rich food supplements. The one reserve - one structure system is obviously a highly simplified model that can only approximate the gross behaviour of real-world physiological systems at best.

9 Cyclic endosymbiosis by specialization

Symbiogenesis, as described here, allows the host to use substrates, which it could not use without the symbionts. The opposite process is specialization on a single substrate, where the endosymbiont is no longer functional. This has occurred for instance in aerobic mitochondriate species that invaded anaerobic environments. In some species the mitochondria evolved into hydrogenosomes, but in others the mitochondria were lost. The loss of plastids has occurred in at least some species of all major groups of organisms, while in some parasitic groups, such as the kinetoplastids, they assume other functions. Specialization on metabolic substrates seems to be linked directly to the loss of genes. The loss of non-functional machinery increases the growth rate [538]; the reduction of the amount of DNA causes a reduction in the time required to copy it, which reduces mean cell size. This size reduction increases the surface area to volume ratio, and substrate uptake is proportional to surface area. Some properties of the symbiont might be retained, however, as testified by mitochondrion-derived genes in species that have lost their mitochondria.

Generally, (endo)symbiosis might be considered to be a process by which metabolic properties are acquired several orders of magnitude faster than by the Darwinian route of mutation and selection [374]. Darwin's mutation/selection route can be particularly cumbersome, because all intermediary stages have to be vital enough to continue the acquisition with incremental steps; almost all metabolic pathways involve several, or even many, enzymes. This provides constraints on the type of properties any particular organism can acquire along the Darwinian route. Such constraints do not apply to acquisition of metabolic traits by endosymbiosis.

Specialization with its accompanying losses of organelles, completes the endosymbiotic cycle, which has been repeated many times in the evolutionary history of life, and has created a bewildering biodiversity.

Multicellularity and body size

Although some individual cells can become quite large, with inherent consequences for physiological design and metabolic performance [204, 475], multicellularity can also lead to really large body sizes. Multicellularity evolved many times in evolutionary history, even among the prokaryotes, but particularly among the eukaryotes. It allows a specialization of cells to particular functions, and the exchange of products is inherently linked to specialization. Think, for instance, of filamental chains of cells in cyanobacteria where heterocysts specialize in N_2 fixation. To this end, specialization requires adaptations for the exclusion of dioxygen and the production of nitrogenase. The existence of dinitrogen-fixation unicellular cyanobacteria shows that all metabolic functions can be combined within a single cell, which is remarkable as its photosynthesis produces dioxygen, inhibiting dinitrogen fixation. A temporal separation of the processes solves the problem, but restricts dinitrogen fixation during darkness; specialization can be more efficient under certain conditions. The mixobacterium *Chondromyces* and the proteobacteria *Stigmatella* and *Mixococcus* have life cycles that remind us of those of cellular slime moulds, involving a multicellular stage, whereas acetinobacteria, such as Streptomyces resemble fungal mycelia (e.g. [126]. Pathogens, such as viruses can kill individual cells without killing the whole organism, which is an important feature of multicellularity, and is basic to the evolution of defense systems.

Cell differentiation is minor in poriferans, reversible in coelenterates and plants, and irreversible in vertebrates. The number of cells of one organism very much depends on the species, and can be up to 1017 in whales [488], which requires advanced communication. Many larger organisms, including opisthokonts (fungi plus animals), tracheophytes, rhodophytes and phaeophytes, evolved elaborate transport systems to facilitate exchange of metabolites among the cells and with the environment. Animals evolved advanced locomotory abilities, which requires accurate coordination by a nervous system. This latter system not only took tasks in information exchange and processing, but also in metabolic regulation. Animals also evolved an immune system, which supplements chemical defenses to fight pathogens.

Differentiation and cellular communication

Multicellularity has many implications. Cells can be organized into tissues and organs, which gives metabolic differentiation once more an extra dimension. It comes with a need for regulation of the processes of growth and apoptosis of cells in tissues [494], in which communication between cells plays an important role. Animals (from cnidarians to chordates) use gap junctions between cells of the same tissue, where a family of proteins called connexins form tissue-specific communication channels. They appear early in embryonic development (in the eight-cell-stage in mammals) and are used for nutrient exchange, cell regulation, conduction of electrical impulses, development and differentiation. Together with the nervous and endocrine systems, gap junctions serve to synchronize and integrate activities. When cell-to-cell communication systems fail, tumours can develop; only a small fraction of tumours result from DNA damage [348]. Plants use plasmodesmata to interconnect cells, which are tubular extensions of the plasma membrane of 40-50 nm in diameter, that traverse the cell wall and interconnect the cytoplasm of adjacent cells into a symplast. Higher fungi form threads of multi-nucleated syncytia, known as mycelia; sometimes septa are present in the hyphae, but they have large pores. Otherwise, the cells of fungi only communicate via the extracellular matrix (Moore, 1998). Rhodophytes have elaborate pit connections between the cells [112] which have a diameter in the range 0.2-40 μm filled with a plug that projects in the cytoplasm on either side. *Ascomycetes* and *Basidiomycetes* have similar pit connections, but lack the plug structure and the cytoplasm is directly connected unlike the situation in rhodophytes.

Emergence of life stages: adult and embryo

Several groups of bacteria evolved to a multicellular state in the form of reproductive bodies (myxobacteria, actinomycetes), chains with cell differentiation (cyanobacteria), mats, films or flocs [66]. When eukaryotization had occurred, multicellularity became complex and arose independently in almost all major taxa. This came with the invention of reproduction by eggs in the form of packages of reserve with an very small amount of structure: the juvenile state thus gave rise to both the adult and the embryo state. Embryos differ from juveniles by not taking up substrates from the environment. That is to say they do not (yet) use the assimilation process for energy and building-block acquisition, although most do take up dioxygen. The spores of endobacteria can be seen as an embryonic stage for prokaryotes. Adults differ from juveniles by allocation to reproduction, rather than further increasing the state of maturity. Unlike dividing juveniles, adults do not reset their state (*i.e.* the amount of structure, reserve and the state of maturity). Animals, notably vertebrates, and embryophytes, notably the flowering plants, provide the embryo fully with reserve material. Egg size, relative to adult size, has proved highly adaptable in evolutionary history.

If the cumulative investment into maturity exceeds a threshold, further allocation to maturity is ceased and mobilized reserve is redirected to reproduction. Logically, and perhaps also biochemically, this threshold corresponds with that of cell division by unicellulates.

The fact that allocation to reproduction is incremental, and eggs are not incrementally small, implies the installation of a buffer with destiny reproduction, and a set of buffer-handling rules. Some organisms produce an egg as soon as this buffer allows, as in some rotifers, while others accumulate over a year, as in corals or mussels, or over several years, as in some trees.

Foetal development in some animals (notably mammals) is a further variation on this theme. Vegetative propagation was invented independently in many taxa; even animals as advanced as the sea cucumber *Holothuria parvula* sport propagation by division [135].

Quite a few references suggest the existence of determinate and indeterminate growth patterns, especially in animals, where no growth occurs during reproduction in determinate growers. These patterns could be captured, in principle, by a change in the value of κ [356]. The combination of weak homeostasis and partitionability still allows that κ is a function of the amount of structure. However, the von Bertalanffy growth curve fits most growth data for isomorphs at constant food availability very well, which means that growth is not at the expense of reproduction and that κ is constant. It simply depends on the value of the maturity threshold for puberty whether or not growth still proceeds during reproduction, so there need not be a fundamental difference in metabolic organization between these patterns.

If growth is of the von Bertalanffy type at a constant low food density, and food availability increases after growth ceases, will an organism resume growth? Many species fail to do so, depending how long growth has already ceased. This loss of metabolic flexibility is possibly linked to the ageing process, and follows similar patterns as, for example, the occurrence of post-reproductive periods in many species. These patterns can be included in the DEB theory by linking parameter values to ageing-induced damage, similar to the strategy that has been shown to be effective for the effects of toxicants [302].

The holometabolic insects are a clear (and possibly the only) example of determinate growers; they insert an extra embryo stage (called the pupal stage) in their life cycle and do not grow as adults. Some species of *Octopus* and *Oikopleura* and some flowering plant species sport suicide reproduction, where growth is suddenly interrupted and some of the structure is rapidly converted to eggs or seeds, typically followed by death. Like torpor and migration, these strategies probably evolved to survive bleak periods.

Further increase in maintenance costs

Multicellular organization and an active life-style, especially in eukaryotes, results in a series of extra maintenance costs. Concentration gradients across the more abundant and dynamic membranes become more important, as well as intracellular transport and movements of the individual. The invasion of the fresh-water habitat required a solution to the osmotic condition. Many eukaryotes use pulsating vacuoles for this purpose. Invasion of the terrestrial habitat required an answer to the problem of desiccation. Many animals and some plants elevate the temperature of parts of their body metabolically to enhance particular physiological functions. Birds and mammals have taken this to extremes. Most maintenance costs are proportional to the amount of structure, but some (osmotic and thermoregulatory work) are proportional to organism's surface area. All these processes

increased maintenance requirements further, but also improved the metabolic performance. Such organisms became less dependent on the local chemical and physical conditions.

Some animals developed ovovivipary, *i.e.* they carry their eggs inside the body during the embryonic stage. This offers much better protection, and the mother is not confined to a particular site during breeding or parental care. Some animals (*e.g. Peripatus*, some sharks, placentalia) developed a placenta to transfer reserve from the mother to the foetal system. Foetal development is similar to that of embryos inside eggs, but their developmental rate is no longer restricted by the availability of reserve [289]. Many parental animals feed their offspring in the early juvenile stages, which is important for nutrition and for the inoculation of symbiotic digestive microorganisms.

Some animals and plants increase their body temperature temporarily (some flowers during gamete and fruit development, insects during flight, some fishes in certain regions of their body) or more permanently (mainly birds and mammals). This was a next step in the evolution of homeostasis, and resulted in a considerable further increase in maintenance costs that had to be balanced by an equivalent increase in their ability to acquire resources. Since cooling is linked to surface area, the impact on the energy budget depends on the body size; this has been quantified in the DEB theory [289] in a straightforward way.

Differentiation

The transition to a multicellular state has been made in almost all large taxa, including prokaryotes. It comes with cell differentiation into tissues and organs; the organs then take the role of organelles. The dynamics of organ sizes can be quantified effectively by further partitioning the flux of mobilized reserve (the κ-rule). If the fraction that is allocated to a particular body part is fixed, and the specific maintenance costs equal those of other body parts, isomorphic growth results. Although this frequently covers the main patterns, deviations can be observed that can be understood by linking the allocation fraction to the relative workload. This even holds for tumours, where the workload is quantified as their maintenance requirement, relative to that of the host [349]. This allocation produces realistic predictions for how tumour growth depends on the physiological state of the host; tumour growth is more aggressive in young (small) individuals, compared to old (large) ones, and in well-fed individuals, compared to those that experience caloric restriction. It also gives realistic predictions for how velum *versus* gut size in bivalve larvae depends on food availability [293] (see Figure 5.8). The relative workload of the velum, which functions in filtering, equals one minus the relative workload of the gut, which functions in food processing. The relative size of the velum and gut adapts rather quickly to the feeding conditions, growth is isomorphic after the adaptation period. The feeding rate of adapted individuals depends on food density according to the Hill's equation, rather than the Holling type II relationship that would result if the relative organ size was constant. By partitioning food handling into a mechanical phase that is sequential to food searching and a digestion phase that is parallel to food searching, the observed differences from the standard Holling type II functional response in fish larvae can be understood [358].

Likewise, the allocation to adipose tissue can be linked to feeding, allocation to the liver to particular dietary components (*e.g.* alcohol in humans), and allocation to muscles

in sportsmen, *etc.*

Plants differentiated their structure into a root for nutrient uptake linked to water uptake and a shoot for gas exchange, photon acquisition and evaporation of water; the latter dominates water uptake by the root, which means that the ratio of the surface area of the root and the shoot appears in the saturation coefficient for nutrient uptake by the roots. In addition plants developed translocation of reserves between root and shoot, which are fixed fractions of the mobilized flux (consistent with the κ-rule for allocation). These links between root and shoot imply compensating development of both types of structure [289]; a reduction in light affects the root more than the shoot, and a nutrient reduction affects the shoot more than the root. Plants typically alter their morphology in predictable ways; they start as V1-morphs immediately after germination, then undergo an isomorphic phase, finally ending as a V0-morph when the neighbouring plants in their habitat prohibit further extension of functional surface area of the roots and shoots. Leaves typically last one year, and fall after recovering (some of) the reserve. This means that plants live syntrophically with the soil biota (especially bacteria and fungi), that feed on this organic rain and release the locked nutrients as waste for renewed uptake by the plants. Moreover, almost all plant species have an endomycorrhiza, *i.e.* specialized fungi of the phylum *Glomeromycetes* that are probably involved in drought resistance and nutrient uptake. The *Brassicacaea*, which are specialists on nutrient-rich soils, do not have endomycorrhizae. Some 30 % of plants also have an ectomycorrhiza and many use animals for pollination and dispersal.

Ageing and sleeping

When the cyanobacteria eventually enriched the atmosphere with dioxygen, many species adapted to this new situation and energy acquisition from carbohydrates was greatly improved by using dioxygen for oxidation in the respiratory chain. Although means to cope with free radicals, such as reactive nitrogen species (RNS), were already present, the handling of reactive oxygen species (ROS) became important to reduce damage to the metabolic machinery and especially to DNA. This especially holds true for tissues of cells with non-reversible differentiation; this excludes *e.g.* plants. Specialized proteins (peroxidase dismutases) were developed and their effectiveness was tuned to compromise between survival of the juvenile period and the use of ROS to generate genetic variability among gametes. The latter is important to allow adaptation to long-term environmental changes that are too large for adaptation within a given genome. Big-bodied species are vulnerable; the body size scaling relationships implied by the DEB theory show that the length of the juvenile period scales with body length among species whereas the reproductive rate decreases with length. Therefore large-bodied species must have efficient peroxidase dismutases and, therefore, reduce the genetic variability among their gametes, while having few offspring. High feeding levels for an individual mean high respiration rates and a short lifespan. Survival probability changes with age in predictable ways [346] and involves acceleration of ageing. This acceleration is linked to mitochondrial damage (in aerobic eukaryotes), which produce ROS, the amount of mitochondria per cell is up-regulated to achieve an adequate production of intermediary metabolites from the TCA cycle [327]; the TCA cycle and the respiratory chain are both inside the mitochondria.

The various evolutionary lines to multicellularity arose with a variety of communication strategies among cells. Many fungi merged their cells in hyphae; heterokonts and plantae (rhodophytes and chlorophytes) linked their cells *via* protoplasm connections and the latter (especially the embryophytes) developed transport systems *via* apoptosis to reallocate metabolites. Animals continued the use of (prokaryotic) gap junctions, which allow for limited transport of particular metabolites only, and developed both a transport system (blood and lymph) and a (relatively) fast signaling system (the neuronal system). The latter allowed for the development of signal processing from advanced sensors (light, sound, smell, electrical field, pain) in combination with advanced locomotory machinery for food acquisition (mostly other organisms or their products). Advanced methods for food acquisition also came with a requirement for learning and the development of parental care. The neuronal system is, however, sensitive to ROS, and requires sleep for repair [519, 520]. Since the required sleeping time tends to be proportional to the specific respiration rate, large-bodied species have more time to search for food. Their speed and the diameter of their home range increases with length, which enhances their ability to cope with spatial heterogeneity. Because the maximum reserve density also increases with length, the time to death by starvation will increase which enhances their ability to copy with temporal heterogeneity. At the extreme, the largest whales leave their Antarctic feeding grounds, swim to oligotrophic tropical waters to calve, feed the calf some 600 l of milk per day for several months, and then swim back with their calf to their feeding grounds where they resume feeding. Such factors partly compensate for the disadvantages of a large body size and the associated high minimum food densities.

From supply to demand systems

Plants evolved extreme forms of morphological and biochemical adaptations to the chemical and physical conditions in their direct environment and remained supply systems. Animals, by contrast, especially birds and mammals, excel in behavioural traits designed to meet their metabolic needs. They evolved into demand systems, "eating what they need", with those needs having reduced variability. This co-evolved with an increase in the difference between standard and peak metabolic rates, closed circulation systems, advanced forms of endothermy, immune systems and hormonal regulation systems. The physical design of these organisms, such as the capacity of transport networks, is designed to meet the peak metabolic performance, but gives little information about standard metabolic performance. The evolutionary history of demand systems makes clear that we can only understand their metabolic performance in the light of that of supply systems. The demand of demand systems represents an evolutionary fixation of the performance of supply systems under "typical" environmental conditions.

Behaviour and time budgets

Animals, especially those functioning at the demand-end of the supply-demand spectrum, can acquire their food so efficiently that time is available for behaviour other than food acquisition and food processing, such as social interaction. The Holling type II functional

response for how feeding rate depends on food density is identical to the Michealis-Menten product formation by enzymes because individuals and enzymes use their time in either searching for substrate or processing of substrate. If other behaviour traits compete for time, predictable deviations from this relationship result. Since specific food uptake is no longer a function of food density only but also of population density, stable coexistence is possible of two species that compete for a single substrate, even in spatially homogeneous and constant environments. Together with the syntrophic basis of coexistence, this can be an important mechanism in the evolution of biodiversity.

The cell-individual-population continuum

The boundaries between cells, individuals, colonies, societies and populations are not sharp at all. Fungal mycelia can cover up to 15 hectares as in the basiodiomycete *Armillaria bulbosa*, but they can also fragment easily. Cellular slime moulds (dictyostelids) have a single-celled free-living amoeboid stage, as well as a multicellular one; the cell boundaries dissolve in the multicellular stage of acellular slime moulds (eumycetozoa), which can now creep as a multi-nucleated plasmodium over the soil surface.

The mycetozoans are not the only amoebas with multi-nuclear stages; *Mastigamoeba* (a pelobiont) is another example[37]. Many other taxa also evolved multi-nucleated cells, plasmodia or stages, e.g. ciliates, Xenophyophores, Actinophryids, *Biomyxa*, Loukozoans, Diplomonads, *Gymnosphaerida*, Haplosporids, *Microsporidia*, Nephridiophagids, *Nucleariidae*, Plasmodiophorids, *Pseudospora*, *Xanthophyta* (e.g. *Vaucheria*), most classes of *Chlorophyta* (*Chlorophyceae*, *Ulvophyceae*, *Charophyceae* (in mature cells) and all *Cladophoryceae*, *Bryopsidophyceae* and *Dasycladophyceae*)) [438, 200]; the *Paramyxea* have cells inside cells.

Certain plants, such as grasses and sedges, can form runners that give off many sprouts and cover substantial surface areas; sometimes, these runners remain functional in transporting and storing resources as tubers, whereas in other cases they soon disintegrate. A similar situation can be found in, for example, corals and bryozoans, where the tiny polyps can exchange resources through stolons.

Behavioural differentiation between individuals, such as between those in syphonophorans, invites to consider the whole colony an integrated individual, whereas the differentiation in colonial insects and mammals is still that loose that it is recognized as a group of coordinated individuals.

These examples illustrate the vague boundaries of multicellularity, and even those of individuality. A sharpening of definitions or concepts may reduce the number of transition cases to some extent, but this cannot hide the fact that we are dealing here with a continuum of metabolic integration in the twilight-zone between individuals and populations. This illustrates that organisms, and especially eukaryotes, need each other metabolically.

Direct syntrophic interactions

The demand of nutrients and energy in the form of carbohydrates has led to many syntrophic relationships between carbohydrate-supplying photoautotrophs and nutrient-supplying

heterotrophs. Pure photoautotrophs are probably rare, if they exist at all; either they have mixotrophic capabilities, or they form associations with heterotrophs. Being able to move independently and over considerable distances, jellyfish, for example, are able to commute between anaerobic conditions at lower water strata for nitrogen intake and higher ones for photosynthesis by their dinozoan endosymbionts supplying them with energy stored in carbohydrates. Dinozoans are engaged in similar relationships with hydropolyps (corals) and molluscs; extensive reefs testify of the evolutionary success of this association.

A close relationship between chlorophytes (or cyanobacteria) and fungi (mainly ascomycetes) evolved relatively recently, i.e. only ca. 450 million years ago, in the form of lichens and *Geosiphon* [511]. The fungal partner specialized in decomposing organic matter, which releases nutrients for the algae in exchange for carbohydrates, not unlike the situation in corals. Similarly, mycorrhizas exchange nutrients against carbohydrates with plants, which arose in the same geological period. The endomycorrhizas (presently recognized as a new fungal phylum, the glomeromycetes) evolved right from the beginning of the land plants; the ectomycorrhizas (ascomycetes and basidiomycetes) evolved only during the Cretaceous. These symbioses seemed to have been essential for the invasion of the terrestrial environment [517].

Some plants can also fix dinitrogen with the help of bacteria, encapsulated in specialized tissues. A single receptor seems to be involved in endosymbiontic associations between plants on the one hand and bacteria and fungi on the other [539], but the recognition process is probably quite complex [437] and not yet fully understood. Associations between the dinitrogen-fixation cyanobacterium *Nostoc* and the fern *Azolla* have been known for some time, but the association with the bryophyte *Pleurozium schreberi* has only recently been discovered [104]; this extremely abundant moss covers most soil in boreal forests and in the taiga. The cyanobacteria are localized in extra-cellular pockets in these examples, but in some diatoms they live intracellularly. See Rai et al. [463] for a review of symbioses between cyanobacteria and plants.

Heterotrophs not only have syntrophic relationships with photoautotrophs, but also with chemolithotrophs. A nice example concerns the gutless tubificid oligochaete *Olavius algarvensis*, with its sulphate-reducing and sulphide-oxidizing endosymbiontic bacteria [122]. These symbionts exchange reduced and oxidized sulphur; the fermentation products of the anaerobic metabolism of the host provide the energy for the sulphate reducers, whereas the organic compounds produced by the sulphide oxidizers fuel the (heterotrophic) metabolism of the host. Taxonomic relationships among hosts can match that among symbionts [120], which suggest considerable co-evolution in syntrophic relationships.When tree leaves fall on the forest floor, fungi release nutrients locked in them by decomposition; the soil fauna accelerates this degradation considerably [580]. Without this activity by fungi and the soil fauna, trees soon deplete the soil from nutrients, as most leaves last for only one year, even in evergreen species. As mentioned, trees, and plants in general, also need mycorrhizas to release nutrients from their organic matrix. Moreover, most of them also need insects, birds or bats and other animals to be pollinated (e.g. [460, 25], and yet other animals for seed dispersal. Thus, berries, for example of *Caprifoliaceae*, *Solanaceae* and *Rosaceae*, are 'meant' to be eaten [527]; some seeds have edible appendices (e.g. *Viola*) to promote dispersal, but others have no edible parts in addition to the seed, such as *Adoxa*

and *Veronica*, and germinate better after being eaten by snails or birds and ants, respectively. Still other seeds stick to animals (e.g. *Boraginaceae*, *Arctium*) for dispersal. Fungi, such as the stinkhorn *Phallus* and the truffle *Tuber*, also interact with animals for their dispersal.

By shading and evaporation, trees substantially affect their microclimate, and thereby allow other organisms to live there as well. This too can be seen as an aspect of metabolism. As mentioned, non-photosynthesizing plastids are still functional in plants; such plants can still have arbuscular mycorrhizas, as are found in the orchid *Arachnitis uniflora* [197]. Although the plant cannot transport photosynthetically produced carbohydrate to their fungal partner *Glomus*, it is obviously quite well possible that other metabolites are involved in the exchange. The complex role of plastids shows that the plant is not necessarily parasitizing the fungus.Like plants, animals need other organisms (e.g. for food).

The processing of food requires symbiosis too. We briefly discuss some aspects. Many animals feed on cellulose-containing phototrophs, but no animal can itself digest cellulose. Most animals have associations with prokaryotes, amoebas and flagellates to digest plant-derived compounds [525]. These micro-organisms transform cellulose to lipids in the anaerobic intestines of their host animal; the lipids are transported to the aerobic environment of the tissues of the animal for further processing. Attine ants even culture fungi to extract cellulases [375]. Many symbioses are still poorly understood, such as the *Trichomycetes*, which live in the guts of a wide variety of arthropods in all habitats [399]; the role of smut fungi (*Ustilaginales*) in their symbioses with plants also seems more complex than just a parasitic relationship [562]. Faeces, especially that of herbivores, represent nutritious food for other organisms. This is because proteins often limit food uptake, implying that other compounds must be excreted; protein supplements to the grass diet of cows can greatly reduce the amount of grass they need.

Organisms specialized on the use of faeces as a resource are known as coprophages. Examples are the bryophyte *Splachnum*, which lives off faeces of herbivores (*S. luteum* actually lives off that of the moose *Alces alces*); the fly *Sarcophaga* which lives off cattle dung; the fungus *Coprinus* which lives off mammalian faeces, similar to beetles of the dung beetle family *Scarabaeidae*.

Dead animals are processed by a variety of other animals; burrowing beetles of the family *Silphidae* specialize in this activity, for instance. Almost all animal taxa engage in carrion feeding, since the chemical make up of organisms does not differ that much; because of their great capacity of moving around, animals are often the first to arrive at the feast. Many examples illustrate that it is just a small step from feeding off dead corpses to that of living off live ones. Predation, a specialization of most animals, has many consequences, and some can actually be 'beneficial' for the prey: nutrient recycling, selection of healthy individuals, reduction of competition by weak individuals, reduction of transmission of diseases, and enhancing the co-existence of prey species are all implications of predation.

Intricate relationships between organisms evolved, especially in prey-predator interactions, such as those between insects and plants (e.g. [509]. A low predation pressure on symbiotic partners enhances their stable co-existence [264], whereas co-existence becomes unstable at a high pressure and easily leads to the extinction of both prey and predator. This points to a co-evolution of parameter values quantifying the dynamics in prey-predator

systems. The time scale of the effects on fitness is essential; short-term positive effects can go together with long-term negative effects of behavioural traits on fitness. Time scales and indirect side-effects that operate through changes in food availability are important aspects that are usually not included in the literature on evolutionary aspects of life history strategies.

Indirect symbiontic syntrophy

In this section, we only give some examples of the many indirect trophic relationships that exist between species. Phytoplankters bind nutrients in the photic zone of the oceans, sink below it, die and are degraded by bacteria. Subsequently, a temporary increase in wind speed brings some of the released nutrients back to the photic zone by mixing and enables photosynthesis to continue. The sinking of organic matter is accelerated by grazing zooplankters. The result of this process is that, over time, phytoplankters build up a nutrient gradient in the water column, that CO_2 from the atmosphere becomes buried below the photic zone, and that organic resources are generated for the biota living in the dark waters below this zone and on the ocean floor. Mixing by wind makes phytoplankters commute between the surface, where they can build up and store carbohydrates by photosynthesis, and the bottom of the mixing zone, where they store nutrients. Reserves are essential here for growth, because no single stratum in the water column is favourable for growth; their reserve capacity must be large enough to cover a commuting cycle, which depends on wind speed. Although nutrient availability controls primary production ultimately, wind is doing so proximately. The rain of dead or dying phytoplankters fuels the dark ocean communities, not unlike the rain of plant leaves fueling soil communities, but then on a vastly larger spatial scale. Little is known about the deep ocean food web; recent studies indicate that cnidarians (jelly fish) form a major component [107].

When part of this organic rain reaches the anoxic ocean floor, the organic matter is decomposed by fermenting bacteria (many species can do this); the produced hydrogen serves as substrate for methanogens (i.e. archaea), which convert carbon dioxide into methane. This methane can accumulate in huge deposits of methane hydrates, which serve as substrate for symbioses between bacteria and a variety of animals, such as the ice worm *Hesiocoeca*, a polychaete. The total amount of carbon in methane hydrates in ocean sediments is more than twice the amount to be found in all known fossil fuels on Earth. If the temperature rises in the deep oceans, the hydrates become unstable and result in a sudden massive methane injection into the atmosphere. This happened e.g. 55 Ma years ago (e.g. [594], the Paleocene-Eocene Thermal Maximum (PETM) event, which induced massive extinction. We are just beginning to understand the significance of these communities on ocean floors and deep underground.

The colonization of the terrestrial environment by plants may in fact have allowed reefs of brachiopods, bryozoans and molluscs (all filter feeders) to flourish in the Silurian and the Devonian (360–438 Ma ago); the reefs in these periods were exceptionally rich [588]. With the help of their bacterial symbionts, the plants stimulated the conversion from rock to soil, which released nutrients that found their way to the coastal waters, stimulated algal growth, and, hence, the growth of zooplankton, which the reef animals, in turn, filtered out of the

water column. Although plant megafossils only appeared in the Silurian, cryptospores, which probably originate from bryophytes were very abundant in the Ordovician (438–505 Ma ago) [534]. So the timing of the terrestrial invasion and the reef development supports this link. The reefs degraded gradually during the time Pangaea was formed toward the end of the Permian, which reduced the length of the coastline considerably, and thereby the nutrient flux from the continents to the ocean. Moreover, large continents come with long rivers, and more opportunities for water to evaporate rather than to drain down to the sea; large continents typically have salt deposits. When Pangaea broke up, new coastlines appeared. Moreover, this coincided with a warming of the globe, which brought more rain, more erosion, and high sea levels, which caused covering of large parts of continents by shallow seas. This combination of factors caused planktontic communities to flourish again in the Cretaceous, and completely new taxa evolved, such as the coccolithophorans and the diatoms. This hypothesis directly links the activities of terrestrial plants to the coastal reef formation through nutrient availability. Although plants reduce erosion on a time scale of thousands of years, they promote erosion on a multi-million years time scale in combination with extreme but very rare physical forces that remove both vegetation and soil. The geological record of the Walvis Ridge suggests that the mechanism of physical-chemical forces that remove the vegetation, followed by erosion and nutrient enrichment of coastal waters in association with recolonization of the rocky environment by plants might also have been operative in e.g. the 0.1 Ma recovery period following the PETM event (Kroon, personal communication).

A direct quantitative relationship exists between the fossil carbohydrates (methane hydrates, coal, oil, gas, all of biotic origin) and dioxygen in the atmosphere. Although dioxygen, a by-product of oxygenic photosynthesis, was doubtlessly very toxic for most organisms when it first occurred freely in the atmosphere; today most life is dependent upon it, both directly, as well as indirectly, such as the ozone shield against UV radiation. So phototrophs generate dioxygen that is used by heterotrophs; again a form of syntrophy.

Effects of life on climate

The evolutionary interrelationships between life and climate are discussed in [291].

Climate modeling mainly deals with energy (temperature) and water balances. Heat and water transport and redistribution, including radiation and convection in atmospheres and oceans, depends on many chemical aspects which means that climate modeling cannot be uncoupled from modeling biogeochemical cycling. I here focus on radiation, as affected via albedo and absorption by greenhouse gases.

Water

Because of its abundance, water is by far the most important greenhouse gas. Its origin is still unclear; some think it originates from degassing of the hot young planet [332], others think from meteoric contributions in the form of carbonaceous chondrites [40], which possibly continues today.

Plants modify water transport in several ways. Although plants can extract foggy water from the atmosphere particularly in arid environments (by condensation at their surface as well as via the emission of condensation kernels), they generally pump water from the soil into the atmosphere, and increase the water capacity of terrestrial environments by promoting soil formation in bare environments (chemically, with help of bacteria [41]) thereby reducing water runoff to the oceans. This became painfully clear during the flooding disasters in Bangladesh, that followed the removal of Himalayan forests in India. On a short time scale, plants greatly reduce erosion; their roots prevent or reduce soil transport by common mild physical forces. In combination with rare strong and usually very temporal physical forces that remove vegetation (fires in combination with hurricanes or floods, for instance), however, plants increase erosion on a longer time scale, because plants enhance soil-formation in rocky environments. Because such 'catastrophes' are rare, they have little impact on short time scales. The effects of plants on climate and geochemistry were perhaps most dramatic during their conquest of dry environments in the middle Devonian. It came with a massive discharge of nutrients and organic matter into the seas, that lead to anoxia and massive extinctions in the oceans [5].

Plants, therefore, affect the nutrient (nitrate, phosphate, silica, carbonates) supply to the oceans in complex ways, and thus the role of life in the oceans in the carbon cycle. Plants pump water from the soil into the atmosphere much faster in the tropics than in the temperate regions because of temperature (high temperature comes with large evaporation), seasonal torpor (seasons become more pronounced toward the poles, so plants are active during a shorter period in the year toward the poles) and nutrients in the soil (plants pump to get nutrients, which are rare in tropical soils).

Plants substantially influence their local environment, and facilitate colonization by other forms of life, which follows a sequence of ecosystem succession. As holds for most forms of life, plants, and especially the flowering plants, need other organisms (fungi, animals) for survival and propagation. Their massive appearance in the Carboniferous greatly affected global climate, via effects on the carbon cycle [39]. Most climate models keep the mean global relative humidity constant at 50%, e.g. [99], but this assumption can be questioned.

Carbon dioxide

Carbon dioxide is the second most important greenhouse gas. Its dynamics involves the global carbon cycle, which is still poorly known quantitatively. This is partly due to the coupling with other cycles.

Carbon dioxide is removed from the atmosphere by chemical weathering of silicate rocks, which couples the carbon and silica cycles. This weathering occurs via wet deposition, and gives a coupling between the carbon and the water cycle. When ocean down-washed calcium carbonate and silica oxide precipitate and become deeply buried by continental drift in earth's mantle, segregation occurs into calcium silicate and carbon dioxide; volcanic activity puts carbon dioxide back into the atmosphere. Geochemists generally hold this rock cycle to be the main long-term control of the climate system.

Westbroek [582] argued that the role of life in the precipitation processes of carbonates

and silica oxide became gradually more important during evolution. Mucus formers (by preventing spontaneous precipitation of super-saturated carbonates) and calcifiers have controlled carbonates since the Cretaceous. Diatoms (and radiolarians) have controlled silicates since the Jurassic [333]. Corals and calcifying plankton (coccolithophores and foraminiferans) have an almost equal share in calcification. In freshwater, charophytes are in this guild. For every pair of bicarbonate ions, one is transformed into carbon dioxide for metabolism, and one into carbonate. Planktonic derived carbonate partly dissolves, and contributes to the build up of a concentration gradient of inorganic carbon in the ocean. This promotes the absorption of carbon dioxide from the atmosphere by seawater.

The dry deposition of carbon dioxide in the ocean is further enhanced by the organic carbon pump, where inorganic carbon is fixed into organic carbon, which travels down to deep layers by gravity. This process is accelerated by predation where unicellular algae are compacted into faecal pellets, and partial microbial decomposition recycles nutrients to the euphotic zone, boosting primary production. The secondary production also finds its way to the deep layers.

Most of the organic matter is decomposed in the deep ocean. The net effect is a depletion of inorganic carbon from the euphotic zone, which promotes the transport of carbon from the atmosphere into the oceans. This process is of importance on a time scale in the order of millennia (the cycle time for ocean's deep water), and so is relevant for assessing effects of an increase of atmospheric carbon by humans. It is less important on much longer time scales.

In nutrient-rich shallow water, organic matter can accumulate fast enough to form anaerobic sediments, where decomposition is slow and incomplete and fossilization into mineral oil occurs. Although textbooks on marine biogeochemistry do not always fully recognize the role of plants in the global carbon cycle, cf [355, p 139], coal deposits in freshwater marshes are substantial enough to affect global climate. Oil formed by plankton and coal by plants mainly occurs on continental edges, and affects climate on the multi-million time scale.

Methane

Methane is the third most important greenhouse gas; 85 % of all emitted methane is (presently) produced by methanogens (in syntrophic relationships with other organisms, sometimes endosymbiotic) in anaerobic environments (sediments, guts) [370, 143]. The flux is presently enhanced by large scale deforestation by humans via termites. Apart from accumulation in the atmosphere, and in fossilized gas, big pools ($2\,10^3$–$5\,10^6$ Pg) of methane hydrates rest on near shore ocean sediments. Since methane can capture infrared radiation 25 times better than carbon dioxide, on a molar basis, a release of the methane hydrates can potentially destabilize the climate system [342]. Oxidation of methane is a chief source of water in the stratosphere [79], where it interferes with radiation.

Like carbon dioxide, the methane balance is part of the global carbon cycle. Since most of life's activity is limited by nutrients, the carbon cycle cannot be studied without involving other cycles. Nitrogen (nitrate, ammonia) is the primary limiting nutrient, but iron might be limiting as well in parts of the oceans [15, 91]. After assuming that dinitrogen

fixing cyanobacteria could eventually relieve nitrogen limitation, Tyrell [561] came to the conclusion that nitrogen was proximately limiting primary production, and phosphate was ultimately doing so. The question remains, however, are cyanobacteria active enough? Many important questions about the nitrogen cycle are still open, even if oceans represent a sink or a source of ammonia, nitrates and nitrous oxide [208]. The latter is after methane, the next most important greenhouse gas, which can intercept infrared radiation 200 times better than carbon dioxide.

Most nutrients enter the oceans via rivers from terrestrial habitats, which couples both systems and makes coastal zones very productive. The surface area of this habitat has obviously been under control by continental drift and seawater level changes, and therefore with ice formation and temperature. These remarks serve to show the link between climate and biochemical cycles.

Dioxygen

Complex relationships exist between the carbon and oxygen cycles. Dioxygen results from photosynthesis, so there is a direct relationship between dioxygen in the atmosphere and buried fossil carbon. The latter probably exceeds dioxygen on a molar basis, because of e.g. the oxidation of iron and other reduced pools in the early history of the earth. Photorespiration links dioxygen to carbon dioxide levels; both gases bind competitively to rubisco and drive carbohydrate synthesis in opposite directions. This effect of dioxygen is possibly an evolutionary accident that resulted from the anoxic origins of rubisco. Spontaneous fires require at least 75 % of present day dioxygen levels, and oxygen probably now sets an upper boundary to the accumulation of organic matter in terrestrial environments, and so partly controls the burial of fossilized carbon [589]. The extensive coal fires in China at 1 km depth, that occur since human memory, illustrate the importance of this process. Model calculations by Berner [38] suggest, however, that dioxygen was twice the present value during the Carboniferous. If true, this points to the control of fossil carbon accumulation by oxygen being weak. The big question is, of course, to what extent humans are perturbing the climate system by enhancing the burning of biomass and fossil carbon. The massive burning of the worlds' rain forests after the latest el Niño event makes it clear that their rate of disappearance is accelerating, despite the world-wide concern.

Albedo

Apart from greenhouse gases, the radiation balance is affected by albedo. Ice and clouds are the main controlling components. Cloud formation is induced by micro-aerosols, which result from combustion processes, volcanoes and ocean spray derived salt particles. Phytoplankton (diatoms, coccolithophorans) affects albedo via the production of dimethyl sulfide (DMS), which becomes transformed to sulphuric acid in the atmosphere, acting as condensation nuclei. The production is associated with cell death, because the precursor of DMS is mainly used in cell's osmo-regulation. Plants, and especially conifers, which dominate in taiga and on mountain slopes, produce isoprenes and terpenes [68], which, after some oxidation transformations, also result in condensation nuclei. Since plants cover a main

part of the continents, plants change the colour, and so the albedo of the earth, in a direct way. Condensation nuclei derived from human-mediated sulfate emissions now seem to dominate natural sources, and possibly counterbalance the enhanced carbon dioxide emissions [93].

Ice affects the climate system via the albedo and ocean level. If temperature drops, ice grows and increases the albedo, which makes it even colder. It also lowers the ocean level, however, which enhances weathering of fossil carbon and increases atmospheric carbon dioxide. This affects temperature in the opposite direction, and illustrates a coupling between albedo, and the carbon and water cycles.

Effects of climate on life

Climate affects life mainly through temperature, and in terrestrial environments, by precipitation and humidity. Nutrient supply and drain is usually directly coupled to water transport. The transport of organisms themselves in water and in air can also be coupled to climate. The effects are in determining both geographical distribution patterns, abundance and activity rates.

The effects of body temperature of physiological rates are well described by the Arrhenius relationship within a species-specific range of temperatures, which approximately results in a two-to-three-fold increase in rate (respiration, feeding, reproduction, growth, etc) for a 10 degrees increase in body temperature. At the lower temperature boundary, most organisms can switch to a torpor state, while instantaneous death results when temperature exceeds the upper boundary. Many species of organism that do not switch to the torpor state, escape bad seasons by migration, some of them traveling on a global scale. Endotherms (birds and mammals) are well known examples of spectacular migrations; their energy budgets are tightly linked to the water balance. The capacity to survive periods of starvation has close links with body size; these periods tend to be proportional to volumetric body length.

Plant production increases in an approximately linear way with annual precipitation, which illustrates the importance of water availability in terrestrial environments. Plants use water for several purposes, one of them being the transport of nutrients from the soil to their roots. This is why the ratio of the surface areas of shoots and roots enters in the saturation constants for nutrient uptake by plants. Precipitation also affects nutrient availability via leakage.

Because multiple reserve systems have to deal with excretion, assimilation is much more loosely coupled to maintenance and growth compared to single reserve systems. The way temperature affects photosynthesis (*i.e.* the formation of carbohydrates from photons, carbon dioxide and water) differs from how it affects growth (synthesis of structure), with the consequence that the excretion of carbohydrates (mobilized from its reserve, but rejected by the SUs for growth) depends on temperature. This means that the importance of the microbial loop is temperature dependent. Single reserve systems, by contrast, do not excrete in this way and so do not have this degree of freedom, with the consequence that all their rates (assimilation, maintenance, growth, reproduction, respiration) depend

on temperature in (more or less) the same way. The logic is in the biochemistry behind the transformation from food to biomass (growth, reproduction). This machinery does not have the flexibility to operate with a temperature-dependent efficiency. Studies on the temperature dependence of rates typically do not consider the mass balance of the system. If temperature affects animal assimilation differently than growth, body composition or product formation would depend on temperature as well; this has never been observed in "lower" animals to our knowledge. Temporal heterogeneity, acclimatisation, the role of reserve in body composition and the separation of effects of food intake and temperature hamper this line of research.

Extensive pampa and savannah ecosystems, as well as the recently formed fijnbos vegetation in Southern Africa require regular fires of a particular intensity for existence. Many plant species require fire to trigger germination.

Local differences between seasons in temperate and polar areas are large with respect to global climate changes during the evolution of the earth, which complicates the construction of simple models that aim to be realistic.

Chapter 9

Living together

Symbiontic relationships

{299}

The number of known symbiontic relationships continues to increase. Mites and collemboles turn out to play a key role in the fertilization of mosses [98].

The flagellate *Hatena* (*Katablepharidophyta*) has the (single) symbiont *Nephroselmis* (*Prasinophyceae, Viridiplantae*). The symbiont retains its nucleus, mitochondria, plastid, and occasionally the Golgi body, but the flagella, cytoskeleton and endomembrane system are lost. Its eye-spot, which is inside the plastid, is always near the apex of the host and the host use it for phototaxis. When the host divides, a one daughter gets the symbiont, and the other develops a feeding apparatus to engulf a new symbiont, after which the feeding apparatus degenerates [425].

The opistobranch *Phyllodesmium* feeds on soft symbiontic corals and houses coral's algal symbionts in its complex midgut. The zooanthellae not only remain active photosynthesically, but also give the slug exactly the same color as its coral prey, which makes it difficult to detect [445]. The opistobranch *Elysia* harbors the chloroplast of its prey *Vaucheria* (*Xanthophyta*). Since *Elysia* parents don't pass the chloroplasts to their offspring, the acquisition of chloroplasts is the first thing to do in its 10-month life.

Derivation of Eq at bottom

{303}

Eq at the bottom and that for M_{V1}/M_{V2} can be derived as follows: We are looking for conditions under which M_{V1}/M_{V2} remains constant, and is independent of the specific growth rate $\dot{r}$. So if M_{V1} is growing at rate $\dot{r}$, M_{V2} must also grow at that rate. This must hold for all rates, so also for $\dot{r} = 0$. If $f = g_1 \dot{k}_{M1}/\dot{k}_{E1}$, we have that $\dot{r}_1 = 0$ (see formula for $\dot{r}_1$ and set numerator equal to zero) and $j_P = \zeta_{PM}\dot{k}_{M1}g_1 + \zeta_{PA}\dot{k}_{E1}f = \dot{k}_{M1}g_1(\zeta_{PM} + \zeta_{PA})$ (see below the formulas for $\dot{r}_1$ and $\dot{r}_2$). We set the numerator of $\dot{r}_2$ equal to zero and obtain $\frac{\dot{k}_{E2}j_P}{j_{P,Am2}}\frac{M_{V1}}{M_{V2}} = \dot{k}_{M2}g_2$. Substitution of j_P and rearranging terms gives

$$\frac{M_{V1}}{M_{V2}} = \frac{g_2}{g_1}\frac{\dot{k}_{M2}}{\dot{k}_{M1}}\frac{j_{P,Am2}}{\dot{k}_{E2}}\frac{1}{\zeta_{PM} + \zeta_{PA}}$$

which is the formula that is presented. Equating the polynomial coefficients in $\dot{r}_1$ to zero, as explained in the text, we have $\frac{\zeta_{PM}}{\zeta_{PA}}\left(\frac{\dot{k}_{M1}}{\dot{k}_E}+\frac{\dot{k}_{M1}}{\dot{k}_{M2}}\right)=1-\frac{\dot{k}_{M1}}{\dot{k}_{M2}}$. Rearrangement of terms gives $\zeta_{PM}=\zeta_{PA}\frac{\dot{k}_{M1}^{-1}-\dot{k}_{M2}^{-1}}{\dot{k}_E^{-1}+\dot{k}_{M2}^{-1}}$, so $\zeta_{PM}+\zeta_{PA}=\zeta_{PA}\frac{\dot{k}_{M1}^{-1}+\dot{k}_E^{-1}}{\dot{k}_E^{-1}+\dot{k}_{M2}^{-1}}$. Substitution into the equation for M_{V1}/M_{V2} directly gives the result in the last line. The formula for M_{E1}/M_{E2} can be derived from the observations that $M_E=M_V m_{Em} f$ (from Table 3.4 at {122}), and the scaled functional response f of the recipient is $\frac{j_P}{j_{P,Am2}}\frac{M_{V1}}{M_{V2}}$. This gives $\frac{M_{E1}}{M_{E2}}=\frac{M_{V1}}{M_{V2}}\frac{m_{Em1}}{m_{Em2}}f\frac{j_{P,Am2}}{j_P}\frac{M_{V2}}{M_{V1}}=\frac{m_{Em1}}{m_{Em2}}\frac{j_{P,Am2}}{j_P}f$. We now substitute j_P, which reduces for $\zeta_{PG}=0$ and $\dot{k}_{E1}=\dot{k}_E$ to $j_P=\zeta_{PM}\dot{k}_{M1}g_1+\zeta_{PA}\dot{k}_E f=f\dot{k}_E\zeta_{PA}\left(1+\frac{\dot{k}_{M2}-\dot{k}_{M1}}{\dot{k}_{M2}+\dot{k}_E}\frac{g_1}{f}\right)$. The latter follows after substitution of ζ_{PM} for the value obtained above. Substitution of $\frac{m_{Em1}}{m_{Em2}}=\frac{M_{Em1}}{M_{Em2}}\frac{M_{V2}}{M_{V1}}$ directly leads to the formula for M_{E1}/M_{E2} that is presented on the bottom line.

Symbioses

{304}

The dynamic aspects of symbioses that are based on syntrophic relationships are studies in depth in [298, 297].

Droop vs DEB

{315}

The demonstration that the one reserve - one structure DEB model for V1-morphs without maintenance reduces to the Droop model is as follows. The Droop equations [121] are:

$$\frac{d}{dt}Q = u-\mu Q \tag{9.1}$$

$$\mu/\mu'_m = 1-k_Q/Q \tag{9.2}$$

$$u/u_m = s/(k_s+s) \tag{9.3}$$

quantity	Droop	DEB
specific growth rate	μ	$\dot{r}$
asymptotic growth rate	μ'_m	$\dot{k}_E$
cell nutrient quota	Q	m_E+n_{XV}
subsistence quota	k_Q	n_{XV}
specific uptake rate	u	j_{XA}
max spec uptake rate	u_m	j_{XAm}
half saturation constant	k_s	K
nutrient concentration	s	X

Since $\dot{k}_E=j_{XAm}/m_{Em}$, see {122}, the specific reserve dynamics (3.55) becomes

$$\frac{d}{dt}m_E=j_{EAm}f-\dot{k}_E m_E$$

For nutrient X (think of elemental nitrogen, for instance), we have $y_{EX}=1$, so $j_{EAm}=j_{XAm}$ and (9.3) shows that $u=j_{EAm}f$. To see that Droop's cell quota kinetics is equivalent to DEB reserve kinetics for zero maintenance costs, $\dot{k}_M=0$, we need to demonstrate that

μQ is equivalent to $\dot{k}_E m_E$, since $\frac{d}{dt}Q$ is equivalent to $\frac{d}{dt}m_E$. Multiplication of (9.2) with Q leads to $\mu Q = \mu'_m(Q - k_Q)$. Since $Q - k_Q$ is equivalent to m_E, we only need to demonstrate that μ'_m is equivalent to $\dot{k}_E$, where μ'_m is the specific growth rate at infinite reserve density. Since $\dot{r} = \dot{k}_e \frac{e-l_d}{e+g} = \frac{\dot{k}_E e - \dot{k}_M g}{e+g}$ with $e = m_E/m_{Em}$ (see {108} and {122}), we indeed have that $\dot{r} \to \dot{k}_E$ for $m_E \to \infty$ (which is obviously not possible in the cell since the maximum reserve density is $m_{Em} = j_{XAm}/\dot{k}_E$). A minor difference between the Droop and the DEB models is the use of units. Where DEB theory uses C-mol (because this is most handy when evaluating mass conservation), Droop's model is frequently applied on (dry) weights.

Droop aimed to relate cell quota to the specific growth rate as observed in chemostats in steady state. He had no dynamic system in mind, and emphasized its empirical nature.

Derivation of Eq (9.19)

{318}

Eq (9.19) can be derived as follows: Notice that the general strategy of the chapter is to start on ground that should be familiar to microbiologists and step by step more DEB elements are introduced. So we have to show that (9.19) reduces to (9.12) by removing DEB elements. The first step is to exclude aging, so $\dot{h}_a = 0$. The second step is to remove reserve, so $[E_m] \to 0$. We work here with compound parameters, rather than with primary ones, so we have to study each of the compound parameters to evaluate the consequences. We have $g = \frac{[E_G]}{\kappa[E_m]}$, so $g \to \infty$. We also have $l_d = \frac{\dot{k}_M g}{\dot{k}_E} = \frac{[\dot{p}_M]}{\kappa[\dot{p}_{Am}]}$, so l_d remains fixed. The implementation of these changes in (9.19) results in $\frac{d}{d\tau}x_1 = Y_g \jmath_{Xm}(f - l_d)x_1 - x_1 = Y_g \frac{f-l_d}{f} \jmath_{Xm} f x_1 - x_1 = Y \jmath_{Xm} f x_1 - x_1$ with $Y = Y_g \frac{f-l_d}{f}$. This latter relationship is given in the table at the bottom of {315} for the Marr-Pirt model. Notice the absence of dots in the equations, because we work in scaled time, that is dimensionless.

Time scale separation

{328}

Simplifying approximations for batch dynamics by Jean-Christophe Poggiale. Assume that we have the following model for V1-morphs in a batch reactor (Figure 9.1)

$$\begin{aligned} \frac{d}{d\tau}x_0 &= I - j_{Xm} f x_1 \\ \frac{d}{d\tau}e &= k_E\,(f - e) \\ \frac{d}{d\tau}x_1 &= \frac{k_E e - k_M g}{e + g} x_1 \end{aligned}$$

Let us assume that e is a fast variable with respect to x_0 and x_1. It follows that e reaches a quasi-steady state value f, which is a function of the slow variables:

$$f\,(x_0) = \frac{x_0}{K_x + x_0}$$

We can thus replace e by f in the third equation, which leads to the two dimensional model (Figure 9.2):

Table 9.1: Definition, values and units of the parameters.

Symbol	Parameter Name	Value	Unit
$\dot{I}$	input rate of substrate	1	$\mathrm{mM\,h^{-1}}$
j_{Xm}	maximum specific uptake rate	0.125	$\mathrm{mM\,h^{-1}}$
K_x	half-saturation constant for uptake	5	mM
$\dot{k}_E$	Reserve turnover rate	0.925	$\mathrm{h^{-1}}$
$\dot{k}_M$	Maintenance turnover rate	0.04	$\mathrm{h^{-1}}$
g	Investment ratio	0.5	-

$$\begin{aligned}\frac{d}{d\tau}x_0 &= I - j_{Xm} f x_1 \\ \frac{d}{d\tau}x_1 &= \frac{(k_E - k_M g)\, x_0 - k_M g K_x}{x_0\,(1+g) + g K_x} x_1\end{aligned}$$

Furthermore, if we assume that x_0 is also fast with respect to x_1, then x_0 also reaches a quasi-steady state value obtained by vanishing the first equation. We thus get $f = \frac{I}{j_{Xm} x_1}$. Finally, we can replace f by its value in the third equation and we consequently a one-dimensional model (Figure 9.3):

$$\frac{d}{d\tau}x_1 = \frac{k_E I}{I + g j_{Xm} x_1}\left(1 - \frac{k_M g j_{Xm}}{k_E I} x_1\right) x_1 = r\,(x_1)\left(1 - \frac{x_1}{K}\right) x_1$$

where

$$r\,(x_1) = \frac{k_E I}{I + g j_{Xm} x_1} \quad \text{and} \quad K = \frac{k_E I}{k_M g j_{Xm}}$$

Bifurcation theory

{345}

Work on the bifurcation analysis of tri-trophic food chains has been extended including omnivory and symbiontic relationships [59, 246, 263, 338, 264]. We also studied bi-trophic food chain in which the prey has reserves [255, 297, 336]. The substantial system consequences of a varying nutritional value of prey for predation is studied in [335]. Nice overviews of bifurcation analysis for population dynamics can be found in [256, 244]. Chaos in a bi-variate prey-predator systems is described in [247],

Closed nutrient-producer-consumer system

When one organism eats another one with a chemical composition that can vary, there is a need to deal with conversion efficiencies of prey into predator in a bit more detail than is usual [297]. Things simplify considerably when, like the basic formulation of DEB theory assumes, biomass can be decomposed into a single reserve and a single structure,

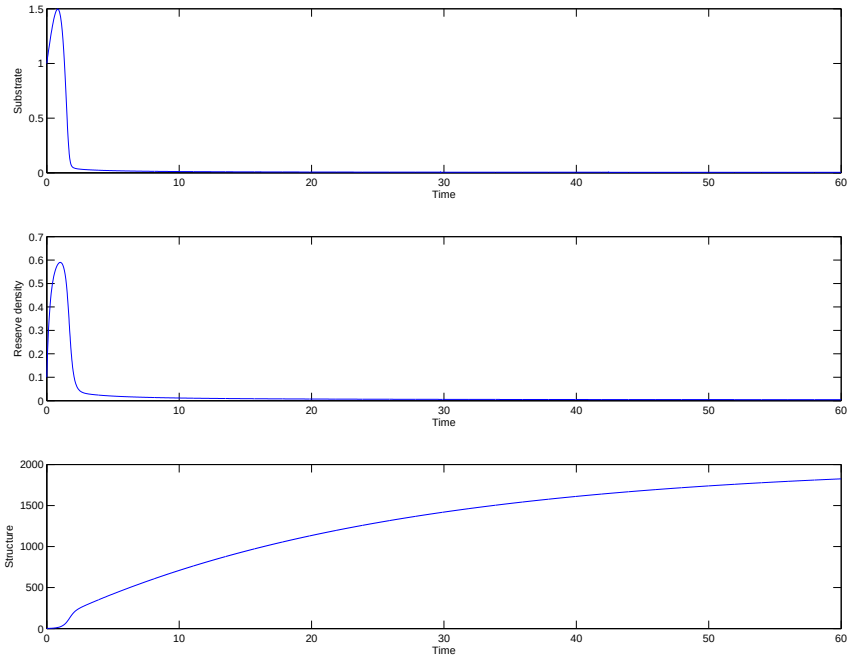

Figure 9.1: This figure shows the dynamics of the standard DEB - model

which do not change in composition. The assimilation process of the predator than should specify how the two components of its prey, together with nutrients from the environment, transform into predator reserves. Think for instance of daphnids feeding on algae. Alga's main carbon component, cellulose, is of no nutritional value for the daphnid. It is the starch and lipids in alga's reserves that are daphnids' main energy sources, while it also needs ammonia and phosphate, for instance, as building blocks. Daphnids can obtain part of these nutrients from the intra-cellular reserves of the alga, sometimes they can also obtain them directly from the environment. So the nutritional value of the alga for the daphnids is not a constant, but varies, and depends on environmental conditions.

The implications of a variable nutritional value of the producer (alga) for the consumer (daphnid) can be illustrated with the simple dynamical system

$$m_N = N/P - n_{NC}\, C/P - n_{NP} \tag{9.4}$$

$$\frac{d}{dt}P = \dot{r}_P P - j_{PA} C \quad \text{with } \dot{r}_P = \frac{\dot{k}_N m_N}{y_{NP} + m_N} \quad \text{and } j_{PA} = \frac{j_{Pm} P}{K + P} \tag{9.5}$$

$$\frac{d}{dt}C = (\dot{r}_C - \dot{h})C \quad \text{with } \dot{r}_C = (1/\dot{r}_{CP} + 1/\dot{r}_{CN} - 1/(\dot{r}_{CP} + \dot{r}_{CN}))^{-1} \tag{9.6}$$

$$\dot{r}_{CP} = y_{CP}\, j_{PA} - \dot{k}_{MP} \quad \text{and } \dot{r}_{CN} = y_{CN}\, m_N\, j_{PA} - \dot{k}_{MN}$$

where consumers' reserve density m_N follows from mass conservation, for a total amount of nutrient N; all nutrient that is not in producers' or consumers' structure is in producers' reserve. The chemical indices n_{NP} and n_{NC} stand for producers' and consumers' nutrient content per carbon. The amount of nutrient in the environment is taken to be negligibly

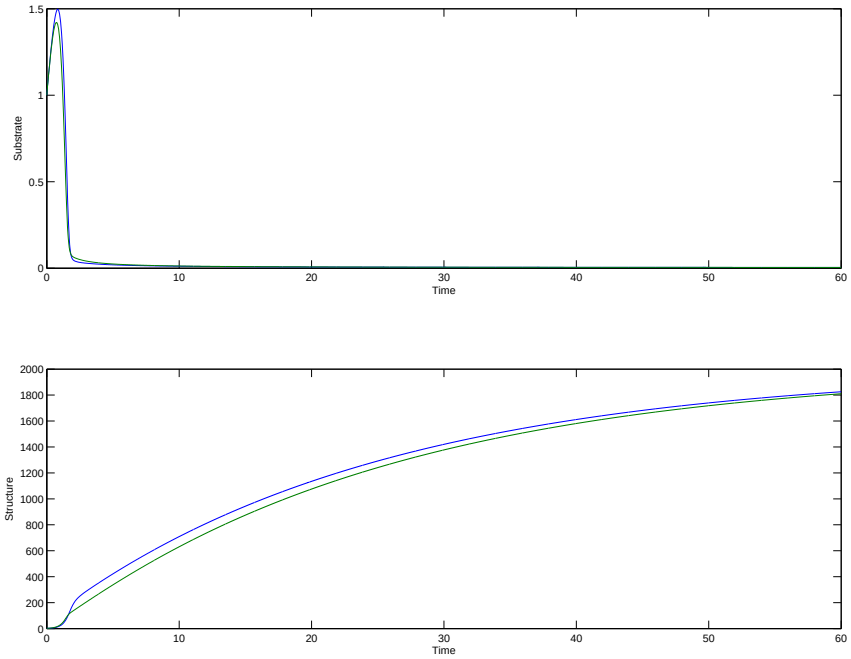

Figure 9.2: This figure compares the 2D-model dynamics to that of the DEB - model.

small. The consumer has a constant hazard rate $\dot{h}$, and dead producers decompose instantaneously. The producers' reserve turnover rate is $\dot{k}_N$, and producers' maintenance is neglected. Consumers' reserves are not taken into account. These simplifications of the DEB theory amount to Droop's kinetics for the consumer (with a very small half saturation constant, and a very large specific maximum uptake rate), and Marr-Pirt's kinetics for the consumer. The Marr-Pirt's kinetics results from the DEB model as a limit for increasing reserve turnover rates. The expression for the growth rate follows from the SU kinetics and the assumption that assimilates from producers' reserve and that from structure are complementary and parallelly processed with a large capacity. There is little need to set a maximum to the capacity here, because that is already set by the maximum specific assimilation rate j_{PAm}. Notice the SU formalism here deals with rates, rather then concentrations, as is basic to its derivation.

Figures 9.4 and 9.6 show the asymptotic dynamics of the system, while Figure 9.5 gives typical orbits. We observe that it shows the typical paradox of enrichment: the system starts oscillating above a certain nutrient level. If consumers require the reserve of the producers, it also has a lower bound for the nutrient level, due to the maintenance costs of the consumer and the system has an upper boundary for nutrient, above which it cannot exist. If the consumers do not require the reserve of the producers, both the homoclinic and the tangent bifurcation points disappear. This means, the upper bound for the nutrient level disappears (the larger the nutrient level, the larger the amplitude of the oscillations, cf [420]) with unrealistic low minima. The lower bound also disappears in the sense that the system goes extinct at very low nutrient levels by a gradual decrease of the consumer population. Notice that consumers cannot invade the producer population with a very

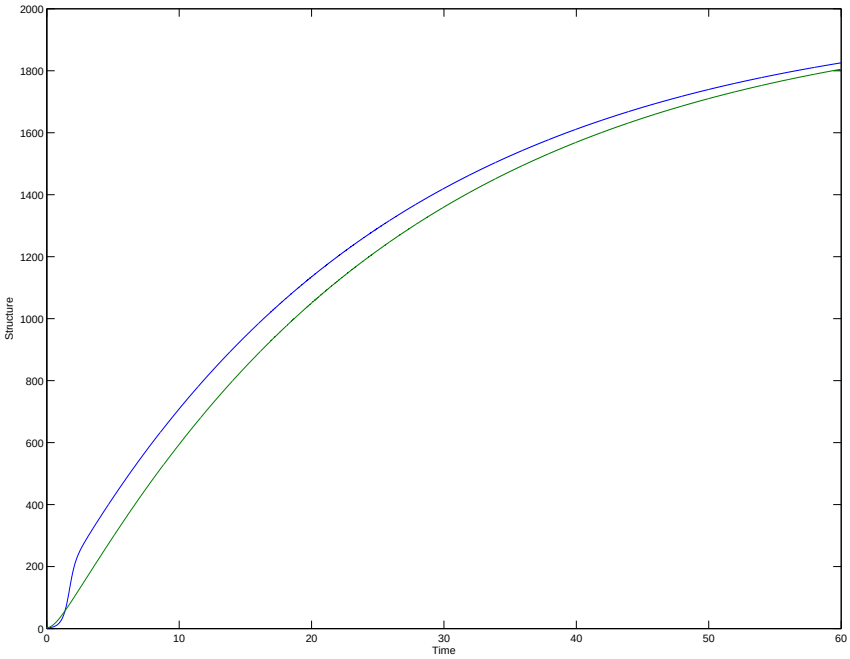

Figure 9.3: This figure compares the logistic-like growth dynamics to that of the DEB - model.

small inoculum size in the case of co-limitation by producers' reserve, but it can in absence of this co-limitation; see Figure 9.4. We can conclude that the nutritional details of the producer/consumer interaction affect their kinetics in a qualitative way. Muller et al [410] discuss a very similar producer-consumer model, which deviates slightly in the specification of consumers' growth (implementation of maintenance and of maximum growth).

Stochastic formulation

The implementation of stochastic events requires the notion of individuals (notably their number), and gives the density of a single producer P_ε and consumer C_ε an explicit and independent role [312].

Table 9.2 gives the possible events F feeding, S searching, D_s dying of C_s and D_h dying of C_h, the intensities $\dot{\lambda}_i$ and the steps sizes at time t. The last process G, the growth of the producers, is supposed to be a deterministic continuous process, not a stochastic point process; the producers continue growing between the Poissonian events, i.e. $\frac{d}{dt}\underline{P} = \dot{r}_P\underline{P}$ where the specific growth rate $\dot{r}_P$ is given in (9.5), producers' reserve density m_N changes as (9.4) and the (variable) yield Y_{CP} is given by $Y_{CP} = \dot{r}_C/j_P$. Between the stochastic jump events m_N, $\dot{r}_P$ and Y_{CP} change smoothly and deterministically, while the consumer densities C_s and C_h remain constant. At a time-incremental basis, $\underline{m}_N$, $\underline{\dot{r}}_P$ and $\underline{Y}_{CP}$ are stochastic, because they are functions of $\underline{P}$ and $\underline{C} = \underline{C}_s + \underline{C}_h$. Together with the initial conditions $P(0)$, $C_s(0)$ and $C_h(0)$, this fully specifies the stochastic dynamics, which we will call the S-model (stochastic model). Again we have the constraint $m_N(0) > 0$ on the initial conditions.

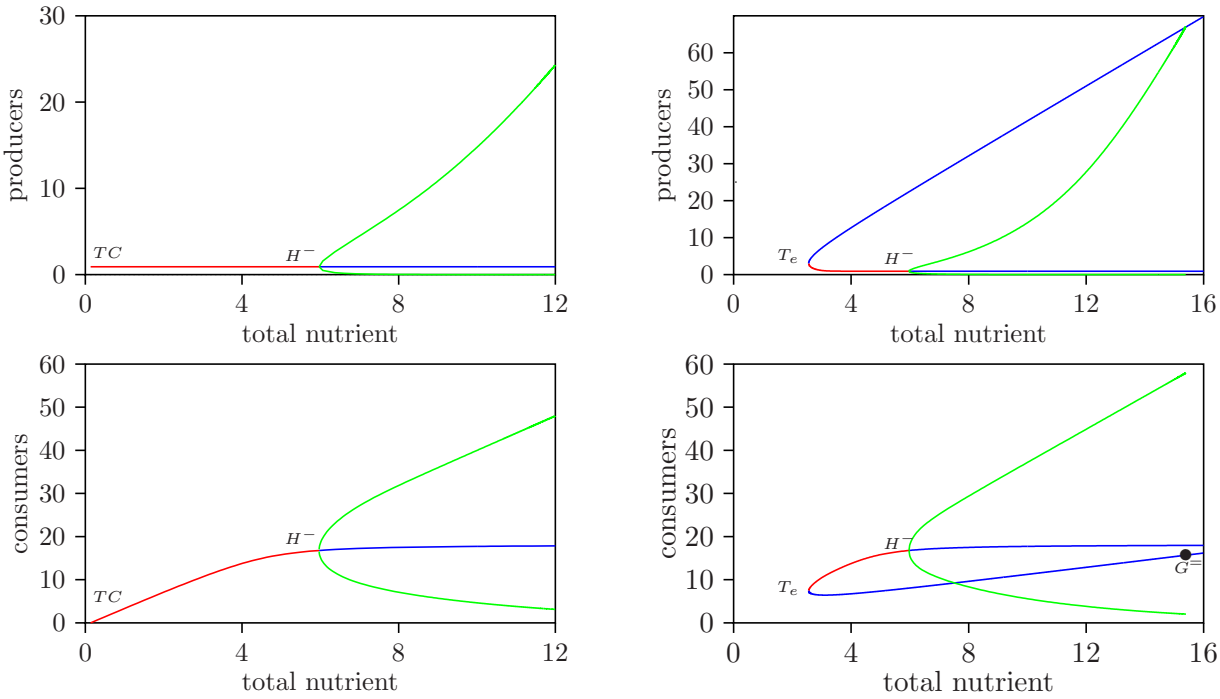

Figure 9.4: The bifurcation diagrams for the producer (top) and the consumer (bottom) dynamics in a closed system, using the total amount of nutrient as bifurcation parameter. The producer follows Droop's kinetics, the consumer follows Marr-Pirt's kinetics and has a constant hazard rate; there is no free nutrient in the environment. Left: The consumer is not limited by producers' reserve, so $\dot{r}_C = \dot{r}_{CP}$. Right: Producers' reserve and structure are complementary for consumers. At very low nutrient levels, the system cannot exist. At intermediary nutrient levels, the system has a point attractor. A transcritical (TC, left) or tangent (T_e, right) and a Hopf bifurcation point (H^-) mark the boundaries of these intermediary nutrient levels. At larger nutrient levels, the system oscillates with increasing amplitude. A homoclinic bifurcation point ($G^=$, right) marks the upper boundary of this interval; the system cannot exist at higher nutrient levels (right), while producers' minima become extremely small for growing nutrients levels (left). Parameters: $\dot{h} = 0.005$ h^{-1}, $n_{NP} = 0.15$ $\frac{\text{mol}}{\text{mol}}$, $n_{NC} = 0.25$ $\frac{\text{mol}}{\text{mol}}$, $y_{CN} = 5.5$ $\frac{\text{mol}}{\text{mol}}$ $y_{CP} = 2$ $\frac{\text{mol}}{\text{mol}}$, $K = 10$ mM, $j_{Pm} = 0.15$ $\frac{\text{mol}}{\text{mol h}}$, $\dot{k}_N = 0.25$ h^{-1}, $\dot{k}_{MP} = 0.02$ h^{-1}, $\dot{k}_{MN} = 0.01$ h^{-1}.

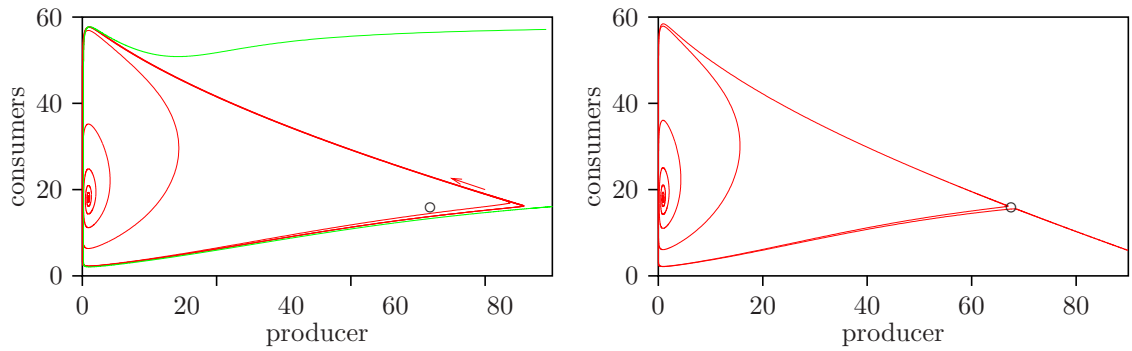

Figure 9.5: Orbits of the producer-consumer system of Figure 9.4 for nutrient levels just below (left, $N = 15.3$ mM) and above (right, $N = 15.5$ mM) the homoclinic bifurcation point. Orbits that start within the stippled separatrix of the top figure result in a stable oscillation (one such an orbit is indicated), while other orbits lead to extinction. This separatrix breaks open for higher nutrients levels (right figure), and all orbits lead to extinction (one such an orbit is indicated). The saddle point, and the spiral source are indicated.

Table 9.2: The possible stochastic events F, S, D_s and D_h, the intensities $\dot{\lambda}_F$, $\dot{\lambda}_S$, $\dot{\lambda}_{D_s}$ and $\dot{\lambda}_{D_h}$ and the steps sizes (dP, dC_s, dC_h), given the state (P, C_s, C_h) of the system at time t. The growth process G is deterministic and continuous. Mass balance restrictions make that the steps in the three variables are coordinated. The coefficient δ_t varies in time, due to stoichiometric constraints on the growth of the consumers from structure as well as varying reserve of the producers. The system is closed for nutrient, so for producers and consumers as well, while nutrient uptake by the producers is large enough to cause negligibly small concentrations of free nutrient.

event type i	F feeding	S searching	D_s dying of C_s	D_h dying of C_h	G growing
intensity $\dot{\lambda}_i$	$\dot{k}\frac{P}{K}\frac{C_s}{C_\varepsilon}$	$\dot{k}\frac{C_h}{C_\varepsilon}$	$\dot{h}_C\frac{C_s}{C_\varepsilon}$	$\dot{h}_C\frac{C_h}{C_\varepsilon}$	$\dot{r}_P\frac{P}{P_\varepsilon}$
change dP	$-P_\varepsilon$	0	0	0	P_ε
change dC_s	$-C_\varepsilon$	C_ε	$-C_\varepsilon$	0	0
change dC_h	$\underline{\delta}_t C_\varepsilon$	$-C_\varepsilon$	0	$-C_\varepsilon$	0

Trajectories for the producer and consumer populations at different values for the total amount of nutrient in the system are given in Figure 9.7. We can see that the Hopf bifurcation point is hardly important for the stochastic models, but the focus point is. Between the focus and the Hopf bifurcation point the deterministic model ports an overshoot behaviour, which lasts longer and has a larger amplitude if closer to the Hopf bifurcation point. Asymptotically, however, the deterministic system settles at the point attractor. The stochastic model, on the contrary, sports irregular semi-oscillatory behaviour in this interval of values for the total amount of nutrient. The oscillations become more regular and the amplitude increases if closer tot the Hopf bifurcation points. Around the focus point the model behaviour changes smoothly, but around the Hopf bifurcation point the asymptotic behaviour of the deterministic model change abruptly. while its transient behaviour and the behaviour of the stochastic model changes smoothly. In summary, the stochastic model responds more smoothly to changes in the total amount of nutrient.

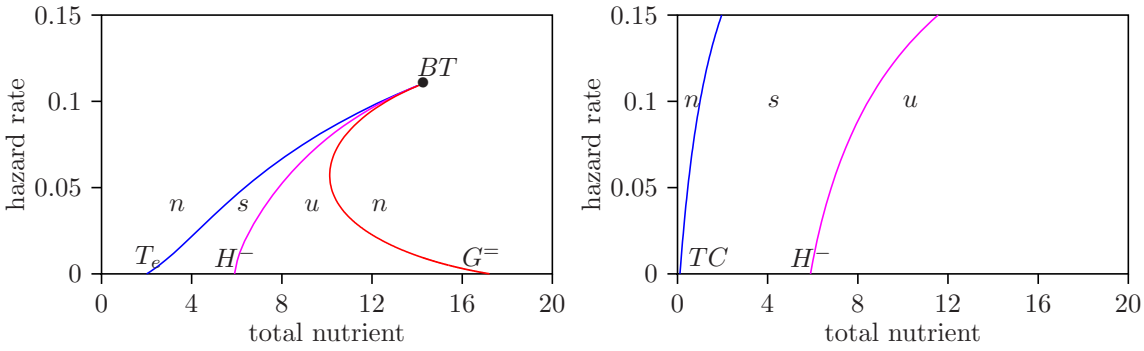

Figure 9.6: The two-dimensional bifurcation diagram for the producer-consumer system as in Figure 9.4, using the total nutrient level and consumers' hazard rate as bifurcation parameters. The consumer requires producers' structure *and* reserve (left) or producers' structure only (right). Three areas are indicated: n no co-existence, s stable co-existence, u unstable co-existence (oscillations). The tangent (T_e), Hopf (H^-) and Homoclinic ($G^=$) bifurcation curves meet in a Bagdanov-Takens point in the top figure; the transcritical (TC) and Hopf (H^-) bifurcation curves diverge in the bottom figure.

Primary production in oceans

{350}

For applications such as the implementation of primary production modules in ocean circulation models, and the study of speciation in an adaptive dynamics context, we felt the need to simplify the canonical community even more till a mono-species community of mixotrophs [311, 559, 558]. Such communities share some characteristics with canonical communities. It turns out that spatial gradient are essential in understanding the speciation of mixotrophs into auto- and heterotrophs. Self-shading seems essential to understand why mixotrophs tend to dominate in oligotrophic environments.

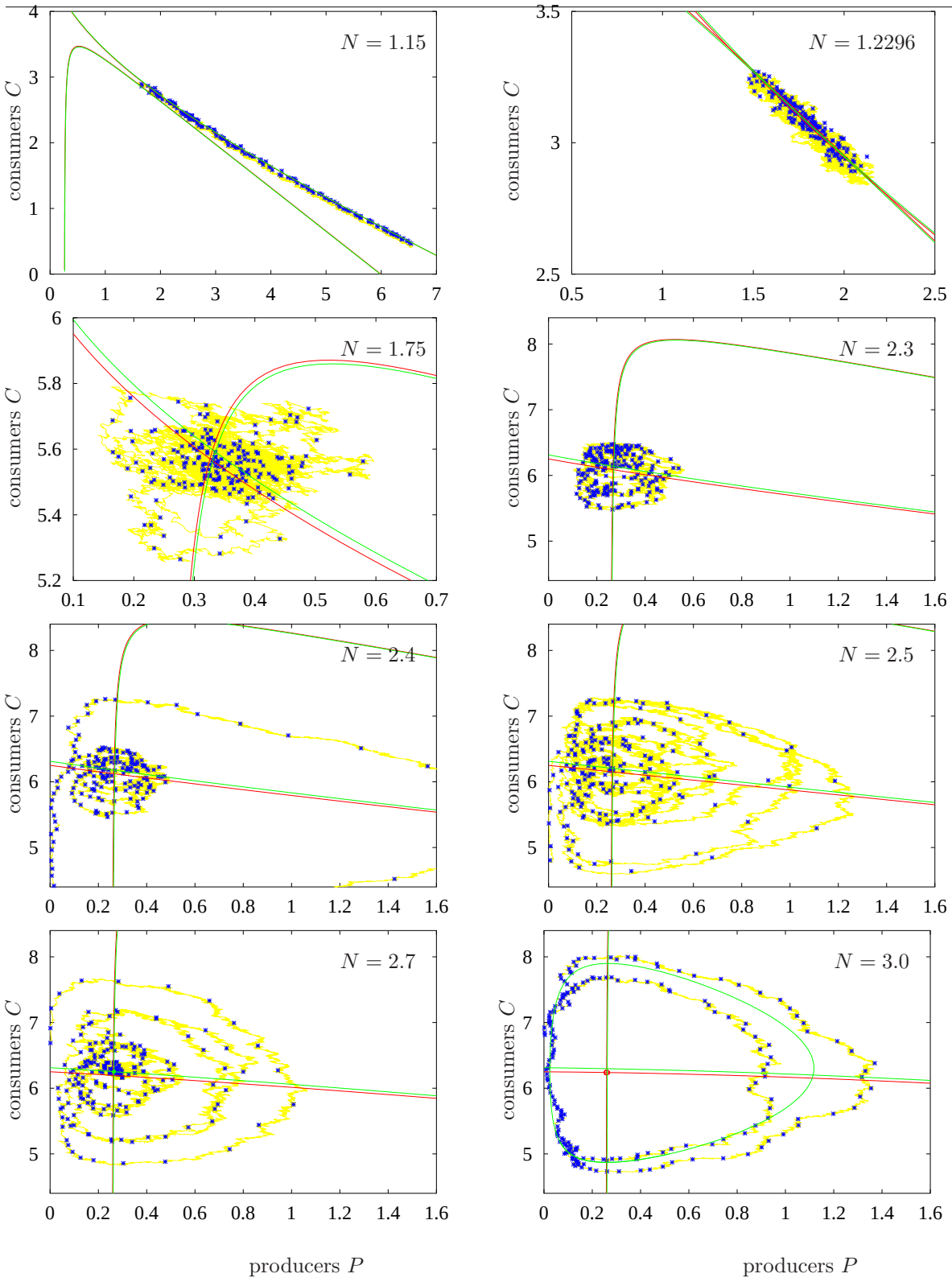

Figure 9.7: The trajectory of the stochastic model for different values for the total amount of nutrient N. The fat dots are the linearly interpolated values with equal time units apart. For low N-values, the start is at the stable equilibrium of the expected value of stochastic model, which is at the intersection of the $\frac{d}{dt}P = 0$ and the $\frac{d}{dt}C_h = 0$ isoclines (while $\frac{d}{dC_h}C_s = 0$; solid curves). For large N-values ($N = 2.7, 3.0$), the start is at a random point of the limit cycle of the NTS-model. The isoclines of the deterministic model are plotted as well (stippled). Notice that for $N = 2.3$ few points of the S-model are at the mean, because of its tendency to cycle. For $N < 2.6$ 1000 time units are used, and 5000 for $N > 2.6$. The various bifurcation points for the total amount of nutrient are:

	tangent	focus	Hopf	global
deterministic	1.217	1.520	3.165	7.11
stochastic	1.229	1.535	2.801	6.96

Chapter 10

Evaluation

Lumping species

{365}

[298] shows that it is possible to merge to two different species that each follow the DEB rules by incremental changes of parameter values across generations such that a single new species emerges that again follows the DEB rules. Since such merging has frequently occurred in evolutionary history, this should be an property of all models that claim to be not species-specific. Net-production models do not have this property. [327] shows that DEB reserves are essential to avoid leaks of metabolites from a cell, if a compound in the catabolic flux is fed to a linear or circular pathway that gives products that are allocated to maintenance and growth. Leaks cannot be avoided in net-production models, which makes it more difficult to make net-production models consistent with biochemical models.

Notation and symbols

Dirac function

{409}, l7

Jacques Bedaux pointed out that the explanation $(x = x_s)/dx \equiv \delta(x - x_s)$ should be introduced, where δ is the Dirac delta function. We then have $\int_{x_1=-\infty}^{x} \delta(x_1 - x_s)\, dx_1 = (x \geq x_s)$.

Notation differences between the first and the second edition

{410}

Some notational differences between first and second editions of the DEB book.

[281]	[289]	interpretation
m	k_M	maintenance rate coefficient
-	m_*	structure-specific molar mass of compound $*$
$\dot{M}$	$\dot{p}_M$	energy flux allocated to maintenance
$\dot{H}$	$\dot{p}_T$	energy flux allocated to heating
$\dot{p}$	$\dot{h}$	individual-specific predation probability rate
K	X_K	half saturation constant
$[G]$	$[E_G]$	energy requirement to grow a unit volume of structure
$\dot{\nu}$	$\dot{k}_E$	specific energy conductance (in V1-morphs)
$\dot{D}$	$\dot{h}$	dilution rate of chemostat
-	$\dot{D}$	diffusivity
$\dot{I}$	$\dot{J}_X$	ingestion rate
W_1	X_W	total biomass density in C-moles per volume

The motivation behind these changes was that the second edition deals more elaborately with masses and mass fluxes, which involves many new symbols. This made it necessary to link the symbol more closely to its dimension group.

The comment for {260} relates to the length symbols.

Notation differences between the second and the third edition

{410}

It turned out to be essential to become more consistent in the signs of mass fluxes and yields. In the second edition, fluxes such as the catabolic flux $\dot{J}_{EC}$ and the food flux $\dot{J}_{XA}$ were typically taken positive. This gave inconsistencies in some cases, which I tried to remove be taking them negative if the level of observation is the whole individual; a negative sign of a flux is linked to the disappearance of that compound from a pool, but this depends on the level of observation. This sign-problem is complex, however, and depends on the level of observation and the choice of state variables (i.e. pools). Parameters are always positive, and yield coefficients written with a lower case y are taken as parameters, but yield coefficients written with an upper case Y are ratios of fluxes (so they are variables, which might vary in time). An example of a subtle consequence is: $\dot{J}_{XA} = \{\dot{J}_{XA}\}L^2$, with $\{\dot{J}_{XA}\} = -\{\dot{J}_{EA}\}/y_{EX}$, where primary parameter $y_{EX} > 0$ and quantity $\{\dot{J}_{XA}\} < 0$. The yield of structure on reserve in the growth process is $Y^G_{VE} = -y_{VE}$, with primary

parameter $y_{VE} > 0$. The negative sign results from the fact that structure appears, but reserve disappears.

The mass-specific fluxes j will be treated as positive, with the consequence that $\dot{J}_{EM} = -j_{EM} M_V$, while $j_{EM} = \dot{k}_M y_{EV}$, because maintenance acts as a sink for reserve. Hazard rates, $\dot{h}$, and energy fluxes, $\dot{p}$, are always taken to be positive.

Since the theory substantially extended, and new variables need to be considered, quite a few new symbols appeared.

Notation and symbols (replacement of original)

Some readers will be annoyed by the notation, which sometimes differs from the one usual in a particular specialisation. One problem is that conventions in e.g. microbiology differ from those in ecology, so not all conventions can be observed at the same time. The symbol D, for example, is used by microbiologists for the dilution rate in chemostats, but by chemists for diffusivity. A voluminous literature on population dynamics exists, where it is standard to use the symbol l for survival probability. This works well as long as one does not want to use lengths in the same text! Another problem is that most literature does not distinguish structural biomass from energy reserves, which both contribute to e.g. dry weight. So the conventional symbols actually differ in meaning from the ones used here.

Few texts deal with such a broad spectrum of phenomena as this book. A consequence is that any symbol table is soon exhausted if one carelessly assigns new symbols to all kinds of variables that show up.

The following conventions are used to reduce this problem and to aid memory.

Symbols

- Variables denoted by symbols that differ only in indices, have the same dimensions. For example M_E and M_V are both moles.
- The interpretation of the leading character does not relate to that of the index character. For example, the M in M_E stands for mass in moles, but in $\dot{k}_M$ it stands for maintenance.
- Some lowercase symbols frequently relate to uppercase ones via scaling; $\{e, E\}$, $\{m, M\}$, $\{j, J\}$, $\{l, L\}$, $\{w, W\}$ and $\{x, X\}$.
- Structure V has a special role in DEB notation. The structural volume V_V is abbreviated as V. Many quantities are expressed per structural mass, volume, or surface area. Likewise the energy of reserve E_E is abbreviated as E.
- Analogous to the tradition in chemistry, quantities which are expressed per unit of structural volume have square brackets, [ ]. Quantities per unit of structural surface area have braces, { }. Quantities per unit of weight have angles, $\langle\,\rangle$, (with indices w and d for wet and dry weight). This notation is chosen to stress that these symbols

refer to relative quantities, rather than absolute ones. They do not indicate concentrations in the chemical sense, because most of the compounds concerned are not soluble.
Parentheses, square brackets and braces around numbers refer to equations, references and pages respectively.

- Rates have dots, which merely indicate the dimension 'per time'. Dots (and primes) do *not* stand for the derivative as in some mathematical and physical texts (see the subsection 'Expressions'). Dots, brackets and braces allow an easy test for some dimensions, and reduce the number of different symbols for related variables. If time has been scaled, i.e. the time unit is some particular value making scaled time dimensionless, the dot has been removed from the rate that is expressed in scaled time.

- Molar values have an overbar.

- Random variables are underscored. The notation $\underline{x}|\underline{x} > x$ means: the random variable $\underline{x}$ given that it is larger than the value x. It can occur in expressions for the probability, $\Pr\{\}$, or for the probability density function, $\phi()$, of distribution function, $\Phi()$.

- Vectors and matrices are printed in bold face. A bold number represents a vector or matrix of elements with that value; so $\dot{\boldsymbol{J}}\mathbf{1}$ is the summation of matrix $\dot{\boldsymbol{J}}$ across columns and $\mathbf{1}^T\dot{\boldsymbol{J}}$ across rows; $\boldsymbol{x} = \mathbf{0}$ means that all elements of $\boldsymbol{x}$ are 0.

- Organic compounds are quantified in C-mol, which stand for the number of C-atoms as a multiple of the number of Avogadro. So 6 C-mol of glucose equals 1 mol of glucose. Notice that for simple compounds, such as glucose we have both the option to express it in mole or C-mole, but for generalized compounds we can only express them in C-mole. So we always use C-mole.

- Yield coefficients are indicated by y if they are constant and by Y if they can vary in time. Moreover, y is taken to be non-negative, while Y can be negative, if one compound is appearing, and the other disppearing. They represent ratios of molar fluxes, so $y_{VE} = J_{EG}/J_{VG}$ is the ratio of the flux of reserve E (here meant to be a type) that is allocated to growth G (here meant to be a process) and the flux of structure V that is synthesized in the growth process. As a consequence we have $y_{EV} = y_{VE}^{-1}$; the yield coefficients y_{**} are treated as positive constant mass-mass couplers. Likewise, we write Y_{WX} for the C-moles of biomass that is formed per consumed C-mole of substrate. This is not constant, however, and depends on the specific growth rate.

Indices

Indices are catenated, the first subscript frequently specifying the variable to which the symbol relates. For example M_V stands for a mole of structural biomass, where V is structural biovolume. Some indices have a specific meaning

$*$	indicates that several other symbols can be substituted.
	It is known as 'wildcard' in computer science.
	As superscript it denotes the equilibrium value of the variable.
$'$	indicates a scaling as superscript.
i, j	are counters that refer to types or species; They can take the values $1, 2, \cdots$
m	stands for 'maximum'. For example $\dot{J}_{Am}$ is the maximum value that $\dot{J}_A$ can attain.
$+$	can refer to the sum of elements, such as $V_+ = \sum_i V_i$, or to addition, such as X_{i+1}.

Indices for compounds refer to

C	carbon dioxide	$C-$	bicarbonate	E	reserve	E_R	reprod. reserve
H	water, maturity	$\mathcal{M}$	minerals	N_H	ammonia	N_O	nitrate
O	dioxygen	$\mathcal{O}$	org. compounds	P	product (faeces)	Q	toxic compound
V	structural mass	X	food				

Indices for processes refer to

a	aging	A	assimilation	C	catabolism	D	dissipation
F	feeding	G	growth	J	mat. maintenance	M	som. maintenance
R	reproduction	$T+$	dissipating heat	T	heating (endotherms)		

Expressions

- An expression between parentheses with an index '+' means: take the maximum of 0 and that expression, so $(x - y)_+ \equiv \max\{0, x - y\}$. The symbol '$\equiv$' means 'is per definition'. It is just another way of writing, you are not supposed to understand that the equality is true.

- Although the mathematical standard for notation should generally be preferred over that of any computer language, I make one exception: the logic boolean, e.g. $(x < x_s)$. It always comes with parentheses and has value 1 if true or value 0 if false. It appears as part of an expression. Simple rules apply, such as

  $(x \leq x_s)(x \geq x_s) = (x = x_s)$

  $(x \leq x_s) = (x = x_s) + (x < x_s) = 1 - (x > x_s)$

  $\int_{x_1=-\infty}^{x} (x_1 = x_s)\, dx_1/dx = (x \geq x_s)$

  $\int_{x_1=-\infty}^{x} (x_1 \geq x_s)\, dx_1 = (x - x_s)_+$

- The following operators occur:

$\frac{d}{dt} X\|_{t_1}$	derivative of X with respect to t evaluated at $t = t_1$
$\frac{\partial}{\partial t} X\|_{t_1}$	partial derivative of X with respect to t evaluated at $t = t_1$
$\mathcal{E} g(\underline{x})$	expectation of a function g of the random variable $\underline{x}$
var $\underline{x}$	variance of the random variable $\underline{x}$: $\mathcal{E}(\underline{x} - \mathcal{E}\underline{x})^2$
cv $\underline{x}$	coefficient of variation of the random variable $\underline{x}$: $\sqrt{\text{var } \underline{x}}/\mathcal{E}\underline{x}$
cov $(\underline{x}, \underline{y})$	covariance between the random variables $\underline{x}$ and $\underline{y}$: $\mathcal{E}(\underline{x} - \mathcal{E}\underline{x})(\underline{y} - \mathcal{E}\underline{y})$
cor $(\underline{x}, \underline{y})$	correlation between $\underline{x}$ and $\underline{y}$: cov $(\underline{x}, \underline{y})/\sqrt{\text{var } \underline{x}\, \text{var} \underline{y}}$
$\boldsymbol{x}^T$	transpose of vector or matrix $\boldsymbol{x}$ (interchange rows and colums)
$\vdots$	catenation across columns: $\boldsymbol{n} = (\boldsymbol{n}_{\mathcal{M}} \vdots \boldsymbol{n}_{\mathcal{O}})$

Units, dimensions and types

The SI system is used to present units of measurements. My experience is that some readers are unfamiliar with the symbol 'a' for year.

In the description of the dimensions in the list of symbols, the following symbols are used:

$-$	no dimension	L	length (of individual)	e	energy ($\equiv ml^2t^{-2}$)
t	time	l	length (of environment)	T	temperature
$\#$	number (mole)	m	mass (weight)		

These dimension symbols just stand for an abbreviation of the dimension, and differ in meaning from symbols in the symbol column. A difference between the dimensions l and L is that the latter involves an arbitrary choice of the length to be measured (e.g. including or excluding a tail). The morph interferes with the choice. The dimensions differ because the sum of lengths of objects for which l and L apply, does not have any useful meaning. The list below does not include symbols that are used in a brief description only. The page number refers to the page where the symbol is introduced.

The choice of symbols relates to dimensions, and not to types. Three types are specified in the description in the list: constant, c, variable, v, and function, f. This classification cannot be rigorous, however. The temperature T, or example, is indicated to be a constant, but it can also be considered as a function of time, in which case all rate constants are functions of time as well. On the other hand, variables such as food density X, can be held constant in particular situations. Variables such as structural biovolume V are constant during a short period, such as is relevant for the study of the process of digestion, but not during a longer period, such as is relevant for the study of life cycles. The choice of type can be considered as a default, deviations being mentioned in the text.

List of frequently used symbols

symbol	dim	type	interpretation
a	t	v	age, i.e. time since gametogenesis of fertilization
a_b	t	v	age at birth (hatching), i.e. end of embryonic stage
a_p	t	v	age at puberty, i.e. end of juvenile stage
$a_\dagger$	t	v	age at death (life span)
$\{\dot{b}\}$	$l^3\#l^3L^{-2}t^{-1}$	c	specific searching rate
$\dot{b}_\dagger$	$l^3\#^{-1}t^{-1}$	c	killing rate by xenobiotic compound
$B_x(a,b)$	-	f	incomplete beta function
c_0	$\# l^{-3}$	c	no-effect concentration of xenobiotic compound in the environment
c_d	$\# l^{-3}$	v	concentration of xenobiotic compound in the water (dissolved)
c_X	$\# l^{-3}$	v	concentration of xenobiotic compound in food
c_V	$\# l^{-3}$	v	scaled concentration of xenobiotic compound in tissue: $[M_Q]P_{dV}$
d_*	$m\,L^{-3}$	c	density of compound $*$
$\dot{D}$	l^2t^{-1}	c	diffusivity
e	-	v	scaled energy density: $[E]/[E_m] = m_E/m_{Em}$

e_0	-	v	scaled energy costs of one egg/foetus: E_0/E_m
e_b	-	v	scaled energy density at birth
e_H	-	v	scaled maturity density: gu_H/l^3
e_R	-	v	scaled energy allocated to reproduction: $E_R E_m^{-1}$
E	e	v	non-allocated energy in reserve
E_0	e	v	energy costs of one egg/foetus
E_m	e	c	maximum non-allocated energy in reserve: $[E_m]V_m$
E_R	e	v	energy in reserve with allocation reproduction
E_J	e	v	accumulated energy investment into maturation
E_J^b	e	v	maturation threshold for feeding (birth)
E_J^p	e	v	maturation threshold for reproduction (puberty)
$[E]$	$e\,L^{-3}$	v	energy density: E/V
$[E_b]$	$e\,L^{-3}$	v	energy density at birth
$[E_G]$	$e\,L^{-3}$	c	volume-specific costs for structure
$[E_m]$	$e\,L^{-3}$	c	maximum energy density
f	-	v	scaled functional response: $f = \frac{X}{X_K+X} = \frac{x}{1+x}$
$\dot{F}$	l^3t^{-1}	v	filtering rate
$\dot{F}_m$	l^3t^{-1}	c	maximum filtering rate
g	-	c	energy investment ratio: $\frac{[E_G]}{\kappa[E_m]}$
$\overline{g}_*$	$e\,\#^{-1}$	c	molar gibbs energy of compound $*$
G	e	v	Gibbs energy of the system
$\dot{h}$	t^{-1}	v	number-specific predation probability rate (hazard rate)
$\dot{h}_a$	t^{-1}	c	aging rate for unicellulars: $\frac{[E_G]}{\kappa\mu_{QC}}\,\frac{\dot{k}_E+\dot{k}_M}{g+1}$
$\ddot{h}_a$	t^{-2}	c	aging acceleration: $\propto \frac{[E_G]}{\kappa\mu_{QC}}$
$\dot{h}_m$	t^{-1}	c	max. throughput rate in a chemostat without complete washout
$\overline{h}_*$	$e\,\#^{-1}$	v	molar enthalpy of compound $*$
H	e	v	enthalpy of the system
j_*	$\#\,\#^{-1}t^{-1}$	v	structure-specific flux of compound $*$: $\dot{J}_*/M_V$
$\dot{J}_*$	$\#\,t^{-1}$	v	flux of compound $*$
$\dot{J}_{*_1,*_2}$	$\#\,t^{-1}$	v	flux of compound $*_1$ associated with process $*_2$
$\dot{\boldsymbol{J}}$	$\#\,t^{-1}$	v	matrix of fluxes of compounds $\dot{J}_{*_1,*_2}$
$\{\dot{J}_{Xm}\}$	$\#L^{-2}t^{-1}$	c	surface-area-specific max ingestion rate
$[\dot{J}_{Xm}]$	$\#L^{-3}t^{-1}$	c	volume-specific maximum ingestion rate: $\{\dot{J}_{Xm}\}V_d^{-1/3}$
k	-	c	maintenance ratio: $\dot{k}_J/\dot{k}_M$
$\dot{k}_e$	t^{-1}	c	elimination rate of xenobiotic compound
$\dot{k}_E$	t^{-1}	c	specific-energy conductance: $\{\dot{p}_{Am}\}V_d^{-1/3}[E_m]^{-1} = [\dot{p}_{Am}]/[E_m]$
$\dot{k}_J$	t^{-1}	c	maturity maintenance rate coefficient
$\dot{k}_M$	t^{-1}	c	somatic maintenance rate coefficient: $[\dot{p}_M]/[E_G]$
K_*	$\#\,l^{-3\,\mathrm{or}\,-2}$	c	saturation coefficient of compound $*$; default: food
l	-	v	scaled body length: $(V/V_m)^{1/3}$
l_b	-	c	scaled body length at birth: $(V_b/V_m)^{1/3}$
l_d	-	c	scaled cell length at division: $(V_d/V_m)^{1/3} = \dot{k}_M g/\dot{k}_E$
l_h	-	c	scaled heating length: $(V_h/V_m)^{1/3}$
l_p	-	c	scaled body length at puberty: $(V_p/V_m)^{1/3}$

L	L	v	physical length: $V^{1/3}/\delta_{\mathcal{M}}$
L_b	L	c	physical length at birth: $V_b^{1/3}/\delta_{\mathcal{M}}$
L_d	L	c	physical length at cell division
L_m	L	c	maximum physical length: $V_m^{1/3}/\delta_{\mathcal{M}}$
L_p	L	c	physical length at puberty: $V_p^{1/3}/\delta_{\mathcal{M}}$
m_*	$\#\#^{-1}$	v	mole of compound $*$ relative to M_V: M_*/M_V
m_{Em}	$\#\#^{-1}$	v	max molar reserve density: $M_{Em}/M_V = [M_{Em}]/[M_V]$
M_*	$\#$	v	mole of compound $*$
$\mathcal{M}(V)$	-	f	shape (morph) correction function: $\frac{\text{real surface area}}{\text{isomorphic surface area}}$
$[M_{Em}]$	$\# L^{-3}$	c	maximum reserve density in non-embryos in C-moles $[E_m]/\mu_E$
$[M_{sm}]$	$\# L^{-3}$	c	maximum volume-specific capacity of the stomach for food
$[M_V]$	$\# L^{-3}$	c	number of C-atoms per unit of structural body volume V
$n_{*_1*_2}$	$\#\#^{-1}$	c	number of atoms of element $*_1$ present in compound $*_2$
$n^0_{*_1*_2}$	$\#\#^{-1}$	c	number of isotopes 0 of element $*_1$ present in compound $*_2$
$n^{0*_3}_{*_1*_2}$	$\#\#^{-1}$	c	number of isotopes 0 of element $*_1$ present in compound $*_2$ in process $*_3$
$\boldsymbol{n}$	$\#\#^{-1}$	c	matrix of chemical indices $n_{*_1*_2}$
N	$\#$	v	(total) number of individuals: $\int_a \phi_N(a)\, da$
$\dot{p}_*$	$e\, t^{-1}$	v	energy flux (power) of process $*$
$\dot{p}_{T+}$	$e\, t^{-1}$	v	total dissipating heat
$\dot{\boldsymbol{p}}$	$e\, t^{-1}$	v	vector of basic powers: $(\dot{p}_A\, \dot{p}_D\, \dot{p}_G)$
$\{\dot{p}_{Am}\}$	$e\, L^{-2} t^{-1}$	c	surface-area-specific maximum assimilation rate
$[\dot{p}_{Am}]$	$e\, L^{-3} t^{-1}$	c	volume-specific maximum assimilation rate: $\{\dot{p}_{Am}\} V_d^{-1/3}$
$[\dot{p}_J]$	$e\, L^{-3} t^{-1}$	c	volume-specific maturity maintenance rate: $\dot{p}_J/V$
$[\dot{p}_M]$	$e\, L^{-3} t^{-1}$	c	volume-specific somatic maintenance rate: $\dot{p}_M/V$
$\{\dot{p}_T\}$	$e\, L^{-2} t^{-1}$	c	surface-area-specific heating rate: $\dot{p}_T\, V^{-2/3}$
$P_{*_1*_2}$	-	c	partition coeff. of a compound in matrix $*_1$ and $*_2$ (moles per volume)
P_{ow}	-	c	octanol/water partition coefficient of a compound
P_{PX}	-	c	faeces/food partition coefficient of a compound
P_{Vd}	$l^3 L^{-3}$	c	biomass/water (dissolved fraction) partition coefficient of a compound
P_{VW}	-	c	structural/total body mass partition coefficient of a compound
$q(c,t)$	-	v	survival probability to a toxic compound
$\dot{r}$	t^{-1}	c	number-specific population growth rate
$\dot{r}_B$	t^{-1}	c	von Bertalanffy growth rate: $(3/\dot{k}_M + 3 f V_m^{1/3}/\dot{v})^{-1} = \dot{k}_M g/3(f+g)$
$\dot{r}_m$	t^{-1}	c	(net) maximum number-specific population growth rate
$\dot{r}_m^\circ$	t^{-1}	c	gross maximum number-specific population growth rate
$\dot{R}$	$\# t^{-1}$	v	reproduction rate, i.e. number of eggs or young per time
$\dot{R}_m$	$\# t^{-1}$	c	max reproduction rate
s	-	v	stress value
s_0	-	c	stress value without effect
$\overline{s}_*$	$e\, T^{-1}\, \#^{-1}$	v	molar entropy of compound $*$
S	$e\, T^{-1}$	v	entropy of the system
t	t	v	time
t_d	t	v	inter division period
t_D	t	c	DNA duplication time
t_g	t	v	gut residence time

t_R	t	v	time at spawning
t_s	t	v	mean stomach residence time
T	T	c	temperature
T_A	T	c	Arrhenius temperature
T_b	T	c	body temperature
T_e	T	c	environmental temperature
u_E	-	v	scaled reserve: $U_E g^2 \dot{k}_M^3 / \dot{v}^2$
u_H	-	v	scaled maturity: $U_H g^2 \dot{k}_M^3 / \dot{v}^2$
U_E	tL^2	v	scaled reserve: $M_E / \{\dot{J}_{EAm}\}$
U_H	tL^2	v	scaled maturity: $M_H / \{\dot{J}_{EAm}\}$
$\dot{v}$	$L\,t^{-1}$	c	energy conductance (velocity): $\{\dot{p}_{Am}\}/[E_m]$
v_H^b	-	c	scaled maturity volume at birth: $\frac{M_H^b g^2 \dot{k}_M^3}{\dot{v}^2 \{\dot{J}_{EAm}\}(1-\kappa)}$
V	L^3	v	structural body volume
V_b	L^3	c	structural body volume at birth (transition embryo/juvenile)
V_d	L^3	c	structural cell volume at division
V_h	L^3	c	structural volume reduction due to heating: $\{\dot{p}_T\}^3 [\dot{p}_M]^{-3}$
V_m	L^3	c	maximum structural body volume: $(\kappa\{\dot{p}_{Am}\})^3 [\dot{p}_M]^{-3} = (\dot{v}/\dot{k}_M g)^3$
V_p	L^3	c	structural body volume at puberty (transition juvenile/adult)
V_w	L^3	c	physical volume
V_∞	L^3	c	ultimate structural body volume
$\mathcal{V}$	L^3	v	maximum structural body volume compared to reference: $z^3 V_{m1}$
w_*	$m\,\#^{-1}$	c	molar weight of compound $*$
W_d	m	v	dry weight of (total) biomass
W_w	m	v	wet weight of (total) biomass
x	-	v	scaled biomass density in environment: X/X_K
X_*	$\#\,l^{-3}$ or -2	v	biomass density of compound $*$ in environment; default: food
X_r	$\#\,l^{-3}$	c	substrate density in feed of chemostat
$y_{*_1*_2}$	$\#\,\#^{-1}$	c	constant yield coefficient that couples molar flux $*_1$ to molar flux $*_2$
$Y_{*_1*_2}$	$\#\,\#^{-1}$	v	yield coefficient that couples molar flux $*_1$ to molar flux $*_2$: $\dot{J}_{*_1}/\dot{J}_{*_2}$
$Y^k_{*_1*_2}$	$\#\,\#^{-1}$	v	yield coefficient that couples molar flux $*_1$ to molar flux $*_2$ in process k: $\dot{J}_{*_1 k}/\dot{J}_{*_2 k}$
z	-	v	zoom factor to compare body sizes
$\alpha^{*_3}_{*_1*_2}$	-	c	reshuffle coefficient for element $*_1$ of compound $*_2$ in process $*_3$
$\beta^{0*_3}_{*_1*_2}$	-	c	odds ratio of isotope 0 of element $*_1$ of compound $*_2$ in transformation $*_3$
$\Gamma(x)$	-	f	gamma function
δ	-	c	aspect ratio
δ_l	-	c	shape parameter of generalized logistic growth
$\delta_{\mathcal{M}}$	-	c	shape (morph) coefficient: $V^{1/3}/L$
$\delta^0_{*_1*_2}$	-	v	fraction of isotope 0 of element $*_1$ in compound $*_2$: $n^0_{*_1*_2}/n_{*_1*_2}$
$\eta_{*_1*_2}$	$\#\,e^{-1}$	c	coefficient that couples mass flux $*_1$ to energy flux $*_2$: $\mu^{-1}_{*_2*_1}$
$\boldsymbol{\eta}$	$\#\,e^{-1}$	c	matrix of coefficients that couple mass to energy fluxes
θ	-	v	fraction of a number of items: $0 \leq \theta \leq 1$
κ	-	c	fraction of catabolic power energy spent on maintenance plus growth
κ_A	-	c	fraction of assimilation that originates from well-fed-prey reserves
κ_E	-	c	fraction of rejected flux of reserves that returns to reserves
κ_R	-	c	fraction of reproduction energy fixed in eggs
μ_*	$e\,\#^{-1}$	c	chemical potential of compound $*$

$\mu_{*_1*_2}$	$e\,\#^{-1}$	c	coefficient that couples energy flux $*_1$ to mass flux $*_2$: $\eta^{-1}_{*_2*_1}$
$\boldsymbol{\mu}_{\mathcal{M}}$	$e\,\#^{-1}$	c	vector of chemical potentials of 'minerals'
$\boldsymbol{\mu}_{\mathcal{O}}$	$e\,\#^{-1}$	c	vector of chemical potentials of organic compounds
ρ	-	c	binding probability of substrate
τ	-	v	scaled age: $a\dot{k}_M$
$\phi_N(a)$	$\#\,t^{-1}$	v	number of individuals of age in interval $(a, a+da)$
$\phi_{\underline{x}}(x)dx$	-	f	probability density of $\underline{x}$ evaluated in x
$\Phi_{\underline{x}}(x)$	-	f	distribution function of $\underline{x}$ evaluated in x: $\int_0^x \phi_{\underline{x}}(x_1)\,dx_1$
$\dot{\sigma}$	$e\,T^{-1}t^{-1}$	v	entropy production of the system
$\zeta_{*_1*_2}$	$\#\,\#^{-1}$	c	coefficient that couples mass flux $*_1$ to energy flux $*_2$: $\mu_E m_{Em} \mu^{-1}_{*_2*_1}$

Bibliography

[1] V. Ahmadjian and S. Paracer. *Symbiosis; An introduction to biological associations.* Univ. Press New England, Hanover, 1986.

[2] O. Alda Alvarez, T. Jager, S. A. L. M. Kooijman, and J Kammenga. Responses to stress of *Caenorhabditis elegans* populations with different reproductive strategies. *Functional Ecology*, **19**:656–664, 2005. , toxicity, individual, population.

[3] O. Alda Alvarez, T. Jager, E. Marco Redondo, and J. E. Kammenga. Assessing physiological modes of action of toxic stressors with the nematode *Acrobeloides nanus*. *Environ. Toxicol. Chem.*, **25**:3230–3237, 2006. .

[4] O. Alda Alvarez, T. Jager, B. Nunez Colao, and J. E. Kammenga. Temporal dynamics of effect concentrations. *Environ. Sci. Technol.*, pages 2478–2484, 2006. .

[5] T. J. Algeo, S. E. Scheckler, and J. B. Maynard. Effects of the middle to late devonian spread of vascular land plants on weathering regimes, marine biotas, and global climate. In P. C. Gensel and D. Edwards, editors, *Plants invade the land; evolutionary & environmental perspectives.*, Critical moments & perspectives in earth history and paleobiology. Columbio University Press, New York, 2001.

[6] M.O. Alver, J. A. Alfredsen, and Y. Olsen. An individual-based population model for rotifer (*Brachionus plicatilis*) cultures. *Hydrobiologia*, **560**:93–108, 2006.

[7] J. P. Amend and E. L. Shock. Energetics of overall metabolic reactions of thermophilic and hyperthermophilic archaea and bacteria. *FEMS Microbiological Reviews*, **25**:175–243, 2001.

[8] A. D. Anbar and A. H. Knoll. Proterozoic ocean chemistry and evolution: A bioinorganic bridge? *Science*, **1137**:1137–1142, 2002.

[9] J. S. Andersen, J. J. M. Bedaux, S. A. L. M. Kooijman, and H. Holst. The influence of design parameters on statistical inference in non-linear estimation; a simulation study based on survival data and hazard modelling. *Journal of Agricultural, Biological and Environmental Statistics*, **5**:323–341, 2000.

[10] R. A. Andersen. Biology and systematicss of heterokont and haptophyte algae. *American Journal of Botany*, **91**:1508–1522, 2004.

[11] A. J. Anderson and E. A. Dawes. Occurence, metabolism, metabolic control, and industrial uses of bacterial polyhydroxylkanoates. *Microbiological Reviews*, **54**:450–472, 1990.

[12] J. O. Andersson and A. J. Roger. A cyanobacterial gene in nonphotosybthetic protests an early chloroplast acquisition in eukaryotes? *Current Biology*, **12**:115–119, 2002.

[13] S. G. E. Andersson, A. Zomorodipour, J. O. Andersson, T. Sicheritz-Pontón, U. Cecilia, M. Alsmark, R. M. Podowski, A. K. Näslund, A.-S. Eriksson, H. H. Winkler, and C. G. Kurland. The genome sequence of *Rickettsia prowazekii* and the origin of mitochondria. *Nature*, **396**:133–143, 1998.

[14] P. W. Atkins. *Physical Chemistry.* Oxford University Press, Oxford, 1990.

[15] H. J. W. de Baar and P. W. Boyd. The role of iron in plankton ecology and carbon dioxide transfer of the global oceans. In R. B. Hanson, H. W. Ducklow, and J. G. Field, editors, *The changing ocean carbon cycle.*, volume 5 of *Internat. Geosphere-biosphere programme book series*, pages 61–140. Cambridge University Press, 2000.

[16] J. Baas, B. P. P. van Houte, C. A. M. van Gestel, and S. A. L. M. Kooijman. Modelling the effects of binary mixtures on survival in time. *Environmental Toxicology & Chemistry*, **26**:1320–1327, 2007.

[17] J. Baas, T. Jager, and S. A. L. M. Kooijman. The statistical properties of NEC estimates if values scatter among individuals. *Water Research*, 2007. subm 2007/06/11.

[18] C. Bacher and A. Gangnery. Use of dynamic energy budget and individual based models to simulate the dynamics of cultivated oyster populations. *J. Sea Research*, **56**:140–155, 2006.

[19] A.N. Baker, F.W.E. Rowe, and H.E.S. Clark. A new class of Echinodermata from New Zealand. *Nature*, **321**:862–864, 1986.

[20] B. Bakker. *Control and regulation of glycolysis in* Trypanosoma brucei. PhD thesis, Vrije Universiteit, 1998.

[21] S. L. Baldauf, D. Bhattachary, J. Cockrill, P. Hugenholtz, and A. G. B. Pawlowski, J. ans Simpson. The tree of life. In J. Cracraft and M. J. Donoghue, editors, *Assembling the tree of life*, pages 43–75. Oxford University Press, Oxford, 2004.

[22] P. Ball. *A biography of water.* Weidenfeld & Nicolson, London, 1999.

[23] H. Baltscheffsky. Energy conversion leading to the origin and early evolution of life: did inorganic pyrophosphate precede adenosine triphosphate? In H. Baltscheffsky, editor, *Origin and Evolution of Biological Energy Conversion.*, pages 1–9. VCH Publishers, Cambridge, 1996.

[24] M. Baltscheffsky, A. Schultz, and H. Baltscheffsky. H^+-PPases: a tightly membrane-bound family. *FEBS Letters*, **457**:527–533, 1999.

[25] F. G. Barth. *Insects and flowers.* Princeton University Press, Princeton, 1991.

[26] E. Battley. Heat capacity measurements from 10 to 300 K and derived thermodynamic functions of lyophilized cells of *Saccharomyces cerevisae* including the absolute entropy and the entropy formation at 298.15 K. *Thermochimica Acta*, **298**:37–46, 1997.

[27] J. J. M. Bedaux and S. A. L. M. Kooijman. Statistical analysis of bioassays, based on hazard modeling. *Environ. & Ecol. Stat.*, **1**:303–314, 1994. , lethal, kinetics, individual.

[28] J. J. M. Bedaux and S. A. L. M. Kooijman. Statistical analysis of bioassays, based on hazard modeling. Abstract, 1994. The XVIIth International Biometric Conference, Hamilton, Canada & Conference on Environmetrics, Burlington, Canada.

[29] J. J. M. Bedaux and S. A. L. M. Kooijman. Stochasticity in deterministic models. In C. R. Rao, G. P. Patil, and N. P. Ross, editors, *Handbook of statistics 12: Environmental statistics.*, pages 561–581. Elsevier Science B. V., Amsterdam, 1994. .

[30] J. R. Beddington. Mutual interference between parasites or predators and its effect on searching efficiency. *Journal of Animal Ecology*, pages 331–340, 1975.

[31] D. Beerling. *The emerald planet.* Oxford University Press, Oxford, 2007.

[32] P. J. L. Bell. Viral eukaryogenesis: Was the ancestor of the nucleus a complex DNA virus? *J. Mol. Evol.*, **53**:251–256, 2001.

[33] P. J. L. Bell. Sex and the eukaryotic cell clycle is consistent with a viral ancestry for the eukaryotic nucleaus. *J. theor. Biol.*, **243**:54–63, 2006.

[34] S. Bengtson. *Early life on earth.* Columbia University Press, New York, 1994.

[35] T. G. Benton, S. J. Plaistow, A. P. Beckerman, C. T. Lapsley, and S. Littlejohns. Chnages in maternal investment in eggs can affect population dynamics. *Proc. R. Soc.*, **272**:1351–1356, 2005.

[36] J. Bereiter-Hahn. Behaviour of mitochondria in the living cell. *Int. Rev. Cytol.*, **122**:1–63, 1990.

[37] C. Bernard, A. G. B. Simpson, and D. J. Patterson. Some free-living flagellates (protista) from anoxic habitatats. *Ophelia*, **52**:113–142, 2000.

[38] R. A. Berner. Atmospheric oxygen, tectonics and life. In S. H. Schneider and P. J. Boston, editors, *Scientists on Gaia.*, pages 161–173. MIT Press, Cambridge, Mass., 1991.

[39] R. A. Berner. The effects of the rise of land plants on atmospheric CO_2 during the paleozoic. In P. G. Gensel and D. Edwards, editors, *Plants invade the land; Evolutionary & environmental perspectives.*, pages 173–178. Columbia University Press, 2001.

[40] R. A. Berner, E. K.and Berner. *Global environment; water, air, and geochemical cycles.* Prentice Hall, New Jersey, 1996.

[41] J. Berthelin. Microbial weathering. In W. E. Krumbein, editor, *Microbial geochemistry.*, pages 233–262. Blackwell Scientific Publ., Oxford, 1983.

[42] D. F. Bertram and R. R. Strathmann. Effects of maternal and larval nutrition on growth and form of planktotrophic larvae. *Ecology*, **79**:315–327, 1998.

[43] J. J. Beun. *PHB metabolism and N-removal in sequencing batch granular sludge reactors.* PhD thesis, University of Delft, 2001.

[44] J. Bigay, P. Guonon, S. Robineau, and B. Antonny. Lipid packing sensed by arfgap1 couples copi coat disassembly to membrane bilayer curvature. *Nature*, **426**:563–566, 2003.

[45] R. J. Bijlsma. *Modelling whole-plant metabolism of carbon and nitrogen: a basis for comparative plant ecology and morphology.* PhD thesis, Vrije Universiteit, Amsterdam, 1999. limitation, individual.

[46] R. J. Bijlsma and H. Lambers. A dynamics whole-plant model of integrated metabolism of nitrogen and carbon. 2. balanced growth driven by C fluxes and regulated by signals from C and N substrate. *Plant and Soil*, **220**:71–87, 2000. , limitation, individual.

[47] R. J. Bijlsma, H. Lambers, and S. A. L. M. Kooijman. A dynamics whole-plant model of integrated metabolism of nitrogen and carbon. 1. comparative ecological implications of ammonium-nitrate interactions. *Plant and Soil*, **220**:49–69, 2000. , limitation, individual.

[48] E. Billoir, A. R. R. Pèy, and S. Charles. Integrating the lethal and sublethal effects of toxic compounds into the population dynamics of *Daphnia magna*: A combination of the debtox and matrix population models. *Ecological Modelling*, **203**:204–214, 2007.

[49] C. W. Birky. The inheritance of genes in mitochondria and chloroplasts: Laws, mechanisms, and models. *Annual Review of Genetics*, **35**:125–148, 2001.

[50] C. J. Bjerrum and D. E. Canfield. Ocean productivity before about 1.9 gyr ago limited by phosphorus adsorption onto iron oxides. *Nature*, **417**:159–162, 2002.

[51] F. F. Blackman. Optima and limiting factors. *Annals of Botany*, **19**:281–295, 1905.

[52] R. E. Blankenship and H. Hartman. Origin and early evolution of photosynthesis. *Photosynthesis Research*, **33**:91–111, 1992.

[53] R. E. Blankenship and H. Hartman. The origin and evolution of oxygenic photosynthesis. *Trends in Biochemical Sciences*, **23**:94–97, 1998.

[54] X. Bodiguel. A mechanistic model of pcb bioaccumulation in the hake: model predictions compared to field data. *J. Sea Res.*, 2009. in prep.

[55] A. H. de Boer, G. W. van der Molen, H. B. A. Prins, H. A. A. J. Korthout, and P. C. J. van der Hoeven. Aluminium fluoride and magnesium, activators of heterotrimeric GTP-binding proteins, affect high-affinity binding of the fungal toxin fusicoccin to the fusicoccin-binding protein in oat root plasma mambranes. *Eur. J. Biochem*, **219**:1023–1029, 1994. kinetics, individual.

[56] M. P. Boer. *The dynamics of tri-trophic food chains.* PhD thesis, Vrije Universiteit, Amsterdam, 2000. bifurcation, population, ecosystem.

[57] M. P. Boer, B. W. Kooi, and S. A. L. M. Kooijman. Food chain dynamics in the chemostat. *Math. Biosci.*, **150**:43–62, 1998. , bifurcation, population.

[58] M. P. Boer, B. W. Kooi, and S. A. L. M. Kooijman. Homoclinic and heteroclinic orbits in a tri-trophic food chain. *J. Math. Biol.*, **39**:19–38, 1999. , bifurcation, ecosystem.

[59] M. P. Boer, B. W. Kooi, and S. A. L. M. Kooijman. Multiple attractors and boundary crises in a tri-trophic food chain. *Mathematical Biosciences*, **169**(2):109–128, 2001.

[60] D. Bontje, B. W. Kooi, M. Liebig, and S. A. L. M. Kooijman. Aquatic indoor microcosm - part 2: Modelling ecotoxicological effects on algae under dynamic nutrient stress. *Aquatic Toxicology*, 2008. , subm, 2007/12/03.

[61] D. Boukal, A. Laugen, U. Dieckmann, and B. Ernande. Modelling population dynamics of farmed Pacific oysters from individual energy allocation; implications of life-cycle closure and inclusion of density dependent food acquisition. *J. Sea Res.*, 2009. in prep.

[62] Y. Bourles, M. Alunno-Bruscia, S. Pouvreau, G. Tollu, D. Leguay, C. Arnaud, P. Goulletquer, and S. A. L. M. Kooijman. Modelling growth and reproduction of the pacific oyster *Crassostrea gigas*: application of the oyster-deb model in a coastal pond. *J. Sea Res.*, 2009. , in prep.

[63] A. J. Boyce, M. L. Coleman, and M. J. Russell. Formation of fossil hydrothermal chimneys and mounds from silvermines, ireland. *Nature*, **306**:545–550, 1983.

[64] B. W. Brandt. *Realistic characterizations of biodegradation.* PhD thesis, Vrije Universiteit, Amsterdam, 2002.

[65] B. W. Brandt, F. D. L. Kelpin, I. M. M. van Leeuwen, and S. A. L. M. Kooijman. Modelling microbial adaptation to changing availability of substrates. *Water Research*, **38**:1003–1013, 2004.

[66] B. W. Brandt and S. A. L. M. Kooijman. Two parameters account for the flocculated growth of microbes in biodegradation assays. *Biotechnology & Bioengineering*, **70**:677–684, 2000.

[67] B. W. Brandt, I. M. M. van Leeuwen, and S. A. L. M. Kooijman. A general model for multiple substrate biodegradation. application to co-metabolism of non structurally analogous compounds. *Water Research*, **37**:4843–4854, 2003. .

[68] G. B. Brasseur, J. J. Orlando, and G. S. Tyndall. *Atmospheric Chemistry and Global Change.* Oxford Univ. Press, 1999.

[69] D. Brawand, W. Wahli, and H. Kaessmann. Loss of egg yolk genes in mammals and the origin of lactation and placentation. *PLOS Biol.*, **6**:0507–0517, 2008.

[70] J. J. Brocks, G. A. Logan, R. Buick, and R. E. Summons. Archean molecular fossils and the early rise of eukaryotes. *Science*, **285**:1033–1036, 1999.

[71] L. T. Brooke, D. J. Call, and L. T. Brooke. *Acute toxicities of organic chemicals to fathead minnow (*Pimephlus promelas*)*, volume IV of *Center for lake superior environmental studies.* University of Wisconsin USA, 1988.

[72] L. T. Brooke, D. J. Call, and L. T. Brooke. *Acute toxicities of organic chemicals to fathead minnow (*Pimephlus promelas*)*, volume V of *Center for lake superior environmental studies.* University of Wisconsin USA, 1990.

[73] L. T. Brooke, D. L. Geiger, D. J. Call, and C. E. Northcott. *Acute toxicities of organic chemicals to fathead minnow (*Pimephlus promelas*)*, volume I of *Center for lake superior environmental studies.* University of Wisconsin USA, 1984.

[74] L. T. Brooke, S. H. Poirrier, and D. J. Call. *Acute toxicities of organic chemicals to fathead minnow (*Pimephlus promelas*)*, volume III of *Center for lake superior environmental studies.* University of Wisconsin USA, 1986.

[75] G. H. Brown and J. J. Wolken. *Liquid crystals and biological structures.* Academic Press, New York, 1979.

[76] J. Bruggeman and S. A. L. M. Kooijman. A biodiversity-inspired approach to aquatic ecosystem modeling. *Limnol Oceanogr*, **52**:1533–1544, 2007. .

[77] J. Bruggeman, A.-W. Omta, L. Pecquerie, H. A. Dijkstra, and S. A. L. M. Kooijman. A simple 0d model for ocean plankton that quantifies the carbon pump and the microbial loop. *Limnol Oceanogr*, 2008. , in prep.

[78] L. J. Buckley. RNA–DNA ratio: an index of larval fish growth in the sea. *Marine Biology*, **80**:291–298, 1984.

[79] S. S. Butcher, R. J. Charlson, G. H. Orians, and G. V. Wlofe. *Global biochemical cycles.* Academic Press, London, 1992.

[80] A. G. Cairns-Smith, A. J. Hall, and M. J. Russell. Mineral theories of the origin of life and an iron sulphide example. *Origins Life and Evolution of the Biosphere*, **22**:161–180, 1992.

[81] D. E. Canfield, K. S. Habicht, and B. Thamdrup. The archean sulfur cycle and the early histroy of atmospheric oxygen. *Science*, **288**:658–661, 2000.

[82] J. F. M. F. Cardoso. *Growth and reproduction in bivalves.* PhD thesis, Groningen University, 2007.

[83] J. F. M. F. Cardoso, H. W. van der Veer, and S. A. L. M. Kooijman. Body size scaling relationships in bivalves: a comparison of field data with predictions by dynamic energy budgets (deb theory). *J. Sea Res.*, **56**:125–139, 2006. .

[84] J. F. M. F. Cardoso, J. IJ. Witte, and H. van der Veer. Intra- and interspecies comparison of energy flow in bivalve species in Dutch coastal waters by means of the Dynamic Energy Budget (DEB) theory. *J. Sea Research*, **56**:182–197, 2007.

[85] S. Casas and C. Bacher. Modelling trace metal (Hg and Pb) bioaccumulation in the mediterranean mussel, *Mytilus galloprovincialis*, applied to environmental monitoring. *J. Sea Research*, **56**:168–181, 2007.

[86] T. Cavalier-Smith. The origin of cells, a symbiosis between genes, catalysts and membranes. *Cold Spring Harbor Symposia on Quantitative Biology*, **52**:805–824, 1987.

[87] T. Cavalier-Smith. A revised six-kingdom system of life. *Biol. Rev.*, **73**:203–266, 1998.

[88] T. Cavalier-Smith. Membrane heredity and early chloroplast evolution. *Trends in Plant Sciences*, **5**:174–182, 2000.

[89] T. A. Cavalier-Smith. Chloroplast evolution: Secondary symbiogenesis and multiple losses. *Current Biology*, **12**:R62 – 64, 2002.

[90] T. A. Cavalier-Smith. The phagotrophic origin of eukaryotes and phylogenetic classification of protozoa. *International Journal of Systematic and Evolutionary Microbiology*, **52**:297–354, 2002.

[91] F. Chai, S. T. Lindley, J. R. Toggweiler, and R. R. Barber. Testing the importance of iron and grazing in the maintenance of the hogh nitrate condition in the equatorial pacific ocean: a physical-biological model study. In *The changing ocean carbon cycle.*, volume 5 of *Internat. Geosphere-biosphere programme book series*, pages 155–186. Cambridge University Press, 2000.

[92] S. Charlat and H. Mercot. *Wolbachia*, mitochondria and sterility. *TREE*, **16**:431–432, 2001.

[93] R.J. Charlson. The vanishing climatic role of dimethyl sulfide. In G. M. Woodwell and F. T. Mackenzie, editors, *Biotic feedbacks in the globalclimatic system.*, pages 251–277. Oxford University Press, 1995.

[94] J. Chela-Flores. First step in eukaryogenesis: Physical phenomena in the origin and evolution of chromosome structure. *Origins of Life and Evolution of the Biosphere*, **28**:215–225, 1998.

[95] L. Chistoserdova, C. Jenkins, M. G. Kalyuzhnaya, C. J. Marx, A. Lapidus, J. A. Vorholt, J. T. Stanley, and M. E. Lidstrom. The enigmatic Planctomycetes may hold a key to the origins of metanogenesis and methylotrophy. *Molecular Biology and Evolution*, **21**:1234–1241, 2004.

[96] B. M. Clark, N. F. Mangelson, L. L. St. Clair, L. B. Rees, G. S. Bench, and J. R. Southon. Measurement of age and growth rate in the crustose saxicolous lichen *Caloplaca trachyphylla* using ^{14}C accelerator mass spectrometry. *The Lichenologist*, **32**:399–403, 2000.

[97] R. E. Criss. *Principles of stable isotope distribution.* Oxford Univerity Press, New York, 1999.

[98] N. Cronberg, R. Natcheva, and K. Hedlund. Microarthropods mediate sperm transfer in mosses. *Science*, **313**:1255, 2006.

[99] T. J. Crowley and G. R. North. *Paleoclimatology.*, volume 18 of *Oxford Monogr. Geol. & Geophys.* Oxford University Press, 1991.

[100] T. Dalsgaard, D. E. Canfield, J. Petersen, B. Thamdrup, and J. Acuna-Gonzalez. N-2 production by the anammox reaction in the anoxic water column of golfo dulce, costa rica. *Nature*, **422**:606–608, 2003.

[101] D. W. Deamer and R. M. Pashley. Amphiphilic components of the murchison carbonaceous chondrite; surface properties and membrane formation. *Origins of Life and Evolution of the Biosphere*, **19**:21–38, 1989.

[102] J. Dean. *Lange's Handbook of Chemistry.* McGraw-Hill, 12^{th} Ed., New York, NY, 1979.

[103] D. L. DeAngelis, R. A. Goldstein, and R. V. O'Neill. A model for trophic interaction. *Ecology*, **56**:881–892, 1975.

[104] T. H. DeLuca, O. Zackrisson, M.-C. Nilsson, and A. Sellstedt. Quantifying nitrogen-fixation in feather moss carpets of boreal forests. *Nature*, **429**:917–920, 2002.

[105] C. F. Delwiche. Tracing the thread of plastid diversity through the tapestry of life. *Am. Nat.*, **154**:S164–S177, 1999.

[106] C. F. Delwiche, R. A. Andersen, D. Bhattacharya, B. D. Mishler, and R. M. McCourt. Algal evolution and the early radiation of green plants. In J. Cracraft and M. J. Donoghue, editors, *Assembling the tree of life*, pages 121–167. Oxford University Press, Oxford, 2004.

[107] C. Dennis. Close encounters of the jelly kind. *Nature*, **426**:12–14, 2003.

[108] E. Derelle, C. Ferraz, P. Lagoda, S. Eycheni, and others. DNA libraries for sequencing the genome of *Ostreococcus tauri* (*Chlorophyta, Prasinophyceae*): the smallest free-living eukaryotic cell. *Journal of Phycology*, **38**:1150–1156, 2002.

[109] R. F. Dill, E. A. Shinn, A. T. Jones, K. Kelly, and R. P. Steinen. Giant subtidal stromatolites forming in normal salinity waters. *Nature*, **324**:55–58, 1986.

[110] J. G. Dillon and R. W. Castenholz. Scytonemin, a cyanobacterial sheath pigment, protects against uvc radiation: implications for early photosynthetic life. *Journal of Phycology*, **35**:673–681, 1999.

[111] G. C. Dismukes, V. V. Klimov, S. V. Baranov, Dasguptam J. Kozlov, Yu. N., and A. Tyryshkin. The origin of atmospheric oxygen on earth: the innovation of oxygenic photosynthesis. *Proceedings of the National Academy of Sciences U.S.A*, **98**:2170–2175, 2001.

[112] P. S. Dixon. *Biology of the Rhodophyta.* Oliver & Boyd, Edinburgh, 1973.

[113] R. Docampo, W. de Souza, K. Miranda, P. Rohloff, and S. N. J. Moreno. Acidocalcisomes - conserved from bacteria to man. *Nature Reviews Microbiology*, **3**:251–261, 2005.

[114] M. Doebeli. A model for the evolutionary dynamics of cross-feeding polymorphisms in microorganisms. *Population Ecology*, **44**:59–70, 2002.

[115] C. D. von Dohlen, S. Kohler, S. T. Alsop, and W. R. McManus. Mealybug β-proteobacterial endosymbionts contain γ-proteobacterial symbionts. *Nature*, **412**:433–436, 2001.

[116] M. H. Donker, C. Zonneveld, and N. M. van Straalen. Early reproduction and increased reproductive allocation in metal-adapted populations of the terrestrial isopod *Porcellio scaber*. *Oecologia*, **96**:316–323, 1993.

[117] W. F. Doolittle. Phylogenetic classification and the universal tree. *Science*, **284**:2124–2128, 1999.

[118] A. E. Douglas. *Symbiotic interactions.* Oxford University Press, 1994.

[119] S. E. Douglas. Plastid evolution: origin, diversity, trends. *Current Topics in Genetics and Development*, **8**:655–661, 1998.

[120] C. L. van Dover. *The ecology of deep-sea hydrothermal vents.* Princeton University Press, Princeton, 2000.

[121] M. R. Droop. Some thoughts on nutrient limitation in algae. *Journal of Phycology*, **9**:264–272, 1973.

[122] N. Dubilier, C. Mulders, T. Felderman, D. de Beer, A. Pernthaler, M. Klein, M. Wagner, C. Erséus, F. Thiermann, J. Krieger, O. Giere, and R. Rudolf Amann. Endosymbiotic sulphate-reducing and sulphide-oxidizing bacteria in an oligochaete worm. *Nature*, **411**:298–302, 2001.

[123] V. Ducrot, A. R. R. Péry, R. Mons, and J. Garric. Energy-based modeling as a basis for the analysis of reproductive data with the midge (*Chironomus riparius*). *ENvironmental Toxicology and Chemistry*, **23**:225–231, 2004.

[124] A. Duisterwinkel. Nieuwe theorie voor toxicologie. *C2w*, **18**(28 Okt):26–27, 2006. .

[125] C. de Duve. *A guided tour of the living cell.* Scientific American Library, New York, 1984.

[126] M. Dworkin. *Developmental biology of the bacteria.* Benjamin-Cummings Publ. Co., California, 1985.

[127] E. M. Dzialowski and P. R. Sotherland. Maternal effects of egg size on emu *Dromaius novaehollandiae* egg composition and hatchling phenotype. *J. Experimental Biology*, **207**:597–606, 2004.

[128] Muller E.B. and Nisbet R. M. Survival and production in variable resource environments. *Bulletin of Mathematical Biology*, **62**:1163–1189, 2000.

[129] K. J. Eckelbarger, P. A. Linley, and J. P. Grassle. Role of ovarian follicle cells in vitellogenesis and oocyte resorption in *Capitella* sp. i (Polychaeta). *Marine Biology*, pages 133–144, 1984.

[130] E. Eichinger. *Bacterial degradation of dissolved organic carbon in the water column: an experimental and modelling approach.* PhD thesis, University de Mediterranee & Vrije Universiteit, Marseille & Amsterdam, 2008. .

[131] M. Eichinger, S. A. L. M. Kooijman, R. Sempéré, and J.-C. Poggiale. Mechanistic model simplification for implementation in biogeochemical models: case of doc degradation by heterotrophic bacteria in a perturbed system. *Ecol. Modelling*, 2008. , subm, 2008/11/13.

[132] D. H. Eikelboom, A. H. Stouthamer, H. B. van Verseveld, and E. B. Muller. High performance bioreactor: A physiological approach to wastewater treatment with zero sludge production by complete sludge retention. Technical Report IMW-P 93/051, TNO, October 1993. Japan-Netherlands Workshop on integrated water management.

[133] S. Einum and I. A. Fleming. Maternal effects of egg size in brown trout (*Salmo trutta*): norms of reaction to environmental quality. *Proceedings: Biological Sciences*, **266**(1433):2095–2095, 1999.

[134] T. M. Embley and R. P. Hirt. Early branching eukaryotes? *Current Opinion in Genetics and Development*, **8**:624–629, 1998.

[135] R. H. Emson and P. V. Mladenov. Studies of the fissiparous holothurian *Holothuria parvula* (Selenka) (*Echinodermata: Holothuroidea*). *Journal of Experimental Marine Biology and Ecology*, **111**:195–211, 1987.

[136] F. van den Ent, L. A. Amos, and J. Löwe. Prokaryotic origin of the actin cytoskeleton. *Nature*, **413**:39–44, 2001.

[137] G. Ernsting, C. Zonneveld, J. A. Isaaks, and A. Kroon. Size at maturity and patterns of growth and reproduction in an insect with indeterminate growth. *Oikos*, **66**:17–26, 1993.

[138] A. G. Evers. *Growth, starvation and storage in microorganisms.* PhD thesis, Vrije Universiteit, Amsterdam, January 1991. population.

[139] A. G. Evers. A model for light-limited continuous cultures: growth, shading and maintenance. *Biotechn. Bioeng.*, **38**:254–259, 1991. limitation, population.

[140] E. Evers and S. A. L. M. Kooijman. Feeding and oxygen consumption in *Daphnia magna*; a study in energy budgets. *Neth. J. Zool.*, **39**:56–78, 1989. DEB, individual.

[141] T. Fenchel. *Origin & early evolution of life.* Oxford University Press, Oxford, 2002.

[142] T. Fenchel and B. L. Finlays. *Ecology and evolution in anoxic worlds.* Oxford University Press, Oxford, 1995.

[143] J. G. Ferry. *Methanogenesis. Ecology, physiology, biochemistry & genetics.* Chapman & Hall, New York, 1993.

[144] M. S. Finkler, J. B. van Orman, and P. R. Sotherland. Experimental manipulation of egg quality in chickens: influence of albumen and yolk on the size and body composition of near-term embryos in a precocial bird. *J. Comp. Physiol. B*, **168**:17–24, 1998.

[145] J. Flye Sainte Marie. *Ecophysiology of Brown Ring Disease in the Manila clam* Ruditapes philippinarum*, experimental and modelling approaches.* PhD thesis, Brest University & Vrije Universiteit, Brest & Amsterdam, 2008. .

[146] J. Flye Sainte Marie. A quantitative evaluation of the energetic cost of the development of brown ring disease in the Manila clam *Ruditapes phillippinarum. J. Sea Res.*, 2009. in prep.

[147] G. L. Flynn and S. H. Yalkowsky. Correlation and prediction of mass transport across membranes i: Influence of alkyl chain length on flux-determining properties of barrier and diffusant. *Journal of Pharmaceutical Sciences*, **61**:838–852, 1972.

[148] P. Forterre. Genomics and the early cellular evolution. the origin of the DNA world. *C. R. Acad. Sci.*, **324**:1067–1076, 2001.

[149] P. Forterre. The origin of DNA genomes and DNA replication proteins. *Current Opinion in Microbiol.*, **5**:525–532, 2002.

[150] P. Forterre. The origin of virusses and their possible roles in major evolutionary transitions. *Virus Res.*, **117**:5–16, 2006.

[151] P. Forterre, A. Bergerat, and P. Lopez-Garvia. The unique DNA topology and DNA topoisomerase of hyperthermophilic archaea. *FEMS Microbiol. Rev.*, **18**:237–248, 1996.

[152] B. Fry. *Stable isotope ecology.* Springer, New York, 2006.

[153] J. A. Fuerst. Intracellular compartmentation in planctomycetes. *Rev. Microbiol.*, **59**:299–328, 2005.

[154] J. Fuhrman. Genome sequences from the sea. *Nature*, **424**:1001–1002, 2003.

[155] M. Fujiwara, B. E. Kendall, and R. M. Nisbet. Growth autocorrelation and animal size variation. *Ecology Letters*, **7**:106–113, 2004.

[156] L. Garby and P. Larsen. *Bioenergetics – its thermodynamic foundations.* Cambridge University Press, 1995.

[157] D. L. Geiger, C. E. Northcott, D. J. Call, and L. T. Brooke. *Acute toxicities of organic chemicals to fathead minnow (*Pimephlus promelas*)*, volume II of *Center for lake superior environmental studies.* University of Wisconsin USA, 1985.

[158] D.L. Geiger, L. T. Brooke, and D. J. Call. *Acute toxicities of organic chemicals to fathead minnow (*Pimephales promelas*)*, volume 2-5 of *Center for Lake Superior Environmental Studies.* Univerity of Wisconsin-Superior, USA, 1985–1990.

[159] A. A. M. Gerritsen. *The influence of body size, life stage, and sex on the toxicity of alkylphenols to* Daphnia magna. PhD thesis, University of Utrecht, The Netherlands, 1997.

[160] A. G. Gibbs. Biochemistry at depth. In D. J. Randall and A. P. Farrell, editors, *Deep-sea fishes.*, chapter 6, pages 239–278. Academic Press, San Diego, 1997.

[161] U. Gille and FV Salomon. Heart and body growth in ducks. *Growth Dev Aging*, **58**(2):75–81, 1994.

[162] S. J. Giovannoni, H. J. Tripp, S. Givan, M. Podar, K. L. Vergin, D. Baptista, L. Bibbs, J. Eads, T. H. Richardson, M. S. Noordewier, M. Rappé, J. M. Short, J. C. Carrington, and E. J. Mathur. Genome streamlining in a cosmopolitan oceanic bacterium. *Science*, **309**:1242–1245, 2005.

[163] D. S. Glazier. Effects of Food, Genotype, and Maternal Size and Age on Offspring Investment in *Daphnia Magna*. *Ecology*, **73**(3):910–926, 1992.

[164] Z. M. Gliwicz and C. Guisande. Family planning in *Daphnia*: resistance to stravation in offspring born to mothers grown at different food levels. *Oecologia*, **91**:463–467, 1992.

[165] F. A. P. C. Gobas and A. Opperhuizen. Bioconcentration of hydrophobic chemicals in fish: relationship with membrane permeation. *Environmental Toxicology and Chemistry*, **5**:637–646, 1986.

[166] K. Grangeré. How the environment contributes to the interannual variability of oyster's physiological state. *J. Sea Res.*, 2009. in prep.

[167] P. J. Graumann. Cytoskeletal elements in bacteria. *Rev. Microbiol.*, **61**:589–618, 2007.

[168] K. Grice, C. Cao, G. D Love, M. E. Böttcher, R. J. Twitchett, E. Grosjean, R. E. Summons, S. C. Turgeon, W. Dunning, and Y. Jin. Photic zone euxinia during the permian-triassic superanoxic event. *Science*, **307**:706–709, 2005.

[169] J. Gruenberg. The endocytic pathway: a mosaic of domains. *Nature Reviews*, **2**:721–730, 2001.

[170] R. Guerrero. Predation as prerequisite to organelle origin: *Daptobacter* as example. In L. Margulis and R. Fester, editors, *Symbiosis as a source of evolutionary innovation.*, chapter 8, pages 106–117. MIT Press, 1991.

[171] R. S. Gupta. What are archaebacteria: life's third domain or monoderm prokaryotes related to gram-positive bacteria? A new proposal for the classification of prokaryotic prganisms. *Molecular Microbiology*, **29**:695–707, 1998.

[172] W.C. Gurney and R. M. Nisbet. Resource allocation, hyperphagia and compensatory growth. *Bulletin of Mathematical Biology*, **66**:1731–1753, 2004.

[173] S. J. Hallam, N. Putnam, C. M. Preston, J. C. Detter, D. Rokhsar, P. M. Richardson, and E. F. DeLong. Revers methanogenesis: Testing the hypothesis with environmentl genomics. *Science*, **305**:1457–1462, 2004.

[174] T. G. Hallam, R. R. Lassiter, and S. A. L. M. Kooijman. Effects of toxicants on aquatic populations. In S. A. Levin, T. G. Hallam, and L. F. Gross, editors, *Mathematical ecology.*, pages 352–382. Springer, London, 1989. ,lethal, sublethal, population.

[175] P. P. F. Hanegraaf. *Mass and energy fluxes in microorganisms according to the Dynamic Energy Budget theory for filaments.* PhD thesis, Vrije Universiteit, Amsterdam, 1997. limitation, population.

[176] P. P. F. Hanegraaf and Muller E. B. The dynamics of the macromolecular composition of biomass. *J. theor. Biol.*, **212**:237–251, 2001.

[177] P. P. F. Hanegraaf, B. W. Brandt, and S. A. L. M. Kooijman. Final report on the project debdeg "realistic characterizations of the biodegradation of compounds" prepared for stw. Technical report, Vrije Universiteit, March 14, 2001. degradation, sewage.

[178] P. P. F. Hanegraaf and B. W. Kooi. The dynamics of a tri-trophic food chain with two-component populations from a biochemical perspective. *Ecol. Modell.*, **152**:47–64, 2002.

[179] P. P. F. Hanegraaf, B. W. Kooi, and S. A. L. M. Kooijman. The role of intracellular components in food chain dynamics. *C. R. Acad. Sci. Ser. III*, **323**:99–111, 2000. , molecule, limitation, population, individual.

[180] P. P. F. Hanegraaf, A. H. Stouthamer, and S. A. L. M. Kooijman. A mathematical model for yeast respirofermentative physiology. *Yeast*, **16**:423–437, 2000.

[181] R. J. F. van Haren. *Application of Dynamic Energy Budgets to xenobiotic kinetics in* Mytilus edulis *and population dynamics of* Globodera pallida. PhD thesis, Vrije Universiteit, June 1995. DEB, individual, population.

[182] R. J. F. van Haren and E. M. L. Hendrikx. Population dynamic models of potato cyst nematodes based on dynamic energy budgets. *Nematologica*, **38**:414, 1992. DEB, population, individual.

[183] R. J. F. van Haren, E. M. L. Hendrix, and H. J. Atkinson. Growth curve analysis of sedentary plant parasitic nematodes in relation to plant resistance and tolerance. In J. Grasman and G. van Straten, editors, *Predictability and Nonlinear Modelling in Natural Sciences and Economics.*, pages 172–183. Kluwer Academic Publishers, Dordrecht, 1994. DEB, individual.

[184] R. J. F. van Haren and S. A. L. M. Kooijman. Feeding history affects xenobiotics accumulation in the marine mussel *Mytilus edulis*: Model development. In D. A. Holwerda, editor, *Physiological and biochemical approaches to the toxicological assessment of environmental pollution.*, pages P1–26, 1990. kinetics, individual.

[185] R. J. F. van Haren and S. A. L. M. Kooijman. Application of the dynamic energy budget model to *Mytilus edulis* (L). *Neth. J. Sea Res.*, **31**:119–133, 1993. , DEB, individual.

[186] R. J. F. van Haren, H. E. Schepers, and S. A. L. M. Kooijman. Dynamic energy budgets affect kinetics of xenobiotics in the marine mussel *Mytilus edulis*. *Chemosphere*, **29**:163–189, 1994. , kinetics, individual.

[187] M. W. Hart. What are the costs of small egg size for a marine invertebrate with feeding planktonic larvae? *American Naturalist*, **146**:415–426, 1995.

[188] H. Hartman. Speculations on the origin and evolution of metabolism. *Journal of Molecular Evolution*, **4**:359–370, 1975.

[189] H. Hartman. Photosynthesis and the origin of life. *Origins of life and the evolution of the biosphere*, **28**:515–521, 1998.

[190] D. W. Hawker and D. W. Connell. Relationships between partition coefficient, uptake rate constant, clearance rate constant and time to equilibrium for bioaccumulation. *Chemosphere*, **14**:1205–1219, 1985.

[191] J. M. Hayes. Global methanotrophy at the archeon-proterozoic transition. In S. Bengtson, editor, *Early life on earth.*, volume 84 of *Nobel Symposium*, pages 220–236. Columbria University Press, New York, 1994.

[192] D. D. Heath, C. W. Fox, and J. W. Heath. Maternal effects on offspring size: Variation through early development of chinook salmon. *Evolution*, **53**(5):1605–1611, 1999.

[193] R. Heinrich and T. A. Rapoport. A linear steady-state treatment of enzymatic chains. general properties, control and effector strength. *Eur. J. Biochem.*, **42**:89–95, 1974.

[194] R. Heinrich and S. Schuster. *The regulation of cellular systems.* Chapman and Hall, New York, 1996.

[195] R. W. Hendrix, M. C. Smith, R. N. Burns, M. E. Ford, and G. F. Hatfull. Evolutionary relationships among diverse bacteriophages: All the worlds phage. *Proceedings of the National Acadeny of Sciences of the USA*, **96**:2192–2197, 1999.

[196] E. H. W. Heugens, T. Jager, R. Creyghton, M. H. S. Kraak, A. J. Hendriks, N. M. van Straalen, and W. Admiraal. Temperature dependent effects of cadmium on *Daphnia magna*: accumulation versus sensitivity. *Environ. Sci. Technol.*, **37**:2145–2151, 2003.

[197] D. S. Hibbet. When good relationships go bad. *Nature*, **419**:345–346, 2002.

[198] H. V. Hill. The possible effects of aggregation on the molecules of haemoglobin on its dissociation curves. *J. Physiol. (London)*, **40**:IV–VII, 1910.

[199] P. H. E. Hobbelen and C. A. M. van Gestel. Using dynamic energy budget modeling to predict the influence of temperature and food density on the effect of Cu on earthworm mediated litter consumption. *Ecological Modelling*, **202**:373–384, 2007.

[200] C. van den Hoek, D. G. Mann, and H. M. Jahn. *Algae; an introduction to phycology.* Cambridge University Press, Cambridge, 1995.

[201] J. A. Hoekstra. *Statistics in ecotoxicology. Quantifying the biological effects of chemicals.* PhD thesis, Vrije Universiteit, November 1993. lethal, sublethal, individual.

[202] J.-H. S. Hofmeyr. Control-pattern analysis of metabolic pathways. flux and concentration control in linear pathways. *Eur. J. Biochem.*, **186**:343–354, 1989.

[203] H. D. Holland. *Early proterozoic atmospheric change. In: Bengtson, S. (ed.) Early life on earth.* Columbia University Press, New York, 1994.

[204] A. B. Hope and N. A. Walker. *The physiology of giant algal cells.* Cambridge University Press, Cambridge, 1975.

[205] J. Hovekamp. *On the growth of larval plaice in the North Sea.* PhD thesis, University of Groningen, 1991.

[206] H. Huber, M. J. Hohn, R. Rachel, T. Fuchs, V. C. Wimmer, and K. O. Stetter. A new phylum of Archaea represented by nanosized hyperthermophilic symbiont. *Nature*, **417**:63–67, 2002.

[207] J. Hugenholtz and L. G. Ljungdahl. Metabolism and energy generation in homoacetogenic clostridia. *FEMS Microbiology Reviews*, **87**:383–389, 1990.

[208] D. A. Jaffe. The nitrogen cycle. In S. S. Butcher, R. J. Charlson, G. H. Orians, and G. V. Wolfe, editors, *Global biogeochemical cycles.*, pages 263–284. Academic Press, London, 1992.

[209] T. Jager. A biology-based appraoch for ecotoxicity QSARs. *Ecotoxicol.*, 2008. , subm 2008/04/15.

[210] T. Jager, O. Alda Alvarez, J. E. Kammenga, and S. A. L. M. Kooijman. Modelling nematode life cycles using dynamic energy budgets. *Functional Ecology*, **19**:136–144, 2005.

[211] T. Jager, T. Crommentuijn, C. A. M. van Gestel, and S. A. L. M. Kooijman. Simultaneous modelling of multiple endpoints in life-cycle toxicity tests. *Environ. Sci. Technol.*, **38**:2894–2900, 2004.

[212] T. Jager, T. Crommentuijn, C. A. M. van Gestel, and S. A. L. M. Kooijman. Chronic exposure to chlorpyrifos reveals two modes of action in the springtail *Folsomia candida*. *Environ. Pollut.*, **145**:452–458, 2007. , lethal, sublethal, individual.

[213] T. Jager, E. H. W. Heugens, and S. A. L. M. Kooijman. Making sense of ecotoxicological test results: towards process-based models. *Ecotoxicology*, **15**:305–314, 2006.

[214] T. Jager and S. A. L. M. Kooijman. Modeling receptor kinetics in the analysis of survival data for organophosphorus pesticides. *Environmental Science & Technology*, **39**:8307–8314, 2005.

[215] D. Jardine and M. K. Litvak. Direct yolk sac volume manipulation of zebrafish embryos and the relationship between offspring size and yolk sac volume. *J. Fish Biology*, **63**:388–397, 2003.

[216] F. Jean. The estimation of deb parameters for the ormer. *J. Sea Res.*, 2009. in prep.

[217] X. Ji, W.-G. Du, and W.-Q. Xu. Experimental manipulation of eggs size and hatling size in the cobra, *Naja naja atra* (*Elapidae*). *Neth. J. Zool.*, **49**:167–175, 1999.

[218] F. M. Jiggins, J. K. Bentley, M. E. N. Majerus, and G. D. D. Hurst. How many species are infected with *Wolbachia*? cryptic sex ratio distorters revealed to be common by intensive sampling. *P. Roy. Soc. Lond. B*, **268**:1123–1126, 2001.

[219] M. de Jong-Brink. Parasites make use of multiple strategies to change energy budgetting in their host. In H. J. Th. et al Goos, editor, *Perspective in Comparative Endocrinology: Unity and Diversity*. Monduzzi Editore, International Proceedings Division., 2001.

[220] B. B. Jørgensen and V. A. Gallardo. *Thioploca* spp.: filamentous sulfur bacteria with nitrate vacuoles. *FEMS Microbiological Ecology*, **28**:301–313, 1999.

[221] H. Kacser and J. A. Burns. The control of flux. *Symp. Soc. Exp. Biol.*, **27**:65–104, 1973.

[222] O. Kandler. The early diversification of life and the origin of the three domains: a proposal. In J. Wiegel and M. W. W. Adams, editors, *Thermophiles: The keys to molecular evolution and the origin of life.*, pages 19–31. Taylor and Francis, Washington, 1998.

[223] S. J. Karakashian. Growth of *Paramecium bursaria* as influenced by the presence of algal symbionts. *Physiol. Zool.*, **36**:52–68, 1963.

[224] J. F. Kasting. Earths early atmosphere. *Science*, pages 920–925, 2001.

[225] M. Kates. The phytanyl ether-linked polar lipids and isopreniod neutral lipids of extremely halophilic bacteria. *Lipids*, **15**:301–342, 1979.

[226] L. A. Katz. The tangled web: Gene genealogies and the origin of eukaryotes. *Am. Nat.*, **154**:S137–S145, 1999.

[227] A.D. Keefe, S.L. Miller, and G. Bada. Investigation of the prebiotic synthesis of amino acids and rna bases from co_2 using fes/h_2s as a reducing agent. *Proceedings of the National Academy of Sciences of the USA*, **92**:11904–11906, 1995.

[228] P. J. Keeling. A kingdoms progress: Archaezoa and the origin of eukaryotes. *BioEssays*, **20**:87–95, 1998.

[229] F. D. L. Kelpin, M. Kirkilionis, and B. W. Kooi. Numerical analysis and parameter estimation of a structured population model with discrete events in the life history. *J. Theor. Biol.*, **207**:217–230, 2000.

[230] M. Kirkpatrick, editor. *The evolution of Haploid-Diploid life cycles.*, volume 25 of *Lectures on Mathematics in the Life Sciences*. American Mathematical Society, Providence, Rhode Island, 1993.

[231] T. Klaniscek, H. Caswell, M. G. Neubert, and Nisbet R. M. Integrating dynamic energy budgets into matrix population models. *Ecological Modelling*, **196**:407–420, 2006.

[232] M. Kleiber. Body size and metabolism. *Hilgardia*, **6**:315–353, 1932.

[233] D. J. Klionsky. Regulated self-canibalism. *Nature*, **431**:31–32, 2004.

[234] C. Klok. Effects of earthworm density on growth, development, and reproduction in *Lumbricus rubellus* (hoffm.) and possible consequences for the intrinsic rate of population increase. *Soil Biology & Biochemistry*, **39**:2401–2407, 2007.

[235] C. Klok, M. Holmstrup, and C. Damgaardt. Extending a combined dynamic energy budget matrix population model with a bayesian approach to assess variation in the intrinsic rate of population increase. an example in the earthworm *Dendrobaena octaedra*. *Environmental Toxicology and Chemistry*, **26**:2383–2388, 2007.

[236] A. J. Kluyver and H. J. L. Donker. Die einheit in der biochemie. *Chemie von der Zelle und Gewebe*, **13**:134–191, 1926.

[237] A. H. Knoll. *Life on a young planet; the first three billion years of evolution on earth.* Princeton University Press, Princeton, 2003.

[238] Y. Koga, T. Kyuragi, M. Nishhihara, and N. Sone. Did archaeal and bacterial cells arise independently from noncellular precursors? a hypothesis stating that the advent of membrane phospholipids with enantiomeric glycerophosphate backbones caused the separation of the two lines of decent. *Journal of Molecular Evolution*, **46**:54–63, 1998.

[239] M. Konarzewski and S. A. L. M. Kooijman. Models for growth in precocial and altricial birds. *J. Ornith.*, **135**(3):324, 1994. DEB, individual.

[240] M. Konarzewski, S. A. L. M. Kooijman, and R. E. Ricklefs. Models for growth. In J. M. Starck and R. E. Ricklefs, editors, *Avian growth and development.*, pages 340–365. Oxford University Press, 1998. , DEB, individual.

[241] A. S. Kondrashov. Evolutionary genetics of life cycles. *Annual Review of Ecology and Systematics*, **28**:391–435, 1997.

[242] W. H. Könemann. *Quantitative structure–activity relationships for kinetics and toxicity of aquatic pollutants and their mixtures in fish.* PhD thesis, Utrecht University, the Netherlands, 1980.

[243] B. W. Kooi. Time scale separation in ecosystem dynamics; final report of van gogh project vgp 62-550. Technical report, Dept. Theor. Biol. VU, Amsterdam, 2002. , aggregation, ecosystem.

[244] B. W. Kooi. Numerical bifurcation analysis of ecosystems in a spatially homogeneous environment. *Acta Biotheoretica*, **51**:189–222, 2003.

[245] B. W. Kooi and M. P. Boer. Discrete and continuous time population models, a comparison concerning proliferation by fission. *J. Biol. Systems*, **3**:543–558, 1995. , bifurcation, population.

[246] B. W. Kooi and M. P. Boer. Bifurcations in ecosystem models and their biological interpretation. *Applicable Analysis*, **77**:29–59, 2001.

[247] B. W. Kooi and M. P. Boer. Chaotic behaviour of a predator-prey system. *Dynamics of Continuous, Discrete and Impulsive Systems, Series B: Applications and Algorithms*, **10**:259–272, 2003.

[248] B. W. Kooi, M. P. Boer, and S. A. L. M. Kooijman. Complex dynamic behaviour of autonomous microbial food chains. *Journal of Mathematical Biology*, **36**:24–40, 1997. , bifurcation, ecosystem.

[249] B. W. Kooi, M. P. Boer, and S. A. L. M. Kooijman. Mass balance equation versus logistic equation in food chains. *J. Biol. Syst.*, **5**(1):77–85, 1997. , population.

[250] B. W. Kooi, M. P. Boer, and S. A. L. M. Kooijman. Consequences of population models on the dynamics of food chains. *Math. Biosci.*, **153**:99–124, 1998. , population, ecosystem.

[251] B. W. Kooi, M. P. Boer, and S. A. L. M. Kooijman. On the use of the logistic equation in food chains. *Bull. Math. Biol.*, **60**:231–246, 1998. , population.

[252] B. W. Kooi, M. P. Boer, and S. A. L. M. Kooijman. Resistance of a food chain to invasion by a top predator. *Math. Biosci.*, **157**:217–236, 1999.

[253] B. W. Kooi, D. Bontje, G. A. K. van Voorn, and S. A. L. M. Kooijman. Sublethal contaminants effects in a simple aquatic food chain. *Ecol. Modelling*, **112**:304–318, 2008. .

[254] B. W. Kooi, T. G. Hallam, F. D. L. Kelpin, C. M. Krohn, and S. A. L. M. Kooijman. Iteroparous reproduction strategies and population dynamics. *Bull. Math. Biol.*, **63**:769–794, 2001.

[255] B. W. Kooi and P. P. F. Hanegraaf. Bi-trophic food chain dynamics with multiple component populations. *Bull. Math. Biol.*, **63**:271–299, 2001.

[256] B. W. Kooi and F. D. L. Kelpin. Structured population dynamics, a modeling perspective. *Comments on Theoretical Biology*, **8**:125–168, 2003.

[257] B. W. Kooi and S. A. L. M. Kooijman. Existence and stability of microbial prey–predator systems. *J. Theor. Biol.*, **170**:75–85, 1994. , bifurcation, ecosystem.

[258] B. W. Kooi and S. A. L. M. Kooijman. The transient behaviour of food chains in chemostats. *J. Theor. Biol.*, **170**:87–94, 1994. , population, ecosystem.

[259] B. W. Kooi and S. A. L. M. Kooijman. Many limiting behaviours in microbial food chains. In O. Arino, M. Kimmel, and D. Axelrod, editors, *Mathematical Population Dynamics.*, Biological Systems, pages 131–148, Wuerz Publ, Winnipeg, Canada, 1995. , bifurcation, ecosystem.

[260] B. W. Kooi and S. A. L. M. Kooijman. Population dynamics of rotifers in chemostats. *Nonlin. Analysis, Theory, Methods & Applications*, **30**(3):1687–1698, 1997. , population, DEB.

[261] B. W. Kooi and S. A. L. M. Kooijman. Discrete event versus continuous approach to reproduction in structured population dynamics. *Theor. Pop. Biol.*, **56**:91–105, 1999.

[262] B. W. Kooi and S. A. L. M. Kooijman. Invading species can stabilize simple trophic systems. *Ecological Modelling*, **133**:57–72, 2000.

[263] B. W. Kooi, L. D. J. Kuijper, M. P. Boer, and S. A. L. M. Kooijman. Numerical bifurcation analysis of a tri-trophic food web with omnivory. *Math. Biosci.*, **177**:201–228, 2002.

[264] B. W. Kooi, L. D. J. Kuijper, and S. A. L. M. Kooijman. Consequences of symbiosis for food web dynamics. *J. Math. Biol.*, **3**:227–271, 2004.

[265] B. W. Kooi, J. C. Poggiale, P. Auger, and S. A. L. M. Kooijman. Aggregation methods in food chains with nutrient recycling. *Ecological Modelling*, **157**:69–86, 2002.

[266] B. W. Kooi and T. A. Troost. Advantages of storage in a fluctuating environment. *Theor Pop. Biol.*, **70**:527–541, 2006. , ecosystem, bifurcation, adaptive dynamics.

[267] B. W. Kooi, H. W. van Verseveld, and S. A. L. M. Kooijman. Fundamenteel onderzoek vermindering slibproduktie. Technical Report RWZI-two-thousant 94-03, STOWA, 1994. sewage, degradation.

[268] S. A. L. M. Kooijman. Nutriënten- en energiehuishouding bij dieren en micro-organismen. *Toegepaste Wetenschappen*, **1(1)**:44–47, 1985. , DEB, individual, population.

[269] S. A. L. M. Kooijman. Toxiciteit op populatie niveau. *Vakblad voor Biol.*, **23**:163–185, 1985. lethal, sublethal, population.

[270] S. A. L. M. Kooijman. Toxicity at population level. In J. Cairns, editor, *Multispecies toxicity testing.*, pages 143–164. Pergamon Press, New York, 1985. , lethal, sublethal, population.

[271] S. A. L. M. Kooijman. Energy budgets can explain body size relations. *J. Theor. Biol.*, **121**:269–282, 1986. , scaling.

[272] S. A. L. M. Kooijman. Population dynamics on the basis of budgets. In J. A. J. Metz and O. Diekmann, editors, *The dynamics of physiologically structured populations.*, Springer Lecture Notes in Biomathematics., pages 266–297. Springer-Verlag, Berlin, 1986. individual, population, DEB.

[273] S. A. L. M. Kooijman. What the hen can tell about her egg; egg development on the basis of budgets. *J. Math. Biol.*, **23**:163–185, 1986. , individual embryo.

[274] S. A. L. M. Kooijman. Kwantitatieve bioenergetika. *SWIM*, **3**(1):2–6, 1988. individual, DEB.

[275] S. A. L. M. Kooijman. Strategies in ecotoxicological research. *Environ. Aspects Appl. Biol.*, **17**(1):11–17, 1988. , lethal, sublethal, individual, population.

[276] S. A. L. M. Kooijman. The von Bertalanffy growth rate as a function of physiological parameters; a comparative analysis. In T. G. Hallam, L. J. Gross, and S. A. Levin, editors, *Mathematical ecology.*, pages 3–45. World Scientific, Singapore, 1988. DEB, individual.

[277] S. A. L. M. Kooijman. Vermindering van slibproductie. H_2O, **22**(22):684, 1989. degradation, sewage.

[278] S. A. L. M. Kooijman. Effects of feeding conditions on toxicity for the purpose of extrapolation. *Comp. Biochem. Physiol.*, **100c**(1/2):305–310, 1991. , kinetics, individual.

[279] S. A. L. M. Kooijman. Oecotoxicologische risicoevaluatie. In N. M. van Straalen and J. A. C. Verkleij, editors, *Leerboek Oecotoxicologie.*, pages 348–356. VU Uitgeverij, Amsterdam, 1991. lethal, sublethal, individual, population, kinetics.

[280] S. A. L. M. Kooijman. Biomass conversion at population level. In D. L. DeAngelis and L. J. Gross, editors, *Individual based models; an approach to populations and communities.*, pages 338–358. Chapman & Hall, 1992. population, DEB.

[281] S. A. L. M. Kooijman. *Dynamic energy budgets in biological systems. Theory and applications in ecotoxicology.* Cambridge University Press, 1993.

[282] S. A. L. M. Kooijman. Effects of temperature on birds. In E. J. M. Hagemeijer and T. J. Verstrael, editors, *Bird Numbers 1992. Distribution, monitoring and ecological aspects.*, pages 285–290. Statistics Netherlands, Voorburg/Heerlen, 1994. DEB, individual.

[283] S. A. L. M. Kooijman. Individual based population modelling. In J. Grasman and G. van Straten, editors, *Predictability and Nonlinear Modelling in Natural Sciences and Economics.*, pages 232–247. Kluwer Academic Publishers, Dordrecht, 1994. population, individual.

[284] S. A. L. M. Kooijman. The stoichiometry of animal energetics. *J. Theor. Biol.*, **177**:139–149, 1995. , limitation, individual, population.

[285] S. A. L. M. Kooijman. An alternative for NOEC exists, but the standard model has to be replaced first. *Oikos*, **75**:310–316, 1996. , lethal, sublethal, individual, population.

[286] S. A. L. M. Kooijman. Process-oriented descriptions of toxic effects. In G. Schüürmann and B. Markert, editors, *Ecotoxicology.*, pages 483–519. Spektrum Akademischer Verlag, 1997. , , lethal, sublethal, individual, population.

[287] S. A. L. M. Kooijman. The dynamic energy budget model. In *Report of the OECD Workshop on Statistical Analysis of Aquatic Toxicity Data.*, volume 10 of *OECD Environmental Health and Safety Publications*, pages 91–98. OECD, 1998. , DEB, individual.

[288] S. A. L. M. Kooijman. The synthesizing unit as model for the stoichiometric fusion and branching of metabolic fluxes. *Biophyscal Chemistry*, **73**:179–188, 1998.

[289] S. A. L. M. Kooijman. *Dynamic Energy and Mass Budgets in Biological Systems.* Cambridge University Press, 2000.

[290] S. A. L. M. Kooijman. Quantitative aspects of metabolic organization; a discussion of concepts. *Philosophical Transactions of the Royal Society B*, **356**:331–349, 2001.

[291] S. A. L. M. Kooijman. On the coevolution of life and its environment. In J. Miller, P. J. Boston, S. H. Schneider, and E. Crist, editors, *Scientists debate Gaia: the next century.*, chapter 30, pages 343–351. MIT Press, Cambridge, Massachusetts, 2004.

[292] S. A. L. M. Kooijman. Samenleven van organismen. In H. Heesterbeek, O. Diekmann, and J. A. J. Metz, editors, *De Wiskundige Kat, de Biologische Muis en de Jacht op Inzicht; verkenningen op het grensvlak van wiskunde en biologie*, pages 63–76. Epsilon-uitgevers, Utrecht, 2004. , symbiosis, ecosystem, DEB.

[293] S. A. L. M. Kooijman. Pseudo-faeces production in bivalves. *J. Sea Research*, **56**:103–106, 2006.

[294] S. A. L. M. Kooijman. What the egg can tell about its hen: embryo development on the basis of dynamic energy budgets. *J. Math. Biol.*, 2008. subm 2007/09/10.

[295] S. A. L. M. Kooijman. *Dynamic Energy Budget theory for metabolic organisation.* Cambridge University Press, 2009. in prep.

[296] S. A. L. M. Kooijman. Social interactions can affect feeding behaviour of fish in tanks. *J. Sea Res.*, 2009. in prep.

[297] S. A. L. M. Kooijman, T. R. Andersen, and B. W. Kooi. Dynamic energy budget representations of stoichiometric constraints to population models. *Ecology*, **85**:1230 – 1243, 2004.

[298] S. A. L. M. Kooijman, P. Auger, J. C. Poggiale, and B. W. Kooi. Quantitative steps in symbiogenesis and the evolution of homeostasis. *Biological Reviews*, **78**:435–463, 2003.

[299] S. A. L. M. Kooijman, J. Baas, D. Bontje, M. Broerse, C. A. M. van Gestel, and T. Jager. Ecotoxicological applications of dynamic energy budget theory. In J. Devillers, editor, *Ecotoxicology Modeling.* Springer, 2008. , to appear.

[300] S. A. L. M. Kooijman, J. Baas, D. Bontje, M. Broerse, C. van Gestel, and T. Jager. Toxico-kinetic models for ecotoxicological applications. In J. Devillers, editor, *Model in ecotoxicology.* Springer, 2007. to appear.

[301] S. A. L. M. Kooijman, J. Baas, D. Bontje, M. Broerse, T. Jager, C. van Gestel, and B. van Hattum. Scaling relationships based on partition coefficients and body sizes have similarities and interactions. *SAR and QSAR in Environ. Res.*, 2007. , to appear.

[302] S. A. L. M. Kooijman and J. J. M. Bedaux. *The analysis of aquatic toxicity data.* VU University Press, Amsterdam, 1996.

[303] S. A. L. M. Kooijman and J. J. M. Bedaux. Analysis of toxicity tests on *Daphnia* survival and reproduction. *Water Res.*, **30**:1711–1723, 1996. , lethal, sublethal, individual.

[304] S. A. L. M. Kooijman and J. J. M. Bedaux. Analysis of toxicity tests on fish growth. *Water Res.*, **30**:1633–1644, 1996. , sublethal, individual.

[305] S. A. L. M. Kooijman and J. J. M. Bedaux. Some statistical properties of estimates of no-effects concentrations. *Water Res.*, **30**:1724–1728, 1996. , lethal, individual.

[306] S. A. L. M. Kooijman and J. J. M. Bedaux. Toxic effects on survival, growth and reproduction; a new approach. *Newsletter Netherlands Centre Alternatives to Animal Use*, **4**:11–12, 1997. , lethal, sublethal, individual, population.

[307] S. A. L. M. Kooijman and J. J. M. Bedaux. Dynamic effects of compounds on animal energetics and their population consequences. In J. E. Kammenga and R. Laskowski, editors, *Demography in Ecotoxicology.*, pages 27–41. Wiley, 2000.

[308] S. A. L. M. Kooijman, J. J. M. Bedaux, A. A. M. Gerritsen, H. Oldersma, and A. O. Hanstveit. Dynamic versus static measures for ecotoxicity. In M. C. Newman and C. Strojan, editors, *Risk Assessment: Logic and Measurement.*, pages 187–224. Ann Arbor Press, 1998. , lethal, sublethal, individual, population, kinetics.

[309] S. A. L. M. Kooijman, J. J. M. Bedaux, A. R. R. Péry, and T. Jager. Biology-based methods. In H. Magaud, editor, *Current approaches in the statistical analysis of ecotoxicity data: A guidance to application.*, volume 54, TC 147/ SC 5/ WG 10/ N0390 of *Series on Testing Assessment*, chapter 7. ISO and OECD, Paris, 2006.

[310] S. A. L. M. Kooijman, J. J. M. Bedaux, and W. Slob. No-effect concentration as a basis for ecological risk assessment. *Risk Analysis*, **16**:445–447, 1996. , lethal, sublethal, population, individual.

[311] S. A. L. M. Kooijman, H. A. Dijkstra, and B. W. Kooi. Light-induced mass turnover in a mono-species community of mixotrophs. *J. Theor. Biol.*, **214**:233–254, 2002.

[312] S. A. L. M. Kooijman, J. Grasman, and B. W. Kooi. A new class of non-linear stochastic population models with mass conservation. *Math Biosci*, 2007. to appear.

[313] S. A. L. M. Kooijman, A. O. Hanstveit, and N. van der Hoeven. Research on the physiological basis of population dynamics in relation to ecotoxicology. *Wat. Sci. Tech.*, **19**:21–37, 1987. individual, population.

[314] S. A. L. M. Kooijman, A. O. Hanstveit, and N. Nyholm. No-effect concentrations in alga growth inhibition tests. *Water Res.*, **30**:1625–1632, 1996. , lethal, sublethal, population.

[315] S. A. L. M. Kooijman and R. J. F. van Haren. Animal energy budgets affect the kinetics of xenobiotics. *Chemosphere*, **21**:681–693, 1990. kinetics, individual.

[316] S. A. L. M. Kooijman and R. Hengeveld. The symbiontic nature of metabolic evolution. In T. A. C. Reydon and L. Hemerik, editors, *Current Themes in Theoretical Biology: A Dutch perspective.*, pages 159–202. Springer, Dordrecht, 2005.

[317] S. A. L. M. Kooijman, N. van der Hoeven, and D. C. van der Werf. Population consequences of a physiological model for individuals. *Funct. Ecol.*, **3**:325–336, 1989. individual, population, DEB.

[318] S. A. L. M. Kooijman, T. Jager, and B. W. Kooi. The relationship between elimination rates and partition coefficients of chemical compounds. *Chemosphere*, **57**:745–753, 2004.

[319] S. A. L. M. Kooijman and B. W. Kooi. Catastrophic behaviour of myxamoebae. *Nonlin. World*, **3**:77–83, 1996. , population.

[320] S. A. L. M. Kooijman, B. W. Kooi, and M. P. Boer. Rotifers do it with delay. the behaviour of reproducers vs dividers in chemostats. *Nonlinear World*, **3**:107–128, 1996.

[321] S. A. L. M. Kooijman, B. W. Kooi, and T. G. Hallam. The application of mass and energy conservation laws in physiologically structured population models of heterotrophic organisms. *J. Theor. Biol.*, **197**:371–392, 1999.

[322] S. A. L. M. Kooijman, B. W. Kooi, H. W. van Verseveld, C. H. Ratsak, E. B. Muller, and D. H. Eikelboom. Afvalwater zuiveren zonder slib te produceren. *Land + Water*, **8**:61–64, 1994. , sewage, degradation.

[323] S. A. L. M. Kooijman and J. A. J. Metz. On the dynamics of chemically stressed populations; the deduction of population consequences from effects on individuals. *Ecotox. Environ. Saf.*, **8**:254–274, 1983. lethal, sublethal, individual, population.

[324] S. A. L. M. Kooijman, E. B. Muller, and A. H. Stouthamer. Microbial dynamics on the basis of individual budgets. *Antonie van Leeuwenhoek*, **60**:159–174, 1991. , individual, population, DEB.

[325] S. A. L. M. Kooijman and R. M. Nisbet. How light and nutrients affect life in a closed bottle. In S. E. Jørgensen, editor, *Thermodynamics and ecological modelling.*, pages 19–60. CRC Publ., Boca Raton, FL, USA, 2000.

[326] S. A. L. M. Kooijman, K. de Raat, and M. I. Willems. Ames test modeling. *Mutations Research*, **130**:217, 1984.

[327] S. A. L. M. Kooijman and L. A. Segel. How growth affects the fate of cellular substrates. *Bull. Math. Biol.*, **67**:57 – 77, 2005.

[328] S. A. L. M. Kooijman, T. Sousa, l. Pecqueri, J. van der Meer, and T. Jager. The estimation of dynamic energy budget parameters, a practical guide. *Func. Ecol.*, 2007.

[329] S. A. L. M. Kooijman, T. Sousa, L. Pecqueri, J. van der Meer, and T. Jager. From food-dependent statistics to metabolic parameters, a practical guide to the use of dynamic energy budget theory. *Biol. Rev.*, 2008. , to appear.

[330] S. A. L. M. Kooijman and T. A. Troost. Quantitative steps in the evolution of metabolic organisation as specified by the dynamic energy budget theory. *Biol. Reviews*, **82**:1–30, 2007.

[331] E. V. Koonin, K. S. Makarova, and L. Aravind. Horizontal gene transfer in prokaryotes: Quantification and classification. *Annual Review of Microbiology*, **55**:709–742, 2001.

[332] K. B. Krauskopf and D. K. Bird. *Introduction to geochemistry.* McGraw-Hill Internat. Editions, New York, 1995.

[333] W. E. Krumbein and D. Werner. The microbial silica cycle. In W. E. Krumbein, editor, *Microbial geochemistry.*, pages 125–157. Blackwell Scientific Publ., Oxford, 1983.

[334] L. D. Kuijper, B. W. Kooi, T. R. Anderson, and S. A. L. M. Kooijman. Stoichiometry and food chain dynamics. *Theoretical Population Biology*, **66**:323–339, 2004.

[335] L. D. J. Kuijper. *The role of trophic flows in food web dynamics.* PhD thesis, Vrije Universiteit, Amsterdam, 2004.

[336] L. D. J. Kuijper, T. R. Anderson, and S. A. L. M. Kooijman. C and N gross efficiencies of copepod egg production studies using a dynamic energy budget model. *J. Plankton Research*, **26**:1–15, 2003.

[337] L. D. J. Kuijper, T. R. Anderson, and S. A. L. M. Kooijman. C and N gross efficiencies of copepod egg production studies using a dynamic energy budget model. *J. Plankton Research*, **26**:213–226, 2004. , limitation, DEB, ecosystem.

[338] L. D. J. Kuijper, B. W. Kooi, C. Zonneveld, and S. A. L. M. Kooijman. Omnivory and food web dynamics. *Ecological Modelling*, **163**:19–32, 2003.

[339] A. Kulminski, K. Manton, I. Akushevich, and A. Yashin. The effect of the organisms' body size and energy reserves in models for population dynamics. *Journal of Biological Systems*, **12**:419–437, 2004.

[340] W. Lampert, E. McCauley, and B. F. J. Manly. Trade-offs in the vertical distribution of zooplankton: ideal free distribution with costs? *Proceedings of the Royal Society of London series B-Biological Sciences*, **270**:765–773, 2003.

[341] N. Lane. *Oxygen, the molecule that made the world.* Oxford University Press, Oxford, 2002.

[342] D. A. Lashof. Gaia on the brink: Biogeochemical feedback processes in global warming. In S. H. Schneider and P. J. Boston, editors, *Scientists on Gaia.*, pages 393–404. MIT Press, Cambridge, Mass., 1991.

[343] G. Ledder, J. D. Logan, and A. Joern. Dynamic energy budget models with size-dependent hazard rates. *Journal of Mathematical Biology*, **48**:605–622, 2004.

[344] J. J. Lee, G. F. Leedale, and P. Bradbury. *An illustrated guide to the Protozoa.* Society of Protozoologists, Lawrence, Kansas, 2000.

[345] I. M. M. van Leeuwen. *Mathematical models in cancer risk assessment.* PhD thesis, Vrije Universiteit, Amsterdam, 2003.

[346] I. M. M. van Leeuwen, F. D. L. Kelpin, and S. A. L. M. Kooijman. A mathematical model that accounts for the effects of caloric restriction on body weight and longevity. *Biogerontology*, **3**:373–381, 2002.

[347] I. M. M. van Leeuwen and S. A. L. M. Kooijman. Final report project DEBtum "realistic characterizations of the tumor-induction potential of chemicals". Technical report, Dept Theoretical Biology, Vrije Universiteit, Amsterdam, 2003. , lethal, sublethal.

[348] I. M. M. van Leeuwen and C. Zonneveld. From exposure to effect: a comparison of modeling approaches to chemical carcinogenesis. *Mutation Research*, **489**:17–45, 2001.

[349] I. M. M. van Leeuwen, C. Zonneveld, and S. A. L. M. Kooijman. The embedded tumor: host physiology is important for the interpretation of tumor growth. *British Journal of Cancer*, **89**:2254–2263, 2003. .

[350] I. van Leeuwen. Vive rápido, muere joven; matemáticas en biología del envejecimiento. *La Gaceta De La RSME*, **10**:71–96, 2007. .

[351] R. A. Leigh and D. Sanders. *The plant vacuole.* Academic Press, San Diego, 1997.

[352] V. Lemesle and J.-L. Gouze. A biochemically based structured model for phytoplankton growth in the chemostat. *Ecological Complexity*, **2**:21–33, 2005.

[353] J. W. Lengeler, G. Drews, and H. G. Schlegel, editors. *Biology of the prokaryotes.* Thieme Verlag, Stuttgart, 1999.

[354] B. Levine and D. J. Klionsky. Development by self-digestion: Molecular mechanisms and biological functions of autophagy. *Developmental Cell*, **6**:463–477, 2004.

[355] S. M. Libes. *An introduction to Marine Biogeochemistry.* Wiley, New York, 1992.

[356] K. Lika and S. A. L. M. Kooijman. Life history implications of allocation to growth versus reproduction in dynamic energy budgets. *Bull. Math. Biol*, **65**:809–834, 2003.

[357] K. Lika and R. M. Nisbet. A dynamic energy budget model based on partitioning of net production. *Journal of Mathematical Biology*, **41**:361–386, 2000.

[358] K. Lika and N. Papandroulakis. Modeling feeding processes: a test of a new model for sea bream (*Sparus aurata*) larvae. *Canadian Journal of Fisheries and Aquatic Science*, **99**:1–11, 2004.

[359] Papandroulakis N Lika K. Modeling feeding processes: a test of a new model for sea bream (*Sparus aurata*) larvae. *Canadian Journal of Fisheries and Aquatic Sciences*, **62**:425–435, 2005.

[360] P. A. Lindahl and B. Chang. The evolution of acetyl-CoA synthase. *Origins of Life and Evolution of the Biosphere*, **31**:403–434, 2001.

[361] M. R. Lindsay, R. J. Webb, M. Strouss, M. S. M. Jetten, M. K. Butler, R. J. Forde, and J. A. Fuerst. Cell compartmentalisation in planctomycetes: novel types of structural organisation for the bacterial cell. *Archives of Microbiology*, **175**:413–429, 2001.

[362] L. G. Ljungdahl. The acetyl-coa pathway and the chemiosmotic generation of atp during acetogenesis. In H. L. Drake, editor, *Acetogenesis.*, pages 63–87. Chapman and Hall, New York, 1994.

[363] H. Lodish, A. Berk, S. L. Zipursky, P. Matsudaira, D. Baltimore, and J. Darnell. *Molecular cell biology.* W. H. Freeman & Co, New York, 2000.

[364] J. Loman. Microevolution and maternal effects on tadpole *Rana temporaria* growth and development rate. *Journal of Zoology*, **257**(01):93–99, 2002.

[365] C. Lopes, A. R. R. Péry, A. Chaumot, and S. Charles. Ecotoxicology and population dynamics: Using DEBtox models in a Leslie modeling approach. *Ecological Modelling*, **188**:30–40, 2005.

[366] A. Lorena. Modelling of micro-algae for carbon sequestration and biofuel production. *J. Sea Res.*, 2009. in prep.

[367] M. Maar, K. Bolding, J. K. Petersen, J. S. L. Hansen, and K. Timmermann. Growth and feed-backs of blue mussels change ecosystem dynamics in a coupled physical-biogeochemical model of Nysted off-shore wind farm, denmark. *J. Sea Res.*, 2009. in prep.

[368] D. Mackay, W. Y. Shiu, and K. C. Ma. *Illustrated handbook of physical-chemical properties and environmental fate for organic chemicals.* Lewis publishers, Inc., Michigan, USA, 1992.

[369] M. T. Madigan, J. M. Martinko, and J. Parker. *Brock Biology of Microorganisms.* Prentice Hall International, New Jersey, 2000.

[370] R. A. Mah, D. M. Ward, L. Baresi, and T. L. Glass. Biogenesis of methane. *Ann. Rev. Microbiol.*, **31**:309–341, 1977.

[371] U.-G. Maier, S. E. Douglas, and T. Cavalier-Smith. The nucleomorph genomes of cryptophytes and chlorarachniophytes. *Protist*, **151**:103–109, 2000.

[372] L. Margulis. *Origins of eukaryotic cells.* Freeman, San Fransico, 1970.

[373] L. Margulis. *Symbiosis in cell evolution.* Freeman, New York, 1993.

[374] L. Margulis and R. Fester, editors. *Symbiosis as a source of evolutionary innovation.* MIT Press, 1991.

[375] M. M. Martin. *Invertebrate-microbial interactions; Ingested fungal enzymes in arthropod biology.* Comstock Publishers & Associates,, Ithaca, 1987.

[376] W. Martin and M. Muller. The hydrogen hypothesis for the first eukaryote. *Nature*, **392**:37–41, 1998.

[377] W. Martin, C. Rotte, M. Hoffmeister, U. Theissen, g. Gelius-Dietrich, A. Ahr, and K. Henze. Early cell evolution, eukaryotes, anoxia, sulfide, oxygen, fungi first (?), and a thee of genomes revisited. *Life*, **55**:193–204, 2003.

[378] W. Martin, T. Rujan, E. Richly, A. Hansen, Cornelsen, S., T. Lins, D. Leister, B. Stoebe, M. Hasegawa, and D. Penny. Evolutionary analysis of arabidopsis, cyanobacterial, and chloroplast genomes reveals plastid phylogeny and thousands of cyanobacterial genes in the nucleus. *Proceedings of the National Academy of Sciences of the USA*, **99**:12246–12251, 2002.

[379] W. Martin and M. Russel. On the origin of cells: a hypothesis for the evolutionary transitions from abiotic geochemistry to chemoautotrophic prokaryotes and from prokaryotes to nucleated cell. *Philosophical Transaction of the Royal Society London B*, **358**:59–85, 2003.

[380] W. Martin and C. Schnarrenberger. The evolution of the calvin cycle from prokaryotic to eukaryotic chromosomes: a case study of functional redundancy in ancient pathways through endosymbiosis. *Current Genetics*, **32**:1–18, 1997.

[381] W. Martin, B. Stoebe, V. Goremykin, S. Hansmann, M. Hasegawa, and K. V. Kowallik. Gene transfer to the nucleus and the evolution of chloroplasts. *Nature (London)*, **393**:162–165, 1998.

[382] M. Matteus. Can we reach consensus between marine ecological models and metabolic theories in ecology?. *J. Sea Res.*, 2009. in prep.

[383] G. L. C. Matthaei. On the effect of temperature on carbon-dioxide assimilation. *Phil. Trans. Roy. Soc. B*, **197**:47–105, 1905.

[384] O. Maury, B. Faugeras, Y.-J. Shin, Poggiale J.-C., T. Ben Ari, and F. Marsac. Modeling environmental effects on the size-structured energy flow through marine ecosystems. part 1: The model. *Progress in Oceanography*, **74**:479–499, 2007.

[385] O. Maury, Y.-J. Shin, B. Faugeras, T. Ben Ari, and F. Marsac. Modeling environmental effects on the size-structured energy flow through marine ecosystems. part 1: Simulations. *Progress in Oceanography*, **74**:500–514, 2007.

[386] J. Maynard Smith, N. H. Smith, M. O'Rourke, and B. G. Spratt. How clonal are bacteria? *Proceedings of the National Academy of Sciences U.S.A*, **90**:4384–4388, 1993.

[387] G. I. McFadden. Primary and secondary endosymbiosis and the origin of plastids. *Journal of Phycology*, **37**:951–959, 2001.

[388] GS McIntyre and RH Gooding. Egg size, contents, and quality: maternal-age and-size effects on house fly eggs. *Can. J. Zool./Rev. Can. Zool*, **78**(9):1544–1551, 2000.

[389] D.A. McQuarrie. Stochastic approach to chemical kinetics. *J. Appl. Prob.*, **4**:413–478, 1967.

[390] J. van der Meer. An introduction to dynamic energy budget (deb) models with special emphasis on parameter estimation. *J. Sea Res.*, **56**:85–102, 2006.

[391] J. van der Meer. Metabolic theories in biology. *Trends in Ecology and Evolution*, **21**:136–140, 2006.

[392] J. van der Meer. Seasonal timing in the reproduction of the bivalve *Macoma baltica*: a model study of fitness consequences. *J. Sea Res.*, 2009. in prep.

[393] E. Meléndez-Hevia. The game of the pentose phosphate cycle: a mathematical approach to study the optimization in design of metabolic pathways during evolution. *Biomedical and Biochemical Acta*, **49**:903–916, 1990.

[394] E. Meléndez-Hevia and A. Isidoro. The game of the pentose phosphate cycle. *Journal of Theoretical Biology*, **117**:251–263, 1985.

[395] J. A. J. Metz and F. H. D. van Batenburg. Holling's 'hungry mantid' model for the invertebrate functional response considered as a Markov process. Part I: The full model and some of its limits. *Journal of Mathematical Biology*, **22**:209–238, 1985.

[396] J. A. J. Metz and F.H. D. van Batenburg. Holling's 'hungry mantid' model for the invertebrate functional response considered as a Markov process. Part II: Negligible handling time. *Journal of Mathematical Biology*, **22**:239–257, 1985.

[397] W. Michaelis, R. Seifert, K. Nauhaus, and others. Microbial reefs in the black sea fuelled by anaerobic oxidation of methane. *Science*, **297**:1013–836, 2002.

[398] R. Mikelsaar. A view of early cellular evolution. *J. Mol. Evol.*, **25**:168–183, 1987.

[399] J. K. Misra and R. W. Lichtwardt. *Illustrated genera of Trichomycetes; fungal symbionts of insects and other arthropods.* Science Publishers, Enfield, NH, USA, 2000.

[400] G. W. van der Molen. *A physiologically-based mathematical model for the long-term kinetics of dioxins and furans in humans.* PhD thesis, Vrije Universiteit, Amsterdam, 1998. kinetics, individual.

[401] G. W. van der Molen, S. A. L. M. Kooijman, and W. Slob. A generic toxicokinetic model for persistent lipophilic compounds in humans: an application to TCDD. *Fundam. Appl. Toxicol.*, **31**:83–94, 1996. , kinetics.

[402] G. W. van der Molen, S. A. L. M. Kooijman, and W. Slob. A human toxicokinetic model for dioxin. *Organohalogen Compounds*, **29**:394–399, 1996. kinetics.

[403] G. W. van der Molen, S. A. L. M. Kooijman, J. Wittsiepe, P. Schrey, , D. Flesch-Janys, and W. Slob. Estimation of dioxin and furan elimination rates from cross-sectional data using a pharmacokinetic model. *J. Exposure Analysis & Environ. Epidemiology*, **10**:579–585, 2000.

[404] F. M. M. Morel. Kinetics of nutrient uptake and growth in phytoplankton. *J. Phycol.*, **23**:137–150, 1987.

[405] Y. Moret, P. Juchault, and T. Rigaud. *Wolbachia* endosymbiont responsible for cytoplasmic incompatibility in a terrestrial crustacean: effects in natural and foreign hosts. *Heredity*, **86**:325–332, 2001.

[406] S. A. Morley, R. S. Batty, and P. Geffen, A. J. anf Tytler. Egg size manipulation: a technique for investigating maternal effects on the hatching characteristics of herring. *J. Fish Biol.*, **55 (suppl A)**:233–238, 1999.

[407] H. J. Morowitz, J. D. Kosttelrik, J. Yang, and G. D. Cody. The origin of intermediary metabolism. *Proceedings of the National Academy of Sciences U.S.A*, **97**:7704–7708, 2000.

[408] G. J. Morton, D. e. Cummings, D. G. Baskin, g. s. Barsh, and M. W. Schwartz. Central nervous system control of food intake and body weight. *Nature*, **443**:289–294, 2006.

[409] E. B. Muller. *Bacterial energetics in aerobic wastewater treatment.* PhD thesis, Vrije Universiteit, 1994. sewage, degradation.

[410] E. B. Muller, R. M. Nisbet, S. A. L. M. Kooijman, J. J. Elser, and E. McCauley. Stoichiometric food quality and herbivore dynamics. *Ecol. Letters*, **4**:519–529, 2001.

[411] E. B. Muller, A. H. Stouthamer, and H. W. van Verseveld. Simultaneous NH_3 oxidation and N_2 production at reduced O_2 tensions by sewage sludge subcultured with chemolithrophic medium. *Biodegradation*, **6**:339–349, 1995. degradation, sewage.

[412] L. Muscatine. Glycerol excretion by symbiotic alge from corals and *Trdacna*, and its control by the host. *Science (Washington, D. C.)*, **156**:516–519, 1977.

[413] L. Muscatine, P. G. Falkowski, and Z. Dubinsky. Carbon budgets in symbiotic associations. *Endocytobiosis*, **2**:649–658, 1983.

[414] L. Muscatine, P. G. Falkowski, J. W. Porter, and Z. Dubinsky. Fate of photosynthetically fixed carbon in light and shade-adapted corals. *Proc. R. Soc. Lond. B.*, **222**:181–202, 1984.

[415] L. Muscatine and H. M. Lenhoff. Symbiosis of hydra and algae. II. Effects of limited food and starvation on growth of symbiotic and aposymbiotic hydra. *Biol. Bull., (Woods Hole)*, **129**:316–328, 1965.

[416] R. G. Nager, P. Monaghan, and D. C. Houston. Within-clutch trade-offs between the number and quality of eggs: experimental manipulations in gulls. *Ecology*, **81**:1339–1350, 2000.

[417] R. G. Nager, P. Monaghan, D. C. Houston, K¿ E. Arnold, J. D. Blount, and N. Berboven. Maternal effects through the avian egg. *Acta Zoologica Sinica*, **52 (suppl)**:658–661, 2006.

[418] A. Narang, A. Konopka, and D. Ramkrishna. New patterns of mixed substrate growth in batch cultures of *Escherichia coli* K12. *Biotechnology & Bioengineering*, **55**:747–757, 1997.

[419] E. G. Nisbet and C. M. R. Fowler. Archaean metabolic evolution of microbial mate. *Proceedings of the Royal Society - Series B*, **266**:2375–2382, 1999.

[420] R. M. Nisbet and W. S. C. Gurney. Model of material cycling in a closed ecosystem. *Nature*, **264**:633–634, 1976.

[421] R. M. Nisbet, E. B. Muller, K. Lika, and S. A. L. M. Kooijman. From molecules to ecosystems through dynamic energy budget models. *J. Anim. Ecol*, **69**:913–926, 2000.

[422] R.M. Nisbet, E. McCauley, W.S.C. Gurney, W. W. Murdoch, and S. N. Wood. Formulating and testing a partially specified dynamic energy budget model. *Ecology*, **85**:3132–3139, 2004.

[423] E. G. Noonburg and R. M. Nisbet. Behavioural and physiological responses to food availability and predation risk. *Evolutionary Ecology Research*, **7**:89–104, 2005.

[424] V. Norris and D. J. Raine. A fission-fusion origin for life. *Origins of Life and Evolution of the Biosphere*, **29**:523–537, 1998.

[425] N. Okamoto and I. Inouye. A secondary symbiosis in progress? *Science*, **310**:287, 2005.

[426] G. J. Olsen and C. R. Woese. Lessons from an archaeal genome: what are we learning from *Methanococcus jannaschii*? *Trends in Genetics*, **12**:377–379, 1996.

[427] A.-W. Omta, J. Bruggeman, H. A. Dijkstra, and S. A. L. M. Kooijman. The physics of the biological carbon pump. *Global Biogeochemical Cycles*, 2007. subm 2006/08/21.

[428] A. W. Omta, J. Bruggeman, S. A. L. M. Kooijman, and H. A. Dijkstra. The biological carbon pump revisited: feedback mechanisms between climate and the redfield ratio. *Geophysical Research Letters*, 2006.

[429] A.-W. Omta, S. A. L. M. Kooijman, and H. A. Dijkstra. Influence of (sub)mesoscale eddies on the soft-tissue carbon pump. *J. Geophys. Res.*, **112**:doi:10.1029/2007JC004189, 2007. .

[430] L. E. Orgel. Self-organizing biochemical cycles. *Proceedings of the National Academy of Science of the USA*, **97**:12503–12507, 2000.

[431] R. Österberg. On the prebiotic role of iron and sulfur. *Origin of Life and Evolution of the Biosphere*, **27**:481–484, 1997.

[432] K. W. Osteryoung and J. Nunnari. The division of endosymbiotic organelles. *Science*, **302**:1698–1704, 2003.

[433] S. Otte, J. G. Kuenen, L. P. Nielsen, H. W. Pearl, J. Zopfi, H. N. Schulz, A. Teska, B. Strotmann, V. A. Gallardo, and B. B. Jørgenssen. Nitrogen, carbon, and sulfur metabolism in natural *Tioploca* samples. *Applied Environmental Microbiology*, **65**:3148–3157, 1999.

[434] B. O. Palsson, H. Palsson, and E. N. Lightfoot. Mathematical modelling of dynamics and control in metabolic networks. III linear eaction sequences. *J. Theor. Biol.*, **113**:231–259, 1985.

[435] D. Pantaloni, C. Le Clainche, and M.-F. Carlier. Mechanism of actin-based motility. *Science*, **292**:1502–1506, 2001.

[436] D. Papineau, J. J. Walker, S. J. Moizsis, and N. R. Pace. Composition and structure of microbial communities from stromatolites of Hamelin Pool in Shark Bay, Wesern Australia. *Applied Environmental Microbiology*, **71**:4822–4832, 2005.

[437] M. Parniske and J. A. Downie. Lock, keys and symbioses. *Nature*, **425**:569–570, 2003.

[438] D. J. Patterson. The diversity of eukaryotes. *Am. Nat.*, **154**:S96–S124, 1999.

[439] L. Pecqerie. Resolving environmental effects on stage transition in anchovy early life history using DEB theory. *J. Sea Res.*, 2009. in prep.

[440] L. Pecquerie. *Bioenergetic modelling of the growth, development and reproduction of a small pelagic fish: the Bay of Biscay anchovy.* PhD thesis, Agrocampus Rennes & Vrije Universiteit, Amsterdam, 2008. .

[441] L. Pecquerie, P. Grellier, P. Petitgas, and S. A. L. M. Kooijman. Anchovy energetics. *Canadian Journal Fisheries and Aquatic Sciences*, 2008. ,in prep.

[442] L Pecquerie, P. Petitgas, P. Grellier, R. Fablet, M. Alunno-Bruscia, and S. A. L. M. Kooijman. Reconstructing food and growth histories from otolith opacity patterns. *Proceedings of the National Academy of Sciences of the United States of America*, 2008. ,in prep.

[443] L. Pecquerie, P. Petitgas, P. Grellier, and S. A. L. M. Kooijman. Environmental effect on von Bertalanffy parameters: the use of bioenergetics to model anchovy growth. *Canadian Journal Fisheries and Aquatic Sciences*, 2008. ,in prep.

[444] L. Pecquerie, P. Petitgas, and S. A. L. M. Kooijman. Environmental impact on spawning duration: application of the dynamice energy budget (deb) theory to the Bay of Biscay anchovy (*Engraulis encrasicolus*). *Marine Ecology Progress Series*, 2008. ,in prep.

[445] E. Pennisi. Plant wannabes. *Science*, **313**:1229, 2006.

[446] A. R. R. Péry, J. J. M. Bedaux, C. Zonneveld, and S. A. L. M. Kooijman. Analysis of bioassays with time-varying concentrations. *Water Res.*, **35**:3825–3832, 2001.

[447] A. R. R. Péry, A. Bethune, J. Gahou, R. Mons, and J. Garric. Body residues: a key variable to analyze toxicity tests with *Chironomus riparius* exposed to copper-spiked sediments. *Ecotoxicology and Environmental Safety*, **61**:160–167, 2005.

[448] A. R. R. Péry, V. Ducrot, R. Mons, and J. Garric. Modelling toxicity and mode of action of chemicals to analyse growth and emergence tests with the midge chironomus riparius. *Aquatic Toxicology*, **65**:281–292, 2003.

[449] A. R. R. Péry, P. Flammarion, B. Vollat, J. J. M. Bedaux, S. A. L. M. Kooijman, and J. Garric. Using a biology-based model (debtox) to analyse bioassays in ecotoxicology: Opportunities & recommendations. *Environ. Toxicol. Chem.*, **21**:459–465, 2002.

[450] A. R. R. Péry and J. Garric. Modelling effects of temperature and feeding level on the life cycle of the midge *Chironomus riparius*: An energy-based modelling approach. *Hydrobiologia*, **553**:59–66, 2006.

[451] A. R. R. Péry, R. Mons, P. Flammarion, L. Lagadic, and J. Garric. A modeling approach to link food availability, growth, emergence, and reproduction for the midge *Chironomus riparius*. *Environmental Toxicology and Chemistry*, **21**:2507–2513, 2003.

[452] A. R. R. Péry, R. Mons, and J. Garric. Energy-based modeling to study population growth rate and production for the midge chironomus riparius in ecotoxicological risk assessment. *Ecotoxicology*, **13**:647–656, 2004.

[453] C. J. M. Philippart, O. G. Bos, E. Gontikaki, and S. A. L. M. Kooijman. The role of phenotypic plasticity in age and size at metamorphosis of the marine bivalve *Macoma balthica*. *Journal of Animal Ecology*, 2005. in prep.

[454] B. K. Pierson, H. K. Mitchell, and A. L. Ruff-Roberts. *Chloroflexus aurantiacus* and ultraviolet radiation: implications for Archean shallow-water stromatolites. *Origins of Life and Evol. of the Biosphere*, **23**:243–260, 1993.

[455] B. J. Pieters, T. Jager, M. H. S. Kraak, and W. Admiraal. Modeling responses of *Daphnia magna* to pesticide pulse exposure under varying food conditions: intrinsic versus apparent sensitivity. *Ecotoxicology*, **15**:601–608, 2006. .

[456] R. Porley and N. Hodgetts. *Mosses & Liverworts.* Collins, 2005. Bryophyta biology Britain.

[457] L. Posthuma, R. A. Verweij, B. Widianarko, and C. Zonneveld. Life-history patterns in metal-adapted *Collembola*. *Oikos*, **67**:235–249, 1993.

[458] S. Pouvreau. What does the DEB model enlighten on the feeding physiology pf *Crassostrea gigas*? *J. Sea Res.*, 2009. in prep.

[459] S. Pouvreau, Y. Bourles, S. Lefebvre, A. Gangnery, and M. Alunno-Bruscia. Application of a dynamic energy budget model to the pacific oyster *Crassostrea gigas*, reared under various environmental conditions. *J. Sea Res.*, **56**:156–167, 2006. , individual, growth, reproduction.

[460] M. Proctor and P. Yeo. *The pollination of flowers.* Collins, London, 1973.

[461] Q. Quammen. *The song of the dodo.* Simon & Schuster, New York, 1996.

[462] Péry A. R. R., Mons R. L., and J. Garric. Modelling of the life cycle of *Chironomus* species using an energy-based model. *Chemosphere*, **59**:247–253, 2005.

[463] A. N. Rai, E. Soderback, and B. Bergman. Cyanobacterium-plant symbioses. *New Phytologist*, **147**:449–481, 2000.

[464] M. S. Rappé, S. A. Connon, K. L. Vergin, and S. J. Giovannoni. Cultivation of the ubiquitous SAR11 marine bacterioplankton clade. *Nature*, **438**:630–633, 2002.

[465] C. H. Ratsak. *Grazer induced sludge reduction in wastewater treatment.* PhD thesis, Vrije Univesteit, September 1994. sewage, degradation.

[466] C. H. Ratsak. Biologische slibvermindering: een duurzame technologie? H_2O, **14**:19–21, 1998. sewage.

[467] C. H. Ratsak. Effects of *Nais elinguis* on the performance of an activated sludge plant. *Hydrobiologia*, **463**:217–222, 2001.

[468] C. H. Ratsak, B. W. Kooi, and S. A. L. M. Kooijman. Modelling the individual growth of *Tetrahymena* sp. and its population consequences. *J. Eukaryotic Microbiol.*, **42**:268–276, 1995. , population, individual.

[469] C. H. Ratsak, B. W. Kooi, and H. W. van Verseveld. Biomass reduction and mineralization increase due to the ciliate *Terahymena pyriformis* grazing on the bacterium *Pseudomonas fluorescens*. *Wat. Sci. Tech.*, **29**:119–128, 1994. , sewage, degradation.

[470] C. H. Ratsak, S. A. L. M. Kooijman, and B. W. Kooi. Modelling of growth of an oligochaete on activated sludge. *Water Res.*, **27**:739–747, 1993. , sewage, DEB, individual.

[471] C. H. Ratsak, S. A. L. M. Kooijman, A. H. Stouthamer, and H. W. van Verseveld. Bacterivorous grazers: A way to reduce sludge-production. In *Proceedings of the First Dutch-Japanese Workshop on the Treatment of Manucipal Waste Water.*, pages 92–103, Heelsum, April 1992. RIZA, STOWA, TUD, RWZI-two-thousand. degradation, sewage.

[472] C. H. Ratsak, K. A. Maarsen, and S. A. L. M. Kooijman. Effects of protozoa on carbon mineralization in activated sludge. *Water Res.*, **30**:1–12, 1996. , sewage, degradation.

[473] D. M. Raup. Geometric analysis of shell coiling: General problems. *J. Paleontol.*, **40**:1178–1190, 1966.

[474] D. M. Raup. Geometric analysis of shell coiling: Coiling in ammonoids. *J. Paleontol.*, **41**:43–65, 1967.

[475] J. A. Raven and C. Brownlee. Understanding membrane function. *Journal of Phycology*, 2001.

[476] J. A. Raven and Z. H. Yin. The past, present and future of nitrogenous compounds in the atmosphere, and their interactions with plants. *New Phytologist*, **139**:205–219, 1998.

[477] W. Reisser, editor. *Algae and symbioses.* Biopress Limited, Bristol, 1992.

[478] W. Reisser, R. Meier, and B. Kurmeier. The regulation of the endosymbiotic algal population size in ciliate-algae associations. An ecological model. In H. E. A. Schenk and W. Schwemmler, editors, *Endocytobiology*, volume 2, pages 533–543. W. de Gruyter, berlin, 1983.

[479] R. F. Rekker. The hydrophobic fragmental constant. its derivation and application. a means of characterizing membrane systems. In W. Th. Nauta and R. F. Rekker, editors, *Pharmacochemistry Library.* Elsevier, Amsterdam, 1977.

[480] J. S. Ren and A. H. Ross. Environmental influence on mussel growth: A dynamic energy budget model and its application to the greenshell mussel *Perna canaliculus*. *Ecological Modelling*, **189**:347–362, 2005.

[481] J.S. Ren and D. R. Schiel. A dynamic energy budget model: parameterisation and application to the Paci c oyster *Crassostrea gigas* in new zealand waters. *Journal of Experimental Marine Biology and Ecology*, 2008. doi:10.1016/j.jembe.2008.04.012.

[482] D. Reznick, H. Callahan, and R. Llauredo. Maternal Effects on Offspring Quality in Poeciliid Fishes. *Integrative and Comparative Biology*, **36**(2):147, 1996.

[483] M. L. Richardson and S. Gangolli. *The dictionary of substances and their effects.* the Royal Society of Chemistry, Cambridge, CB4 4WF, 1995.

[484] D. Rickard, I.B. Butler, and A. Olroyd. A novel iron sulphide switch and its implications for earth and planetary science. *Earth and Planetary Science Letters*, **189**:85–91, 2001.

[485] B. Rico-Villa. Growth dynamic energy budget (DEB) model for the larvae of Pacific oyster *Crassostrea gigas*. *J. Sea Res.*, 2009. in prep.

[486] M. A. Riley and J. E. Wertz. Bacteriochins: Evolution, ecology and application. *Annu. Rev. Microbiol.*, **56**:117–137, 2002.

[487] N. Risgaard-Petersen, A. M. Langezaal, S. Ingvardsen, M. C. Schmid, M. S. M. Jetten, H. J. M. op den Camp, J. W. M. Derksen, E. Piña Ochoa, S. P. Eriksson, L. P. Nielsen, N. P. Revsbech, T. Cedhagen, and G. J. van der Zwaan. Evidence for complete denitrification in a benthic foraminifer. *Nature*, **443**:93–96, 2006.

[488] M. Rizzotti. *Early evolution.* Birkhauser Verlag, Bazel, 2000.

[489] N. Rodriguez-Ezpeleta, H. Brinkmann, S. C. Burey, G. Roure, B. abd Burger, W. Loffelhardt, H. J. Bohnert, H. Philippe, and B. F. Lang. Monophyly of primary photosynthetic eukaryotes: green plants, red algae, and glaucophytes. *Current Biology*, pages 1325–1330, 2005.

[490] A. J. Roger. Reconstructing early events in eukaryotic evolution. *Am. Nat.*, **154**:S146–S163, 1999.

[491] A. h. Romano and T. Conway. Evolution of carbohydrate metabolic pathways. *Research in Microbiology*, **147**:448–455, 1996.

[492] M. C. Rossiter. Environmentally-based maternal effects: a hidden force in insect population dynamics? *Oecologia*, **87**(2):288–294, 1991.

[493] M. C. Rossiter. Maternal Effects Generate Variation in Life History: Consequences of Egg Weight Plasticity in the Gypsy Moth. *Functional Ecology*, **5**(3):386–393, 1991.

[494] M. E. Rothenberg and Y.-N. Jan. The hyppo hypothesis. *Nature*, **425**:469–470, 2003.

[495] M. J. S. Rudwick. The growth and form of brachiopod shells. *Geol. Mag.*, **96**:1–24, 1959.

[496] M. J. S. Rudwick. Some analytic methods in the study of ontogeny in fossils with accretionary skeletons. *Paleont. Soc., Mem.*, **2**:35–59, 1968.

[497] J. B. Russel and G. M. Cook. Energetics of bacterial growth: Balance of anabolic and catabolic reactions. *Microbiological Reviews*, **59**:48–62, 1995.

[498] M. J. Russell and A. J. Hall. The emergence of life from iron monosulphide bubbles ar a submarine hydrothermal redox and pH front. *Journal of the Geological Society London*, **154**:377–402, 1997.

[499] M. J. Russell and A. J. Hall. From geochemistry to biochemistry: chemiosmotic coupling and transition element clusters in the onset of life and photosynthesis. *The Geochemical News*, **133**(October):6–12, 2002.

[500] M. J. Russell, Daniel R. M., A. J. Hall, and J. A. Sherringham. A hydrothermally precipitated catalytic iron sulfide membrane as a first step toward life. *Journal of Molecular Evolution*, **39**:231–243, 1994.

[501] F. Ryan. *Darwins blind spot.* Texere, New York, 2003.

[502] Ren J. S. and Ross A. H. A dynamic energy budget model of the pacific oyster *Crassostrea gigas*. *Ecol. Model*, **142**:105–120, 2001.

[503] G. W. Saunders and M. H. Hommersand. Assessing red algal supraordinal diversity and taxonomy in the context of contemporary systematic data. *American Journal of Botany*, **91**:1494–1507, 2004.

[504] M .A. Savageau. *Biochemical Systems Analysis.* Addison-Wesley Publishing Company., Reading, MA, 1976.

[505] J. Schalk. *A study of the metabolic pathway of anaerobic ammonium oxidation.* PhD thesis, University of Delft, 2000.

[506] D. E. Schindel. Unoccupied morphospace and the coiled geometry of gastropods: Architectural constraint or geometric covariance? In R. M. Ross and W. D. Allmon, editors, *Causes of evolution. A Paleontological perspective*. The University of Chicago Press, 1990.

[507] P. Schönheit and T. Schafer. Metabolism of hyperthermophiles. *World Journal of Microbiology & Biotechnology*, **11**:26–57, 1995.

[508] M. A. A. Schoonen, Y. Xu, and J. Bebie. Energetics and kinetics of the prebiotic synthesis of simple organic and amino acids with the fes-h2s/fes2 redox couple as a reductant. *Origins of Life and Evolution of the Biosphere*, **29**:5–32, 1999.

[509] L. M. Schoonhoven, T. Jermy, and J. J. A. van Loon. *Insect-plant biology; From physiology to ecology.* Chapman and Hall, London, 1998.

[510] H. N. Schulz and B. B. Jørgensen. Big bacteria. *Annual Reviews of Microbiology*, **55**:105–137, 2001.

[511] A. Schüßler. Molecular phylogeny, taxonomy, and evolution of geosiphon pyriformis and arbuscular mycorrhizal fungi. *Plant and Soil*, **244**:75–83, 2002.

[512] R. P. Schwarzenbach, P. M. Gschwend, and D. M. Imboden. *Enviromental oranic chemistry.* John Wiley & sons, Inc., New York, 1993.

[513] P. Sébert. Pressure effects on shallow-water fishes. In D. J. Randall and A. P. Farrell, editors, *Deep-sea fishes.*, chapter 7, pages 279–324. Academic Press, San Diego, 1997.

[514] L. A. Segel. Diffuse feedback from a diffuse informational network. In L. A. Segel and I. Cohen, editors, *Design Principles for the Immune System and Other Distributed Autonomous Systems*, pages 203–226. Oxford University Press, 2001.

[515] D. Segré, D. Ben-Eli, D. W. Deamer, and D. Lancet. The lipid world. *Origins of Life and Evolution of the Biosphere*, **31**:119–145, 2001.

[516] M. Selig, K. B. Xavier, H. Santos, and P. Schnheit. Comparative analysis of embden-meyerhof and entnerdoudoroff glycolytic pathways in hyperthermophilic archaea and the bacterium *Thermotoga*. *Archives of Microbiology*, **167**:217–232, 1997.

[517] M.-A. Selosse and F. Le Tacon. The land flora: a phototroph-fungus partnership? *Trends in Ecology and Evolution*, **13**:15–20, 1998.

[518] Y. Shen and R. Buick. The antiquity of microbial sulfate reduction. *Earth-Science Reviews*, **64**:243–272, 2004.

[519] J. M. Siegel. The REM sleep-memory consilidation hypothesis. *Science*, **294**:1058–1063, 2001.

[520] J. M. Siegel. Why we sleep. *Scientific American*, **289**(5):72–77, 2003.

[521] A. G. Simpson and A. J. Roger. Eukaryotic evolution: getting to the root of the problem. *Current Biology*, **12**:R691 – 693, 2002.

[522] A. G. B. Simpson, J. van den Hoff, C. Bernard, H. R. Burton, and D. J. Patterson. The ultrastructure and systematic position of the euglenozoon *Postgaardi mariagerensis*, Fenchel et al. *Arch. Protistenkd.*, **147**:213–225, 1996.

[523] P. G. Simpson and W. B. Whitman. Anabolic pathways in methanogens. In J. G. Ferry, editor, *Methanogenesis.*, pages 445–472. Chapman and Hall, New York, 1993.

[524] B. Sinervo. The evolution of maternal investments in lizards: an experimental and comparative analysis of egg size and its effects on offspring performance. *Evolution*, **44**:279–294, 1990.

[525] D. C. Smith and A. E. Douglas. *The biology of symbiosis.* Arnold, London, 1987.

[526] D. J. Smith and G. J. C. Underwood. The production of extracellular carbohydrates by estuarine benthic diatoms: the effects of growth phase and light and dark treatment. *Journal of Phycology*, **36**:321–333, 2000.

[527] B. Snow and D. Snow. *Birds and berries.* Poyser, Calton, 1988.

[528] T. Sousa. *Thermodynamics as a Substantive and Formal Theory for the Analysis of Economic and Biological Systems.* PhD thesis, Technical University, Vrije Universiteit, Lisbon, Amsterdam, 2007. .

[529] T. Sousa, T. Domingos, and S. A. L. M. Kooijman. From empirical patterns to theory: A formal metabolic theory of life. *Phil. Trans. R. Soc. B*, 2008. , to appear.

[530] T. Sousa, R. Mota, T. Domingos, and S. A. L. M. Kooijman. The thermodynamics of organisms in the context of DEB theory. *Physical Review E*, **74**:1–15, 2006.

[531] J. I. Sprent. *The ecology of the nitrogen cycle.* Cambridge studies in ecology. Cambridge University Press, Cambridge, 1987.

[532] J. T. Staley, M. P. Bryant, N. Pfennig, and J. G. Holt. *Bergeys manual of systematic bacteriology.* Williams and Wilkins, Baltimore, 1989.

[533] A. Stechmann and T. Cavalier-Smith. Rooting the eukaryote tree by using a derived gene fusion. *Science*, **297**:89–91, 2002.

[534] P. Steemans and C. H. Wellman. Miospores and the emergence of land plants. In B. Webby, F. Paris, M. L. Droser, and I. C. Percival, editors, *The great Ordovician biodiversification event.*, pages 361–366. Columbia University Press, New York, 2004.

[535] E. T. Steenkamp, J. Wright, and S. L. Baldauf. The protistan origins of animals and fungi. *Molecular Biology and Evolution*, **23**:93–106, 2006.

[536] J. W. Stiller, D. C. Reel, and J. C. Johnson. A single origin of plastids revisited: convergent evolution in organellar genome content. *Journal of Phycology*, **39**:95–105, 2003.

[537] D. K. Stoecker and M. W. Silver. Replacement and aging of chloroplasts in *Strombidium capitatum* (*Ciliophora: Oligaotrichida*). *Marine Biology*, **107**:491–502, 1990.

[538] A. H. Stouthamer and S. A. L. M. Kooijman. Why it pays for bacteria to delete disused DNA and to maintain megaplasmids. *Antonie van Leeuwenhoek*, **63**:39–43, 1993.

[539] S. Stracke, C. Kistner, S. Yoshida, et al. A plant receptor-like kinase required bor both bacterial and fungal symbiosis. *Nature*, **417**:959–962, 2002.

[540] M. Strous. *Microbiology of anaerobic ammonium oxidation.* PhD thesis, Delft University of Technology, 2000.

[541] M. Strous and M. S. M. Jetten. Anaerobic oxidation of mathane and ammonium. *Annual Reviews of Microbiology*, **58**:99–117, 2004.

[542] L. Stryer. *Biochemistry.* W. H. Freeman and Comp., New York, 1988.

[543] M. R. Sullivan, J. B. Waterbury, and S. W. Chisholm. Cyanophages infecting the oceanic cyanobacterium *Prochlorococcus. Nature*, **424**:1047–1050, 2003.

[544] H. Tappan. Possible eucaryotic algae (*Bangiophycidae*) among early Proterozoic microfossils. *Geological Society of America Bulletin*, **87**:633–639, 1976.

[545] F. J. R. Taylor. Implications and extensions of the serial endosymbiosis theory of the origin of eukaryotes. *Taxon*, **23**:229–258, 1974.

[546] J. W. Taylor, J. Spatafora, K. O'Donnell, F. Lutzoni, T. James, D. S. Hibbert, D. Geiser, T. D. Bruns, and M. Blackwell. The fungi. In J. Cracraft and M. J. Donoghue, editors, *Assembling the tree of life*, pages 171–194. Oxford University Press, Oxford, 2004.

[547] P. Taylor, T. E. Rummery, and D. G. Owen. Reactions of iron monosulfide solids with aqueous hydrogen sulfide up to 160°c. *Journal of Inorganic and Nuclear Chemistry*, **41**:1683–1687, 1979.

[548] T. F. Thingstad, H. Havskum, K. Garde, and B. Riemann. On the strategy of "eating your competitor": a mathematical analysis of algal mixotrophy. *Ecology*, **77**:2108–2118, 1996.

[549] R. V. Thomann. Bioaccumulation model of organic chemical distribution in aquatic food chains. *Environmental Science & Technology*, **23**:677–707, 1989.

[550] P. G. Thomas and T. Ikeda. Sexual regression, shrinkage, re-maturation and growth of spent female *Euphausia superba* in the laboratory. *Mar. Biol.*, **95**:357–363, 1987.

[551] Y. Thomas, J. Mazurié, S. Pouvreau, C. Bacher, and M. Alunno-Bruscia. Modelling the growth of *Mytilus edulis* (L.) by coupling a Dynamic Energy Budget model with satellite-derived environmental data. *J. Sea Res.*, 2009. in prep.

[552] D'Archy W. Thompson. *Growth and form.*, volume I & II. Cambridge University Press, 1917.

[553] A. G. M. Tielens, C. Rotte, J. J. van Hellemond, and W. Martin. Mitochondria as we dont know them. *Trends in Biochemical Sciences*, **27**:564–572, 2002.

[554] C. Tolla. *Bacterial populations dynamics modelling: applied to the study of bioturbation effects on the nitrogen cycle in marine sediments.* PhD thesis, University of Marseille & Vrije Universiteit, Amsterdam, 2006.

[555] C. Tolla, S. A. L. M. Kooijman, and J. C. Poggiale. A kinetic inhibition mechanism for the maintenance process. *J. Theor. Biol.*, **244**:576–587, 2007.

[556] T. Troost. *Evolution of community metabolism.* PhD thesis, Vrije Universiteit, Amsterdam, 2006. .

[557] T. A. Troost, U. Dieckmann, and B. W. Kooi. Joint evolution of predator body size and prey-size preference. *Evolutionary Ecology*, 2008. , to appear, evolution, adaptive dynamics.

[558] T. A. Troost, B. W. Kooi, and S. A. L. M. Kooijman. Ecological specialization of mixotrophic plankton in a mixed water column. *Am. Nat.*, **166**:E45–E61, 2005. , AD, bifurcation, ecosystem.

[559] T. A. Troost, B. W. Kooi, and S. A. L. M. Kooijman. When do mixotrophs specialize? adaptive dynamics theory applied to a dynamic energy budget model. *Math. Biosci.*, **193**:159–182, 2005. , AD, bifurcation, ecosystem.

[560] T. A. Troost, B. W. Kooi, and S. A. L. M. Kooijman. Bifurcation analysis can unify ecological and evolutionary aspects of ecosystems. *Ecol. Mod.*, **204**:253–268, 2007. , adaptive dynamics, bufircation theory, ecosystem.

[561] T. Tyrell. The relative influences of nitrogen and phosphorous on oceanic primary production. *Nature*, **400**:525–531, 1999.

[562] K. Vánky. *Illustrated genera of smut fungi.*, volume 1 of *Cryptogamic Studies*. Gustav Fischer Verlag, Stuttgart, 1987.

[563] H. van der Veer and M. Alunno-Bruscia. The DEBIB project: Dynamic Energy Budgets in Bivalves. *Journal of Sea Research*, **56**:81–84, 2006.

[564] H. van der Veer, J. F. M. F. Cardoso, and s. A. L. M. Kooijman. Physiological performance of plaice *Pleuronectes platessa* (L.) can be predicted by Dynamic Energy Budgets. *J. Sea Res.*, 2009. in prep.

[565] H. van der Veer, J. F. M. F. Cardoso, and J. van der Meer. The estimation of DEB parameters for various Northeast Atlantic bivalve species. *J. Sea Research*, **56**:107–124, 2006.

[566] H. W. van der Veer, S. A. L. M. Kooijman, W. C. Leggett, and J. van der Meer. Body size scaling relationships in flatfish as predicted by dynamic energy bugets (deb theory): implications for recruitment. *J. Sea Research*, **50**:255–270, 2003.

[567] H. W. van der Veer, S. A. L. M. Kooijman, and J. van der Meer. Intra- and interspecific comparison of energy flow in north atlantic flatfish species by means of dynamic energy budgets. *J. Sea Research*, **45**:303–320, 2001.

[568] T. A. Villareal. Evaluation of nitrogen fixation in the diatom genus *Rhizosolenia* ehr. in the absence of its cyanobacterial symbiont *Richelia intracellularis* schmidt. *J. Plank. Res.*, **9**:965–971, 1987.

[569] T. A. Villareal. Nitrogen fixation of the cyanobacterial symbiont of the diatom genus *Hemiaulus*. *Mar. Ecol. Prog. Ser.*, **76**:201–204, 1991.

[570] K. Vink, L. Dewi, J. J. M. Bedaux, A. Tompot, M. Hermans, and N. M. van Straalen. The importance of the exposure route when testing the toxicity of pesticides to saprotrophic isopods. *Environ. Toxicol. Chem.*, **14**:1225–1232, 1995. kinetics, lethal, sublethal, individual.

[571] J. A. G. M. de Visser, A. ter Maat, and C. Zonneveld. Energy budgets and reproductive allocation in the simultaneous hermaphrodite pond snail, *Lymnaea stagnalis* (L.): A trade-off between male and female function. *Am. Nat.*, **144**:861–867, 1994. , DEB, individual, population.

[572] T. J. Vrede, D. Dobberfuhl, S. A. L. M. Kooijman, and J. J. Elser. Fundamental connections among organism c:n:p stoichiometry, marcomolecular composition and growth. *Ecology*, **85**:1217 – 1229, 2004.

[573] G Wächtershäuser. Pyrite formation, the first energy source for life. a hypothesis. *Systematic and Applied Microbiology*, **10**:207–210, 1988.

[574] G Wächtershäuser. Evolution of the 1st metabolic cycles. *Proceedings of the National Academy of Sciences U.S.A*, **87**:200–204, 1990.

[575] T. G. Waddell, P. Repovic, E. Meléndez-Hevia, R. Heinrich, and F. Montero. Optimization of glycolysis: A new look at the efficiency of energy coupling. *Biochemical Education*, **25**:204–205, 1997.

[576] M. R. Walker. Stromatolites: The main geological source of information on the evolution of the early benthos. In S. Bengtson, editor, *Early life on earth.*, volume 84 of *Nobel Symposium*, pages 270–286. Columbria University Press, New York, 1994.

[577] P. Ward. Precambrian strikes back. *NewScientist*, (9 Feb):40–43, 2008.

[578] J. Warham. The crested penguins. In B. Stonehouse, editor, *The biology of penguins*, pages 189–269. MacMillan Publishing Co., London, 1975.

[579] T. F. Weis. *Cellular biophysics.*, volume I Transport. MIT Press, Cambridge, Massachusetts, 1996.

[580] J. van Wensum. *Isopods and pollutants in decomposing leaf litter.* PhD thesis, Vrije Universeit, Amsterdam, 1992.

[581] J. H. Werren. Evolution and consequences of *Wolbachia* symbioses in invertebrates. *Am. Zool.*, **40**:1255–1255, 2000.

[582] P. Westbroek. *Life as a geological force; dynamics of the Earth.* W. W. Norton & Co, New York, 1991.

[583] J. N. C. Whyte, J. R. Englar, and B. L. Carswell. Biochemical-composition and energy reserves in *Crassostrea-gigas* exposed to different levels of nutrition. *Aquaculture*, **90**:157–172, 1990.

[584] J. W. M. Wijsman, E. Brummelhuis, and A. C. Smaal. Application of a DEB model for cockles to simulate growth in the Oostersclde estuary. *J. Sea Res.*, 2009. in prep.

[585] C. R. Woese. A proposal concerning the origin of life on the planet earth. *Journal of Molecular Evolution*, **12**:95–100, 1979.

[586] C. R. Woese. Archaebacteria. *Scientific American*, **6**:98–122, 1981.

[587] C. R. Woese. On the evolution of cells. *Proceedings of the National Academy of Sciences U.S.A.*, **99**:8742–8747, 2002.

[588] R. Wood. *Reef evolution.* Oxford University Press, Oxford, 1999.

[589] T. R. Worsley, R. D. Nance, and J. B. Moody. Tectonics, carbon, life, and climate for the last three billion years: A unified system? In S. H. Schneider and P. J. Boston, editors, *Scientists on Gaia.*, pages 200–210. MIT Press, Cambridge, Mass., 1991.

[590] J. Xiong, W. M. Fisher, K. Inoue, et al. Molecular evidence for the early evolution of photosynthesis. *Science*, **289**:1724–1730, 2000.

[591] S. H. Yoon, J. D. Hacket, C. Ciniglia, G. Pinto, and D. Bhattacharya. The single, ancient origin of chromist plastids. *Proceedings of the National Academy of Sciences U.S.A.*, **99**:15507–15512, 2002.

[592] S. H. Yoon, J. D. Hacket, C. Ciniglia, G. Pinto, and D. Bhattacharya. A molecular timeline for the origin of photosynthetic eukaryotes. *Molecular Biology and Evolution*, **21**:809–818, 2004.

[593] T. Yoshinaga, A. Hagiwara, and K. Tsukamoto. Effect of periodical starvation on the survival of offspring in the rotifer *Brachionus plicatilis*. *Fisheries Science*, **67**:373–374, 2001.

[594] J. C. Zachos, M. W. Wara, S. Bohaty, M. L. Delaney, et al. A transient rise in tropical sea surface temperature during the paeocene-eocene thermal maximum. *Science*, **302**:1551–1554, 2003.

[595] Y.J. Zhao, H. Y. Wu, H. L. Guo, Xu. M., K. Cheng, and H. Y. Zhu. Vacuolation induced by unfavorable pH in cyanobacteria. *Progress in Natural Ncience*, **11**:931–936, 2001.

[596] C. Zonneveld. *Animal energy budgets: a dynamic approach.* PhD thesis, Vrije Universiteit, December 1992.

[597] C. Zonneveld. Modelling the kinetics of non-limiting nutrients in microalgae. *J. Mar. Syst.*, **9**:121–136, 1996. , limitation, population.

[598] C. Zonneveld. Modeling effects of photoadaptation on the photosynthesis-irradiance curve. *J. Theor. Biol.*, **186**:381–388, 1997. , limitation, ecosystem.

[599] C. Zonneveld. A cell-based model for the chlorophyll 'a' to carbon ratio in phytoplankton. *Ecol. Modell.*, **113**:55–70, 1998. , limitation, population.

[600] C. Zonneveld. Light-limited microalgal growth: a comparison of modeling approaches. *Ecol. Modell.*, **113**:41–54, 1998. , limitation, population.

[601] C. Zonneveld. Photoinhibition as affected by photoacclimation in phytoplankton: a model approach. *J. Theor. Biol.*, **193**:115–123, 1998. , limitation, population.

[602] C. Zonneveld, H. A. van den Berg, and S. A. L. M. Kooijman. Modeling carbon cell quota in light-limited phytoplankton. *J. Theor. Biol.*, **188**:215–226, 1997. , limitation, ecosystem.

[603] C. Zonneveld and S. A. L. M. Kooijman. Application of a general energy budget model to *Lymnaea stagnalis*. *Funct. Ecol.*, **3**:269–278, 1989. individual, DEB.

[604] C. Zonneveld and S. A. L. M. Kooijman. Body temperature affects the shape of avian growth curves. *J. Biol. Syst.*, **1**:363–374, 1993. , DEB, individual.

[605] C. Zonneveld and S. A. L. M. Kooijman. Comparative kinetics of embryo development. *Bulletin of Mathematical Biology*, **3**:609–635, 1993.

[606] G. Zubay. *Origins of life on earth and in the cosmos.* Academic Press, San Diego, 2000.